

# **I**nternational Iodine Workshop

Full Proceedings



**For Official Use**

**NEA/CSNI/R(2016)5**

Organisation de Coopération et de Développement Économiques  
Organisation for Economic Co-operation and Development

**30-May-2016**

**English text only**

**NUCLEAR ENERGY AGENCY  
COMMITTEE ON THE SAFETY OF NUCLEAR INSTALLATIONS**

**INTERNATIONAL IODINE WORKSHOP: Full Proceedings**

*This document only exists in PDF*

**JT03396860**

**Complete document available on OLIS in its original format**

*This document and any map included herein are without prejudice to the status of or sovereignty over any territory, to the delimitation of international frontiers and boundaries and to the name of any territory, city or area.*

NEA/CSNI/R(2016)5  
For Official Use

English text only

## ORGANISATION FOR ECONOMIC CO-OPERATION AND DEVELOPMENT

The OECD is a unique forum where the governments of 34 democracies work together to address the economic, social and environmental challenges of globalisation. The OECD is also at the forefront of efforts to understand and to help governments respond to new developments and concerns, such as corporate governance, the information economy and the challenges of an ageing population. The Organisation provides a setting where governments can compare policy experiences, seek answers to common problems, identify good practice and work to co-ordinate domestic and international policies.

The OECD member countries are: Australia, Austria, Belgium, Canada, Chile, the Czech Republic, Denmark, Estonia, Finland, France, Germany, Greece, Hungary, Iceland, Ireland, Israel, Italy, Japan, Luxembourg, Mexico, the Netherlands, New Zealand, Norway, Poland, Portugal, the Republic of Korea, the Slovak Republic, Slovenia, Spain, Sweden, Switzerland, Turkey, the United Kingdom and the United States. The European Commission takes part in the work of the OECD.

OECD Publishing disseminates widely the results of the Organisation's statistics gathering and research on economic, social and environmental issues, as well as the conventions, guidelines and standards agreed by its members.

## NUCLEAR ENERGY AGENCY

The OECD Nuclear Energy Agency (NEA) was established on 1 February 1958. Current NEA membership consists of 31 countries: Australia, Austria, Belgium, Canada, the Czech Republic, Denmark, Finland, France, Germany, Greece, Hungary, Iceland, Ireland, Italy, Japan, Luxembourg, Mexico, the Netherlands, Norway, Poland, Portugal, the Republic of Korea, the Russian Federation, the Slovak Republic, Slovenia, Spain, Sweden, Switzerland, Turkey, the United Kingdom and the United States. The European Commission also takes part in the work of the Agency.

The mission of the NEA is:

- to assist its member countries in maintaining and further developing, through international co-operation, the scientific, technological and legal bases required for a safe, environmentally friendly and economical use of nuclear energy for peaceful purposes;
- to provide authoritative assessments and to forge common understandings on key issues, as input to government decisions on nuclear energy policy and to broader OECD policy analyses in areas such as energy and sustainable development.

Specific areas of competence of the NEA include the safety and regulation of nuclear activities, radioactive waste management, radiological protection, nuclear science, economic and technical analyses of the nuclear fuel cycle, nuclear law and liability, and public information.

The NEA Data Bank provides nuclear data and computer program services for participating countries. In these and related tasks, the NEA works in close collaboration with the International Atomic Energy Agency in Vienna, with which it has a Co-operation Agreement, as well as with other international organisations in the nuclear field.

This document and any map included herein are without prejudice to the status of or sovereignty over any territory, to the delimitation of international frontiers and boundaries and to the name of any territory, city or area.

Corrigenda to OECD publications may be found online at: [www.oecd.org/publishing/corrigenda](http://www.oecd.org/publishing/corrigenda).

© OECD 2016

---

You can copy, download or print OECD content for your own use, and you can include excerpts from OECD publications, databases and multimedia products in your own documents, presentations, blogs, websites and teaching materials, provided that suitable acknowledgment of the OECD as source and copyright owner is given. All requests for public or commercial use and translation rights should be submitted to [rights@oecd.org](mailto:rights@oecd.org). Requests for permission to photocopy portions of this material for public or commercial use shall be addressed directly to the Copyright Clearance Center (CCC) at [info@copyright.com](mailto:info@copyright.com) or the Centre français d'exploitation du droit de copie (CFC) [contact@cfcopies.com](mailto:contact@cfcopies.com).

---

## COMMITTEE ON THE SAFETY OF NUCLEAR INSTALLATIONS

The NEA Committee on the Safety of Nuclear Installations (CSNI) is an international committee made up of senior scientists and engineers with broad responsibilities for safety technology and research programmes, as well as representatives from regulatory authorities. It was created in 1973 to develop and co-ordinate the activities of the NEA concerning the technical aspects of the design, construction and operation of nuclear installations insofar as they affect the safety of such installations.

The committee's purpose is to foster international co-operation in nuclear safety among NEA member countries. The main tasks of the CSNI are to exchange technical information and to promote collaboration between research, development, engineering and regulatory organisations; to review operating experience and the state of knowledge on selected topics of nuclear safety technology and safety assessment; to initiate and conduct programmes to overcome discrepancies, develop improvements and reach consensus on technical issues; and to promote the co-ordination of work that serves to maintain competence in nuclear safety matters, including the establishment of joint undertakings.

The priority of the CSNI is on the safety of nuclear installations and the design and construction of new reactors and installations. For advanced reactor designs, the committee provides a forum for improving safety-related knowledge and a vehicle for joint research.

In implementing its programme, the CSNI establishes co-operative mechanisms with the NEA Committee on Nuclear Regulatory Activities (CNRA), which is responsible for issues concerning the regulation, licensing and inspection of nuclear installations with regard to safety. It also co-operates with other NEA Standing Technical Committees, as well as with key international organisations such as the International Atomic Energy Agency (IAEA), on matters of common interest.



## ACKNOWLEDGEMENTS

### WORKSHOP ORGANIZING COMMITTEE

JACQUEMAIN Didier	(IRSN, France)
KISSANE Martin	(NEA)
VAN DORSSELAERE Jean-Pierre	(NUGENIA/SARNET)

### WORKSHOP SCIENTIFIC COMMITTEE (MEMBERS OF THE ORGANIZING COMMITTEE AND)

ALBIOL Thierry	(IRSN, France)
DICKINSON Shirley	(NNL, UK)
HERRANZ Luis Enrique	(CIEMAT, Spain)
FUNKE Friedhelm	(AREVA GmbH, Germany)
GLOWA Glenn	(CNL, Canada)
GUPTA Sanjeev	(Becker Technologies, Germany)
HOSHI Harutaka	(NRA, Japan)
HOTTA Akitoshi	(NRA, Japan)
KARKELA Teemu	(VTT, Finland)
LIND Terttaliisa	(PSI, Switzerland)
POWERS Dana	(SNL, USA)
SALAY Michael	(USNRC, USA)
SONG JinHo	(KAERI, Korea)

### FUNDING

The workshop was co-funded by the European Commission – Joint Research Centre, the French “Institut de Radioprotection et de Sûreté Nucléaire” and the Nuclear Energy Agency (NEA) of the OECD.



## LIST OF ACRONYMS

BDBA	Beyond Design Basis Accident
CIEMAT	Centro de Investigaciones Energéticas, Medioambientales y Tecnológicas (Spain)
DBA	Design Basis Accident
BIP	Behaviour of Iodine Project (a NEA joint project)
BWR	Boiling-Water Reactor
CNL	Canadian Nuclear Laboratories
CRPPH	NEA Committee on Radiation Protection and Public Health
CSNI	NEA Committee on the Safety of Nuclear Installations
DF(s)	Decontamination Factor(s) (in FCVS)
EC	European Commission
(F)CVS	(Filtered) Containment Venting System
FP	Fission Product
HBU	High Burn-Up
IRSN	Institut de Radioprotection et de Sûreté Nucléaire (France)
ISTP	International Source Term Programme (a co-operative research programme)
KAERI	Korea Atomic Energy Research Institute
LWR	Light-Water Reactor
MCCI	Molten-Core-Concrete Interaction
MOX	Mixed OXide Fuel
NEA	Nuclear Energy Agency of the OECD
NNL	National nuclear laboratory (UK)
NRA	Nuclear Regulation Authority (Japan)
NPP	Nuclear Power Plant
OECD	Organisation for Economic Cooperation and Development
Org-I	Organic Iodides
PRG	Programme Review Group (of the BIP or STEM joint projects)
PSI	Paul Scherrer Institute (Switzerland)
RCS	Reactor Coolant System
SA	Severe Accident
SAM(M)	Severe-Accident Management (Measures)
SARNET	Severe-Accident Research NETwork
SFP	Spent-Fuel Pool
SNL	Sandia National Laboratories (USA)
ST	Source Term

STEM	Source-Term Evaluation and Mitigation project (a NEA joint project)
TGT	Thermal Gradient Tube
THAI	Thermal hydraulics, Hydrogen, Aerosol, Iodine project (a NEA joint project)
USNRC	United States Nuclear Regulatory Commission
VTT	Technical Research Centre of Finland
WGAMA	CSNI Working Group on Analysis and Management of Accidents
WPNEM	CRPPH Working Party on Nuclear Emergency Matters

## EXECUTIVE SUMMARY

The international Iodine Workshop organized by the French “Institut de Radioprotection et de Sûreté Nucléaire”, the Nuclear Energy Agency of the OECD, the NUGENIA-SARNET network and the European Commission through the Joint Research Centre (Petten) was held in Marseille (France) from 30 March to 1 April 2015.

The scope and objectives of the workshop were to:

- review and discuss the outcomes of recently concluded and on-going national and international research programmes related to iodine and ruthenium behaviour during NPP accidents including DBA (Design Basis Accident) and BDBA (Beyond Design Basis Accident);
- review and discuss the associated progress made in related modelling in NPP accidents;
- review and discuss the implications for source term evaluations and assessment of accident management measures (for radiological impact reduction through, e.g., FCVS implementation);
- identify safety-significant issues in the field not yet sufficiently covered that would induce gaps or potential weaknesses in accident analysis and assessment of accident management measures, including for the long-term phases of an accident;
- share source-term evaluation results and related uncertainties assessments;
- contribute to the dissemination of knowledge gained in the field and promote the best use of knowledge updates for accident analysis and management.

The workshop enjoyed the participation of 76 experts from research organizations, industry, safety authorities and their technical safety organizations from Belgium, Canada, Finland, France, Germany, Italy, Japan, Poland, Republic of Korea, Spain, Sweden, Switzerland, UK, USA and two international organizations EC and NEA. Thirty-one technical papers were presented.

The workshop objectives relative to reviewing and discussing the state of the art knowledge of iodine and ruthenium behaviour in NPP accidents gained through research projects and progress made in the related modelling were well fulfilled. In addition, highlighting remaining open issues and assessing their coverage through on-going and planned research activities was well considered with, in particular, discussions concerning the NEA BIP (Behaviour of Iodine Project)-3, STEM-2 and THAI-3 follow-on proposals and recommendations for future work. The workshop also contributed, and will continue contributing through publication of the summary report, to knowledge sharing and dissemination in the field.

However, contributions concerning applications of research results for improving accident analyses and management were limited in number and scope. This led workshop experts to formulate recommendations to foster international exchanges and actions to assess more thoroughly implications of progress on ST research for NPP accident management; in addition to this, recommendations were also made for further investigations on some technical issues.

## **Main conclusions by topic**

### ***Iodine and ruthenium release from fuel***

The existing large database on FP release from fuel highlights that volatile FPs (I, Cs, Te) tend towards complete release in SAs involving significant fuel degradation while release of semi-volatile FPs (Mo, Ba, Ru) is strongly dependent on oxido-reducing conditions, with Mo and Ru release tending to be large in oxidizing conditions. Semi-volatile FP-release modelling has still to be improved. Recently obtained data are challenging hypotheses used in accident analyses for volatile FPs (notably Cs) release for DBA, BDBA with limited fuel degradation and for FP release in oxidizing conditions.

### ***Iodine and ruthenium transport in the RCS***

Much progress was made on understanding and modelling of gas-phase iodine chemistry in the RCS. SA system codes benefited from model developments related to the effect of Mo on Cs and I chemistry and transport. Data were generated to treat the kinetics and thermodynamic modelling of influential reactions for the Cs, Mo, B, I, H, O chemical system. The kinetic database is being extended to treat Ag, In and Cd effect on iodine transport and chemistry. All these developments aim at providing better predictions of the gaseous iodine fractions at the RCS break in a SA – which is highly scenario dependent and affected by carrier gas composition, compounds resulting from control rod degradation and other FPs - and reduce related uncertainties on iodine ST evaluations.

Some progress in understanding Ru transport was obtained from experimentation. The issue is to develop models able to calculate Ru re-emission from RCS deposits as Ru rapidly deposits on RCS surfaces after its release from the fuel. The Ru source to the containment would then be very dependent on such re-emission processes. However, experiments closer to reactor conditions are necessary to provide data for the development of applicable models.

A remaining important issue is the development of a pragmatic research approach to tackle complex heterogeneous processes (interactions of gas species with surfaces and aerosols in the RCS) and assess the effect of re-suspension/re-volatilization/decomposition of deposits resulting from mechanical, thermal and dose loadings. These may be important delayed sources of FPs (I, Cs and Ru) to the containment potentially contributing to the ST in later stages of the accident, notably in case of FCVS use. Limited experimentation on Cs and Ru re-vaporization processes was and is being performed. This is proposed to be continued for Ru in the STEM-2 project. However, performing reactor-relevant experiments and developing models still appear challenging due to the complexity of the involved processes and the importance of dealing with representative surface states and deposits.

A test was performed to investigate gaseous iodine release for SGTR accidents. Calculations have shown the lack of validation of existing iodine chemistry models in the aqueous phase for DBA conditions in the RCS (low doses and concentrations, high temperatures, additives effects).

### ***Iodine and ruthenium behaviour in the containment***

The knowledge gained on the containment gas phase (aerosols and gases/vapours) during all stages of the accident should help assess releases through containment leaks and through FCVS. Following PHEBUS FP, research focused on gas-phase and heterogeneous processes (interaction of gaseous iodine with paints and organic iodides (Org-I) production, with reactive aerosols, iodine-oxide ( $I_xO_y$ ) particle formation/decomposition, gaseous iodine release by decomposition of deposited aerosols by radiation). The research was recently conducted in the ISTP, NEA BIP-1 and BIP-2, THAI-1 and THAI-2 and STEM projects. Gas-phase processes are reasonably well covered by past, on-going and planned research (with the proposed NEA BIP-3, STEM-2, THAI-3 follow-on projects) with a focus on inorganic gaseous iodine species,  $I_xO_y$ , Org-I and gaseous ruthenium tetroxide ( $RuO_4$ ) behaviour. Significant progress has been

made through all these projects on the understanding and modelling of such processes. Part of the gained knowledge is implemented in SA system codes.

Following the Fukushima accident, considering potential long-term loss of containment heat removal systems, questions were raised on FP remobilization from deposits on containment surfaces and from sumps/suppression pools during long-term stages of a SA, notably in relation to assessing FP release during containment venting. This contributed to the definition of research projects intending to increase knowledge on such processes. This is included in the BIP-3, STEM-2 and THAI-3 projects.

Less work was recently performed on containment aqueous-phase chemistry in SA as the main source of volatile iodine was considered to be in the gas phase. The effect of impurities in sumps on iodine volatility was investigated, notably showing a low effect for chlorine and generating data to model nitrate/nitride effects. Recently, following Fukushima's accident, questions were raised as to the effect of seawater compounds on water-phase chemistry concerning the FP-scrubbing efficiency in suppression pools and in liquid-type FCVS considering evolving hydrodynamics and chemical conditions during the accident and considering the long-term aqueous-phase chemistry in relation to long-term accident management (corrosion reactions and leaching of corium/debris).

The effect of seawater is currently investigated in Japan with possible effects of bromine on iodine chemistry. Work in this field will continue in the coming years to develop the corresponding models.

The effects of evolving hydrodynamic and chemical conditions on FP pool scrubbing efficiency in suppression pools and FCVS during a SA were, are or will be partly investigated. However, the modelling of hydrodynamics, with existing modelling unable to represent flow instabilities which may strongly affect FP scrubbing efficiencies, has to be improved. There are presently only limited concerted research actions in the field, with the notable exception of the EU-PASSAM project covering some aspects, and a larger collaboration would certainly be beneficial to progress on scrubbing modelling.

### ***FP Filtration in FCVS***

Important efforts were led in the past for the development and qualification of FCVS but questions remain as to the efficiency and robustness of such systems in SA conditions as they may be envisaged post-Fukushima. For some countries where safety criteria associated with releases are more stringent, there is a search for more efficient filtration to further reduce radiological consequences. Such issues, with the assessment of innovative filtration technologies, are being covered in current research projects. There are also some specific FCVS national developments notably in Japan and in the Republic of Korea.

The knowledge-base related to “delayed” in-containment re-volatilization and re-suspension processes of radionuclides from RCS and containment surfaces and containment pools is being extended through on-going and future research programmes.

As for filtration, besides aerosols, specific attention is being given to Org-I and IxOy particles as they may contribute significantly to the ST in some accidents. Possible contribution of ruthenium-oxide species to the ST is also under investigation.

### ***Iodine chemistry in the environment***

Little attention was given to iodine chemistry in the environment for the assessment of its dispersion and related radiological consequences. Due to the complexity of the chemical systems to be treated and the lack of validation of the existing preliminary modelling, the potential impact of iodine chemistry in the environmental on radiological consequences has to be further assessed. If the impact is shown to be strong, a pragmatic approach to model it will have to be developed.

### ***SA system codes ST models validation***

Questions were raised about the level of detail required in models for system codes and the effect of uncertainties in the models on the calculated ST and consequences. For “end-user” applications such as radiological consequence assessments and emergency planning, the models have to be simple and conservative. However, even the apparently simple models have to be based on a good understanding and representation of the iodine behaviour, sometimes at the level treated by the more detailed models, in order to ensure that the important phenomena are correctly taken into account and scaled.

### ***Reference ST evaluations and emergency response tools***

Final objectives of the ST research are to contribute to the consolidation of reference ST calculations used, notably, for design of protection measures and of fast-running calculation tools used to support emergency response. The question of the methodology of implementation of ST-research outcomes into these tools and of the assessment of their robustness remains a key issue.

### **Main recommendations**

Experts consider that models able to better predict the kinetics of FP release from fuel would be valuable for the evaluation of consequences of accidents with limited fuel degradation (incl. DBA) and with oxidizing conditions (incl. SFP) and their management. Analyses of existing data (e.g., VERDON tests) should be deepened to propose future research in the field.

Experts recommend conducting further assessments of the importance of oxidizing accident scenarios which could result in significant Ru release to the environment.

Experts recommend designing research to test the validity of aqueous-phase iodine-chemistry models in DBA conditions.

Experts recommend conducting further assessments to assess the potential effect of “delayed” FP re-emission from RCS and containment surface deposits and sumps on ST evaluations and focus the research in the field to be relevant to reactor applications, integrating existing knowledge, on-going and planned research.

For scrubbing FCVSs, the effect of evolving hydrodynamic and chemical conditions in SAs on scrubbing efficiency requires further investigations. Experts also recommend fostering collaborations on pool-scrubbing model development in relation to assessing FP retention in suppression pools and in FCVSs in SAs. Such models should also be of relevance for FP retention in SGTR.

Experts recommend strengthening collaborative analytical activities, if possible joined integrated activities between projects, using the available international programmes results, highlighting that such activities were in the last years limited in scope.

Experts recommend organizing further exchanges to deepen the assessment of the validity of ST-related models implemented in SA system codes notably by addressing:

- the definition of a reference code-validation matrix for iodine behaviour in the RCS and containment;
- the necessary level of detail for the modelling of the complex iodine behaviour for plant calculations;
- the model validation for plant calculations (scaling issue) by performing, e.g., a SA system-code benchmarking exercise for defined reactor-like scenarios notably to assess the impact of recent developments of chemical models.

Experts recommend strengthening knowledge exchange between the ST-research and the environmental-chemistry communities.

Concerning ST calculations, the experts recommend strengthening exchanges on source term evaluations performed for NPPs in various countries (results and methodologies) and on quantification of remaining uncertainties on the related modelling, this in view of checking that the ST research is properly focused and no key issue overlooked.

Concerning fast-running tools for emergency response, the workshop experts recommend strengthening links between the ST-research community and the emergency response 'end-users'.



## TABLE OF CONTENTS

LIST OF ACRONYMS .....	7
EXECUTIVE SUMMARY .....	9
TABLE OF CONTENTS .....	15
BACKGROUND AND SCOPE OF THE WORKSHOP.....	17
PARTICIPATION IN THE WORKSHOP.....	19
SUMMARY OF TECHNICAL SESSIONS .....	21
Session 1:main lessons from experimental programmes on iodine and ruthenium behaviour in a severe accident and research perspectives .....	21
Session 2:iodine transfer to aqueous phase, aqueous-phase chemistry.....	27
Session 3:organic iodide formation and partitioning, chemistry and interactions with aerosols, droplets and surfaces in the gas phase .....	29
Session 4:filtered containment venting systems .....	33
Session 5:recent developments in iodine chemistry modelling in severe accidents and applications to source-term and radiological-consequences evaluations .....	35
SUMMARY STATUS REPORTS OF NEA BIP-2 AND OECD/STEM PROGRAMMES .....	37
NEA BIP-2 and follow-up - G. Glowa (CNL).....	37
NEA STEM and follow-up - C. Mun (IRSN).....	38
SUMMARY, CONCLUSIONS AND RECOMMENDATIONS .....	43
APPENDIX 1: WORKSHOP AGENDA .....	51
APPENDIX 2: LIST OF PARTICIPANTS.....	55
APPENDIX 3: PAPERS BY TECHNICAL SESSIONS .....	65
Session 1:main lessons from experimental programmes on iodine and ruthenium behaviour in a severe accident and research perspectives .....	67
Session 2:iodine transfer to aqueous phase, aqueous-phase chemistry.....	181
Session 3:organic iodide formation and partitioning, chemistry and interactions with aerosols, droplets and surfaces in the gas phase .....	213
Session 4:filtered containment venting systems .....	275
Session 5:recent developments in iodine chemistry modelling in severe accidents and applications to source term and radiological consequences evaluations .....	339



## **BACKGROUND AND SCOPE OF THE WORKSHOP**

The international OECD/NEA-NUGENIA-SARNET Iodine Workshop was organized jointly by the French “Institut de Radioprotection et de Sûreté Nucléaire” (IRSN), the Nuclear Energy Agency (NEA) of the OECD, the NUGENIA-SARNET network and the European Commission through the Joint Research Centre (JRC) of Petten. It was held in Marseille (France) from March 30, 2015 till April 1, 2015. Stakeholders involved in improving understanding of iodine behaviour and mitigating iodine release in a nuclear power plant (NPP) accident judged appropriate to organize such an event in view of:

- the recent termination of many research initiatives in the field: the International Source Term Programme (ISTP), the NEA Behaviour of Iodine Project phase 2 (BIP-2), the NEA Thermal-hydraulics, Hydrogen, Aerosol, Iodine Project phase 2 (THAI-2), the European Commission (EC) Severe Accident Research Network of Excellence phase 2 funded within the 7<sup>th</sup> Framework Programme (SARNET-2 in FP7), which all ended in 2014, and the NEA Source Term Evaluation and Mitigation Project phase 1 (STEM-1), which will end in June 2015;
- the recent launching, driven notably by the Fukushima accident, of research initiatives related to the design or improvement of filtered containment venting systems (FCVSS), which provide a means to preserve the containment and mitigate radioactive releases when an accident at a NPP results in containment over-pressurization: the EC PASSAM FP7 project, the French MIRE project which were launched in 2013 and many other national initiatives notably in Europe, Japan, Switzerland and the Republic of Korea;
- the on-going elaboration of future research international ventures, notably in the frame of the NEA safety research projects: BIP-3, STEM-2 and THAI-3;
- questions raised after the Fukushima accident relative to iodine releases and related radiological consequences.

The scope and objectives of the workshop were to:

- Review and discuss the outcomes of recently concluded and on-going national and international research initiatives (PHEBUS FP/ISTP, SARNET-2, NEA BIP-2, STEM and THAI-2, EC PASSAM, national projects, etc.) related to iodine – and, for some of them, ruthenium – behaviour during NPP accidents including design basis accidents (DBA) and beyond design basis accidents (BDBA);
- Review and discuss the associated progress made in iodine and ruthenium chemistry modelling in NPP accidents;
- Review and discuss the implications of the main research outcomes (experiments and model development/assessment) for source term evaluations and assessment of accident management measures (for radiological impact reduction through, e.g., the implementation of FCVS) both for DBA and BDBA;

- Highlight open issues of safety significance in the field and confirm that they are well-covered by on-going or planned research activities, notably through the NEA BIP-3, STEM-2 and THAI-3 proposals. Check that these activities are as far as possible conducted in an integrated and optimized way (e.g., in facilities with complementary capabilities);
- Contribute to the dissemination of knowledge gained in the field;
- Share recently updated knowledge on iodine and ruthenium chemistry (as well as on chemistry of other elements - fission products and structure materials - that will affect it) in NPP accidents, including release from the fuel, transport in the reactor coolant system, behaviour in the containment and release to the environment through containment leak paths or containment venting systems (CVS), filtered or unfiltered;
- Promote the best use of knowledge updates for accident analysis and management;
- Share source term evaluation results made in various countries (e.g., as part of deterministic or PSA level 2 studies) and related uncertainties assessments;
- Identify safety-significant issues in the field not yet sufficiently covered that would induce gaps or potential weaknesses in accident analysis and assessment of accident management measures, including the consideration of the long-term phases of an accident.

Because one of the objectives of the workshop was to review and discuss the main outcomes of the completed NEA BIP-2 project and the finishing STEM project (last test completed in April 2015) as well as the pertinence of the follow-up research initiatives, the BIP-3 and STEM-2 projects, the workshop should also fulfil the objectives of the final summary workshop for the BIP-2 and STEM projects.

## **PARTICIPATION IN THE WORKSHOP**

Thirty-one technical papers were presented in five technical sessions (see the agenda in Appendix 1). Authors were members of research organizations, industry, safety authorities and their technical safety organizations. The workshop enjoyed the participation of 76 experts from Belgium, Canada, Finland, France, Germany, Italy, Japan, Poland, Republic of Korea, Spain, Sweden, Switzerland, United Kingdom, United States of America and two international organizations EC and NEA (participants are shown in Appendix 2). The technical papers are provided in Appendix 3.



## SUMMARY OF TECHNICAL SESSIONS

### Session 1: main lessons from experimental programmes on iodine and ruthenium behaviour in a severe accident and research perspectives

**Session Chairs: T. Albiol (IRSN), H. Hoshi (NRA)**

Session 1 consisted of ten presentations. Main outcomes are reported hereafter as well as chairmen views on pending issues.

1.1 – Main outcomes relative to iodine behaviour from the VERDON/ISTP programme - Y. Pontillon (CEA) et al. Four VERDON FP release tests were successfully performed by CEA from 2011 to 2014 in the frame of the ISTP programme. The programme objectives were to study (1) FP release from high burn-up UO<sub>2</sub> and MOX fuels, in particular for low volatile FP and (2) impact of air ingress on FP behaviour which is expected to enhance the release of highly radiotoxic FP, such as ruthenium, as well as to re-volatilise volatile FP (iodine, caesium) previously deposited in the RCS. Three VERDON tests covering the first topic were performed: VERDON-1 with UO<sub>2</sub> fuel at 72 GWd/t in reducing conditions, VERDON-3 and VERDON-4 on a 60 GWd/t MOX fuel respectively in steam (oxidizing) and hydrogen (reducing) conditions. The VERDON-2 test, covering the air ingress topic, was performed on a 60 GWd/t MOX fuel, using a more complex experimental circuit including thermal gradient tubes (TGTs) downstream the furnace where the fuel sample is heated. The main outcomes of the experimental programme related to iodine and caesium behaviour are:

- earlier and faster releases of highly volatile FP (I, Cs) – also for semi-volatile FP such as Mo and Ba - for MOX and high burn-up (HBU) UO<sub>2</sub> fuel compared to average burn-up UO<sub>2</sub> fuel - releases are the fastest with MOX fuel with in particular larger than expected caesium releases measured at the 1200°C temperature plateau in VERDON 3 and 4 tests;
- faster releases of highly volatile FP with increasing oxygen potential of the carrier gas – the carrier gas oxygen potential also strongly affects semi-volatile FP releases such as that of Mo and Ba, Mo release being promoted in oxidizing conditions (Mo behaviour is underlined there as Mo is affecting Cs and I chemistry in the RCS);
- re-vaporisation of iodine deposited in the TGT during the air ingress phase of VERDON 2;
- low gaseous iodine fractions (~ 1% of the iodine inventory) were measured in VERDON-3 and 4 (MOX fuels) where release started at very low temperature (~ 300°C) and accelerated above ~ 600°C.

An additional air ingress test, VERDON-5, will be performed in 2015 with HBU UO<sub>2</sub> fuel (same fuel as VERDON-1) with similar experimental arrangements as the VERDON-2 test, to compare the ruthenium release and FP re-volatilisation with those obtained for MOX fuel in air.

These results of the VERDON programme are presently under analyses. However, they raise questions as to the hypotheses one should consider for the volatile FP releases for design basis accidents

(DBA), beyond design basis accident (BDBA) with limited fuel degradation (e.g., when core cooling can be recovered before significant fuel melting) and accidents in oxidizing conditions (including loss of cooling in spent fuel pools (SFPs)).

1.2 – Research on the transport and chemistry of iodine in the primary circuit and containment conditions at VTT - T. Karkela (VTT) et al. The behaviour of iodine in a SA is studied at VTT as regards RCS chemistry, containment chemistry and filtration (in relation to FCVS use). It was shown that FP deposits on RCS surfaces can act as a source of gaseous iodine (long-term source), that gaseous iodine (inorganic and organic) can transform in the containment to aerosol particles due to oxidation (by reacting with air radiolysis products), that particle deposits on containment surfaces can act as a source of gaseous iodine (even in the absence of radiation) and that particulate and gaseous iodine can be filtered with a modified Wet Electrostatic Precipitator (WESP) filter. All those processes that may significantly impact the iodine source term are still the subject of research.

1.3 – Main findings of the IRSN experimental programmes performed on iodine chemistry in severe accident conditions – A.C. Grégoire (IRSN) et al. IRSN performed the CHIP programme in the ISTP frame to study iodine chemistry in the RCS during a SA. The programme was terminated in 2014 and was conducted notably to explain the unexpected gaseous iodine fractions measured in the PHEBUS FP tests in the containment during the fuel degradation. The results supported the development of a comprehensive model for the homogeneous gas phase chemistry of the (I, Cs, B, Mo, O, H) system able to reproduce PHEBUS tests observations. A proper estimation of the gaseous iodine fractions in the RCS necessitates treatment of kinetic limitations, of the effect of B and Mo on I and Cs chemistry (Mo playing a major role in oxidizing conditions by the formation of  $\text{CsMoO}_4$ ) and of the effect of the carrier gas composition – notably the relative  $\text{H}_2/\text{H}_2\text{O}$  content. All this is now included in the ASTEC system code and partly in other system codes (MELCOR). On-going work concerns the effect of Ag-In-Cd control rod elements on iodine chemistry in the RCS (CHIP+ programme which started in 2014).

IRSN performed experiments in the frame of the ISTP and NEA STEM programmes in the EPICUR facility to study iodine chemistry in the containment during a SA. Experimentation in the STEM programme related to iodine has recently been completed. These programmes were conducted to gain knowledge on organic iodides and iodine oxides formation/decomposition in the containment atmosphere and on radio-induced iodine re-volatilisation from aerosols deposited on containment walls. These processes were identified from PHEBUS FP tests analysis as potential major contributors to the gaseous iodine remaining in suspension in the containment. The results supported the development of a model for the organic iodides formation/decomposition which is now included in the ASTEC system code. On-going and future work are now focusing on the effect of paint ageing on organic iodides formation, on the deposited aerosols and iodine oxides stability under radiation (NEA STEM2 proposal, see 1.10) and on medium-term iodine releases by re-vaporisation of RCS deposits (French MiRE programme).

1.4 – THAI Experiments on volatility, distribution and transport behaviour of iodine and fission products in the containment - S. Gupta (Becker) et al. The THAI facility provided a significant amount of data on coupled-effects tests investigating thermal-hydraulics, hydrogen combustion risk and mitigation, aerosol and iodine behaviour in a LWR containment. Based on THAI experimental results, progress has been demonstrated in modelling of aerosol and iodine behaviour and their coupling with containment thermal hydraulics in severe accident analysis codes, such as COCOSYS-AIM, ASTEC-IODE, MELCOR-INSPECT, and others. The improved models have demonstrated reliable simulation of complex experiments, e.g., analysis of NEA THAI2 test investigating molecular iodine interaction with non-reactive ( $\text{SnO}_2$ ) and reactive (Ag) aerosols, and EU-SARNET/SARNET2 code-benchmark exercises involving THAI data on iodine/surface interactions, iodine mass transfer, iodine oxides behaviour and iodine transport in multi-compartment behaviour.

A follow-up of the NEA THAI2 project is currently under discussion. Hydrogen-related investigations on PAR performance in counter-current flow conditions and hydrogen deflagration tests in two-compartment system are proposed. Additionally, in light of the Fukushima Daiichi accident, experimental investigations are foreseen to study the re-entrainment of fission products (aerosols and gaseous  $I_2$ ) from water pool at elevated temperature due to continuous heat-up of pool or depressurization-induced (venting) boiling. Another planned experiment is related to “delayed” source term in order to investigate re-suspension of aerosols as well as iodine deposits from steel/painted surfaces due to hydrogen combustion.

1.5 – A summary of the PSI investigations on iodine chemistry in the presence of impurities and additives - T. Lind (PSI) et al. PSI experimental methods include lab-scale facilities (also in hot cell), lab-scale bubble column and intermediate and full height Filtered Containment Venting System (FCVS) facilities. PSI experimental programmes investigated iodine retention in FCVS, organic iodides ( $CH_3I$ ) decomposition by hydrolysis and radiolysis and effect of impurities ( $N_2O$ ,  $NO_3^-$ ,  $Cl^-$ ) on the iodine volatility. Data on organic iodides decomposition were used to develop/validate the corresponding models for system codes. Data on effect of  $N_2O$ ,  $NO_3^-$  on iodine volatility were reported in the SARNET frame and are considered adequate to develop the corresponding modelling. Chloride ions were shown to have little or no effect on the iodine volatility. The latest research focused on the use of additives for improved retention of organic iodides in liquid FCVS.

1.6 – Recent Findings on Ruthenium Chemistry in a Severe Accident - T. Karkela (VTT) et al. An overview of recent experimental results from VTT, IRSN, CEA, MTA EK and CHALMERS (integral, semi integral and separate effect experiments) was presented. The chemistry of radiotoxic ruthenium in a severe nuclear power accident has actively been investigated especially during the last decade. The Ru studies have covered the release from the fuel, the transport in the primary circuit and the behaviour in the containment building. The gathered experimental data have been used to understand the key parameters governing the Ru chemistry in a severe accident (SA) and to develop/validate models for SA analysis codes. The collaboration on the international level in the frame of SARNET and SARNET-2 has been intensive on the subject. Detailed studies on separate phenomena have been conducted, e.g., as part of ISTP and NEA STEM programmes. Furthermore, PHEBUS FP tests have produced valuable data on integral phenomena.

The large-scale integral and semi-integral experiments have confirmed that Ru release depends strongly on carrier gas composition. Ru may be largely released from an irradiated fuel sample when conditions result in significant fuel oxidation, this may occur in particular when steam-rich gas or air is involved. In addition, the oxidation of  $UO_2$  fuel seems to lead to a higher and faster Ru release than in case of MOX fuel as evidenced by VERDON results. As mentioned earlier, an additional test, VERDON5 will be performed in 2015 to confirm this difference.

If Ru is released from the fuel in significant amount, it was shown both from analytical and integral tests to interact and deposit fast on surfaces offered by RCS piping (with and without FP deposits) and aerosol particles (e.g., Ag containing particles). In the containment building, most of the ruthenium is expected to end up as deposits on the containment surfaces and in the sump. However, even if the major part of Ru is deposited or in particulate form after its release from the fuel, analytical experiments evidenced higher gaseous ruthenium fractions (in the form of  $RuO_4$ , stable at low temperature) than what can be expected from thermodynamic equilibrium calculation. Oxidizing conditions in the RCS (presence of air) and in the containment (presence of oxidant air radiolysis products) favour ruthenium oxidation to higher oxidation states, including the gaseous  $RuO_4$  form.

Additional investigations are proposed as part of the NEA STEM2 proposal (see 1.10) to quantify whether significant fractions of gaseous ruthenium ( $RuO_4$ ) may be transferred to the containment and released to the environment through leaks or FCVS and have a significant radiological impact.

1.7 – Thoughts on Ruthenium – M. Salay (USNRC) et al. Research on ruthenium focus on its transport once released from the fuel and provides considerable information on  $\text{RuO}_4$  behaviour. However, it has yet to be demonstrated that Ru release under prototypic conditions could substantially affect source term. Research seems to be lacking in some areas such as detailed analyses of scenarios that could lead to air ingress, transport of air to fuel rods and fuel itself and clad and fuel relocation behaviour.

1.8 – The Main Outcomes of the NEA Behaviour of Iodine Project – G. Glowa (CNL) et al. The main field of investigation of the phase 2 of the BIP programme which ended in 2014 was the interaction of iodine with paint and organic iodides formation in the containment during a severe accident. In the first phase of the project, adsorption onto epoxy paint – that are commonly used as coatings in NPPs - and formation of  $\text{CH}_3\text{I}$  from irradiated epoxy paint were investigated. The important role of water in these processes was evidenced. BIP-2 investigated the same processes, with emphasis on developing a more mechanistic understanding of organic iodide production during irradiation of iodine-loaded paint. Epoxy paint is a complex mixture of polymeric compounds and it is difficult to know where and how iodine is interacting and how methyl iodide is formed.

It can be concluded from BIP-2 results that while iodine seems to preferentially associate with the nitrogen-containing functional groups (amines, amides) in the paint, reactions with many parts of the complex paint structure are possible. Obtained results can help explain differences in sorption behaviour between various epoxy paints. While iodine may react with various chemical compounds on and within the paint, the resulting organic iodides can break down under radiation to form methyl iodide. The methyl iodide formation does not appear to be a specific reaction associated with a particular bonding site or functional group, but rather seems to be a common degradation product during a complex free radical degradation process. These results can be used to guide the development of computer models and provide data for their validation.

The data shows that there are similarities in the iodine-paint interaction between the epoxy paints studied, which allows some optimism for the development of a generic iodine-paint model. However, the results also suggest that the treatment of the paint (e.g., pre-irradiation), and differences in the chemical makeup of the paint (i.e., type of hardener) can affect its behaviour with respect to iodine. It is proposed to investigate remaining issues regarding organic iodides formation in the containment in the frame of complementary NEA BIP-3 and STEM-2 initiatives (see 1.9 and 1.10).

1.9 – The Behaviour of Iodine Project: A Proposal for BIP-3 – P. Yakabuskie (CNL) et al. Recently, there have been several NEA initiatives to study the behaviour of iodine in containment: the THAI (THAI-1 and THAI-2), STEM and BIP (BIP-1 and BIP-2) projects. Despite considerable advancements in the understanding of this topic over the past decade, there are still outstanding gaps in knowledge that warrant further investigation. Based on acquired knowledge, CNL is proposing in a phase 3 of the BIP project to further explore the effects of paint ageing and pre-irradiation, total dose and dose rate, humidity and wetting of painted surfaces and the presence of competing species (e.g.,  $\text{NO}_x$ ,  $\text{Cl}_2$ ) on adsorption and desorption processes. Radiolytic studies relating to  $\text{CH}_3\text{I}$  production and degradation in the gas phase are as well proposed. Stronger analytical activities than in the BIP-2 project are foreseen to promote the use of experimental data for model development/validation and ST computations. The BIP-3 project is expected to run for a 3-year term from mid-2015 to mid-2018.

1.10 – NEA STEM Project and its Follow-up STEM-2 – C. Mun (IRSN) et al. IRSN is proposing a phase 2 for the STEM project focusing on unresolved relevant Source Term (ST) issues after STEM<sup>1</sup>, BIP-2 and

---

<sup>1</sup> It was agreed, prior to the STEM project start, to split the project into two phases, as the initial proposal was too large to be covered in 4 years. The present STEM phase 2 proposal considers the initial proposal and outcomes of STEM phase 1 and BIP and THAI phase 1 and 2 projects.

THAI-2 projects completion: effect of paint ageing (normal operation and pre-irradiation on iodine trapping and release under irradiation (proposed testing complementary to BIP-3); effect of irradiation on stability/destruction of iodine aerosols (iodine oxides as well as multi-components iodine aerosols); ruthenium re-vaporisation from RCS deposits with more prototypic conditions than in the previous STEM phase (study of oxidizing conditions and representative RCS surfaces to develop predictive models for ST evaluations). An Analytical Working Group should be set up to allow stronger analytical activities than in the previous STEM phase and to promote the use of the experimental results in some ST computations. This STEM follow-up project is expected to run for a four-year term from mid-2015 to mid-2019.

### **Conclusion and recommendations from the Chairmen**

Knowledge on iodine and ruthenium chemistry in a severe accident has progressed considerably through various experimental programmes in the last decade. A large data set has been produced that is not yet fully integrated by analysts. One limitation is the restricted access to some of the produced data. Collaborative work for the development/validation of related models for severe-accident system codes – such as ASTEC, MAAP, MELCOR - and for the assessment of gains in accuracy of source-term evaluations should be reinforced. The necessary level of detail for the modelling of the complex behaviour of iodine and ruthenium and the model validity for plant application (scaling issue) should be further addressed. It could be recommended to develop a standard code-validation matrix related to iodine behaviour in a severe accident. Sharing the outcomes of performed and future international collaborative programmes as well as knowledge transfer to new generations appears to be of key importance.



## Session 2: iodine transfer to aqueous phase, aqueous-phase chemistry

**Session Chairs: F. Funke (AREVA GmbH), J. Song (KAERI)**

Session 2 consisted of three presentations, one about fission product transport in the containment in wet conditions, and the other two about formation of volatile iodine by seawater radiolysis in containment sumps in severe accident conditions, an issue raised by the Fukushima Daiichi accident.

2.1 – Iodine and Silver Wash-Down Modelling in COCOSYS-AIM by Use of THAI Results – G. Weber (GRS) et al. G. Weber (GRS) presented new and revised models of fission products transport and reactions at wet walls or in sumps, using data from THAI projects. The models are already or will be implemented in COCOSYS.  $I_2$  deposition onto wet paint during steam condensation is described by a new water layer model. The model considers all relevant chemical reactions in the water layer as well as iodine adsorption onto paint covered by water layer either in the form of film or rivulets. The model was successfully checked on the THAI test Iod-24, where two different wall condensation rates on two painted surface areas were established at the same time. For the wash-down on non-soluble aerosol particles by draining condensate, the new model AULA was developed, based on a model for sediment transport applied in geology. Particles erode and are washed down when a critical flow velocity is exceeded. Two flow types are considered, rivulets and films. For a first validation, laboratory tests performed in support of the large-scale THAI test AW-3 were analysed with AULA. The new AULA model is able to calculate erosion and wash-down of non-soluble aerosols by rivulets and closed films. First results indicate that wash-off from floors is not efficient in accident conditions. It was concluded that further wash-down tests are required with a realistic reactor typical aerosol of compact particles consisting of soluble and insoluble materials. The reaction model of silver with molecular iodine ( $I_2$ ) in sump was enlarged by implementing a new parameter, the reactive surface of silver particles in a sump. The reactive surface is reduced when Ag particles are deposited on the sump bottom. A post-test calculation of the THAI test AW-3, where suspended and precipitated silver particles were contacted with  $I_2$ , agreed well with the results.

Highlights from the discussion were (i) the need for an appropriate nodalization of zones to model the rivulets and films, and (ii) that the fission-product behaviour at the PHEBUS FP tests condensers should also be analysed in the future using the new wash-off models.

2.2 – Effect of Constituents of Seawater on Formation of Volatile Iodine by Aqueous Phase Radiation Chemistry – K. Hata (JAEA) et al. K. Hata (JAEA) presented model calculations on the effects of constituents of seawater on the formation of volatile iodine ( $I_2$ ) by aqueous phase radiation chemistry. The aqueous model was extended to include the reactions of the seawater constituents. The gamma-radiolysis of seawater model solutions at ambient temperature and doped with iodide ( $I^-$ ) was calculated to simulate effects on iodine volatility. It was comprehensively demonstrated that the production of  $I_2$  is affected by a number of constituents. In particular, bromide promotes the production of  $I_2$ , but chloride does not. Hydrogen carbonate influences the  $I_2$  production through its role in determining the pH value. The  $H_2$  production is promoted by  $I^-$ . The pH of the seawater effectively determines the  $I_2$  yields. It was concluded that the injection of seawater into a pool containing iodide can have a significant impact on the iodine source term.

In the discussion it was commented that the chloride result was consistent with previous work, and that borate could be relevant in radiolytic  $I_2$  formation due a catalytic influence. Organic constituents of seawater, which could be precursors of organic iodides and which were not included in this study, could be of importance in future work, but the organic iodide production could also be suppressed by the scavenging of oxidizing radicals from water radiolysis by organic molecules.

2.3 – Formation and Release of Molecular Iodine in Aqueous Phase Chemistry during Severe Accident With Seawater Injection – K. Kido (JAEA) et al. K. Kido (JAEA) used the KICHE code to perform calculations on the radiolytic formation of gaseous I<sub>2</sub> as function of the mixing ratio of RCS water with seawater, to simulate the situation of seawater injection into a degraded core. Calculations show that the I<sub>2</sub> production increases with the fraction of seawater. Effects from bromide and hydrogen carbonate were similar to those found in the previous presentation by Hata et al. Dissolved oxygen drastically reduced the I<sub>2</sub> yield by catalytically consuming hydroxyl radicals, while dissolved carbon dioxide promoted the I<sub>2</sub> production by reducing the pH value. The calculated effect of chloride, which was also treated in the discussion, seems to be small as in the previous paper by Hata et al.

### **Session 3: organic iodide formation and partitioning, chemistry and interactions with aerosols, droplets and surfaces in the gas phase**

**Session Chairs: G. Glowa (CNL), M. Salay (USNRC)**

Six interesting papers, contributed by Chalmers, NNL, AREVA, and KAERI, were presented during Session 3 dealing with containment gas phase processes. These papers covered both experimental and modelling efforts on the subjects of the formation and destruction of organic iodides, adsorption of molecular iodine onto paints and aerosols, the volatilization of molecular and organic iodine from sprays, and the development of materials that could reduce the gaseous iodine such as silver impregnated silica gels or paints modified to produce a lower quantity of organic iodides. The topics covered by these papers differed significantly, and as such, will be discussed separately.

3.1 – Chalmers Project on Volatile Organic Iodine Species Behaviour and Retention under Severe Nuclear Accident Conditions in LWR – S. Tietze (Chalmers University).

3.2 – OIPHA-I and II Model – Mathematical Models to Describe the Partitioning and Hydrolysis Behaviour of Organic Iodides Between Gaseous and Aqueous Phase - S. Tietze (Chalmers University).

The first two papers were presented by Chalmers University. The first paper covered experimental work in the areas of formation and chemistry of organic iodides from paint constituents. It reviewed the chemistry of paint and the potential mechanisms for organic iodide formation along with discussing potential modifications to the paints, namely increasing the use of ring structures and aromatics, that would be expected to result in a lower rate of organic iodide formation. It presented experimental results in various areas including sorption and leaching of organic iodides and looked at different approaches to improving wet containment filtration methods. The second presentation described the early development of the OIPHA code. This code calculates the mass transfer of organics between the gaseous and aqueous phases along with hydrolysis. Models of gas-phase and aqueous-phase radiolysis and iodine-surface interactions with paints are planned.

3.3 – The Radiolysis of Gaseous Methyl Iodide in Air – S. Bowskill (NNL). National Nuclear Laboratories presented two papers concerning the gas phase radiolysis of iodine species in air. The 3<sup>rd</sup> paper presented experimental results while the 4<sup>th</sup> paper (below) discussed the model development and simulations of several experimental series. The experiments involved the measurement of the radiolytic decomposition of methyl iodide as a function of O<sub>2</sub>(g) concentration, temperature, liquid water volume, dose rate, and surface area to gas volume ratio. The decomposition rates were found to be comparable to that of previous work. No significant effect of temperature was observed, but increasing the concentration of O<sub>2</sub>, the surface-area to gas volume, and the water vapour concentration all decrease the decomposition rate. The decomposition exhibited a square-root dependence on dose rate. The rate of decomposition of ethyl iodide (C<sub>2</sub>H<sub>5</sub>I) was found to be similar to that of methyl iodide. Overall, no significant sensitivities were observed so that the measured rates are considered to be applicable to containment situations. The results of these experiments have been used to develop a mechanistic model of methyl iodide decomposition described in the fourth paper.

3.4 – The IODAIR Model for Radiolysis of Gaseous Iodine Species in Air: Data Comparison and Predictions – S. Dickinson (NNL). The fourth paper described the IODAIR model and provided the simulations of several experiments including the Harwell experiments discussed above, PARIS tests, as well as BIP tests. The model gives good agreement with experimental measurements of gaseous I<sub>2</sub> decomposition during irradiation at relatively high starting concentrations. However, at lower concentrations the extent of decomposition is overestimated. The model also gives good agreement with measurements of the radiolytic destruction of CH<sub>3</sub>I in air, and reproduces the observed increase in rate at

low O<sub>2</sub> concentrations. Mechanisms are proposed to account for the experimentally-observed dose rate dependence, and for the effect of humidity. Although it has been reported in the literature, the model could not reproduce the formation of CH<sub>3</sub>I from mixtures of CH<sub>4</sub> and I<sub>2</sub>.

3.5 – Interaction of Gaseous I<sub>2</sub> with Painted Surfaces and Aerosols in Large-Scale THAI Tests – F. Funke (AREVA GmbH). The fifth paper detailed recent experiments in the THAI experimental facility (no radiation) regarding the interaction of molecular iodine with wet and dry paint, and with aerosols of differing reactivity. German Gehopon epoxy paint was used for these experiments and was aged by heat treatment to a 15 year equivalent. In agreement with BIP tests, the adsorption of molecular iodine on dry paint exhibited a large effect of humidity, and the iodine was mainly chemisorbed and therefore strongly bound. Molecular iodine was observed to adsorb onto wet paint at a similar overall rate to dry paints exposed to high relative humidity. This observation helped in the development of a water-layer model. Molecular iodine adsorption on different aerosols was measured. Both high-reactivity (Ag) and low-reactivity (SnO<sub>2</sub>) aerosols were used to represent potentially bounding reactivities for nuclear aerosols. Although little adsorption was observed on the non-reactive aerosol, the reactive aerosol absorbed molecular iodine at rates comparable to paint. The THAI experiments are used to help develop AIM-3, the iodine code within COCOSYS.

3.6 – Effect of Water-droplet Sizes on the Migration of Volatile I<sub>2</sub> and CH<sub>3</sub>I – H.-J. Im (KAERI). The final paper in session 3 primarily addressed the effect of water droplet sizes on molecular iodine and methyl iodide volatilization but also addressed techniques for making filter materials. The transfer of both molecular and methyl iodine was lower for smaller droplets. Silver nanoparticles were successfully embedded in silica gels for potential use as iodine adsorbents in filter systems. These adsorbents are now ready for testing.

### **Importance of the research**

Due to the integrated nature of the various iodine phenomena that lead to the prediction of the chemical form and concentration of iodine in the containment environment, the implications for the research presented in session 3 are closely linked to the conclusions of the workshop.

The iodine concentration directly affects the amount of iodine that can be released from the containment to the environment, and thus the dose to workers and the public. The chemical form of the iodine in containment depends on multiple processes that affect the location of iodine in containment and, thus, the concentration of iodine in the containment atmosphere.

Understanding the mechanisms for the formation and destruction of organic iodides and adsorption of iodine onto paints and aerosols are, therefore, crucial to understanding not only the chemical form, but also the concentration of iodine in the containment atmosphere subject to release.

After the Fukushima Daiichi accident, many countries are installing or upgrading Filtered Containment Venting Systems (FCVS) that can relieve containment pressure while minimizing fission product release. Understanding the processes ongoing in containment filters along with the speciation entering the filter are needed to predict the reduction in dose that the filtration systems provide because they exhibit different performance for different iodine chemical forms. Session 3 had a strong focus on the behaviour of organic iodides, which are considered to have low decontamination factors in several types of filtration systems.

The models that are being used to fully capture all the observed phenomena are quite complex and involve hundreds of reactions. These full reaction sets are far too complex to be practically included in a system

code of the type used to calculate releases for reactor accidents. Therefore, simplified or reduced equation sets that capture the dominant trends must be developed for use in system codes.

### **Conclusion and recommendations from the chairmen**

Despite the long history of post-accident iodine behaviour research, and the complexity of the full models, gaps remain in understanding of some of the fundamental phenomena that govern iodine behaviour in containments. Some of the areas requiring further research were discussed in Session 3:

- Formation of organic iodides from paint constituents;
- Formation of CH<sub>3</sub>I in the gas phase from CH<sub>4</sub>;
- Interaction of I<sub>2</sub> with paints and aerosols;
- Gas phase CH<sub>3</sub>I and I<sub>2</sub> radiolysis;
- Potential mitigation strategies.

Several of these items are the subjects of proposed OECD projects including THAI-3, STEM-2 and BIP-3. It is recommended that these international projects receive continued support. Not only do these projects generate experimental data required to develop and validate SA codes computer models and to reduce uncertainties on ST evaluations, but they also provide a forum in which experts throughout the world can exchange knowledge and ideas.



#### Session 4: filtered containment venting systems

**Session Chairs: T. Lind (PSI), L.E. Herranz (CIEMAT)**

A total of six papers were presented in the session. The sources of those papers were diverse: 2 from industry (Westinghouse and AREVA), 3 from research institutes (KAERI and PSI) and 1 from a joint project of the 7<sup>th</sup> Framework Programme of EURATOM (PASSAM). Accordingly, the major messages sent across might be grouped in three categories: progress in industrial devices optimization and/or development, aspects to consider when coming to an effective implementation of FCVS and potential improvement of mitigation from research.

4.1 – Westinghouse Molecular Sieve Technology – A. Andren (Westinghouse). Westinghouse presented the molecular sieve technology as the means chosen to trap effectively volatile Organic Iodides (Org-I). Different configurations of this technology have been built (i.e., cylindrical and box types) to couple it to their traditional wet and dry filters. A number of tests have been carried out in the presence of steam, radiation and high temperatures and they seem to anticipate that DFs from 5 to 50 would be reachable for Org-I, depending on zeolite bed depth, in FCVS working conditions. No degradation of zeolite material has been observed whenever they are kept in dry conditions by keeping a N<sub>2</sub> atmosphere.

4.2 – Improved Iodine Retention at Filtered Containment Venting – P. Zeh (AREVA GmbH). AREVA outlined the improvement achieved in their system performance by adding a new stage for gaseous iodine, particularly volatile Organic Iodine (Org-I). The system consists of three stages: a Venturi scrubber (aerosols and I<sub>2</sub> retention), a metal-fibre filter (fine particles re-suspended and/or escaping from the pool) and a sorbent section (trapping of remaining volatile iodine of any kind). The last experiment conducted focused on Org-I retention under different temperature, pressure and steam fractions; after more than 50 tests, they reported DFs higher than 50. The whole system has been tested at large scale to avoid any scaling effect in their results.

4.3 – Design on the Performance Test of Filter Containment Venting System – K.-S. Ha (KAERI).

4.4 – Thermal-hydraulic Effect on Iodine Retention in the Filtered Containment Venting System – Y.-S. Na (KAERI). KAERI highlighted many related aspects to potential source term to environment: the relevance of containment integrity, the importance of bypass sequences, the close link between thermal-hydraulics and any FCVS performance, etc. In the final part of their presentation, they presented the current status in Korea concerning the development of an enhanced FCVS system, the ongoing studies concerning implementation, with emphasis placed on the component performance when scaled up. A number of innovative ideas were introduced that are still under investigation, like the use of two filtering vessels or the external cooling of the scrubber systems. On line with this work they have already started modelling of FCVS performance with the MELCOR code in a OPR 1000 NPP. Even though the results presented were still preliminary, this approach might assist in assessing the thermal-hydraulic boundary conditions on a wet scrubber performance.

4.5 – Investigation of Iodine Retention in a Filtered Containment Venting System in the VEFITA Test Programme – D. Suckow (PSI). PSI showed their progress in the investigation of an alternative means for capturing volatile Org-I in water pools based on finding the right combination of sodium thiosulfate (Na<sub>2</sub>S<sub>2</sub>O<sub>3</sub>) and Aliquat336, the second one being responsible for accelerating Org-I mass transfer to the water and fixing of iodide ions. After getting successful results in lab scale tests, in the near future they will determine the novel method performance in more representative conditions of an FCVS through using a 1:1 in height facility called VEFITA. A test matrix has already been built and analytical work to characterize major FCVS thermal-hydraulic variables is ongoing.

4.6 – The European PASSAM Project on Atmospheric Source Term Mitigation: Half-Way Progress and Main Results – T. Albiol (IRSN). The PASSAM project is investigating, within the 7<sup>th</sup> Framework Programme of EURATOM, the potential optimization and enhancement of Source Term mitigation systems in case of a severe accident. Coordinated by IRSN, it empirically explores both traditional (pool scrubbing and sand filters) and innovative (acoustic agglomeration, high pressure sprays, wet electrostatic precipitators and advanced zeolites) methods, in addition to combined methods (i.e., wet + dry filtration). Some results have been already obtained, but it is still too early to set any firm conclusion regarding the systems under investigation. Particular emphasis is being placed on understanding the phenomena responsible for retention in realistic severe-accident conditions in the short and long term of a severe accident.

In summary, the session delivered new and innovative results for the FCVS design and implementation. Commercial FCVSs can be equipped with a filtration stage for retention of volatile organic iodides with the possibility of tailoring the decontamination factor for each application. The operation of such filtration stages has been experimentally proven in a wide range of conditions. Open issues remain the source term of organic iodides to such filters, as well as the long-term behaviour of the filters and the retained iodine species. Alternative methods for retention of organic iodides are being investigated. In addition, several innovative FCVS designs and source term mitigation methods were presented, and further research is on-going to determine the feasibility, scale-up potential, and the collection efficiency of such systems.

## **Session 5: recent developments in iodine chemistry modelling in severe accidents and applications to source-term and radiological-consequences evaluations**

**Session Chairs: S. Dickinson (NNL), D. Jacquemain (IRSN)**

This session comprised two papers on the development of models for iodine chemistry in the containment, and four papers in describing the application of models of varying degrees of complexity to calculate the releases or radiological consequences from design basis and severe accidents.

5.2 – Iodine Behaviour in the Circuit and Containment: Modelling Improvements in the Last Decade and Remaining Uncertainties – L. Bosland (IRSN).

5.3 – Containment Iodine Chemistry – M. Salay (USNRC).

The modelling development papers presented by Bosland and Salay focused on the specific aspects of the behaviour of iodine where the authors consider that additional data and models are needed to complete an adequate representation of the behaviour of iodine in containment. These included modelling of chemistry in the RCS to improve prediction of the gaseous iodine source to the containment, and a number of heterogeneous phenomena in the containment that have an impact on the concentration and chemical speciation of iodine in the containment atmosphere in the medium term. In some cases, experimental programmes are underway or planned to address the issues; in others, models are being developed on the basis of information available from other fields of study. The discussion of these papers raised questions about the level of detail required in the models, and the effect of uncertainties in the containment chemistry models on the calculated source terms and consequences.

5.1 – Iodine Chemistry in Design Basis Faults – A. Zodiates (EDF Energy).

5.4 – Application of the COCOSYS Iodine Chemistry Model AIM-3 to PWR Containment Analyses Using New Validation Results of RTF and CAIMAN Experiments – H. Dimmelmeier (AREVA GmbH).

5.5 – Iodine Source Term Computations with ASTEC, Link with PSA Level 2 Tools and Fast Running Source Term Tools For Emergency Organisation – K. Chevalier-Jabet (IRSN).

The papers presented by Zodiates, Dimmelmeier and Chevalier-Jabet described the application of models to calculate iodine releases from containment. These papers highlighted the differences in complexity of the models, depending on their application, and in particular the importance of simplicity and conservatism for “end-user” applications such as radiological consequence assessments and emergency planning. However, even the apparently simple models have to be based on a good understanding of the behaviour of iodine, at the level treated by the more detailed models, in order to ensure that the important phenomena are taken into account and correct extrapolations are made from experimental data. Data from PHEBUS FP, SARNET and recent NEA programmes such as BIP, STEM and THAI are thus used to inform the development of the higher-level codes. An example was highlighted in which the application of data measured for severe-accident conditions may not be conservative in design-basis conditions, suggesting the need for additional data on iodine volatility from solutions at low dose rate, low concentration and high temperature.

5.6 – In What Extent the Iodine Reactivity in the Atmosphere Can Impact the Radiological Consequences – J. Trincal (IRSN).

The final paper of the session, presented by Trincal, showed that the complex chemistry of iodine continued after it was released to the environment, and could have an important impact on the dispersion and deposition behaviour controlling the biological uptake of radioiodine. Furthermore, there is a large

overlap between the gas-phase chemistry provoked by the radiation field within the containment, and by UV radiolysis in the atmosphere. This paper provoked discussion about the different drivers for predicting the gaseous iodine species in containment, since these calculations implied that the environmental fate would be the same for organic and inorganic iodine. In contrast, the distribution between organic and inorganic iodine is an important consideration in the efficiency of mitigation systems.

## SUMMARY STATUS REPORTS OF NEA BIP-2 AND OECD/STEM PROGRAMMES

At the NEA BIP-2 and STEM Programme Review Group (PRG) meetings in September 2014, it was decided that the upcoming OECD/NEA-NUGENIA/SARNET International Workshop on iodine behaviour would be an excellent forum to present and discuss the final outcomes of the two projects and the proposal for the follow-ups. The final summary status reports of both projects are presented hereafter as well as the proposed topics for the follow-ups and the related discussions.

### NEA BIP-2 and follow-up - G. Glowa (CNL)

The primary objective of the NEA BIP project operated by CNL (formerly AECL) was to investigate the interactions between iodine and containment paints, including iodine sorption behaviour and the subsequent formation of organic iodides. The first phase of BIP (BIP-1, July 2007 - March 2011) focused on the interaction between iodine and epoxy paints. Epoxy paints are commonly used surface coatings within nuclear reactor containment buildings throughout the world. In particular, experiments investigating the role of water on the iodine deposition velocities and the formation of methyl iodide from irradiated paint showed that adsorbed water strongly promoted both the sorption and organic iodide formation processes.

BIP-2 (July 2011 – September 2014) investigated the same processes as BIP-1, with emphasis on developing a more mechanistic understanding of organic iodide production during irradiation of iodine-loaded paint. Epoxy paint is a complex mixture of polymeric compounds and it is difficult to know where and how iodine is interacting and how methyl iodide is formed. To isolate the influence of various functional groups present in epoxy paint, polymer samples having simple, but representative, structures (such as amide groups) were used as model compounds for comparative testing. The samples were exposed to  $I_2(g)$  and irradiated to determine the rate of methyl iodide formation. In addition to the polymer tests, tests were performed with epoxy paint at 80°C (for comparison to EPICUR tests) with different iodine loading schemes (to help our understanding of the effect of water) and with paint that was pre-exposed to  $Cl_2$  or  $NO_2$  (to simulate the effect of reactive species expected within containment).

Several spectroscopic techniques were utilized in BIP-2 to investigate iodine-paint surface interactions. Scanning electron microscopy was used to determine coupon surface morphology, energy dispersive x-ray analysis measured the depth of penetration of the iodine into the paint layer, and gas chromatography-mass spectroscopy was used to study solvent release from 20-year-old epoxy paint.

BIP-2 members have indicated that the BIP-2 project has been used to further their general understanding of post-accident iodine behaviour and aid in the interpretation of integral tests such as PHEBUS FP. The data are also used for the development and validation of iodine models within severe accident system codes such as MELCOR, ASTEC-IODE, COCOSYS, and RAIM.

It was also highlighted at this workshop that the organic iodide source term in containment is required as input for designers of filtered containment venting systems (FCVS). Organic iodides have a low decontamination factor in such systems, so they are relatively important contributors to environmental releases as compared to aerosol forms and molecular iodine ( $I_2$ ).

It should be noted that, while the inclusion of a detailed, mechanistic model to describe iodine-paint interactions is not a realistic objective for many of our iodine codes, the ability to qualitatively describe the underlying chemical processes provides support for the use of empirical models.

In addition to presenting the final results of the BIP-2 project, a preliminary proposal for a follow-up project (BIP-3) was presented. The proposal contained topics that were previously identified and ranked by the BIP-2 PRG and focused on:

- Improving our ability to simulate iodine adsorption and desorption behaviour over a range of conditions:
  - Paint ageing (“natural”, thermal, and irradiation)
  - Long irradiations
- Predicting CH<sub>3</sub>I behaviour (formation and degradation) in accident conditions:
  - Paint ageing
  - Wet/dry cycling
- Investigating the effect of contaminants (e.g., NO<sub>x</sub>, Cl<sub>2</sub>).

The complementarity with the STEM-2 proposal topics was also considered in the project proposal.

The workshop allowed further comment and discussion by a wider group of iodine experts. This rigorous process provided an opportunity to evaluate the technical scope of the BIP-3 programme while ensuring the efficient use of our combined resources. Specific workshop discussions related to BIP-3 topics included:

Importance of gas-phase reactions - It is clear that gas-phase reactions are important for the determination of the speciation and concentration of iodine in the gas phase. Items related to the effects of gas phase contaminants such as Cl<sub>2</sub> and NO<sub>x</sub> within the BIP-3 programme will be retained. The presence of CO(g) due to the molten corium concrete interaction has been identified as a reactive species in containment. The prospect of studying aspects of CO reactions with iodine species will be discussed by the BIP members.

Gas phase methyl iodide degradation - It is clear that this process is important for the determination of the gas phase methyl iodide concentration. New information presented at this workshop suggests that the remaining uncertainty in the degradation rate is not significant for the calculation of iodine source term. As a result, this topic will be removed from the BIP-3 proposal.

A code-comparison exercise - It was reiterated at this workshop that the sharing of analytical work was not a strong component of BIP-2. Furthermore, it was noted that an iodine code comparison exercise has not been performed in a while. In the absence of new appropriate experimental data, a comparison of a simple theoretical scenario could provide some guidance to ongoing experimental and code development work. The BIP-3 analytical group may be an appropriate venue for such an exercise.

In conclusion, this international OECD/NEA-NUGENIA/SARNET Iodine Workshop provided an excellent opportunity to share the results and discuss the path forward for the BIP project. A modified proposal will be submitted through the NEA for expressions of interest in BIP-3.

#### **NEA STEM and follow-up - C. Mun (IRSN)**

The STEM (Source Term Evaluation and Mitigation) NEA project operated by the French “Institut de Radioprotection et de Sûreté Nucléaire” (IRSN), was launched mid-2011 in order to improve the evaluation of Source Term (ST) for a severe accident (SA) on a nuclear power plant and to reduce uncertainties on specific phenomena related to the chemistry of two fission products which may be major contributors to the radiological consequences: iodine and ruthenium. Concerning these two radionuclides, three main issues were addressed: i/ middle-term iodine behaviour in the containment with specific

attention to the stability of deposited iodine aerosol particles under radiation (radiation induced decomposition producing gaseous iodine species), ii/ short and middle-term iodine-paint interactions under radiation (organic iodides production), iii/ ruthenium transport chemistry in order to determine the speciation of Ru, in particular the partition between gaseous and condensed forms, during its transport through the Reactor Cooling System (RCS).

Concerning the STEM iodine research, semi-integral experiments were carried out in the EPICUR facility. These tests were first focused on the releases of volatile molecular iodine ( $I_2$ ) and organic iodides (Org-I) from representative epoxy painted coupons loaded with molecular iodine and also with iodine aerosols species ( $CsI/I_xO_y$ ) to assess their thermal and radiolytic stability. Main outcomes of the programme are:

- New data from long duration irradiation tests which can be used to develop accurate kinetic models of gaseous iodine (molecular and organic iodides) release from paints in the containment with consideration of short-term and “delayed” releases. New models based on STEM data were already implemented in the ASTEC SA system code (IRSN) and in the RAIM iodine chemistry code (KINS);
- Demonstration that iodine aerosol ( $CsI$ ,  $I_xO_y$ ) decomposition processes in the containment are major processes affecting the volatile iodine concentrations in suspension in the containment and that a proper modelling of these processes has to be developed. Some kinetics data of the decomposition processes were obtained and a preliminary modelling was implemented in the ASTEC code.

Recent ASTEC calculations performed by IRSN with the new modelling developed based on STEM data showed a better understanding of the iodine behaviour in the containment for the integral PHEBUS FP tests series with an iodine volatility which would be essentially driven by organic iodides formation/decomposition at paint and in the gas phase,  $I_xO_y$  formation/decomposition in the gas phase and other iodine aerosols decomposition.

The additional knowledge and improvements for calculation tools derived from the STEM project should allow a more robust assessment of radioactive releases and consequences in a SA. Indeed, the STEM project contributed to fill some gaps of knowledge on production of gaseous iodine in the containment from important processes – these processes were previously identified through an IRSN study coupling ASTEC and SUNSET (uncertainty evaluation tool) as major contributors to the remaining uncertainties on ST evaluations - which were not earlier thoroughly investigated.

As underlined during the workshop, the gained knowledge is expected to allow a better appreciation of releases by containment leaks and through FCVS during all phases of an accident. A specific emphasis was put on iodine oxides and organic iodides filtration since these species are expected to have a rather low decontamination factor in FCVS (both French sand bed filters and pool-scrubbing filters) and may be main contributors to iodine environmental releases.

Concerning the STEM ruthenium research, a series of vaporization and re-vaporization analytical experiments were performed in the START test facility. The effect of the oxygen potential on the deposits formation was assessed, as well as the kinetics of Ru transport after vaporization and the kinetics of re-vaporization from the deposits in a transport tube simulating the RCS.

As already demonstrated by previous international or national experimental programmes, ruthenium species released from the core in oxidizing conditions can reach the containment and form volatile ruthenium tetroxide. The transport in the RCS is one of the key process driving gaseous ruthenium formation and eventually its release to the environment. The STEM ruthenium research allowed gaining knowledge on the key parameters impacting the transport kinetics, the partition between gaseous  $RuO_4$  and particles of  $RuO_2$  and the extent of the re-vaporization process of deposited species in a transport tube. It was shown in particular that, despite the fact that most of the volatilised ruthenium deposits fast on the

transport tube, a few % of it, produced either by vaporisation or re-vaporisation, may eventually be transported as a gaseous fraction downstream to the tube exit (simulating the break to the containment).

Based on STEM results, a preliminary Ru transport model through the RCS was developed and implemented in the ASTEC system code. Considering these developments, a preliminary PSA level 2 assessment was made by IRSN to appreciate Ru contribution to the radiological consequences for a French 1300 MWe NPP (presented at the 2015 ERMSAR conference). It was shown that, even when gaseous ruthenium fractions reaching the containment represents only a few % of the core inventory (order of magnitude of STEM data), Ru isotopes are with iodine ones major contributors to the radiological consequences.

Following the presentation of the main outcomes of the STEM project, a preliminary proposal for a follow-up project (STEM-2) was presented and discussed. It was reminded that initially two phases for the STEM project were defined at the STEM expert meeting held in October 2010: the first one from mid-2011 till mid-2015 and the second one (STEM-2) till mid-2018 to complete the first phase. Based on recent progresses made in the ST area, notably based on the NEA BIP-2 and STEM programmes, topics for STEM-2 proposal could be identified or consolidated and ranked by the STEM PRG members with the objective to fill main remaining knowledge gaps affecting ST evaluations. The complementarity with the BIP-3 proposal topics was also considered in the project elaboration.

Following the last STEM PRG meeting discussions, the second phase would possibly be performed from mid-2015 to mid-2019 focussing on:

- The effect of the ageing of paints on iodine behaviour: i.e., irradiation tests (medium and long terms irradiation periods) on paints aged in representative reactor conditions and loaded with iodine. Some limited data reported in the literature indicate that paint ageing may strongly impact iodine adsorption/desorption kinetics and organic iodides production – and consequently potential iodine releases;
- The study of iodine aerosol stability:
  - iodine oxides radiolytic decomposition;
  - iodine oxides decomposition by carbon monoxide;
  - radiolytic oxidation of multi-components iodine aerosols.

As the first phase of the project demonstrated, these processes may strongly affect the iodine fraction (amount and speciation) in suspension in the containment – and consequently potential iodine releases. Data generated in the first phase of the project have to be analysed to develop kinetics models able to reproduce aerosol decomposition processes for all phase of the accident (including the MCCI phase).

- Complementary tests on ruthenium re-vaporization from RCS stainless steel surfaces for highly oxidizing conditions. Data generated in the first phase of the project have to be completed for more representative conditions.

The workshop brought further discussion and debate and thus induced an additional evaluation of the technical scope of the STEM-2 proposal leading to consolidation & update of the proposal:

#### Iodine oxide decomposition by carbon monoxide:

The study of the effect of CO on iodine oxides decomposition appeared as an important issue as CO concentrations in the containment can be several orders of magnitude higher than volatile iodine concentrations during the MCCI phase. It also appeared during the discussion that the hydrogen generated during the accident (by the Zircaloy oxidation during early phases and by MCCI later) may also affect the iodine oxides decomposition despite possible hydrogen consumption by mitigation means (PARS or

igniters) when these are implemented. The effect of both gases on iodine oxide stability has to be further assessed.

Prototypical conditions for ruthenium re-vaporisation tests:

While the probability of “air ingress” accident scenarios was debated between experts during the workshop, providing more conclusive answers relative to the ruthenium issue – which is considered by some experts as an important objective by itself – requires the performance of more representative tests than in the first phase of the STEM project. This may be a challenge to achieve as one would like to consider RCS representative surfaces for deposition, the presence of representative aerosols particles and proper gas composition including oxidant conditions. This will require a careful design of the experiments for that specific investigation.

Analytical work:

It was also underlined during the workshop that analytical work to provide a final comprehensive analysis of the results with implications for ST evaluations including mitigation aspects should be promoted.

In conclusion, the international OECD/NEA-NUGENIA/SARNET Iodine workshop provided an excellent opportunity to present the main outcomes of the first phase of the STEM project and to discuss, between all experts in the field, the main issues that should be investigated during the second phase of the project. Following the experts’ remarks expected on an initial STEM-2 proposal distributed at the Workshop, an updated STEM-2 proposal will be submitted as a basis for launching the STEM-2 project.



## SUMMARY, CONCLUSIONS AND RECOMMENDATIONS

### **Fulfilment of Workshop objectives**

It was recognized that the workshop objectives relative to reviewing and discussing the state of the art knowledge of iodine and ruthenium behaviour in NPP accidents gained through research projects and progresses made in the related modelling were well fulfilled. Also, highlighting remaining open issues and assessing their coverage through on-going and planned research activities was well considered with in particular discussions concerning the NEA BIP-3, STEM-2 and THAI-3 proposals and recommendations for future works reported hereafter. The workshop also contributed, and will continue contributing through the summary report publication, to knowledge sharing and dissemination in the field.

However, it was underlined that contributions concerning research results applications for improving accident analyses and management were limited in number and scope, with the notable exception of an IRSN presentation of the status of different tools used for source term evaluations and emergency planning presented in the last session. This led workshop experts to formulate some general recommendations to foster international exchanges and actions to assess more thoroughly research progresses implications for NPP accident management. This comes in addition to recommendations on technical issues which need, according to these experts, additional research efforts in the future.

### **Conclusions and recommendations**

#### *Iodine and ruthenium release from fuel*

The existing large database on FP release from fuel experiments (CRL, HI/VI, PHEBUS FP, VEGA, VERCORS, etc.) was recently completed by the ISTP/VERDON test series focusing on HBU and MOX fuel. VERDON results confirm that highly volatile FP (I, Cs, Te) should tend to completely release in a SA resulting in significant fuel degradation and that semi-volatile FP (Mo, Ba, Ru) release is strongly dependent on oxido-reducing conditions, with Mo and Ru release tending to be large in oxidizing conditions – Ru release requiring fuel oxidation and being lower for MOX fuel than for UO<sub>2</sub> fuel.

Results of the VERDON programme are still under analysis. However, they raise questions as to the hypotheses one should consider for the volatile FP release (notably for Cs) for DBA, BDBA with limited fuel degradation (e.g., when core cooling can be recovered before significant fuel melting) and for accidents in oxidizing conditions (including loss of cooling in spent fuel pool (SFP) with interest, in such a situation, in assessing margins before intervention).

The existing FP release database was used by the past to develop simplified or more mechanistic FP release models. These models should be tested against VERDON tests results in the near future. However, in order to progress significantly in the existing modelling and to incorporate the major effects on FP release kinetics (such as fuel BU effect and oxidizing potential effect), a detailed mechanistic approach requiring substantial development would be necessary.

For the time being, except for the VERDON-5 additional test, which should be performed in 2015 to complete the existing VERDON database (release from HBU fuel with an air oxidation phase, boron effect on FP transport), no other international initiative to address the above listed issues is planned for the near

future. An initiative proposing the development of a mechanistic approach relating fuel microstructure evolutions and FP release mechanisms in accident transients was proposed within the last EC H2020 call (INFORMS project) but it was not funded by the EC.

Workshop experts discussed the usefulness of simplified analytical testing (using e.g., fuel simulants) to progress in the field. No strong recommendation was made at the workshop concerning research for iodine and ruthenium release from the fuel considering that:

- analyses of the VERDON test series has still to be completed;
- filling knowledge gaps concerning FP behaviour (Cs, I, Ru) in the RCS and the containment as well as in FCVS is expected to provide more gain on ST evaluations for SA;
- also, as already mentioned, for Ru, the importance one should attribute to oxidizing accident scenarios, which would result in significant Ru release and transport to the containment, should be further assessed. This resulted in a recommendation formulated when discussing research for Ru transport in the RCS (see next section).

***Nevertheless, it is recognized that models able to predict FP release kinetics from fuel would be valuable tools for the evaluation of consequences of accidents with limited fuel degradation (including DBA) and with oxidizing conditions (including SFP) and their management.*** Analyses of existing data (in particular VERDON) should be deepened to design future research in the field.

### ***Iodine and ruthenium transport in the RCS***

#### *a. Homogeneous chemistry and heterogeneous process (reactions with surfaces and aerosols) in the gas phase in a SA*

Much progress was reported at the workshop in the understanding and modelling of homogeneous iodine gas phase chemistry in the RCS, notably from ISTP/CHIP data analyses and involving in some cases supporting theoretical chemistry. System codes such as ASTEC and MELCOR benefited from model developments in that respect related to the effect of Mo on Cs and I chemistry and transport. Data were generated to treat the Cs, Mo, B, I, H, O chemical system (CHIP/ISTP) and models are implemented in ASTEC considering both kinetics and thermodynamics modelling of influential reactions. The database is being extended by IRSN to treat Ag, In and Cd effect on iodine transport and chemistry (CHIP+ programme and theoretical developments). All these developments aim at providing better predictions of the gaseous iodine fractions at the RCS break in a SA – which may be highly scenario dependent as evidenced by PHEBUS FP observations (with strong effect of carrier gas composition, of compounds resulting from control rod degradation (including Ag, In, Cd, B elements), of other FPs (Mo)) - and reduce related uncertainties on iodine source term evaluations.

Presently, SA system codes have implemented with different levels of detail the gained information. ASTEC in its latest version includes a revised modelling of kinetics and thermodynamics of the Cs, Mo, B, I, H, O system which was validated against CHIP and PHEBUS FP data with significant progress obtained notably in reproducing the iodine behaviour for PHEBUS FP tests. The approach used was not to implement kinetics for all chemical reactions but only for the most influential reactions. This way, code calculations times are not significantly impacted despite detailed calculations of the chemical system.

The required level of detail of the modelling of RCS chemistry, notably for SA system codes, was discussed. Even if some uncertainty evaluations performed prior to these developments using coupled ASTEC/SUNSET tools indicated that calculated iodine releases may be in some accident scenarios strongly dependent on gaseous iodine fractions at the RCS break, comparative reactor-like (BWRs- PWRs) SA system code calculations in their present stage of development for typical accident scenarios would provide some input to such a debate and help further assessment of the gain for ST evaluations. ***The workshop experts recommended that some SA system code benchmarking exercise be organized for***

*defined reactor-like scenarios to assess the effect of recent chemical-model developments on ST evaluations.* This recommendation was raised on several occasions during the workshop as it does not relate solely to assessing the progress made in RCS chemistry modelling.

Some progress in understanding of Ru transport from experimentation performed at VTT, MTA EK Chalmers University and IRSN was obtained. The issue is to develop models able to calculate Ru re-emission from RCS deposits as Ru is known to deposit very fast on RCS surfaces after its release from the fuel. The Ru source to the containment would then be very dependent on such re-emission processes. However, experiments in more representative conditions (RCS surfaces and oxidizing conditions) are necessary to provide data for the development of models applicable to the reactor case. This is proposed as a part of the STEM-2 project.

As discussed earlier, the importance of the Ru issue was debated as some experts pointed out that the importance of oxidizing accident scenarios, which could result in significant Ru release and transport to the containment, should be further assessed. Others consider that the potentially important contribution of Ru to radiological consequences even when considering a limited release of it (few % of the core inventory) – as evidenced by some L2 PSA evaluations - is sufficient to justify research efforts to either close the issue or provide tools to assess possible ruthenium contribution to radiological consequences. ***The workshop experts recommended conducting further assessments as to the importance of oxidizing accident scenarios which could result in significant ruthenium release to the environment.***

More generally, an important issue that was underlined during the workshop discussions relates to the necessity to develop a pragmatic research approach to treat complex heterogeneous processes involving interactions of gas species with surfaces and aerosols in the RCS and considering possible re-suspension/re-volatilization/decomposition of deposits resulting from mechanical, thermal and dose loadings. These may be important delayed source of FP (I, Cs and Ru) to the containment - when significant deposits have occurred in the RCS during release phases (probably more relevant for Cs and Ru, Cs re-volatilization was evidenced in some PHEBUS FP tests) – potentially contributing to the ST in later phases of the accident, notably in case of FCVS use. It is indeed generally hypothesized in calculations supporting ST evaluations that radioactive aerosols and gas species are depleted by fast deposition processes in the containment leading to substantial reduction of suspended concentrations in the first hours following their release to the containment.

Limited experimentation on Cs and Ru re-vaporization processes is being performed in the French MiRE and the NEA STEM projects. This is proposed to be continued for Ru in the STEM-2 project. However, doing experiments and developing models relevant to reactor situations still appear challenging notably due to the complexity of the involved processes and the potential importance of dealing with representative surface states and deposits.

***The workshop experts recommended conducting further assessments to appreciate the potential effect of FP re-emission from RCS deposits on ST and to focus the experimental research in the field – to be relevant to the reactor case - integrating existing knowledge, on-going and planned research.***

#### *b. Aqueous phase chemistry in DBA*

Specific testing was performed as part of the NEA THAI-2 programme to investigate gaseous iodine release for the case of SGTR accidents (flashing conditions at the break induced by RCS depressurization). Calculations performed for the test preparation have evidenced the lack of validation of existing iodine chemical models in the aqueous phase for RCS conditions relevant for DBA (low doses and low concentrations, elevated temperatures (> 200°C), additives effects). This was also concluded from investigations conducted by EDF Energy. ***The workshop experts recommended designing research to test the validity of iodine chemical models for aqueous phase chemistry in DBA conditions.***

### ***Iodine and ruthenium behaviour in the containment***

#### *a. Homogeneous chemistry and heterogeneous process (reactions with surfaces and aerosols) in the gas phase in a SA*

In that field, gained knowledge on containment gas phase content (aerosols and gas) is expected to help appreciate releases through containment leaks and through FCVS during all phases of the accident, including long term phases (e.g., MCCI), considering changing gas phase composition ( $H_2$ ,  $H_2O$ ,  $CO$  and  $CO_2$  production and consumption), effects of dose, of SAMM (e.g., steam production resulting from corium cooling in and ex-vessel, sprays) and of energetic events (e.g., hydrogen combustion) on FP remobilization from deposits on containment walls.

Following PHEBUS FP, research on iodine containment chemistry focused on gas phase processes (interaction of gaseous iodine with paints and organic iodides (Org-I) production, interaction with reactive aerosols (e.g., Ag-containing particles), iodine oxides ( $I_xO_y$ ) formation/decomposition, gaseous iodine release by radiolytic decomposition of deposited aerosols) as the PHEBUS tests analysis indicated they determined the gaseous iodine evolution - whereas a lot of research efforts were earlier put on aqueous phase chemistry (gaseous iodine was initially assumed to be essentially produced by radiolytic processes in the sumps following iodine aerosols deposition there). The research was recently notably conducted in the ISTP/Ru, ISTP/EPICUR, NEA BIP-1 and BIP-2, THAI-1 and THAI-2 and STEM. The above processes are considered reasonably well covered by past, on-going and planned research (notably with the proposed NEA BIP-3, STEM-2, THAI-3) with a focus on inorganic gaseous iodine species, iodine oxides particles ( $I_xO_y$ ), organic iodides (Org-I) and gaseous ruthenium tetroxide ( $RuO_4$ ) behaviour. Significant progresses have been made through all these programmes on the understanding and modelling of Org-I,  $I_xO_y$ ,  $RuO_4$  production/decomposition. Part of the gained knowledge is implemented in SA system codes. As for RCS chemistry, ***the workshop experts recommended that some SA system code benchmarking exercise be organized for defined reactor-like scenarios to assess the effect of recent chemical models developments on ST evaluations.***

Following the Fukushima accident and considering potential long term loss of containment heat removal systems, questions have been raised on possible FP remobilization from deposits on containment surfaces and sumps/suppression pools during long term phases of a SA and notably in relation to assessing FP release during containment venting. This resulted in the definition or reorientation of research projects intending to increase knowledge on such processes. This is in particular included in the NEA BIP-3, STEM-2 and THAI-3 projects.

Complementary BIP-3, STEM-2 and THAI-3 projects have been presented and discussed at the workshop. Proposals for BIP-3 and STEM-2 have been distributed to the workshop participants and offered for comments. They were already discussed and reviewed by BIP-2 and STEM partners. The THAI-3 proposal was already extensively discussed at an expert meeting in November 2014. These three complementary projects will be focusing on:

- formation/decomposition of Org-I through homogeneous and heterogeneous processes - including paint ageing effect – (BIP-3/STEM-2);
- reemission of gaseous iodine from iodine aerosols deposits under radiation (STEM-2);
- formation/decomposition of  $I_xO_y$  including CO effect (MCCI phase) and assessment of  $H_2$  effect (STEM-2);
- effect of impurities ( $Cl_2$ ,  $NO_x$ ) on gas phase reactions involving iodine (BIP-3);
- remobilization of gaseous iodine from containment sumps or suppression pools either due to continuous heat-up or due to depressurization-induced (venting) boiling (THAI-3);
- effect of hydrogen deflagration on FP remobilization from wall deposits (THAI-3).

The workshop experts recognize that the follow-on proposals are well targeted to tackle some of the raised issues. Some comments were made which helped improve the focus of the proposals as reported earlier in the programmes summary section. Proposals remained open for comments till the end of April 2015 with the objective of having the project proposals finalized by the operators (CNL for BIP-3, IRSN for STEM-2 and Becker Technologies for THAI-3) by mid-2015 after taking account of the workshop discussions and any additional relevant expert comments. The operators intend to launch the projects over the second half of 2015 (BIP-3, STEM-2) or early 2016 (THAI-3). It is also recognized that the proposed experiments will only partly cover the issues listed above. There are also some specific national developments that will tackle such issues with, e.g., new containment facilities under development in Japan and Republic of Korea with the intention to investigate more challenging conditions than studied in existing facilities (e.g., containment gas-phase temperatures of 200°C or higher as measured during the Fukushima's accident).

***The workshop experts recommended conducting further assessments to assess the potential effect of “delayed” FP re-emission from containment surface deposits and sumps on ST evaluations and focus the research in the field – to be relevant to the reactor case - integrating existing knowledge, on-going and planned research.***

***The workshop experts further recommended to strengthen collaborative analytical activities, if possible joined integrated activities between projects, using the available results of international programmes, highlighting that such activities were in recent years limited in scope.***

#### *b. Aqueous-phase chemistry in SA*

As discussed earlier, following the PHEBUS FP tests, less work was performed on aqueous-phase chemistry in SA as the main source of volatile iodine was considered to be in the gas phase. The effect of impurities in containment sumps on iodine volatility was investigated at PSI, notably showing the low effect of chlorine content and generating data to tackle nitrate/nitride effects. Recently, following the Fukushima accident, questions were raised as to the effect of seawater compounds on water-phase chemistry during the accident concerning the FP-scrubbing efficiency in suppression pools and in liquid-type FCVS considering evolving thermal-hydraulic and chemical conditions during the accident and concerning the long-term aqueous-phase chemistry in relation to long-term accident management (corrosion reactions and leaching of corium/debris).

The effect of seawater is currently investigated in Japan as presented at the workshop with possible effects of bromine on iodine chemistry. Work in this field will continue in Japan in the coming years to develop the corresponding models.

The effects of changing thermal hydraulic (changing flow hydrodynamics) and chemical conditions (composition, doses, pH, oxido-reducing potential) on FP pool-scrubbing efficiency in suppression pools and FCVS during a SA were, are and will be partly investigated in research programmes (e.g., EC PASSAM, NEA THAI-3 and national initiatives on pool scrubbing experimentation and modelling in France, Germany, Japan, Republic of Korea, Spain and Switzerland). Analytical work performed to date on scrubbing experiments shows the necessity to improve modelling of the hydrodynamics of scrubbing, with existing modelling unable to represent flow instabilities which may strongly affect FP scrubbing efficiencies. There is presently only limited concerted research actions on pool scrubbing in the PASSAM project, and in the future in the THAI-3 project, and a larger collaboration in the field would certainly be beneficial to progress faster on scrubbing modelling. At a later stage, modelling FP scrubbing will require a coupling between hydrodynamic models with modelling of chemical reactions in the liquid phase.

Investigations of the long-term aqueous-phase chemistry in relation to the long-term accident management (corrosion reactions and leaching of corium/debris) are being or will be conducted in Japan. There was no specific recommendation in this field as the subject was not thoroughly discussed.

*The workshop experts recommended fostering collaborative initiatives on pool-scrubbing models development in relation to assessing FP retention in suppression pools and in FCVS in SA. Such models should also be of relevance to dealing with FP retention in SGTR with flooded secondary side.*

### ***FP Filtration in FCVS***

FCVSs implemented before Fukushima were mainly designed to manage long-term pressure build-up in the containment; new FCVS may perhaps be designed to deal with more challenging conditions (management of early phases of an accident, cycling or long-term use in SA conditions). The robustness, the safe use and the reliability of FCVS for such conditions should be further assessed either to improve existing systems or to propose upgraded design requirements for future systems.

The well-known existing filtration technologies, e.g., scrubbers, deep-bed filtration and different sorption systems were presented at the workshop. Part of the information concerning the existing filtration-systems performance and qualification is proprietary and was not disclosed by FCVS designers. However, two major aspects can be underlined concerning existing systems:

- most of the available systems were designed based on knowledge existing in the late 1980s; some have been updated depending on the system design and implementation (based on consideration of the results of relevant research and plant safety reviews notably additional filtration stages to modify the overall filtration efficiency); and
- given the possible extension of the domain of FCVS use, the demonstration of the systems' performance should be extended to more challenging conditions.

In different countries, ST evaluations are factored into accident analysis, used for FCVS regulatory assessment and as a guide for design and operation requirements of FCVS. ST evaluations in general are a part of PSA level 2 studies. These studies typically include the FCVS performance in reducing the ST, though the system is generally not separately examined. It is worth stressing, as discussed earlier, that the knowledge-base related to “delayed” in-containment re-volatilization and re-suspension processes for radionuclides/aerosols from RCS and containment surfaces and containment pools (sumps and suppression pools) is being extended through on-going and future research programmes (notably in the NEA BIP, STEM and THAI projects and the EC PASSAM project).

As for FCVS filtration, besides aerosols, specific attention is being given to organic iodides and iodine-oxide particles as they may contribute significantly to the ST in some accidents (notably, in the NEA BIP, STEM and EC PASSAM projects). Possible contribution of ruthenium-oxide species to the ST is also under investigation in on-going research programmes (notably in NEA STEM).

Important efforts were made for the development and qualification of FCVS by industry but questions remain as to the efficiency and robustness of such systems in SA conditions as these may be envisaged post-Fukushima. For some countries where safety criteria associated with releases are more stringent, there might be a search for more efficient filtration to further reduce radiological consequences. Such issues, with the assessment of innovative filtration technologies, are being covered in the EC PASSAM and French MiRE project. There are also some specific FCVS national developments notably in Japan and in the Republic of Korea.

Except for the specific recommendation on the need to foster collaborative efforts on FP scrubbing modelling in FCVS (see previous section), experts considered that on-going research on FCVS is well focused.

Recommendations on research tackling “delayed” re-emission processes in relation to ST assessment with FCVS use were listed in earlier sections. ***In particular for scrubbing FCVS, the effect of changing chemical conditions in SA on scrubbing efficiency requires further research efforts.***

### ***Iodine chemistry in the environment***

If a lot of development had been made to model iodine chemistry in the RCS and in the containment in a SA for ST applications, little attention has been given to iodine chemistry in the environment, i.e., after its release from the containment, for the assessment of its dispersion and related radiological consequences. Preliminary work based on existing knowledge of atmospheric iodine chemistry indicates that the radiological consequences due to iodine may be strongly dependent on the iodine chemistry in the environment. Due to the complexity of the chemical systems to be treated, it is necessary at this stage to further assess the potential impact of iodine chemistry in the environment on radiological consequences and define, if the impact is demonstrated to be strong, a pragmatic approach to model it. As a first step, ***the workshop experts recommended strengthening knowledge exchange between the ST research community and the environmental-chemistry community.***

### ***SA system codes ST models validation***

The discussions at the workshop raised questions about the level of detail required in the models, and the effect of uncertainties in the RCS and containment chemistry models on the calculated source terms and consequences. For “end-user” applications such as radiological consequence assessments and emergency planning, the models have to be simple and conservative. However, even the apparently simple models have to be based on a good understanding and representation of the behaviour of iodine, at the level treated by the more detailed models, in order to ensure that the important phenomena are correctly taken into account and scaled.

It was noted that international code benchmarking exercises had been performed in the past on specific RTF, THAI and PHEBUS FP tests and provided important lessons and that further benchmarking exercises are proposed for some THAI tests in the NUGENIA/SARNET frame. However, in order to address more specifically the scaling issue, benchmarking exercises for well selected reactor-like scenarios would be of higher value.

***Experts recommended organizing further exchanges to deepen the assessment of the validity of ST related models implemented in severe accident system codes – such as ASTEC, MAAP, MELCOR – notably by addressing:***

- ***the definition of a reference code-validation matrix for iodine behaviour<sup>2</sup> in RCS and containment;***
- ***the necessary level of detail for the modelling of the complex iodine behaviour for plant calculations;***
- ***the model validation for plant calculations (scaling issue) by performing, e.g., some SA system-code benchmarking exercise for defined reactor-like scenarios notably to assess the effect of recent chemical models development.***

### ***Reference ST evaluations and emergency response tools***

Final objectives of the ST research is to contribute to the consolidation of reference ST calculations used notably for protection measures design and of fast running calculation tools used as support to emergency response. The question of the methodology for the implementation of ST research outcomes into reference ST calculations and into fast running tools and of the assessment of their robustness was judged a key issue.

---

<sup>2</sup> As was done through an NEA exercise for containment thermal hydraulics.

Concerning ST calculations, *the experts recommended strengthening exchanges on source term evaluations performed for NPPs in various countries (results and methodologies) and on related quantification of remaining uncertainties on the related modelling*, this in view of checking that the ST research is properly focused and that no remaining important issue has been forgotten. The phase 2 of the NEA BSAF project which will start mid-2015 will concentrate on the assessment of radioactive substances releases and dispersion in the environment during the Fukushima Daiichi's accident and will contribute to this objective.

Concerning fast-running tools for emergency response, *the workshop experts recommended strengthening links between the ST research community and the emergency response community*. Initiatives in this field should be promoted following the conclusions of the NEA FASTRUN benchmarking exercise conducted for fast-running emergency response tools that was organized by the WGAMA and WPNEM (report NEA/CSNI/R(2015)19). Also, they should complement work that will be performed through the FASTNET project, which will start mid-2015 and is funded in the EC H2020 frame, dealing with methodological developments of more advanced prognostic/diagnosis emergency response tools.

## APPENDIX 1: WORKSHOP AGENDA

### MONDAY MARCH 30, 2015

<b>Registration</b>	8:30-9:00
<b>Welcome, opening remarks</b> <i>(D. Jacquemain, IRSN; J.P. Van Dorsselaere, NUGENIA/SARNET, N. Blundell, OECD/NEA)</i>	9:00-9:20
<b>Session 1 Main lessons from experimental programmes on iodine and ruthenium behaviour in a severe accident and research perspectives</b> <i>Session Chairs: T. Albiol (IRSN), H. Hoshi (NRA)</i>	
1.1 Main Outcomes Relative to Iodine Behavior from the VERDON/ISTP Programme (Y. Pontillon, CEA)	9:20-9:45
1.2 Research on the Transport and Chemistry of Iodine in Primary Circuit and Containment Conditions at VTT (T. Karkela, VTT)	9:45-10:10
1.3 Main Findings of the IRSN Experimental Programmes Performed on Iodine Chemistry in Severe Accident Conditions (A.C. Grégoire, IRSN)	10:10-10:35
1.4 THAI Experiments on Volatility, Distribution and Transport Behavior of Iodine and Fission Products in the Containment (S. Gupta, Becker Tech.)	10:35-11:00
<i>Coffee Break</i>	11:00-11:30
1.5 A Summary of the PSI Investigations on Iodine Chemistry in the Presence of Impurities and Additives (T. Lind, PSI)	11:30-11:55
1.6 Recent Findings on Ruthenium Chemistry in a Severe Accident (T. Karkela, VTT)	11:55-12:20
1.7 Thoughts on Ruthenium Research (M. Salay, USNRC)	12:20-12:45
<i>Lunch</i>	12:45-14:00
1.8 The Main Outcomes of the OECD Behavior of Iodine Project (G. Glowka, CNL)	14:00-14:25
1.9 The Behavior of Iodine Project: a Proposal for BIP3 (P.A. Yakabuskie, CNL)	14:25-14:50
1.10 OECD/STEM Project and Its Follow-up STEM2 (C. Mun, IRSN)	14:50-15:15
<i>Coffee Break</i>	15:15-15:45
<b>Session 2 Iodine transfer to aqueous phase, aqueous-phase chemistry</b> <i>Session Chairs: F. Funke (AREVA GmbH), J. Song (KAERI)</i>	
2.1 Iodine and Silver Wash-Down Modelling in COCOSYS-AIM by Use of THAI Results (G. Weber, GRS)	15:45-16:10
2.2 Effect of Constituents of Seawater on Formation of Volatile Iodine by Aqueous Phase Radiation Chemistry (K. Hata, JAEA)	16:10-16:35

- 2.3 Formation and Release of Molecular Iodine in Aqueous Phase Chemistry during Severe Accident With Seawater Injection (K. Kido, JAEA) 16:35-17:00

**End of day 1** 17:00

## TUESDAY MARCH 31, 2015

### Session 3 Organic iodide formation and partitioning, chemistry and interactions with aerosols, droplets and surfaces in the gas phase

*Session Chairs: G. Glowa (CNL), M. Salay (NRC)*

- 3.1 Chalmers Project on Volatile Organic Iodine Species Behaviour and Retention under Severe Nuclear Accident Conditions in LWR (S. Tietze, Chalmers Univ.) 9:00-9:25
- 3.2 OIPHA-I and II Model – Mathematical Models to Describe the Partitioning and Hydrolysis Behaviour of Organic Iodides Between Gaseous and Aqueous Phase (S. Tietze, Chalmers Univ.) 9:25-9:50
- 3.3 The Radiolysis of Gaseous Methyl Iodide in Air (S. Bowskill, NNL) 9:50-10:15
- Coffee Break* 10:15-10:45
- 3.4 The IODAIR Model for Radiolysis of Gaseous Iodine Species in Air: Data Comparison and Predictions (S. Dickinson, NNL) 10:45-11:10
- 3.5 Interaction of Gaseous I<sub>2</sub> with Painted Surfaces and Aerosols in Large-Scale THAI Tests (F. Funke, AREVA GmbH) 11:10-11:35
- 3.6 Effect of Water-droplet Sizes on the Migration of Volatile I<sub>2</sub> and CH<sub>3</sub>I (H.-J. Im, KAERI) 11:35-12:00

*Lunch* 12:00-13:15

### Session 4 Filtered containment venting systems

*Session Chairs: T. Lind (PSI), L.E. Herranz (CIEMAT)*

- 4.1 Westinghouse Molecular Sieve Technology (A. Andren, Westinghouse) 13:15-13:40
- 4.2 Improved Iodine Retention at Filtered Containment Venting (P. Zeh, AREVA GmbH) 13:40-14:05
- 4.3 Design on the Performance Test of Filter Containment Venting System (K.-S. Ha, KAERI) 14:05-14:30
- 4.4 Thermal-hydraulic Effect on Iodine Retention in the Filtered Containment Venting System (Y.-S. Na, KAERI) 14:30-14:55
- 4.5 Investigation of Iodine Retention in a Filtered Containment Venting System in the VEFITA Test Programme (D. Suckow, PSI) 14:55-15:20
- 4.6 The European PASSAM Project on Atmospheric Source Term Mitigation: Half-Way Progress and Main Results (T. Albiol, IRSN) 15:20-15:45

*Coffee Break* 15:45-16:15

### Session 5 Recent developments in iodine chemistry modelling in severe accidents and applications to source term and radiological consequences evaluations

*Session Chairs: S. Dickinson (NNL), D. Jacquemain (IRSN)*

- 5.1 Iodine Chemistry in Design Basis Faults (A. Zodiates, EDF Energy) 16:15-16:40

5.2 Iodine Behaviour in the Circuit and Containment: Modelling Improvements in the Last Decade and Remaining Uncertainties (L. Bosland, IRSN)	16:40-17:05
5.3 Containment Iodine Chemistry (M. Salay, USNRC)	17:05-17:30
<b>End of day 2</b>	17:30

### WEDNESDAY APRIL 1, 2015

**Session 5 cont. Recent developments in iodine chemistry modelling in severe accidents and applications to source term and radiological consequences evaluations**  
*Session Chairs: S. Dickinson (NNL), D. Jacquemain (IRSN)*

5.4 Application of the COCOSYS Iodine Chemistry Model AIM-3 to PWR Containment Analyses Using New Validation Results of RTF and CAIMAN Experiments (H. Dimmelmeier, AREVA GmbH)	9:00-9:25
5.5 Iodine Source Term Computations with ASTEC, Link with PSA Level 2 Tools and Fast Running Source Term Tools For Emergency Organisation (K. Chevalier-Jabet, IRSN)	9:25-9:50
5.6 In What Extent the Iodine Reactivity in the Atmosphere Can Impact the Radiological Consequences (J. Trincal, IRSN)	9:50-10:15
<i>Coffee Break</i>	10:15-10:45
<b>Session 6 General Discussion – conclusions of the workshop (all)</b> <i>Session Chairs: L. E. Herranz, D. Jacquemain, M. Kissane</i>	10:45-12:30
<i>Lunch</i>	12:30-13:45
<b>End of day 3</b>	13:45



**APPENDIX 2: LIST OF PARTICIPANTS****BELGIUM**

Dr ADORNI Martina  
 BEL V  
 Rue Walcourt 148  
 Brussels  
 BELGIUM  
 Phone: +3225280384  
 E-mail: martina.adorni@belv.be

Ms OURY Laurence  
 TRACTEBEL ENGINEERING (GDF Suez)  
 Avenue Ariane 7  
 1200 Bruxelles  
 BELGIUM  
 Phone: +3227737775  
 E-mail: laurence.oury@gdfsuez.com

**CANADA**

Mr GLOWA Glenn  
 CANADIAN NUCLEAR LABORATORIES  
 Chalk River Laboratories  
 286 Plant Road  
 Chalk River, Ontario, K0J 1J0  
 CANADA  
 Phone: +16135848811 ext. 46052  
 E-mail: glenn.glowa@cnl.ca

Dr YAKABUSKIE Pamela  
 CANADIAN NUCLEAR LABORATORIES  
 Chalk River Laboratories  
 286 Plant Road  
 Chalk River, Ontario, K0J 1J0  
 CANADA  
 Phone: +16135843311 ext 43146  
 E-mail: pam.yakabuskie@cnl.ca

**FINLAND**

Mr AUVINEN Ari  
 VTT TECHNICAL RESEARCH CENTRE  
 OF FINLAND  
 Biologinkuja 7  
 P.O. Box 1000  
 FI-02044 VTT, Espoo  
 FINLAND  
 Phone: +358207225785  
 E-mail: ari.auvinen@vtt.fi

Mr KÄRKELÄ Teemu  
 VTT TECHNICAL RESEARCH CENTRE  
 OF FINLAND  
 Biologinkuja 7  
 P.O. Box 1000  
 FI-02044 VTT, Espoo  
 FINLAND  
 Phone: +358207225718  
 E-mail: teemu.karkela@vtt.fi

**FRANCE**

Dr EZZIDI Alexandre  
AREVA NP  
1 place Jean Millier  
92084 Courbevoie  
France  
Phone: +33134967733  
E-mail: alexandre.ezzidi@areva.com

Mr DUCROS Gérard  
CEA  
CE Cadarache, bâtiment 315  
13108 Saint-Paul-lez-Durance Cédex  
France  
Phone: +33442256150  
E-mail: gerard.ducros@cea.fr

Dr HANUS Eric  
CEA  
CE Cadarache  
13108 Saint-Paul-lez-Durance Cédex  
France  
Phone: +33442254566  
E-mail: eric.hanus@cea.fr

Mrs BOSCHIERO Marie-Hélène  
EDF  
12-14 avenue Dutrievoz  
69628 Villeurbanne Cédex  
France  
Phone: +33472827163  
E-mail: marie-helene.boschiero@edf.fr

Mrs MAURICE Aubélia  
EDF  
12-14 avenue Dutrievoz  
69100 Villeurbanne  
France  
Phone: +33472827375  
E-mail: aubelia.maurice@edf.fr

Dr TOURNIAIRE Bruno  
EDF  
SEPTEN  
12-14 avenue Dutrievoz  
69628 Villeurbanne  
France  
Phone: +33472827884  
E-mail: bruno.tourniaire@edf.fr

Dr GALLAIS-DURING Annelise  
CEA  
DEN/CAD/DEC/SA3C/LAMIR  
CE Cadarache, bâtiment 315  
13108 Saint-Paul-lez-Durance Cédex  
France  
Phone: +33442254993  
E-mail: annelise.gallais-during@cea.fr

Mr PONTILLON Yves  
CEA  
DEN/CAD/DEC/SA3C/LAMIR  
CE Cadarache, bâtiment 315  
13108 Saint-Paul-lez-Durance Cédex  
France  
Phone: +33442257226  
E-mail: yves.pontillon@cea.fr

Mr FORTIN Matthias  
EDF  
SEPTEN, TE/CE  
12-14 avenue Dutrievoz  
69628 Villeurbanne  
France  
Phone: +33472824764  
E-mail: matthias.fortin@edf.fr

Ms ROZEL Christelle  
EDF  
SEPTEN  
12-14 avenue Dutrievoz  
69628 Villeurbanne  
France  
Phone: +33472827065  
E-mail: christelle.rozel@edf.fr

Mr ALBIOL Thierry  
 IRSN  
 PSN-RES/SEREX  
 CE Cadarache, bâtiment 328  
 BP 3  
 13115 Saint-Paul-lez-Durance Cédex  
 France  
 Phone: +33442499794  
 E-mail: thierry.albiol@irsn.fr

Mr CANTREL Laurent  
 IRSN  
 PSN-RES/SAG/LETR  
 CE Cadarache, bâtiment 702  
 BP 3  
 13115 Saint-Paul-lez-Durance Cédex  
 France  
 Phone: +33442199450  
 E-mail: laurent.cantrel@irsn.fr

Mr COUSIN Frédéric  
 IRSN  
 PSN-RES/SAG/LETR  
 CE Cadarache, bâtiment 702  
 BP 3  
 13115 Saint-Paul-lez-Durance Cédex  
 France  
 Phone: +33442199479  
 E-mail: frederic.cousin@irsn.fr

Dr GERYES Tony  
 IRSN  
 BU-DCI  
 31 avenue de la division Leclerc  
 92260 Fontenay-aux-Roses  
 France  
 Phone: +33787106500  
 E-mail: tony.geryes@irsn.fr

Dr HASTE Tim  
 IRSN  
 PSN-RES/SAG/LETR  
 CE Cadarache, bâtiment 702  
 BP 3  
 13115 Saint-Paul-lez-Durance Cédex  
 France  
 Phone: +33442199567  
 E-mail: tim.haste@irsn.fr

Dr BOSLAND Loïc  
 IRSN  
 PSN-RES/SAG/LETR  
 CE Cadarache, bâtiment 702  
 BP 3  
 13115 Saint-Paul-lez-Durance Cédex  
 France  
 Phone: +33442199446  
 E-mail: loic.bosland@irsn.fr

Mrs CHEVALIER-JABET Karine  
 IRSN  
 PSN-RES/SAG/LETR  
 CE Cadarache, bâtiment 702  
 BP 3  
 13115 Saint-Paul-lez-Durance Cédex  
 France  
 Phone: +33442199364  
 E-mail: karine.chevalier-jabet@irsn.fr

Dr FLEUROT Joëlle  
 IRSN  
 PSN-RES/SAG/LETR  
 CE Cadarache, bâtiment 702  
 BP 3  
 13115 Saint-Paul-lez-Durance Cédex  
 France  
 Phone: +33442199521  
 E-mail: joelle.fleurot@irsn.fr

Dr GREGOIRE Anne-Cécile  
 IRSN  
 PSN-RES/SEREX/L2EC  
 CE Cadarache, bâtiment 328  
 BP 3  
 13115 Saint-Paul-lez-Durance Cédex  
 France  
 Phone: +33442199740  
 E-mail: anne-cecile.gregoire@irsn.fr

Dr JACQUEMAIN Didier  
 IRSN  
 PSN-RES/SAG  
 CE Cadarache, bâtiment 702  
 BP 3  
 13115 Saint-Paul-lez-Durance Cédex  
 France  
 Phone: +33442199565  
 E-mail: didier.jacquemain@irsn.fr

Mrs MONSANGANT-LOUVET Céline  
IRSN  
Centre de Saclay  
BP 68  
91192 Gif-sur-Yvette Cedex  
France  
Phone: +33169082913  
E-mail: celine.monsanglant-louvet@irsn.fr

Dr MORIN Sandrine  
IRSN  
PSN-RES/SEREX/L2EC  
CE Cadarache, bâtiment 328  
BP 3  
13115 Saint-Paul-lez-Durance Cédex  
France  
Phone: +33442199620  
E-mail: sandrine.morin@irsn.fr

Dr MUN Christian  
IRSN  
PSN-RES/SEREX/L2EC  
CE Cadarache, bâtiment 328  
BP 3  
13115 Saint-Paul-lez-Durance Cédex  
France  
Phone: +33442199624  
E-mail: christian.mun@irsn.fr

Mr TRINCAL Julien  
IRSN  
PSN-RES/SAG/LETR  
CE Cadarache, bâtiment 702  
BP 3  
13115 Saint-Paul-lez-Durance Cédex  
France  
Phone: +33442199187  
E-mail: julien.trincal@irsn.fr

Mr VAN DORSSELAERE Jean-Pierre  
IRSN  
PSN-RES  
CE Cadarache, bâtiment 250  
BP 3  
13115 Saint-Paul-lez-Durance Cédex  
France  
Phone: +33442199709  
E-mail: jean-pierre.van-dorsselaere@irsn.fr

Mr VEILLY Edouard  
IRSN  
31 avenue de la division Leclerc  
92260 Fontenay-aux-Roses  
France  
Phone: +33158357162  
E-mail: edouard.veilly@irsn.fr

Mr VOLA Didier  
IRSN  
PSN-RES/SAG  
CE Cadarache, bâtiment 702  
BP 3  
13115 Saint-Paul-lez-Durance Cédex  
France  
Phone: +33442199714  
E-mail: didier.vola@irsn.fr

Dr STREKOWSKI Rafal  
MARSEILLE UNIVERSITY  
Université Aix-Marseille  
Campus Saint-Charles  
3 place Victor Hugo  
13331 Marseille  
France  
Phone:  
E-mail: rafal.strekowski@univ-amu.fr

## GERMANY

Dr DIMMELMEIER Harald  
AREVA GmbH  
Henri-Dunant-Strasse 50  
D-91058 Erlangen  
GERMANY  
Phone: +49913190095035  
E-mail: harald.dimmelmeier@areva.com

Mr FUNKE Friedhelm  
AREVA GmbH  
Paul-Gossen-Strasse 100  
91052 Erlangen  
GERMANY  
Phone: +49913190097681  
E-mail: friedhelm.funke@areva.com

Dr ZEH Peter  
AREVA GmbH  
Paul-Gossen-Strasse 100  
91052 Erlangen  
GERMANY  
Phone: +49913190097690  
E-mail: peter.zeh@areva.com

Dr GUPTA Sanjeev  
BECKER TECHNOLOGIES GmbH  
Koelner strasse, 06  
65760 Eschborn  
GERMANY  
Phone: +496196936115  
E-mail: gupta@becker-technologies.com

Mrs BECK Sara  
GRS  
Schwertnergasse 1  
50667 Köln  
GERMANY  
Phone: +492212068722  
E-mail: sara.beck@grs.de

Dr WEBER Gunter  
GRS  
Forschungszentrum  
Boltzmannstrasse 14  
D-85748 Garching  
GERMANY  
Phone: +498932004506  
E-mail: gunter.weber@grs.de

Mr POSS Gerhard  
BECKER TECHNOLOGIES GmbH  
Koelner strasse, 06  
65760 Eschborn  
GERMANY  
Phone: +496196936101  
E-mail: poss@becker-technologies.com

Mr LOVASZ Liviusz  
GRS  
Boltzmannstr. 14  
85748 Garching  
GERMANY  
Phone: +498932004458  
E-mail: liviusz.lovasz@grs.de

Dr WEBER Sebastian  
GRS  
Boltzmannstr. 14  
85748 Garching  
GERMANY  
Phone: +498932004438  
E-mail: sebastian.weber@grs.de

## INTERNATIONAL ORGANIZATIONS

Dr SIMOLA Kaisa  
EUROPEAN COMMISSION  
JOINT RESEARCH CENTRE  
P.O. Box 2  
NL 1755 ZG Petten  
The Netherlands  
Phone: +31224565180  
E-mail: kaisa.simola@ec.europa.eu

Mr BLUNDELL Neil  
OECD NUCLEAR ENERGY AGENCY  
Le Seine St-Germain  
12 boulevard des îles  
9213 Issy-les-Moulineaux  
France  
Phone: +33625043143  
E-mail: neil.blundell@oecd.org

Dr KISSANE Martin  
OECD NUCLEAR ENERGY AGENCY  
12 boulevard des îles  
92130 Issy-les-Moulineaux  
France  
Phone: +33145241054  
E-mail: martin.kissane@oecd.org

## ITALY

Mr GONFIOTTI Bruno  
UNIVERSITY OF PISA  
Largo Luciano Lazzarino  
56122 Pisa  
ITALY  
Phone: +393331716086  
E-mail: bruno.gonfiotti@for.unipi.it

## JAPAN

Dr HATA Kuniki  
JAPAN ATOMIC ENERGY AGENCY  
2-4 Shirane Shirakata  
Tokai-mura, Naka-gun  
Ibaraki 319-1195  
JAPAN  
Phone: +81292826778  
E-mail: hata.kuniki@jaea.go.jp  
Dr HOSHI Harutaka  
NUCLEAR REGULATION AUTHORITY  
Roppogi-First Bldg  
1-9-9 Roppongi, Minato-ku, Tokyo  
JAPAN  
Phone: +81351142224  
E-mail: harutaka\_hoshi@nsr.go.jp

Dr KIDO Kentaro  
JAPAN ATOMIC ENERGY AGENCY  
2-4 Shirane Shirakata  
Tokai-mura, Naka-gun  
Ibaraki 319-1195  
JAPAN  
Phone: +81292826159  
E-mail: kido.kentaro@jaea.go.jp  
Mr NUKATSUKA Shigehiro  
ENERGIS Co., Ltd.  
16-12, Shimbashi 6-Chome  
Minato-ku, Tokyo 105-0004  
JAPAN  
Phone: +81368802312  
E-mail: shigehiro\_nukatsuka@mshi.co.jp

**POLAND**

Ms SKOLIK Katarzyna  
 AGH UNIVERSITY  
 OF SCIENCE AND TECHNOLOGY  
 al. A. Mickiewicza 30  
 30-059 Cracow  
 POLAND  
 Phone: +48662631850  
 E-mail: kskolik@agh.edu.pl

Mr MALICKI Mateusz  
 PAA NATIONAL ATOMIC ENERGY  
 AGENCY  
 ul. Krucza 36  
 00-522 Warszawa  
 POLAND  
 Phone: +48226959924  
 E-mail: malicki@paa.gov.pl

Mr WLOSTOWSKI Mateusz  
 PAA NATIONAL ATOMIC ENERGY  
 AGENCY  
 ul. Krucza 36  
 00-522 Warszawa  
 POLAND  
 Phone: +48226959724  
 E-mail: wlostowski@paa.gov.pl

**REPUBLIC OF KOREA**

Dr HA Kwang Soon  
 KOREA ATOMIC ENERGY  
 RESEARCH INSTITUTE  
 989-111 Daedeok-daero  
 Yuseong-gu  
 Daejeon, 305-353  
 REPUBLIC OF KOREA  
 Phone: +82428688653  
 E-mail: tomo@kaeri.re.kr

Dr NA Young Su  
 KOREA ATOMIC ENERGY  
 RESEARCH INSTITUTE  
 989-111 Daedeok-daero  
 Yuseong-gu  
 Daejeon, 305-353  
 REPUBLIC OF KOREA  
 Phone: +82428688522  
 E-mail: ysna@kaeri.re.kr

Dr LEE Jongseong  
 KOREA INSTITUTE OF NUCLEAR SAFETY  
 62 Gwahak-ro, Yuseong-gu,  
 Daejeon 305-338  
 REPUBLIC OF KOREA  
 Phone: +82428680670  
 E-mail: jongseong@kins.re.kr

Dr IM Hee-Jung  
 KOREA ATOMIC ENERGY  
 RESEARCH INSTITUTE  
 Nuclear Chemistry Research Division  
 Deokjin-dong  
 Yuseong-gu  
 Daejeon, 305-353  
 REPUBLIC OF KOREA  
 Phone: +82428684740  
 E-mail: imhj@kaeri.re.kr

Dr SONG JinHo  
 KOREA ATOMIC ENERGY  
 RESEARCH INSTITUTE  
 989-111 Daedeok-daero  
 Yuseong-gu  
 Daejeon, 305-353  
 REPUBLIC OF KOREA  
 Phone: +82421041849396  
 E-mail: dosa@kaeri.re.kr  
 Mr LEE Seongnyeon  
 KOREA INSTITUTE OF NUCLEAR SAFETY  
 62 Gwahak-ro, Yuseong-gu,  
 Daejeon 305-338  
 REPUBLIC OF KOREA  
 Phone: +82428680817  
 E-mail: adult@kins.re.kr

**SPAIN**

Dr HERRANZ Luis E.  
CIEMAT  
Head of Unit for Nuclear Safety Research  
Division of Nuclear Fission  
Department of Energy  
Avenida Complutense, 40  
28040 MADRID, SPAIN  
Phone: +34913466219  
E-mail: luisen.herranz@ciemat.es

**SWEDEN**

Dr ANDREN Anders  
WESTINGHOUSE ELECTRIC SWEDEN AB  
SE 721 63 Västerås  
SWEDEN  
Phone: +46732367765  
E-mail: andrenal@westinghouse.com

Dr EKBERG Christian  
CHALMERS UNIVERSITY  
TECHNOLOGY  
Chemical and Biological Engineering  
Energy and Materials  
Kemivägen 4  
41296 Göteborg  
SWEDEN  
Phone: +46317722801  
E-mail: che@chalmers.se

Mr KAJAN Ivan  
CHALMERS UNIVERSITY of TECHNOLOGY  
Kemivägen 4  
41296 Göteborg  
SWEDEN  
Phone: +46723709988  
E-mail: kajan@chalmers.se  
Mrs TIETZE Sabrina  
OF CHALMERS UNIVERSITY OF  
TECHNOLOGY  
Nuclear Chemistry  
Department of Chemical and Biological  
Engineering  
Kemivägen 4  
41296 Göteborg  
SWEDEN  
Phone: +46735214168  
E-mail: sabrina.tietze@chalmers.se

Dr GLANNESKOG Henrik  
VATTENFALL AB  
Gullbergs Strandgata 6  
se-401 27  
Gothenburg  
SWEDEN  
Phone: +46706252487  
E-mail: henrik.glanneskog@vattenfall.com

**SWITZERLAND**

Mr ZIEGER Tobias  
CCI AG  
Itaslenstrasse 9  
8362 Balzers  
SWITZERLAND  
Phone: +41792764155  
E-mail: tobias.zieger@imi-critical.com

Dr LIND Terttaliisa  
PAUL SCHERRER INSTITUT  
OHSA / C11  
CH-5232 Villigen PSI  
SWITZERLAND  
Phone: +41563102650  
E-mail: terttaliisa.lind@psi.ch

Dr SUCKOW Detlef  
PAUL SCHERRER INSTITUT  
5232 Villigen PSI  
OHSA/C04  
SWITZERLAND  
Phone: +41563104145  
E-mail: detlef.suckow@psi.ch

#### **UNITED STATES**

Dr SALAY Michael  
U.S. NUCLEAR REGULATORY  
COMMISSION  
MS: C3-A07M  
11555 Rockville Pike  
Rockville, MD 20852-2739  
U.S.A  
Phone: +13012517543  
E-mail: michael.salay@nrc.gov

#### **UNITED KINGDOM**

Dr DOUGALL Alex  
EDF ENERGY  
Barnett Way  
Barnwood, Gloucester GL4 3RS  
UNITED KINGDOM  
Phone: +441452652694  
E-mail: alexandra.j.dougall@edf-energy.com

Mr PRIOR Robert  
R.P. SAFETY CONSULTING LTD  
2 Elwick Road  
Ashford TN23 1PD  
Kent  
UNITED KINGDOM  
Phone: +447827292920  
E-mail: bob.prior@rpsafetyconsulting.com

Ms BOWSKILL Susannah  
NATIONAL NUCLEAR LABORATORY  
B168, Harwell Oxford Science Campus  
Didcot, OX11 0QT  
UNITED KINGDOM  
Phone: +441925289995  
E-mail: susannah.r.bowskill@nnl.co.uk

Dr DICKINSON Shirley  
NATIONAL NUCLEAR LABORATORY  
B168, Harwell Oxford Science Campus  
Didcot, OX11 0QT  
UNITED KINGDOM  
Phone: +447894598707  
E-mail: shirley.dickinson@nnl.co.uk

Mr IHARA Takafumi  
TOKYO ELECTRIC POWER COMPANY  
Berkeley Square House  
Berkeley Square  
London W1J 6BR  
UNITED KINGDOM  
Phone: +447917816226  
E-mail: ihara.takafumi@tepco.co.jp

Dr ZODIATES Anastasios  
EDF ENERGY  
Barnett Way  
Barnwood, Gloucester GL4 3RS  
UNITED KINGDOM  
Phone: +441452653915  
E-mail: tasos.zodiates@edf-energy.com



**APPENDIX 3: PAPERS BY TECHNICAL SESSIONS**



**Session 1: main lessons from experimental programmes on iodine and ruthenium behaviour in a severe accident and research perspectives**

## MAIN OUTCOMES RELATIVE TO IODINE BEHAVIOUR FROM THE VERDON/ISTP PROGRAMME

Y. Pontillon\*, S. Bernard, A. Gallais-During, B. Gleizes, E. Hanus and G. Ducros  
CEA, DEN, DEC, F-13108 Saint-Paul-lez-Durance, France

\*Corresponding author, tel: (+33) 442257226, Email:yves.pontillon@cea.fr

**Abstract** – *Following the TMI-2 accident in 1979, numerous programmes have been launched in France and abroad, in order to quantify the release or fission products (FP) from irradiated fuel and to better assess the source term under severe accident conditions. In France, the CEA has conducted the VERCORS programme, composed of 17 separate effect tests (SET), which is considered to be complementary to the integral-type PHEBUS-FP tests programme. After the successive shutdowns of the VERCORS (2002) and PHEBUS-FP (2004) facilities, a thorough identification of the remaining uncertainties in source term assessment and modelling was established by CEA, EDF and IRSN. This work led to the launch of the International Source Term Programme (ISTP).*

*The ISTP is composed of SET, taken in charge by IRSN and CEA. The CEA part of this programme is the VERDON programme dedicated to: (1) FP release from high burn-up UO<sub>2</sub> and MOX fuels, in particular for low volatile FP and (2) impact of air ingress on FP behaviour, which is expected to enhance the release of highly radiotoxic FP, such as ruthenium, as well as to re-volatilise volatile FP (iodine, caesium) previously deposited in the primary circuit. This VERDON programme has been carried out in a new laboratory of the CEA Cadarache, where two dedicated hot cells and one glove box have been built for this purpose. Three VERDON tests covering the first topic (FP release) were performed: VERDON-1 (September 2011) on UO<sub>2</sub> at 72 GWd/t in reducing conditions, VERDON-3 (April 2013) and VERDON-4 (October 2014) on a 60 GWd/t MOX fuel respectively under steam oxidising and hydrogen reducing conditions. The VERDON-2 test (June 2012), covering the air ingress topic, was performed on a 60 GWd/t MOX fuel, using a more complex experimental circuit including in particular thermal gradient tubes downstream the furnace where the fuel sample is heated.*

*The main outcomes relative to the iodine behaviour identified from this experimental programme are presented, focusing in particular on the following aspects:*

- *Release kinetics*
  - *observed for high burn-up UO<sub>2</sub> fuel and MOX fuel, compared to the kinetics measured on standard UO<sub>2</sub> fuel in the previous VERCORS programme,*
  - *at lower temperature simulating a LOCA,*
- *The iodine deposits and re-volatilisation observed in VERDON-2, following the air injection,*
- *The gaseous iodine fraction measured at the outlet of the VERDON circuit, simulating the entrance in the containment.*

## I. INTRODUCTION

One of the most important areas of research concerning a hypothetical severe accident in a Light Water Reactor (LWR), on both a French and an international level, is determining the source term, i.e. quantifying the nature, release rate and global released fraction of fission products (FP) and other radioactive materials. This is in great part due to the consequences of the Three Mile Island (1979), Chernobyl (1986) and more recently Fukushima accidents. In the course of this type of scenario, the chain of events can effectively result in primary coolant boiling and draining, meaning that it is no longer cooling the core. One direct result is the core melting and the release of FP and structural and/or activated control rod elements (*e.g.* activation products, AP) into the containment building. If there is a failure in the various protective barriers, the FP/AP can leak out of the containment building and be released into the environment.

A large numbers of research programmes have thus been undertaken on this subject in various countries. In line with this approach, IRSN (France) has been the driving force and has conducted programmes specifically focusing on determining the source term, with particular efforts devoted to **understanding the mechanisms** that lead to the release of FP, since only a very complete knowledge of the phenomena governing the behaviour of FP/AP under such constraints will make it possible to define the actions that need to be planned (and/or performed) to minimise emissions and optimise the protection of both the people and the environment. The HEVA [1]/VERCORS [2] programmes were thus initiated by the CEA. VERCORS has considerably broadened the field of application by exploring higher temperatures and by testing a wider range of fuels (UO<sub>2</sub>, MOX, debris bed configurations, high burn-ups) in a more complex experimental installation with improved instrumentation. It was composed of 17 tests which were conducted over 14 years, in accordance with 3 experimental phases. A first series of six tests (VERCORS 1 to VERCORS 6) was conducted between 1989 and 1994 on UO<sub>2</sub> fuels in a higher temperature range than the preceding HEVA phase, close to the fuel

relocation [3]. This series made it possible to integrate certain FP with low volatility into the HEVA results database. Two series of tests – VERCORS HT and RT – were then conducted alternately throughout 1996-2002 allowing the data base extension up to the less volatile FP.

These analytic experiments simulating severe LWR accidents were financed jointly by IRSN and EDF. Their aim was to quantify the released fraction and release rates of FP from irradiated nuclear ceramics (UO<sub>2</sub> or MOX, typically three PWR pellets in their original cladding), quantify the nature of the gases and aerosols emitted (particle size analysis and chemical composition), and understand how the fuel degrades. These experimental sequences were carried out in a very high activity cell and were commonly considered to be complementary to the PHEBUS FP [4] integral tests and comparable with certain tests carried out abroad: HI/VI [5] in the United States, VEGA [6] in Japan or the programme conducted at the CRL in Canada [7]. The experimental results of this programme are used to (a) define the envelope values for released fraction within the scope of assessing reference source terms for all French PWRs, and (b) validate the semi-empirical or mechanistic models regarding FP release and transport while qualifying the simulation codes by integrating these models [8], [9], [10], [11].

However, major uncertainties still remain in some fields, concerning the assessment of risks for populations and the environment [12]. As a consequence, it has been decided to build a co-operative research programme between teams involved in severe accident (SA) phenomenology all over the world (US-NRC, IRSN, CEA, EDF, GDF Suez, PSI, European Commission, EAEL, KAERI), based on separate-effect experiments and called “International Source Term Program (ISTP)”. The results of these separate-effect experiments would allow improving models used for Source Term evaluation studies. Four main R&D research axes have been included in this programme: (1) iodine behaviour in the RCS and the containment, (2) study of the boron carbide effect on fuel degradation and FP release, (3) study of the air effect on fuel and FP behaviour

and (4) study of the fission product release from the fuel.

As far as the source term quantification is concerned, four VERDON tests were considered. They are devoted to FP release from high burn up  $UO_2$  fuel, MOX fuels and air ingress scenario. They were performed in the new VERDON laboratory at the CEA Cadarache Centre. After having described this new VERDON laboratory (section II), an overview of the four ISTP VERDON tests is proposed (section III). In the last part of the paper (section IV), the main outcomes relative to the iodine behaviour identified from this experimental programme will be presented, focusing in particular on three main aspects:

- Release kinetics
  - observed for high burn-up  $UO_2$  fuel and MOX fuel, compared to the kinetics measured on standard  $UO_2$  fuel in the previous VERCORS programme,
  - at lower temperature simulating a LOCA type accident,
- The iodine deposits and re-volatilisation observed in VERDON-2, following the air injection,
- The gaseous iodine fraction measured at the outlet of the VERDON circuit, simulating the entrance in the containment.

## II. THE VERDON LABORATORY

The four ISTP VERDON tests were conducted between 2011 and 2014 in an entirely new laboratory at the CEA Cadarache Centre in the LECA-STAR facility [13]. It is constituted of two high activity cells (called C4 and C5) and a gloves-box, as illustrated in Figure 1. The C4 cell is dedicated to the sample reception, pre/post-tests gamma scanning and loop elements storage. The C5 cell contains the experimental circuit itself (i.e. VERDON loop, including two configurations). It is dedicated to the accidental sequence realisation and to on-line measurements. The glove-box main functions are to analyse and store the fission and carrier gases.

The VERDON loop in its release configuration is illustrated in Figure 2. This experimental loop is constituted of (along the path of gas flow): (a)

the fluid injection system, (b) the furnace, (c) an aerosol filter located directly on the top of the furnace (Its filtering part is constituted of stainless steel poral<sup>®</sup> which function is to stop all the fission products under aerosol forms. The aerosol filter is heated at  $150^{\circ}C \pm 10\%$ ), (d) a May-Pack filter, filled with zeolite (impregnated with silver) in order to trap potential molecular iodine and heated at  $150^{\circ}C \pm 10\%$  to avoid condensation, (e) a condenser the function of which is to condense steam from the experimental gas and to recover the water for analysis, (f) a final safety filter, which filtering part is constituted of stainless steel poral<sup>®</sup>, in order to stop any residual trace of fission products (other than gaseous Xe, Kr). Upstream from the condenser, the circuit is constituted of stainless steel tubes heated at  $150^{\circ}C \pm 10\%$ . Downstream, the condenser is linked to the final safety filter. Outside of the cell, a “linking line” is used to make the junction between the C5 cell and the gloves box.

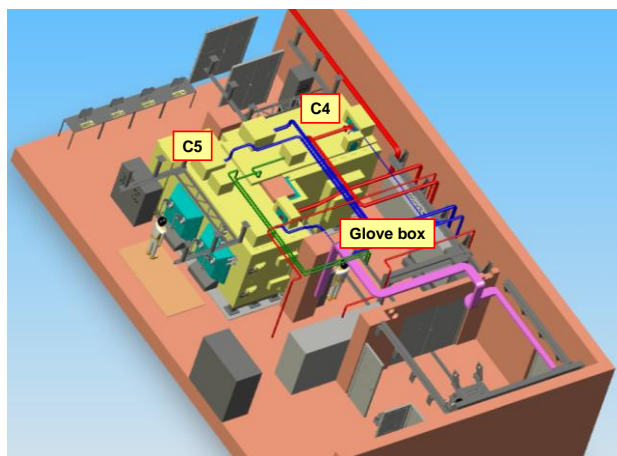


**Figure 1: Schematic view of the VERDON laboratory**

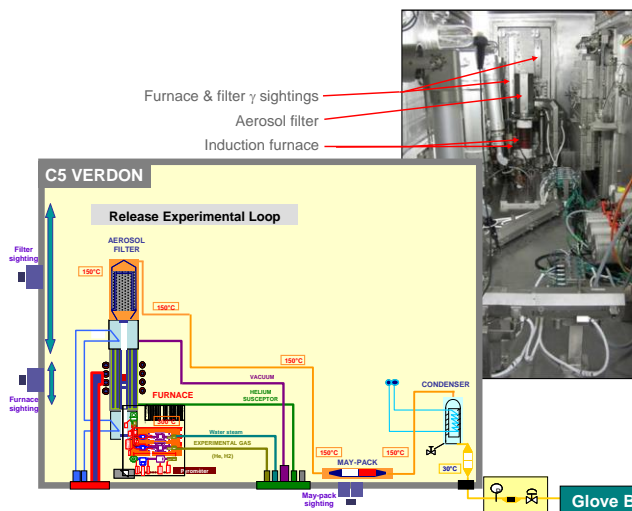


**Figure 2: The so-called release experimental loop (CER)**

The VERDON loop in its transport configuration is illustrated in Figure 3. In addition to FP release objective, this experimental loop is also dedicated to the study of FP deposits and their potential re-volatilisation. It is constituted above the furnace of: (a) a section heated at 700°C; (b) a multiple thermal gradient tubes (TGTM) in which the temperature along the outlet of four Inconel tubes (700 mm length, ~20 mm diameter) is linearly decreasing from 730°C to 140°C.

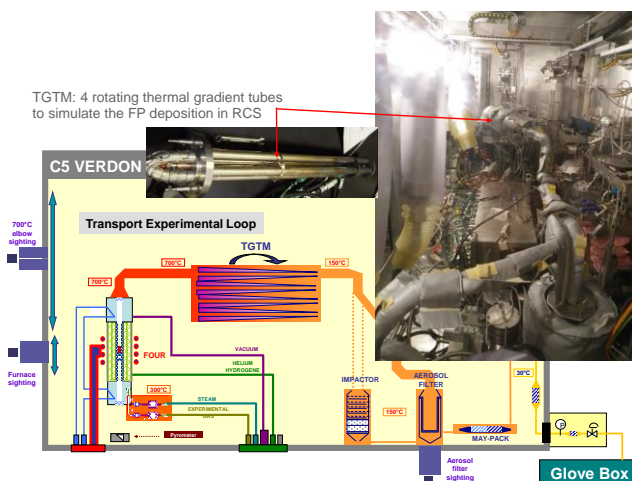


**Figure 3: The so-called transport experimental loop (CET)**

Downstream from the TGTM, the fluid goes through a 150°C heated Inconel section and goes successively to: (a) an aerosol filter or (b) a cascade impactor composed of a succession of 6 impaction stages designed to collect the aerosols on drilled discs with decreasing diameter openings from 1.2 mm to 0.2 mm, two successive batteries of beds designed to collect submicronics aerosols and finally a Poral® filter (grade-3). The impactor operates for few minutes at the end of the test in order to quantify the particle size distribution of the aerosols. It is heated to allow 150°C in the impactor. The May-Pack filter and the condenser are similar to those of the release loop and located downstream of the aerosols filter and cascade impactor. Downstream, the condenser is linked to a P4VP filter made of “polyvinylpyridine” in order to trap the potential gaseous ruthenium tetra-oxide potentially produced during the experiment.

In both configurations, the VERDON furnace is based, as the previous VERCORS one, on induction technology. Schematically, it is constituted of a coil surrounding a tungsten susceptor tube, which is the heating component of the furnace. A high frequency power supply generates a current in the coil. By electromagnetic coupling, a current is generated into the susceptor tube and the corresponding electric energy is converted to thermal energy by Joule effect, leading to the heating of the susceptor tube. Then, the fuel sample, located at the centre of the susceptor tube, is heated, mostly by thermal radiation.

FP release kinetics is measured by means of three complementary on line gamma spectrometry stations and one micro gas chromatography apparatus.

One gamma station is aimed directly at the fuel sample and used during all the test. This gamma station makes it possible to qualitatively measure the FP remaining in the fuel as a function of temperature, which explains why a relatively imprecise quantification of the release kinetics was obtained<sup>3</sup>. The two advantages of this station

<sup>3</sup> At least 10% release have to be recorded by this station to guarantee a significant value, particularly

come (i) from its ability to measure directly at the source (all the FP were measured, unlike at the other stations where deposits upstream could occur) and (ii) for its ability to indicate the precise moment when the fuel relocates by detecting the disappearance (or significant decrease) in the signal from non-volatile FP. This last point was well illustrated in the case of the VERCORS series [2, 14]. This gamma station is also used in order to perform pre and post qualitative gamma scanning of the sample inside the furnace respectively before and after the accidental sequence.

One other gamma station is aimed at the large-capacity aerosol filter. It provides a very precise measurement of the FP deposited at this point, where most of the volatile FP were found. It is highly complementary with the previous station (fuel sight).

The last gamma station is aimed at the May-Pack (CER configuration only and allows measuring potential gaseous iodine during the test.

The gas analysis can be also performed on-line by a micro gas chromatograph ( $\mu$ GC) localized inside the glove box. The  $\mu$ -GC extends the analysis of active gases to all the gases.

### III. THE FOUR VERDON ISTP TESTS

For the four VERDON-ISTP tests (Table 1), the sample was taken on a  $UO_2$  or a MOX fuel rod, previously irradiated in a PWR operated by the French operator EDF. The sample consists of two irradiated pellets in their original cladding and two half-pellets of depleted (and un-irradiated) uranium dioxide located at each end of the sample and held there by crimping the cladding so that the cladding is not fully sealed. Before the experimental sequence, the sample was re-irradiated at low linear power (15 to 20 W/cm) in the OSIRIS material testing reactor for about a week, in order to recreate the short half-life FPs without any in-pile release. As a consequence, these FPs (i.e.  $^{99}Mo$ ,  $^{132}Te$ ,  $^{133}I$ ,  $^{131}I$ ,  $^{140}Ba...$ ), important for their radiobiological

---

as the changes in the object geometry measured during heating (swelling, fracturing, then fuel collapse, etc.) significantly complicates the quantitative use of the measurement, just like the axial migration of the FP.

effects, are measurable by using on-line gamma spectrometry during the experiment. The fuel sample used for VERDON-1 was a high burn up  $UO_2$  fuel very similar to VERCORS-RT6 (same fuel assembly, same power history, and very close burn up). For VERDON-2 to -4, the samples were made up of a fuel section taken at the same span of a MOX fuel rod so that they are identical. The main parameters explored throughout the 4 tests during the program were mainly the maximal temperature, the oxidizing-reducing conditions of the carrier fluid, the high burn-up and the nature of the fuel sample ( $UO_2$  or MOX). For the four tests, an intermediate temperature plateau was performed at 1500°C (in a steam and hydrogen atmosphere for VERDON-1 and -3, pure steam for VERDON-2 and -4) in order to fully oxidize the cladding before the temperature ramps up to the final phase of the test. The duration of this intermediate plateau was about 10-15 minutes, except for VERDON-1 for which it was 50 minutes long.

During the first VERDON-1 test, the good performances of the VERDON loop in terms of tightness, thermal-hydraulics, furnace ceramics behavior, etc... and of the gamma scanning and sighting have been clearly demonstrated. As a consequence it was asserted that the VERDON facility was technology-approved. The comparison with VERCORS RT6 (same fuel, same thermal history, same atmosphere, etc...) has been possible and conclusive: similar FP released fractions at 1500°C. The VERDON loop was then qualified in "release configuration", in continuity with VERCORS experiments.

The VERDON-2 test concerns high burn up MOX fuel behavior - and corresponding FP release and transport - under air ingress conditions. One of the main goals of this test concerns the transport/re-volatilization study of ruthenium and previously deposited volatile fission products in the RCS of a nuclear power plant, thanks to the TGTM of the Transport configuration.

VERDON-3 and -4 are two complementary experiments. Their main objective is the quantification of FP release from a high burn up MOX fuel under steam oxidizing conditions for VERDON-3 and hydrogen reducing conditions for VERDON-4. Both tests were conducted at

high temperature but without reaching global fuel relocation and with a follow-up of semi-volatile fission products in order to expect interesting post-test micro-analysis. They were performed with the Release Circuit.

Table 1: Main characteristics of the 4 VERDON-ISTP tests

Test	Fuel	Circuit	Atmosphere end of test	Max Temperature	Main Objectives
VERDON-1 (30/09/2011)	UO <sub>2</sub> , 72 GWd/t Re-irradiated (OSIRIS)	Release	Reducing, H <sub>2</sub> /H <sub>2</sub> O molar ratio = 10	2600°C	High burn-up effect on FP release / Complementary to Vercors RT6
VERDON-2 (27/06/2012)	MOX, 60 GWd/t	Transport	Mixed steam-air conditions: 50-50%	2100°C	Air ingress / Ru release / Iodine revolatilisation
VERDON-3 (17/04/2013)	Re-irradiated (OSIRIS)	Release	Oxidising H <sub>2</sub> O/H <sub>2</sub>	2300°C	MOX effect on FP release / Complementary tests under steam-hydrogen atm
VERDON-4 (16/10/2014)		Release	Reducing H <sub>2</sub> O/H <sub>2</sub>	2500°C	

As far as UO<sub>2</sub> fuels are concerned, according to the released fractions measured by on-line gamma station and thanks to the data obtained via pre and post-test gamma scannings, the FP general classification determined during the VERCORS series, in relation to their released fractions and specific behaviours, is confirmed here with:

- Volatile FP (including fission gases, iodine, caesium, antimony, tellurium, cadmium, rubidium and silver) all have a high or even almost complete release for temperatures representative of a SA. The nature of the test (fuel type, initial geometry, atmosphere at the end of the test, etc.) essentially affects the release kinetics of these species and has little effect on the released fraction once this temperature level has been reached during the test.
- Semi-volatile FP such as molybdenum, rhodium, barium, palladium and technetium have released fraction that can attain 50% to 100%, but their redeposit are close to the emission point. In addition, the high sensitivity of the kinetics and released fraction regarding the oxidising conditions of the tests – already demonstrated during the VERCORS programme – were confirmed with VERDON. For instance, Mo release increased under oxidising conditions through the formation of volatile species. On the contrary, the release for rhodium and barium increased under reducing conditions. This

latter point seems to be less pronounced during VERDON tests on MOX fuels.

- Low volatile FP such as ruthenium, niobium, strontium, yttrium, lanthanum, cerium and europium have low, yet significant, released fraction of around 3% to 10% on average, but these values can attain 20-40% in the case of some FP under particular conditions, e.g. oxygen potential or high burn-up. In addition, the FP in this category are essentially re-deposited in the high temperature section of the test loop, i.e. near the fuel (emission point). Furthermore, it also appears that reducing conditions encourage the release of strontium, cerium, europium and lanthanum, whereas oxidising conditions enhance the ruthenium release.
- Non-volatile FP include zirconium, neodymium and praseodymium. Their released fractions are too low to be measured by gamma spectrometry under even the severest of the test grids used here.

Besides, one has to note that VERDON program highlights some FP specific release behaviours from MOX fuels. In particular:

- The relatively low release rate of Ru during VERDON-2 (air ingress scenario),
- High release kinetics, beginning at rather low temperature, for volatile (I, Cs, Te) and semi-volatile (Mo) FP,
- Unexpected Ba behaviour during VERDON 2 and 3 with practically the same release (i.e. whatever the atmosphere of the test),
- Specific iodine behaviour, as described in the following section.

#### IV. MAIN OUTCOMES RELATIVE TO THE IODINE BEHAVIOUR

The main outcomes relative to the iodine behaviour identified thanks to the ISTP “VERDON” programme are principally:

- Release kinetics
  - observed for high burn-up UO<sub>2</sub> fuel and MOX fuel, compared to the kinetics measured on standard UO<sub>2</sub> fuel in the previous VERCORS programme,

- at lower temperature simulating a LOCA type thermal history.
- The iodine deposits and re-vaporisation observed in VERDON-2, following the air injection,
- The gaseous iodine fraction measured at the outlet of the VERDON circuit, simulating the entrance in the containment.

These three main aspects are described successively below.

### **Release kinetics of Iodine (and Caesium) and Iodine release (versus Caesium) at low temperature**

Iodine and caesium FPs are of great importance with regard to the radiological consequences following a severe accident in a LWR core. They are composed of isotopes with very different half-lives:

- Short half-life for iodine (from 1 hour for  $^{134}\text{I}$  to 8 days for  $^{131}\text{I}$ ); the short-term radiological effects are very high in the first few days following an accident, but are negligible after 1 month. Iodine carries 15% of the core's decay heat 1 day after the emergency shutdown; In addition, iodine is of high concern according to its ability to be released and/or produced under gaseous forms in the containment.
- Long half-life for caesium (30 years for  $^{137}\text{Cs}$ ); the radiological effects, which are low in the short term (there are nevertheless  $^{138}\text{Cs}$  and  $^{136}\text{Cs}$  with respective half-lives of 30 min and 13 days) stretch into long term over several decades.

Although the global release of these two FP did not depend (or only very little) on the test conditions at temperatures of more than 2,300°C, it was quite different for their **release kinetics**. Inter-comparison of all the tests in the VERCORS/VERDON grid makes it possible to highlight:

- that for temperature superior than 1200°C, the release kinetics of Cs and I are almost identical,
- the influence of key parameters - such as the burn-up, atmosphere, fuels (MOX or  $\text{UO}_2$ ), and its initial geometry (intact or debris bed)

- on the release kinetics. It was also possible to identify the influence of one of these parameters on another. From a general point of view, the release rate increases with the burn up, in oxidizing condition and with MOX compared to  $\text{UO}_2$  fuels.

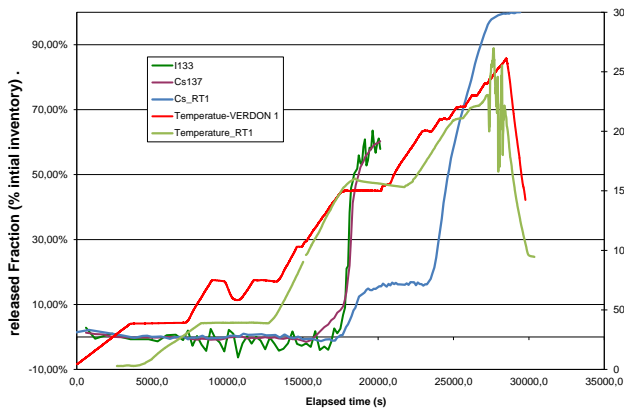
To illustrate the impact of the burn-up on the release kinetics of iodine and caesium, Figure 4a compares tests VERDON-1 ( $\text{UO}_2$  6 cycles) and VERCORS RT1 ( $\text{UO}_2$  4 cycles which can be considered as reference test with a moderate burn-up). An unequivocal effect on the rate of iodine's and caesium's release kinetics is visible. At the end of the cladding oxidation plateau, caesium release was around four times higher for VERDON-1 than for RT1.

The influence of the nature of the fuels (MOX versus  $\text{UO}_2$ ) is also perfectly highlighted by the comparison between tests VERDON -2, -3 -4 (MOX fuels at 60 GWd/t) and VERCORS RT1. Whatever the atmospheres of the tests and up to the end of the cladding oxidation plateau, the volatiles (Cs/I) FP release kinetics is faster for MOX compared to  $\text{UO}_2$  fuels (Figure 4b).

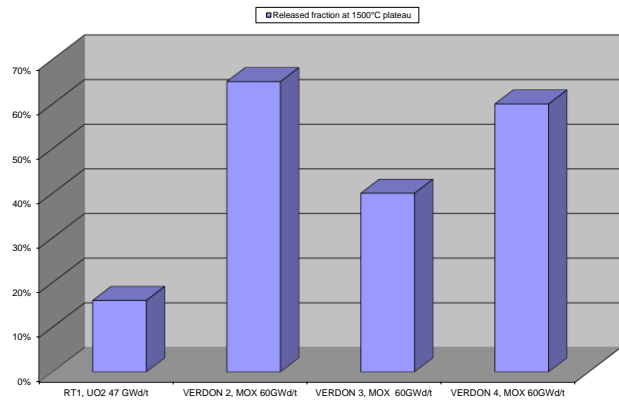
The influence of the atmosphere (oxidizing or reducing) is also perfectly highlighted by the comparison between tests VERDON-3 and VERDON-4 during the so-called oxidation plateau. These tests are effectively similar from the viewpoint of both the fuel used (identical fuel rods) and the temperature ramp history up to end of the 1500°C plateau. The comparisons are thus direct. A marked difference in the release for VERDON-3 (Mixed  $\text{H}_2\text{O}/\text{H}_2$  atmosphere) was measured in relation to VERDON-4 (more oxidizing conditions, steam), with respectively around 40% and 60% respectively for VERDON-3 and VERDON-4.

The "LOCA" plateau (15 min at 1200°C), performed for VERDON 3 and 4, makes it possible to highlight a discrepancy between the iodine ( $^{131}\text{I}$ ,  $^{133}\text{I}$ ) and caesium ( $^{134}\text{Cs}$ ,  $^{137}\text{Cs}$ ) behaviour. At this stage, a 10% release has been recorded for the caesium whereas the iodine seems not to be released. This can be interpreted as a difference in the behaviour between long (caesium) and short (iodine) half-life species:

- Long half-life nuclides are quasi uncreated during the irradiation in the OSIRIS MTR. Thus, their repartition inside the MOX pellets is mainly determined by the fuel thermal history during base irradiation in EDF nuclear power plant. In the case of the caesium, diffusion occurs to the grain boundaries and its distribution inside the MOX pellet includes inter- and intra-granular parts. In addition, a strong axial and radial migration leading to an accumulation at the pellets boundaries has been observed on this particular rod. This behaviour can explain the early release recorded during the “LOCA” plateau.
- Short half-life nuclides, unlike the previous ones, completely disappear from the MOX pellets a few days after the end of the power plant irradiation. Thus, their repartition inside the VERDON fuel sample is only due to the MTR irradiation and they are mainly located in intra-granular position of the MOX pellets. This repartition inside the fuel microstructure can explain the delay in the release of the short half-life iodine species compared to the long half-life caesium ones.



(a)



(b)

Figure 4 : (a) I and Cs Release kinetics for VERDON-1 and VERCORS RT1 (b) Release at 1500°C (after 10 minutes plateau) during VERDON -2, -3, -4 and VERCORS RT1.

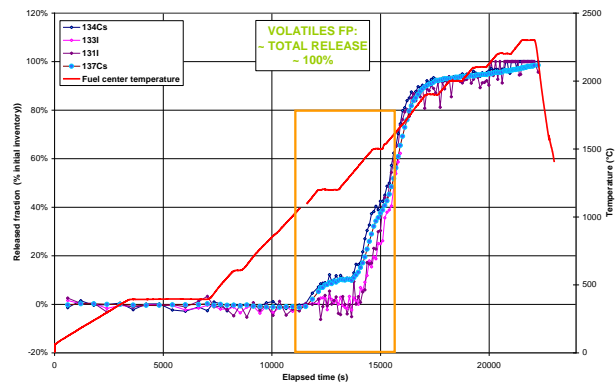


Figure 5 : I and Cs release rate at low temperature simulating LOCA conditions (VERDON-3).

One can note that this is the first time that this specific behaviour of I compared to Cs is recorded at this level of temperature. That can have a significant impact, regarding the source term, in LOCA type conditions according to the corresponding half-life.

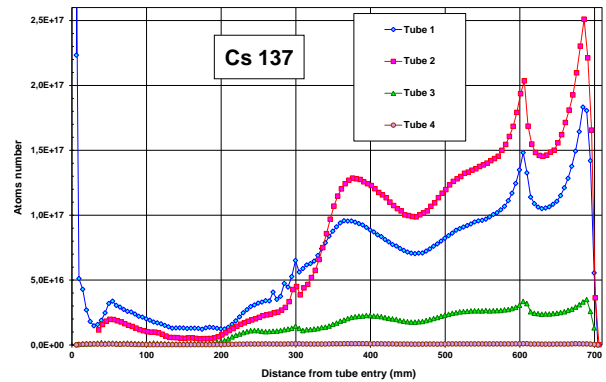
**Iodine deposits re-volatilization during VERDON-2**

The VERDON-2 thermal-hydraulic sequence is displayed on Figure 6a. Phase 1 and 2 were similar to VERDON-1 test without H<sub>2</sub> injection. Phase 3, under steam conditions, was dedicated to the measurement of release, transport and deposit of FPs without air injection. The first TGT rotation occurred (tubes 1-2 to tubes 2-3) at the end of this phase. Phase 4, under air and steam conditions (molar ratio of 1 between steam and air) has been maintained for 70 minutes. Phase 5 was then performed up to 2100°C. The

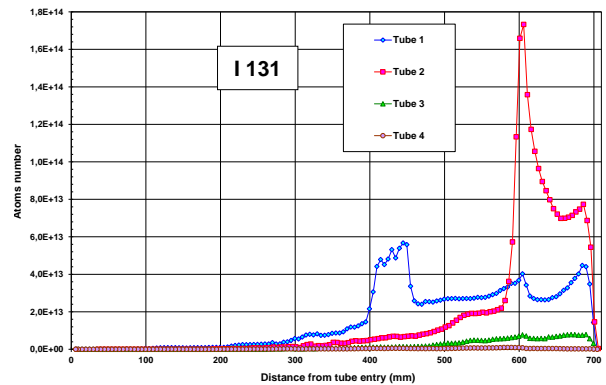
2100°C plateau lasted for 90 minutes. During this plateau, the TGTM was turned after 60 minutes (tubes 2-3 to tube 3-4) and after the rotation, the tubes 3 and 4 stayed during 30 minutes under the same atmosphere to be able to study the FP deposits and their potential re-volatilisations.

The transport of volatile FPs (caesium and iodine) along the TGTM is very different. For Cs, the deposit profile is qualitatively similar in each tube (almost the totality of caesium was released at 2000°C), showing no effect of air injection (Figure 6b), whereas for iodine, one can observe (Figure 6c) that the highest <sup>131</sup>I deposits were located in the middle of tube 1 and at the outlet of tube 2.

The central deposit observed on tube 1 has been completely re-volatilized during the air injection since it no longer appeared on tube 2. Deposits on tube 3 are very low, which shows that deposits at the outlet of tube 2 have been also re-volatilized at the end of the test. This latter point clearly highlights the difference, in terms of transport, which exists between Cs and I, difference which can impact chemistry occurring in the RCS during a severe accident.

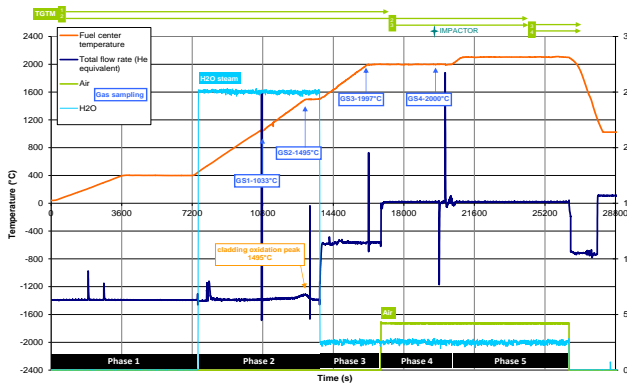


(b)



(c)

Figure 6 : (a) VERDON-2 thermal-hydraulic sequence, <sup>137</sup>Cs and <sup>131</sup>I deposit along the four TGTM tubes respectively for (b) and (c)



(a)

**Gaseous iodine fraction monitored during VERDON tests.**

As explained above, the May-Pack gamma station is dedicated to the iodine behaviour and more particularly to its gaseous species as far as only gaseous FP remain in the experimental loop downstream the aerosol filter. As displayed in Figure 7, continuous accumulation of gaseous iodine is recorded by this gamma station during VERDON-3 (similar behaviour has been also recorded latter during VERDON 4). It is important to notice that only iodine has been detected in the may-pack filter, no other nuclides are present. It is the first time along the VERCORS and VERDON programs that iodine has been recorded on-line on the May-Pack filter (only post-test measurements previously), highlighting here a very early arrival of gaseous iodine. Based on a rough comparison with VERDON-2, the total amount of gaseous iodine trapped in the May-Pack filter of VERDON-3

can be estimated to around 1% of the iodine initial inventory.

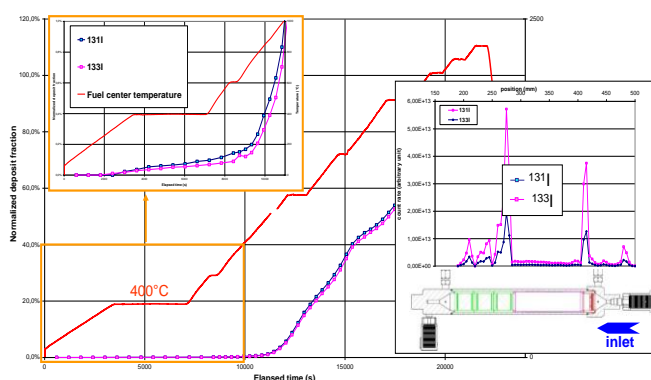


Figure 7 : Gaseous Iodine behaviour during VERDON3

## V. CONCLUSION/PERSPECTIVES

Four ISTEP-VERDON tests were conducted between 2011 and 2014 in an entirely new laboratory at the CEA Cadarache Centre in the LECA-STAR facility. These tests were dedicated to: (1) FP release from high burn-up UO<sub>2</sub> and MOX fuels, in particular for low volatile FP and (2) impact of air ingress on FP behaviour, which is expected to enhance the release of highly radiotoxic FP, such as ruthenium, as well as to re-volatilise volatile FP (iodine, caesium) previously deposited in the primary circuit. After having described this new VERDON laboratory, an overview of the four ISTEP VERDON tests was proposed. Then the main outcomes relative to the iodine behaviour identified from this experimental programme have been presented.

From a general point of view, the main insights gained from the VERDON tests are: (1) high release kinetics, beginning at low temperature, for volatile (I, Cs) and even for semi-volatile (Mo, Ba) FPs, for high burn-up UO<sub>2</sub> and MOX fuels; (2) re-volatilization of iodine deposited in the thermal gradient tubes has been observed during air injection in VERDON-2 test; (3) gaseous iodine has been quantified downstream the VERDON circuit simulating its release into the containment for VERDON 3 and 4.

To complement the experimental data concerning FP release and transport from high burn-up fuel under air ingress conditions a new test is considered. This "Air ingress" test, called VERDON-5, will be performed on UO<sub>2</sub> fuel

(same high burn-up fuel as VERDON-1), using the Transport Circuit and similar atmosphere conditions as for the VERDON-2 test.

Besides, thanks to the high quality of the results gained from this experimental loop together with the fact that the VERDON laboratory is unique in the world for studies performed on re-irradiated nuclear fuels up to temperature representative of a SA it is possible to investigate new field of research such as for instance: LOCA type experiments under air/steam atmosphere, air ingress scenario at moderate and low temperature, coupling between release and fuel degradation. These new topics are currently under evaluation.

## REFERENCES

- [1] Leveque et al., 1994. "The HEVA experimental programme". Nucl. Technol. 108, 33-44
- [2] Y. Pontillon, G. Ducros, P.P. Malgouyres, 2010. "Behaviour of fission products under severe PWR accident conditions: the VERCORS experimental programme - Part 1: General description of the programme - Part 2: Release and transport of fission gases and volatile fission products - Part 3: Release of low-volatile fission products and actinides", Nucl. Eng. Des. 240 (2010) 1843-1881.
- [3] Ducros et al., 2001. "Fission Product release under severe accidental conditions; general presentation of the program and synthesis of VERCORS 1 to 6 results". Nucl. Eng. Des. 208, 191-203
- [4] Schwarz et al., 2013. "PHEBUS-FP final seminar, special issue", Annals of Nuclear Energy 61 (2013) 1-230.
- [5] Lorenz R.A., Osborne M.F., 1995. "A summary of ORNL fission product release tests with recommended release rates and diffusion coefficients". Report ORNL/TM-12801 - Nureg/CR-6261
- [6] A. Hidaka, 2011. "Outcome of VEGA Program on Radionuclide Release from Irradiated Fuel under Severe Accident Conditions", Journal of Nuclear Science and Technology, vol. 48, (2011), 85-102

- 
- [7] Lui Z. et al., 1994. "A summary of CRL fission product release measurements from UO<sub>2</sub> samples during post-irradiation annealing (1983-1992)". Report COG-92-377
- [8] Veshchunov, et al., 2003. "Development of the mechanistic code MFPR for modelling fission product release from irradiated UO<sub>2</sub> fuel (part 1). Development and validation of new models". In: Proceedings of ENS Topfuel 2003, Würzburg, Germany
- [9] Dubourg, R., Nicaise, G., 2003. "Development of the mechanistic code MFPR for modelling fission product release from irradiated UO<sub>2</sub> fuel (part 2). Application to integral tests VERCORS 4-5 and PHEBUS FPTO". In: Proceedings of ENS Topfuel 2003, Würzburg, Germany
- [10] Brillant G., Marchetto C., Plumecocq W., 2010. "Ruthenium release from fuel in accident conditions", Radiochim. Acta, 98(5), p.267-275, 2010
- [11] Beuzet E. et al., 2012. "Ruthenium release modelling in air and steam atmospheres under severe accident conditions using the MAAP4 code", Nucl. Eng. Des. 246 (2012) 157-162
- [12] Clement, B., "The Phebus Fission Product and Source Term International Programs", Int. Conf. Nuclear Energy for New Europe 2005 Bled, Slovenia, September 5-8, 2005
- [13] ] M.P. Ferroud-Plattet et al., 2009, "CEA VERDON Laboratory at Cadarache: new hot cell facilities devoted to studying irradiated fuel behaviour and fission product releases under simulated accident conditions", Proc. HotLab Int. Conf., Prague, Czech Republic, 2009.
- [14] Pontillon, Y., et al., 2005. "Study of the active role played by UO<sub>2</sub>-ZrO<sub>2</sub>-PF interactions on irradiated fuel collapse temperature from VERCORS tests". J. Nucl. Mater. 344, 265-273.

## RESEARCH AT VTT ON THE TRANSPORT AND CHEMISTRY OF IODINE UNDER PRIMARY CIRCUIT AND CONTAINMENT CONDITIONS

Teemu Kärkelä<sup>(1)\*</sup>, Mélyny Gouëlle<sup>(1)</sup>, Jarmo Kalilainen<sup>(1)</sup>, Pekka Rantanen<sup>(1)</sup>, Ari Auvinen<sup>(1)</sup>

<sup>(1)</sup> VTT Technical Research Centre of Finland, Espoo, Finland

\*Corresponding author, tel: (+358) 20 722 5718, Fax: (+358)20 722 7026, Email:teemu.karkela@vtt.fi

**Abstract** –*The behaviour of fission products (FPs) during a severe nuclear power plant accident has been studied at VTT for the past 30 years. The focus has been on the transport and chemistry of gaseous compounds and aerosols in the primary circuit and the containment. In the past containment aerosols have been studied e.g. with intermediate scale facilities AHMED and VICTORIA. In primary circuit the studies have included resuspension and revaporisation phenomena as well as retention of FPs in steam generators. In recent years the main interest has been on ruthenium and iodine, because of their high radiotoxicity and possibility to form gaseous compounds.*

*FPs deposited on primary circuit surfaces may be released back into the gas phase, even after a long time from the beginning of a severe accident. Therefore high temperature chemistry of iodine has been studied with EXSI-PC facility. It was found out that when using CsI as a precursor with Ag, B<sub>2</sub>O<sub>3</sub> or MoO<sub>3</sub> the release of gaseous iodine even at 400 °C was significant. Boron seemed to react with caesium forming a solid, glassy compound and thus the release of gaseous iodine was enhanced. The effect of chemical reactions on primary circuit surfaces on the transport of FPs is not well-considered in current severe accident codes.*

*Gaseous iodine reacts with air radiolysis products, such as ozone, in the gas phase of containment. The radiolytical oxidation of elemental and organic iodine was investigated using EXSI-CONT facility. The formation of iodine oxide aerosol particles in air by UV(c) radiation was detected on-line in the experiments. The main gaseous reaction products from the radiolytical oxidation of CH<sub>3</sub>I were methanol and formaldehyde. Further studies on the oxidation by beta radiation with BESSEL facility verified the formation of iodine containing particles. During a severe accident, a part of the nucleated iodine oxide particles in the atmosphere will deposit on the various surfaces of containment. It was found that the desorption of iodine from the particles deposited on painted surface was enhanced by gamma radiation.*

*The filtration of gaseous and particulate iodine has been investigated using a wet electrostatic precipitator (WESP) technique. The filtration efficiency of a modern WESP can be higher than 99.9 % for the particles. To trap gaseous iodine in this study, additional ozone is fed to the gas flow in order to oxidize all gaseous iodine to iodine oxide particles. The newly formed particles are mixed with a spray of water droplets. Inside the filtration unit of WESP, large droplets and particles are charged and driven to the collection electrode. The droplets are very efficient in trapping small particles, for which charging efficiency may otherwise be too low for effective filtration. As a result of the first filtration experiments, 95 % of iodine was filtered with the WESP. The remaining 5 % of iodine was transported through the filter in a gaseous form.*

## I. INTRODUCTION

In Fukushima Daiichi nuclear plant cooling of the reactor cores at units 1, 2 and 3 was lost due to station black out. Since the cooling could not be restored in time, fuel damage took place in all three reactors and fission products were partly released from the core. As expected in a such severe accident, the highest contribution to the source term to the environment was partly from iodine isotopes.

Traditionally, it has been assumed that in a severe accident most iodine would be released from the fuel. Release to the containment would take place mostly as aerosol particles with gaseous/vapour compounds fraction of about 5% [1]. Particulate iodine is expected to be removed from the gas phase of the containment by engineered safety systems as well as by natural aerosol processes like settling and diffusio-phoresis. Particulate and gaseous iodine would finally end up in sump waters and remain there if alkaline conditions are maintained. However, most iodides (except AgI, TlI and CuI) are very water soluble. Unfortunately, iodine water chemistry is also very complicated as it can assume several different oxidation states. In case of acidification of the water e.g. from nitric acid formation and other radiolytic processes, molecular iodine would partition back to the atmosphere. It might also form volatile organic iodides. Rate of release from water would increase as the sump temperature would approach the boiling point.

Phébus FP program provided opportunity to test these expectations in iodine chemistry with realistic configurations and chemical environment. In Phébus FP tests iodine was indeed mostly released to the model containment as aerosol particles with gaseous iodine species making up few percent of the overall release. The release rate of iodine as well as aerosol sedimentation were also consistent with current severe accident modelling. Contrary to the expectations, gaseous iodine depleted from the atmosphere much faster than expected in the early phase of the tests. More alarmingly, a steady-state concentration of iodine in containment atmosphere was reached in all Phébus FP tests. The sump pH did not seem to

influence the iodine partition in the gas phase. In addition, iodine concentration in the gas phase increased when the sump was condensing and decreased when it was evaporating. One would expect exactly opposite behaviour, if the source of the iodine is from the sump. In addition, silver iodide precipitated in the sump, when AIC (AgInCd) control rod was applied in the tests. With B<sub>4</sub>C control rod most iodine released into the model containment was in gaseous form.

Based on the results from Phébus FP program a number of hypothesis on iodine behaviour were formulated [2]. It was suggested that:

- 1) Either the painted surface or the steel walls acted as the source of the persistent gas phase iodine species in the tests.
- 2) Radiolytic processes destroyed gas phase molecular iodine and organic iodide to form iodine oxide or iodine nitroxide particles. These particles further coagulated and settled or were removed by other natural processes.
- 3) The source of gaseous iodine from the circuit was either chemical reactions in the gas stream or on the surfaces of the tube walls.

Only by mechanistic understanding of iodine behaviour the consequences of a severe accident can efficiently be mitigated.

## II. FISSION PRODUCT TRANSPORT STUDIES AT VTT

The behaviour of fission products (FPs) during a severe nuclear power plant accident has been studied at VTT for the past 30 years. The focus in experiments has been on the transport and chemistry of FPs in the primary circuit and the containment.

In the past containment aerosols have been studied e.g. with intermediate scale facilities AHMED [3] and VICTORIA [4]. The objective was to study the behaviour of hygroscopic and inert aerosols at different relative humidities and temperatures. In studies at primary circuit conditions the experiments have included resuspension and revaporisation phenomena as well as retention of FPs in steam generators [5, 6].

In recent years the interest in experiments has been on ruthenium and iodine, because of their

high radiotoxicity and possibility to form gaseous compounds. In these studies have been focused on to find out in which form FPs are transported. In addition, the effect of various parameters, such as temperature, humidity and radiation, on the speciation of fission products have been studied. The adsorption and desorption of iodine from iodine oxide aerosol deposition on painted containment surface has also been investigated. The recent activities of VTT on iodine behavior in a SA are described in the following chapters. The focus in the work has been e.g. to test the hypothesized mechanisms formulated on the basis of Phébus FP program (see above).

### III. PRIMARY CIRCUIT CHEMISTRY OF IODINE

After fission products have been released from the overheated and molten fuel, they are transported through the reactor coolant system and FPs will reach areas at lower temperature. As a consequence, vapour condensation and particle nucleation processes takes place in the gas flow. If vapour condensation takes place close to the surfaces of primary circuit, a layer of condensate can be formed on the circuit surface. Particles in the gas flow may also deposit on the circuit surfaces together with control rod and structural materials. The release of gaseous iodine from precursor mixtures simulating deposits in primary circuit conditions have been investigated with EXSI-PC facility [7-12]. A list of the recently conducted experiments is presented in Table 1.

TABLE I: recently conducted experiments on primary circuit chemistry of iodine.

Precursors	Temperature [°C]	Atmosphere*
CsI	650	A, B and C
CsI	650	A, B and C
CsI	550	A, B and C
CsI	400	A, B and C
CsI + MoO <sub>3</sub>	650	A, B and C
CsI + Mo	650	A, B and C
CsI + Mo	650	A, B and C
CsI + Ag	650	A, B and C
CsI + Ag	400	A, B and C
AgI	650	A, B and C
AgI	400	A, B and C
CsI+Ag+MoO <sub>3</sub>	400	A, B and C

CsI + B <sub>2</sub> O <sub>3</sub>	650	A, B and C
CsI + B <sub>2</sub> O <sub>3</sub>	650	A, B and C
CsI + B <sub>2</sub> O <sub>3</sub>	400	A, B and C
CsI + Cd	650	A and C
Cd	650	A and C
CsI + Cd	400	A, B and C
Cd	400	A, B and C
CsI + CsOH	650	A and C

\* The composition of atmosphere is explained in Table 2.

The crucible containing the precursors was heated up to 400 °C, 550 °C or 650 °C in the reaction furnace. The furnace tube used in the experiments was made of alumina or stainless steel (AISI 304), which was pre-oxidized in a steam flow before the experiment. The reaction product particles were collected on PTFE filters with 5 µm pore size, and the gaseous reaction products were trapped in two consecutive bubbling bottles (0.2 M NaOH and 0.02 M Na<sub>2</sub>S<sub>2</sub>O<sub>3</sub> water solution), which located downstream the aerosol filters. Additional toluene trap was used in some experiments. The elemental composition of both samples was analyzed with Inductively Coupled Plasma Mass Spectrometer (ICP-MS). Experiments included three different gaseous atmosphere conditions, with different fractions of steam, argon and hydrogen, shown in Table 2.

TABLE II

Gas flow rates (NTP conditions 0 °C and 1013 mbar) and volume fractions (at 100 °C and 1013 mbar) fed to the reaction furnace.

		Condition		
		A	B	C
<b>Argon</b>	Flow rate [l/min, NTP]	3.3	3.2	2.9
	Gas vol-%	86.7	83.9	76.1
<b>Steam</b>	Mass flow rate [g/min]	0.3	0.3	0.3
	Gas vol-%	13.3	13.5	13.4
<b>H<sub>2</sub></b>	Flow rate [l/min, NTP]	0	0.1	0.4
	Gas vol-%	0	2.6	10.5

In experiments with only CsI precursor, the overall release of iodine decreased significantly when temperature was decreased to 400 °C. As a consequence, the transport of iodine containing

particles (CsI) was very low. Nevertheless, a small amount of gaseous iodine was observed to be released from the precursor even at 400 °C. In that specific case, the fraction of gaseous iodine was higher than the fraction of aerosols. The addition of Ag to CsI precursor at 650 °C resulted in the similar release of CsI aerosol as with pure CsI precursor, whereas the transport of gaseous iodine decreased. Some amount of silver was found on filter in aerosol form, probably as AgI, which could explain the observed decrease in gaseous iodine transport. At 400 °C reaction temperature, the release of gaseous iodine was much higher compared to the experiment at 650 °C and almost no iodine containing aerosol particles were formed, see Figure 1. Most likely, the lower reaction temperature reduced significantly the vaporization of Cs, I and Ag compounds. Similar behaviour was observed when CsI precursor, mixed with additional MoO<sub>3</sub>, was heated to 400 °C. Addition of metallic Mo seemed to increase the release of gaseous iodine as well.

The formation of vitreous caesium borate compound was noticed, when a mixture of CsI and B<sub>2</sub>O<sub>3</sub> was heated to 650 °C. This could contribute to the formation of possible blockages in the circuit or containment. Such a boron-rich partial blockage was observed in the rising line before the steam generator inlet in Phébus FPT3 test. Also as a result of boron trapping most of caesium in the crucible, a high fraction of gaseous iodine was transported to the bubbling bottle. The release of gaseous iodine remained high even at 400 °C.

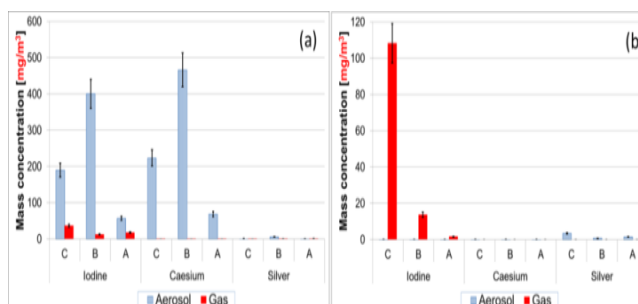


Fig. 1. Iodine, cesium and silver mass concentrations, transported in gaseous and particulate forms, in the experiments at (a) 650 °C and (b) 400 °C. Conditions were in order from C to A. [9]

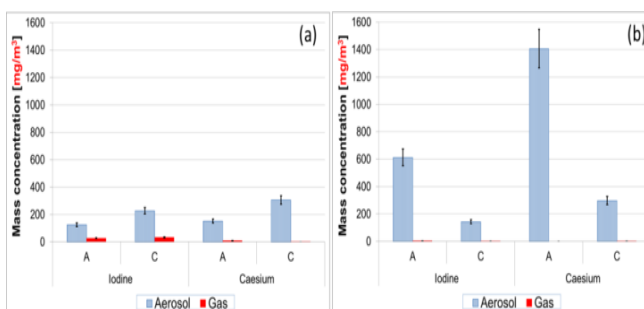


Fig. 2. Iodine and caesium mass concentrations (aerosol and gas) at 650 °C with caesium to iodine molar ratio of (a) 1.0 and (b) 1.6. Conditions A and C only. [12]

The transport of cadmium was significantly increased by the presence of caesium iodide, whereas CsI aerosol transport was decreased only slightly. 10 to 60 times more cadmium reached the sampling lines than in the experiment with only cadmium. As it was observed, most of cadmium was condensed on the facility's surfaces before the sampling lines in the cadmium experiment. Thus, it is highly probable that the vaporised cadmium had condensed on caesium iodide particles and transported to the filter. A fraction of cadmium was transported as cadmium hydroxide Cd(OH)<sub>2</sub>, that was verified by XRD. Addition of Cd to CsI precursor seemed to result in a higher transport of gaseous iodine, but the formation of Cd-I compound was not detected.

The amount of gaseous iodine was barely detectable when the initial Cs/I molar ratio was higher than 1 (addition of CsOH to CsI precursor), see Figure 2. The effect of the atmospheric composition was noticed as well; when hydrogen was present in the carrier gas (condition C), the amount of aerosols (caesium and iodine) released from the crucible was significantly decreased.

#### IV. CONTAINMENT CHEMISTRY OF IODINE

Volatile iodine can form several compounds with other fission products, control rod and structural materials in the primary circuit. Therefore, e.g. in case of a tube break, iodine can be transported to the containment atmosphere both in gaseous and particulate forms. It is very likely that iodine at

least partly deposits on painted surfaces of a reactor containment building during a severe accident. In such a case, molecular iodine can be released from these deposits (e.g. particle deposits) back to the gas phase under varying temperature, chemical and radiation conditions in a severe accident. Furthermore, iodine may also react with painted surfaces to form organic iodine species. These organic species are another possible source of volatile iodine, which may increase the fraction of iodine in the gas phase. Therefore, it is important to study the transport of iodine in containment conditions. This is being investigated in collaboration between VTT and Chalmers University of Technology (Sweden). First results have shown, that the release of gaseous iodine from IO<sub>x</sub> and CsI deposits on various metal and aged paint surfaces increased with the temperature and the release was enhanced by gamma radiation. Another question is, whether these released iodine compounds are transported as gaseous molecules or as aerosol particles resulting from reactions with air radiolysis products. To answer this last question several experiments were conducted in cooperation with Chalmers University of Technology [13, 14]. In experiments molecular iodine and methyl iodide were fed into the VTT's EXSI-CONT facility in an air mixture. In some experiments the flow contained also a low fraction of water vapor. The reactions took place in a quartz tube heated either to 50 °C, 90 °C or 120 °C. UV-light was used as a source of radiation to produce ozone from oxygen. A separate generator was also applied to reach higher ozone concentrations. VTT has carried out further studies on the radiolytical oxidation of I<sub>2</sub> and CH<sub>3</sub>I by beta radiation in oxygen at 20 °C with a new BESSEL facility [15, 16]. In experiments gaseous sample was irradiated for 1 hour to 4 days and afterwards the formed gaseous and aerosol reaction products were analysed with online devices.

As a result of CH<sub>3</sub>I experiments with EXSI-CONT, there was a clear trend in the formation of gaseous reaction product species. The main gaseous reaction products were methanol and formaldehyde. Especially at elevated temperature other reaction products, such as formic acid and methyl formiate, became important as well. Increasing amount of reaction product species were

detected while the concentration of ozone was increased. The measured gaseous reaction product species in experiments at 50 °C to 120 °C are presented in Figure 3. Similarly, the mass concentration of aerosols increased as well, thus aerosol nucleation was enhanced, see Figure 4. Also, increase in temperature seemed to increase the aerosol mass concentration. This is probably partly due to more efficient decomposition of gaseous CH<sub>3</sub>I and subsequent aerosol formation with ozone. The formation of gaseous reaction products was efficient in this study, even though the residence time of the flow inside the facility was only approx. 7 seconds. It seemed that thermal decomposition reactions further enhanced the formation of reaction products.

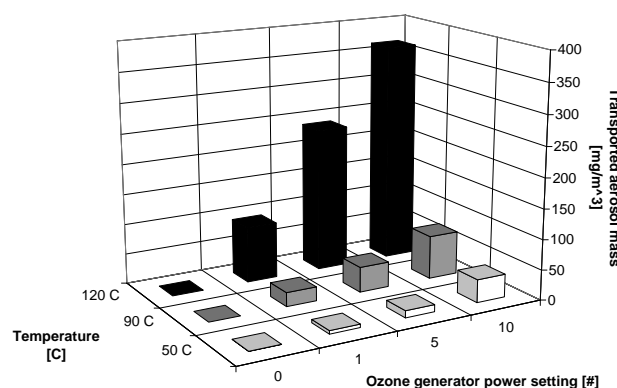


Fig. 4. The measured aerosol mass concentration while the temperature of EXSI-CONT facility and the power setting of ozone generator were varied. [14]

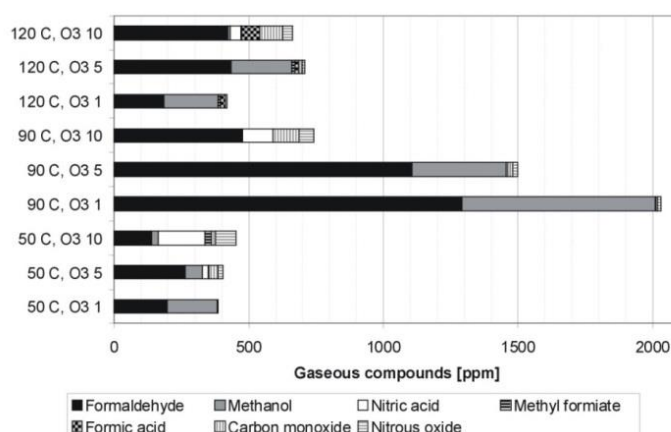


Fig. 3. The gaseous reaction products (in ppm) from the oxidation of methyl iodide with ozone. The temperature of EXSI-CONT facility and the power setting of ozone generator are presented on vertical axis. [14]

In the beta irradiation experiments with BESSEL facility, it was found out that the concentration

of formed particles (ca. 10 nm to 50 nm in diameter) decreased very slowly with increasing irradiation time, see Figure 5. It seemed that an equilibrium was reached between gas phase iodine compounds and iodine species deposited on wall surfaces. At that equilibrium the rate of new particle formation was low. When the facility was purged with oxygen, a new formation of particles was observed in every  $\text{CH}_3\text{I}$  experiment. It suggested that the radiolysis reaction products were limiting the particle formation. Oxygen, a precursor of ozone when irradiated, was also needed for the nucleation to take place, since the new particle formation was not observed without irradiation or when the atmosphere was pure nitrogen. The formed particles were highly water soluble and volatile. These findings could also partially explain the constant concentration of iodine, which was observed in the gas phase of containment at the end of every Phébus FP test.

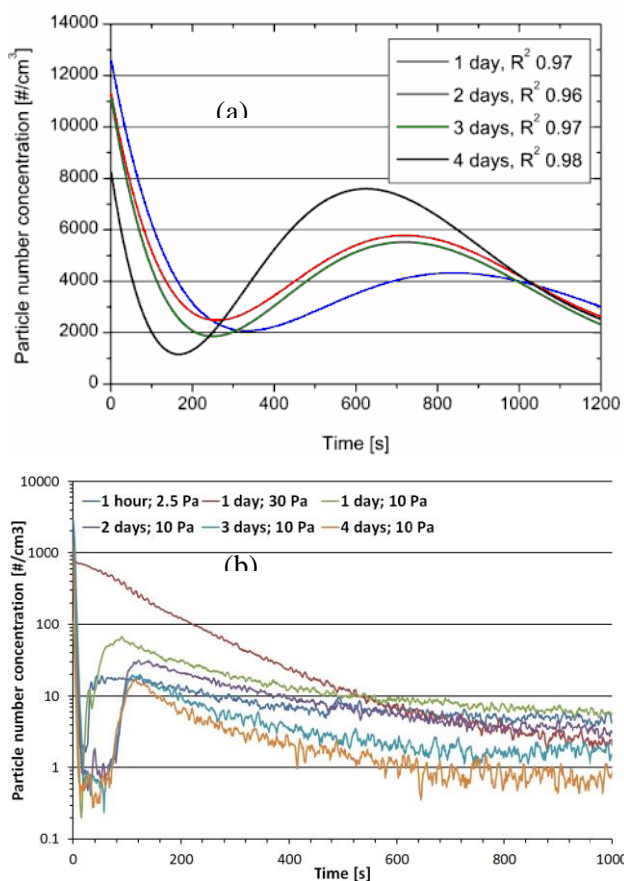


Fig. 5. The number concentration of the formed aerosols after the exposure of gaseous (a)  $\text{CH}_3\text{I}$  [15] and (b)  $\text{I}_2$  [16]

precursors to beta radiation in oxygen atmosphere at 20 °C. The irradiation period ranged from 1 hour to 4 days. The initial vapour pressure of  $\text{CH}_3\text{I}$  was approx. 4 kPa, whereas the vapour pressure of molecular iodine ranged from 2.5 Pa to 30 Pa.

## V. FILTRATION OF GASEOUS AND PARTICULATE IODINE

In the containment atmosphere, part of gaseous iodine compounds is radiolytically decomposed mainly by gamma rays and beta particles originating from fission products. As a result of radiolytical oxidation, gaseous iodine can be transformed to e.g. iodine oxide particles. Due to the high contribution of radiotoxic iodine to the possible source term, the retention of iodine containing compounds and thus the prevention of their release to the environment is of primary importance. Currently, VTT is studying the filtration of both gaseous and particulate iodine with a new filtration system. This technique can be used to filter e.g. other FP aerosols as well. The efficiency of the system is being evaluated in EU PASSAM project, which aims at demonstrating the ability of innovative systems to achieve larger source term attenuation.

The basic studies on iodine oxidation at VTT have produced a significant amount of data and knowledge on the behaviour of iodine in a severe accident. The knowledge is being used to enhance the filtration efficiency of the wet electrostatic precipitator (WESP) technique. In the conventional ESP technique, particles are charged with ions and in the electric field charged particles drift to the collection electrode. For small particles, less than 1  $\mu\text{m}$  in diameter, charging efficiency may be too low for effective filtration. These particles are filtered with an ion wind principle. Momentum of the ions travelling to the collection electrode drives small aerosol particles there as well.

The conventional ESP technique can also be used to filter gaseous pollutants when the gas flow is pre-treated before the filtration unit. The water droplets fed into the system adsorb gaseous impurities. The effect can be enhanced by injecting additives with the water. Inside the filtration unit large droplets are charged and driven to the collection electrode. The droplets are also very efficient in trapping small particles.

The gaseous compounds can also be oxidized to form solid particles which are filtered with the ESP technique. Both proposed methods are being studied now for the decontamination of gaseous species in containment conditions. Gaseous iodine is oxidized with additional ozone and water droplets are fed to the gas flow just before the filtration unit of WESP.

The first experiments were carried out with  $\text{TiO}_2$  and  $\text{I}_x\text{O}_y$  aerosols, see Figure 5. The applied electric voltage between the electrodes, the residence time of particles inside the ESP chamber and the injection of water droplets before the ESP chamber were varied in the experiments. The injection of water droplets significantly increased the trapping efficiency of  $\text{TiO}_2$  particles for applied electric voltage less than 15 kV (negative). In the iodine experiments, a gas flow containing elemental iodine (2.2 l/min, 16 ppm) was mixed with ozone (3 l/min, > 1000 ppm) in order to oxidize all gaseous iodine to iodine oxide particles. The gas flow was further diluted and the total flow rate through the WESP was 86 l/min (20 s residence time). As a result of the first filtration experiments, close to 100 % of the formed  $\text{I}_x\text{O}_y$  particles was filtered with the WESP when the applied electric voltage was in a range from -10 kV to -25 kV.

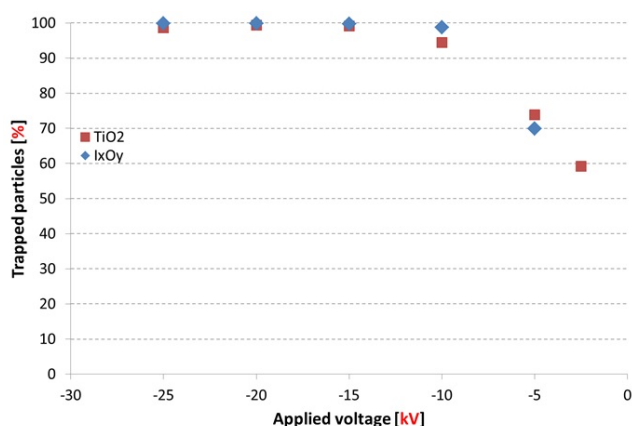


Fig. 5. Evolution of the fraction of trapped  $\text{TiO}_2$  and  $\text{I}_x\text{O}_y$  particles with the WESP filter as a function of the applied electric voltage between the electrodes. [17]

Currently, the main focus is on testing the trapping of gaseous molecular ( $\text{I}_2$ ) and organic ( $\text{CH}_3\text{I}$ ) iodine with the WESP filter. In those experiments the filter will also be exposed to representative containment conditions, such as

high temperatures and various steam fractions in a gas flow.

## VI. SUMMARY AND CONCLUSIONS

Phébus FP program raised a number of questions that could not be answered by the current severe accident analysis tools. Based on the experimental observations several hypothesis e.g. on iodine behaviour in the primary circuit as well as within the containment were formulated. These hypotheses must be experimentally tested and not just parameterized.

Some of these hypotheses have been experimentally verified by VTT. One of the uncertainties was the effect of reactions on primary circuit surfaces on the fraction and timing of iodine release into the containment atmosphere. In the experiments, a difference in the release of iodine in the primary circuit conditions at 400 °C, 550 °C and 650 °C temperatures was detected. Iodine seemed to be released almost completely in gaseous form at lower temperature despite the used precursor mixtures. This surprising observation suggests that the FP deposits on the surfaces of primary circuit may act as a source of volatile iodine for a long period since the beginning of severe accident. However, an excess amount of Cs to I seemed to reduce the formation of gaseous iodine at 650 °C. Results on the radiolytical oxidation of gaseous molecular and organic iodine by beta radiation, and complementary experiments with ozone and UV radiation, verified the formation of aerosol particles, which was one of the formulated hypotheses after Phébus FP experiments. The diameter of nucleated particles ranged from ca. 10 nm to 50 nm. These very small particles were highly water soluble and volatile.

Recent studies by VTT have produced new information on the chemistry and transport of iodine in severe accident conditions. These results are needed e.g. in order to explain the observed behaviour of iodine in the experiments of Phébus FP program. However, the most important impact of these results will be on the development of severe accident analysis codes. Previously, the lack of information has prevented to taking into consideration the FP deposits on

primary circuit surfaces and iodine oxide particles both in the containment gas phase and on the containment surfaces as a short and long term source of volatile iodine. The new information on the iodine chemistry developed have been utilized e.g. in the development of electric filtration technique for gaseous and particulate iodine species. The efficiency of this Finnish innovation is currently evaluated in EU PASSAM project.

#### ACKNOWLEDGMENTS

The financial support of VTT Technical Research Centre of Finland, The Finnish Research Programme on Nuclear Power Plant Safety (SAFIR2014), Nordic Nuclear Safety Research Programme (NKS-R) and Severe Accident Research NETwork of excellence (SARNET) is acknowledged.

#### NOMENCLATURE

AHMED = Aerosol and heat transfer measurement device

BESSEL = Beta irradiation vessel

EXSI-CONT = Experimental study on iodine chemistry – containment

EXSI-PC = Experimental study on iodine chemistry - primary circuit

ESP = Electrostatic precipitator

FP = fission product

ICP-MS = Inductively coupled plasma mass spectrometer

NTP = Normal temperature and pressure

PTFE = Polytetrafluoroethylene

UV-light = Ultraviolet light

VICTORIA = Facility for studies on LWR containment aerosol behaviour

WESP = Wet electrostatic precipitator

XRD = X-ray diffraction

#### REFERENCES

1. B. Clément, L. Cantrel, G. Ducros, F. Funke, L. Herranz, A. Rydl, G. Weber, C. Wren,

“State of the art report on iodine chemistry”, NEA/CSNI/R(2007)1 (2007).

2. R. Y. Lee and M. Salay, “Findings on iodine behaviour in design basis and severe accidents”, Presented to the Advisory Committee on Reactor Safeguards 8.5.2008, U.S.NRC

3. J. Mäkynen, J. Jokiniemi, P. Ahonen, E. Kauppinen, R. Zilliacus, “AHMED experiments on hygroscopic and inert aerosol behaviour in LWR containment conditions: experimental results”, *Nuclear Engineering and Design*, **178**, pp. 45-59 (1997).

4. J. Mäkynen, J. Jokiniemi, E. Kauppinen, H. Tuomisto, T. Routamo, “LWR aerosol experiments at VICTORIA model containment”, *Journal of Aerosol Science*, **28**, pp. 715 (1997).

5. T. Raunio, “Experimental Study on Fine Particle Resuspension in Nuclear Reactor Safety”, Master’s Thesis (2007)

6. D. Bottomley, R. Dickson, T. Routamo, J. Dienstbier, A. Auvinen, N. Girault, “Revaporisation issues: On Overview”, *Proc. of the 2nd European Review Meeting on Severe Accident Research, ERMSAR 2007*, Germany (2007).

7. T. Kärkelä and A. Auvinen, “Experimental study on iodine chemistry (EXSI) – Facility for primary circuit experiments”, VTT-R-02791-09 (2009).

8. J. Kalilainen, T. Kärkelä, P. Rantanen, J. Forsman, A. Auvinen and U. Tapper, Part “Primary circuit chemistry of iodine,” *Proc. Of the SAFIR2010, The Finnish Research Programme on Nuclear Power Plant Safety 2007-2010*, Final report, 312-320 (2011).

9. J. Kalilainen, P. Rantanen, T. Kärkelä, M. Lipponen, A. Auvinen and J. Jokiniemi, “Effects of molybdenum and silver on iodine transport in primary circuit on severe nuclear accidents”, VTT-R-00425-12 (2012).

10. J. Kalilainen, T. Kärkelä, R. Zilliacus, U. Tapper, A. Auvinen and J. Jokiniemi, "Chemical reactions of fission product deposits and iodine transport in primary circuit conditions", *Nuclear Engineering and Design* **267**, 140-147 (2014).
11. M. Gouëlle, J. Kalilainen, P. Rantanen, T. Kärkelä, and A. Auvinen, "Experimental study on the behaviour of CsI on primary circuit surfaces and effects of cadmium on iodine transport during a severe nuclear accident", VTT-R-00630-14 (2014).
12. M. Gouëlle, J. Kalilainen, T. Kärkelä and A. Auvinen, "Experimental Study on the Behaviour of CsI on Primary Circuit Surfaces: Effects of Cadmium and Caesium Hydroxide on Iodine Transport during a Severe Nuclear Accident", VTT-R-00424-15 (2015).
13. T. Kärkelä, J. Holm, A. Auvinen, C. Ekberg, H. Glänneskog, U. Tapper and R. Zilliacus, "Gas phase oxidation of elemental iodine in containment conditions". *In Proc. of the ICON17*, Brussels, **2**, 719 – 727 (2009).
14. T. Kärkelä, J. Holm, A. Auvinen, R. Zilliacus, T. Kajolinna, U. Tapper, H. Glänneskog and C. Ekberg, "Gas phase reactions of organic iodine in containment conditions", *In Proc. Of the ICAPP2010*, San Diego, **2**, 1084 – 1091 (2010).
15. T. Kärkelä, A. Auvinen, T. Kekki, P. Kotiluoto, J. Lyyränen and J.K. Jokiniemi, "Radiolytical oxidation of gaseous iodine by beta radiation", Submitted to *Radiochimica Acta* (2015).
16. T. Kärkelä, M. Gouëlle, T. Kekki, P. Kotiluoto and A. Auvinen, "Formation of HNO<sub>3</sub>, O<sub>3</sub> and IOx particles by beta radiation", VTT-R-00641-15 (2015).
17. M. Gouëlle, T. Kärkelä, J. Hokkinen and A. Auvinen, Presentation in the 5th management team meeting of EU PASSAM project (2015).

**MAIN FINDINGS OF THE IRSN EXPERIMENTAL PROGRAMMES PERFORMED  
ON IODINE CHEMISTRY IN SEVERE ACCIDENT CONDITIONS**

Colombani J, Grégoire A.C<sup>\*</sup>, Morin S.

*Institut de Radioprotection et de Sûreté Nucléaire, Saint-Paul Lez Durance, France*

*<sup>\*</sup>Corresponding author, tel: (+33) 442199740, Fax: (+33) 442199163, Email: anne-  
cecile.gregoire@irsn.fr*

**Abstract** – *Over the past two decades, IRSN has sustained large efforts on Severe Accident (SA) research dedicated to the evaluation of the “Source Term” (ST). The overall aim of this ST work is to better predict potential releases of fission products into the containment atmosphere and finally into the environment, with a special attention to iodine species.*

*Large efforts achieved so far have clearly improved the understanding of iodine behaviour in SA conditions. Iodine is known to be almost entirely released from the degraded core, with significant early releases during the accident transient. Depending on the chemical composition of the flow passing through the Reactor Coolant System, a significant amount of volatile iodine species is potentially transported from the primary circuit up to the containment building. In the containment atmosphere, main iodine species (molecular iodine, organic iodides, and iodine aerosols species) have been identified as well as their main processes of formation, deposition and decomposition: volatile iodine species are quickly adsorbed onto the containment surfaces and/or transferred into the sump, they may also react with the air/steam radiolytic products, yielding soluble iodine oxides particles that are then transferred to the sump or that settle on containment surfaces. The adsorbed species may also lead again to the formation of volatile species. All these processes are linked and have been evidenced experimentally.*

## I. INTRODUCTION

Due to its high volatility and radiotoxicity, iodine is a major contributor to the short and middle term radioactive releases to the environment in case of Severe Accident (SA) on a Nuclear Power Plant (NPP). In the 80-90's, after the Three Mile Island accident, a vast amount of research dealt with severe accident source term. As far as iodine is concerned, the main findings indicate that iodine releases from the reactor core could amount to 60-70% of its core inventory in case of SA and that it would be almost exclusively transported as CsI in the Reactor Coolant System (RCS) [1].

Since then, many experimental programmes have been performed by IRSN in cooperation with international partners. The understanding of the "SA processes" considerably evolved after having performed the series of Phébus Fission Products (FP) integral tests that were undertaken to investigate key phenomena governing NPPs SA from core degradation to the late phase and particularly the iodine chemistry [2].

To complete and better understand the volatile iodine formation, deposition and decomposition main processes highlighted in the Phébus tests, the International Source Term Program (ISTP), was launched in 2005 [3]. Small scale experiments have been performed at IRSN to examine the behaviour of iodine in the RCS (CHIP-program) and in the reactor containment building (EPICUR program). Then, the OECD/STEM (Source Term Evaluation and Mitigation) program was launched in 2011.

## II. IODINE BEHAVIOUR IN THE PHEBUS FPT0/1/2/3 TESTS – MAIN FEATURES

The Phébus FP programme was initiated in 1988 and four tests were performed in a bundle configuration in the Phébus facility [4].

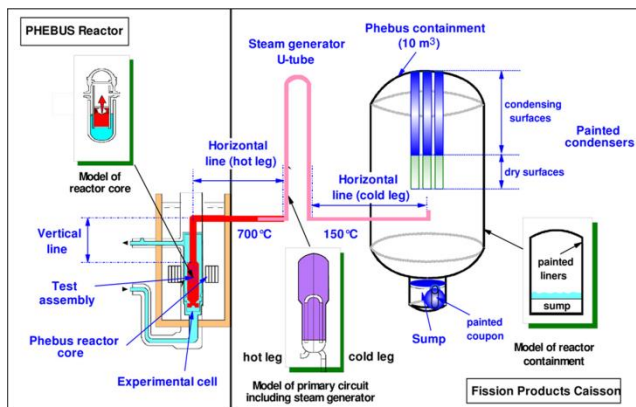


Fig. 1 Schematics of the experimental circuit in the Phébus FP - bundle tests FPT0/1/2/3 [5].

This facility [5], scaled down by a factor 5000 relative to a 900MWe pressurized water reactor, allowed the study of fuel degradation, the release of FPs and their transport and behaviour through the RCS and in the containment building with a specific attention to iodine radiochemistry (see Fig.1). Experiments FPT-0 to FPT-3 used a 1 m high bundle of 21 fuel rods including a control rod in the central position. Radioactive materials exiting the bundle during its degradation were transported to a single inverted U-tube simulating a steam generator and then to a 10 m<sup>3</sup> vessel simulating a reactor containment. The 1/5000 scaling ratio is also valid for the volume of the containment atmosphere, the surface area of the painted condensing surfaces and the interfacial area between the sump and the atmosphere.

The main features of the test matrix are displayed in Table I. Concerning the core, the main parameters were the nature of the coolant (steam-rich or steam-poor with a high or a low steam flow rate) and the material composition of the control rod: Silver-Indium-Cadmium (SIC) or Boron Carbide (B<sub>4</sub>C). These variables potentially had a direct impact on the iodine behaviour in the primary circuit. Indeed, the redox conditions prevailing in the RCS varied strongly with the extent and the duration of the main hydrogen phase due to Zircaloy-clad oxidation. Furthermore, iodine reactivity may be directly influenced by the release of the other FPs (Cs, Mo, Te) and control rod materials (Ag, In, Cd or B). Concerning the containment and subsequently the late phase iodine chemistry, the main parameters were the sump pH and its thermal-hydraulic conditions.

TABLE I: Phébus test matrix [5]

Test	Fuel /degradation conditions	Primary circuit	Containment
FPT-0	Fresh Fuel/ SIC rod /steam-rich conditions (2g/s)	non-condensing steam generator	pH5
FPT-1	BR3 fuel, 23 GWd/tU/ SIC rod/ steam rich (2g/s)	As FPT-0	pH5
FPT-2	As FPT-1 but steam poor conditions (0.5 g/s) and low boric acid flow	As FPT-1 with effect of boric acid	pH9/ evaporating sump
FPT-3	As FPT-1 with B <sub>4</sub> C rod and steam poor (0.5 g/s)	As FPT-0	pH5/ evaporating sump

Each test started with a pre-conditioning phase consisting of a re-irradiation of the fuel bundle to generate a representative short lived FP inventory. This was followed by a transition period to adjust the circuit thermal hydraulic conditions. The experimental phase itself started with the degradation phase (4-5 hours long) during which

fuel degradation and material release to the containment were studied. After containment isolation, it was followed by a “long term” phase divided into an aerosol phase (2 days) dedicated to the analysis of aerosols deposition mechanisms, a washing phase (20 min) which aimed at collecting aerosols into the sump, and a chemistry phase (2 days) devoted to the analysis of iodine chemistry.

### II.1 Iodine behaviour in the circuit (degradation phase)

Iodine is considered as a volatile FP with an integral release fraction ranging from 78 to 90% of its initial fuel inventory (i.i.) [6]. The release kinetics gained from on-line measurements in the hot leg indicates that it is closely linked to the hydrogen release for FPT0/1/2 with an early release concomitant with the first Zircaloy oxidation phase (characterized by a strong hydrogen release) [7]. On the contrary, for FPT3, the first significant iodine release (also observed for xenon) was delayed until after the hydrogen peak. This difference may be accounted for a different timing in fuel degradation events or for the formation of different iodine species [7] - fig.2.

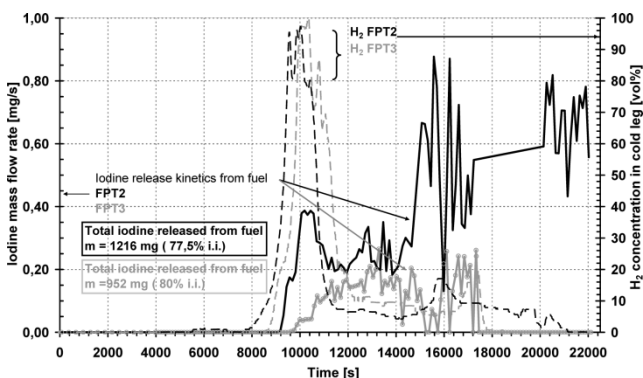


Fig. 2 Iodine mass flow rate in hot leg during FPT2/3 tests [7].

The iodine transport kinetics in the cold leg was strongly correlated to the flow rate determined in the hot leg in FPT0/1. On the contrary, in FPT2/3, the transport kinetics in the cold leg was much smoother, owing to a significantly reduced steam injection in FPT2/3 compared to FPT0/1 and to enhanced iodine retention in the steam generator.

Iodine retention in the Phébus circuit is moderate [7]: the transported iodine fraction from the bundle to the containment vessel was the highest for the FPT1/2 tests accounting for respectively 72% and 77% of the released iodine. For FPT3, this fraction was significantly lower (43%), following the large deposition of boron-containing materials and subsequent partial blockage in this region [6, 7] before the late oxidation phase. The main areas of

iodine deposition are characterized by a sharp thermal gradient at high temperatures [7]. Thus, the iodine deposition fractions were the highest in the steam generator rising section, accounting for at least 50% of the total iodine deposited in the circuit. A second main significant zone of iodine retention was observed at the bundle outlet characterized by a sharp thermal gradient from ~1600 down to 700 °C.

Three main iodine forms (aerosols, vapours and gases) have been transported in the Phébus primary circuit with proportions that varied depending on the tests (linked to redox conditions, material release kinetics). Iodine vapours forms condense between 700 and 150 °C whereas the gaseous forms may be transported up to the containment vessel.

Iodine was mainly transported in vapour form at 700 °C for FPT0/1/2 [7]. Analysis of thermal gradient tube samplings and thermal transition lines (700-150°C) provided complementary information on the nature of these vapour species. CsI condensation peaks were highlighted in several FPT2/FPT3 samplings. Besides this species, other iodine condensations peak were clearly identified indicating that this species was not the only iodine vapour species transported through the circuit hot leg [7].

TABLE II

Overview of iodine behaviour in Phébus tests [6], [7], [8]

Test	FPT0	FPT1	FPT2	FPT3
Release from bundle (%i.i)	>91	90	72	79
RCS deposits (% i.i) distribution in the RCS (%/ total deposited iodine)	28 UP +VL: n.m. HL +SG : 76 CL+UP+VL: balance	26 UP +VL : 21 HL +SG : 76 CL: balance	15.7 UP +VL : 27 HL +SG : 35-62 <sup>a</sup> CL: balance	44.9 UP +VL: 13 HL +SG : 17-51 <sup>a</sup> CL: balance
Main iodine forms transiting the RCS <sup>b</sup> (aerosol/vapour/gas %/total I over the transient)	HL > 700 °C : Aerosol : few% Vapour + gas : dominant CL ~ 150 °C : Aerosol : <98 Gas > 2 <sup>d</sup>	HL > 700 °C : Aerosol : 6-12 Vapour + gas :88-94 CL ~ 150 °C : Aerosol : dominant Gas : negligible <sup>d</sup>	HL > 700 °C : Aerosol :11-44 Vapour 56-89 Gas < 0.3 CL ~ 150 °C : Aerosol : ~99.9 Gas : 0.1 <sup>d</sup>	HL > 700 °C : Aerosol :13 Vapour : 42 Gas : 45 CL ~ 150 °C : Aerosol :5 Gas :95
Injection into the Containment (%i.i.) gaseous iodine (% c.i.) <sup>c</sup>	63 33 <sup>d</sup>	64 4 <sup>d</sup>	56.7 0.6 <sup>d</sup>	34.1 80
Containment distribution at the end of the test Gaseous (% c.i.)				
Stainless Steel Wall (% c.i.)	0.1	~0.14	~0.02	~0.09
Elliptic floor (% c.i.)	n.m	2	7	13.7
Sump (% c.i.)	n.m.	5.6	54	0
Painted condenser dry (% c.i.)	n.m.	92.3	28	17
Painted condenser wet (% c.i.)	n.m.	0.2	0.4	15.8
Painted sump coupon (% c.i.)	16	1	3.2	38.2
	n.m.	1.2	1.9	1.3

RCS = model Reactor Cooling System comprising: UP = Upper Plenum, VL = Vertical Line, HL = Hot Leg, SG = Steam Generator, CL = Cold Leg

<sup>a</sup> respectively lower bound and upper bound retention in the SG from measured iodine deposition in the rinsing section of the SG and from circuit mass balance between the HL and the CL; <sup>b</sup> Circuit data; FPT0/ 1/2 tests: trends and value ranges; for FPT3 test : quantitative data; <sup>c</sup> containment data, c.i. containment inventory; <sup>d</sup> : discrepancies between circuit and containment data concerning gaseous fraction : circuit data may underestimate the transported gaseous iodine fraction.

This observation is also consistent with caesium found transported mainly in an aerosol form at this location. The FPT3 test results, for which half of the iodine was transported through the hot leg-point in a vapour form and half in a gaseous form, clearly depart from the previous Phébus test results. The use of a B<sub>4</sub>C control rod in FPT3, instead of SIC, could be an explanation in the formation of gaseous iodine forms. Indeed both the favoured combination of caesium with boron (that may also have occurred in FPT2 where a boric acid steady flow was injected) and the absence of materials such as silver, indium and cadmium (that are known to have a great affinity for iodine) could promote the persistence of gaseous iodine species such as HI or I<sub>2</sub>.

In the cold leg only iodide aerosols and gaseous iodine are expected. In the FPT0/1/2 circuit cold leg, most of the iodine was transported in an aerosol form towards the containment vessel, with a very low gaseous iodine fraction. In FPT3, as expected from iodine forms measured in the hot leg, iodine was found to be transported in the circuit cold leg mainly in gaseous form (95%).

## II.2 Atmospheric Iodine behaviour and deposition in the containment

In all tests, more than half of the iodine fuel inventory reached the containment (Table II). During the fuel degradation, an early presence of gaseous iodine in the containment was observed in all tests with a maximum observed during or just after the main Zircaloy oxidation phase for FPT0/1/3 tests and during the second oxidation phase for FPT2 [8]. Though the potential chemical transformation of iodides entering the containment (where specific conditions prevailed dose rate and oxygen concentration) cannot be excluded, this gaseous iodine may be also likely formed in the RCS, probably linked to non-equilibrium chemical effects. In FPT3, the gaseous iodine fraction was much higher pointing to the essential role of control rod material on iodine chemistry in the RCS. The lower gaseous iodine fraction measured during the FPT2 main Zircaloy oxidation phase as compared to previous FPT0/1 tests might be explained by the lower steam injection that both implies slower and more progressive fuel degradation as well as higher transit times of fission products in the primary circuit. Whatever the iodine fraction and nature (aerosol or gas) injected into the containment atmosphere, the efficiency of the various sinks finally leads to a significant depletion of atmospheric iodine until very low and constant

residual concentrations are reached. Depletion mechanism is dominated i/ by aerosol gravitational deposition on the elliptic floor for FPT0/1/2 tests where aerosols were the dominant form of iodine ; ii/ to a lesser extent, by aerosols deposition on the stainless steel surfaces for FPT2 due to smaller aerosol sizes compared to FPT1; iii/ and by adsorption/absorption on the atmospheric painted condensers (and to a lesser extent on the stainless steel walls) for FPT3 where high gaseous iodine fraction was injected into the containment.

At the end of the test, the fraction deposited on the containment surfaces represent about 3-10% c.i. for FPT1-2 and 70% c.i. for FPT3. Low amounts of iodine remained on the elliptic floor except for FPT2 due to a non-efficient washing.

The low residual concentrations of gaseous iodine are similar in all tests (ranging from 8 10<sup>-10</sup> mol(I)/L for FPT1 to 2 10<sup>-11</sup> mol(I)/L for FPT0) indicating an equilibrium between source and sink mechanisms. The most efficient depletion phenomenon during the late phases of the tests, was found to be the sump chemistry.

## II.3 Gaseous iodine speciation

For FPT0/FPT1, if at short and midterm phases, both molecular and organic iodine concentrations were similar, the organic iodide became dominant after the washing phase and throughout the long term phase. On the contrary for FPT2/FPT3, the dominant form of gaseous iodine was always molecular.

The painted atmospheric surfaces were the main source of organic iodides. But even in the FPT3 test characterized by a high amount of iodine adsorbed on paints, the organic iodide fraction did not exceed 20% gaseous iodine and its concentration significantly decreases throughout the test down to very low constant concentration in the long term by radiolytic destruction. The immersed painted surfaces apparently did not act as a significant organic iodide source.

Organic iodides formed preferentially in tests where there was no evaporation from the sump and no steam condensation on the containment surfaces (FPT0/1). Tests performed with sump evaporation and condensation on containment surfaces (FPT2/3) yielded reduced organic iodide fractions. This observation is consistent with a reduced organic iodide formation from wet painted surfaces.

### II.3 Iodine behaviour in the sump

At the end of test, iodine sump inventory represented a significant fraction of the containment inventory for all tests (see Table II). The solubility of iodine in the sump decreased from the early aerosol phase towards the final washing phase, indicating the formation of insoluble species. Indeed, silver originated from control rod was found to have played a key role in iodine sump chemistry in irreversibly binding the iodine to form an insoluble iodine species (AgI). Iodine was found to be more insoluble when the Ag/I ratio was high and the pH acidic as in FPT0/1 tests [8] so that very little water soluble iodine species was detected at the end of those tests. In FPT2, a smaller insoluble iodine fraction (~1/3 of final iodine sump inventory) was found linked to a lower Ag/I molar ratio in the sump compared to previous tests. In FPT3, despite the very low Ag/I ratio (0.35), a low fraction of non soluble iodine forms were also detected after the washing phase.

No significant iodine relovatilization from the sump was observed. The reaction of iodine with silver in FPT0/1 (irreversible formation of insoluble species) and the sump alkaline conditions in FPT2 (chemical hydrolysis of volatile iodine species into non-volatiles iodates) may have prevented iodine relovatilization for those tests. In FPT3, the low iodine inventory and the lower dose rates in the sump may have also prevented iodine relovatilisation.

To assess the main remaining uncertainties on iodine source term evaluation the CHIP and STEM experimental research programs on iodine chemistry are still on-going.

### III. EXPERIMENTAL WORK PERFORMED IN THE CHIP FACILITY

Based on the Phébus-FP experiments as reported in section II, the presence of early gaseous iodine in the containment vessel can possibly be attributed to pre-existing gaseous iodine in the primary circuit. The release of gaseous iodine from the RCS may be due to a more complex iodine chemistry than expected or even to possible kinetics limitations as the chemical system undergoes very strong thermo-hydraulic changes in SA conditions. In order to develop and validate models of FP behaviour in the primary circuit, the ISTP/CHIP experimental program [3] was launched to obtain more information on iodine speciation under different circuit boundary conditions in presence of different fission products (Cs, Mo, I, ...) and control rod

materials (B, Cd, In, Ag) and to evidence possible kinetics limitations.

#### III.1 Test facilities

In the CHIP facility [10] and the small scale test bench, the elements are transported in a controlled thermal gradient. These benches are designed as an open system with a continuous flow of reagents (see Fig.2).

The chemical elements, including the carrier gas ( $H_2/H_2O$ /inert gas), are heated at  $1600^\circ C$  in a High Temperature (HT) zone. At this temperature, all the species are under gaseous form at thermodynamic chemical equilibrium. Downstream of the HT zone, the fluid is cooled down in the so-called "transport zone" where chemical reactions take place producing aerosols and gases. Particles and gases are then collected and separated before being analysed by offline chemical techniques. The main test parameters are: i/the molar flow rate or the concentration of the elements injected in the line, ii/the residence time of the flow and the thermal gradient profile of the fluid in the transport zone, iii/ the composition of the carrier gas (mixture of steam/He or steam/He/ $H_2$ ).

The steam/carrier gas mixture is directly fed at the inlet of the high temperature alumina tube. The reagents of interest are vaporised in external generators connected to the main line.

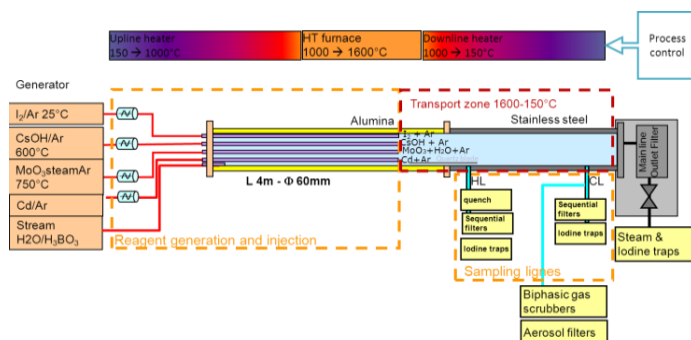


Fig. 3 CHIP PL facility – General design.

Gaseous iodine is obtained by sublimation of molecular iodine pellets heated at  $25^\circ C$  and swept by a low argon flow. Molecular iodine is then released in the HT zone with a mass flow rate representative of SA conditions ( $\sim 5 \cdot 10^{-8}$  to  $1 \cdot 10^{-7}$  mol/s). Caesium vapours are produced by vaporization at  $500^\circ C$  of initially dehydrated caesium hydroxide; the vapours are then transported in an argon flow. Molybdenum vapours are obtained by vaporization at  $750^\circ C$  of molybdenum trioxide, in a low argon/steam flow. Boron is delivered by a steam generator producing

either a mixture of steam/carrier gas or a mixture of steam/ $\text{H}_3\text{BO}_3$ /carrier gas by vaporization of a boric acid aqueous solution. In the steady state, these generators produce a stable mass flow rate of each reagent. The vaporised reagents are mixed together in the HT zone.

The main line is equipped with an integral quartz aerosol filter and by gas scrubbers filled with a sodium hydroxide solution (1 M) in order to trap the gaseous iodine species. The pressure in the CHIP facility usually set around 2 bars, is regulated by a control valve located downstream of the main filter.

Three sampling lines have been implemented, which can be sequentially operated:

- the Hot Leg sampling line (HL) devoted to fluid sampling at 500-700 °C (inlet of the downstream tube) and corresponding to hot leg break conditions;
- the Cold Leg sampling line (CL) devoted to fluid sampling in the 150 °C (outlet of the downstream tube) and corresponding to cold leg break conditions;
- the Organic Line (CL-OL) implemented as a branch on the cold leg sampling line (150 °C) and devoted to gaseous iodine speciation.

After the test, the facility is dismantled and each part is leached to establish a reliable element distribution from the high temperature mixing zone down to the outlet gas scrubbers. As iodine can only be stabilised in alkaline media, the leaching is performed with diluted NaOH. Caesium and boron species are also quantitatively recovered by these operations but molybdenum oxides are only partly recovered. The solutions are then analysed by ICP MS (Inductively Coupled Plasma – Mass Spectrometry) for elemental quantification. A selection of samplings (sequential filters and aerosols deposits in the main line) is preserved for aerosols characterisation (determination of morphology, composition and speciation).

The principle of the small scale bench is similar to CHIP facility. It consists of a high temperature furnace equipped with an alumina tube and implemented with lines allowing injection of  $\text{I}_2$  and CsOH vapours in a given carrier gas flow.  $\text{I}_2$  vapours were generated with the same device as for the CHIP line and CsOH vapours were directly generated in the main line by vaporisation of dehydrated CsOH placed in a crucible. In the transport zone, a similar temperature profile as for

the CHIP line is obtained. Several sampling lines are implemented at the main line outlet (150°C). They are similar to the organic lines of the CHIP facility, except that here, all the flow transiting the main line is directed to a given sampling line. Test conduct and post-test operations are the same as for the CHIP facility.

## III.2 Mains results

### III.2.1 IOH and CsIOH system

A first series of tests was performed in the small scale bench in oxidising (steam) or reducing (hydrogen) atmosphere with the injection of molecular iodine only. At high temperature,  $\text{I}_2$  is cracked to form mainly atomic iodine (calculation at thermodynamical equilibrium). Recombination occurs at lower temperatures in the transport zone and lead to the formation of more stable species as  $\text{I}_2$  or HI. Summary of the results are displayed in Table III. For both atmospheres, significant iodine deposition was observed (around 35%). As expected from calculations at thermodynamic equilibrium, the carrier gas composition clearly influences the nature of the released of gaseous iodine. Molecular iodine is expected with oxidizing conditions whereas the release of hydrogen iodide is expected with reducing conditions. Kinetics limitations were clearly evidenced in both conditions. Indeed, a measurable fraction of released iodine is under HI form (~10%) in oxidizing condition and under  $\text{I}_2$  form (~20%) in reducing condition. The main parameter that governs the extent of the kinetics limitations seems to be the  $\text{H}_2\text{O}$  or H/I ratio, as the other thermal hydraulic parameters that could influence kinetics limitations (residence time or temperature gradient) were similar. In oxidising conditions, the remaining HI fraction at 150°C (representative of cold leg break) decreases as the  $\text{H}_2\text{O}/\text{I}$  ratio increases indicating that the system is drawn towards thermodynamic equilibrium. In reducing conditions, the  $\text{I}_2$  released increasing with the H/I ratio indicates also kinetics limitations (paper in progress [9]).

Knowing the IOH system, the influence of caesium on gaseous iodine persistence was studied. Small scale tests were performed with an excess of Cs relative to I (to be representative of SA conditions). No gaseous iodine was observed in conditions of a cold leg break whatever the atmosphere condition (reducing or oxidizing, cf. Table III). The thermodynamical modelling at equilibrium correctly predicts the experimental results, indicating there is no kinetic limitation for iodine/caesium reactivity.

### III.2.2 Mo and B CsIOH system

Some elements are identified as caesium trap and thus can prevent the formation of CsI, such as molybdenum or boron. It was thus decided to study more complex systems involving additional elements to the initial CsIOH system. The aim is to identify the systems leading to the persistence of significant gaseous iodine fraction at the break. Mo is present in large quantities in the fuel, in excess relative to Cs and then can be released in significant amount particularly under RCS oxidizing condition [11-12].

A first series of tests was performed in the small scale bench with concomitant injection of CsI and MoO<sub>3</sub> in presence of steam [11]. It has been observed that the presence of molybdenum, even in low amounts, significantly increases the fraction of released gaseous iodine.

Complementary experiments were performed in the CHIP facility allowing thus an excess of Cs relative to iodine as observed in the Phébus tests. The CHIP tests main results are presented in Table III. The influence of the atmosphere was explored with tests performed in oxidising conditions (steam) and on tests performed in more reducing conditions.

In oxidizing condition, with a low excess of Mo relative to Cs, up to 90% of iodine is released as gaseous species mainly as I<sub>2</sub> and HI. The aerosols collected at 150°C were composed of molybdenum oxides and of various forms of caesium molybdates (Cs<sub>2</sub>Mo<sub>n</sub>O<sub>3n+1</sub>, n≥2) as already observed in similar tests on small bench. No CsI particles were detected. Molybdenum reacts with caesium to produce caesium molybdates, so caesium is not available to react with iodine, and the gaseous iodine fraction remains high.

TABLE III

Overview of the CHIP program tests [9], [10],[12]

System	IOH		CsIOH	MoCsIOH		BCsIOH	
Test loop	Small bench Oxidising	Small bench Reducing	Small bench Oxidising/ Reducing	CHIP Oxidising	CHIP Reducing	CHIP Oxidising	
Carrier gas composition (%Vol.)	H <sub>2</sub> O/Ar 50/50	Ar/H <sub>2</sub> 97.3/2.7	H <sub>2</sub> O/Ar or Ar/H <sub>2</sub>	H <sub>2</sub> O/He/Ar 51/44/5	H <sub>2</sub> O/H <sub>2</sub> /Ar 2.5/2.5/95	H <sub>2</sub> O/Ar 50/50	
Element ratio HT zone	O/I~15000	H/I~9900	Cs/I~2 to 4	Cs/I~4 Mo/Cs~3.2	Cs/I~4.2 Mo/Cs~3.7	Cs/I~2.3 B/Cs~19	
Element ratio sampling lines	-	-	Cs/I~2	Cs/I~ 2.7 Mo/Cs~3.3	Cs/I~3.2 Mo/Cs~3.1	Cs/I~2 B/Cs~35	
Deposition in the main line	I Cs Mo or B	33% - -	36% - -	50% 70% -	0% 27% 25%	38% 52% 66%	30% 35% 2%
Iodine form	I <sub>g</sub> I <sub>aerosol</sub>	67% -	64% -	0% 50%	90% 10%	1% 61%	1% 69%
Iodine gaseous speciation	I <sub>2</sub> HI	9/10 1/10	2/10 8/10	- -	~2/3 ~1/3	0 -	1 0

As soon as the atmosphere becomes more reducing, gaseous iodine released strongly decreases even in presence of MoO<sub>3</sub>. CsI remains the dominant form of transported iodine. Molybdenum was significantly reduced to the (+V) and (+IV) oxidation states and caesium polymolybdates were also detected. .

On the contrary, large excess of B leads to the release of only ~1% of gaseous iodine (BCsIOH test, cf Table III). Molecular iodine has been identified as the main species, but the existence of other gaseous species (HI, HOI) cannot be excluded. The weak influence of B on gaseous iodine persistence at the cold leg break was also observed during the Phébus FPT2 test, performed with a boric acid injection in excess relative to Cs (B/Cs ~19). It seems that only very large release of boron (B >> Cs) may lead to a significant gaseous iodine fraction at the cold leg break. Even if the formation of caesium metaborate may be expected, these species could not be directly evidenced [10].

Cadmium, indium or silver may also contribute to a strong lowering of gaseous iodine at the circuit cold leg break, more CHIP tests are in progress performed in order to study their influences.

#### IV. EPICUR EXPERIMENTS

Based on the Phébus experiments as reported in section II, several iodine species (molecular iodine, aerosols) are transferred into the containment building during a SA. The objectives of the EPICUR tests performed in the framework of ISTP and STEM programs are to obtain results on formation, deposition and decomposition processes of iodine species released in the containment vessel. The ISTP/EPICUR experiments were particularly dedicated to study the behaviour under radiation of iodine species transferred into the sump (in the containment sump, iodine in soluble compounds is dissolved as non-volatile iodide: I<sup>-</sup>). The STEM/EPICUR tests were dedicated to study the release under radiation of iodine species (molecular iodine or iodine aerosols species) deposited onto painted surfaces in the containment atmosphere. After a brief description of the EPICUR facility, this section

gives an overview of the results of the experiments carried out so far to investigate the formation of molecular iodine (I<sub>2</sub>) and organic iodide species (RI) from the sump or from painted surfaces in the containment atmosphere under various conditions.

##### IV.1 Experimental set-up

The experimental set-up used to study the release of volatile iodide species consists of a loop containing a panoramic irradiator, an electro-polished stainless steel irradiation vessel (4.8l), connected through electro-polished stainless-steel tubes to a selective iodine filtration system, called Maypack (Fig. 3).

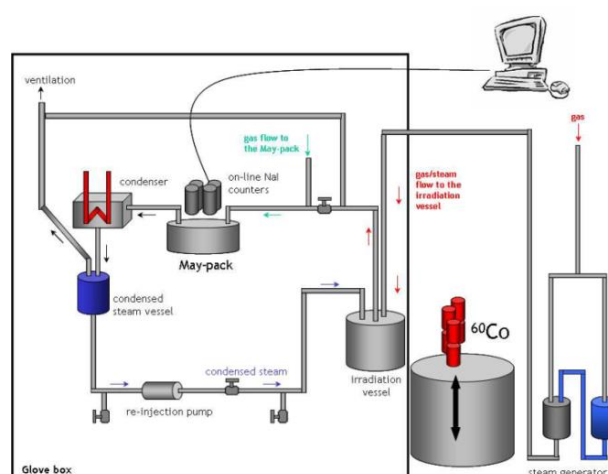


Fig. 3: Simplified view of the experimental EPICUR loop

The irradiation vessel subjected to the dose rate from the irradiator simulates the reactor containment. In the first set of experiments, the sump is simulated by an aqueous iodine solution. In the second set of experiments, the surfaces of the containment are simulated by an EPOXY painted stainless steel coupon placed in the gaseous phase of the irradiation vessel.

The panoramic irradiator containing <sup>60</sup>Co sources is designed to deliver an average dose rate of several kGy.h<sup>-1</sup> to represent the effect of radiation related to the presence of fission products in the reactor containment during a SA.

The sump solution or the painted coupons are placed in the temperature-controlled irradiation vessel connected through stainless steel tubing to the May-pack. Via this device the volatile species produced in the irradiation vessel are

transferred to different species-selective filters in order to trap molecular iodine I<sub>2</sub> (Knit-mesh filter with silver clad copper) and organic iodide RI (KI impregnated charcoal filter). Thanks to the use of <sup>131</sup>I to label iodine used to load the sump or the painted coupons (see § IV.2), continuous  $\gamma$ -measurements are performed on the May-pack filter stages (NaI counters are placed above each filtration stage of the May-pack device) in order to follow on-line the release of the different species volatilized and trapped on the selective filters.

At the end of the irradiation phase, the iodine filtration system is recovered. The different filters, the loaded sump or coupon and the rinsing solutions of the irradiation vessel and of the experimental loop are also  $\gamma$ -counted after the test in order to compare these post-test measurements with the on-line measurements and to calculate the iodine mass balance.

#### IV.2 Samples preparation

Two kinds of tests were performed on the releases of iodine species from the sump or painted coupon, loaded with iodine.

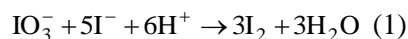
The sump was simulated with a solution of sodium iodide (NaI<sup>127</sup>I) prepared in a boric acid solution (0.2 mol.l<sup>-1</sup>) and labelled with radioactive iodine (<sup>131</sup>I). The pH was adjusted to 5.0 or 7.0 by adding H<sub>2</sub>SO<sub>4</sub> or NaOH. 2 litres of this solution were introduced in the irradiation vessel and placed on the experimental loop.

The painted coupons were 56 mm in diameter and 3 mm thick (total geometrical surface of 50 cm<sup>2</sup>). They were made of black steel and recovered with 2 layers of Centrepox N (40  $\mu$ m) and 1 layer of Hydrocentrifugon (50  $\mu$ m) paints. Centrepox N and Hydrocentrifugon paints are epoxy type paints used in the French nuclear plants. Centrepox N is used as a sub-layer to avoid the corrosion of the surfaces. The painted coupons were preheated at 130°C in a dry atmosphere for 96 h prior to the labelling phase and the irradiation phase.

Some tests were performed using quartz or stainless steel coupons. These coupons were first cleaned with demineralized water then with alcohol and then dried. No other treatment (pre-heating phase) was performed on the quartz or

stainless steel coupon before the loading with labelled iodine and the irradiation phase.

The coupons were loaded either with molecular iodine (I<sub>2</sub>) or aerosol species (CsI). Molecular iodine was produced from the Dushman reaction (1) in presence of labelled iodine (<sup>131</sup>I) using a sodium iodide and a sodium iodate solution:



The CsI aerosols were produced via an aerosol generator from a CsI solution prepared using a commercial powder solubilized in water and in presence of labelled iodine (<sup>131</sup>I).

Then, the <sup>131</sup>I loaded coupon was introduced in the irradiation vessel and placed on the experimental loop.

#### IV.3 Experimental conditions of radiation

The experimental conditions of the EPICUR tests are detailed in Table IIV. The objectives of these tests were to study the impact of several parameters under radiation on the formation of organic iodide and molecular iodine from iodine species transferred into the sump (dissolved in the sump or deposited onto immersed painted surfaces) or from iodine species deposited onto painted surfaces in the containment atmosphere. The gases used for these experiments (to transfer volatile species produced in the irradiation vessel towards the Maypack) were argon or high purity air.

Table IIV: experimental conditions of the EPICUR tests

	Phase or support	Iodine species	T (°C)	[I] <sub>i</sub> (mol.l <sup>-1</sup> or mol.m <sup>-2</sup> )
Sump	Liquid phase	I-	80 or 120	10 <sup>-4</sup> or 10 <sup>-5</sup>
	Liquid phase + immersed paint			
Painted surfaces in the containment atmosphere	Paint	I <sub>2</sub> or CsI		10 <sup>-2</sup> or 10 <sup>-3</sup> or 10 <sup>-4</sup>
	Quartz or stainless steel	CsI		

## IV.4 Results and discussions

### IV.4.1 Sump radiolysis – ISTP/EPICUR experiments

Iodine behaviour under radiation in the sump has been extensively studied in the past three decades [13-19]. Parameters such as dose rate, pH, solutes concentration, presence of oxygen or temperature were investigated as they can modify the yield of primary radiolysis products and thus the volatility of iodine. Results obtained in ISTP/EPICUR experiments focused on the molecular iodine release from the sump (iodide in liquid phase) under radiation were presented in an earlier paper [20]. Results indicated that the molecular iodine release decreased strongly with increasing pH in the studied experimental conditions. Sump temperature and oxygen content had a less important impact on the molecular iodine release. Finally, the influence of the initial iodine concentration in the liquid phase was also investigated. Results suggested that its influence on the molecular iodine transfer rate was rather small in the iodine concentration range  $10^{-4}$  -  $10^{-5}$  mol.l<sup>-1</sup>. The observations made in this article were consistent with those of previous researchers. Further ISTP/EPICUR experiments focused on the release of organic iodides under radiation from immersed painted surfaces were performed (liquid phase + immersed paint). These experiments showed no significant release of volatile organic iodides from painted coupons immersed in a liquid phase.

### IV.4.2 Painted surfaces in the containment atmosphere radiolysis - STEM/EPICUR experiments.

The STEM/EPICUR experiments focused on the releases of volatile molecular iodine (I<sub>2</sub>) and organic iodides (RI) from coupons loaded with molecular iodine [21] or iodine aerosols species (CsI) and placed in the gaseous phase of the irradiation vessel, under a long duration period (≥ 30 hours) to evaluate medium term releases.

Six tests were performed on the releases from epoxy painted coupons loaded with I<sub>2</sub>. Seven tests were performed on the releases from epoxy painted coupons loaded with CsI aerosols but also with quartz or stainless steel coupons, in

order to study the aerosols decomposition without paint interactions. The effect of parameters of main interest (temperature, relative humidity, initial concentration of iodine deposited on the sample surface) on the releases of I<sub>2</sub> and RI and of the global volatilization (defined as the difference between the initial quantity deposited on the coupon before irradiation and the quantity of iodine remaining on the coupon after irradiation) are presented and discussed below.

#### IV.4.2.1 Releases from painted coupons loaded with I<sub>2</sub>

Figure 4 shows the general trend of the releases kinetics of I<sub>2</sub> and RI from epoxy painted coupons under radiation. Figure 4 shows two kinetics: the releases are rapid during the first hours of the irradiation phase and then kinetics decrease.

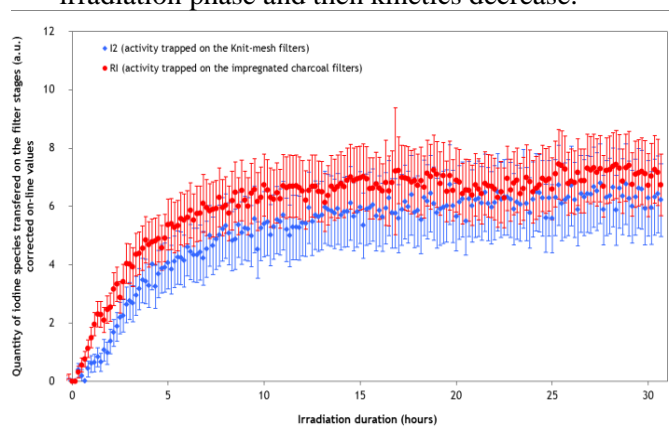


Fig. 4: General trend of the RI and I<sub>2</sub> releases

The study of the impact of initial iodine surface concentration on the coupon on the releases showed that the fraction of organic iodide released was stable for initial iodine surface concentrations lower than  $10^{-3}$  mol(I).m<sup>-2</sup> then it decreased for higher initial iodine surface concentrations; whereas the fraction of molecular iodine released and the global volatilization increased when the initial iodine surface concentration on the coupon increased. These results may be explained taking into account the molecular iodine interaction with the Epoxy paint during the loading phase. Different chemical sites are suspected for iodine-paint interaction [22]:

- chemical sites responsible for the I<sub>2</sub> release during the irradiation phase (the reactions or

interactions between Iodine and paint are reversible);

- chemical sites responsible for the RI release during the irradiation phase (the reactions or interactions between iodine and paint are not reversible, mechanisms and chemical recombination from the iodine bounded to the paint lead to the formation of RI).

The trend towards an increase in the RI fraction released at lower initial iodine surface concentration on the coupon would suggest that a larger fraction of iodine is bounded to the chemical sites responsible for RI release when the surface concentration is decreased. This in turn indicates a preferential interaction of iodine with these sites, rather than with reversible sites as discussed above. Saturation of these preferred sites could have been reached after a certain initial iodine surface concentration on the coupon. Further adsorption would then occur on other chemical sites identified above, leading to a relative decrease of the RI release.

When the relative humidity increased from 20 to 60%, the organic iodide release and the global volatilization decreased, the molecular iodine release decreased moderately. This may be explained as follows: water vapour may polarize iodine and make easier its interaction with polar groups of paint (chemisorption) which could therefore lead to lower releases.

When the temperature increased from 80 to 120°C, the global volatilization and the molecular iodine release decreased drastically; whereas the organic iodide release was not significantly affected. A possible explanation is that iodine interaction with paint is enhanced with a higher temperature, favouring chemical reactions with higher activation energy, leading to a decrease in the molecular iodine release at higher temperature [22].

#### *IV.4.2.2 Releases from coupons loaded with CsI*

The general trend of the I<sub>2</sub> and RI releases from epoxy painted coupons loaded with CsI under radiation showed only one kinetics: the releases of I<sub>2</sub> and RI are constant during the irradiation phase.

The study of the impact of the CsI concentration loaded on the epoxy painted surface showed that

the decrease of the CsI concentration by a factor of 24 and/or of the CsI particles size (by a factor of about 10) on the epoxy painted coupon leads to a decrease of the releases of iodine species by a factor of 3: an important decrease of the fraction of molecular iodine volatilized and a more moderate decrease of the fraction of organic iodides volatilized were observed. This decrease of the volatilization of iodine species could be due to the interactions between CsI aerosols and epoxy paint but this hypothesis cannot be confirmed at this stage of the study.

The irradiation of aerosols of CsI deposited on a quartz or a stainless steel coupon led to an almost total volatilization of iodine species whereas the irradiation of aerosols of CsI deposited on a painted coupon (epoxy paint) led to a partial volatilization. This difference of behaviour may be due to different interaction processes between CsI aerosols and the surface of coupons of different nature (epoxy paint or quartz or stainless steel).

The increase of relative humidity from 20% to 50% promoted molecular iodine release from a quartz coupon whereas the increase of the temperature from 80°C to 120°C did not affect significantly the fraction of molecular iodine released from a stainless steel coupon, taking into account all experimental uncertainties.

## V. SUMMARY AND PERSPECTIVES

Short term iodine processes are well predicted for various accident scenarios. Indeed, from a “circuit” point of view, the CHIP program highlighted the fact that in certain conditions, a direct gaseous iodine release in the containment building cannot be excluded – as already observed in at least one of the Phébus tests. The presence of fission products as Mo or B and the nature of the atmosphere (oxidizing or reducing) have a strong influence on this release. Moreover, kinetic limitations may also play a role as evidenced from the study of the gas phase iodine reactivity.

Regarding the iodine behaviour in the containment, the ISTP/EPICUR tests highlighted that molecular iodine could be released from the sump and that molecular iodine and organic iodides could be released from painted surfaces according to various phenomena and kinetics.

CHIP and STEM/EPICUR programs have produced numerous results which help to greatly improve the understanding of iodine behaviour in Phébus program and therefore in severe accident conditions. The ongoing STEM/EPICUR tests are focused on the iodine oxide aerosols stability under radiation and might show a significant volatilization of molecular iodine from these IOx species. Phenomenological models have been developed and implemented in simulation tools like the ASTEC severe accident code.

However, qualifying the potential mid-term releases of volatile iodine species (fission products reevaporation from the RCS, radiolytic degradation of iodine aerosols in the containment) still needs further knowledge. Therefore, experimental works on iodine chemistry in SA conditions are still ongoing at IRSN.

The CHIP program is extended as CHIP + focusing on the influence of control rods materials (silver, cadmium, and indium) on iodine chemistry in the RCS. Within the mitigation and outside releases in case of SA (MIRE) project, the mid-term potential iodine releases due to reevaporation of RCS deposits is investigated. An extension of the current OECD/STEM program is foreseen in collaboration with an extension of the OECD/BIP2 program. The effect of paint ageing on iodine trapping and release under irradiation and the effect of irradiation on stability of iodine aerosols will be the main subjects on iodine behaviour to be studied by IRSN.

#### ACKNOWLEDGMENTS

Authors acknowledge the partners of the Phébus and the International Source Term Program: Electricité de France, the Commissariat à l’Energie Atomique, the European Community, the US Nuclear Regulatory Commission, the Atomic Energy of Canada Limited, Suez-Tractebel and the Paul Scherrer Institute.

Authors acknowledge also the OECD hosting the STEM project. Authors acknowledge for their support the Electricité De France, the Atomic Energy of Canada Limited, the Teknologian tutkimuskeskus VTT (Finland), The Nuclear Research Institute (Czech Republic), the

Gesellschaft für Anlagen – und Reaktorsicherheit (Germany), the Korea Atomic Energy Research Institute, the Korea Institute for Nuclear Safety, The US Nuclear Regulatory Commission.

#### REFERENCES

1. L. SOFFER, *et al.*, “Accident Source Term for Light Water Nuclear Power Plants”, NUREG-1465 (1995).
2. M. SCHWARZ, *et al.*, Phebus FP: A severe accident research program for current and advanced light water reactors. Nuclear Engineering and Design, 187, 47. (1999).
3. B. CLEMENT and R. ZEYEN, The Phebus Fission Product and Source Term International Programs. In : Proceedings of International Conference on Nuclear Energy for New Europe, Bled, Slovenia, 5-8 September. (2005).
4. B. CLEMENT and R. ZEYEN “The objectives of the Phébus Experimental program and the main lessons learned, Annals of Nuclear Energy, 61, 4-10”(2013)
5. P. MARCH and B. SIMONDI TEISSEIRE “Overview of the facility and experiments performed in Phébus FP”, Annals of Nuclear Energy, 61, 11-22 (2013).
6. A.C. GREGOIRE and T. HASTE “Material release from the bundle in Phébus FP”, Annals of Nuclear Energy, 61, 63–74 (2013).
7. N. GIRAULT and F. PAYOT, “Insights into iodine behaviour and speciation in the Phébus primary circuit”, Annals of Nuclear Energy, 61, 143–156(2013)
8. B. SIMONDI TEISSEIRE *et al.*, “Iodine behavior in the containment in PHébus FP tests”, Annals of Nuclear Energy, 61, 157-169 (2013).
9. A.C. GREGOIRE, *et al.* “Studies on the thermokinetic of the IOH system in the conditions representative of the RCS in nuclear severe accident conditions”, *in progress*.
10. A.C. GREGOIRE, H. MUTELLE, “Experimental study of the [B, Cs, I, O, H] and [Mo, Cs, I, O, H] systems in the primary

- circuit of a PWR in conditions representative of a severe accident”, Proceedings of International Conference on Nuclear Energy for New Europe, Ljubljana, Slovenia, 5-7 September (2012).
11. M. GOUELLO, *et al.* « Analysis of the iodine gas phase produced by interaction of CsI and MoO<sub>3</sub> vapours in flowing steam”, *Nuclear Engineering and Design*, 263, 462-472 (2013).
  12. A.C. GREGOIRE *et al.*, « Studies on the role of molybdenum on iodine transport in the RCS in nuclear severe accident conditions, *Annals of Nuclear Energy*, 117-129 (2015).
  13. C.B. ASHMORE *et al.*, “Measurements of the radiolytic oxidation of CsI using sparging apparatus: part II”. AEA-TSD-0516, *AEA Technology* (1995).
  14. C.B. ASHMORE *et al.*, “Measurements of the radiolytic oxidation of aqueous CsI using a sparging apparatus”, *Nuclear Technology*, 129, (3), 387-397 (2000).
  15. C.B. ASHMORE *et al.*, “Measurements of the radiolytic oxidation of CsI using sparging apparatus: part III”, AEAT-1268, *AEA Technology* (1997).
  16. W.G. BURNS *et al.*, “The radiolysis of aqueous solutions of caesium iodide and caesium iodate”, AERE-R-13520, *Harwell* (1990).
  17. Lucas M., “Radiolysis of cesium iodide solutions in conditions prevailing in a pressurized water reactor severe accident”, *Nuclear Technology*, 82, 157-161 (1988).
  18. G.J. EVANS *et al.*, “The volatilization of iodine species over dilute iodide solutions”, *Canadian Journal of Chemical Engineering*, 71, 761-765 (1993).
  19. F. TAGHIPOUR *et al.*, “Iodine behavior under conditions relating to nuclear reactor accidents”, *Nuclear Technology*, 137, 3, 181-193 (2002).
  20. S. GUILBERT *et al.*, “Radiolytic oxidation of iodine in the containment at high temperature and dose rate”, *Proceedings of the International Conference Nuclear Energy for New Europe*, Portorož, Sept. 10-13, Slovenia (2007).
  21. J. COLOMBANI *et al.*, “Experimental study of organic iodide volatilization from painted surfaces present in the containment during a severe accident”, *Proceedings of the 6<sup>th</sup> European Review Meeting on Severe Accident Research*, Avignon, 2-4 October, France (2013).
  22. BOSLAND L. *et al.*, “Towards a mechanistic interpretation of the iodine – paint interactions”, *Proceedings of the 4<sup>th</sup> European Review Meeting on Severe Accident Research*, Bologna, 11-12 May, Italia (2010).

## THAI EXPERIMENTS ON VOLATILITY, DISTRIBUTION AND TRANSPORT BEHAVIOUR OF IODINE AND FISSION PRODUCTS IN THE CONTAINMENT

S. Gupta<sup>(1),\*</sup>, F. Funke<sup>(2)</sup>, G. Langrock<sup>(2)</sup>, G. Weber<sup>(3)</sup>, B. von Laufenberg<sup>(1)</sup>, E. Schmidt<sup>(1)</sup>, M. Freitag<sup>(1)</sup>, G. Poss<sup>(1)</sup>

<sup>1</sup>Becker Technologies GmbH, Koelner Strasse 6, 65760 Eschborn, Germany, <sup>2</sup>AREVA GmbH; Paul-Gossen-Straße 100, 91052 Erlangen, Germany, <sup>3</sup>Gesellschaft für Anlagen- und Reaktorsicherheit (GRS)mbH, Forschungsgelände, 85748 Garching, Germany

\*Corresponding author, Tel: (+49) 6196936115, Fax: (+49) 6196936100, Email: gupta@becker-technologies.com

**Abstract** – *In case of a hypothetical severe accident in a nuclear light water reactor, the kinetics of reactions of iodine species entering from primary side to the containment is complex and mainly influenced by the thermal hydraulic conditions and the type of gaseous, aqueous and solid materials available for interaction, e.g. gas components, decontamination paint, aerosols, and water pools. Resulting physical and chemical processes have an influence on the iodine volatility and subsequently on the iodine and aerosol inventory in the containment atmosphere. The availability of experimental data investigating above-mentioned effects in large scale experimental facility is very sparse and thus desirable for the further development and validation of iodine and aerosol models incorporated into integral accident analysis codes.*

*In this context, 49 experiments conducted so far in the THAI facility provide a basis to understand the source term relevant iodine and aerosol behaviour inside the containment. The THAI test facility allows investigating various accident scenarios, ranging from turbulent free convection to stagnant stratified containment atmospheres and can be combined with simultaneous use of hydrogen, iodine and aerosol issues. Main component of the THAI test facility is a 60 m<sup>3</sup> stainless steel vessel, 9.2 m high and 3.2 m in diameter, with exchangeable internals for multi-compartment investigations. The maximum design pressure of the vessel is 14 bar at 180 °C which allows to conduct H<sub>2</sub> deflagration tests. The facility is approved for the use of radiotracer I-123 which enables the measurement of time resolved iodine behavior down to very low concentration levels.*

*THAI experiments related to iodine and aerosol issues cover a wide spectrum of accident scenarios and provide relevant data for validation and development of iodine and aerosol models implemented in the severe accident analysis codes. The adsorption and desorption of iodine on steel and painted surfaces under different thermal-hydraulic conditions in single- and multi-compartment volumes, the mass exchange of iodine between gaseous and liquid phases, interaction between iodine and airborne aerosol particles, dry and wet resuspension of aerosols from surfaces and water pools, iodine and aerosols interaction with an operating PAR, formation of iodine oxides by reaction between iodine and ozone, and iodine release from a flashing jet are examples of the phenomena and processes which have been investigated in the THAI tests.*

*Based on THAI experimental results, important progress has been demonstrated in modelling of aerosol and iodine behaviour and their coupling with containment thermal hydraulics in severe accident analysis codes, such as COCOSYS-AIM, ASTEC-IODE, MELCOR-INSPECT, and others. The improved models have demonstrated reliable simulation of complex experiments, e.g. analysis of NEA THAI 2 test investigating molecular iodine interaction with non-reactive (SnO<sub>2</sub>) and reactive (Ag) aerosols, and EU-SARNET/SARNET2 code-benchmark exercises involving THAI data on iodine/surface interactions, iodine mass transfer, iodine oxide behaviour and iodine transport in multi-compartment behaviour.*

*A follow-up of NEA THAI 2 project is currently under discussion. Hydrogen related investigations on PAR performance under counter-current flow conditions and hydrogen deflagration tests in two-compartment*

*system are proposed. Additionally, in light of Fukushima Daiichi accident, experimental investigations are foreseen to study the release of fission product (aerosols and gaseous I<sub>2</sub>) from water pool at elevated temperature due to continuous heat-up of pool or depressurization (venting) induced boiling. Another planned experiment is related to “delayed” source-term in order to investigate re-emission of aerosols as well as iodine deposits from steel/painted surfaces due to hydrogen combustion.*

*The present paper provides an overview of the THAI experiments related to iodine and aerosol issues performed in the frame of national and NEA joint projects. From the comprehensive THAI experimental database, a selection of typical results is presented to illustrate the multi-functionality of the THAI facility and the broad variety of iodine and aerosol related experimental investigations.*

## I. INTRODUCTION

The local iodine concentration and iodine species behaviour in the containment is governed by several chemical and physical processes and mainly determined by the presence of radiation, thermal hydraulic conditions and the type of gas and materials available for interaction, such as gas-mixtures, decontamination paint, water pools and their chemical boundary conditions e.g. pH, surfactants. Estimation of fission product source-term requires precise information about amount, composition and release time of the volatile radioactive species which could be present inside containment and become available for release to the environment during an accident either due to a containment leakage or via controlled release pathways (e.g. containment venting).

Safety analysis tools based on coupled thermal hydraulic, aerosol and iodine codes (e.g. COCOSYS-AIM, ASTEC-IODE, MELCOR-INSPECT, and others) are employed to simulate iodine and aerosol transport and distribution behavior in the containment and the source term to the environment. The performance of these safety analysis codes for a real reactor application is often validated through large scale experiments reasonably representative of dominant accident sequences or conditions. Large scale experiments used for validation purpose need to consider the impact of physical processes which govern the mixing of containment atmosphere such as, forced convection, natural convection, condensation for an accurate prediction of iodine and aerosol transport and distribution behavior.

In this context 49 experiments related to iodine and aerosol issues have been conducted in the THAI (Thermal-hydraulics, Hydrogen, Aerosols, and Iodine) test facility. An overview of the iodine and aerosol related tests conducted up to now in the THAI test facility is given in Table 1. THAI offers the opportunity for the coupling of different processes or phenomena which may occur under accident conditions. Thermal hydraulic and iodine effects, for example, are coupled for an investigation of iodine distribution in a steam-air-hydrogen containment atmosphere with natural and/or forced convection and with or without wall

condensation. Experiments on iodine mass transfer between gas space and sump have been carried out under well controlled thermal hydraulic test conditions, stratified or well-mixed sump, and for different convection states of sump water motion. Another example out of a multitude of possibilities is the interaction of molecular iodine, and/or aerosols with safety devices, such as, spray, passive autocatalytic recombiners (PAR), pressure suppression pool, installed inside the containment as accident mitigation systems.

In the present paper, from the comprehensive THAI experimental database, a selection of typical results is presented to illustrate the multifunctionality of the THAI facility and the broad variety of iodine and aerosol related experimental investigations.

## II. THAI TEST FACILITY

THAI is a technical-scale containment test facility designed and built to address hydrogen and fission product issues under Design Basis Accident (DBA) and Severe Accident (SA) conditions. Main component of the facility is a 60 m<sup>3</sup> stainless steel vessel, 9.2 m high and 3.2 m in diameter, with exchangeable internals for multi-compartment investigations. At the lower end of the vessel a sump compartment is attached. Figure 1 depicts the THAI test vessel with its standard internals: a 4 m high inner steel cylinder (divided into two 2 m sections, ID 1380 mm, 10 mm thick wall), open at its upper and lower end, supported by six columns (915 mm long pipes of 60 mm OD), and four condensate trays fixed in the annulus between vessel wall and inner cylinder at elevation  $H = 4$  m. These internal structures are removable. The vessel is designed for a maximum overpressure of 14 bar at 180 °C and can withstand moderate hydrogen deflagrations. The facility is approved for the use of I-123 radiotracer which enables the measurement of time resolved iodine behavior.

The cylindrical part of the test vessel is equipped with three independent heating/cooling mantles over the height for controlled wall temperature conditioning by means of external thermal oil circuits. The heating/cooling power of each

jacket is determined from measurements of oil mass flow and inlet/outlet temperature difference. Top and bottom of the vessel can be heated electrically. The sump water can be heated and recirculated at different flow rates. The outer sides of the vessel are thermally insulated by 12 cm mineral wool to minimize the heat losses. Typical heat losses are in the order of 8 kW at 110 °C operation temperature. A large top flange of 1.4 m diameter and two man holes provide access to the interior of the vessel for modifications of internals, installation of test components, e.g. PAR, and instrumentation. Measuring flanges on five levels and at five circumferential positions allow installation of in-situ optical and conventional instrumentation, and of sampling lines.

The size of the test vessel is large enough to establish inhomogeneous atmosphere conditions (e.g. stratification) as well as natural convection flow loops by controlled wall heating and cooling. The vessel dimensions, its modular multi-compartment configuration and the well-controlled boundary conditions facilitate coupling of flow distribution studies with fission products to investigate the influence of independent thermal-hydraulic conditions prevailing in different compartments on fission product deposition and resuspension behaviour in the presence of steel, painted surfaces and water pools.

#### Feed systems

Feed systems are available for injection of steam, air, gas (e.g. N<sub>2</sub>, O<sub>2</sub>, He, H<sub>2</sub>, O<sub>3</sub>), iodine and aerosol at variable positions. A 108 kW steam generator provides up to 36 g/s saturated steam for release into the test vessel. Elemental iodine (I<sub>2</sub>) is labelled with I-123 radiotracer by melting the solid I<sub>2</sub> together with I-123 placed inside a small glass flask. The injection of gaseous radio-labelled I<sub>2</sub> into the gas phase of the THAI vessel is then performed by hot carrier gas (e.g. synthetic air, helium). Injection of radio-labelled I<sub>2</sub> into the sump water is carried out by using a cold aqueous I<sub>2</sub> solution in a pressure vessel placed inside a glove box, which can be directly connected to the vessel sump. The THAI facility is equipped with various aerosol generation techniques to produce severe accident prototypical poly-disperse aerosols (CsI, Ag,

LiNO<sub>3</sub>, SnO<sub>2</sub>, etc.) at specified thermal-hydraulic conditions and aerosol mass concentration up to 4 g/m<sup>3</sup>.

#### Instrumentation

Conventional thermal hydraulic instrumentation is provided for pressure, fluid and wall temperature, relative humidity, feed mass flow, wall heating/cooling power, water level and condensate mass flow measurements. It is supplemented by a thermal conductivity based gas sampling system for continuous light-gas (H<sub>2</sub>, He) concentration monitoring and with oxygen concentration analyzers based on electrochemical detection principle. Furthermore, a spectral photometer (FASP) is available for in-situ measurements of fog droplet size and airborne liquid water content. For flow measurements THAI can be equipped with vane wheel transducers for point velocity measurements, a 2-D Laser Doppler Anemometer (LDA) for velocity profile measurement, and a Particle Image Velocimetry (PIV) for velocity field measurement.

Iodine distribution measurements are mainly based upon radioactive iodine I-123 which is used as a tracer for inactive iodine, and liquid or gas samples are taken at numerous locations for immediate gamma-ray evaluation. To avoid errors by adsorption of gaseous iodine within the sampling lines several small gas scrubbers are installed at the measuring points inside the test vessel. They are filled with an aqueous iodine absorber (alkaline sodium thiosulphate) which retains the iodine from the gas sample sucked through the liquid. Filling, draining and purging of the scrubbers, and gas flow control are managed from outside. The iodine concentration in the vessel atmosphere is determined from the amount of I-123 tracer in the absorber liquid and from the gas flow through the scrubber. In addition, external Maypack filters are applied to discriminate molecular, organic and aerosol-borne iodine in the test vessel atmosphere. Samplings from condensates in trays, collecting tanks, and from sump water at different heights allows offline evaluation of I-123. Furthermore, I-123 sensitive scintillation detectors are focused onto deposition coupons mounted inside the vessel and are monitoring online the iodine deposits through glass windows. The material of

the surface of the deposition coupons is chosen to be representative for the tests objectives, such as steel, paint or aerosol covered. Coupons can be heated or cooled by independent steam and water based circuits to study iodine desorption and surface wash-down behaviour. Additionally, specific chemical trace analyses of iodine (including iodine speciation measurements) are performed on-site or at AREVA's Radiochemical Laboratory, Erlangen, Germany.

Aerosol concentration is measured by filter samplers which are installed outside the THAI vessel. Additionally, an in-line aerosol concentration measurement is performed by laser light extinction measurement, which provides a continuous and non-intrusive measurement. Low-pressure cascade impactors are used for determining the aerosol particle size distribution. A condensation nuclei counter and a differential mobility analyzer are available for measuring aerosol particles in sub-micron range.

### III. SINGLE AND MULTI-COMPARTMENT IODINE DISTRIBUTION AND BEHAVIOUR

Iodine is transported in the containment by gas and water flows under stratified or mixed boundary conditions. There will be locally different chemical and thermal-hydraulic conditions for processes such as chemical reactions of iodine, iodine deposition and resuspension at walls and iodine mass transfer to and from sumps. As a consequence iodine will be distributed non-homogeneously, and gaseous concentrations, wall deposits or concentrations in sumps will be different in different compartments of reactor containment.

THAI experiments cover both single- and multi-compartment iodine distribution experiments. Experiments conducted in a single compartment with homogeneously mixed atmosphere may lack coupling of above-mentioned phenomena with locally varying thermal-hydraulic conditions as expected in a multi-compartment containment structure but provide useful database for optimization of a particular phenomenon or process in iodine models. An extensive THAI database is available on iodine interaction with steel and painted surfaces in single- compartment configuration under a wide spectrum of thermal-

hydraulic conditions. On the basis of THAI experimental data, appropriate models considering both physisorption and chemisorption reactions have been developed and implemented in the COCOSYS/AIM code [1]. For example, results obtained in several single-compartment THAI iodine tests with dry air and steel environment facilitated optimization of the iodine depletion velocity constants and the implementation of a resuspension term in COCOSYS/AIM. The model was extended by use of the data from two steel samples measured in the NEA BIP programme [2]. Figure 2 shows good agreement achieved in the comparison of COCOSYS results with one of the THAI I<sub>2</sub>/steel interaction test Iod-18, indicating that all important aspects necessary for evaluating iodine/steel interaction under dry and wet test conditions are considered in the model. In this test, I<sub>2</sub> interaction with steel was measured as function of relative humidity over a broad range of relative humidity from dry air up to superheated steam/air mixture. The influence of natural and turbulent atmosphere convection states on iodine deposition and resuspension behavior was separately studied in THAI test Iod-22. The test data indicate overall negligible influence between natural and turbulent convection states on I<sub>2</sub>/steel deposition and resuspension behaviour under the investigated experimental conditions.

Iodine/paint model in COCOSYS/AIM which has also been partly developed based on THAI data also describes the interaction of I<sub>2</sub> with dry painted surfaces based upon physisorption followed by chemisorption analogously to the iodine/steel model. Figure 3 shows the comparison of the COCOSYS/AIM prediction with experimental data of THAI test Iod-15. This test was conducted at 100 °C and with 45 % relative humidity. A good agreement between the analyses and the experiment is confirmed. However, when the same model was applied against THAI test Iod-17 which had been conducted with a large variation in relative humidity (60-70 % in the initial test phase and 15-20 % in a late test phase), the modelled iodine desorption was found to be too strong as compared to the experimental results. The effect of relative humidity was not yet considered in the model, but the availability of more recent THAI

tests suggests a significant dependency of iodine deposition on paint from very dry to nearly saturated conditions [3].

In continuation to the single-compartment iodine tests, so far seven multi-compartment iodine tests have been conducted in THAI. Varied test parameters were relative humidity (also including partly condensation at walls) and surface types (stainless steel from vessel walls and internals or also additional painted surfaces), and coupling with aerosol behaviour. In THAI multi-compartment tests, the iodine distribution by atmospheric flows is measured in the THAI vessel sub-divided into 5-compartments consisting of a dome, upper and lower annulus, sump and a dead end room (inner cylinder covered at the top). A general sketch of iodine multi-compartment tests is given in Figure 4.

The first four iodine multi-compartment tests (Iod-10, Iod-11, Iod-12, and Iod-19) were conducted in an almost identical test configuration and with stainless steel (163 m<sup>2</sup>) environment. The first iodine multi-compartment test, Iod-10 was conducted in a dry air atmosphere with helium tracer and in 5-compartment geometry, whereby a low air humidity was set through a rather cold sump compartment. The next two THAI tests Iod-11 and Iod-12 investigated the influence of humidity on the iodine resuspension from the wall. The distribution behaviour of iodine in a steam/air atmosphere with a rather high relative humidity, yet without wall condensation, was investigated in test Iod-11. In the third multi-compartment test Iod-12, additionally the influence of wall condensation was investigated. Test Iod-11 was repeated as Iod-19 after a time interval of three years in order to check the reproducibility and a possible change of the stainless steel wall with respect to iodine reactions. Thermal hydraulic and iodine results could be reproduced very well. It was also concluded that the steel surface of the THAI vessel had not changed significantly with respect to interactions with iodine during other tests performed meanwhile.

In multi-compartment iodine tests, the test strategy was generally to start with a stratified phase with high temperature in the dome compartment and low temperatures below. In the subsequent mixing phase, wall heating, helium or

steam injection were operated to mix up the atmosphere, and the temperature and relative humidity conditions were maintained in a third test phase over longer time until end of the test. The distribution behaviour of gaseous I<sub>2</sub> and its homogenisation over the whole vessel during these test phases was monitored.

The vertical temperature profiles as measured during different test phases of Iod-11 test are shown in Figure 5. At the beginning of the *stratified phase*, about 1 g of gaseous I<sub>2</sub> was injected into the dome within 10-15 minutes. The beginning of injection was the start of the test time (t = 0). Test results indicate that part of the I<sub>2</sub> was adsorbed on the steel surface but almost no I<sub>2</sub> reached the lower compartments during *thermal stratification phase*. The iodine inventory accumulated in dome can be assumed as a source of iodine for the subsequent test phases. In the *transient phase* the mixing of the vessel atmosphere was stimulated by a controlled injection of heat, helium and steam. The vessel atmosphere was heated by the middle and lower vessel jackets and the sump water was heated electrically. Helium injection was carried out in the bottom compartment to support the atmospheric mixing and to serve as a tracer for atmospheric mixing. The released helium was rapidly distributed by the convective flows and after three hours it was completely mixed (Figure 6). In contrast, iodine behaved differently and indicated inhomogeneous concentration distribution in the vessel atmosphere. This inhomogeneous mixing is due to I<sub>2</sub> adsorption and desorption processes onto/from the steel surfaces which delays the transport of gaseous I<sub>2</sub> between the compartments. This delayed I<sub>2</sub> transport lasted until the end of the test. In the *mixed phase* the well mixed conditions were maintained by keeping atmospheric and sump temperatures nearly stationary. The I<sub>2</sub> distribution in the vessel changed only gradually, but the concentration decreased in all compartments due to chemisorption at the steel surfaces. At the end of the mixed phase the I<sub>2</sub> concentration in the dome was still one order of magnitude higher than in the lower compartments. In the lower compartments the I<sub>2</sub> concentration differed up to a factor 2, which is clearly above the measurement error of ± 30 %.

The THAI multi-compartment tests Iod-11 and Iod-12 have been analysed and interpreted in the THAI benchmark performed in the frame of SARNET2 [4]. In addition to the large user effect observed on the results, the benchmark results also highlighted the need of detailed modelling of iodine adsorption/desorption reactions at steel surfaces. The iodine/steel model is already available in COCOSYS-AIM 3. Under wet conditions, i.e. with wall condensation, in addition to the improved iodine/steel model at dry surfaces, optimization of iodine models with regard to iodine wash-down behavior to precisely model  $I_2$  reaction with wet painted surfaces was also required, and this was investigated in THAI tests Iod-21 and Iod-24. Experimental results and their application for iodine model validation and development are discussed in [3, 5]. The need for detailed thermal-hydraulic modelling to calculate the correct relative humidity and atmospheric flow rates was also identified. Relative humidity provides a basis for the correct application of the iodine/steel model and thus to accurately simulate the  $I_2$  transport in a multi-compartment geometry. Similar iodine multi-compartment tests with partly painted surface were also suggested.

In the meantime, THAI multi-compartment iodine tests Iod-27A, Iod-28 and Iod-30 including painted surfaces have been conducted. At the time of  $I_2$  injection, relative humidity in the thermally stratified dome compartment varies from < 1 % (Iod-27A) to > 90 % (Iod-28 and Iod-30). In Iod-30, multi-compartment iodine behaviour is studied in the presence of high relative humidity (but without wall condensation) and with silver aerosol. The effect of  $I_2$  removal from containment atmospheres by interaction with aerosols has been studied in two THAI tests using inert aerosol  $SnO_2$  (Iod-25) and reactive aerosol Ag (Iod-26). Main experimental findings on reaction of  $I_2$  interaction with dry and painted surfaces and aerosols are discussed in [3].

#### IV. $I_2$ MASS TRANSFER BETWEEN SUMP AND GAS

$I_2$  mass transfer between the sump and the atmosphere is an important process which governs the iodine equilibrium concentrations in the containment atmosphere. Mass transfer of volatile iodine species ( $I_2$ , organic iodide) can be significantly influenced by the prevailing containment thermal-hydraulics, chemical conditions in sump, and sump water flow regimes, e.g. quiescent or agitated sump. Volatility of iodine species from sump increases as water temperature increases or pH in the water pool decreases. Under condensing conditions, some iodine species deposited over containment surfaces will be washed into the sump. Some of these processes have been subjected to detailed investigation in THAI tests.

In the Iod-9 mass transfer test conducted in the THAI test facility, test phases were designed to address the following main processes:  $I_2$  adsorption onto and desorption from the stainless steel vessel walls with and without wall condensation, the mass transfer of molecular iodine from the gas into two different sumps, and the iodine transport into the sumps during condensing conditions at the walls. The main sump with a volume of 0.625 m<sup>3</sup> was stagnant, then recirculated. A second sump was small, flat (52 liter/1m<sup>2</sup>) and unstirred. Gaseous iodine was injected at the start of the test into a superheated steam/air atmosphere (relative humidity 30-40 %) at 1.5 bar pressure and 90 °C temperature with dry walls. Repartitioning of the iodine was observed in the gaseous phase at the wall and in the sumps. In the final washing test phase steam was injected at different mass flow rates to study the  $I_2$  deposition at wet steel walls. The resulting locally measured minimum and maximum condensate rates from defined surface area were 1.8E-5 kg/m<sup>2</sup>s and 2.8E-4 kg/m<sup>2</sup>s, respectively. In addition to the atmospheric iodine concentration, the simultaneous iodine transport with the falling wall water film into the sump was also measured.

Test Iod-9 was analysed within the frame of the European SARNET project and valuable insights were obtained for severe accident analysis codes with integrated semi-empirical approach based

iodine models (COCOSYS/AIM, ASTEC/IODE) as well as mechanistic approach based iodine model (LIRIC) [6]. Measured and simulated iodine concentration in gas atmosphere is shown in Figure 7. Employed codes fairly well simulated the iodine transport and behaviour in THAI test Iod-9 in the gaseous and water phases, and also on the surfaces in the gaseous phase. Figure 7 also shows that wall condensation with fast wet iodine adsorption caused fast iodine depletion in the atmosphere. As in other THAI tests, the distribution of gaseous  $I_2$  was strongly inhomogeneous because of local steam injection and locally different wall condensation. Analysis results demonstrated the need to improve modelling of  $I_2$  mass transfer with particular focus on coupling of iodine mass transfer coefficient with sump flow conditions and iodine wash-down behavior from surfaces. The importance of a correct modelling of  $I_2$ /steel reactions under dry and wet conditions by different codes was highlighted. Under wet conditions, i.e. with wall condensation, iodine wash-down has to be considered. Codes with inadequate modelling capability on iodine wash-down behavior and wrongly predicted condensate mass flow rates indicated wrongly predicted iodine concentration in the sump.

Mass transfer of molecular iodine at the water pool-gas interface as a function of water motion has been investigated in THAI test Iod-23. In the test,  $I_2$  was initially dissolved in a water volume and the amount of gaseous iodine transferred from water to gas side was measured by instantaneously collecting the gas-borne iodine on a filter. From the iodine accumulation on the filter, the iodine mass flow and the mass transfer coefficient could be evaluated. Two different states of water motion were repeatedly established: a stagnant pool, and an agitated pool with well-defined flow distribution, in order to cover a wide range of conditions for  $I_2$  mass transfer. The measurements show that the mass transfer coefficient is strongly dependent upon the water motion, with much higher values for the agitated pool. The experimental data can also be correlated by means of a water surface film renewal model superimposed to the two-film theory [7].

## V. FISSION PRODUCT WASH DOWN BEHAVIOUR

Depending on the accident scenario and the prevailing thermal hydraulic conditions, aerosol entering into reactor containment may consist of particles of various sizes and may be composed of more than one species. Aerosol particles deposited on floors and walls in the containment are washed off by water flow (condensate) into puddles or small water pools in the containment sub-compartments. From there they are washed down via existing drains and other paths into the sump. Only a few per cent of the aerosol mass is transferred directly into the sump by sedimentation. The potential of a particular fission product to be re-released from the containment sump during a severe accident may depend on several factors, such as, accident sequence, other chemical substances such as aerosols, surfactants present in the sump, chemical boundary conditions, e.g. sump water redox potential, pH, and the prevailing thermal-hydraulic conditions. Fission product transport in the containment atmosphere dominates the distribution of dose rate, decay heat and hence humidity in the containment which in turn has a large influence on the aerosol depletion behaviour. Therefore, understanding of iodine and aerosol wash-down behaviour is important for source term assessment. Wash-down of soluble aerosols like CsI from surfaces is comparatively simple as the aerosol particles are dissolved in the condensate and drained downwards inside the containment. More complex is the behaviour of insoluble materials, such as  $SnO_2$  and Ag as wash-down process depends on condensate and aerosol characteristics among others. In case of iodine wash-down there is an additional influence of chemical reactions with the decontamination paint in the presence of wall condensate.

The THAI aerosol wash-down (AW) tests addressed the main phenomenon related to the wash-down process of soluble and insoluble aerosols deposited under superheated thermal hydraulic conditions on flat surfaces or in a small pool (initially dry during aerosol injection and deposition phase). The thermal-hydraulic conditions were established in such a way that wash-down of deposited aerosols occur only by

steam condensing over the vessel mantles and no volume condensation takes place during steam injection. The condensate drained out from the plates and the puddle was analysed separately for determining the aerosol concentration. Tests were conducted with single component aerosols of different solubility (CsI, Ag), and aerosol mixture (CsI/SnO<sub>2</sub>).

For the wash-down tests, standard internals (inner cylinder and four lateral condensate trays) had been removed to allow free unobstructed environment for aerosol deposition on specially designed plate sections and small puddle. Steam condenses and runs down vertical THAI vessel walls. In the lower part of the THAI vessel, horizontal deposition surfaces for aerosols were installed in the form of interconnecting sections made of stainless steel. Out of the total 20 stainless steel sections used to occupy the THAI vessel cross section, 16 sections form a flat surface (plate section) and 4 sections form a water puddle (39 mm deep, volume: 26.9 litre). The stainless steel sections and the puddle were inclined with a downward gradient of about 2°. The surface area of each stainless steel section is 0.37 m<sup>2</sup>. The material of horizontal deposition surfaces was stainless steel in AW test, whereas in AW2 & AW3 tests horizontal deposition surfaces were coated with artificially aged decontamination paint with an estimated age of 15 years.

In the first test phase aerosol injection was carried out and sufficiently long time was allowed to let the aerosol particles depositing over surfaces. The mass median diameters of the airborne aerosols were in the range of 1.0 - 2.0 µm with geometric standard deviations in between 1.5 - 2.0 for the three tests. At the end of the aerosol deposition phase, the achieved horizontal surface loadings were 80 g/m<sup>2</sup> CsI (AW), 30 g/m<sup>2</sup> CsI/60 g/m<sup>2</sup> SnO<sub>2</sub> (AW2), and 35 g/m<sup>2</sup> Ag (AW3), respectively. The specific surface loading of the vertical walls was about 10 times lower than on the horizontal surfaces, which is in accordance with the ratio of vertical to horizontal surface area in THAI vessel (approximately 10). The mass flow rate of steam was kept constant at 14 g/s (AW) and 17 g/s (AW2 & AW3).

For soluble aerosol CsI, test results indicate that wash-down from horizontal surfaces was complete but aerosol concentration in the puddle runoff water decreased much slower and shows draining out of CsI even after a day-long washing period. In other words, the puddle water acts as an intermediate storage of dissolved CsI, which leads to a considerable delay in the aerosol transport. In test AW2 conducted with CsI/SnO<sub>2</sub> aerosol mixture, results on wash-down behaviour of soluble CsI aerosol were in agreement with the AW test. However, wash-down of non-soluble aerosols (SnO<sub>2</sub>, Ag) remained far from being complete in tests AW2 and AW3. Test results both for soluble and insoluble aerosols indicate an initial concentration spike implying higher aerosol removal followed by a long transient of continuous low aerosol removal. Decrease in aerosol concentration does not occur smoothly but exhibit timely peaks which could be linked to the rivulet formation and dissolution mechanisms observed during the tests.

In AW2 test, considering complete wash-down of aerosols from the vertical surfaces, the estimated total wash-down efficiency of the aerosol mixture from deposition surfaces was of the order of 50 % consisting to a large extent of the soluble CsI aerosol. The unwashed aerosol mass which remained on the surfaces consisted of 95 % of the non-soluble SnO<sub>2</sub> aerosol.

The main processes which were found to have an influence on the observed aerosol wash-down behaviour included condensation induced flow patterns, such as rivulets or closed water films, in case of rivulets – which was the prevailing case during the tests – their formation and dissolution mechanisms, partial aerosol wash-down as compared to closed water-film, and strong retention of even soluble aerosols in the water filled puddle [5, 8]. The THAI tests on aerosol wash down were accompanied by two lab-test programs in which parameter variations like aerosol loading, condensate mass flow, particle sizes and surface coating were investigated. A major outcome of these tests was the observation of long-lasting stability of rivulets in the presence of non-soluble aerosols surface loadings. Furthermore, the width of the individual rivulets scales with surface inclination, but not with condensate mass flow.

The wash-down behaviour of molecular iodine from vertical surfaces was first studied during a dedicated test phase of the THAI test Iod-9. Tests results indicate an increase in the aqueous iodine concentration due to steam condensation on the main sump surface and the surrounding walls. However, the doubling of the steam injection rate from 15 g/s to 30 g/s in the test phase dedicated to study wash-down behaviour did not lead to an additional increase in the iodine concentration. The iodine wash-down behaviour and its influence on iodine distribution was not very well understood by the iodine codes used for Iod-9 post-test analysis [6].

Later on, two THAI tests Iod-21 and Iod-24 were conducted for detailed investigation on iodine wash-down behaviour. The parameters varied included dry or wet painted surfaces and variation in condensate rate over the painted surfaces. One of the main outcomes from Iod-24 test was that the iodine adsorption onto paint can be higher with a low condensation rate than high condensate rate. The iodine wash-down versus condensate rate behaviour observed in Iod-24 as well as in Iod-9 could be explained by limited wash-down efficiency which could be achieved with stable rivulets and also due to the fact that the wet  $I_2$  adsorption velocity does not rise linearly with the condensation rate.

Furthermore, in the THAI experiment AW3, investigation on wash-down behaviour of the non-soluble aerosol was extended by investigating the effect of washed down Ag aerosol on the fixation of volatile iodine ( $I_2$ ) in the sump water in a second part of the test. Regarding the  $I_2$ -Ag reaction in sump, the specific surface area of the silver particles settled at the bottom of the sump, relevant in the iodine/silver model has been identified as one of the influential uncertain parameters determined in the uncertainty and sensitivity study on a COCOSYS-AIM calculation on PHEBUS test FPT1 [9]. In THAI test AW3, the  $I_2$ /Ag reaction rate in the case of  $I_2$  being dissolved in stagnant water above a layer of settled Ag particles was measured, first results and modelling are provided in [5].

The THAI experimental investigations related to iodine and aerosol wash-down as well as  $I_2$ -Ag reaction in sump have provided relevant data for

the optimisation and further development of iodine and silver wash-down models in COCOSYS/AIM-3 code.

## VI. IODINE-OZONE INTERACTION AND IODINE OXIDE BEHAVIOUR

Radiolytic processes occurring inside containment have the potential to convert gas phase molecular iodine and organic iodide into iodine oxide or iodine nitroxide particles (“IOx”). This gas to particle conversion has been investigated in the THAI tests Iod-13 and Iod-14 [10]. As no radiation source is available in THAI, the radiation field was simulated by directly injecting ozone ( $O_3$ ) as a representative of air radiolysis products into the THAI vessel, where it reacted with the gaseous  $I_2$ . The two tests were conducted at an atmospheric temperature of 100 °C and a relative humidity of 60 – 70 %. In test Iod-13 ozone was injected into the  $I_2$ -loaded atmosphere. In Iod-14 test, ozone was injected first to a high concentration level expected to immediately oxidise all  $I_2$ . The test results indicate that iodine behaviour in Iod-13 is mainly governed by the gaseous iodine, as the ozone concentration was low. However, in Iod-14 test performed with ozone-saturated conditions,  $I_2$  is rapidly converted into IOx and the behaviour of the atmospheric iodine is governed by iodine oxides as aerosol particles. The observed iodine oxides form submicron particles with mean volume related diameter of about 0.35  $\mu\text{m}$ . Over time, agglomeration of particles is observed but the IOx concentration depleted slowly (indicating efficient diffusive deposition rather than sedimentation) under the investigated test conditions and in the absence of other nuclear aerosols.

Uncertainty still remains regarding the effect of gas composition on IOx compounds and related iodine volatility, which are partly considered for investigation in the planned NEA STEM2 project (see paper by C. Mun in this workshop). Different conditions depending on reactor design as well as during an accident can be expected such as inert versus non-inert containment atmospheres, presence of CO from fires and MCCI or  $H_2$  from zircaloy oxidation. Additional experiments under comprehensive accident conditions will be required to understand the

effect of gas composition on conversion of IOx compounds back into gaseous iodine species.

#### VII. INTERACTION BETWEEN FISSION PRODUCTS AND AN OPERATING PASSIVE AUTOCATALYTIC RECOMBINER (PAR)

During an accident, the prevailing thermal hydraulic conditions and the extent of fission products interaction with PAR units may either jeopardize their performance or lead to constitute an additional potential source term. For the purpose of safety analysis and the management of mitigation measures these interaction processes must be known by means of experiments under realistic test conditions. Such experimental data are required to be subjected to detailed plant scale analysis for evaluating the possible impact on source term to the environment in the event of an accident. In this context, two THAI experiments HR-31 and HR-32 were specifically designed to study the fission product interaction with an operating PAR.

The HR-31 test series consisted of two tests for investigating the thermal conversion of iodine aerosol (CsI) to gaseous iodine (I<sub>2</sub>) while passing through an operating PAR. Related PAR research based on thermochemical analysis indicated that CsI aerosol particles in a size range typically present in the containment atmosphere can be vaporized at temperature of 800 °C within residence times of 0.1s - 0.5s which are typical of a PAR operation [11].

Test boundary conditions were established in particular to achieve high catalyst temperatures (> 800°C) to maximize CsI conversion, which requires high hydrogen concentrations (8 to 9 vol %) at the PAR inlet. The gas mixture in the vessel atmosphere was rendered inert by adding steam (> 60 %) to avoid H<sub>2</sub> ignition risks during the experiment. The conversion yield of aerosol-borne CsI to gaseous iodine has been calculated according to the Eq. 1, by using the measured concentration of gaseous iodine at PAR outlet and the relationship of gas densities at PAR inlet and PAR outlet as follows:

$$\text{Conversion (\%)} = \frac{C_{I_{\text{gas}}}(PAR_{\text{out}})}{C_{CsI_{\text{aerosol}}}(PAR_{\text{in}})} \cdot \frac{\rho_{PAR_{\text{in}}}}{\rho_{PAR_{\text{out}}}} \cdot 100 \quad (1)$$

The evaluation with Eq. 1 considers that no gaseous iodine enters the PAR. This has also been confirmed by gaseous iodine concentration measurements in the vicinity of the PAR inlet.

The measured particle Sauter mean diameter at the PAR inlet was in the range of 0.6 - 0.8 µm. Considering the PAR inlet cross-section dimension and the measured inlet velocity, residence time of about 0.15 sec was estimated in between two catalyst plates. The test results indicate the conversion rates of CsI aerosol to gaseous iodine in the range of 1 - 3 %.

Another important result of THAI experiments HR-31 was the shifting in aerosol particle distribution to lower Sauter mean diameter at the PAR outlet.

The second experiment (HR-32) was designed to investigate the poisoning effects of fission product on PAR performance. The PAR poisoning test considered challenging test conditions which are conceivable during a severe accident. Subjected conditions for the test included PAR exposure to fission products at very low inlet H<sub>2</sub> concentration (< 2 vol %), elevated concentration of realistic aerosol mixture (hygroscopic and inert aerosols), use of reactive molecular iodine, and saturated steam conditions prevailing inside the test vessel. Test phases were defined to ensure fission products arrival at PAR inlet before the onset of PAR recombination occurs.

During the tests, the PAR was exposed to high concentrations (1.5 g/m<sup>3</sup> - 2.5 g/m<sup>3</sup>) of insoluble tin oxide (SnO<sub>2</sub>) aerosol, highly hygroscopic lithium nitrate (LiNO<sub>3</sub>) droplets, steam and radio-labelled molecular iodine (injected amount 1.7E-6 g/l). Test results indicate that PAR H<sub>2</sub> depletion efficiency remained unaffected and comparable to the results of the other PAR tests with the identical thermal-hydraulic conditions but without aerosols and iodine. The onset of recombination was delayed and occurred at inlet hydrogen concentration of about 4.0 vol % and under saturated steam conditions. However, the delay in H<sub>2</sub> recombination onset was also

observed for other PAR-tests conducted with comparable thermal hydraulic conditions in the presence of saturated steam content but without fission products.

### VIII. AEROSOL RESUSPENSION

In the event of a severe accident, aerosols deposited onto containment walls or trapped into water pools may be re-entrained or re-suspended to containment atmosphere depending on an accident transient. Aerosol “wet” resuspension may occur either due to extreme sump water heating, e.g. by core melt, or in case of rapid depressurization, e.g. due to containment venting. Other processes which may result into “dry” resuspension of already deposited aerosols into the containment atmosphere include atmospheric currents induced by hydrogen deflagrations or by other phenomena like steam explosions. Among other effects, resuspension may result into an increase in aerosol concentrations in the containment atmosphere which in turn may have an influence on the radiological source term from containment to the environment.

Wet resuspension of aerosols from boiling sump has been investigated in seven tests (TH-14 – TH-17 and TH-25.1 – TH-25.3) conducted so far in the THAI test facility. The tests were conducted by using aerosol material of different chemical nature: CsCl, KI, Cs<sub>2</sub>SO<sub>4</sub>, and Li<sub>2</sub>SO<sub>4</sub> salts as soluble aerosols and non-soluble aerosol suspension of calcium carbonate (CaCO<sub>3</sub>) with two different primary mass-median diameters of 0.065 µm and 0.9 µm. The test configuration for wet aerosol resuspension tests and main steps followed during test progression are shown in Figure 8. The resuspended fraction refers to the fission products in droplets and is defined as a product of entrainment factor (mass ratio of released droplets and released gas) and aerosol enrichment factor (ratio of concentration in droplets and in sump water). Resuspension was effected by injecting steam at the bottom of the sump. The investigated superficial velocities (defined as the volume flow of the released gas and steam bubbles per unit area of the pool) ranged from 0.024 m/s to 0.13 m/s with higher values representing churn turbulent flow regime. For soluble aerosols, the entrainment factor

obtained during THAI test cases confirmed former REST laboratory-scale test data with entrainment factors varying between 1.5E-05 and 1.0E-04 for the investigated range of gas superficial velocity from 0.044 m/s to 0.185 m/s [12]. As shown in Figure 9, a decreasing trend of the resuspension fraction for insoluble particles was found as the superficial velocity increases. The effect of primary particle sizes on the resuspension fraction was found to be rather small compared to the effect of the superficial velocity. The largest values obtained at a superficial velocity of 0.024 m/s were approximately 4.1E-4 and reduce to 1.9E-5 for high superficial velocities of about 0.13 m/s. Test results indicate that mainly very small aerosols in the range of 0.06 µm - 0.11 µm (mass median diameter) are released from a boiling pool, which in turn might remain airborne for a long time. Such a small particle size represents unfavourable value for the design of the accident management measure filtered containment venting because filters normally show a minimum efficiency in this particle size range (“Filter gap”).

The varied test parameters in the THAI “wet” aerosol resuspension tests did not consider the effect of chemical boundary conditions, e.g. pH, surfactants concentrations on the fission product scrubbing and release behaviour from water pools. Further experiments will be required as chemical boundary conditions may have significant impact on the fission product release fraction either by modifying the fission product speciation or by changing the bubble dynamics in water pool and the splashing process at the water surface.

Experimental investigations on fission product pool scrubbing and water pool hydrodynamics for selected accident scenarios are underway in the currently running projects, e.g. EU-PASSAM. The THAI water pool hydrodynamics (WH) tests [14] have been focused on investigating fluid-dynamic features produced by a gas/steam discharge in water pools. The experimental investigations covered various phenomena, such as complete and incomplete steam condensation, thermal stratification in the water pool, bubble-column induced gas-liquid hydrodynamics, and air blowdown behaviour in

the water pool to quantify dynamic pressure loadings.

Dry aerosol resuspension experiments in THAI test facility investigate the interaction of aerosols with hydrogen deflagrations. The experimental configuration and the test methodology used for the three THAI tests AER-1, AER-3 and AER-4 investigating dry aerosol resuspension is shown in Figure 10. In the first step, a layer of aerosol depositions has been prepared on a floor close to the vessel bottom by injecting CsI aerosol into the test vessel and subsequent settling over a 24 hours period. Then the 5.5 m long vertical deflagration tube has been filled with a hydrogen-air mixture. In step 2, after ignition at the lower end of the deflagration tube the hydrogen-air mixture burns in upward direction towards the closed top end. The burnt gases expand and escape through the bottom pipe and are directed by a slit nozzle in horizontal direction over the aerosol deposits. The escaping gas jet velocities over the deposition plate are in the range of 17 m/s to 67 m/s. Significant portions of the deposited aerosol become re-suspended, and the resulting aerosol concentration in the gas atmosphere is measured by bulk-filter sampling. Before initiation of the deflagration, majority of the aerosol particles had been deposited over surfaces and only very fine particles contribute to the measured low mass concentration in the gas atmosphere. Immediately after the deflagration, the measured particle size shows a large fraction of coarse particles. The test conditions before and after ignition in AER-1, AER-3, and AER-4 tests are compiled in Table 2.

By using THAI experimental data, a source term calculation was performed with COCOSYS [13]. For the calculation purpose, a hydrogen deflagration was assumed in a KONVOI type reactor. The performed COCOSYS calculations show that high air velocities produced by energetic deflagration may resuspend already deposited aerosols resulting into an increase of the released aerosol mass up to a factor of 10 higher than aerosol mass available for release without resuspension.

The potential impact of hydrogen deflagration on oxidation behaviour of metal iodides (e.g. CsI) and any effect on iodine volatility by changing

its speciation were not considered in the THAI aerosol resuspension tests. However, THAI PAR tests (see section VII) as well as previous experimental investigations reported in [15] on interaction between hydrogen combustion and metal iodides showed a conversion yield of up to 75 % depending on the investigated H<sub>2</sub> concentrations, aerosol compositions and aerosol particles size. However, the influence of various parameters (aerosol concentration, aerosol size, co-aerosol effect, and influence of steam content) was mentioned to be not very well understood and therefore additional experiments are required to further investigate potential impact of hydrogen deflagration induced thermal conditions on oxidation behaviour of metal iodides as well as on iodine speciation under containment typical geometry and gas atmosphere (e.g. paint, aerosols, steam).

## IX. CONCLUSION AND PERSPECTIVES

The main objectives of the experiments in the THAI test facility are to supply safety-relevant information in the area of hydrogen and fission product transport under prototypical severe accident conditions. The THAI dimensions and its operational features facilitate providing database on phenomena oriented and coupled effects experiments for validation and further development of coupled thermal hydraulic, aerosol and iodine codes used for severe accident analyses. In the present paper, an overview has been provided on the THAI experiments investigating volatility, distribution and transport behaviour of iodine and aerosols in the containment.

THAI experiments fill gaps and also enlarge the existing knowledge on iodine behaviour in gas/liquid phase under severe accident typical thermal hydraulic conditions and interactions with exposed steel/painted surfaces, gas mixtures, radiolysis by-product ozone, water pools, and aerosols. Based on THAI experimental findings, important progress has been achieved in aerosol and iodine modelling and their coupling with containment-typical thermal hydraulics. The improved models have demonstrated reliable simulation of complex experiments, e.g. hydrogen distribution experiment (ISP-47 and NEA THAI code

benchmark), hydrogen combustion behaviour (ISP-49), hydrogen mitigation by PARs (NEA THAI-2 code benchmark), iodine/surface interactions, iodine mass transfer, and iodine transport and multi-compartment behaviour (EU-SARNET and EU-SARNET2).

In the currently running national project, extension of the THAI test facility to two-vessel geometry is planned. The extended THAI facility will retain its unique experimental features, e.g. use of H<sub>2</sub> and iodine I-123 tracer, differential wall heating/cooling. Moreover, by establishing independent desired flow and temperature conditions in two vessels, it will be possible to approach realistic similarities to reactor scenarios. Experimental investigation on wash-out behaviour of iodine by water spray is also planned to be tested as a function of the spray water chemistry, i.e. the difference of spraying with fresh water and recirculated sump water.

A follow up of the recently concluded NEA THAI 2 project is currently under discussion to resolve remaining open issues in the fields of thermal hydraulics, hydrogen deflagration, Passive Autocatalytic Recombiner performance, aerosols and iodine. Some of the proposed experiments will benefit from the extended THAI test facility. The fission product topics are proposed to include aspects of fission product release from hot water pools and of gaseous iodine in complex boundary conditions including the presence of aerosol and the effect of hydrogen deflagration. The coupled-effects nature of the proposed fission product experiments would be valuable in improving the prediction capabilities of the severe accident analysis tools.

#### ACKNOWLEDGMENTS

THAI experimental research programme is funded by the German Federal Ministry for Economic Affairs and Energy, on the basis of a decision of the German Bundestag (Projects number 1501218, 1501272, 1501325, 1501326, 1501361, 1501420, 1501455). The sponsorship by the countries of the NEA THAI and NEA THAI2 is gratefully acknowledged.

#### REFERENCES

1. G. Weber and F. Funke, "The iodine model AIM-3 in COCOSYS – an overview", 3<sup>rd</sup> COCOSYS workshop, GRS, Garching, June 23 – 25 (2009).
2. OECD/NEA, "Behaviour of iodine project, final summary report. Nuclear safety", NEA/CSNI/R(2011)11 (2012).
3. F. Funke, S. Gupta, G. Weber, G. Langrock, G. Poss, "Interaction of gaseous I<sub>2</sub> with painted surfaces and aerosols in large-scale THAI tests", *Proceedings of the International OECD-NEA/NUGENIA-SARNET Workshop on the Progress in Iodine Behaviour for NPP Accident Analysis and Management*, Paper no. 3-5, Marseille, France, March 30 - April 1 (2015).
4. G. Weber, L. E. Herranz, M. Bendiab, M. Fontanet, F. Funke, B. Gonfiotti, I. Ivanov, S. Krajewski, A. Manfredini, S. Paci, M. Pelzer, T. Sevón, "Thermal-hydraulic-iodine chemistry coupling: insights gained from the SARNET benchmark on the THAI experiments Iod-11 and Iod-12", *Nuclear Engineering and Design*, 265, 95 – 107 (2013).
5. G. Weber, F. Funke, W. Klein-Hessling, S. Gupta, "Iodine and silver wash-down modelling in COCOSYS-AIM by use of THAI results", *Proceedings of the International OECD-NEA/NUGENIA-SARNET Workshop on the Progress in Iodine Behaviour for NPP Accident Analysis and Management*, Paper no. 2-1, Marseille, France, March 30 - April 1 (2015).
6. G. Weber, L. Bosland, F. Funke, G. Glowa, T. Kanzleiter, "ASTEC, COCOSYS, and LIRIC interpretation of the iodine behaviour in the large-scale THAI test Iod-9", *Proceedings of 17<sup>th</sup> International Conference on Nuclear Engineering*, ICONE-17, Brussels, Belgium, July, 12 - 16 (2009).
7. K. Fischer, M. Freitag and H. S. Kang. Mechanistic model of iodine mass transfer at pool surfaces. In *Nuclear Engineering and Design*, 278, 627-631, (2014).
8. M. Hoehne and G. Weber, "Interpretation of the THAI CsI aerosol wash down test AW by COCOSYS analyses", *NEA THAI project final seminar*, Paris, 06 - 07 October (2010).
9. G. Weber, B. Krzykacz-Hausmann, F. Funke, W. Klein-Hessling, "Uncertainty and Sensitivity Analysis on the Iodine Model in the Containment Code COCOSYS", *NUTHOS-10 Conference*, Okinawa, Japan, December 14-18 (2014).

10. F. Funke, G. Langrock, T. Kanzleiter, G. Poss, K. Fischer, A. Kühnel, G. Weber, H.-J. Allelein, "Iodine oxides in large-scale THAI tests", *Nuclear Engineering and Design*, 245, 206-222 (2012).
11. J.C. Sabroux and F. Deschamps, "Iodine chemistry in hydrogen recombiners", *Eurosafe forum on Nuclear safety*, Brussels (2005).
12. H. Bunz, M. Koyro, B. Propherer, W. Schöck, W. Wagner-Amb, "Resuspension of fission products from sump water", *Final Report, European Commission EUR 14635 EN* (1992).
13. H. Nowack, and H.-J. Allelein, "Dry aerosol resuspension after a hydrogen deflagration in the containment", *Proceedings of international conference on nuclear energy for new Europe*, Slovenia, September 10 – 13 (2007).
14. S. Gupta, B. Balewski, K. Fischer, G. Poss, "Experimental investigations of BWR pressure suppression pool behaviour under loss of coolant accident conditions", *Proceedings of ICAPP-11 conference*, Paper 11389, Nice, France (2011).
15. Committee on the Safety of Nuclear Installations, OECD Nuclear Energy Agency, "Effects of hydrogen combustion on fission products and aerosols", *Technical note by a group of experts*, Report number NEA/CSNI/R (93) 6 (1993).

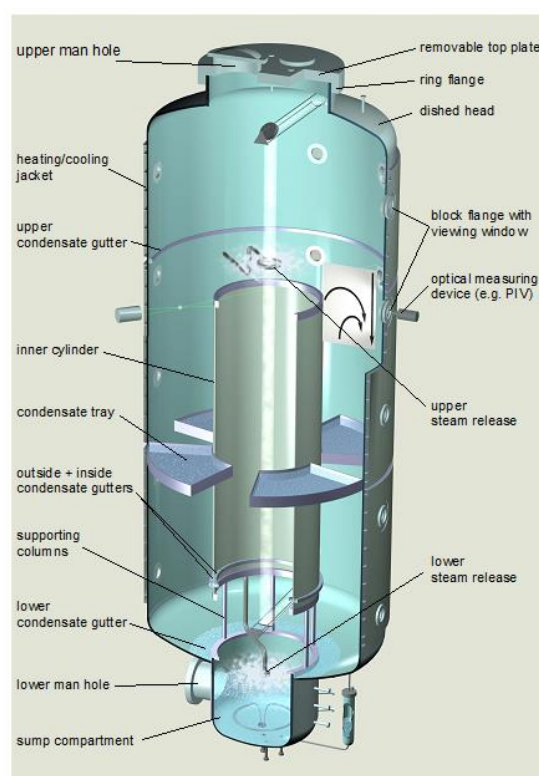


Figure 1: THAI test vessel with standard internals

Table 1: Overview of THAI tests investigating iodine and other fission product related issues. Tests not specifically marked have been conducted in the frame of national THAI projects (2000-2015).

Topic	THAI test	Main condition
I <sub>2</sub> deposition onto steel	Iod-6, Iod-7, Iod-9 (first phase) Iod-16, Iod-18	Dry steel walls; temperature and humidity transients
	Iod-22	Dry steel walls; atmospheric convection forced by a blower
	Iod-8	Wet steel walls; weak and strong wall condensation
I <sub>2</sub> deposition onto paint	Iod-15, Iod-17, Iod-20	Large painted areas at dry condition; temperature and humidity transients
	Iod-21, Iod-24	Large painted areas at wet condition; different wall condensation rates
I <sub>2</sub> /ozone reaction	Iod-13, Iod-14	IO <sub>2</sub> aerosol formation and behavior at different I <sub>2</sub> to O <sub>3</sub> ratios; superheated atmosphere
	Iod-9 (second phase) Iod-23	I <sub>2</sub> transfer from atmosphere into sump; sump stratified and mixed
I <sub>2</sub> mass transfer gas/sump		I <sub>2</sub> transfer from sump to atmosphere; influence of sump water motion (stratified and agitated)
I <sub>2</sub> deposition onto aerosols	Iod-25 (OECD/NEA THAI2)	I <sub>2</sub> deposition onto non-reactive SnO <sub>2</sub> aerosol
	Iod-26 (OECD/NEA THAI2)	I <sub>2</sub> deposition and chemisorption onto reactive Ag aerosol
I <sub>2</sub> transport in a multi-compartment geometry	Iod-10	I <sub>2</sub> distribution in 5-compartment geometry with steel walls at dry atmosphere (Iod-10), humid atmosphere (Iod-11) and with wall condensation (Iod-12)
	Iod-11 (repetition) Iod-12	
	Iod-27a	I <sub>2</sub> distribution in 5-compartment geometry painted areas and steel walls at very dry atmosphere (Iod-27a), humid atmosphere (Iod-28) and with an additional Ag aerosol injection (Iod-30)
	Iod-28	
I <sub>2</sub> transport in a multi-compartment geometry with painted areas	Iod-30	
Gaseous iodine release by a flashing jet	Iod-29 (OECD/NEA THAI2)	Quantification of gaseous iodine release under thermal hydraulic conditions of a steam generator tube rupture during reactor shutdown. Simulation of 40 bar pressure drop by use of an external pressure vessel
Iodine/Passive Autocatalytic Recombiner (PAR) interaction	HR-31 (OECD/NEA THAI)	Superheated, high CsI aerosol concentration, catalyst surface > 800 °C; CsI conversion to gaseous iodine
	HR-32(OECD/NEA THAI)	Saturated test condition, inert and hygroscopic aerosols mixture; PAR poisoning
Aerosol wash down	AW (OECD/NEA THAI)	Wash-down of soluble CsI aerosol by wall condensate; retention in a puddle
	AW2	Wash-down of a mixed CsI /SnO <sub>2</sub> aerosol (soluble/insoluble) by wall condensate; retention in a puddle
	AW3 (part 1)	Wash-down of insoluble Ag aerosol by wall condensate
	AW3 (part 2)	Reaction of iodine with particulate Ag in sump at mixed and stagnant conditions
	AW4	Airborne CsI aerosol washout by spray

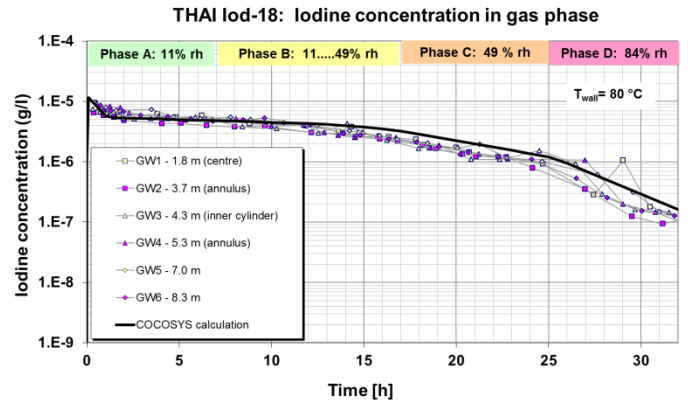


Figure 2: Comparison of COCOSYS I<sub>2</sub> /steel model with data from THAI Iod-18

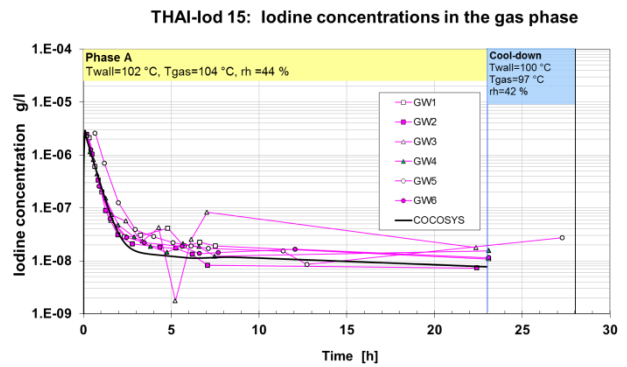


Figure 3: Comparison of COCOSYS I<sub>2</sub> /paint model with data from THAI Iod-15

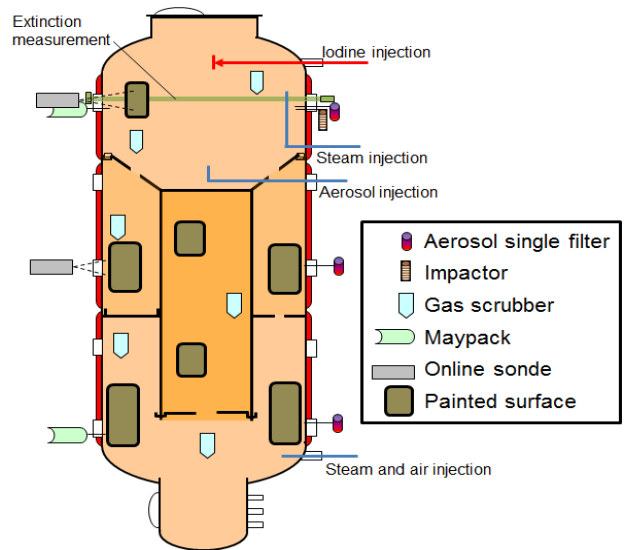


Figure 4: An example of THAI test configuration used in Iod-30 iodine multi-compartment test conducted in the presence of high relative humidity and aerosol

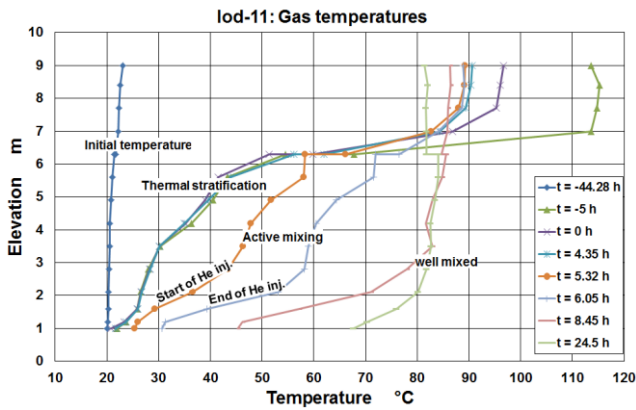


Figure 5: Vertical profile of gas temperatures measured during different test phases in Iod-11 test

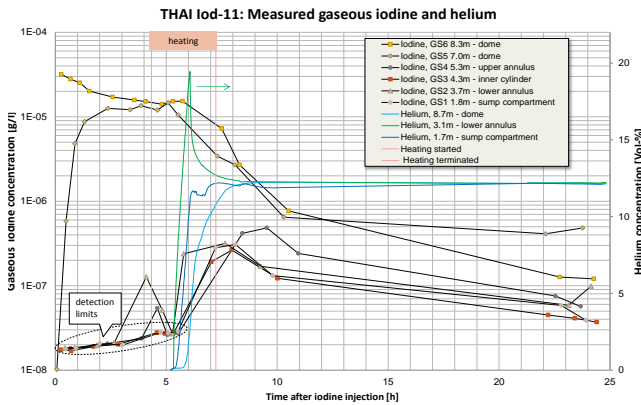


Figure 6: Iodine and helium concentrations measured during different test phases in Iod-11 test

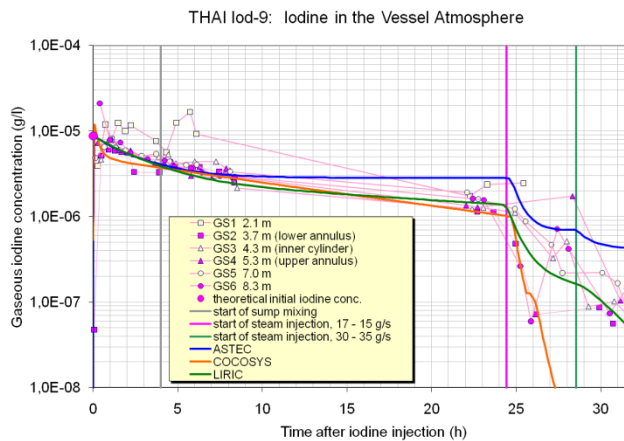


Figure 7: Comparison of measured iodine concentration in gas atmosphere in Iod-9 test with simulation results of COCOSYS, ASTEC and LIRIC [6]

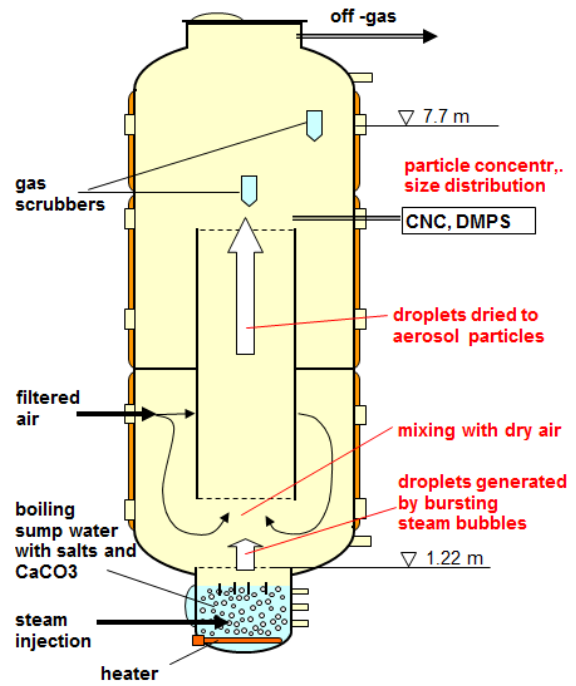


Figure 8: THAI test configuration as used in wet aerosol resuspension tests

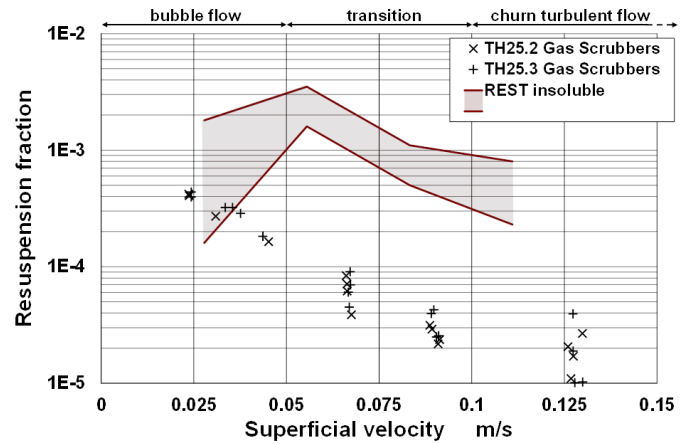


Figure 9: Calcium carbonate resuspension fractions derived from gas scrubber based measurements

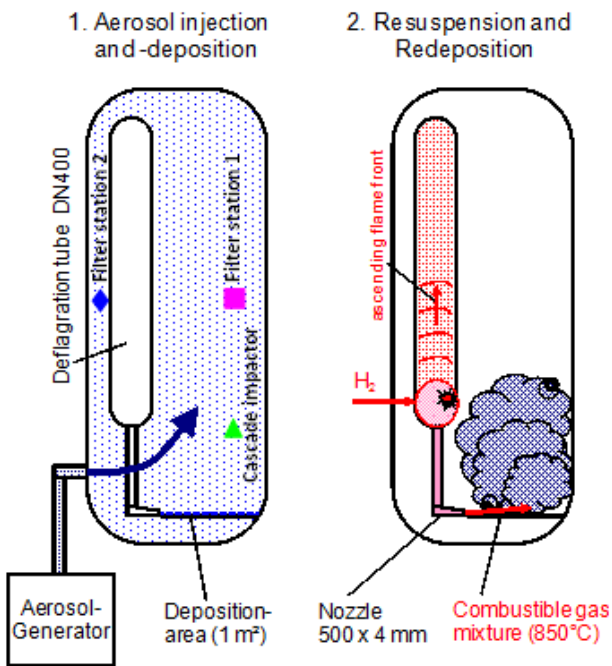


Table 2: Dry aerosol resuspension tests: selected test conditions before and after the deflagration

... Deflagration		Aer-1	Aer-3	Aer-4
Surface loading before...	g/m <sup>2</sup>	14.4	19.8	10.6
Air-borne aerosol concentration before ...	g/m <sup>3</sup>	0.0044	0.0035	0.0013
MMD d <sub>50,3</sub> before ...	µm	0.938	0.814	0.715
Temperatur	°C	875	810	750
Blown-out area	mm x mm	500 x 1000	600 x 1300	500 x 500
Air-borne aerosol concentration after ...	g/m <sup>3</sup>	0.0807	0.2419	0.0424
MMD d <sub>50,3</sub> after ...	µm	1.526	1.857	1.547

Figure 10: THAI test configuration and main steps of the test procedure used in dry aerosol resuspension tests

## A SUMMARY OF THE PSI INVESTIGATIONS ON IODINE CHEMISTRY IN THE PRESENCE ON IMPURITIES AND ADDITIVES

T. Lind<sup>\*1</sup>, B. Jäckel<sup>1</sup>, D. Suckow<sup>1</sup>, S.Guentay<sup>2</sup>

<sup>1</sup>Paul Scherrer Institute, Villigen-PSI, Switzerland

<sup>\*</sup>Corresponding author, tel: (+41)310 2650, Email terttaliisa.lind@psi.ch

<sup>2</sup>Presently at: Innovative Technology Development GmbH, Switzerland

**Abstract** – An extensive experimental research project was carried out at PSI in the late 1990s´ until 2008 to investigate the behaviour of different iodine species in water pools. The first part of the project was devoted to generation of an easy and effective preparation of labeled organic iodide aqueous solution, iodine speciation analysis techniques, and experiments to study the basic decomposition mechanism of methyl iodide  $CH_3I$  by water hydrolysis and radiolysis. In the later stages, the effect of different impurities in the water on the iodine volatility was investigated. The latest research had its emphasis on the use of additives for improved retention of organic iodides in the water pools, and the mitigation of the release of iodine species under conditions relevant to filtered containment venting systems. In addition, a dedicated tool, PSIIodine, was developed for interpretation of the experimental results.

Many of the results of the investigations have been already reported in the open literature and in the research programs such as SARNET. This work will be shortly summarized here. Some unpublished work mainly related to the iodine and organic iodide retention in the filtered containment venting systems are presented, and conclusions are made based on the results.

## I. INTRODUCTION

PSI has conducted several experimental and modelling research programs on iodine chemistry and iodine / iodide retention since the 1990's. Experimental investigations have covered the range from very small-laboratory scale investigations to 1:1 height scale experiments for filtered containment venting systems (FCVS), and from inactive species to irradiation experiments in the PSI Hot laboratory. A mechanistic PSIodine code has been developed to interpret the results of the experimental investigations. In this paper, we will give an overview of the developments mainly after year 2002. The latest work on characterization of the FCVS operation as well as development of a method for improved organic iodide retention in the FCVS are presented in a separate paper in this publication (Suckow et al., 2015).

At PSI, the research on iodine chemistry after the year 2002 has mainly concentrated on the effect of impurities on the volatility of the different iodine species in aqueous solutions, decomposition of methyl iodide in water solutions in the presence of additives, and characterization of the retention of iodine and iodides in the FCVS. This work has been preceded and accompanied by fundamental investigations devoted to generation of an easy and effective preparation of labeled organic iodide aqueous solution, iodine speciation analysis techniques, as well as experiments studying the basic decomposition mechanisms of  $\text{CH}_3\text{I}$  by water hydrolysis and radiolysis. The results have demonstrated the repeatability of the literature results and extended the database to other conditions, such as in-situ beta-irradiation effects. Special emphasis has been to characterize the behaviour of organic iodides, mainly  $\text{CH}_3\text{I}$ , and to investigate the effects of different additives with the aim to increase the  $\text{CH}_3\text{I}$  decomposition rate.

## II. EXPERIMENTAL METHODS

The experimental work was carried out in different facilities representing different scales. Fundamental investigations of iodine chemistry in water pools was carried out in small laboratory-scale devices and in the hot cells.

Intermediate scale tests were carried out to study the effect of gas flow through the water pools with realistic residence times at two different facilities. The retention of iodine and organic iodide in FCVS was investigated in 1:1 height scale experimental facility.

Here we describe the facilities and experiments in two different scales, the small laboratory-scale and the 1:1 height scale.

### *Small laboratory-scale set-up*

Two types of reaction vessels were employed for the experiments in the small laboratory-scale. A specially-designed reaction vessel, and commercially available small bottles which are employed in the pharmaceutical industry were used.

The specialized reaction vessel in the irradiation chamber of the gamma cell, Figure 1., in the PSI's Hot Laboratory was used for several tests involving irradiation of mixtures of initially non-volatile iodide and various accident-relevant compounds. It was also used to pre-irradiate investigated reagents. The vessel contains a frit near its inside bottom to pass bubbles of a selected gas through the irradiated or unirradiated solution (sparging). The gas then passes out of the vessel and into a glass tube containing a solid-phase absorber selected for either  $\text{I}_2$  or  $\text{CH}_3\text{I}$  absorption for activity measurements. The gas flow rate was electronically controlled. Such a facility also enabled determination of the mass transfer coefficients of  $\text{I}_2$  and  $\text{CH}_3\text{I}$  for the particular reaction vessel in use. The reaction vessel was also jacketed to perform experiments at higher temperatures.

The majority of experiments were carried out in glass pharmaceutical bottles of capacity  $37 \text{ cm}^3$ . The bottle was closed by a PTFE (Polytetrafluoroethylene)-lined rubber septum cap. This cap enabled experiments with still and sparged test solutions. Two syringe needles pierce the septum cap. They are connected to the regulated gas flow and tube containing the solid phase material to trap volatile iodine species respectively. Thus sparging either

during or after irradiation or after a pre-defined period for the thermal (unirradiated) reactions can be carried out.

For the tests, aqueous solutions were prepared from analytical grade reagents, e.g., CsI, KNO<sub>3</sub>, KNO<sub>2</sub>, CsCl, B(OH)<sub>3</sub> without further purification. Water was doubly distilled from demineralised water. The sparging gases used were argon, nitrous oxide and air of 99.999% purity. For air-sparged experiments, synthetic air was used (80% N<sub>2</sub>, 20% O<sub>2</sub>). A tracer <sup>131</sup>I was used to determine the distribution of iodine species in the gas phase and in the solution by activity measurements. For this purpose, gas phase species were collected in an activated carbon filter impregnated with tri-ethylene-diamine (TEDA).

To control the pH of the water, test solutions were usually buffered. The required initial pH from 7 to 9 was obtained by boric acid and sodium borate mixtures, or by sodium hydroxide addition to boric acid solution. The higher initial pH was obtained by either sodium hydroxide or sodium carbonate addition. For tests in the highly acidic range of pH 2 to 4, sulphuric acid or nitric acid were used at appropriate concentrations.

More detail of the facility, methods and measurements are given by Cripps et al., 2010.



Figure 1. The reaction vessel shown within the irradiation chamber of PSI's  $\gamma$ -irradiation cell.

### *1:1 height scale FCVS facility*

The retention on iodine (I<sub>2</sub>) and methyl iodide in the FCVS was investigated in the 1:1 height scale, reduced diameter facility, Figure 2. In order to represent the most important hydrodynamic features of the FCVS, the facility had all the internals of a commercial FCVS, including the injection nozzle, water pool with mixing elements, and different components of the droplet separators. The water level above the injection orifice could be varied.

The full height of the facility enabled a similar residence time for the gas as in the real scale FCVS. The volume and flow rate scaling factor of the facility was 1:124. The facility dimensions are given in Table 1. The operation pressure of the facility was 5 bar(abs), and temperature 200°C. The carrier gas was air / nitrogen, steam, or a mixture of steam and air / nitrogen.

The experiments for iodine / CH<sub>3</sub>I retention in the FCVS were carried out using the relevant additives in the water, namely, Na<sub>2</sub>S<sub>2</sub>O<sub>3</sub> for retention of iodine compounds, and Na<sub>2</sub>CO<sub>3</sub> to control the pH.

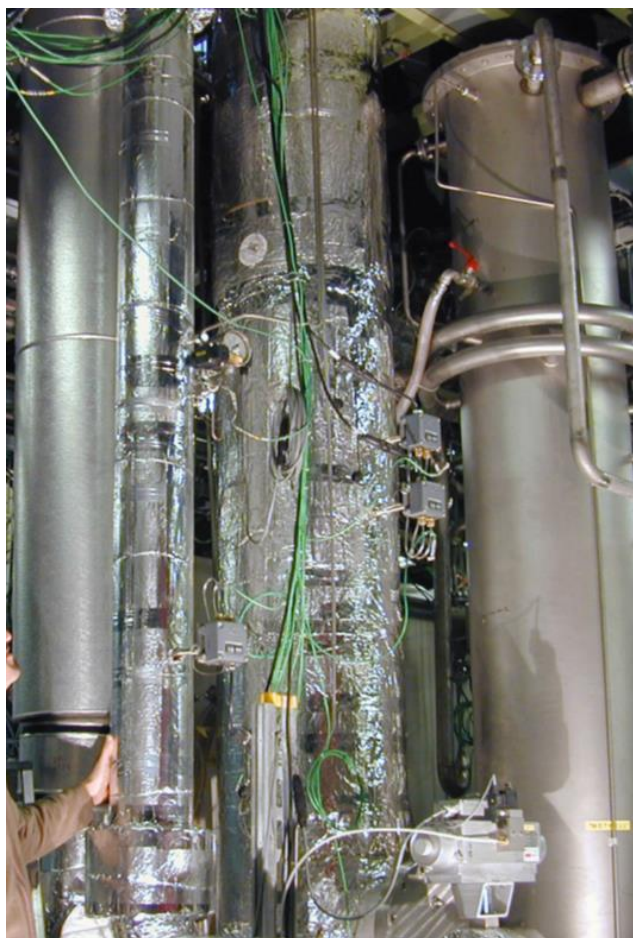


Figure 2. The 1:1 height scale FCVS facility used to determine retention of iodine and CH<sub>3</sub>I

The gaseous elemental iodine was generated by dissolving iodine crystals in about 100 ml alcohol. The resultant solution was then poured into the feed tank to provide a desired elemental iodine concentration in water. Similarly the organic iodide was generated by mixing organic iodide solution in a known amount of demineralised water. The mixer in the 70 l tank secured a homogenous mixture of water and methyl iodide; otherwise a segregation of the phases might take place.

Depending on the experiment one or both components of the iodine was mixed in the liquid feed tank. The liquid mixture was then pumped into a two-component spray nozzle to spray the water in form of extremely fine droplets. The spray nozzle was attached to the mixing chamber of the DRAGON II facility. The gas needed for disintegrating the water jet into fine droplets was hot nitrogen. Additional nitrogen flow was heated and directly fed into the mixing chamber. The walls of the mixing chamber were heated up to avoid steam condensation as well as providing additional energy for droplet evaporation. The desired organic iodide or elemental iodine concentration in the steam-nitrogen mixture flow was adjusted by selecting a feasible combination of spray flow rate and the dissolved organic iodide or elemental iodine concentration in the sprayed water.

The retention of iodine and methyl iodide in the test section was determined by measuring simultaneously iodine / CH<sub>3</sub>I concentration at the test section inlet and outlet. Iodine concentration was measured with selective iodide ion electrodes. For the electrodes, the sample gas was bubbled through a scrubber filled with water doped with ascorbine acid. The methyl iodide concentration was measured with a mass spectrometer.

Table 1. FCVS facility dimensions and operation conditions

Inner diameter [m]	0.27-0.40
Height [m]	6.0
Cross sectional flow area [m <sup>2</sup> ]	0.06-0.13
Number of injection nozzles	1
Average gas velocity [m/s]	0.26-0.57
Pressure [bar,abs]	4.9
Gas temperature [°C]	152
Gas flow rate [kg/h]	350

### III. RESULTS OF THE EXPERIMENTAL PROGRAMMES

Several experimental programmes were carried out at PSI in the different scales as described in the previous section. The focus of the work was partly on the FCVS efficiency for different

iodine compounds, and partly on understanding the iodine chemistry on a more general context with a recent focus on the effect of impurities on iodine volatility. In this section we give an overview of the activities in these areas.

### ***Iodine and organic iodide retention in the FCVS***

Iodine (I<sub>2</sub>) and organic iodide (CH<sub>3</sub>I) retention in the FCVS was investigated in five tests in which either I<sub>2</sub>, CH<sub>3</sub>I, or both were used. CH<sub>3</sub>I was used to represent the organic iodides as the most volatile of them. The temperature in the tests was varied in the range 70-120°C, and the FCVS inlet pressure was 4.4 bar (abs). The steam mass fraction in the gas flow was approximately 0.7-0.8, and the total flow rate 325-350 kg/h. The additives relevant to FCVS were used in the water in the wet scrubber, i.e., Na-thiosulfate for retention of iodine, and Na<sub>2</sub>CO<sub>3</sub> for pH control in the tests when high pH was used. No other additives were used in the water. The experimental conditions are given in Table 2.

Table 2. Experimental conditions in the I<sub>2</sub> and CH<sub>3</sub>I retention tests in the FCVS.

Test #	I <sub>2</sub>	CH <sub>3</sub> I	Na <sub>2</sub> S <sub>2</sub> O <sub>3</sub>	Na <sub>2</sub> CO <sub>3</sub>
B01	Yes	-	Yes	-
B02	-	Yes	Yes	Yes
B03	Yes	Yes	Yes	Yes
B04	-	Yes	Yes	Yes
B05	Yes	-	Yes	-

Table 2. continues. Experimental conditions in the I<sub>2</sub> and CH<sub>3</sub>I retention tests in the FCVS.

Test #	Water level [m]	Water T [°C]	pH
B01	0.9	120	4.5-5.5
B02	0.9	120	9
B03	1.2	120	9
B04	0.75-1.6	70, 120	9
B05	2.1	120	4.5-5.5

The experiments showed the dependence of gaseous elemental iodine retention on the pH of the water in the wet scrubber, and the water level above the injection orifice, Figure 3. All the iodine retention tests were carried out at the water temperature of about 120°C, see Table 2.

The measured decontamination factors for iodine were around 300-400 with the water level of 1.2 m above the orifice at the initial pH of 11.25 (pH at 20°C). The higher water level would increase the decontamination factor (DF). Consequently, it can be seen that given a sufficient water level above the injection orifice and a high pH in the wet scrubber, high retention of iodine in the wet scrubber can be achieved.

Organic iodide (CH<sub>3</sub>I) retention was investigated in three experiments. The retention was found to depend on the water level and temperature. When the water temperature decreased to 70°C and below, and the water level above the injection orifice was approximately 1 m or less, the CH<sub>3</sub>I retention was low with the decontamination factors 2-10. With the water level of 1.6 m and more, and T = 120°C, decontamination factor was more than 10. The effect of pH on the retention of CH<sub>3</sub>I was not investigated in this experimental program.

Based on the tests, it was concluded that with the existing FCVSs, sufficient retention of gaseous elemental iodine can be achieved when the water level in the wet scrubber can be maintained at a high level, and the pH is high. However, the retention of CH<sub>3</sub>I without any further actions is relatively modest. It has to be noted that other organic iodides than methyl iodide were not investigated. They are typically less volatile than methyl iodide, and are therefore considered to pose less challenges in terms of environmental releases. Following this investigation, it was decided to concentrate the PSI efforts in the iodine research on finding solutions to retain CH<sub>3</sub>I more efficiently in the FCVS and other water reservoirs, such as suppression pools in BWRs.

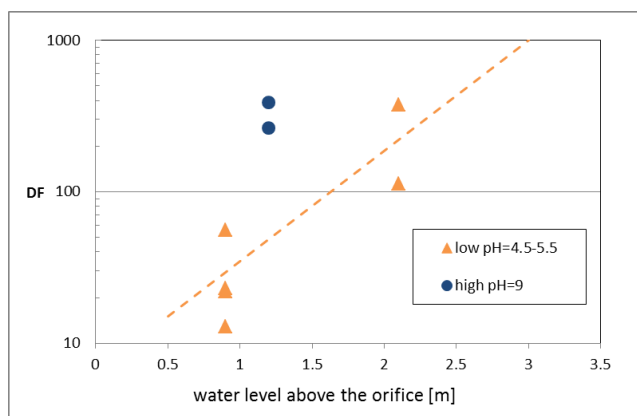


Figure 3. Retention of elemental iodine in the FCVS 1:1 height scale facility (tests B01, B03, B05, Table 2). The dependence of the decontamination factor on the water level above the injection orifice and the pH.

#### *Small-scale experiments for the decomposition of CH<sub>3</sub>I*

PSI has participated in the iodine research by performing basic investigations devoted to generation of an easy and effective preparation of labeled organic iodide aqueous solution, iodine speciation analysis techniques, and experiments studying the basic decomposition mechanism of CH<sub>3</sub>I by water hydrolysis and radiolysis. The results have demonstrated the repeatability of the literature results and extended the database to other conditions, such as in-situ beta-irradiation effects. The effects of different additives were investigated with the aim to increase the CH<sub>3</sub>I decomposition rate.

In this section, we give examples of the PSI work on decomposition of CH<sub>3</sub>I by water hydrolysis and radiolysis. The use of additives to increase CH<sub>3</sub>I retention in water pools will be presented separately. For the hydrolysis, the effect of i) temperature, ii) pH, and iii) initial CH<sub>3</sub>I concentration was studied. The results are given in the form of decomposition rate of CH<sub>3</sub>I as determined based on the laboratory experiments [Cripps et al., 2010]. Tests were also carried out with additives in the water, such as Na<sub>2</sub>S<sub>2</sub>O<sub>3</sub>.

The effect of temperature on the decomposition of CH<sub>3</sub>I is shown in Figure 4. It

shows that the total estimates of first and second order CH<sub>3</sub>I hydrolysis rate constants at up to pH 9 are very slow at 25°C, but increase rapidly up to 90°C. For example, at pH 9, after 6 days at 22°C, only about 4% of the initial CH<sub>3</sub>I was decomposed, but 13% was decomposed after only 45 minutes at 70°C. When comparing the reaction rate constants at pH 5 and pH 9 with the predicted rates, determined using the Borkowski equation [Borkowski, 1985], shown in Figure 4, and with literature data [Parsly, 1971], our measured data is in agreement with the literature data within the scatter and uncertainties of both sources. The literature data suggest that at temperatures from 70°C to 150°C, the hydrolysis rate increases further by a factor of about 103.

The effect of temperature on the hydrolysis of CH<sub>3</sub>I was also investigated with added Na<sub>2</sub>S<sub>2</sub>O<sub>3</sub> in the water to apply the results to FCVS. Figure 5 shows the comparison with literature predictions. The discrepancy at higher temperatures was attributed by the authors to the experimental difficulties at high temperatures.

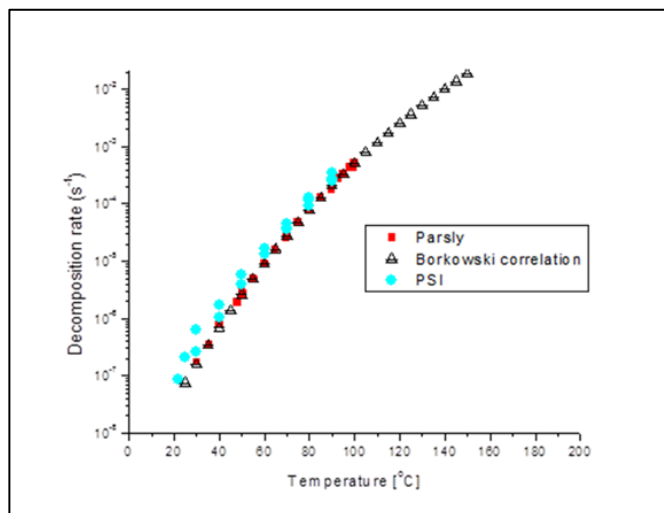


Figure 4. CH<sub>3</sub>I hydrolysis rates at pH 9 vs. temperature, comparison of the literature and PSI data.

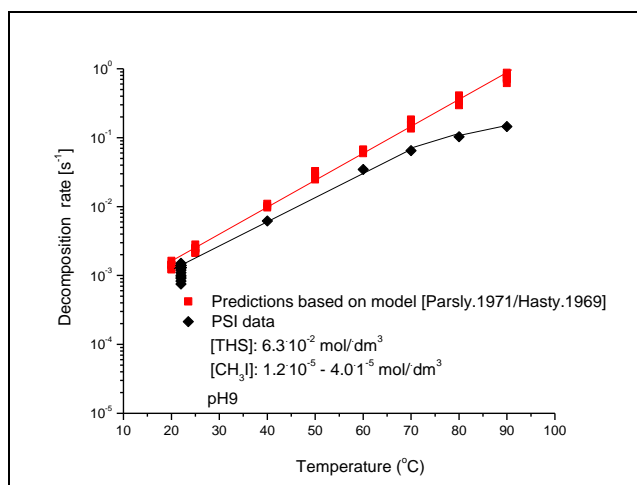


Figure 5.  $\text{CH}_3\text{I}$  decomposition rates vs. temperature with  $\text{Na}_2\text{S}_2\text{O}_3$  added in the water, comparison of the prediction based on literature and PSI experimental data.

Several experiments were conducted to determine the effect of pH on the hydrolysis rate. The data show that the hydrolysis reaction rates at pH 5 and pH 9 are relatively similar. These small rate differences are approximately repeated at different temperatures. From pH 9 to 14, the decomposition rates become higher: by about 1000 times larger at pH 14 than that at pH 9. This trend is in agreement with the predicted rate constants at 25°C. The increased decomposition rate is presumably due to the high  $\text{OH}^-$  concentration at  $\text{pH} > 11$ . For experiments with  $\text{pH} \geq 11$ , sodium bicarbonate was also used, since it is used in containment venting filter solutions of some Swiss NPPs.

The pH dependence was also determined with the added  $\text{Na}_2\text{S}_2\text{O}_3$  in the water, Figure 6. The decomposition of  $\text{CH}_3\text{I}$  does not show significant dependence on the pH except for some reduced decomposition at a very low  $\text{pH} < 2$ .

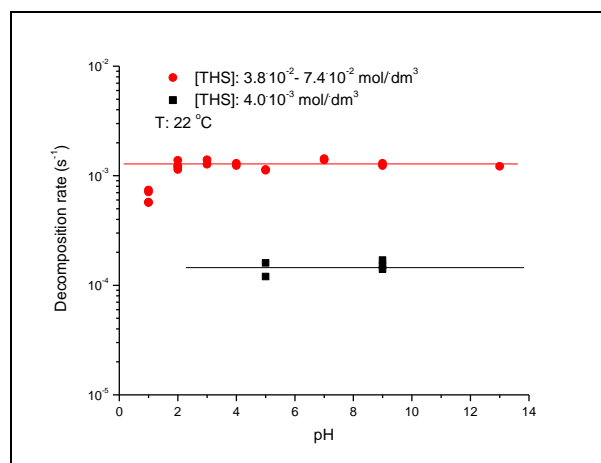


Figure 6.  $\text{CH}_3\text{I}$  decomposition rates vs. pH for different  $\text{Na}_2\text{S}_2\text{O}_3$  concentrations at 22 °C.

Further tests were carried out to determine the dependence of the  $\text{CH}_3\text{I}$  decomposition rate on the concentration of  $\text{CH}_3\text{I}$  and  $\text{Na}_2\text{S}_2\text{O}_3$ . Figure 7 shows that within the experimental uncertainty, the  $\text{CH}_3\text{I}$  decomposition rate does not depend on the initial  $\text{CH}_3\text{I}$  concentration.

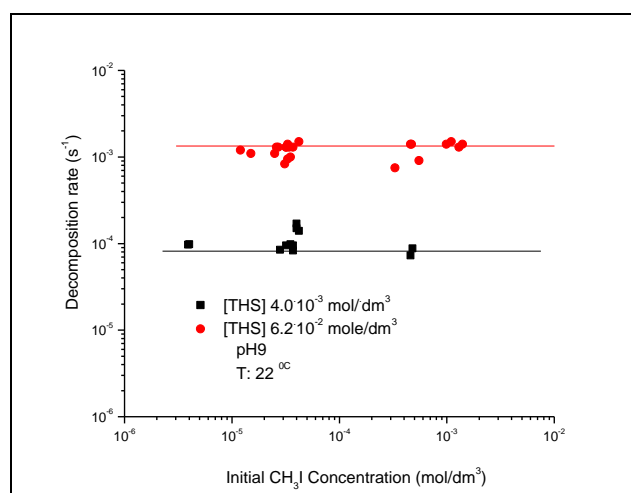


Figure 7.  $\text{CH}_3\text{I}$  decomposition rates vs.  $\text{CH}_3\text{I}$  for two  $\text{Na}_2\text{S}_2\text{O}_3$  concentrations at 22°C.

$\text{CH}_3\text{I}$  decomposition by radiolysis was investigated with and without additives in the water. At  $\text{pH} = 9$  and  $T = 22^\circ\text{C}$ , the decomposition increases with the cumulated dose, Figure 8.

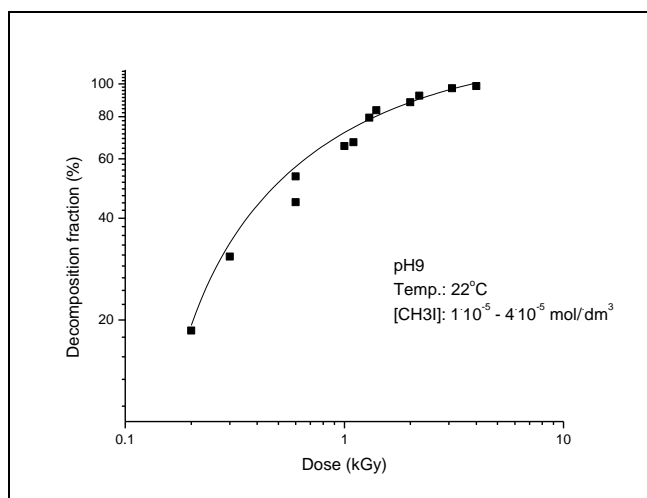


Figure 8.  $\text{CH}_3\text{I}$  decomposition fraction versus radiation dose.

#### *Effect of impurities on iodine behaviour*

In the containment atmosphere and sump during a postulated severe reactor accident, many elements, fission product compounds and structural materials, collectively known as ‘impurities’ are anticipated and measured in gaseous, dissolved or solid form [Hanniet-Girault and Repetto, 1999; Jacquemain et al., 2000]. Via various transport pathways, these constituents may end up in the sump, suppression pool, or FCVS. Once resident in aqueous solution, the potential effects of these ions as well as the effects of their products on iodine chemistry should be understood. To increase this understanding, PSI investigated the effect of the impurities nitrate, nitrite and chloride ions and associated species on iodine volatility by performing experiments (both sparged and unsparged) and by modelling chemical reactions. The species for investigation were as follows:

- I. nitrate ions;
- II. nitrite ions;
- III. chloride ions;
- IV. modelling of other dissolved fission products measured in the sumps of Phébus FP tests.

This work has been reported in the SARNET frame in a nine part report [Cripps et al., 2010] and appeared as a scientific publication

[Cripps et al., 2011], and therefore, only a short summary of the main results is given here.

The experimental study consisted of small-scale irradiations of CsI, boric acid and tracer containing aqueous solutions. Baseline tests were first carried out without nitrate or nitrite ions to obtain results to confirm expected iodine behaviour by correlation with predicted results, which were generated by concurrently developed code PSIodine. The solutions were sparged with  $\text{N}_2\text{O}$ , argon and air to provide different net oxidation systems and to remove volatile iodine for measurement. The baseline experiments showed the expected results and the prediction with the model agreed mainly well with the experimental data. Therefore it was concluded that sufficient baseline results showed that the experimental facility and the iodine reactions modelled in the PSIodine code provided a useful basis to investigate the effects of impurities in irradiated solutions on iodine release.

Both experimental and predicted results clearly showed that nitrate or nitrite ions in argon-sparged and irradiated iodide solutions containing boric acid lower iodine volatility up to an initial  $\text{NO}_3^-$  concentration of  $5.0 \times 10^{-3} \text{ mol dm}^{-3}$ , Figure 9. Using a low CsI concentration ( $4.0 \times 10^{-5} \text{ mol.dm}^{-3}$ ) estimated in containment sump during a postulated severe-accident, an initial nitrate concentration ( $10^{-3} \text{ mol.dm}^{-3}$ ) and pH 7.1, 3.6 % volatile iodine was produced by argon sparging at a dose of 20.5 kGy. In contrast, 80% volatile iodine was formed at a dose of 12 kGy in the absence of nitrate ions. Since the radiation chemistry of  $\text{N}_2\text{O}$ -saturated iodide solutions is well established and the measured volatile iodine yields and final pH correlated very well with the PSIodine code predictions, the effect of added nitrite ions to these solutions provided results which support the correct choice of relevant reactions for inclusion in the nitrate-model. As a result, the authors concluded that the nitrate and nitrite reactions could be included in the iodine chemistry codes.

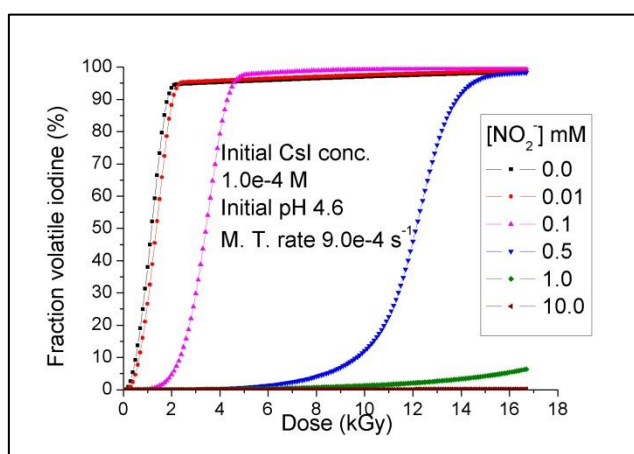


Figure 9. Predicted volatile iodine yields versus dose (kGy) as a function of the initial nitrite concentration (Cripps, 2010).

Chlorine ions in the water were found to have little or no effect on the iodine volatility. There was one unresolved issue of a small increase in cumulative volatility of iodine at a very low pH of 2.5 when both chloride and nitrate were present in the solution [Cripps et al., 2010]. Using only chloride as the impurity, the highest cumulative volatile iodine fraction was observed at the pH of 4.0. Figure 10 shows with the initial pH of 2.5 the fraction of  $I_2$  reaching almost 90% in the test when both chloride and nitrate were used, as well as the corresponding modelling result. When pH was increased in the tests with both chloride and nitrate, the cumulative  $I_2$  fraction was decreased.

The authors noted that as the experiments were mainly carried out with very low concentrations of the reacting species, some the experimental results should be considered as tentative. Also, many of the tests were not repeated, and therefore, for firm conclusions, more tests should be carried out to show the reproducibility of the results.

The experimental and predicted results of this work give sufficient evidence to underline the importance of the effects of nitrate and nitrite ions in irradiated CsI solutions.

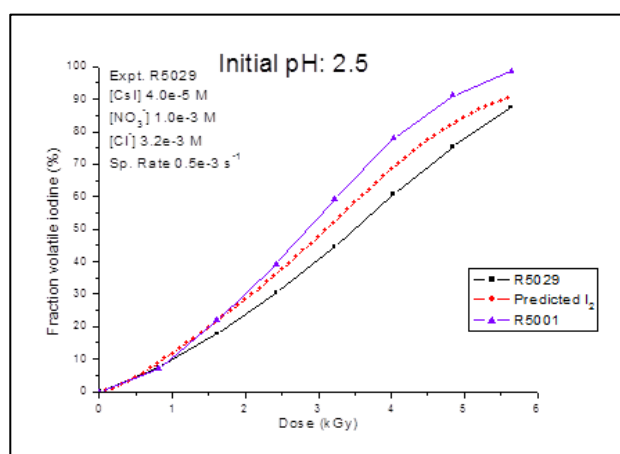


Figure 10. Measured and predicted  $I_2$  fractions when using chloride and nitrate (R5029) or chloride only (R5001) as the impurities in the solution at pH 2.5.

#### IV. PSIODINE CODE

A mechanistic computer code PSIOdine was developed to interpret the results obtained from bench-scale, gas-sparged and irradiated iodide solutions [Cripps et al., 2011]. The code models reactions for the iodine oxidation states  $-1$  to  $+5$  in solution under strong ( $N_2O$ -saturated) and weak oxidising (argon- and air-saturated) conditions. An empirical model was developed to transport  $I_2$  and other species from solution to the gas space by gas bubbles (sparging). By using measured  $I_2$  mass transfer rates for specific reaction vessels, the need to apply assumptions, e.g., uniform and estimated bubble sizes and concentration, diffusion coefficients, was circumvented. By using the same  $I_2$  transfer rate for irradiation of CsI solutions with and without additional ions, data for volatile iodine yields for initial chemical conditions can be compared. Reaction rate changes due to solution evaporation are also modelled. The predicted and experimental data ( $I_2$  fractional releases, pH changes and  $H_2O_2$  formation) correlate well for initial CsI concentrations from  $4.0 \times 10^{-5}$  to  $1.0 \times 10^{-3}$  mol  $dm^{-3}$  and for pH 4.6–7.1 in weak oxidising systems (argon- and air-sparged solutions). Data correlations for strong oxidising conditions ( $N_2O$ -saturated CsI solutions) are also satisfactory. However, the authors recommend that further experiments and model development are necessary to improve data correlations under

conditions particularly relevant to postulated severe accidents in containment.

More details on the PSIodine model is given by Cripps et al., 2011.

## V. CONCLUSIONS

Methods were developed for experimental iodine and  $\text{CH}_3\text{I}$  investigations in different scales. The small laboratory-scale methods were tested by comparing with literature data for  $\text{CH}_3\text{I}$  decomposition by hydrolysis and radiolysis. Further experiments were carried out under severe accident and FCVS relevant conditions.

The small laboratory-scale investigations on the effect of impurities on iodine volatility under irradiation have shown that both nitrite and nitrate ions in the water decrease the formation of volatile iodine. Chlorine in the water has little effect on the iodine volatility. Models for this effect can be implemented in the codes for prediction of iodine behaviour.

The retention of iodine and methyl iodide in the FCVS was investigated in a 1:1 height scale facility. If sufficient water level and high pH can be maintained in the wet scrubber, the retention of iodine is high. The retention of methyl iodide in the wet scrubber using only the chemicals which are typically present in the water of the wet scrubber, e.g.,  $\text{Na}_2\text{S}_2\text{O}_3$  and  $\text{NaOH} / \text{Na}_2\text{CO}_3$ , is limited even at high water temperatures. Consequently, additional substances in the water, or other methods should be used to increase retention of organic iodides in FCVSs.

## ACKNOWLEDGMENTS

This work has been carried out during many years by a large group of scientists many of whom have already retired. A large fraction of the work was carried out by Robin Cripps and Horst Bruchertseifer which is respectfully acknowledged. Over the years, the funding for the work came from various sources, and it is not possible to list here all of them, but we sincerely thank them all. Last, we would like to thank the personnel of the PSI Hot laboratory for providing laboratory resources for this work.

## NOMENCLATURE

BWR = Boiling Water Reactor

DF = Decontamination Factor

FCVS = Filtered Containment Venting System

## REFERENCES

1. D. Suckow, J. Yang, M. Furrer, T. Lind. „Investigation of Iodine Retention in a Filtered Containment Venting System in the VEFITA test program”. OECD-NUGENIA/SARNET workshop on “Progress in Iodine behaviour for NPP Accident Analysis and Management”, Marseille, March 30-April 1, 2015.
2. Borkovski, R. “Untersuchungen zum chemischen Verhalten des Methyljodides bei schweren Störfällen in Druckwasserreaktoren”, KfK Report 3968, Karlsruhe (1985), Germany.
3. R. Cripps, B. Jäckel, H. Bruchertseifer, S. Guntay, 2010. Experimental Results and Model Predictions of Nitrate, Nitrite and Chloride Effects on Iodine Radiolysis Reactions Part 1: Baseline Experiments. Report SARNET2-ST-P3, PSI TM-42-10-03, PSI, Villigen, Switzerland.
4. R. Cripps, B. Jäckel, H. Bruchertseifer, S. Guntay, 2010. Experimental Results and Model Predictions of Nitrate, Nitrite and Chloride Effects on Iodine Radiolysis Reactions Part 2: N<sub>2</sub>O Sparged CsI Solutions Containing Nitrite. Report SARNET2-ST-P4, PSI TM-42-10-04, PSI, Villigen, Switzerland.
5. R. Cripps, B. Jäckel, S. Guntay, 2010. Experimental Results and Model Predictions of Nitrate, Nitrite and Chloride Effects on Iodine Radiolysis Reactions Part 3: Ar-Sparged CsI Solutions Containing Nitrate. Report SARNET2-ST-13, PSI TM-42-10-07, PSI, Villigen, Switzerland.

6. R. Cripps, B. Jäckel, S. Güntay, 2010. Experimental Results and Model Predictions of Nitrate, Nitrite and Chloride Effects on Iodine Radiolysis Reactions Part 4: Air-Sparged CsI Solutions Containing Chloride. Report SARNET2-ST-14, PSI TM-42-10-08, PSI, Villigen, Switzerland.
7. R. Cripps, B. Jäckel, S. Güntay, 2010. Experimental Results and Model Predictions of Nitrate, Nitrite and Chloride Effects on Iodine Radiolysis Reactions Part 5: Air-Sparged CsI Solutions Containing Nitrate. Report SARNET2-ST-15, PSI TM-42-10-09, PSI, Villigen, Switzerland.
8. R. Cripps, B. Jäckel, S. Güntay, 2010. Experimental Results and Model Predictions of Nitrate, Nitrite and Chloride Effects on Iodine Radiolysis Reactions Part 6: Air-Sparged CsI Solutions Containing Nitrate and nitrite. Report SARNET2-ST-16, PSI TM-42-10-10, PSI, Villigen, Switzerland
9. R. Cripps, B. Jäckel, S. Güntay, 2010. Experimental Results and Model Predictions of Nitrate, Nitrite and Chloride Effects on Iodine Radiolysis Reactions Part 7: Air-Sparged CsI Solutions Containing Nitrate and Chloride. Report SARNET2-ST-17, PSI TM-42-10-11, PSI, Villigen, Switzerland.
10. R. Cripps, B. Jäckel, S. Güntay, 2010. Experimental Results and Model Predictions of Nitrate, Nitrite and Chloride Effects on Iodine Radiolysis Reactions Part 8: Air-Sparged CsI Solutions Containing Nitrate and / or Chloride. Report SARNET2-ST-18, PSI TM-42-10-12, PSI, Villigen, Switzerland.
11. R. C. Cripps, B. Jäckel, S. Güntay, 2011. On the radiolysis of iodide, nitrate and nitrite ions in aqueous solution: An experimental and modelling study. Nucl. Eng. Design, 241, pp. 3333-3347.
12. R. C. Cripps, B. Jäckel, S. Güntay, 2011. The PSIodine Code: A computer program to model experimental data on iodine and other species in irradiated CsI solutions sparged with argon, air, or nitrous oxide. Nucl. Eng. Design, 241, pp. 4306-4325.
13. Parsly, L.F., 1971. "Chemical and physical properties of methyl iodide and its occurrence under reactor accident conditions (A summary and annotated bibliography)", ORNL-NSIC-82, (1971).
14. N. Hanniet-Girault and G. Repetto, FPT0 Final Report, IPSN/DRS/SEA/SEA/1/99, Phebus report PH-PF IP/99/423, 1999.
15. D Jacquemain, S Bourdon, A de Bremaeker and M Barrachin, FPT1 Final Report, IPSN/DRS/SEA/1/00, Phebus report PH-PF IP/00/479, 2000.

## RECENT FINDINGS ON RUTHENIUM CHEMISTRY IN A SEVERE ACCIDENT

Teemu Kärkelä<sup>(1)\*</sup>, Christian Mun<sup>(2)</sup>, Gérard Ducros<sup>(3)</sup>, Nóra Vér<sup>(4)</sup>, Marie-Noëlle Ohnet<sup>(2)</sup>, Ivan Kajan<sup>(5)</sup>, Sidi Souvi<sup>(2)</sup>

<sup>(1)</sup>VTT Technical Research Centre of Finland, Espoo, Finland, <sup>(2)</sup>Institut de Radioprotection et de Sécurité Nucléaire, Saint-Paul Lez Durance, France, <sup>(3)</sup>Commissariat à l'énergie atomique et aux énergies alternatives (CEA), Saint-Paul Lez Durance, France, <sup>(4)</sup>Centre for Energy Research (EK), Hungarian Academy of Sciences (MTA), Budapest, Hungary, <sup>(5)</sup>Chalmers University of Technology, Göteborg, Sweden  
\*Corresponding author, tel: (+358) 20 722 5718, Fax: (+358) 20 722 7026, Email:teemu.karkela@vtt.fi

**Abstract** – The chemistry of radiotoxic ruthenium in a severe nuclear power accident has actively been investigated especially during the last decades. The Ru studies have covered the release from a fuel, the transport in the primary circuit and the behaviour in the containment building. The gathered experimental data have been utilized to understand the key parameters governing the Ru chemistry in a severe accident (SA) and to check the ability of the existing models of SA analysis codes to explain the experimental results. To further increase the knowledge on Ru behaviour, the collaboration on international level has been intensive. Lately, the widest and most active networks have been EU SARNET and EU SARNET2. The valuable effort of these networks on sharing information of e.g. national programs and on interpreting the experimental results is continued in EU NUGENIA program. More detailed studies on separate phenomena have been conducted e.g. as part of NEA STEM/START and ISTP/VERDON programs. Furthermore, Phébus FP tests have produced valuable data on integral phenomena.

The large-scale integral and semi-integral experiments have confirmed that Ru release depends strongly on carrier gas. Ru is significantly released from an irradiated fuel sample under oxidizing conditions, in particular when air is involved. In addition, the oxidation of UO<sub>2</sub> fuel seems to lead to a higher Ru release than in case of MOX fuel. Ruthenium can be transported to the containment atmosphere both in gaseous and particulate forms. The small-scale separate-effect experiments gave a detailed view on Ru transport. A high fraction of ruthenium was detected as particles at the outlet of the model primary circuit in an air atmosphere. However, the observed gaseous Ru fraction is higher than what could be expected based on thermodynamic equilibrium calculations. Further studies on the effect of flow residence time in a temperature gradient for the equilibrium of Ru oxides have been conducted.

The effect of other fission products in the gas phase, as well as FP deposits on the surface of primary circuit, on the Ru transport has been investigated. For example, caesium containing deposits seemed to trap gaseous ruthenium effectively. Similarly in case of control rod residues, silver particles in the gas phase of the circuit acted as a sink for gaseous Ru. In an air ingress accident, the effect of air radiolysis products on the Ru chemistry becomes important. As the main air radiolysis products can be considered as oxidizing agents, their ability to oxidize the lower oxides of Ru to higher oxidation state has been examined.

Most of Ru in the containment building ends up as deposits on the containment surfaces and in the sump. Experiments on the radiolytical revaporisation of ruthenium deposits on the epoxy paint surface indicated the release of gaseous ruthenium and it was enhanced under humid atmosphere and elevated temperature. It appeared that the products of air radiolysis caused by  $\gamma$ -radiation promoted the formation of gaseous ruthenium from Ru oxide deposits on paint in a higher amount than could be expected by pure ozone action. Concerning the irradiation tests of perruthenate aqueous solutions, they indicated the formation of gaseous Ru by  $\gamma$ -radiolysis products in solution.

## I. INTRODUCTION

In case of a severe accident (SA) in a nuclear power plant (NPP), when the coolant is lost, fuel will heat-up rapidly leading to a release of some of the fission products that have accumulated in the fuel during a normal operation of NPP. In oxidizing conditions, the release of Ru is probable by formation of volatile ruthenium oxides. The radiotoxicity of these oxides is high both in the short and the long term due to isotopes:  $^{103}\text{Ru}$  with a half-life of 39.3 days and  $^{106}\text{Ru}$  with a half-life of 373.6 days. In order to limit the possible source term, it is of interest to understand the behavior of ruthenium oxides when they are released from the fuel, transported through the reactor coolant system (RCS) or carried along to the atmosphere of containment building.

To increase the knowledge on Ru behavior in SA conditions, the collaboration on international level has been intensive. The effect of oxidizing atmosphere on source term has been one of the high priority open issues in the framework of EC SARNET and SARNET2 (Severe Accident Research NETwork of Excellence) projects [1]. These networks acted as a forum for sharing information of national programs and on interpreting the experimental results. This international collaboration is continued in the frame of EU NUGENIA program. More detailed studies on separate phenomena have been conducted e.g. as part of NEA STEM/START and ISTP/VERDON programs. Furthermore, Phébus FP tests have produced valuable data on integral phenomena.

The large-scale integral tests of the Phébus FP program [2] studied the degradation of real fuel bundle and the release, transport and deposition of FPs, e.g., ruthenium, as well as structural materials and control rod materials in the model of primary circuit and containment building. The tests were conducted under steam-rich or steam-poor atmospheres and under low pressures ( $\sim 0.2$  MPa). The interpretation of the huge amount of experimental data is ongoing.

The four VERDON tests [3] of the International Source Term Program (ISTP) were devoted to the study of fission products release from high burn-

up  $\text{UO}_2$  and MOX fuels. The semi-integral VERDON-2 test was in particular dedicated to study the impact of air ingress following a lower head failure on the ruthenium release from the fuel and its transport/revaporisation in the primary circuit.

The transport of Ru in primary circuit conditions has been studied in separate-effect tests with small-scale experimental facilities as a part of SARNET [4-7] and NEA STEM/START programs [8, 9]. Ruthenium was oxidized at high temperature under dry or humid air atmosphere close to atmospheric pressure with specific attention being paid to the transport of Ru through a thermal gradient tube (TGT). The effect of other fission products and control rod materials on the transport of Ru was also investigated. A newly initiated NKS-ATR activity [10], under the Nordic Nuclear Safety Research (NKS) program, produces information on the effect of aerosols and air radiolysis products on the transport of Ru.

As part of SARNET projects, an extensive set of experiments was carried out to understand the behaviour of ruthenium tetroxide when reacting and thus depositing on containment paint and metal surfaces. Furthermore, the revaporisation of Ru from the deposits, the distribution of gaseous  $\text{RuO}_4$  between gas and liquid phases, as well as the revaporisation of Ru from the sump of containment building, were examined. [11, 12, 13]

This paper summarizes the main results of these recent experimental studies on the behaviour of Ru in severe accident conditions. Also the main phenomena governing Ru deposition in circuit conditions are presented.

## II. Ru RELEASE FROM FUEL

### II.A PHÉBUS FP - RELEASE

The overall objective of the well-known international Phébus FP programme [2] was to simulate phenomena starting from the meltdown of an irradiated  $\text{UO}_2$  fuel assembly in steam flow up to the releases outside of the containment through the transfer of radioactive products coming from the RCS and their subsequent

behaviour in the containment. The release of ruthenium occurred mainly in the late oxidation phase where temperatures are the highest, as expected for low-volatile elements (here fuel oxidation plays a role). Ru release from the test section was low [14]. However, this underestimates the release from the fuel itself, as Ru can be released from high temperature zones in the bundle and deposit downstream on cooler surfaces (upper parts of the fuel rods as well as in the circuit). The low steam injection rate in some tests (~0.5 g/s) specifically favoured significant deposition of Ru in the upper sections of the degraded fuel bundle. With the higher steam injection rate (~2.0 g/s) used in other tests deposition occurred rather in the downstream sections of the circuit. This indicates that the partition of deposits between the fuel bundle and the circuit proper depends on the prevailing thermal hydraulic conditions, which may change with time, thus one cannot consider the circuit and bundle regions independently when considering how much Ru would reach the containment.

## II.B ISTP/VERDON

The International Source Term Program has been launched in 2005 with the aim to reduce the uncertainties relative to Source Term assessment under LWR severe accident conditions. Among the R&D research axes addressed in this program, four VERDON tests devoted to the study of Fission Products (FP) release from high burn-up UO<sub>2</sub> and MOX fuels were performed from 2011 to 2014. The VERDON-2 test was in particular dedicated to study the impact of air ingress following a lower head failure on the ruthenium release from the fuel and its transport/revaporisation in the primary circuit.

The four VERDON tests of the ISTP were conducted in a new hot cell at the CEA Cadarache center, specially built for this purpose (Figure 1) [3].

In both configurations, downstream of the filter, the fission gases (Xe, Kr) and the potential gaseous forms of iodine or ruthenium are transported at 150 °C by the fluid flow along the

circuit. Gaseous iodine is trapped in the May-Pack filter on successive sites of this specific filter according to its chemical forms (molecular or organic) and RuO<sub>4</sub> in a dedicated filter made of polyvinylpyridine. After a security filter, the injected and produced non-condensable gas (He, H<sub>2</sub>, air ...) and the released fission gases are directed outside the cell up to the glove box where they are finally analyzed and stored in a 3m<sup>3</sup> storage vessel.

The accident sequence is simulated by heating the fuel sample in a high frequency furnace under conditions representative of a severe accident, in a fluid flow, which could be a mixture of helium, water steam, hydrogen and air. The fuel sample consists of two irradiated pellets in their original cladding and two half-pellets of depleted (and un-irradiated) uranium oxide placed at each end of the sample and held there by crimping the cladding so that the cladding is not fully sealed.

Two different and complementary circuits are available:

1) The Release Circuit (Figure 1a), which is devoted to the precise characterization of the FP release by means of a total aerosol filter heated at 150°C and being located just above the furnace, allows the precise quantification of the released fraction by gamma spectrometry and/or chemical analysis directly after the test. VERDON-1, -3 and -4 were performed with this circuit.

2) The Transport Circuit (Figure 1b), which enables the study of FP transport in the primary circuit of a nuclear power plant, through a series of 4 thermal gradient tubes (TGTMs) that can be operated sequentially with two in parallel in order to study FP deposit as well as revaporisation [15]. In order to be representative of the hot leg and cold leg temperatures under severe accident conditions, the temperature along these tubes linearly decreases from 700°C at the entrance to 150°C at the exit, and is monitored by a series of thermocouples located every 100 mm. Downstream from the TGTMs, the fluid is transported at 150°C to an aerosol filter or to a cascade impactor where the particle size distribution of the aerosols is quantified. The air ingress VERDON-2 test was performed with this circuit.

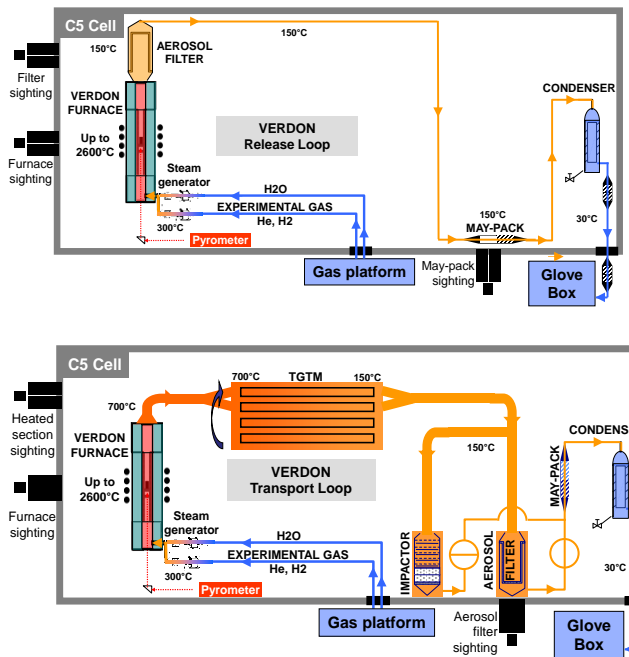


Fig. 1. VERDON hot cell: a) Release Circuit, b) Transport Circuit

Before the experimental sequence, the sample is re-irradiated at low linear power (15 to 20 W/cm) in the OSIRIS material testing reactor for about a week, in order to recreate the short half-life FPs without any in-pile release. As a consequence, these FPs (i.e.  $^{99}\text{Mo}$ ,  $^{103}\text{Ru}$ ,  $^{132}\text{Te}$ ,  $^{133}\text{I}$ ,  $^{131}\text{I}$ ,  $^{140}\text{Ba}$ ...), important for their radiobiological effects, are measurable by using on-line gamma spectrometry during the experiment.

## II.C Ru FINDINGS FROM THE VERDON-2 TEST

The VERDON-2 test was performed using a MOX fuel at 60 GWd/t. The thermal-hydraulic sequence (Figure 2) was composed of two main phases [16]:

1) The first phase under pure steam, including an oxidation plateau at 1500°C, followed by a second 15 minute plateau at 2000°C, simulating SA conditions before the lower head failure. The first TGTM rotation occurred (tubes 1-2 to tubes 2-3) at the end of this phase, in order to study the

volatile FP deposits (mainly iodine, tellurium, caesium) and their potential reevaporation following the air ingress phase.

2) The second phase under mixed air-steam (50%-50% molar ratio): the 2000°C plateau has been maintained for additional 70 minutes. Since the Ru release had not reached the “stop criterion” of 60% released, another plateau at 2100°C was performed for 90 minutes. During this plateau, the TGTM was turned after 60 minutes (tubes 2-3 to tube 3-4) and after the rotation, the tubes 3 and 4 stayed during 30 minutes under the same atmosphere to be able to study the potential reevaporation of  $\text{RuO}_2$  deposits.

The Ru release started with the air ingress phase during the 2000°C plateau, as shown in Figure 3, and reached about 70% of the initial inventory at the end of the sequence. The release rate slightly increased between the 2000°C and 2100°C plateaus. From a general point of view, the ruthenium kinetics seems to be relatively low compared to what could be expected due to the final temperature and atmosphere of the test (2.5 hours under mixed steam-air conditions, 1 hour at 2000°C and 1.5 hour at 2100°C). This low value can be the consequence of the MOX nature of the fuel, as it was confirmed in VERDON-3 (see chapter II.D).

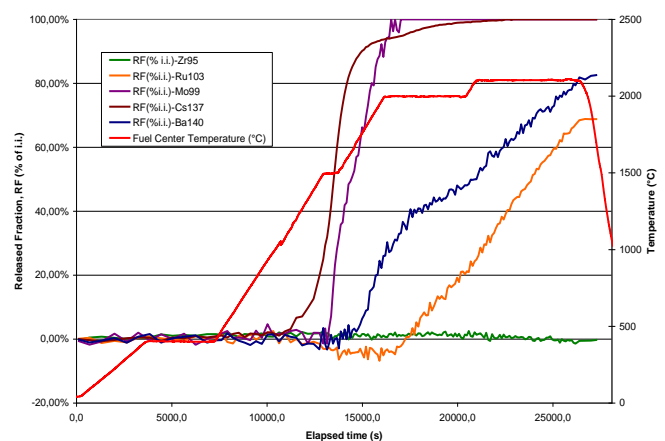


Fig. 3. Ru release kinetics, along with Cs (volatile FP), Mo, Ba (semi-volatile FP) and Zr (non-volatile FP)

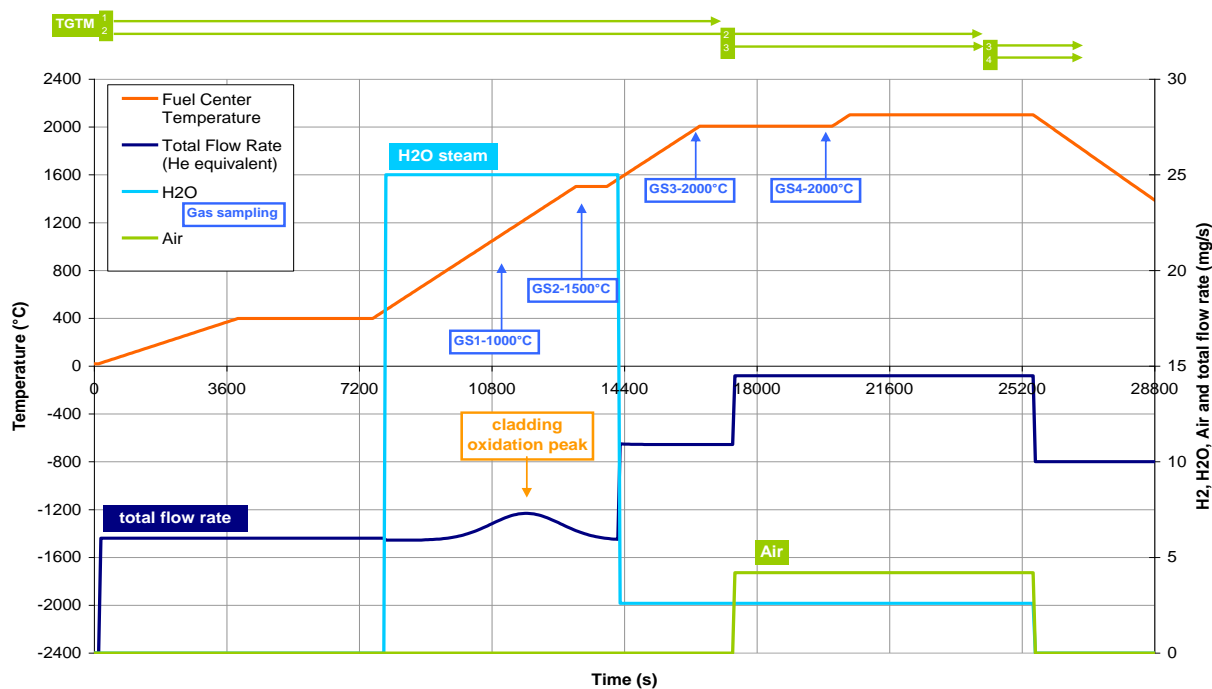


Fig. 2 Thermal-hydraulic sequence of the VERDON-2 test

The transport of Ru can be analysed through the deposits along the thermal gradient tubes. It can be seen in Figure 4, that  $^{103}\text{Ru}$  did not deposit in tube 1, which is consistent with a release that started with the air injection. The profiles of tubes 2 and 3 are similar with a large accumulation in the mid-plane area of the tubes. The quantity of deposits in tube 3 are greater than those in tube 2, which is normal considering its longer period of use. Tube 4 shows a rather homogeneous profile of low amplitude. The sum of the profiles for tubes 2 and 4 is similar to tube 3, which shows there was no significant revaporisation of ruthenium deposits at the end of the test.

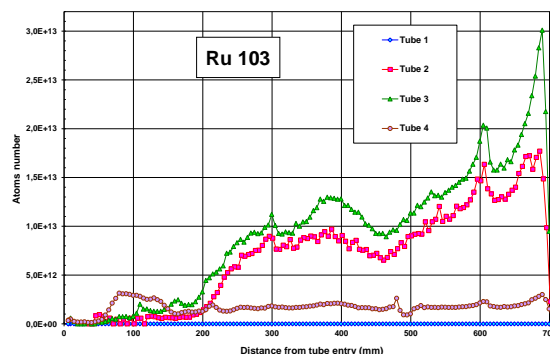


Fig. 4. Distribution of  $^{103}\text{Ru}$  along the TGTM tubes.

To further study the transport of Ru, the filter located downstream the condenser was analysed. This filter was totally free from Ru, indicating that no gaseous  $\text{RuO}_4$  was transported so far.

#### II.D LOWER Ru RELEASE FROM MOX FUEL IN VERDON-3 TEST

The VERDON-3 test was performed with the same MOX fuel as VERDON-2, but under pure steam conditions up to 2300°C. Only a few percent of Ru was released from this test, which is very low in comparison with the Ru release

measured in similar conditions with  $\text{UO}_2$  fuel, for instance on VERCORS HT2 (65%) and VERCORS RT6 (28%) [17]. This result confirms the lower Ru release in case of MOX fuel compared to  $\text{UO}_2$  fuel, probably linked to a difference in the oxidation of the fuel matrix.

Considering the observed behavior of MOX fuel relative to the Ru release, it has been proposed to complement the VERDON data base with a new VERDON-5 test, which will be similar to the VERDON-2 test, but using a high burn-up  $\text{UO}_2$  fuel at 70 GWd/t (same fuel as VERDON-1). In addition, boron will be injected during the initial phase under steam. This supplementary objective will address the impact of  $\text{B}_4\text{C}$  rods degradation on the fission products chemistry in the primary circuit, resulting in a potentially higher gaseous iodine fraction entering the containment. This test will be performed by the CEA in 2015.

### III. Ru TRANSPORT IN PRIMARY CIRCUIT

#### III.A PHÉBUS FP - TRANSPORT

The overall transmission of ruthenium to the containment in the Phébus FP tests was only a few percent of the initial bundle inventory, whereas the corresponding transmission e.g. for the volatile elements Cs and I was roughly up to 20 and 30 times higher respectively [18]. Ruthenium was deposited significantly and progressively from the exit of the bundle to the entrance to the containment. Distribution of Ru deposits along the circuit was mainly concentrated where the temperatures of the wall and fluid decrease strongly, i.e. just above the bundle where the fluid cools from  $\sim 2000$  °C to  $\sim 700$  °C and, in the hot leg of the steam generator, from  $\sim 700$  °C to  $\sim 150$  °C. In the vertical line, simultaneously developing flows and changes in geometry (successive reductions in tube diameter) enhance deposition. The main processes in the circuit are: chemical transformation of vapours, vapour condensation onto structures as well as nucleation to form aerosols, or onto aerosols, aerosol agglomeration (primarily by diffusion), and thermophoretic deposition. Low steam injection rate increased the deposition of Ru. Solubility measurements on the Ru circuit deposits showed consistent non-

soluble behaviour both in the hot and cold legs. There are no data available on the speciation. Overall, taking also into account results of separate-effect tests such as VERCORS (CEA), experimental data show that, contrary to other low volatile elements, under certain thermal hydraulic oxidising/reducing conditions, a fraction of Ru can be transported well downstream of the fuel into the coldest regions of the primary circuit, as noted for example in [19]. Concerning physical form, Ru was observed to be transported almost exclusively as an aerosol.

#### III.B SMALL-SCALE FACILITIES

The transport of ruthenium in a primary circuit has been studied in VTT [4, 5], MTA EK's RUSSET [6, 7] and in START [8, 9] separate-effects programmes. The START program is a part of the Source Term Evaluation and Mitigation (STEM) project hosted by OECD and operated by IRSN. The corresponding experimental facilities are presented in Figure 5. Both horizontal and vertical tubular flow furnaces have been used. In VTT experiments, the furnace tube was made of alumina ( $\text{Al}_2\text{O}_3$ ) and the thermal gradient tube (TGT) was of stainless steel. MTA EK and IRSN used quartz tubing which withstands the relevant thermal and chemical loads and allows observing and analyzing deposits along the tube. In VTT experiments, the Ru deposit profile was analysed with the help of  $^{103}\text{Ru}$  gammatracer. The inner diameter of the tubing was roughly 6 to 8 times higher in VTT and START experiments than in RUSSET tests. However, the flow rate was also significantly lower in RUSSET tests, 0.171 NI/min compared to 5 NI/min and 1.84 NI/min of VTT and START tests, respectively. Thus, all facilities were operated in a laminar flow regime.

The source of Ru was either anhydrous  $\text{RuO}_2$  powder, gaseous  $\text{RuO}_4$  or metallic Ru powder which was oxidized at high temperatures in air-containing atmospheres (air and/or steam as carrier gas). The oxidation temperature in VTT experiments was varied in a range from 827 °C to 1427 °C (outlet at 20 °C), whereas RUSSET and START tests were conducted at 1100 °C (outlet at 100 °C) and 1200 °C, respectively. The temperature of the tube downstream the reaction

furnace was controlled down to 150/250 °C in START tests. The following Ru speciation and transport through a TGT to the containment conditions were investigated. The influences of several other FP components and different surfaces (quartz, stainless steel (EN 1.4301), zirconium/niobium binary alloy (E110), alumina, oxidised metal, and surfaces with RuO<sub>2</sub>, Mo or Cs deposits) on the decomposition and re-vaporisation of ruthenium oxides along a temperature gradient zone have also been investigated, specifically in RUSSET tests. The transported aerosol particles were collected either on filter and/or trapped in an alkaline solution together with the gaseous Ru. The aerosol number/mass size distributions and their corresponding number/mass concentrations were also analysed online in VTT Ru transport experiments.

In general, the Ru vaporization kinetics was observed to be linear in steam/air mixtures and it was dependent on the steam content. The highest release rate of ruthenium was detected in dry air. Ru release was very low when oxidised at ca. 800 °C. At temperatures between 1000 to 1100 °C ruthenium was primarily transported in gaseous form. The partial pressure of gaseous RuO<sub>4</sub> at the circuit outlet, corresponding to containment conditions, was in the range of 10<sup>-6</sup> to 10<sup>-7</sup> bar (in

VTT and RUSSET tests). This is several orders of magnitude higher than expected from thermodynamic equilibrium calculations and thus the surface-catalysed decomposition process of RuO<sub>4</sub> to RuO<sub>2</sub> was not fast enough to follow entirely the thermal equilibrium. This clearly indicates the need to consider the effect of temperature gradients in the RCS and residence time in the circuit on the fraction of gaseous Ru. This is currently being investigated in START program [9].

In tests below the oxidation temperature of 1100 °C, less than a tenth of the released Ru was transported as particles in VTT tests. However, no solid Ru was detected at the circuit outlet in RUSSET tests. The transported aerosol fraction (of the released Ru) increased and was two to four times higher when the oxidation temperature increased from ca. 1200 °C to 1400 °C. Gaseous Ru seemed to react on the surface of the SS tube, on top of which RuO<sub>2</sub> particles had been deposited. Thus Ru transport through the model primary circuit took place almost entirely as particles when Ru was oxidized at temperatures higher than 1200 °C. However, the partial pressure of the transported RuO<sub>4</sub> remained in the range of 10<sup>-6</sup> to 10<sup>-8</sup> bar.

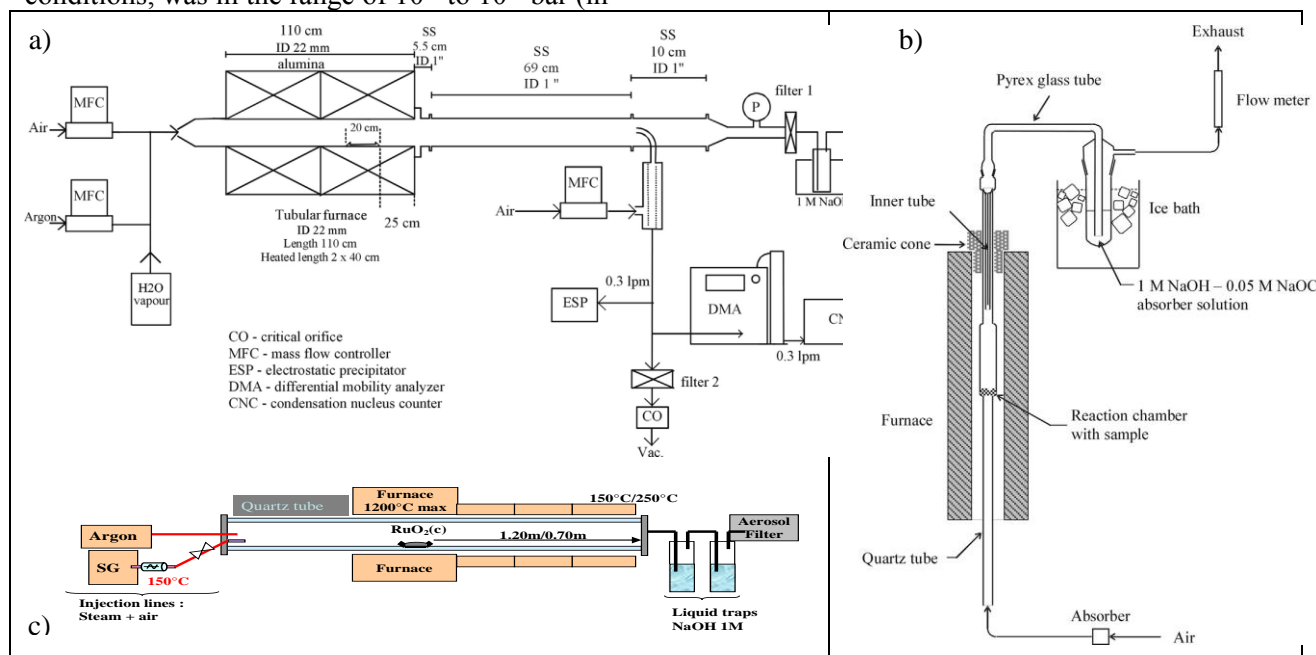


Fig. 5. Experimental facilities for Ru transport studies (operated close to 1 atm): a) VTT Ru transport, b) RUSSET and c) START

The presence of steam in the gas flow enhanced the transport of gaseous ruthenium. In the long duration tests of START programme, the existence of transient phenomena on Ru transport was observed in the short term. The transport of RuO<sub>2</sub>

aerosol was decreased after the 1st hour of tests and thus the gaseous fraction increased from 50 % to 93 %. The fraction of the Ru released from the RuO<sub>2</sub> crucible that was deposited inside the facility ranged from 75 % to 97 %. This tendency of the Ru to deposit was enhanced at low oxidation temperature. It is very likely that in tests at 1027 °C ruthenium was primarily transported in gaseous form. The typical Ru deposition profiles together with the computational results of the tests are presented in Figure 6. The main phenomena governing the transport of pure Ru in the circuit were explained with CFD computations and they are presented in [5].

Revaporisation of the deposited RuO<sub>2</sub> particles was found to be a very significant source of gaseous ruthenium oxides. After Ru was

revaporised from the TGT surfaces at notably lower temperature than the furnace set-point of 1227 or 1427 °C at beginning of the TGT, the fraction of Ru transported in gaseous form was as high as 65% in VTT experiments. This indicated that the surfaces of RCS may act as a source of volatile ruthenium species even in the late phase of an accident. The steam content of the gas flow seemed to enhance the transport of gaseous Ru again. The revaporisation behavior of ruthenium is being investigated in detail in START program [9].

In RUSSET tests, the presence of other FPs in the high temperature oxidation zone decreased the partial pressure of RuO<sub>4</sub> in the outlet air over the SS surface in the temperature gradient zone compared with the pure Ru oxidation. For all types of surfaces investigated, the maximum concentration of RuO<sub>4</sub> in the outlet flow appeared with a time delay if other FPs were present. Furthermore, a stainless steel surface which was pre-coated

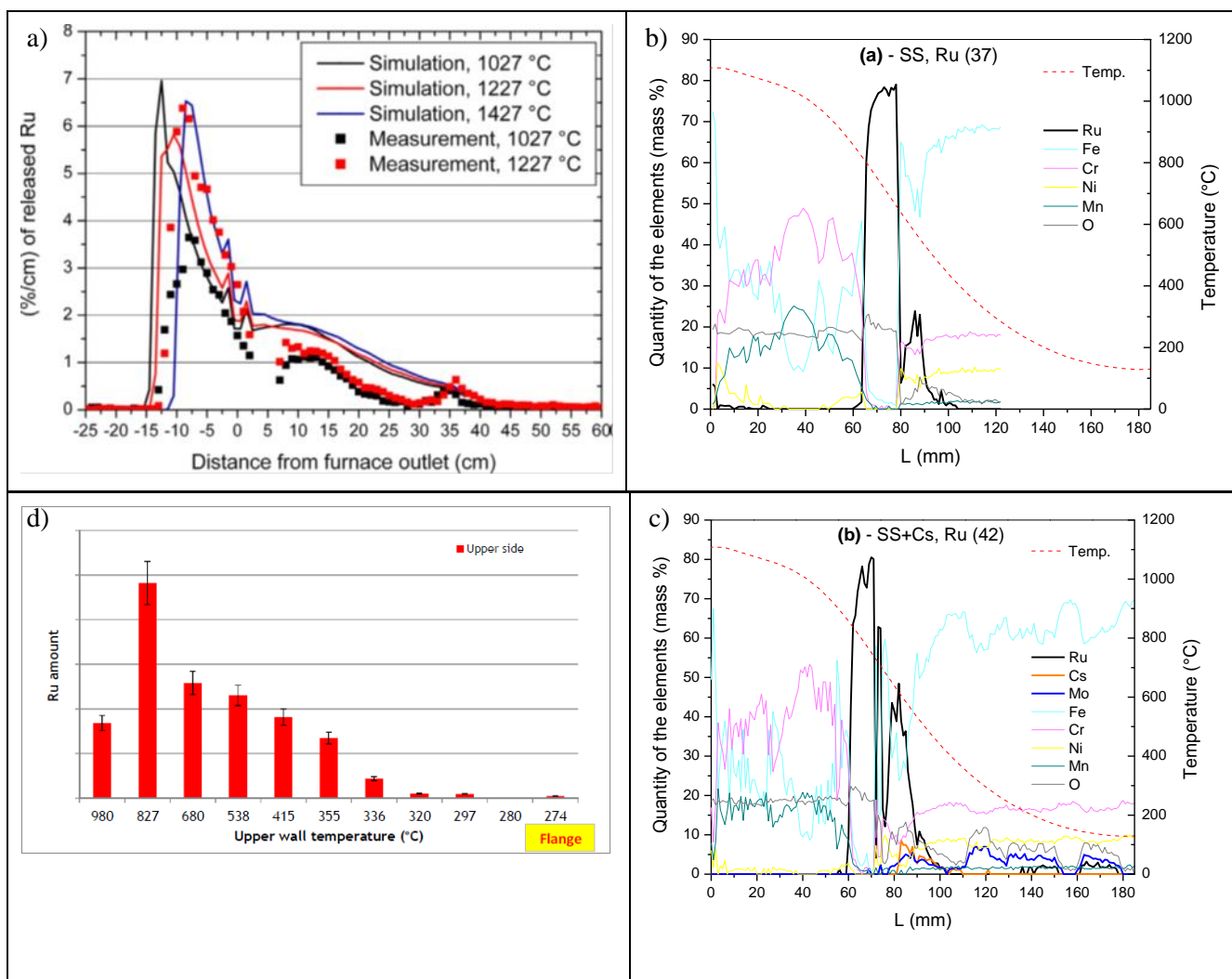


Figure 6. The typical Ru deposition profiles in experiments: a) VTT Ru transport, b) RUSET; distribution on steel surface after pure Ru oxidation, c) RUSET; distribution on Cs coated steel surface after pure Ru oxidation, and d) START.

with caesium trapped Ru efficiently between about 485 and 640 °C, see Figure 6c. Also a sample of CsI powder at ca. 100-150 °C trapped gaseous Ru efficiently in VTT tests. The formation of  $\text{Cs}_2\text{RuO}_4$  was proposed in both cases.

In the newly initiated NKS-ATR activity [10] by VTT and Chalmers the aim is to study the effect of aerosols and air radiolysis products on the transport of gaseous and particulate ruthenium species through a model RCS. All experiments done so far were conducted with VTT's Ru transport facility at 1227 °C with slightly humid air (saturated at 20 °C) as the main carrier gas. The preliminary results show that the impact of additional  $\text{NO}_2$  gas feed (75 ppm volume) to the

flow of Ru oxides (in humid air) was significant both on the transport of Ru through the facility and on the speciation of the transported ruthenium. Transport of gaseous  $\text{RuO}_4$  was increased significantly, whereas at the same time the amount of aerosols reaching the filter was decreased. However, the release of Ru from the crucible was similar as in an experiment without  $\text{NO}_2$ . This indicates that the molar ratio of  $\text{RuO}_3/\text{RuO}_4$  in the gas flow had changed. A proposed explanation is based on the oxidation of  $\text{RuO}_3$  to  $\text{RuO}_4$  by  $\text{NO}_2$ . On the other hand, when only pure Ag particles (diameter 0.5-1.0  $\mu\text{m}$ ) were fed to the humid air flow, the transport of  $\text{RuO}_4$  decreased significantly. Most likely, gaseous  $\text{RuO}_4$  had reactively condensed on the surface of Ag particles as  $\text{RuO}_2$ . Addition of both

Ag particles and NO<sub>x</sub> in a form of AgNO<sub>3</sub> droplets (which decomposed to Ag and NO<sub>3</sub> when heated) to the flow of Ru oxides (in humid air) enhanced the transport of gaseous RuO<sub>4</sub> as well, but not as much as in case of NO<sub>2</sub> feed. In these experiments (with NO<sub>2</sub> or AgNO<sub>3</sub>), the observed transport of gaseous Ru seemed to be several orders of magnitude higher than in the previous experiments with only pure Ru oxides in the air atmosphere [4, 5]. These results indicate that the composition of gaseous atmosphere in the primary circuit has a significant effect on the amount and chemical form of ruthenium transported to the containment during a SA.

#### IV. Ru BEHAVIOUR IN THE CONTAINMENT

An extensive study on the behavior of Ru in containment conditions has recently been conducted by Chalmers University of Technology (2007-2014), [11, 12]. In these experiments, the interaction of RuO<sub>4</sub> with different containment surface materials and the following chemical speciation of the formed ruthenium rich layer were investigated. Additionally, the possible revaporisation of ruthenium from these deposits on surfaces when exposed to gamma radiation was studied. The other part of experiments was focused on the distribution ratio of ruthenium tetroxide between gas and liquid phases in the facility simulating a containment building.

Gaseous RuO<sub>4</sub> was generated prior to all experiments due to the unstable nature of this compound. After the interaction of RuO<sub>4</sub> vapor with the Al, Cu, Zn and epoxy paint samples at temperature of 25 °C and at relative humidity of 99%, a black colored ruthenium rich layer was observed on the samples. XPS analysis of the ruthenium deposits on the containment surface samples revealed that the surface of deposits was composed of ruthenium dioxide in its hydrated form. The formed compound was ruthenium hydroxo-oxide, in which ruthenium was in the oxidation state +IV. This was probably due to the hygroscopic nature of RuO<sub>2</sub> and high humidity of atmosphere during the interaction of RuO<sub>4</sub> with the studied surfaces. The chemical speciation of the deposits was the same regardless the surface material. However, in case of epoxy paint the

hydration of RuO<sub>2</sub> was higher than on metal samples. The crystal structure analysis of the deposits by EXAFS supported also the formation of hydrated form of RuO<sub>2</sub>. Since the deeper layers of the deposits could be analysed with this method, the inner structure was identified to be of RuO<sub>2</sub>. This verified that only the surface of RuO<sub>2</sub> deposits was strongly hydrolyzed.

The affinity of RuO<sub>4</sub> towards Zn, Cu and Al was studied with the help of <sup>103</sup>Ru. In general, the affinity of RuO<sub>4</sub> towards these metals was increased when the humidity of the atmosphere was increased, see Table I. At humidity of ca. 3%, the deposited amount of ruthenium was up to 3 times higher in case of aluminium than on copper or zinc surfaces. However, the highest affinity of RuO<sub>4</sub> towards aluminium was observed at dry conditions.

TABLE I

Affinity of RuO<sub>4</sub> towards metals in humid and dry atmospheres

		Zinc	Copper	Aluminium
Humid	Ru/sample (µg/cm <sup>2</sup> )	15.3 ± 0.3	18.0 ± 0.3	31.6 ± 0.6
	Ru/sample (µg/cm <sup>2</sup> )	13.2 ± 0.2	12.1 ± 0.2	24.8 ± 0.5
	Ru/sample (µg/cm <sup>2</sup> )	18.5 ± 0.3	19.2 ± 0.4	38.9 ± 0.7
Dry	Ru/sample (µg/cm <sup>2</sup> )	2.73 ± 0.5	9.42 ± 0.2	103.29 ± 0.7
	Ru/sample (µg/cm <sup>2</sup> )	0.76 ± 0.02	0.39 ± 0.1	86.78 ± 0.6
	Ru/sample (µg/cm <sup>2</sup> )	2.23 ± 0.4	2.45 ± 0.5	98.35 ± 0.7

The revaporisation experiments were focused on the release of Ru from deposits on epoxy paint (deposit speciation described above) when exposed to gamma radiation. It was proposed, that Ru deposits would be oxidized back to Ru +VIII, and thus volatile RuO<sub>4</sub> would be formed, by the generated oxidizing air radiolysis products. The dose rate of a gamma source (Gammacell 220, 60Co) was ca. 14 kGy·h<sup>-1</sup>. The effect of cumulative radiation dose up to 264 kGy was investigated. Temperature in the irradiation chamber was 44 °C. A beaker with ruthenium deposit on epoxy paint sample was placed into Erlenmeyer flask. The bank was afterwards placed into the gamma field. In addition, the impact of humidity on the revaporised fraction of Ru was examined. In

those experiments, 30ml of 1M KOH solution was injected into the Erlenmeyer flask. The solution acted both as a source of humidity and as an effective trap for volatile ruthenium released from the samples. As a result, a strong impact of humidity on the fraction of Ru revaporised was noticed, see Figure 7, and the fraction seemed to increase linearly as a function of the received radiation dose. In case of dry atmosphere, virtually no revaporisation of Ru was detected regardless of the received dose.

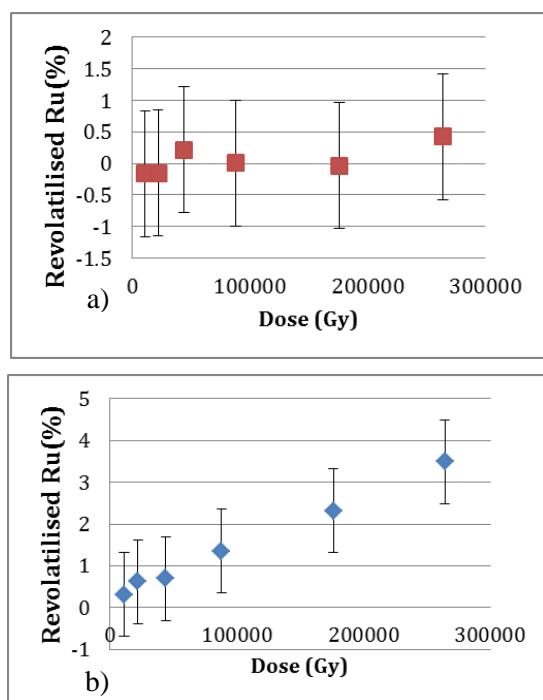


Fig. 7. Revaporised fraction of ruthenium induced by gamma radiation in (a) dry and (b) humid atmospheres.

The observed results were explained by the role of hydroxyl radical produced in humid conditions. Hydroxyl radical with the reduction pair  $\cdot\text{OH}/\text{H}_2\text{O}$  (standard oxidation potential for the couple  $E^\circ=1,4\text{V}$ ) is a strong oxidizing agent with an ability to revaporise ruthenium from the deposit. When the results were compared with the previous results of IRSN [13], it was noticed that a lower fraction of revaporised ruthenium per unit of received dose was obtained in the current study. As temperature in the experiments was significantly lower than in the previous experiments (44 °C vs 90 °C), it was proposed that temperature can affect strongly the kinetics of ruthenium re-oxidation process. It was also

concluded by IRSN [13] that radiolysis promotes the formation of ruthenium tetroxide in a higher amount than could be expected by pure ozone action (about one order of magnitude). The enhancement of Ru revaporisation phenomenon under radiation was explained by the presence of  $\text{O}\cdot$  and/or  $\text{OH}\cdot$  radicals in a higher extent because of additional production by direct radiolytic reactions in air/steam atmospheres.

The distribution of  $\text{RuO}_4$  between gas and liquid phases and especially the corresponding partition coefficient ( $k_D$ ) were determined in a temperature range from 20 to 50 °C. The experiments were performed using an experimental set-up simulating a BWR containment building, shown in Figure 8. All surfaces of the set-up were made of glass. In the experiments gas phase was a mixture of nitrogen and oxygen ( $\text{O}_2$  fraction less than 5%) and liquid phase was composed of Milli-Q water. Gaseous  $\text{RuO}_4$  (spiked with  $^{103}\text{Ru}$ ) was introduced to the system by sublimation of condensed  $\text{RuO}_4$  from the surface of a glass vial. The distribution of Ru between gas and liquid phases was continuously measured with two NaI(Tl) detectors. When Ru was introduced to the system at 20 °C, it was immediately transported into the liquid phase. After five minutes, the concentration of Ru in the gas phase had decreased below a detection limit. A similar phenomenon was also seen at higher temperatures. The concentration of ruthenium in the liquid phase was decreased to ca. 25% after two hours. This behavior was explained by as a reduction of  $\text{RuO}_4$  to solid  $\text{RuO}_2$  that was deposited and accumulated on the glass surfaces of the set-up. The visual observation of black deposit layers on the inner glass surfaces and the analysis with HPGe detector confirmed the deposition of Ru.

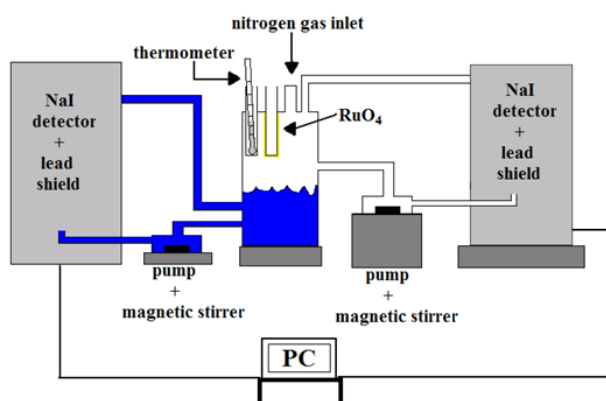


Fig. 8. Experimental set-up for the  $\text{RuO}_4$  distribution experiments.

In experiments without the liquid phase, it took more than 200 minutes until the concentration of Ru in the gas phase had decreased to the detection limit of NaI(Tl) detector. This indicates that  $\text{RuO}_4$  can remain in the gas phase of dry system for a long time when compared to a system with a water phase as well. Based on the experiments deposition velocities were also calculated [11].

Some exploratory irradiation tests of liquid phases containing ruthenium species have been carried out by IRSN [13] in order to check the potential oxidation reaction of Ru aqueous species up to the +VIII oxidation state [ $\text{RuO}_4(\text{g})$ ]. The objective was limited to qualitatively evidence whether or not the sump has the ability to be a source of volatile Ru under radiation. Concerning the preparation of aqueous Ru solutions, the concentration of ruthenium was set to  $10^{-4}$  mol/l according to the expected concentration in the sump in SA conditions [20]. Two pH values, 4 and 10, were studied.  $\text{KRuO}_4$  powder was dissolved into boric acid solution of 0.2 mol/l with respect to boron. The alkaline solution was a mixture of  $\text{KRuO}_4$  powder dissolved into potassium hydroxide solution (KOH) of 0.05 mol/l with a boric acid of 0.2 mol/l with respect to boron. Finally, pH values were adjusted by addition of pure  $\text{HNO}_3$  or LiOH solution of 5 ppm (wt). The aqueous Ru sample was then exposed to gamma radiation ( $^{60}\text{Co}$ ) in a glass ampoule and the released Ru was trapped in KOH solution (0.2 mol/l) located in the other compartment of the ampoule.

Results on the irradiation tests of perruthenate solutions clearly showed that the reevaporation of Ru from the sump is possible. A notable Ru fraction was detected both in liquid trap and on inner surfaces of the glass ampoules despite the pH of Ru solutions and the radiation dose. The measured fraction of reevaporated Ru ranged between 5 and 13%. Furthermore, the presence of Ru precipitates was observed in the liquid trap (mainly) and on glass surfaces at the end of every experiment. Therefore, the extent of Ru reevaporation may appear quite surprising, when taking into account that the observed precipitates may result from the formation of reducing agents under radiation. However, these experiments were exploratory at this stage, and some questions remain open, for example, the role of pH and the effect of radiation dose on the formation of  $\text{RuO}_4$ . Further studies concerning Ru behavior in aqueous phase under radiolysis will be needed to improve the knowledge of Ru aqueous chemistry in SA conditions. In particular, the uncontrolled formation of Ru precipitates needs to be understood beforehand.

#### V. Ru TRANSPORT MODELLING

It must be emphasized that VTT and RUSSET series of ruthenium transport tests clearly demonstrated that the decomposition of  $\text{RuO}_4$  to  $\text{RuO}_2$  was not complete and did not follow thermal equilibrium. The experimentally observed high fraction of gaseous Ru transported through a model primary circuit to the containment should also be considered in severe accident simulation codes. Ru deposition patterns calculated by VTT with the Computational Fluid Dynamics (CFD) software package FLUENT were very close to the experimental results when the hypothesis was to investigate diffusion-limited  $\text{RuO}_2$  and  $\text{RuO}_3$  transport and deposition to the TGT surfaces [21], see Figure 6a. The kinetics of ruthenium conversion to  $\text{RuO}_4$  was assumed to be so slow that the conversion was of secondary importance during the relatively brief cooling phase. Simulation studies verified that the deposition occurred mainly as diffusion-limited reactive condensation of  $\text{RuO}_3(\text{g})$  to  $\text{RuO}_2(\text{c})$ , when the temperature decreased below approx. 800 °C:  $2 \text{RuO}_3 \rightarrow 2 \text{RuO}_2 + \text{O}_2$ . Condensation of  $\text{RuO}_2$ , deposition of  $\text{RuO}_2$  particles and reaction of  $\text{RuO}_4$  with surfaces

(circuit and particles) were other minor deposition processes. The roles of buoyancy and thermophoresis on the deposition of RuO<sub>2</sub> particles, which were nucleated in the gas phase of the circuit, became important when the temperature gradient was high, e.g. at the outlet of the furnace.

## VI. CONCLUSION

In experiments on the effect of atmosphere on the release of Ru from the fuel, a significant release of Ru from the irradiated MOX fuel was observed in air ingress conditions (VERDON-2). The cladding of fuel pellet samples was oxidized prior to reaching the high temperature conditions in the course of test. When the test was repeated in steam conditions (VERDON-3), only a few percent of Ru was released. That is very low in comparison with the Ru release from UO<sub>2</sub> fuel in similar conditions in VERCORS tests. It was concluded that probably the lower release of Ru from MOX fuel than from UO<sub>2</sub> fuel is linked to a difference in the oxidation of the fuel matrix. In large-scale integral Phébus FP tests ruthenium release from the irradiated UO<sub>2</sub> fuel under steam conditions was fairly limited as is typical for a low-volatile element. In addition, a significant fraction of it was deposited on the upper parts of the fuel bundle instead of being transported to the model primary circuit. Ruthenium deposited significantly and progressively from the exit of the bundle to the entrance to the containment. The deposits were mainly located in places where the temperatures of the wall and the fluid decrease strongly, such as the area above the fuel bundle and the hot leg of the steam generator. Concerning the physical form of Ru transported to the coldest regions of the circuit, Ru was observed to be almost exclusively as an aerosol. In VERDON-2 no deposition of Ru was observed to take place in the TGT before the air ingress phase, which is consistent with the Ru release observations. Afterwards, an accumulation of Ru on tube surfaces was noticed in the course of the test. Ruthenium was not observed downstream the condenser (coupled with a May-Pack filter in the upstream) at the circuit outlet, thus indicating that no gaseous Ru was transported so far.

In the separate-effect tests ruthenium transported through the circuit mainly as aerosol particles (>99%) when the Ru source was oxidized above

1227 °C. When the oxidation took place at a rather moderate temperature, 1000–1100 °C, a significant fraction of Ru was transported as gaseous RuO<sub>4</sub>. The oxidizing air radiolysis products can further increase the fraction of gaseous Ru. Ruthenium deposited on the circuit surfaces in the form of RuO<sub>2</sub>. Simulation studies verified that the deposition occurred mainly as diffusion-limited reactive condensation of RuO<sub>3</sub>(g) to RuO<sub>2</sub>(c), when the temperature decreased below approx. 800 °C. Other minor deposition processes were also identified. On the other hand, Ru was also re-vaporised from the deposits and the gaseous fraction of the transported Ru was high.

After RuO<sub>4</sub> had been interacted with metals (Al, Zn, Cu) and epoxy paint surfaces at room temperature with high relative humidity, the formation of black colored Ru deposits was observed. A detailed analysis indicated that the surface of deposits was in a hydrated form of RuO<sub>2</sub>, whereas the deeper structure was still of RuO<sub>2</sub>. The affinity of RuO<sub>4</sub> towards metals was increased by humid conditions. The highest affinity was towards aluminium, although it seemed to trap RuO<sub>4</sub> even better in dry conditions. When the epoxy paint surface with Ru deposit was exposed to gamma radiation at ca. 50 °C, Ru release was observed but only in humid conditions. That was explained by the role of strong oxidizing hydroxyl radical formed in humid conditions due to radiation. Also, the amount of gaseous RuO<sub>4</sub> remaining in the gas phase was strongly dependent on the water content of the system in a temperature range from 20 to 50 °C. When RuO<sub>4</sub> was fed to the gas phase, it remained there for a long time in case of a dry system in comparison to a system with a water pool and a gaseous volume above it – simulating a containment building. RuO<sub>4</sub> was immediately transported to the water pool, in which it was also reduced to solid RuO<sub>2</sub> and deposited on available surfaces. The release of Ru from a perruthenate aqueous solution due to gamma radiation was qualitatively examined. In case of alkaline or acidic solution, simulating a containment sump, a notable fraction of Ru was released in gaseous form. The presence of Ru precipitates in liquid trap and on the surfaces of the set-up was observed in every test.

Data obtained from the above-mentioned - performed and ongoing - separate-effect, semi-integral and fully-integral programs will constitute a support to the model developments and contribute to the validation effort. The upcoming VERDON-5 tests is of specific interest as it examines the effect of air ingress on FPs release from UO<sub>2</sub> fuel, and the following transport through a TGT, and thus it supplements the existing database of integral experiments.

#### ACKNOWLEDGMENTS

This work was conducted in the framework of EC SARNET and SARNET2, ISTP/VERDON, NEA STEM/START and NKS-R (Nordic Nuclear Safety Research – area of Reactor Safety) projects.

The Phébus FP programme was initiated in 1988 by IRSN, in cooperation with the Commission of the European Communities (EC), using the Phébus facility operated by CEA (France), with contributions from EdF (France), USNRC (USA), CANDU Owners Group (Canada), JNES and JAEA (Japan), KAERI (Korea), HSK (now ENSI) and PSI (Switzerland).

#### REFERENCES

1. W. Klein-Heßling, M. Sonnenkalb, D. Jacquemain, B. Clément, E. Raimond, H. Dimmelmeier, G. Azarian, G. Ducros, C. Journeau, L.E. Herranz Puebla, A. Schumm, A. Miasoedov, I. Kljenak, G. Pascal, S. Behta, S. Guntay, M.K. Koch, I. Ivanov, A. Auvinen, I. Lindholm, Conclusions on severe accident research priorities. *Ann. Nucl. Energy* 74, 4–11 (2014).
2. B. Clément, R. Zeyen, The objectives of the Phébus FP experimental programme and main findings. *Ann. Nucl. Energy* 61, 4–10 (2013).
3. M.P. Ferroud-Plattet, J. Bonnin, A. Gallais-During, S. Bernard, J.P. Granjean, G. Ducros, “CEA VERDON Laboratory at Cadarache: new hot cell facilities devoted to studying irradiated fuel behaviour and fission product releases under simulated accident conditions”, *Proc. Int. Conf. HotLab International Conference, Prague, Czech* (2009).
4. U. Backman, M. Lipponen, A. Auvinen, U. Tapper, R. Zilliacus, J.K. Jokiniemi, On the transport and speciation of ruthenium in high temperature oxidizing conditions. *Radiochimica Acta* 93, 297–304 (2005).
5. T. Kärkelä, N. Vér, T. Haste, N. Davidovich, J. Pyykönen, L. Cantrel, Transport of ruthenium in primary circuit conditions during a severe NPP accident, *Ann. Nucl. En.* 74, pp. 173-183 (2014).
6. N. Vér, L. Matus, M. Kunstár, J. Osán, Z. Hózer, A. Pintér, Influence of fission products on ruthenium oxidation and transport in air ingress nuclear accidents, *J. Nucl. Mater.* 396, 208-217 (2010).
7. N. Vér, L. Matus, A. Pintér, J. Osán, Z. Hózer, Effects of different surfaces on the transport and deposition of ruthenium oxides in high temperature air, *J. Nucl. Mater.* 420, 297-306 (2012).
8. B. Clément, B., Simondi-Teisseire, STEM: an IRSN project on source term evaluation and mitigation. *Trans. Am. Nucl. Soc.* 103, 475–476 (2010).
9. O. Leroy, M.N. Ohnet, S. Planteur-Kieffer, “Study of the Ruthenium transport under prevailing conditions in the primary circuit in case of a PWR severe accident”, 7<sup>th</sup> European Review Meeting on Severe Accident Research (ERMSAR-2015), Marseille, France, 24-26 March 2015.
10. [http://www.nks.org/en/nksr/current\\_activities/atr.htm](http://www.nks.org/en/nksr/current_activities/atr.htm), 26.5.2015.
11. J. Holm, Investigation of the behaviour of gaseous I<sub>2</sub> and RuO<sub>4</sub> in different atmospheres, in *Nuclear Chemistry* (2009), Chalmers University of Technology.
12. I. Kajan, RuO<sub>4</sub> interaction with surfaces in the containment of nuclear power plant, Licentiate Thesis, Technical report no 2014:8, ISSN nr: 1652-943X. (2014).
13. C. Mun, L. Cantrel, C. Madic, Radiolytic oxidation of ruthenium oxide deposits. *Nuclear Technology*, 164(2): p. 245-254 (2008).
14. A.-C., Grégoire, T. Haste, Material release from the bundle in Phébus FP, *Ann. Nucl. En.* 61, pp. 63-74 (2013).
15. A. Gallais-During, J. Bonnin, P.-P. Malgouyres, S. Morin, S. Bernard, B. Gleizes, Y. Pontillon, E.

- Hanus, G. Ducros, “Performances and First Results of Fission Products Release and Transport Provided by the VERDON Facility” *Nucl. Eng. Des.*, 277, pp. 117-123 (2014).
16. A. Gallais-During, S. Bernard, B. Gleizes, Y. Pontillon, J. Bonnin, P.-P. Malgouyres, S. Morin, E. Hanus, G. Ducros, “Overview of the VERDON-ISTP Program and main insights from the VERDON-2 air ingress test”, 7th European Review Meeting on Severe Accident Research (ERMSAR-2015), Marseille, France, 24-26 March, 2015.
  17. Y. Pontillon, G. Ducros, “Behaviour of fission products under severe PWR accident conditions: the VERCORS experimental programme, Part 3: Release of low-volatile fission products and actinides”, *Nucl. Eng. Des.* 240, pp. 1867–1881 (2010).
  18. T. Haste, F. Payot, P.D.W. Bottomley, Transport and deposition in the Phébus FP circuit, *Ann. Nucl. En.* 61, pp. 102-121 (2013).
  19. P. Giordano, A. Auvinen, G. Brilliant, J. Colombani, N. Davidovich, R. Dickson, T. Haste, T. Kärkelä, J.S. Lamy, C. Mun, D. Ohai, Y. Pontillon, M. Steinbrück, N. Vér, Recent advances in understanding ruthenium behaviour under air-ingress conditions during a PWR severe accident, *Prog. Nucl. En.* 52, pp. 109-119 (2010).
  20. C. Mun, “Etude du comportement du produit de fission ruthénium dans l’enceinte de confinement d’un réacteur nucléaire, en cas d’accident grave,” PhD Thesis, Université de Paris XI (2007).
  21. T. Kärkelä, J. Pyykönen, A. Auvinen, J. Jokiniemi, Analysis of flow fields, temperatures and ruthenium transport in the test facility, VTT-R-00947-08 (2008).

## THOUGHTS ON RUTHENIUM IN NUCLEAR ACCIDENTS

Michael Salay\*, Richard Lee, and Dana Powers  
U. S. Nuclear Regulatory Commission,  
Rockville, Maryland, USA

\*Corresponding author; tel: (+1) 301-415-2408, Fax: (+1) 301-415-6671, Email: Michael.Salay@nrc.gov

**Abstract** – Ruthenium is considered to be released in accidents involving exposure of hot fuel to air which is considered to occur in air ingress accidents or spent fuel pool drain-down or boil-off scenarios. In the past several years considerable research has been conducted regarding the transport of ruthenium upon release. Ruthenium release analyses have also been conducted using pre-oxidized cladding. Aspects of ruthenium release that have received less attention, including gas transport behavior, the impact of gas consumption, and clad behavior, are discussed.

## I. INTRODUCTION

Radioactive isotopes of ruthenium can have significant radiological effects if released extensively from irradiated reactor fuel under accident conditions. Alpert *et al.* [1986] estimated that for equal release fraction of 10% of core inventory, the release of ruthenium during a severe reactor accident would have about three times the effect of radioactive iodine release on lung dose and an effect equivalent to that of cesium for latent cancers. That is, ruthenium release could affect both prompt and latent fatalities if the release from the degrading reactor core was similar on a fractional basis to the releases of cesium and iodine. This finding and similar findings from other considerations of the radiological effects of ruthenium [Leggett, 2012] have prompted some interest in the behavior of ruthenium under reactor accident conditions. Most of these studies presuppose that ruthenium has been released from degrading reactor fuel and focus on the behavior of the radionuclide in the reactor coolant system and in the reactor containment.

Once released, ruthenium behavior can be complicated. The complication stems from the many oxidation states the element can adopt depending on the chemical environment. Volatile ruthenium tetroxide,  $\text{RuO}_4$ , has a formal oxidation state of +8. Much of the study of ruthenium in aqueous solution has focused on the oxidation states of +2 to +6 [Rard, 1985]. Ruthenium-bearing aerosols are expected to have ruthenium in the +4 valence state, usually as ruthenium dioxide,  $\text{RuO}_2$ , or its various hydrates. This complexity of the oxidation states of ruthenium is reminiscent of the complexities of oxidation states of iodine under accident conditions.

The wide range of ruthenium chemistry becomes accessible under accident conditions because of the range of possible chemical conditions in the reactor coolant system and in the reactor containment depending on the details of reactor accident conditions. Furthermore, conditions of temperature and pressure may be altered by accident management measures of varying levels of effectiveness. Further complications arise because of the vast range of chemical species that

can be released under accident conditions along with ruthenium. Certainly releases of other inorganic species of variable oxidation states can be expected including releases of large amounts of tin, chromium, manganese, and iron as well as other fission products such as iodine. Organic species including ketones and alcohols can be expected to be present in the reactor containment because of the steam oxidation and pyrolysis of organic materials including paint, lubricants, and cable insulation. Finally, there is the additional complication of intense radiation fields in both the gas phase and the condensed phase. Radiolytic processes can be expected to produce both oxidants and reductants that will affect the chemical behavior of ruthenium.

Unraveling the potentially complicated behavior of ruthenium under reactor accident conditions sufficiently well to support predictive modeling appears to be a formidable chore. It could be necessary to undertake this effort if it can be established that ruthenium releases for significant classes of reactor accidents can be comparable to the releases of more familiar radionuclides such as iodine and cesium. The balance of this paper provides some thoughts on the types of considerations that will need to be made in order to establish that significant ruthenium releases from degrading reactor fuel are possible and that there is an attendant need to understand well the details of ruthenium behavior in the reactor coolant system and in reactor containments.

## II. RUTHENIUM IN REACTOR FUEL

Ultimately, ruthenium is generated by the fission process in reactor fuel. It is, however, not an important primary product of fission. Most is produced by the decay of molybdenum through technetium. These elements are, then, always closely associated in the fuel. They are also of low solubility in the fluorite lattice of hyperstoichiometric fuel typical of thermal reactors [Kleykamp, 1993]. Somewhat higher solubilities especially of ruthenium are possible in hypostoichiometric fuel of fast reactors [Olander, 1982]. Because of the low solubility, once a threshold of burnup is surpassed, ruthenium can be detected in the so-called ‘white phases’ of fuel [Kleykamp *et al.*, 1985]. These are

nodules of alloys of Mo, Ru, Rh, Tc, and Pd. Other elements may be present including zirconium and barium to modest levels. A ‘typical’ composition for light water reactor fuel suggested by Sasa *et al.* [1980] in terms of mole fraction is  $x_{\text{Mo}} = 0.429$ ,  $x_{\text{Tc}} = 0.131$ ,  $x_{\text{Ru}} = 0.177$ ,  $x_{\text{Rh}} = 0.049$ ,  $x_{\text{Pd}} = 0.026$ ,  $x_{\text{Ba}} = 0.063$  and  $x_{\text{Zr}} = 0.041$ . Compositions are variable depending on burnup [Kleycamp *et al.*, 1985] and the radial thermal gradient in fuel pellets during normal operations [Zhou, 2010]. It is also typical to detect two populations of alloy nodules. Larger nodules (1-5  $\mu\text{m}$ ) are found in pores and on grain boundaries. Very much smaller nodules can be seen within the fuel grains themselves. The relative amounts of these two types of nodules depend on burnup and linear heating rate of the fuel.

The vapor pressure of pure ruthenium is not high even at temperatures sufficient to cause extensive degradation of reactor fuel:  $\sim 10^{-4}$  bar at 2833 K [Hultgren *et al.*, 1973]. Alloying of the ruthenium in the nodules will further reduce the vapor pressure of ruthenium metal by dilution and by chemical interactions among the alloy constituents [Rand and Potter, 1981]. Consequently, ruthenium release by direct vaporization of the metal is thought to be insignificant for reactor accidents. This does not preclude some transport of metal vapors within the fuel from hotter to cooler regions. Vapors encountering metals such as the zirconium cladding will alloy with these metals.

### III. VAPORIZATION AS RUTHENIUM OXIDE

Ruthenium can form a variety of oxide vapor species [Garisto, 1988] with partial pressure well in excess of the vapor pressure of pure ruthenium:  $\text{RuO}$ ,  $\text{RuO}_2$ ,  $\text{RuO}_3$ , and  $\text{RuO}_4$ . At a fixed oxygen potential, the dominant oxide vapor species is the monoxide at the highest temperatures expected in reactor accidents. Higher oxides become dominant at progressively lower temperatures. The tetroxide is the dominant vapor species at temperatures below about 800 K.

The partial pressures of these ruthenium oxide species are quite low within the fuel during

normal operations. Even under the steam-hydrogen atmospheres characteristic of reactor accidents, the partial pressures are too low to drive risk-significant releases of ruthenium from the fuel. Indeed, significant releases of ruthenium were not detected during the accident at Three Mile Island. Significant ruthenium releases have not been observed in tests of reactor fuel degradation including the PBF tests conducted by the Idaho National Engineering Laboratory [Hobbins *et al.*, 1993], the HI/VI tests conducted by the Oak Ridge National Laboratory [Osborne *et al.*, 1985], or the recent Phébus-FP tests conducted in France. Except at the very highest temperatures and steam partial pressures expected to arise in reactor accidents, atmospheres of steam and hydrogen cannot produce sufficiently high oxygen potentials to drive significant releases of ruthenium.

To get significant releases of ruthenium from irradiated reactor fuel it is necessary to have higher oxygen potentials than can be produced typically by atmospheres of steam and hydrogen at plausible pressures and temperatures. Sufficiently high oxygen potentials can be produced if even small amounts of air are mixed with steam. High releases of ruthenium from irradiated reactor fuel in air were first demonstrated in early experiments at Oak Ridge National Laboratory [Lorenz *et al.*, 1980]. A more dramatic demonstration was reported by Cox *et al.* [1991]. They exposed heated CANDU fuel to air. Once the rather thin zirconium alloy cladding on the CANDU fuel was oxidized, nearly complete release of ruthenium was observed at even modest temperatures relative to those expected to arise in fuel during severe reactor accidents. In both the experiment reported by Cox *et al.* and the experiments reported by Lorenz *et al.*, ruthenium release was accompanied by releases of copious amounts of uranium vaporized by oxidation of the fuel to the volatile hexavalent state –  $\text{UO}_3$ .

The demonstration experiments by Cox *et al.* and those reported by Lorenz *et al.* show that it is possible to get extensive ruthenium release. As issue becomes the types of reactor accidents that can lead to air being present in the steam atmosphere during core degradation. The reactor accident at Three Mile Island demonstrated that

during severe reactor accidents substantial core degradation and relocation to the lower plenum of the reactor vessel could occur along the centerline of the reactor core while fuel about the periphery of the core remained largely intact. Should the relocated core debris penetrate the reactor vessel, it would be possible for air from the reactor containment to enter the reactor vessel by natural circulation and expose the residual fuel in the vessel to high oxygen potentials.

High ruthenium releases, then, are possible during the most severe reactor accidents that progress to the point that the reactor vessel is penetrated by core debris. This, of course, is a subset of reactor accidents involving reactor fuel degradation. The accident at Three Mile Island as well as risk analyses [NRC, 1990] show that important fractions of reactor accidents involving fuel melting are arrested prior to reactor vessel breach.

Other accidents that have been hypothesized to involve exposure of inadequately cooled, irradiated, reactor fuel to air include refueling accidents involving the loss of coolant feed, spent fuel pool accidents involving loss of coolant inventory, and rupture of casks for dry storage of spent fuel.

#### IV. MASS TRANSPORT AND COMPETITIVE REACTIONS

The availability of high oxygen potentials in the gas phase is clearly a necessary condition for extensive ruthenium release from irradiated reactor fuel. It is not a sufficient condition. For extensive vaporization of ruthenium from alloy nodules in the fuel to occur, the high oxygen potentials must exist in the vicinity of the nodules. There are significant mass transport limitations and competitive reactions that are barriers to the establishment of high oxygen potentials adjacent to the alloy nodules containing ruthenium.

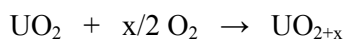
The most obvious of these barriers is the zirconium alloy cladding on the fuel. Zirconium will react with oxygen and nitrogen in the atmosphere. The oxidation of zirconium by air is grossly similar to the oxidation of zirconium by

steam. In detail, there are differences [Steinbrück *et al.*, 2004]. For the conditions of interest, the detailed chemical kinetics are of less interest since reaction of air with the cladding will be limited most likely by gas-phase mass transport. Until the cladding is oxidized, it will 'getter' air from the gas phase and prevent high oxygen potentials developing in the vicinity of ruthenium alloy nodules within the fuel. The barrier to extensive ruthenium releases posed by zirconium reaction with the air is especially significant for boiling water reactors. Boiling water reactors use zirconium alloys for both cladding the fuel and for structures in the core region. Typically, boiling water reactors have about three times as much zirconium in the core region as do pressurized water reactors. It is noteworthy that there have not yet been reports of important releases of ruthenium from fuel in the Fukushima Dai-ichi reactors even though air may have entered the cores of the reactors during the accidents at this site.

The reaction of air with zirconium is about 70% more exothermic than is the reaction of steam with zirconium. It is possible, then, that temperatures in the cladding will be driven to the melting point of the cladding alloy more quickly in steam-air mixtures than in steam-hydrogen mixtures. Melting of the cladding below the zone of reaction with the oxidizing gas could lead to liquefaction of the fuel. There would be a significant loss of surface area for release of radionuclides and even relocation of the fuel from the high temperature zone of the reactor core. On the other hand, melting of the underlying metal could lead to the rapid draining of cladding and directly expose the irradiated reactor fuel to an atmosphere with a high oxygen potential. Powers *et al.* [1994] considered these two possibilities for clad behavior when exposed to air and concluded that there was insufficient phenomenological understanding to predict confidently the course of accident progression. They suggested that to develop reliable models integral tests involving degradation of many fuel rods in air would be needed.

Exposure of reactor fuel to air-steam mixtures is also not sufficient to lead to extensive ruthenium release. A simple examination of Ellingham diagrams [Ewart *et al.*, 1976] shows that many

things in reactor fuel will react with and deplete air from the gas phase before ruthenium can be oxidized. The fuel itself will have to be oxidized to a hyperstoichiometric state consistent with the oxygen potentials needed to produce high partial pressures of ruthenium-bearing vapors:



At the temperatures of interest, the diffusion of oxygen in the fluorite lattice of reactor fuel is sufficiently high that an oxidation front does not develop [Lay, 1970]. Rather, the whole body of fuel must be oxidized before the necessary condition for ruthenium vaporization exists.

Competitive with the process of developing the elevated oxygen potentials in the vicinity of the ruthenium nodules is the slumping and relocation of reactor fuel at high temperature. Slumping of the fuel reduces the surface area available for fission product vaporization to the atmosphere of the reactor vessel and coolant system. It also brings molten fuel into contact with metals that can alloy with ruthenium. Relocation can remove core debris from the high temperature regions of the reactor core. At the very least, slumping and relocation of core debris can limit the time available for extensive ruthenium release.

## V. CONCLUSIONS

For ruthenium release to have a significant effect on the consequences of reactor accidents, the release must be extensive – comparable to anticipated releases of iodine and cesium. It is evident from available information that prolonged exposure of reactor fuel to unlimited amounts of air can lead to extensive release of radioactive ruthenium. There is, however, insufficient information available to judge the likelihood of extensive ruthenium release from reactor fuel during accidents. It is evident that there are multiple barriers to the development of necessary and sufficient conditions for extensive ruthenium release. There are important limitations on the amount of fuel exposed to conditions conducive to extensive ruthenium release and the amount of time that high rates of ruthenium release could persist. It is, then, difficult to formulate a risk-informed justification for the expenditure of resources that will be

needed to understand adequately for predictive modeling the potentially complicated behavior of ruthenium once it has been released from reactor fuel.

## REFERENCES

1. D.J. Alpert, D.I. Chanin, and L.T. Richie, Relative Importance of Individual Elements to Reactor Accident Consequences Assuming Equal Release Fractions, NUREG/CR-4467, SAND85-2575, Sandia National Laboratories, Albuquerque, NM, March 1986.
2. D.S. Cox, C.E.L. Hunt, Z. Liu, N.A. Keller, R.D. Barrand, R.F. O'Connor, and F.C. Iglesias, *Fission product releases from UO<sub>2</sub> in air and inert conditions at 1700-2350 K: Analysis of the MCE-1 experiment*, AECL-10438, Atomic Energy of Canada Limited report, Pinawa, Manitoba, 1991.
3. F.T. Ewart, R.G. Taylor, J.M. Horspool and G. James, "The Chemical Effects of Composition Changes in Irradiated Oxide Fuel Materials II – Fission Product Segregation and Chemical Equilibria", *J. Nucl. Mater.*, **61**; 254-270, 1976.
4. F. Garisto, *Thermodynamic behavior of ruthenium at high temperatures*, AECL-9552, Atomic Energy of Canada Limited, Pinawa, Manitoba, 1988.
5. R.R. Hobbins, D.A. Petti, and D.L. Hagrman, "Fission Product Release From Fuel Under Severe Accident Conditions", *Nuclear Technology*, **101**; 270, 1993.
6. R. Hultgren, P.D. Desai, D.T. Hawkins, M. Gleiser, and K.K. Kelly, *Selected Values of the Thermodynamic Properties of the Elements*, American Society for Metals, Ann Arbor, Michigan, 1973.
7. H. Kleykamp, "The solubility of selected fission products in UO<sub>2</sub> and (U,Pu)O<sub>2</sub>", *J. Nucl. Mater.*, **206**;82-86, 1993.
8. H. Kleykamp, J.O. Paschoal, R. Pejsa, and F. Thommler, "Composition and Structure of Fission Product Precipitates in Irradiated Oxide Fuel: Correlation with Phase Studies in the Mo-Ru-Rh-Pd and BaO-UO<sub>2</sub>-ZrO<sub>2</sub>-MoO<sub>2</sub> Systems", *J. Nucl. Mater.*, **130**;426-433, 1985.

9. K.W. Lay, "Oxygen Chemical Diffusion Coefficient of Uranium Dioxide", *J. Amer. Ceram. Soc.*, **53**; 369-373, 1970.
10. R.W. Leggett, "The biokinetics of ruthenium in the human body", *Radiation Protection and Dosimetry*, **148**;4,389-402, 2012.
11. R.A. Lorenz, J.L. Collins, A.P. Malinauskis, O.L. Kirkland, and R.L. Towns, *Fission Product Release from Highly Irradiated LWR Fuel*, NUREG/CR-0722 R1, Oak Ridge National Laboratory, Oak Ridge, Tennessee, 1980.
12. NRC, Severe Accident Risks: An Assessment for Five U.S. Nuclear Power Plants, NUREG-1150, U.S. Nuclear Regulatory Commission, Washington, DC, 1990.
13. D.R. Olander, "A Mechanistic Analysis of Ruthenium Transport in  $UO_2$ ", *Nuclear Science and Engineering*, **82**; 190-205, 1982.
14. M.F. Osborne, J.L. Collins, R.A. Lorenz, K.S. Norwood, J.R. Travis, and C.S. Webster, *Data Summary Report for Fission Product Release Test HI-5*, NUREG/CR-4037, Oak Ridge National Laboratory, Oak Ridge, Tennessee, 1985.
15. D.A. Powers, L.N. Kmetyk, and R.C. Schmidt, *A Review of the Technical Issues of Air Ingression During Severe Reactor Accidents*, NUREG/CR-6218, Sandia National Laboratories, Albuquerque, NM, 1994.
16. M.H. Rand and P.E. Potter, "Thermodynamics and Phase Diagrams of Mo-Pd-Ru and Related Systems", *Physica*, **103B**; 21-30, 1981.
17. J.A. Rard, "Chemistry and Thermodynamics of Ruthenium and Some of Its Inorganic Compounds and Aqueous Species", *Chemical Reviews*, **85**;1-39, 1985.
18. P. Sasa, A.W. Cronenberg, M.G. Stevenson, "On the Volatilization Potential of Metallic Inclusions Found in Irradiated  $UO_2$  Fuel During Overheating Events", *Nuclear Technology*, **48**; 233-250.
19. M. Steinbrück, A. Meier, U. Stegmaier, and L. Steinback, *Experiments on the Oxidation of Boron Carbide at High Temperature*, FZKA-6979. Forschungszentrum Karlsruhe GmbH, Karlsruhe, Germany, 2004.
20. S.Y. Zhou, *The Redistribution of Ruthenium in  $UO_2$  in a Temperature Gradient*, LBL-12193, Lawrence Berkeley National Laboratory, Berkeley, California, 2010.

**THE MAIN OUTCOMES OF THE OECD BEHAVIOUR OF IODINE PROJECT**

G.A. Glowa\*, C.J. Moore, D. Boulianne  
Canadian Nuclear Laboratories, Chalk River, Canada

\*Corresponding author, tel: (+1) 613-584-3311(ext. 46052), Glenn.Glowa@cnl.ca

**Abstract** – *The second phase of the OECD Behaviour of Iodine Project (BIP) ended in September 2014. The primary objective of this project was to investigate the interactions between iodine and containment paint, including iodine sorption behaviour and the subsequent formation of organic iodides.*

*In the first phase of BIP, BIP-1 focused on the interaction between iodine and epoxy paints. Epoxy paints are commonly used surface coatings within nuclear reactor containment buildings throughout the world. In particular, experiments investigating the role of water on the deposition velocities and formation of methyl iodide from irradiated paint showed that adsorbed water strongly affected both the sorption and organic iodide formation processes.*

*BIP-2 investigated the same processes, with emphasis on developing a more mechanistic understanding of organic iodide production during irradiation of iodine-loaded paint. Epoxy paint is a complex mixture of polymeric compounds and it is difficult to know where and how iodine is interacting and how methyl iodide is formed. To isolate the influence of various functional groups present in epoxy paint, polymer samples having simple, but representative, structures (such as amide groups) were prepared. The samples were exposed to I<sub>2</sub>(g) and irradiated to determine the rate of methyl iodide formation. In addition to the polymer tests, tests were performed with epoxy paint at 80°C (for comparison to EPICUR tests) with different iodine loading schemes (to help our understanding of the effect of water) and with paint that was pre-exposed to Cl<sub>2</sub> or NO<sub>2</sub> (to simulate the effect of reactive species expected within containment).*

*Several spectroscopic techniques were utilized in BIP-2 to investigate iodine-paint surface interactions. Scanning electron microscopy was used to determine coupon surface morphology, energy dispersive x-ray analysis measured the depth of penetration of the iodine into the paint layer, and gas chromatography-mass spectroscopy was used to study solvent release from 20-year-old epoxy paint.*

*This paper will discuss the main outcomes of BIP. The results from the BIP experimental program can be used to guide the development of computer models and provide data for model validation.*

## I. INTRODUCTION

An Organization for Economic Cooperation and Development (OECD) status report on iodine behaviour published in February 2007 concluded that, although the understanding of iodine behaviour in containment had advanced considerably over the past several decades, there were still some areas where

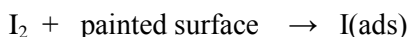
further investigation was warranted [1]. There have recently been several international initiatives (or programs) that have addressed this topic, including the Phébus International Source Term Project, the OECD THAI (Thermalhydraulics Hydrogen Aerosol Iodine) Project, and the OECD STEM (Source Term Evaluation and Mitigation) Project.

The Behaviour of Iodine Project (BIP) was initiated to investigate aspects of the iodine-paint interaction. Although a few other containment surfaces are tested, BIP focuses on epoxy paint, which is a commonly used coating within containment buildings throughout the world. Epoxy paint is a complex mixture of polymeric compounds, and the nature of its interaction with iodine is not known precisely. In BIP, several types of epoxy paint were tested, which should help determine if similarities exist to the extent that a common modelling methodology can be adopted.

The main technical objectives for BIP-2 were to obtain a more detailed and mechanistic understanding of (a) iodine adsorption onto, and desorption from, containment surfaces and (b) organic iodide formation.

### (a) Iodine adsorption

Painted surfaces are an important iodine sink in the post-accident containment building. The adsorption of iodine on paint is often simplified as:



The I(ads) refers to the adsorbed phase of iodine, and often includes several chemical forms, including iodine that is covalently bound, physically bound, and involved with charge transfer complexes. In the aqueous phase, iodine hydrolyzes to compounds such as HOI [2], which have been implicated as a reacting species [3]. Iodine is known to be reactive with various

functional groups including ethylene, carbonyl, phenol, epoxide and amine groups.

Results from BIP-1 show that relative humidity is an important factor determining the rate of deposition of iodine on epoxy paint. The results also show that there is some variability in the deposition velocity on various types of epoxy paint. After exposure to iodine, much of the iodine is strongly retained on painted surfaces and is presumed to be covalently bonded. In BIP-2, the site specificity of iodine bonding was evaluated. Polymeric model compounds with chemical structures characteristic of epoxy paint were chosen for study. Knowing how the iodine is bound may provide mechanistic insights into how to model the process and how organic iodides are formed when iodine-loaded paint is irradiated.

### (b) Organic iodide formation

The mechanism of organic iodide production from irradiated iodine-loaded paint is not fully understood. Possibilities include a radiation-induced reaction of iodine associated with a particular functional group, or a radiation-induced reaction taking place between iodine and residual paint solvents.

In BIP-1, progress was achieved quantifying the rates of formation for methyl iodide from irradiated paint. It was found that the methyl iodide concentration, determined by a balance between a fast formation and destruction rate, changed as a function of time during irradiation. It was also observed that the presence of residual water affected the methyl iodide production rate. Tests using coupons loaded with iodine by contact with aqueous solution had higher organic iodide formation rates than gas-loaded coupons. Water may be required to mobilize paint solvents trapped within the paint matrix, or may be required for an aqueous-phase process within the paint pores.

BIP-2 studies were designed to provide insight into how organic iodides are formed by studying organic iodide production on simple polymeric model compounds. In addition, some tests with painted samples included an irradiation phase at

80°C to allow comparison to tests carried out in the EPICUR<sup>(4)</sup> facility.

The results of BIP-2 include qualitative insights, which can be used to guide model design, and quantitative data (such as deposition velocities) that are necessary input for iodine behaviour models. A mechanistic understanding of these phenomena improves our ability to explain results to our regulatory agencies, and supports the application of these results to conditions outside of the tested range (e.g., extrapolation to a wider selection of epoxy coatings and to larger-scale experiments and containment conditions).

The BIP-2 project officially started in April 2011 and ended in September 2014. The member nations included Belgium, Canada, Finland, France, Germany, Japan, Korea, Spain, Sweden, the United Kingdom and the United States. The total budget of the project was about 900k€, half of which was contributed by Canada. Good progress was achieved regarding the understanding of the nature of iodine bonding on paint, and on the formation of organic iodides.

## II. TESTS PERFORMED

Two main types of tests were performed under BIP-2: adsorption tests (AD), where the sorption behaviour of iodine on various surfaces was measured, and irradiation tests (RAD), where iodine-loaded coupons were exposed to <sup>60</sup>Co gamma radiation to investigate the formation of organic iodides.

For both types of test, iodine was adsorbed onto the coupon surfaces by immersing the samples in aqueous solutions containing I<sub>2</sub>, or by exposing the samples to an airstream containing I<sub>2</sub> using a specially-designed adsorption apparatus. Gas-phase iodine loading was typically performed at 70°C and 70% relative humidity.

Test names generally include the type of test (AD or RAD), the coupon type (see Table 1), an

A or G to identify if the coupon was exposed to iodine in the aqueous (A) or gas (G) phase, and a sequential number to identify replicate tests. For example RAD-EPX-A-1, identifies irradiation test 1, using epoxy resin loaded by contact with an aqueous solution containing I<sub>2</sub>.

TABLE 1: Coupon Types

Name	Coupon Material
GW	Epoxy paint (Gehopon EW10)
EPICUR	Epoxy paint (Hydrocentrifugon Ripolin 901)
ORG	Epoxy paint (Amerlock 400)
NYLON	Nylon 6/6
POLY	Polypropylene
EPX	DOW DER 661 epoxy resin
EPX2	Amine-cured epoxy resin (DOW DER 332 cured with triethylenetetramine)
EPX3	DOW DER 667 epoxy resin

For typical irradiation experiments, a glass vessel containing pre-loaded coupons (Fig. 1) and laboratory air was irradiated at ambient temperature in a Gammacell 220 <sup>60</sup>Co irradiator<sup>(5)</sup>. Gas samples were removed periodically for methyl iodide analysis by Gas Chromatography (GC). Sampling was accomplished using a gas-tight syringe via a gas-sampling septum located at the top of the irradiation vessel. At the end of the irradiation, the gas-phase iodine was analyzed using a gas-phase iodine speciation procedure.

The vessel used for the 80°C irradiation tests included a thermo-well to accommodate a thermocouple for temperature control. For these special tests, a small amount (200 µL) of water was added to the vessel, prior to the heating phase, in order to raise the relative humidity. Humidity was not measured during irradiation. However, water loss during the heat-up phase was quantified during commissioning tests and the water additions were adjusted to yield 60% RH.

<sup>(4)</sup> EPICUR (Experimental Project on Iodine Chemistry Under Irradiation) experiments are currently performed in France within the OECD STEM Project. These experiments study organic iodide formation using a complementary experimental methodology.

<sup>(5)</sup> The Gammacell 220 <sup>60</sup>Co irradiator was distributed by MDS Nordion.



Fig. 1. Open Irradiation Vessel with Coupons.

Full experimental details are available in the BIP data reports and in the BIP-1 Final Summary Report [4].

### III. POLYMER COUPONS

Epoxy paint is a complex mixture of polymeric compounds. In order to isolate the influence of various functional groups present in epoxy paint, coupons were prepared from various polymers.

**Epoxy Resin:** Epoxy resin material is a major component of epoxy paint. DOW DER™ 661, a low molecular weight Di-Glycidyl Ether of Bisphenol-A (DGEBA), was chosen as representative of the epoxy resins found in epoxy paint (Fig. 2). A higher melting point epoxy resin (DER 667) was used for the gas-phase iodine adsorption tests performed at 70°C.

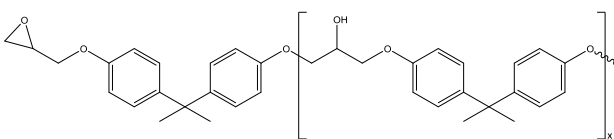


Fig. 2. Chemical Representation of an Epoxy Resin Formed from Bisphenol-A and Epichlorohydrin

**Nylon 6/6:** Nylon 6/6 is a polyamide consisting of repeating units containing 12 carbon atoms and 2 amide groups. This material was chosen because structurally similar polyamides are a component of Amerlock 400 epoxy paint.

™ DER is a registered trademark of the DOW Chemical Company.

**Amine-cured epoxy polymer:** Coupons were prepared from a polymer made by mixing DOW DER 332 (a low molecular weight liquid DGEBA) with TETA (triethylenetetramine). This material was studied in order to investigate the importance of the amine functional group.

**Polypropylene:** This material is simply a long chain aliphatic polymer formed from propene. Polypropylene does not contain any special functional groups, but has many methyl groups. It was chosen to represent any aliphatic portions of epoxy paint.

### IV. RESULTS OF AQUEOUS IODINE ADSORPTION TESTS

Adsorption/desorption measurements on the selected polymers were carried out using aqueous I<sub>2</sub> solutions to evaluate the influence of the various functional groups on iodine adsorption and desorption in the absence of radiation. An overview of the aqueous adsorption and desorption measurements is shown in Fig. 3 and compared to epoxy paint results from BIP-1. Coupons were exposed to saturated I<sub>2</sub> solutions (<sup>131</sup>I trace labelled) containing 0.01 M KH<sub>2</sub>PO<sub>4</sub>, adjusted to pH 6. All polymers and paints tested adsorb iodine as I<sub>2</sub> from the aqueous phase. Untreated Gehopon epoxy paint had similar adsorption behaviour to the Amerlock and Ripolin epoxy paints. It should be noted, however, that iodine adsorbed faster onto untreated Gehopon as compared to heat-treated samples (coupons were heat treated at 160°C for 21 hours to simulate 15 years of ageing).

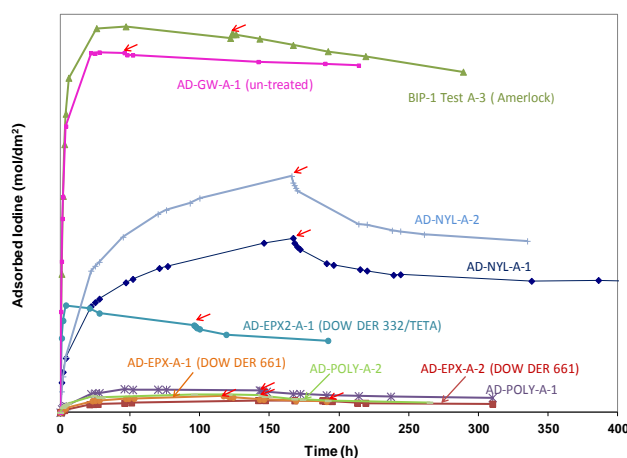


Fig. 3. Aqueous I<sub>2</sub> adsorption and desorption on polymers and epoxy paint (red arrows indicate the initiation of the desorption phase).

The overall adsorption capacity for iodine adsorbed from a saturated  $I_2$  solution was greatest for epoxy paints with somewhat less adsorption by nylon, reduced adsorption by the amine-cured epoxy resin (DOW DER 332/TETA) and significantly less by the DOW DER 661 epoxy resin and polypropylene (Fig. 3). This result suggests that the nitrogen-containing functional groups are important for iodine adsorption on epoxy paint.

In some cases it appears that the surface iodine concentration decreases slightly during the adsorption phase. This observation can be caused by a depletion of the concentration of the reactant ( $I_2$ ) or number of active sites on the coupon surface, while desorption is occurring concurrently. For paints, the maximum loading that could be achieved was limited by the available  $I_2$  in solution.

#### V. RESULTS OF GASEOUS IODINE ADSORPTION TESTS

The adsorption of iodine onto the various polymers at the standard 70°C and 70% RH conditions are shown in Fig. 4, in comparison with Amerlock and Ripolin paint (BIP-1 G-4, G-12). Although the adsorption rate was only ~ 1/5 of that observed for paint, Nylon 6/6 was the only polymer tested with significant gas-phase iodine adsorption. In fact, the adsorption onto polypropylene and the epoxy resins was so low that it was not possible to achieve the target loading for the RAD series tests.

Experiments performed under low temperature, low humidity conditions (30°C and 30% RH) yielded extremely low or undetectable adsorption rates. Iodine adsorption was similar for polypropylene and Nylon 6/6, and undetectable for DOW DER 661 epoxy.

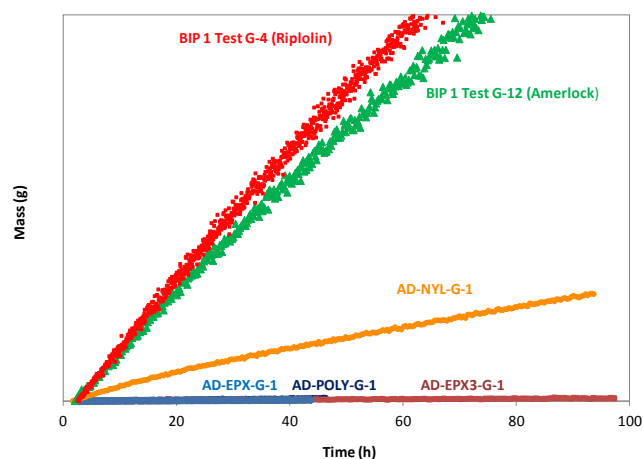


Fig. 4. Iodine Adsorption at 70°C and 70% RH for Polymers and Epoxy Paint.

The remaining tests in this series studied the effect of humidity on gas-phase adsorption. Experiments showed that the effect of humidity on iodine retention for amine-cured epoxy was small. The same was the case for polypropylene and the uncured high molecular weight epoxy resin (DOW DER 667). Only Nylon 6/6 exhibited a clear effect of humidity during gas-phase iodine exposure. The deposition rate increases with an increase in relative humidity. Although the iodine adsorption rate was significantly less than for paint (~1/10), the effect of water was comparable to that observed for Amerlock (Fig. 5).

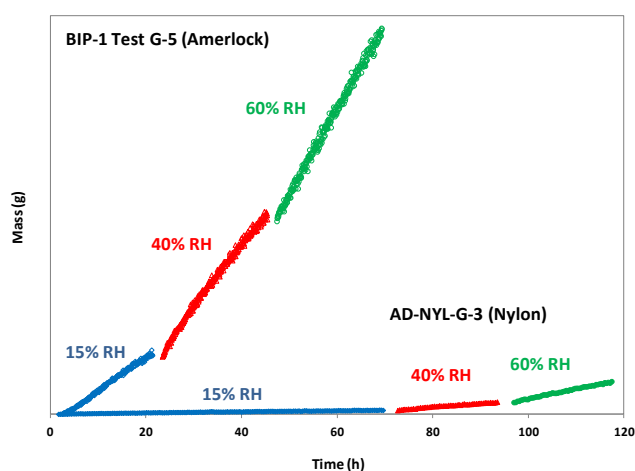


Fig. 5. Effect of Humidity on  $I_2$  Adsorption at 70°C and 15-40-60% RH for Nylon and Amerlock Paint.

## VI. RESULTS OF IRRADIATION TESTS

**Polymer Irradiation Tests**

The polymer irradiation tests were performed to gain insight into which functional groups within epoxy paint could be important for  $\text{CH}_3\text{I}$  production. Fig. 6 shows  $\text{CH}_3\text{I}$  production during the polymer tests. Because the surface loading was variable, a plot of the same data normalized to the initial iodine loading is also useful (Fig. 7). These plots can be used to help identify which structures within the paint are important for organic iodide production.

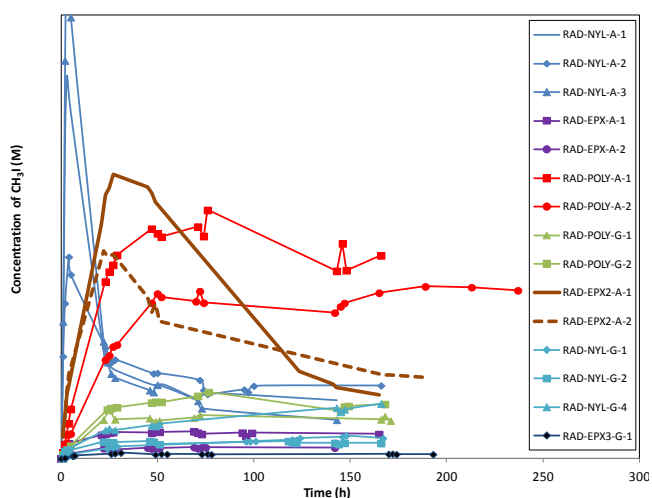


Fig. 6.  $\text{CH}_3\text{I}$  Concentration as a Function of Time (Polymer tests).

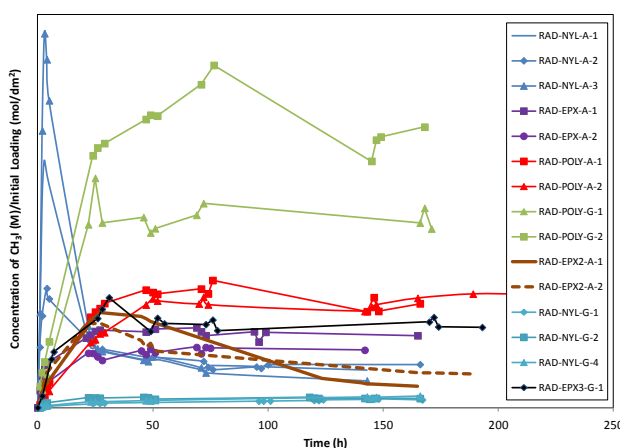


Fig. 7.  $\text{CH}_3\text{I}$  Concentration (Normalized to the Initial Iodine Surface Loading) as a Function of Time (Polymer tests).

Several observations can be made from Figures 6 and 7.

- Nylon (poly-amide) behaves most like paint in terms of quantity and evolution of  $\text{CH}_3\text{I}$ . The nylon tests show the initial sharp peak often observed for aqueous-loaded painted coupons, and the low steady-state concentration typical of gas-loaded painted coupons.
- For aqueous-phase exposure, polypropylene coupons took much longer to load than other coupons. This loading behaviour can be attributed to the chemical structure of polypropylene, which is a long chain aliphatic polymer with no functional groups (but many methyl groups). The aqueous-loaded polypropylene coupons were among the highest  $\text{CH}_3\text{I}$  producers. In the gas phase, the target iodine surface concentration was never achieved, even after  $\sim 70$  hours of iodine exposure. However, when normalized to the initial iodine surface concentration, the gas-loaded polypropylene coupons were the highest  $\text{CH}_3\text{I}$  producer (Fig. 7).
- Epoxy resin is the backbone of the epoxy paint structure. It contains aromatic rings, ether linkages, alcohol groups and epoxides at the chain ends. Aqueous-loaded epoxy coupons did not show the initial sharp peak in  $\text{CH}_3\text{I}$  evolution characteristic of painted coupons, and the quantity produced was low. Gas-loaded epoxy had the lowest  $\text{CH}_3\text{I}$  formation rate of all the polymers, mainly due to the very low iodine surface concentration achieved during the loading stage.
- The amine-cured epoxy produced more  $\text{CH}_3\text{I}$  than the epoxy resin, but when normalized to the iodine surface loading, the  $\text{CH}_3\text{I}$  production is about the same. The amine-cured epoxy also showed an early peak in the  $\text{CH}_3\text{I}$  production, although less sharp than observed for nylon. Amine-cured epoxy was formed by mixing liquid epoxy resin with an amine hardener. Therefore, the polymer contains the functional groups of the epoxy resin plus amine groups.

The polymer tests suggest that all parts of the complex paint structure have the ability to participate in both iodine adsorption and  $\text{CH}_3\text{I}$  production. However, some functional groups may be more important because they more readily adsorb iodine or because they have a

structure that is more favourable for  $\text{CH}_3\text{I}$  formation.

Perhaps the biggest surprise was the relatively high  $\text{CH}_3\text{I}$  formation from polypropylene. Very little adsorption was expected (as there is no functional groups with the ability to react with iodine, other than double bonds at the chain ends). Polypropylene, however, contains an abundance of methyl groups that may enhance  $\text{CH}_3\text{I}$  production during irradiation.

The results suggest that the initial peak observed with aqueous-loaded paint is associated with the amide, and perhaps the amine, portions of the paint polymer.

### Paint Irradiation Tests

In BIP-2, several tests on painted coupons were performed to augment the results of BIP-1. There were five tasks:

1. *Investigate the behaviour of Gehopon paint relative to the other epoxy paints tested in BIP-1.*

RAD-GW-A-1 and RAD-GW-A-2 were performed with painted coupons prepared in Germany with Gehopon paint. The irradiations were performed at  $80^\circ\text{C}$  and about 60% relative humidity. RAD-GW-A-1 showed the early peak normally associated with aqueous-loaded coupons, with a similar  $\text{CH}_3\text{I}$  formation rate as other paints (Fig. 8). RAD-GW-A-2 used pre-irradiated coupons, and had very high  $\text{CH}_3\text{I}$  production. High  $\text{CH}_3\text{I}$  formation was also observed for pre-irradiated nylon (RAD-NYL-G-4), Ripolin (RAD-EPICUR-A-3) and Amerlock (BIP-1) coupons (further discussed in Section VII).

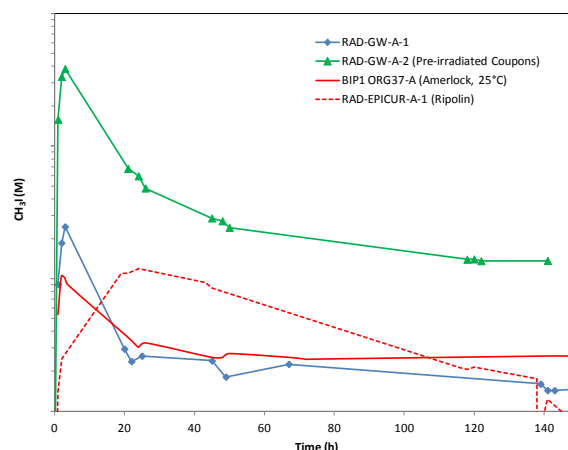


Fig. 8.  $\text{CH}_3\text{I}$  Production during Tests Performed with Gehopon Paint in Comparison to Amerlock and Ripolin (Logarithmic scale).

Qualitatively, Gehopon paint behaves similarly to other epoxy paints, supporting the concept of a common epoxy-iodine paint model. However, the high organic iodide formation suggests that factors such as paint age, heat treatment and pre-irradiation may need to be considered within the model.

2. *Perform Ripolin irradiations at  $80^\circ\text{C}$  to investigate the effect of temperature.*

The irradiation vessel was modified to allow irradiations at  $80^\circ\text{C}$ , in order to determine if the irradiation temperature affects the  $\text{CH}_3\text{I}$  production. The tests facilitate the comparison of the BIP tests to the EPICUR (Experimental Program on Iodine Chemistry Under Irradiation) tests performed in France. Several tests performed with Ripolin at  $80^\circ\text{C}$  are compared with tests performed at  $25^\circ\text{C}$  in Fig. 9. The results do not conclusively show a large effect of temperature. The results suggest a small increase in  $\text{CH}_3\text{I}$  production at the higher temperature and an enhanced  $\text{CH}_3\text{I}$  production from the pre-irradiated coupons.

Although the temperature is expected to affect the mass transport and diffusion aspects of organic iodide formation, the results suggest that it does not affect the fundamental chemistry. The radiation dose to the paint, which is not affected by the temperature, is the primary driver of methyl iodide production.

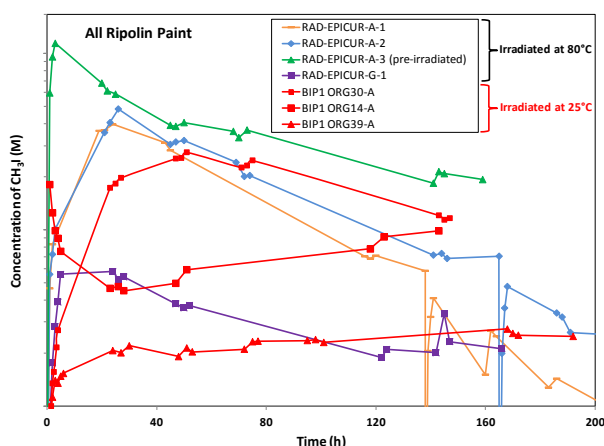


Fig. 9.  $\text{CH}_3\text{I}$  Formation during Tests Performed with Ripolin Coupons at 25 and 80°C (Logarithmic scale).

### 3. Perform additional tests to understand the effect of water on $\text{CH}_3\text{I}$ production.

Test ORG43-A included coupons loaded in the aqueous phase and subsequently dried in a desiccator. The resulting  $\text{CH}_3\text{I}$  production is similar to that of a gas-loaded coupon (i.e., low production and no initial peak) and indicates that water must be available during irradiation in order to form the high initial peak, typical of aqueous-loaded paints (Fig. 10). Test ORG44-A was similar, but received a second aqueous loading at 150 h, and was not dried. The resulting  $\text{CH}_3\text{I}$  peak at 150 h is further confirmation that residual water greatly affects  $\text{CH}_3\text{I}$  production and that the opportunity for a later ‘peak’ is not influenced by previous drying or irradiation.

In addition to these two irradiation tests, a short series of experiments was performed on some surplus ~20-year-old Ripolin coupons originally prepared for Phébus Radioiodine Test Facility tests. Headspace GCMS (Gas Chromatography Mass Spectroscopy) analysis of the coupons heated to 50°C showed two or three large peaks and many very small peaks. The main peaks in the chromatogram had mass spectra consistent with *ortho* and *para*-xylene, while other peaks indicate the presence of toluene, methyl isobutyl ketone, butyl acetate and other compounds related to xylene (e.g., mesitylene, ethyl benzene). Much more release was observed for water-soaked coupons than dry coupons (irradiated or un-irradiated). The release of trapped paint solvents may be one reason for the enhanced  $\text{CH}_3\text{I}$  production rate in water-soaked

coupons. Iodine compounds were not detected in the headspace of any of the vessels containing the iodine-soaked coupons.

As it has been shown to greatly affect organic iodide production, the influence of water may need to be considered within post-accident iodine behaviour models because, within containment, epoxy paint will be submerged or exposed to condensation and water sprays.

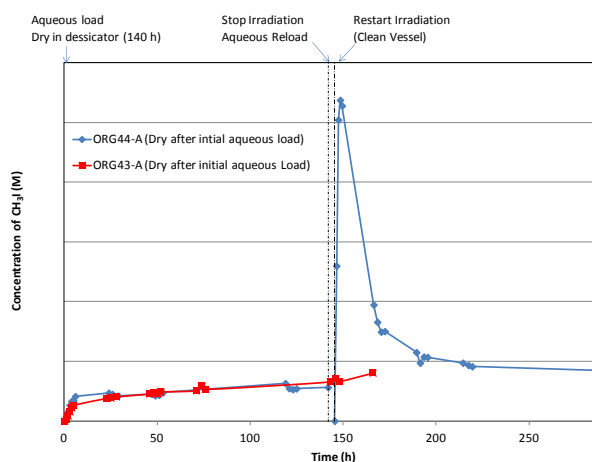


Fig. 10.  $\text{CH}_3\text{I}$  Formation during Painted Coupon Tests.

The enhanced detection of paint solvents from water-soaked coupons offers an explanation and possible modelling strategy for increased organic iodide production in aqueous-loaded RAD tests. However, it must be noted that increased iodine production was also observed during the nylon radiation tests. It is not known if residual solvents or other chemicals are trapped within the nylon polymer. Future tests performed with solvent-free paint (pre-leached or thermally treated) may help determine if residual solvents are important.

### 4. Tests using oxidized forms of iodine on paint.

Oxidized forms of iodine will be present in containment as a product of iodine oxidation in both the liquid and gas phases. The reaction between  $\text{I}_2(\text{g})$  and  $\text{O}_3(\text{g})$  is known to produce aerosols consisting of compounds like  $\text{I}_4\text{O}_9(\text{s})$  and  $\text{I}_2\text{O}_5(\text{s})$ , which can settle on painted surfaces within containment. In contact with water, the solids will dissolve and hydrolyze into compounds including  $\text{HIO}_3$ .

Experiments RAD-IOX-1 and RAD-IOX-2 explored the possibility that, in contact with

paint, these compounds contribute to the formation of organic iodides. For test RAD-IOX-1, painted coupons were sprinkled with  $I_2O_5(s)$ , while for test RAD-IOX-2, coupons were loaded by immersion in  $10^{-3}$  M  $HIO_3$ . Although low,  $CH_3I$  production was observed in both cases, indicating that  $I_2$  need not be the adsorbed iodine species in order to form methyl iodide. The  $HIO_3$  and  $I_2O_5$  may be reacting directly with the paint, or may be undergoing conversion to more reactive species during irradiation or by interaction with residual water.

##### 5. Tests with coupons pre-exposed to $Cl_2$ & $NO_2$ .

RAD-CHLOR-G-S was a scoping test to investigate how chlorine gas, thought to be produced during a reactor accident by the degradation of cable insulation, might affect the interactions between iodine and paint. For this test, Amerlock coupons were exposed to 5 ppm  $Cl_2(g)$  in air at  $70^\circ C$  and 70% RH for one hour prior to the usual iodine loading and irradiation. The concentration ( $1.8 \times 10^{-7}$  M  $Cl_2$ ) is an order of magnitude larger than the usual iodine-loading concentration of  $10^{-8}$  M. Fig. 11 shows that the  $CH_3I$  production from this test is within the normal range for gas-loaded coupons. The chlorine did not have any observable effect on the coupon or on  $CH_3I$  production. Methyl chloride, a potential product of radiolysis following  $Cl_2$  exposure, was not detected by GC analysis during the test.

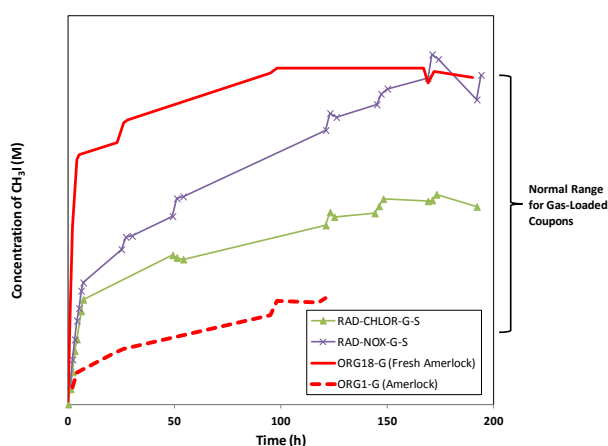


Fig. 11.  $CH_3I$  production from Amerlock coupons in the presence and absence of  $Cl_2$  or  $NO_2$ .

RAD-NOX-G-S was a scoping test that investigated the effect of air radiolysis products

on  $CH_3I$  production. For this test, Amerlock coupons were exposed to 5 ppm  $NO_2(g)$  in air at  $70^\circ C$  and 70% RH prior to the usual iodine loading and irradiation. Fig. 11 shows that this concentration of  $NO_2$  had a negligible effect on  $CH_3I$  production at this concentration. No additional products were detected in the GC samples taken during the irradiation.

The results of these scoping tests show that a 1 h pre-exposure to 5 ppm  $NO_2$  or  $Cl_2$  does not affect the subsequent iodine paint interactions. These concentrations were chosen to be approximately representative of that expected in containment; however, further study may be required to determine if these concentrations represent conservative values.

##### Iodine Compound Irradiation Tests

Small quantities of pure, commercially-available, iodine-containing organic compounds were irradiated in air to gain insight into what types of structures can produce methyl iodide upon irradiation. Compounds included iodophenol, iodobenzyl alcohol, iodoethanoic acid, iodopropionic acid, 1-iodobutane, 2-iodobutane, 2-iodo-2-methylpropane, iodoacetamide, iodoethane, iodoethanol, and (iodomethyl)trimethylammonium iodide.

A small amount of each compound was placed in a small, glass vial equipped with a septum. During irradiation, gas samples were removed periodically to determine the methyl iodide concentration by GC.

It was found that methyl iodide was produced from all iodine compounds irradiated. The production rate was generally higher for volatile compounds, which may be related to the simple chemical structure of the volatile compounds. For example, it is easy to rationalize that fewer steps would be required to make methyl iodide from an aliphatic compound than an aromatic compound. These results suggest that gas-phase radiolysis reactions may contribute to  $CH_3I$  production.

## VII. PRE-IRRADIATION

In several tests throughout BIP-1 and BIP-2, coupons were pre-irradiated prior to iodine loading. In all cases, the coupons tended to have

higher  $\text{CH}_3\text{I}$  production, in comparison to tests performed without pre-irradiation.

- During BIP-1, pre-irradiated Amerlock paint produced higher than average steady-state  $\text{CH}_3\text{I}$  concentrations.
- AD-GW-A-2 had higher  $\text{CH}_3\text{I}$  production than RAD-GW-A-1.
- RAD-EPICUR-A-3 had higher  $\text{CH}_3\text{I}$  production than RAD-EPICUR-A-1 or RAD-EPICUR-A-2.
- Pre-irradiated nylon (RAD-NYL-G-4) had higher  $\text{CH}_3\text{I}$  production than samples without pre-irradiation.

The accumulation of radiation damage to the polymer enhances the formation rate of  $\text{CH}_3\text{I}$  and may be one reason that the  $\text{CH}_3\text{I}$  concentration increases as dose to the coupon accumulates during the test.

#### VIII. SEM/EDX Analysis

As part of the work for BIP-2, some experiments were performed on aged Ripolin coupons (~20 years old) that were originally prepared for the Phébus FP project for tests performed in the Radioiodine Test Facility. Coupons were exposed to various combinations of water, iodine and irradiation. Some of the coupons were examined by Scanning Electron Microscopy (SEM) and Energy Dispersive X-ray (EDX) spectrometry. Samples were cut using a slow-speed diamond saw (for metallurgical sample preparation) to expose the cross-sectional area of the paint so that the penetration depth of iodine could be measured. Various observations were made:

- Paint appears porous under high magnification (Fig. 12).
- Elemental EDX data show that paint is mainly C, O, Si, Ti (nitrogen is difficult to detect).

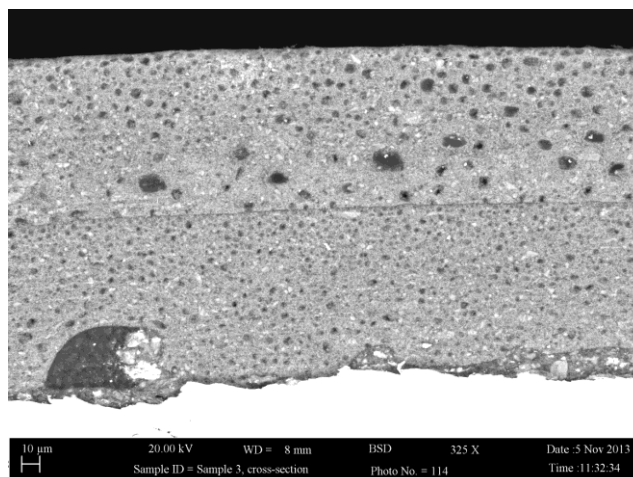


Fig. 12. SEM Image of the Cross Section of a Ripolin Paint Layer.

- Thickness of the paint layer is variable over the surface of the coupon.
- Two-layer compositions can be observed within the paint (Fig. 12). These layers are thought to correspond to the primer and topcoat.
- Several metals are detected at low concentrations, with some present only in the primer layer (e.g., Mg, Pb).
- Iodine is not simply trapped on the paint surface, but penetrates more than 100  $\mu\text{m}$  (Fig. 13). Iodine concentration (after exposure to an  $\text{I}_2$  solution) decreases as a function of depth and seems to penetrate only the topcoat. This depth of penetration may help explain why a large fraction of iodine does not desorb during irradiation.

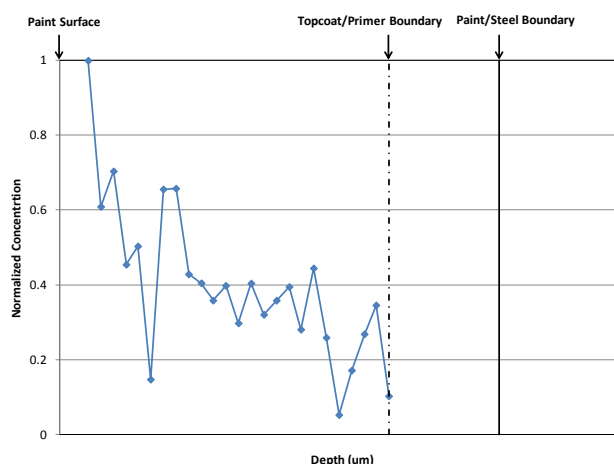


Fig. 13. Iodine penetration into epoxy paint.

## IX. CONCLUSIONS

The results from the final phase of BIP-2 build on the observations from BIP-1. Some conclusions derived from BIP-2 (organized by test series) include:

### Gas Phase Adsorption

- Iodine does adsorb onto the selected polymers, although at slower rates than is typical for epoxy paints.
- At 70°C and 70% RH, the adsorption rate of iodine on pure epoxy resin (DOW DER 667) is similar to polypropylene, while adsorption on nylon and amine-cured epoxy is significantly faster.
- Only nylon has similar behaviour to paint with respect to deposition velocity dependence on relative humidity (i.e., deposition rate increases with increasing relative humidity).

From this information, we can conclude that, while iodine seems to preferentially associate with the nitrogen-containing functional groups (i.e., amine, amide), reaction with many parts of the complex paint structure are possible. This can help explain the differences in sorption behaviour between various epoxy paints, and may help explain the observed methyl iodide formation rates.

### Aqueous Phase Adsorption

- All polymers and paints tested adsorb iodine as I<sub>2</sub> from the aqueous phase.
- Iodine adsorption on nylon is fast, but slower than that on Amerlock paint.
- Amine-cured epoxy polymer adsorbs iodine more rapidly than the unmodified epoxy resin.
- The iodine adsorption rate for epoxy and polypropylene are lower than the amine-cured epoxy polymer and significantly slower than for nylon or epoxy paint.

Similar to gas phase adsorption, we can conclude that, while aqueous iodine seems to preferentially associate with the nitrogen-containing functional groups, reaction with many parts of the complex paint structure are possible. This can help explain the differences in sorption behaviour between various epoxy paints.

### Coupon Irradiation Tests

- CH<sub>3</sub>I production is not limited to a single bonding site or functional group within the paint structure. The mechanism for the radiolytic production of CH<sub>3</sub>I appears to be complex and cannot be unambiguously ascribed to any specific functional group in the polymer structures.
- CH<sub>3</sub>I production has been observed during experiments performed with several different epoxy paints (Amerlock, Ripolin, Epigrip, and Gehopon).
- CH<sub>3</sub>I production has been observed during experiments performed with several model polymers, even when the initial iodine loading concentration is very low.
- The initial CH<sub>3</sub>I peak associated with aqueous-loaded paint coupons is clearly observed for nylon (a polyamide polymer). Many epoxy paints contain polyamide constituents.
- The shape of the methyl iodide evolution curve for both aqueous and gas-loaded nylon resembles that observed for epoxy paints.
- The initial CH<sub>3</sub>I peak associated with aqueous-loaded paint coupons was not observed during aqueous-loaded epoxy resin coupon tests. Although all epoxy paints contain a form of epoxy resin, it appears that this component is not responsible for the observed CH<sub>3</sub>I peak.
- Amine-cured epoxy yields more methyl iodide than the uncured epoxy resin.
- Residual water following submersion is required for the CH<sub>3</sub>I peak associated with aqueous loading. Drying the coupons after aqueous loading negates the CH<sub>3</sub>I peak.
- Soaking promotes the release of paint solvents (as observed in the GCMS study of aged Ripolin coupons). This phenomenon is a possible explanation for the high initial production rate of CH<sub>3</sub>I observed during irradiation for aqueous loaded paints.
- Methyl iodide production is slightly larger when Ripolin coupons are irradiated at 80°C (relative to room temperature). The significance of this small increase is not known.
- Pre-irradiating coupons prior to iodine loading generally increases the CH<sub>3</sub>I

production (observed for Amerlock, Ripolin, Gehopon and Nylon coupons).

- Gehopon epoxy paint behaves similar to other epoxy paints but has higher CH<sub>3</sub>I production. This observation may be associated with the heat treatment and pre-irradiation.
- Exposure to Cl<sub>2</sub> and NO<sub>2</sub> at 5 ppm (in air) does not seem to affect organic iodide production from irradiated coupons.
- CH<sub>3</sub>I is detected when Amerlock coupons are loaded with oxidized forms of iodine such as HIO<sub>3</sub> and I<sub>2</sub>O<sub>5</sub>. These chemical species may be converted to more reactive forms of iodine during the irradiation.

These observations suggest that while iodine may react with various chemical compounds on and within paint, the resulting organic iodides can break down under irradiation to form methyl iodide. The methyl iodide formation does not appear to be a specific reaction associated with a particular bonding site or functional group, but rather seems to be a common degradation product during a complex free radical degradation process.

The results from the coupon irradiation tests can be used to guide the development of computer models and provide data for their validation.

The data shows that there are similarities in the iodine-paint interaction between the epoxy paints studied, which allows some optimism for the development of a generic iodine-paint model. However, the results also suggest that the treatment of the paint (e.g., pre-irradiation), and differences in the chemical makeup of the paint (i.e., type of hardener) can affect its behaviour with respect to iodine.

While the BIP-2 work has progressed our understanding of the iodine-paint interactions, some areas for further study have been identified including expanding our knowledge of:

- Various paint “ageing” mechanisms;
- Reactants that compete for active sites on the paint;
- Formation and destruction of methyl iodide in the gas phase.

These areas will be discussed in a separate paper (Yakabuskie et al., in these proceedings) and will

be proposed as part of the potential BIP-3/STEM-2 project.

## ACKNOWLEDGMENTS

We would like to thank the BIP members for their financial and intellectual contributions over the years.

## NOMENCLATURE

BIP = Behaviour of Iodine Project

DGEBA = Di-Glycidyl Ether of Bisphenol-A

EDX = Energy Dispersive X-Rays

EPICUR = Experimental Project on Iodine Chemistry Under Irradiation

GC = Gas Chromatography

GCMS = Gas Chromatography Mass Spectroscopy

OECD = Organisation for Economic Co-operation and Development

SEM = Scanning Electron Microscopy

STEM = Source Term Evaluation and Mitigation

TETA = Triethylenetetramine

THAI = Thermalhydraulics Hydrogen Aerosol Iodine

## REFERENCES

1. B. Clément, L. Cantrel, G. Ducros, F. Funke, L. Herranz A. Rydl, G. Weber and J.C. Wren, “State of the Art Report on Iodine Chemistry”, Nuclear Energy Agency Report, NEA/CSNI/R(2007)1, (2007).
2. J.C. Wren, J.M. Ball, G.A. Glowa, “The Chemistry of Iodine in Containment”, Nucl. Tech., **129**, 297 (2000).
3. J.C. Wren, J. Paquette, D.J. Wren, G.G. Sanipelli, “The Formation and Volatility of Organic Iodides”, Proc. of the Specialists’ Workshop on Iodine Chemistry in Reactor Safety, UK Atomic Energy Authority, Harwell, England, p. 333 (1985).
4. G.A. Glowa and C.J. Moore, “NEA Behaviour of Iodine Project Final Summary Report” Nuclear Energy Agency Report NEA/CNSNI/R(2011)11 (2012).

**THE BEHAVIOUR OF IODINE PROJECT: A PROPOSAL FOR BIP-3**

P.A. Yakabuskie\*, C.J. Moore, G.A. Glowa  
Canadian Nuclear Laboratories, Chalk River, Canada

\*Corresponding author, tel: (+1) 613-584-3311 (ext. 43146), Pam.Yakabuskie@cnl.ca

**Abstract** – *Continued improvement of existing computer models for predicting post-accident fission product behaviour in containment relies on a comprehensive understanding of all relevant phenomena and high-confidence data. Unexpected iodine behaviour observed during the international Phébus FP program highlighted the need for a greater understanding of iodine behaviour. Recently, there have been several NEA initiatives to study the behaviour of iodine in containment: the THAI (Thermalhydraulics, Hydrogen, Aerosol, Iodine) project, the STEM (Source Term Evaluation and Mitigation) project and the Behaviour of Iodine Projects (BIP-1 and BIP-2). Despite considerable advancements in our understanding of this topic over the past several decades, there are still outstanding gaps in our knowledge that warrant further investigation.*

*Several topics of interest for a potential third phase of the NEA Behaviour of Iodine Project (BIP-3) were recently assembled and a poll of the BIP-2 Programme Review Group was conducted to gauge the relative interest in each area. The poll results provided a prioritized ranking of research topics that has helped inform the proposed BIP-3 research program. While the preliminary topics were not limited to studies of iodine behaviour, the proposed research areas for BIP-3 are complementary to the completed BIP-1 and BIP-2 programs, and focus mainly on remaining questions surrounding the iodine-paint interaction.*

*In particular, we intend to further explore the effects of paint ageing and pre-irradiation, total dose and dose rate, humidity and wetting of painted surfaces and the presence of competing species (e.g., NO<sub>x</sub>, Cl<sub>2</sub>) on adsorption and desorption processes. Radiolytic studies relating to CH<sub>3</sub>I production and degradation in the gas phase are also recommended. An outline for the proposed BIP-3 program will be discussed in detail.*

## I. INTRODUCTION

The NEA Behaviour of Iodine Project (BIP) was created to investigate the interactions between iodine and paint. The adsorption of iodine onto epoxy paint and the subsequent radiolytic production and release of organic iodides from painted containment surfaces were of particular interest. A database of iodine deposition data was accumulated in BIP-1 and expanded in BIP-2. Additionally, BIP-2 probed the mechanisms of iodine-paint interactions, and improved our understanding of the nature of iodine bonding on paint. Key results from the first two phases of the BIP are available [1, 2]. (See paper by Glowa et al., in these proceedings [1]).

In addition to BIP, several other NEA initiatives have contributed to our understanding of iodine behaviour in containment, including the THAI (Thermalhydraulics, Hydrogen, Aerosol, Iodine) and the STEM (Source Term Evaluation and Mitigation) projects. The development of a computational model that can universally reproduce the experimental observations from each of these projects is the primary long-term goal. However, many key questions surrounding iodine behaviour remain unresolved, and additional data is required to improve our modeling capabilities [3].

Canadian Nuclear Laboratories (CNL) is proposing a 3-year project (BIP-3) to build upon the progress made to date in the Behaviour of Iodine Projects. The size and funding structure will be similar to BIP-2, which was completed in September 2014. The project scope will address outstanding modeling issues and provide an opportunity to build upon work initiated in BIP-2.

At the conclusion of the BIP-2 programme, a selection of topics for inclusion in the BIP-3 program was prioritized by the group members. The proposed topics of study are required to further improve the understanding of post-accident iodine behaviour in nuclear reactor containment buildings with a particular focus on iodine adsorption, desorption and organic iodine generation from interaction with paints.

Topics for BIP-3 have been chosen to make effective use of our existing facilities and expertise. It should be noted that other important

and unresolved topics, such as the stability of iodine-containing aerosols, are better handled within the OECD-STEM project.

## II. PROPOSED TOPICS

Paint is an important iodine sink in containment; therefore, kinetic data that describes the iodine-paint interaction is needed to simulate post-accident iodine behaviour. Thus far, BIP has provided deposition velocities for a variety of epoxy paints under various conditions. The topics suggested for BIP-3 are related to the iodine-paint interaction, specifically sorption behaviour and the formation of organic iodides. Closely related to these topics are the effects of paint ageing, residual water and the competitive effect of reactive species such as  $\text{Cl}_2$  and  $\text{NO}_x$ .

This section will introduce the proposed study topics that received the highest ranking from the BIP-2 program review group, and their rationale.

### Iodine Desorption Behaviour

In the absence of irradiation, gas phase iodine desorption from epoxy paint has been observed under the conditions of both BIP and STEM tests (25 to 80 °C).

A typical gas phase adsorption and desorption profile ( $\text{I}_2$  loading concentration of  $10^{-8}$  M) is shown in Fig. 1. It is also clear from STEM tests that the release of both inorganic and organic forms of iodine is promoted by irradiation.

In BIP-3, we propose that the relationship between iodine loading concentration and fraction desorbed (without irradiation) be systematically determined. This data is required in order to properly quantify the radiolytic release process and improve the interpretation of results from BIP and STEM tests.

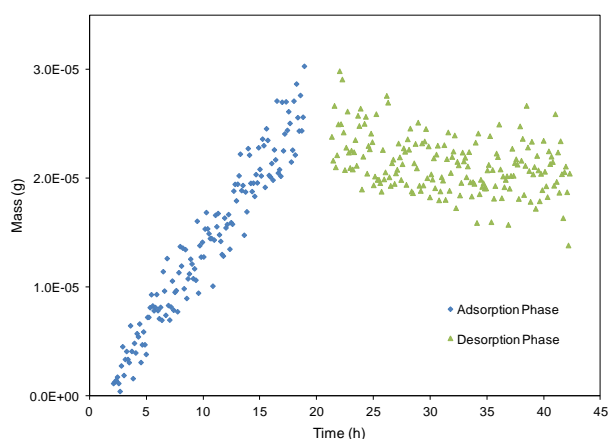


Fig.1. Iodine adsorption and desorption on aged Amerlock paint at 30 °C and 80% RH (BIP-1 Test G-19).

#### Adsorption Capacity

Although saturation of paint with iodine is not anticipated on post-accident containment surfaces, it is useful to know the adsorption capacity of paint as an input for modeling. The adsorption capacity is a fundamental parameter that defines the number of available active sites. Adsorption measurements can be performed using the iodine adsorption apparatus (gas phase) and using repetitive aqueous loadings. Iodine will be adsorbed for various lengths of time (some long term), followed by desorption. By altering the temperature, humidity and gas concentration (both higher and lower than previous tests) the capacity (and initial deposition velocity) can be measured over a wide range of conditions. An example of a long-term gas phase exposure test (~100 hours) is shown in Fig. 2 ( $I_2$  loading concentration of  $10^{-8}$  M).

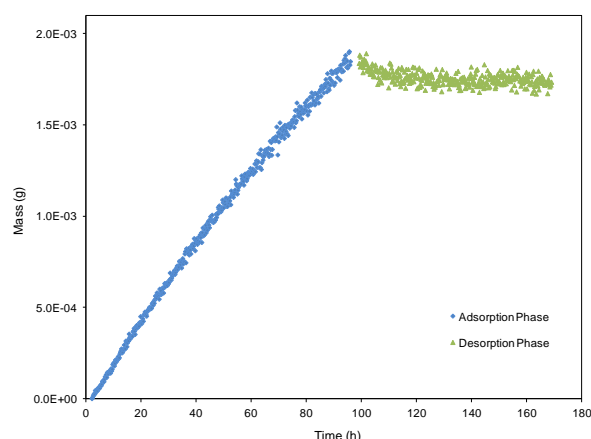


Fig. 2. Iodine adsorption and desorption on fresh Amerlock paint at 70 °C and 70% RH (BIP-1 Test G-12).

#### Iodine Retention during Long Irradiations

For modelling purposes, it is useful to determine how much iodine is retained on paint at long irradiation times. This fraction could affect the design of an iodine model; any iodine that is permanently fixed will affect simulation results, especially for accident scenarios lasting many weeks. Long-duration irradiations will be performed on iodine-loaded painted coupons to determine if some iodide is permanently retained.

It is not known if the rate of iodine loss from an irradiated paint surface is linear, exponential or if a fraction is permanently bound. This information can affect the simulated gas phase organic iodide concentration and the design of any model to simulate this phenomenon. Thus far, BIP tests have been limited to ~150-200 h (at 1-4 kGy/h). We propose increasing the total dose to the extent practical.

#### Paint Ageing

Most members of the BIP-2 programme review group are interested in studying the effects of paint ageing on sorption and organic iodide production. The effects of ageing, both in-service ageing and ageing processes that occur during reactor accidents, can significantly impact the interactions of iodine with paint [3]. Thermal, chemical and radiation- induced changes to the paint can influence:

- the quantity and accessibility of residual solvents for reaction,
- the number of available active sites for surface chemical reactions,
- oxidation of some functional groups on the outer surfaces, and
- mechanical paint degradation (chalking, checking, cracking, flaking, blistering or delamination).

To date many iodine experiments have been performed with relatively fresh paint (e.g., Radioiodine Test Facility (RTF), BIP and STEM experiments). Some experiments have utilized thermal-curing processes to accelerate ageing, but it is not definitively known how well this simulates the ageing of in-service paint. The chemistry of thermally-cured paint may be different from that of more naturally aged paint. However, it should be noted that, in the initial stages of some accident cases, the containment paint may be subjected to high temperatures.

#### Paint Ageing – Effect on Sorption Behaviour and $\text{CH}_3\text{I}$ Production

Paint ageing standards [4, 5] may contain useful procedures for simulating the mechanical aspects of paint ageing, but may not accurately simulate the chemical changes to paint during routine operation. Alternatively, artificial ageing techniques using thermal treatment are commonly used to accelerate the degradation processes associated with long-term service. Previous BIP studies investigating the effects of paint ageing have used painted coupons that had simply aged for extended periods in a laboratory setting.

We propose tests with new and aged paints to gain a further understanding of the effects of ageing on iodine adsorption and  $\text{CH}_3\text{I}$  production. The effect of thermal and laboratory ageing techniques will be compared.

#### Paint Ageing – Effect of Pre-irradiation on Sorption Behaviour

We propose that the effect of irradiation on iodine adsorption behaviour be determined at high doses. There are some indications in earlier

work that the iodine adsorption rate decreases for pre-irradiated specimens at doses approaching 1 MGy [6]. To date, our results do not suggest that adsorption of iodine on paint will decrease with dose. However, measurements are required at doses higher than in previous BIP studies to determine if adsorption is reduced above some critical dose.

#### Paint Ageing – Effect on Residual Solvents

Residual solvents trapped in the paint matrix have been implicated as a source of reactants for the production of organic iodides during paint irradiations. Curing time (ageing) influences the availability of solvents that can be leached from the paint surface during exposure to liquid water. For vinyl-painted coupons exposed to water, Wren et al. [7] found that the release of MIBK (methyl isobutyl ketone), a major paint thinner constituent, was reduced as a result of ageing (Fig. 3). Proposed tests will compare the amount of releasable solvents from new, aged and pre-irradiated epoxy paint to determine the effect of these treatments on the release of residual solvents. Solvent release as a function of submersion time can be investigated.

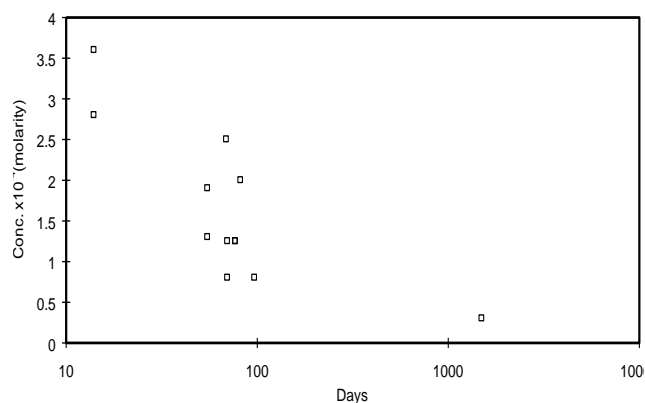


Fig. 3. The final steady-state concentration of MIBK released from vinyl-painted coupons as a function of age [7].

#### $\text{CH}_3\text{I}$ Radiolysis

When organic iodides such as  $\text{CH}_3\text{I}$  are released from irradiated paint, they are subject to degradation by reaction with air radiolysis products. This degradation strongly influences the accumulation of organic iodides in the gas

phase, and must, therefore, be considered within iodine behaviour models. Kinetic data (i.e., radiolytic destruction rate) measured in BIP-1 agrees with other literature values under the conditions tested. Fig. 4 shows typical results for a multiple injection test to quantify the rate of gas phase methyl iodide degradation (BIP-1, Test ORG32-M).

It has been hypothesized that water vapor can change the concentrations of air radiolysis products such that the degradation rate of gas phase  $\text{CH}_3\text{I}$  is decreased. Because accident scenarios generally involve the release of steam, we propose that the effect of humidity (and perhaps other added impurities) be further studied in BIP-3. The quantification of this process under various conditions will help extract organic iodide formation rates from earlier BIP and RTF experiments.

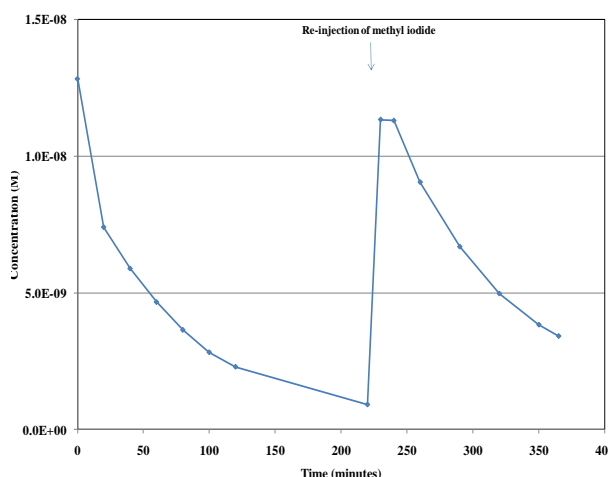


Fig 4.  $\text{CH}_3\text{I}$  concentration as a function of time during irradiation.

#### $\text{CH}_3\text{I}$ Formation in the Gas Phase

The possibility that organic iodides are formed in the gas phase is generally dismissed due to the large concentration of  $\text{O}_2$  relative to  $\text{I}_2$  (i.e., the  $\text{O}_2$  outcompetes the  $\text{I}_2$  for any organic radicals formed). However, work by Bartoniček and Habersbergerová [8, 9] shows that methyl iodide formation is detected in irradiated mixtures of air, methane and  $\text{I}_2$ .

In BIP-3 we propose to investigate the process by irradiating dilute mixtures of  $\text{I}_2$  and  $\text{CH}_4$  in humid air. The detection of small concentrations ( $\sim 10^{-12}$  M) of methyl iodide is possible using our gas chromatograph system.

#### Competition with Reactive Containment Gas Species ( $\text{Cl}_2$ , $\text{NO}_x$ )

In BIP-2, exploratory tests were performed to study how reactive containment species such as  $\text{Cl}_2$  (from cable pyrolysis), and  $\text{NO}_2$  (from air radiolysis) affects the iodine-paint interaction. In these tests, Amerlock coupons were exposed to 5 ppm  $\text{Cl}_2(\text{g})$  or  $\text{NO}_2(\text{g})$  in air at 70 °C and 70% RH for one hour prior to the usual iodine loading and irradiation. The results showed no significant change to iodine sorption or  $\text{CH}_3\text{I}$  formation.

In BIP-3, we propose tests with higher concentrations of competing species (up to 1000 times the concentration of iodine). Post-accident containment could contain iodine at a much smaller concentration than other gas phase impurities. These competing species may occupy available sites on the paint surface, reducing the sites available for iodine adsorption. The influence of competing species is critical to the modeling of iodine behaviour under realistic accident conditions.

#### Effect of Wet/Dry Cycling

BIP-1 and -2 showed that the method used for loading iodine on paint affected the formation of methyl iodide during irradiation. Painted coupons loaded by submersion in iodine solutions had higher initial  $\text{CH}_3\text{I}$  production compared to coupons loaded by exposure to gas phase  $\text{I}_2$ .

Further tests in BIP-2 showed that the  $\text{CH}_3\text{I}$  production arising from coupons loaded by exposure to an aqueous iodine solution, but subsequently dried, more closely resembled that of coupons loaded by exposure to gas phase  $\text{I}_2$ . The  $\text{CH}_3\text{I}$  concentration profiles during BIP-2 tests ORG43-A and ORG44-A are similar to that observed for gas-loaded coupons (i.e., low production and no initial peak), Fig. 5.

However, after a second aqueous phase iodine loading in BIP-2 Test ORG-44, the high initial peak in  $\text{CH}_3\text{I}$  concentration, typical of aqueous-loaded paints, was observed. This indicates that water must be available during irradiation in order to form the peak.

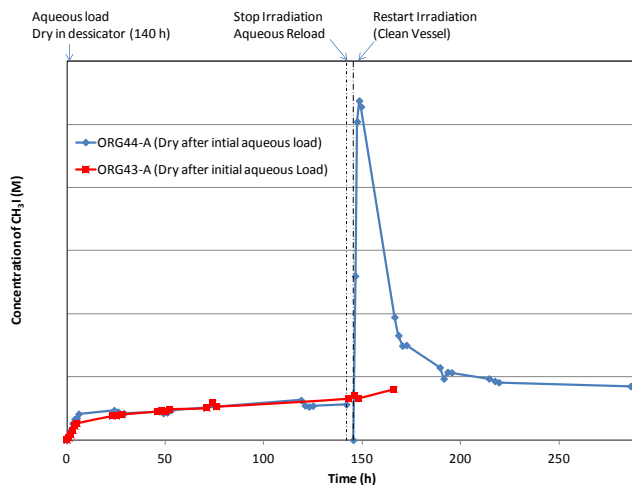


Fig. 5.  $\text{CH}_3\text{I}$  formation during painted coupon tests.

To complete the series, we propose to wet coupons that were loaded by exposure to gas phase  $\text{I}_2$ . This case is intended to be representative of containment walls that are wetted by sprays or condensation.

### III. CONCLUSIONS

A new 3-year NEA project (BIP-3) is being proposed to build upon the progress made in previous Behaviour of Iodine Projects. The proposed topics for study address important and unresolved topics related to iodine-paint interaction as prioritized by the BIP-2 program review group. It should be noted, however, that the program is not intended to be static; the test matrix will evolve based on test results. A portion of the test matrix will be unpopulated to allow new ideas to be added during the project life.

### ACKNOWLEDGMENTS

Thanks to BIP members for their support and guidance during BIP-1 and BIP-2 and for their ranking and comments regarding the proposed BIP-3 program.

### NOMENCLATURE

BIP = Behaviour of Iodine Project

CNL = Canadian Nuclear Laboratories

FP = Fission Product

MIBK = Methyl Isobutyl Ketone

NEA = Nuclear Energy Agency

OECD = Organisation for Economic Co-operation and Development

RTF = Radioiodine Test Facility

STEM = Source Term Evaluation and Mitigation

THAI = Thermalhydraulics, Hydrogen, Aerosol, Iodine

### REFERENCES

1. G.A. Glowa and C.J. Moore, "NEA Behaviour of Iodine Project Final Summary Report," *Nuclear Energy Agency Report*, NEA/CNSI/R(2011)11 (2012).
2. G.A. Glowa, C.J. Moore and D. Boulianne, "The Main Outcomes of the OECD Behaviour of Iodine Project", This Conference, Paper 1.8 (2015).
3. L. Bosland, S. Dickinson, G.A. Glowa, L.E. Herranz, H.C. Kim, D.A. Powers, M. Salay and S. Tietze, "Iodine-Paint Interactions during Nuclear Reactor Severe Accidents," *Annals of Nuclear Energy*, **74**, 184 (2014).
4. AFNOR, "Peintures pour l'industrie nucléaire: essai de tenue à des conditions accidentelles de référence (réacteur à eau sous pression) et de répartabilité". *Association Française de Normalisation*, AFNOR NF T30-900, ISSN 0335-3931, (1996).
5. ASTM, "Standard test method for evaluating coatings used in light-water nuclear power plants at simulated design basis accident (DBA) conditions". *American Society for Testing and Materials International*, ASTM-D3911-08, West Conshohocken, PA. (2008).
6. A.B. Aleksandrov, N.I. Ampelogova, M.A. Karaseva, V.G. Kritskii and N.G. Petrik, "The effect of physicochemical conditions on the absorption of molecular iodine by

- protective varnish and paint coatings during accidents at a nuclear power station with a VVER-640 reactor,” *Therm. Eng.*, **42**, 12, 991-996 (1995).
7. J.C. Wren, D.J. Jobe, G.G. Sanipelli, and J.M. Ball, “Dissolution of Organic Compounds from Vinyl, Epoxy and Polyurethane Coated Surfaces,” *Nucl. Technol.*, **125**, 991-996 (1999).
  8. B. Bartoníček and A. Habersbergerová, “Investigation of the Formation Possibilities of Alkyl Iodides in Nuclear Power Plants,” *Radiat. Phys. Chem.*, **28**, 5, 591 (1986).
  9. B. Bartoníček and A. Habersbergerová, “Formation of Methyl Iodide by Ionizing Radiation,” *Proc. of the 4<sup>th</sup> Working Meeting on Radiation Interactions*, p. 49, Leipzig, Germany (1987).

## OECD/STEM PROJECT AND ITS FOLLOW-UP STEM2

*Christian MUN<sup>(1)\*</sup>, Loïc BOSLAND<sup>(1)</sup>, Laurent CANTREL<sup>(1)</sup>, Juliette COLOMBANI<sup>(1)</sup>, Olivia LEROY<sup>(1)</sup>,  
Marie-Noelle OHNET<sup>(1)</sup>, Thierry ALBIOL<sup>(1)</sup>*

*(1) Institut de Radioprotection et de Sûreté Nucléaire (IRSN), PSN-RES, St Paul lez Durance, 13115, France*

*Corresponding author, Tel: (+33)4.42.19.96.24, christian.mun@irsn.fr*

**Abstract** –*The STEM (Source Term Evaluation and Mitigation) OECD project operated by IRSN, has been launched mid-2011 in order to gain confidence into the Source Term (ST) evaluation and to reduce uncertainties on specific phenomena dealing with the chemistry of two major fission products: iodine and ruthenium, in the event of a severe accident (SA) on a nuclear power plant. These data are also useful to design mitigation means like FCVS or others and also to evaluate the gain of potential deployed mitigation means. More precisely, the STEM project consists in providing additional knowledge and improvements of calculation tools in order to allow a more robust diagnosis and prognosis of the progression of a SA, and a better evaluation of potential releases of radioactive materials. Initially, two phases were defined at the expert meeting in October 2010: the first one from mid-2011 to mid-2015 and the second one (STEM2) up to mid-2018. The first phase addressed three main issues: i/ middle-term iodine releases with specific attention to the chemical stability of iodine aerosol particles under radiation (transformation into gaseous iodine species), ii/ short and medium-term iodine-paint interactions under irradiation, iii/ ruthenium transport chemistry in order to determine the speciation of Ru, in particular the partition between gaseous and condensed forms, during its transport through the Reactor Cooling System (RCS). This paper presents the main outcomes of the STEM first phase. Together with recent results of other R&D programs in the field, notably the OECD/BIP2, STEM results have helped to define more precisely major remaining issues that are proposed to be investigated during the second phase of the project. The paper provides a description of the updated proposal for the second phase of the project that will be conducted from mid-2015 to mid-2019.*

## I. INTRODUCTION

The STEM (Source Term Evaluation and Mitigation) OECD project [1] operated by the “Institut de Radioprotection et de Sûreté Nucléaire” (IRSN), has been launched mid-2011 in order to improve the evaluation of Source Term (ST) for a severe accident (SA) on a nuclear power plant and to reduce uncertainties on specific phenomena dealing with the chemistry of two major fission products: iodine and ruthenium. More precisely, the STEM project consists in providing additional knowledge and improvements for calculation tools in order to allow a more robust diagnosis and prognosis of radioactive releases in a SA. Initially, two phases were defined at the expert meeting held in October 2010: the first one from mid-2011 till mid-2015 and the second one (STEM2) till mid-2018. The first phase addressed three main issues: i/ medium-term iodine releases with specific attention to the chemical stability of iodine aerosol particles under radiation (radiation induced decomposition producing gaseous iodine species), ii/ short and medium-term iodine-paint interactions under irradiation, iii/ ruthenium transport chemistry in order to determine the speciation of Ru, in particular the partition between gaseous and condensed forms, during its transport through the Reactor Cooling System (RCS). In the past four years, kinetics of iodine release from paints and aerosol decomposition kinetics have been quantified. New phenomena have also been identified whose influence on iodine volatility could be significant. Concerning the ruthenium part, the effect of the oxygen potential on the deposits formation has been assessed, as well as the kinetics of Ru transport after vaporization and kinetics of revaporization from the deposits in a thermal gradient tube. More precisely, after presenting the main outcomes of the STEM first phase, this paper gives insights on the main issues that are proposed to be investigated during the updated second phase, i.e. from mid-2015 to mid-2019.

Based on recent R&D results in the ST area, notably those of the OECD/BIP2 and STEM programs, topics for STEM2 have been identified, proposed and ranked by the STEM partners to fill main remaining knowledge gaps

affecting ST evaluations. It should be noted that some of the identified issues, such as for example the effect of pre-irradiation of paints on iodine paint adsorption behaviour, the  $\text{CH}_3\text{I}$  formation in the gaseous phase, or the competition with reactive containment gaseous species ( $\text{Cl}_2$ ,  $\text{NO}_x$ ), are proposed to be studied in the OECD-BIP3 proposal [2], which is complementary to the STEM2 proposal.

Let us note that in addition to STEM, several other NEA initiatives have contributed recently to the understanding of iodine behaviour in the containment building, including the THAI2 (Thermalhydraulics, Hydrogen, Aerosol, Iodine) and the BIP/BIP2 (Behaviour of Iodine Project) projects [19] [20]. The duration and the cost of STEM2 are similar to that of STEM1. A merging of the STEM2 and BIP3 proposals in order to provide in a single project offering a more complete coverage of ST remaining issues is under discussion. If a single project is finally proposed, two operating agents, IRSN and CNL, would operate the project.

## II. MAIN OUTCOMES OF STEM/IODINE PART

The STEM/IODINE experiments, carried out in the EPICUR facility, were focused on the releases of volatile molecular iodine ( $\text{I}_2$ ) and organic iodides (RI) from representative painted coupons loaded with molecular iodine [3] or iodine aerosol species ( $\text{CsI}/\text{IO}_x$ ) and placed in the gaseous phase of an irradiation vessel for  $\geq 30$  hours to evaluate medium term releases. Six tests were performed to study the releases of iodine from epoxy painted coupons loaded with  $\text{I}_2$ . Seven tests were performed to study the releases of iodine from CsI aerosols deposited on epoxy painted coupons, but also deposited on quartz and stainless steel coupons to make easier the data interpretation by preventing any interaction with paint. One test was performed with  $\text{IO}_x$  deposited on quartz and three more are still to be performed. For CsI, the effect of the parameters of main interest (temperature, relative humidity, initial concentration of iodine deposited on the sample surface) on the releases of  $\text{I}_2$  and RI (and on the global volatilization, defined as the difference between the initial quantity deposited on the coupon before irradiation and the quantity of iodine remaining

on the coupon after irradiation) are presented and discussed below. Further details are given in [4].

### II.1. Releases from painted coupons loaded with $I_2$

Figure 1 shows the general trend of the release kinetics under radiation of  $I_2$  (blue curve) and RI (red curve) from epoxy painted coupons pre-loaded with  $I_2$ . Two phases are clearly identified: one at short term for which fast release kinetics is observed and one at mid-term ( $> 10$  hours) with slower kinetics.

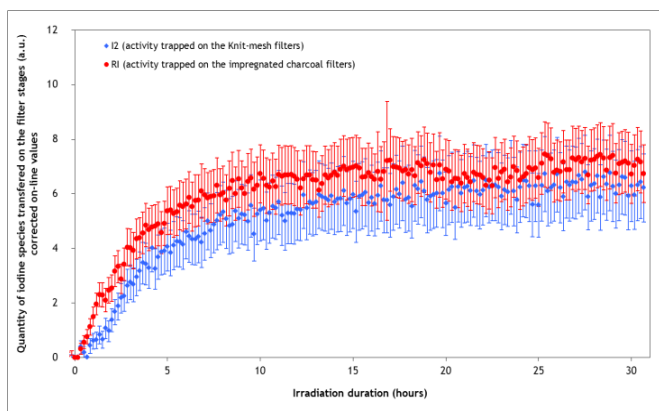


Fig. 1: General trend of the RI and  $I_2$  releases under radiolysis.

The study of initial iodine surface concentration onto the coupon on the releases showed a different impact for  $I_2$  and RI releases. Indeed, the organic iodides release was rather low ( $< 5\%$ ) with small variations (close to a factor 2, depending on the initial concentration), whereas the percentage of molecular iodine released and the global volatilization increased significantly when the initial iodine surface concentration on the coupon increased [3]. These results may be explained taking into account the molecular iodine interaction with the Epoxy paint during the loading phase. Different chemical sites are suspected for iodine-paint interaction [5]:

- chemical sites responsible for the  $I_2$  release during the irradiation phase (the reactions or interactions between iodine and paint are reversible),
- chemical sites responsible for the RI release during the irradiation phase (the reactions or interactions between iodine and paint are not reversible, and lead to the formation of RI).

The trend towards an increase in the RI fraction released at lower initial iodine surface concentration on the coupon would suggest that a larger fraction of iodine is bounded to the chemical sites responsible for RI release when the surface concentration is lower. This in turn indicates a preferential interaction of iodine with these sites, rather than with reversible sites as discussed above. Saturation of these preferred sites could be reached after a certain amount of iodine has deposited on the coupon. Further adsorption would then occur on other chemical sites identified above, leading to a relative decrease of the RI release. When the relative humidity increased from 20 to 60%, the organic iodide release and the global volatilization, mainly due to  $I_2$  release, decreased moderately. This may be explained as follows: steam may polarize iodine and ease its interaction with polar groups of paint (chemisorption) which could therefore lead to lower releases. When the temperature increased from 80°C to 120°C, the global volatilization and the molecular iodine release decreased significantly; whereas the organic iodide release was not significantly affected. A possible explanation is that iodine interaction with paint is enhanced with a higher temperature, favouring chemical adsorption reactions and leading to a decrease in the molecular iodine release at higher temperature [5].

### II.2 Releases from coupons loaded with CsI under radiation

It is recalled that the importance of this process was suspected following analysis of the PHEBUS-FP tests but was not quantified up to now; that is why tests investigating effects of irradiation on deposited CsI were performed in STEM. The results showed that the irradiation of aerosols of CsI deposited on a quartz or a stainless steel coupon led to an almost rapid and total volatilization of iodine species whereas the irradiation of aerosols of CsI deposited on a painted coupon (epoxy paint) led to a partial volatilization. This difference of behavior may be due to different interaction processes between CsI aerosols and the surface of coupons of different nature (epoxy paint or quartz or stainless steel). The general trend of the  $I_2$  and RI

releases showed only one release kinetics for each species whatever the nature of the coupon. The study of the impact of the CsI concentration loaded on the epoxy painted coupon showed that a decrease of the CsI concentration by a factor 24 and/or of the CsI particles size on the epoxy painted coupon leads to a decrease of the releases of iodine species by a factor of 3. An important decrease of the fraction of molecular iodine volatilized and a more moderate decrease of the fraction of organic iodides volatilized were observed. This decrease of the volatilization of iodine species could be due to the interactions between CsI aerosols and epoxy paint and/or by the adsorption of gaseous  $I_2$  on the painted coupon once formed near the surface by CsI decomposition. The increase of relative humidity from 20% to 60% promoted molecular iodine release from CsI deposited on a quartz coupon whereas the increase of the temperature from 80°C to 120°C did not affect significantly the fraction of molecular iodine released from a stainless steel coupon; whatever the studied boundary conditions, CsI is totally oxidized into  $I_{2(g)}$  in a few hours.

### II.3 Releases from coupons loaded with IOx

Air radiolysis leads to the formation of air radiolytic products like  $NO_2$ ,  $O_3$  or  $HNO_3$  [6] as well as shorter-lived radical intermediates that can oxidize iodine and lead to iodine oxides (IOx) particles formation, that sediment onto surfaces [7]. IOx are small aerosol particles, whose composition and chemical behavior, particularly under irradiation; are not well known. A specific device to generate this kind of aerosols has been designed by IRSN and then experiments could be performed in the EPICUR facility. The results have shown that IOx particles partly decompose under irradiation. Further investigations are thus necessary to better understand this potential additional source of volatile iodine species as their speciation and behaviour might be modified by the conditions (temperature, humidity and dose rate) over the irradiation time.

## III. MAIN OUTCOMES OF STEM/RU PART

In the frame of the STEM/RUTHENIUM program aimed at ruthenium transport studies

[8], a series of vaporization and re-vaporization experiments have been performed in the START test facility (see Fig. 2). Ru is vaporized from a crucible in a furnace at 1200°C, and then transported through a thermal gradient quartz tube, leading to an outlet temperature of 150°C to 250°C depending on the tests. The main studied parameters were the carrier gas which was a steam-air mixture at different ratios, the type of thermal gradient (“abrupt” or “smooth”) in the tube, and finally the tube material.

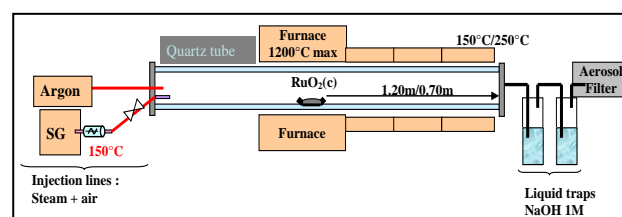


Fig. 2: Scheme of the START test facility.

After a detailed characterization of the heating phase with argon flow, the Ru vaporization kinetics in the furnace with oxidizing conditions was characterized for different carrier gas mixtures ( $H_2O/air$ ) and can be considered linear and steam content dependent. The dry air condition is the most favourable condition for the vaporization of  $RuO_2$  from the crucible at 1200°C. A good reproducibility was obtained for the vaporization test with steam/air gaseous mixture and for one hour duration.

During the vaporization study with an “abrupt” thermal profile, the long duration tests (7 hours) have shown the existence of transient phenomena during the 1<sup>st</sup> hour, confirming thus the necessity to study the ruthenium chemistry for several hours to catch the precise phenomenology. Whatever the gaseous mixture, most of the vaporized Ru is deposited in the quartz tube. The total Ru transported downstream of this tube (gas and aerosols, including Ru deposited on the dipping tube located between the tube and the liquid traps) represents a few percent of the Ru mass vaporized for long duration tests, and is mainly under gaseous form, which confirms the potential important impact of this process on Ru release. Concerning the vaporization tests, no significant effect of steam could be evidenced on the transported Ru fractions to the liquid traps; however, the total Ru amount transported is larger in the presence of steam. Moreover, this

study allowed the measurement of the deposit profiles depending on the wall temperature and did not reveal any effect of the gas mixture (with or without steam) on the Ru deposit profile in the quartz tube.

Two-thirds of the tests have been performed with a re-vaporization phase, consisting of sweeping the steam-air mixture into the tube containing Ru deposits (without generating ruthenium from the crucible). Contrary to the vaporization, no transient phenomenon was observed during this re-vaporization phase. Whatever the gaseous mixture, the Ru amount deposited in the quartz tube after re-vaporization tests represents always the major part of the initial inventory. Contrary to the vaporization tests, two peaks of Ru deposit were observed. The first peak at high temperature was detected as in the vaporization tests (~850°C) and the second peak was observed in the lower range of temperature ~450°C. In addition, this study highlighted the importance of the gaseous mixture composition during the Ru deposit formation and consequently on the re-vaporization phase. The amount of Ru transported during the re-vaporization phase is lower than in the direct vaporization phase; nevertheless, the speciation is a crucial issue as in this last case the ruthenium is only transported under gaseous form, and potentially during a quite long period (which remains to be defined more precisely). Contrary to the vaporization tests, there is a gaseous composition effect on the Ru transported during the re-vaporization tests: it is favoured by air rich mixtures. The Ru experimental mass balances for all the START tests are quite well estimated (about 80%). Finally, the total Ru transported (gas and aerosols) at the tube outlet after vaporization and re-vaporization in long duration experiments amounted to several percent of the initial inventory, in the conditions studied during this first STEM phase.

#### IV. PROPOSED TOPICS FOR STEM2

##### IV.1. STEM2/IODINE topics

As clearly indicated in [9], the modeling of key phenomena concerning iodine chemistry has been recently updated or added in the ASTEC code [10], i.e. mainly: i/. Interaction of I<sub>2</sub> and CH<sub>3</sub>I with paint under irradiation, ii/. Formation

and radiolytic decomposition of gaseous and deposited iodine oxides aerosols, iii/. Radiolytic conversion of gaseous I<sub>2</sub> into CH<sub>3</sub>I, iv/. Interaction of I<sub>2</sub> with steel and aerosols. Despite these recent significant progresses obtained or validated with the results of the first phase of the STEM program, knowledge of some processes is not sufficient to quantify their impact on iodine ST estimations; that is why in the frame of the STEM follow-up project it is proposed to investigate further the specific issues described hereafter.

##### - Paint ageing

For paints, natural ageing in normal operating conditions as well as their change during a nuclear accident (under irradiation, high temperature and humidity rate) might modify the paint capacity to trap iodine and/or produce RI. This could lead to a modified iodine volatility. The study of Aleksandrov [11] indicates that pre-irradiating an epoxy paint between 0.1kGy and 1 MGy before adsorbing iodine leads to an I<sub>2</sub> adsorption kinetics that is decreased by one order of magnitude. Except this study, no quantitative information is available in the literature although the BIP and BIP2 programs [19] [20] have mentioned the same tendency for iodine adsorption. One can also assume a potential effect on the release kinetics as suggested by BIP2 program [20]: CH<sub>3</sub>I release was found to be significantly increased in the short term whereas no data was published for I<sub>2</sub>. That is why IRSN proposed to perform some experiments with the objective to verify if high doses (> 100 – 1000 kGy) might lead to significant chemical modifications in the paint, and to assess to what extent the iodine releases kinetics (I<sub>2</sub> and CH<sub>3</sub>I) could be modified by the dose received by the paint before and all along the accident.

##### - Iodine oxides radiolytic decomposition

As it has been shown that IO<sub>x</sub> particles partly decompose under irradiation and might lead to gaseous molecular iodine, a more complete understanding of their radiolytic stability is necessary. Moreover, due to the lack of knowledge on the precise composition and evolution of I<sub>x</sub>O<sub>y</sub> species (which might significantly impact their behaviour), a more analytical study, based on surface

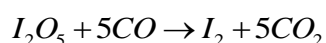
characterizations analysis, is also needed in order to better estimate the size and composition of such aerosols under different conditions. IRSN has thus proposed to study this decomposition phenomenon with a mixed approach:

- irradiation tests in the EPICUR facility by measuring on-line the release kinetics of  $I_2$  and  $CH_3I$  with the objective to study the influence of the dose, temperature and specifically higher humidity rates in order to reach and/or exceed the deliquescence point.

- surface characterizations analysis to determine the speciation of the adsorbed species.

- Iodine oxides decomposition by carbon monoxide

Various authors have reported the  $I_2O_5$  decomposition by carbon monoxide [12] [13] (and other gaseous organic compounds like propane, butane, benzene...) as being complete at ambient temperature:



This reaction might play a significant role on iodine volatility as carbon monoxide can be present in significant amount (several orders of magnitude over the iodine volatile concentration) in the containment by: i/. the  $B_4C$  absorbs degradation (for some PWRs and BWRs) and, ii/. the molten corium-concrete interactions in the containment. However, the precise speciation of  $IxOy$  into the containment building remains unclear (pure  $I_2O_5$ ,  $I_4O_9$ , and/or a mix between hydrated forms and non-hydrated forms...), as well as the extent of the interaction of these non- $I_2O_5$  species with CO. It has to be evaluated if, in the conditions of a severe accident (temperature, humidity, CO concentration in the gaseous phase and IOx composition and concentration on the surfaces), this reaction might lead to significant volatile iodine release or not.

- Radiolytic oxidation of multi-components iodine aerosols

According to PHEBUS-FP tests mainly, multi-components iodine aerosols are formed and/or transported in the Reactor Coolant System (RCS) to the containment building during the accidental sequence. Their radiolytic stability has never been checked and they might contribute to iodine

volatility before settling or once deposited onto surfaces. After having evidenced during the first phase of STEM the release kinetics of iodine from CsI decomposition and having gained first insights concerning IOx decomposition, it is necessary to carry out experiments with these more representative iodine aerosols, in order to complete the current modeling for iodine ST estimations. That is why IRSN proposes to study the multi-components iodine aerosols, or at least other metallic iodide aerosols than CsI. From a safety point of view, it is crucial to evaluate how much volatile iodine could be released under irradiation from these deposited mixed iodine soluble aerosols and/or mixed iodine {insoluble+soluble} aerosols on dry/wet surfaces.

#### IV.2. STEM2/Ru topics

As already demonstrated by experimental data [14][15][16][17], ruthenium species released from the core can reach the containment and form some volatile ruthenium tetroxide. The transport in the RCS is one of the key phenomena impacting ST calculations. The first phase of STEM/RUTHENIUM generated information on the key parameters impacting the transport kinetics, the partition between  $RuO_4$  and particles of  $RuO_2$  and the extent of the revaporization process of deposited species in the thermal gradient quartz tube. A preliminary Ru transport model through the RCS has been recently elaborated [18] ; nevertheless data are not complete and not representative enough to be confident for the extrapolation to reactor case situations. As detailed in [18], a first attempt was made to integrate possible Ru source-term in PSA-2 tools and it was concluded that ruthenium radiological consequences could be significant. That is why in the frame of STEM2/Ru, IRSN proposes some complementary tests, mainly based on the revaporization processes, and focused on:

- a higher representativity of the deposition surface, i.e. stainless steel.

- the use of stronger oxidizing conditions, like those induced by air radiolysis products (i.e.  $O_3$ ,  $NO_x$ ,...) in order to increase the oxygen potential and thus be closer to the radiolytic conditions occurring in the RCS. Indeed, it is important to

keep in mind that in the presence of passive autocatalytic recombiners operating, the molar excess of O<sub>2</sub> could be quite limited during the time window where they operate, therefore the main re-vaporization processes of Ru deposits could be linked to the oxidative action of OH radicals resulting from steam radiolysis, instead of an oxidative action of oxygen directly.

- the use of representative “gaseous pollutants” (i.e. seed particles, silver aerosols...) that could significantly impact the RuO<sub>4</sub>(g) behaviour.

#### V. CONCLUSIONS

Following STEM, the second phase of the project, named STEM2 is being proposed in the NEA framework. This 4-year follow-up project should be focussed on medium- and long-term releases and with three main items as prioritized by the STEM Program Review Group: i/ effect of the ageing of paints on iodine behaviour: i.e. irradiation tests on paints aged in representative reactor conditions and loaded with iodine, to confirm iodine releases processes observed with un-aged paints (including adsorption/desorption kinetics) , ii/ iodine aerosol radiolytic decomposition (IO<sub>x</sub> species as well as multi-components iodine aerosols, and by extension also the iodine oxides decomposition by carbon monoxide), iii/ ruthenium revaporization processes occurring with RCS stainless steel surfaces and highly oxidizing conditions. It has also to be noted that an analytical working group should be set up to promote a final comprehensive analysis of the results for reactor case ST evaluation including mitigation aspects. Finally, conditions of experimental investigations should be consolidated following the recommendations of the International OECD-NEA/NUGENIA-SARNET Workshop on the Progress in Iodine Behaviour for NPP Accident Analysis and Management.

#### ACKNOWLEDGMENTS

Authors are grateful to the OECD. Authors acknowledge for their support and guidance all the STEM project partners: the Electricité De France, the Canadian Nuclear Laboratories, the Teknologian tutkimuskeskus VTT (Finland), The Nuclear Research Institute (Czech Republic), the Gesellschaft für Anlagen – und Reaktorsicherheit

(Germany), the Korea Atomic Energy Research Institute, the Korea Institute for Nuclear Safety, The US Nuclear Regulatory Commission.

#### REFERENCES

1. B. Clement and B. Simondi-Teisseire, “STEM: An IRSN project on source term evaluation and mitigation”, Transactions of the American Nuclear Society - 2010 ANS Annual Meeting; Las Vegas, NV, U.S.; November 7-11th, 103, 475-476, (2010).
2. P.A. Yakabuskie, C.J. Moore, G.A. Glowa, “The Behaviour of Iodine Project: A proposal for BIP3”, *Proc. of the Int. OECD-NEA/NUGENIA-SARNET Workshop on the Prog. in Iodine Behaviour for NPP Acc. Anal. and Manag. - March 30, April 1 - Marseille (France), (2015).*
3. J. Colombani et al., “Experimental study of organic iodide volatilization from painted surfaces present in the containment during a severe accident”, *Proceedings of the 6<sup>th</sup> European Review Meeting on Severe Accident Research, Avignon, 2-4 October, France (2013).*
4. J. Colombani, A.C. Grégoire, S. Morin, “Main findings of the IRSN experimental programs performed on iodine chemistry in severe accident conditions”, *Workshop on the Prog. in Iodine Behaviour for NPP Acc. Anal. and Manag. - March 30, April 1 - Marseille (France), (2015).*
5. L. Bosland et al., “Towards a mechanistic interpretation of the iodine – paint interactions”, *Proceedings of the 4<sup>th</sup> European Review Meeting on Severe Accident Research, Bologna, 11-12 May, Italia (2010).*
6. F. Funke, S. Gupta, *and al.*, “Interaction of gaseous I<sub>2</sub> with painted surfaces and aerosols in large-scale THAI tests”, *Proc. of the Int. OECD-NEA/NUGENIA-SARNET Workshop on the Prog. in Iodine Behaviour for NPP Acc. Anal. and Manag. - March 30, April 1 - Marseille (France), (2015).*
7. L. Bosland, F. Funke, *and al.*, “PARIS project: Radiolytic oxidation of molecular iodine in containment during a nuclear

- reactor severe accident: Part 2: Formation and destruction of iodine oxides compounds under irradiation – experimental results modelling”, *Nucl. Eng. Des.*, 241, (9), p. 4026-4044, (2011).
8. O. Leroy, M.N. Ohnet, S. Planteur-Kieffer, “Study of the Ruthenium transport under prevailing conditions in the primary circuit in case of a PWR severe accident”, *ERMSAR 2015 conference, Marseille (France)*.
  9. L. Bosland, L. Cantrel “Iodine behaviour in the circuit and containment: Modeling improvements in the last decade and remaining uncertainties”, *Proc. of the Int. OECD-NEA/NUGENIA-SARNET Workshop on the Prog. in Iodine Behaviour for NPP Acc. Anal. and Manag. - March 30, April 1 - Marseille (France), (2015)*.
  10. L. Cantrel, F. Cousin, and al., “ASTECV2 severe accident integral code: Fission product modelling and validation”, *Nucl. Eng. & Des.*, 272, p. 195-206, (2014).
  11. A. B. Aleksandrov, N. I. Ampelogova, and al., “The effect of physicochemical conditions on the absorption of molecular iodine by protective varnish and paint coatings during accidents at a nuclear power station with a VVER-640 reactor”, *Therm. Eng.*, 42, (12), p. 991-996, (1995).
  12. C. M. Stevens and L. Krout, “Method for the determination of the concentration and of the carbon and oxygen isotopic composition of atmospheric carbon monoxide”, *Int. J. Mass Spect. & Ion Phys.*, 8, p. 265-275, (1972).
  13. H. J. Kavanaugh, J. W. Dahlby, and al., “The gravimetric determination of carbon in uranium-plutonium carbide materials”, *LA-7981 - Los Alamos Scientific Laboratory*, (1980).
  14. Y. Pontillon, G. Ducros, “Behaviour of fission products under severe PWR accident conditions. The VERCORS experimental programme—Part 3: Release of low-volatile fission products and actinides”, *Nucl. Eng. Des.* 240(7), pp. 1867-1881 (2010).
  15. N. Vér, L. Matus, M. Kunštár, J. Osán, Z. Hózer, A. Pintér, “Influence of fission products on ruthenium oxidation and transport in air ingress nuclear accidents”, *Journal of Nuclear Materials.*, 396, pp. 208-217 (2010).
  16. C. Mun, L. Cantrel, C. Madic, “Radiolytic oxidation of ruthenium oxide deposits”, *Nuclear Technology* 164, pp. 245-254 (2008).
  17. T. Kärkelä, Ruthenium databook – version 1.0, SARNET2-ST-D8.7 report (*EU Severe Accident Research Network of Excellence 2*) (2013).
  18. F. Miradji, F. Cousin, S. Souvi, V. Vallet, J. Denis, V. Tanchoux, L. Cantrel. “Modelling of Ru behaviour in oxidative accident conditions and first source term assessments”, *ERMSAR 2015 conference, Marseille (France)*.
  19. G. Glowa, C. J. Moore, and al., “The main outcomes of the OECD Behaviour of Iodine Project”, *Proc. of the Int. OECD-NEA/NUGENIA-SARNET Workshop on the Prog. in Iodine Behaviour for NPP Acc. Anal. and Manag. - March 30, April 1 - Marseille (France), (2015)*.
  20. G. Glowa, C. J. Moore, and al., “The main outcomes of the OECD Behaviour of Iodine (BIP) Project”, *Annals of Nuclear Energy*, 61, p. 179-189, (2013).



**Session 2: iodine transfer to aqueous phase, aqueous-phase chemistry**

## IODINE AND SILVER WASH-DOWN MODELLING IN COCOSYS-AIM BY USE OF THAI RESULTS

G. Weber<sup>(1)\*</sup>, F. Funke<sup>(2)</sup>, W. Klein-Hessling<sup>(3)</sup>, S. Gupta<sup>(4)</sup>

<sup>(1)</sup>*Gesellschaft für Anlagen- und Reaktorsicherheit (GRS) gGmbH, Garching, Germany,*

<sup>(2)</sup>*AREVA GmbH, Erlangen, Germany,* <sup>(3)</sup>*Gesellschaft für Anlagen- und Reaktorsicherheit (GRS) gGmbH, Cologne, Germany,*

<sup>(4)</sup>*Becker Technologies GmbH, Eschborn, Germany*

\*Corresponding author, Tel: (+49)89 32004 506, Fax: (+49)89 32004 300, Email: [gunter.weber@grs.de](mailto:gunter.weber@grs.de)

**Abstract** – *An accurate prediction of the iodine source term requires not only an adequate simulation of all iodine reactions in the containment but also a precise calculation of thermal hydraulics and aerosol behavior and their interaction with iodine chemistry [1]. Wet deposition of iodine species on containment surfaces, their reaction with the decontamination paint and the wash-down by draining condensate are important interaction processes.*

*In COCOSYS-AIM the models for wet iodine deposition onto paint, for iodine and silver wash-down and for the iodine/silver reaction have been revised using findings and data from several large-scale THAI tests. In this paper three models are highlighted.*

*First, a new water layer model for I<sub>2</sub> deposition onto paint by steam condensation is described. It considers all relevant chemical reactions in the water film as well as iodine adsorption onto paint covered by water film and rivulets. The model was first checked on the THAI tests Iod-24 with two painted cooling elements making different wall condensation rates possible at the same time.*

*Second, the new model AULA for the wash-down of insoluble aerosols like silver particles has been developed. It is based on a model for sediment transport applied in geology. Particles erode and are washed down when a critical flow velocity is exceeded. Two flow types are considered: rivulets and films. For a first validation a THAI AW-3 laboratory test was analyzed with AULA.*

*Third, the reactive surface of silver particles in a sump has been implemented in the model for the iodine/silver reaction. The reactive surface is reduced when Ag particles are deposited on the sump bottom.*

*The revision of the iodine and silver wash-down modelling is expected to reduce significantly the uncertainty in the iodine source term prediction with COCOSYS-AIM.*

## I. INTRODUCTION

During a severe accident in a LWR iodine and other fission products are released into the containment together with large amounts of steam and non-condensable gases. The steam condenses on the cold structures and the condensate flows down the walls and over floors and finally reaches the main sump at the containment bottom. Together with the condensing steam gaseous molecular iodine ( $I_2$ ), particulate iodine (CsI, IOx) and other aerosols are transferred into the wall condensate and transported downwards. Since the surface of the main sumps is rather small compared to all deposition areas in a containment (about 3 % in a German Konvoi PWR) most of the nuclear material, i.e. fission products, control rod and structure materials, is settled on the surfaces in the containment at first and finally washed down into the main sump.

The wash-down process governs the distribution of the fission products between structures, elevated water pools and the main sump. Fission products in the water phase produces steam due to the decay heat while decay heat released from dry structures causes a dry heating of the containment. Furthermore distribution and relocation of radionuclides is important to assess radiation damages of local components like electronic devices, seals, etc. The wash-down processes interact with several other thermal hydraulic and aerosol processes in the containment. Therefore an accurate modelling of the wash-down is relevant for a reliable simulation of the iodine behaviour in the containment and the source term.

At wall condensation two flow patterns can occur: droplet condensation with rivulet formation and water films. Both are treated in the new models described in this paper.

In the containment code COCOSYS including the iodine module AIM-3 wash-down processes are currently modelled only in a simplified way [2,3]. For instance the iodine deposition onto wet paint is calculated by a constant rate, chemical reactions in the condensate layer are not

considered and the wash-down of insoluble aerosols is modelled empirically.

Therefore a new wash-down concept has been developed comprising three models which have been verified on several tests:

- Iodine water layer model (THAI Iod-21 and Iod-24)
- Wash-down model for insoluble aerosols AULA (German: “Abwaschen unlöslicher Aerosole” (THAI AW-2, first part of AW-3 including laboratory tests)
- Model for the reactive surface of silver particles in sumps (PHEBUS FPT1 and second part of AW-3)

The iodine water layer model describes the deposition of gaseous iodine onto paint by wall condensation, all relevant iodine reactions within a water film and with the paint and the iodine transport with the draining condensate.

AULA simulates the erosion of insoluble aerosols by flowing condensate. Ag and Ag/AgOx aerosols which react with iodine are of special interest.

In an extension of the iodine/silver model the reduction of the reactive surface of particles settled on the sump bottom is described.

## II. WATER FILM AND RIVULETS

The major part of the surfaces in LWR containments is coated with decontamination paint based on Epoxy resins. With steam condensation the hydrophobic surface of the paint promotes the formation of droplet condensation. If a cluster of droplets becomes too heavy it moves downwards forming a local rivulet which gathers other droplets on its way. The classical closed water film is only occasionally created, e.g. with high condensation rates. The two different flow types have different wash-down efficiencies for soluble and insoluble aerosol particles, which are considered in the new models.

Rivulet formation is the prevailing condensation type in a LWR. Rivulets on vertical walls occur stochastically at different locations. In the long run a large part of the wall surface will be covered by the individual rivulet tracks. Rivulets

on slightly inclined surfaces are broader, they flow slower and their tracks are more stable.

Fig. 1 a) and b) show droplet condensation and rivulet tracks on a vertical wall coated with German GEHOPON paint at two different wall condensation rates in the THAI test Iod-24 [4]. In b) with the higher condensation rate, droplets are smaller. The photographs c) and d) show rivulets on slightly inclined steel and painted plates with previously deposited CsI aerosol. The plates are 1.2 m long and about 0.3 m wide. On both plates two stable rivulets were formed. The time after the start of wash-down is given in min:sec [5].

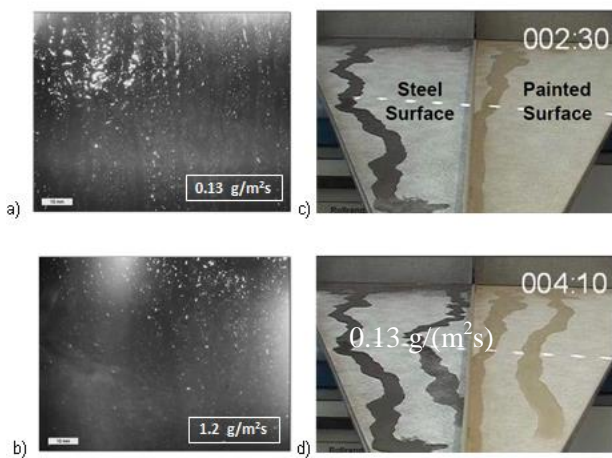


Fig. 1 Droplet condensation and rivulet formation on a vertical painted wall at different wall condensation rates (a, b) and rivulets on slightly inclined plates covered with CsI aerosol (c, d).

In Tab.1 characteristics of rivulets and water films under severe accident conditions are compiled. The values are calculated assuming a wall condensation rate of  $5.E-4 \text{ kg}/(\text{m}^2\text{s})$ . Rivulets are about 10 times faster than water films, but their tracks are narrow.

Tab.1 Characteristics of condensate flow types in a LWR containment (approximate values)

Flow type	Vertical wall		Floor (2% inclined)	
	Rivulet	Water film	Rivulet	Water film
Width	3 mm	large	3 cm	large
Thickness	1 mm	0.1 mm	2 mm	0.3 mm
Mean velocity	1 m/s	0.1 m/s	0.3 m/s	0.03m/s

### III. I<sub>2</sub>/PAINT REACTION AT WALL CONDENSATION

The current AIM model for the I<sub>2</sub> reaction with wet paint during wall condensation is described by the reaction scheme depicted in Fig.2. E.g. the I<sub>2</sub> deposition onto wet paint is given by reaction rate (RR) 4, desorption by RR 62. One fraction of the I<sub>2</sub>(g) deposited into the water film is washed down into the water pool (RR 44) another fraction is converted to I before it moves into the pool. In the model the I<sub>2</sub> fraction is constant and washed off instantaneously. This model has two main restrictions:

- The reactions do not depend on the wall condensation rate.
- Chemical reactions within the water film are not considered. An exception is the simplified modelled I<sub>2</sub>(w) → I(w) reaction.

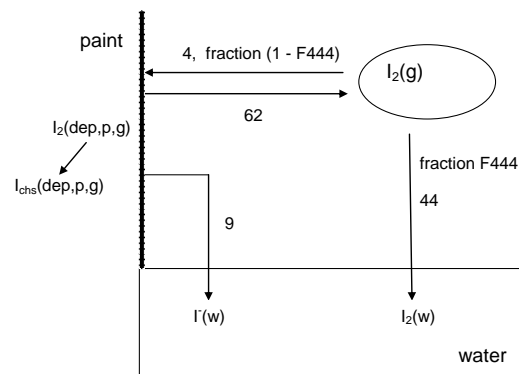


Fig.2 Current I<sub>2</sub>/wet paint interaction and wash-down model in AIM-3

In an ASTEC calculation on PHEBUS test FPT1 the water film along the painted wet condenser was explicitly modelled for the first time [6]. The main objective was to demonstrate the large amount of gaseous I<sub>2</sub> produced by radiolytic oxidation of I from CsI dissolved in the water film. The higher dose rate from the deposited iodine and other fission products in the water film was considered. This simple water film model was not coupled to the containment thermal hydraulics and the build-up of the water film as well as the deposition and the wash-down of fission products were not calculated. Nevertheless, the good results with this early model are a motivation for the new water layer model in COCOSYS.

### III.A New iodine water layer model

In the new water layer model droplets and films are simulated uniformly by a thin water layer. The area of each layer complies with the COCOSYS nodalisation. It can be 10 m<sup>2</sup> to several 100 m<sup>2</sup> in a large LWR containment. The thickness of each layer is calculated dynamically taking into account its orientation (wall or floor) and the wall condensation rate. Surplus condensate is drained through drain junctions into the layer below.

Assuming homogeneous steam condensation at high vertical containment walls the thickness and the flow velocity of the rivulets respectively the water film are increasing from top to bottom. This situation can be handled by defining several water layers one above the other. The mean thickness of each layer and the condensate flow rates between the layers are calculated by the thermal hydraulic module of COCOSYS. In case of rivulets in the model the water is assumed to be distributed over the wall segment.

The iodine species concentration in each water layer is balanced from sources and sinks caused by the condensate flows, transfer from the atmosphere and adsorption onto the immersed paint (Fig.3). Each layer is treated as if it were well mixed. If the volatile iodine concentration exceeds the equilibrium with the gas phase gaseous iodine is transferred into the atmosphere. Local iodine concentration differences in the containment maybe reduced by the wash down and transfer processes. Decisive for the homogeneous chemical reactions in the water layer respectively the reactions with the paint are the local aqueous species concentrations.

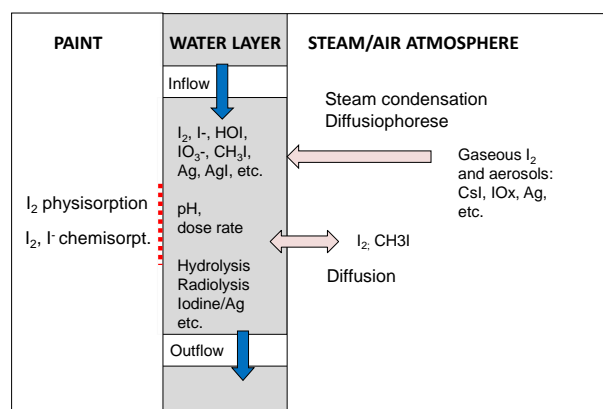


Fig.3 Drawing illustrating the new water layer model

The iodine species in each individual water layer are treated like in the main sump. In the water layer iodine reactions, i.e. hydrolysis, radiolysis, iodine/silver reaction and others, as well as the I<sub>2</sub> and CH<sub>3</sub>I mass transfer to the gas phase are modelled. At present the same reaction rate constants as for the main sump are used unless new water layer specific measurements are available.

Moreover, a possible dry out of the water layer is considered. At dry out gaseous iodine species (I<sub>2</sub>, CH<sub>3</sub>I) are released completely to the atmosphere. Non-volatile substances like CsI, Ag and AgI become immobile and all the chemical water phase reactions are suppressed until the layer is filled by new condensate again.

The I<sub>2</sub>(g) transport is a combination of iodine diffusion and the transport with the condensing steam (Stefan-flow). The I<sub>2</sub> diffusion velocity in the atmospheric boundary layer close to the water layer is identical with the gas side mass transfer coefficient. The combined adsorption velocity becomes [7]:

$$k_{ad} = \frac{R}{1-e^{-R}} k_g \quad (1)$$

with

$$R = \frac{v_{Stef}}{k_g} \quad \text{and} \quad v_{Stef} = \frac{G_{cond}}{\rho_{st}}$$

- $k_{ad}$  I<sub>2</sub> adsorption velocity into the water layer under condensing conditions, m/s
- $G_{cond}$  Condensation steam flux to wall, kg/(m<sup>2</sup>s)
- $k_g$  Gas side mass transfer coefficient for I<sub>2</sub>, m/s (AIM default: 1.4E-3 m/s)
- $v_{Stef}$  Stefan velocity of condensing steam, m/s
- $\rho_{st}$  Steam density, kg/m<sup>3</sup>

$k_g$  is identical with the  $I_2$  adsorption velocity by diffusion at dry conditions. Fig. 4 shows the  $I_2$  adsorption rate into the water layer upon the surfaces (paint, steel, etc.) as function of the condensate rate according to Eq. 1. For low condensation rates  $k_{ad}$  equals  $k_{dif}$ . Although the two wall condensation rates used in Iod-24, differ by a factor 9.2 the  $k_{ad}$  ratio is only 1.7, i.e. the  $I_2$  concentration in the condensate is higher with the low wall condensation rate.

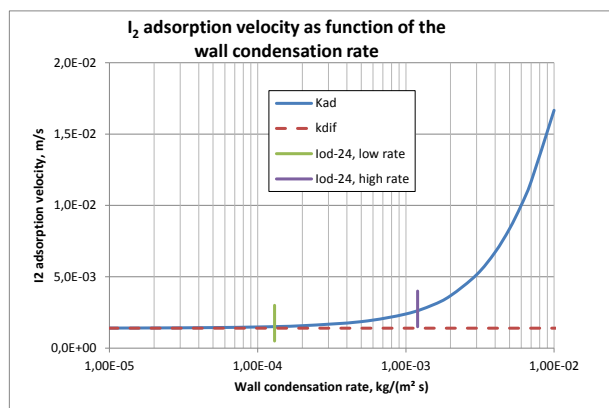


Fig. 4 Iodine adsorption by diffusion and condensation

In a COCOSYS-AIM nodalisation the water layers are relatively large and the condensate is assumed to be homogeneously distributed. Thus in the model droplets and rivulets are simulated by a water layer with parameters (thickness, flow velocity) different from water films.

### III.B Validation

In the THAI test Iod-24 the deposition of gaseous  $I_2$  onto paint under condensing condition was measured. Two cooling elements with a total surface area of  $3.7 \text{ m}^2$  each were coated with German GEHOPON paint and installed in the vessel. The paint was thermally aged to 15 years. The gas atmosphere was superheated and the relative humidity was maintained constant throughout the test at 90% by continuous injection of steam at a constant mass flow rate. Steam was released into the vessel (Fig. 5). The surface of the elements was kept on different temperatures below the saturation point achieving nearly constant condensates rates of  $0.13 \text{ g/m}^2\text{s}$  and  $1.2 \text{ g/m}^2\text{s}$ . More details on this test and a description of the similar Iod-21 can be found in [4].

At stable condensing conditions  $0.55 \text{ g}$  of gaseous  $I_2$  traced with some radioactive I-123 was injected (time  $t = 0$ ). With the condensing steam  $I_2$  was transported to the painted cooling elements. One fraction was adsorbed on the paint the other fraction drained with the condensate and was diverted outside the vessel and measured. The iodine on the elements was measured online by gamma-detectors through glass windows in the vessel.

After 14 hours, the cooling of the painted surfaces and steam injection were stopped and the painted surfaces dried out in order to measure possible iodine desorption

For the COCOSYS-AIM calculation of the test a 9-compartment nodalisation of the THAI vessel was worked

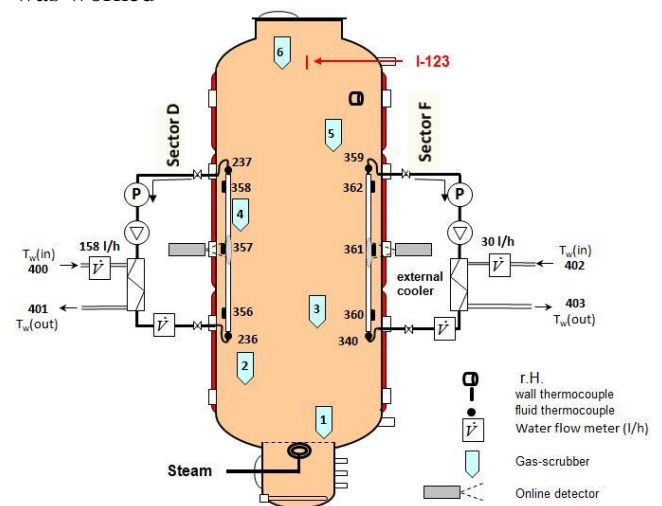


Fig. 5 Vessel configuration with two painted cooling elements in test Iod-24

out. In two zones heat conducting structures represented the two cooling elements. The paint, the condensate layer and the surrounding gas space were simulated with the new water layer model. The water layer thickness was given with  $6.5E-5 \text{ m}$  according to measurements by Becker Technologies. For the pH of the condensate layer the measured value of  $\text{pH} = 4.5 - 5$  was used. Additionally a release of reductive substances from the GEHOPON paint was assumed. The substances had been measured under comparable conditions in earlier tests [8]. They can reduce  $I_2(w)$  quickly to the non-volatile  $I(w)$ .

The iodine mass deposited onto the paint is well calculated by the new water layer model for the

high and the low wall condensation rates (Fig. 6 and Fig. 7). It is remarkable that the deposited iodine mass with a low condensation rate is 56 % higher than that with a high rate. The reason is that the iodine concentration in the condensate with the low rate is higher than that with the high rate, as the wet  $I_2$  adsorption velocity does not rise linearly with the condensation rate (s. Fig. 4). This unexpected behavior is well calculated with the new model. Only for the high condensation rate the mass is about 10 % underestimated.

Iod-24 further shows that adsorbed iodine is not washed-off by pure condensing steam. The iodine physisorbed on paint is rapidly chemisorbed and fixed.

#### IV. WASH-DOWN OF AEROSOLS

During a reactor accident the condensate flowing down washes off the nuclear aerosols, transport them into lower compartments and finally into the reactor sump. The efficiency of the wash-down process depends on the particle properties (size, density, and solubility), surface orientation (wall, floor), thermal hydraulic conditions

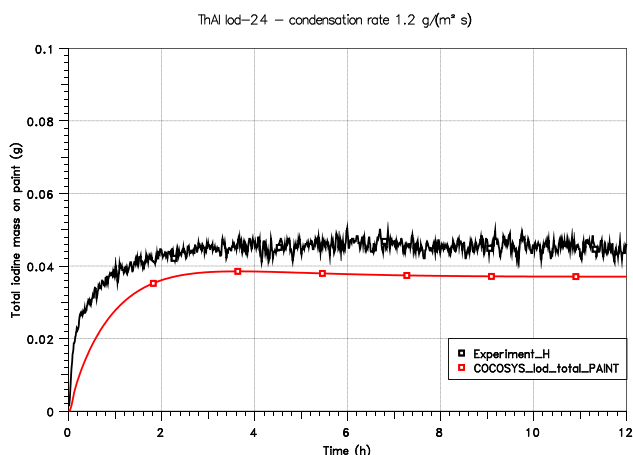


Fig. 6 Iod-24: Total iodine mass on the paint with high condensation rate

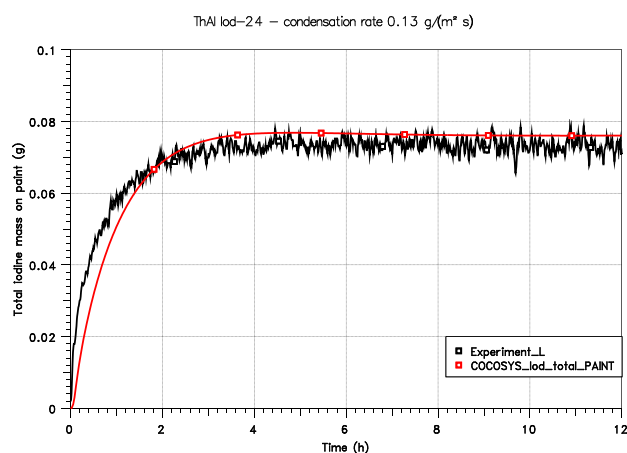


Fig. 7 Iod-24: Total iodine mass on the paint with low condensation rate.

(condensation rate, temperature), flow type (rivulet, film), nature of surface (smooth, rough), etc.

The wash-down processes for soluble and insoluble aerosols are rather different. **Soluble (hygroscopic) material**, like CsI, is quickly dissolved and transported with the condensate. In COCOSYS-AIM the dilution process is simplified treated assuming an instantaneous and complete dissolution of soaked particles. Small puddles and larger pools might retard the condensate and the dissolved material on their way down.

Under reactor conditions the wash-down is significantly more efficient for soluble than for insoluble aerosols as shown by THAI tests AW-1, AW-2 and AW-3 [9]. The model in COCOSYS-AIM for soluble aerosols was successfully validated on AW-1 with CsI and AW-2 with the aerosol mixture CsI + SnO<sub>2</sub> [10].

The wash-down of **insoluble aerosols** like Ag and AgOx particles is more complex because the erosion process depends on both, the hydrodynamic of the condensate and the particle properties.

The current wash-down model for insoluble aerosols in COCOSYS-AIM describes the process in a rather simplified way. Particle erosion rate and wash-down efficiency have to be given by the user.

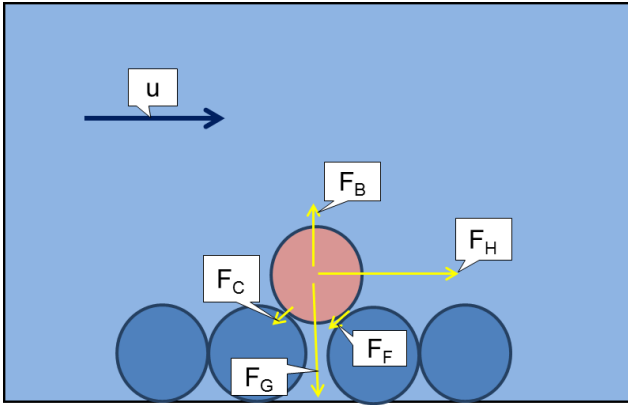


Fig. 8 Forces acting on a settled particle in a water flow ( $F_A$  buoyancy,  $F_S$  hydrodynamic force,  $F_G$  gravity,  $F_R$  friction and  $F_K$  cohesion).

The new wash-down model AULA [11] is based on an approach used in geology to describe the transport of sediments in water flows. A particle erodes when the hydrodynamic force and the buoyancy exceed the forces of gravity, friction and cohesion (Fig. 8). This type of problem was first solved by A. Shields by formulating a criterion [12]. This Shields criterion says that the erosion of a settled particle starts when the flow velocity directly above the particle bed exceeds a critical value. This criterion is valid for a large range of particle sizes and flow velocities

IV.A The AULA model

According to the Shields criterion the erosion of a particle from a structure or from a bed of particles takes place if the shear velocity at the particle bed exceeds the critical shear velocity.  $u_{*,c}(d_p)$  is calculated with the Shields equation for the critical shear stress.

$$u_* > u_{*,c}(d_p) \text{ (Particles erode)}$$

- $u_*$  Shear velocity at the particle bed, m/s
- $u_{*,c}$  Critical shear velocity at the particle bed, m/s
- $d_p$  Mean particle diameter, m

The Shields criterion is valid for particles between 1  $\mu\text{m}$  and about 1 cm. If the criterion is met for a cluster of equal particles, all particles will erode at the same time.

The Shields equation cannot be solved analytically. Several approximations are available. Here the one of Shields, Rouse and

Guo [13] is applied. With the dimensionless auxiliary parameter

$$R_* = \frac{d_p \sqrt{0.1(s-1)gd_p}}{\nu} \quad (2)$$

and the density ratio

$$s = \rho_p / \rho_w$$

the critical dimensionless shear stress, known as Shields parameter, becomes

$$\tau_{*,c} = \frac{0.1}{(R_*)^{2/3}} + 0.054 \left[ 1 - \exp\left(-\frac{(R_*)^{0.52}}{10}\right) \right]$$

- $\rho_p$  effective density of particles,  $\text{kg/m}^3$
- $\rho_w$  density of water,  $\text{kg/m}^3$
- $R_*$  Dimensionless parameter, Rouse-Reynolds-number
- $\tau_{*,c}$  Dimensionless critical shear stress (Shields parameter)

Finally the critical shear velocity is given by

$$u_{*,c} = \sqrt{\tau_{*,c}(s-1)g d_p} \quad (4)$$

For particles between 1 and 10  $\mu\text{m}$  the critical shear velocity depends only slightly on the particle size, i.e. all particles will start to erode nearly at the same flow velocity. The density of the aerosol material has a significant impact on the critical shear velocity. While 10  $\mu\text{m}$  particles with a density of 2000  $\text{kg/m}^3$  erode at a critical shear velocity of 0.8 cm/s particles with 10000  $\text{kg/m}^3$  (e.g. Ag) need a shear velocity of 2.2 cm/s (Fig. 9).

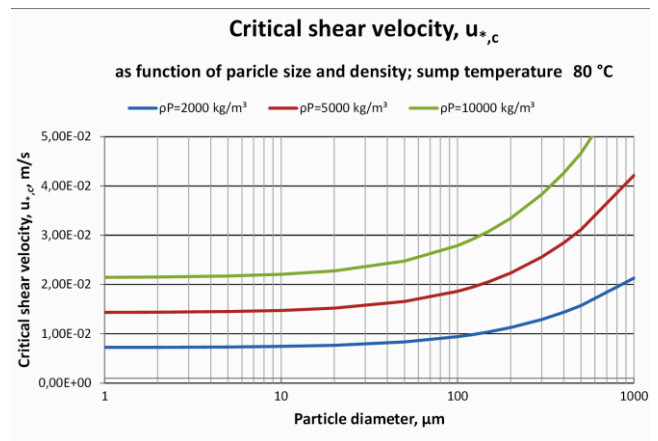


Fig. 9 Critical shear velocity for different aerosol particles.

For cohesive particles the erosion process lasts significantly longer. Most particles  $< 50 \mu\text{m}$  are cohesive (attraction between particles) and/or adhesive (attraction between particles and wall). Behaviour and modelling of the cohesive particles are described below.

The shear velocity of the condensate flows (rivulets and water films) close to the structure can be calculated by use of the mean flow velocity. The thickness of the condensate flow is given by the continuity equation which can be applied for both, rivulets and films by using different flow widths.  $\beta$  is the angle between the wall surface and the vertical direction.

$$\delta = \sqrt[3]{\frac{3 \nu \dot{m}_w}{g W \rho_w \cos\beta}} \quad (5)$$

- $\delta$  Thickness of condensate flow, m  
 $\dot{m}_w$  Condensate mass flow, kg/s  
 $W$  Flow width, m  
 $\nu$  Kinematic viscosity of water,  $\text{m}^2/\text{s}$   
 $g$  Acceleration due to gravity,  $\text{m}/\text{s}^2$

With the condensate thickness the mean flow velocity is calculated

$$u = \frac{\delta^2 g \cos\beta}{3 \nu} \quad (6)$$

The deduction of the shear velocity depends on the type of flow. Because of the slight roughness of the decontamination paint surface, smooth turbulent flows can be expected. The shear velocity for hydraulically smooth flows is calculated by use of a parabolic flow velocity profile.

$$u_* = u \frac{\kappa}{\ln\left(\frac{u_* \delta}{\nu}\right) + 5.2} \quad (7)$$

$\kappa$  is the Karman constant,  $\kappa = 0.41$  and 5.2 is an integration constant. Since  $u_*$  appears on both sides of the equation, it has to be solved by iteration.

Small nuclear particles deviate from the ideal Shields conditions, because of the cohesive and adhesive forces which are not considered. To overcome this problem in AULA the mass erosion rate  $k_E$  based on Shields' parameter is used. This rate was introduced by Ariathurai (cited in [14]) for cohesive particles.

$$k_E = k_{E,0} \frac{(u_*^2 - u_{*,c}^2)}{u_{*,c}^2} \quad \text{for } u_* > u_{*,c} \quad (8)$$

and  $k_E = 0$  for  $u_* \leq u_{*,c}$

- $k_E$  Aerosol mass erosion rate,  $\text{s}^{-1}$   
 $k_{E,0}$  Erosion constant,  $\text{s}^{-1}$

By use of the mass erosion rate the erosion of cohesive particles is initialized by the Shields criterion and goes on until the total aerosol mass has eroded. The erosion constant  $k_{E,0}$  is the time constant for the decreasing erosion process. Formally  $k_{E,0}$  is the mass erosion rate at the shear velocity  $\sqrt{2}$ -times of  $u_{*,c}$ . With a small  $k_{E,0}$  the erosion process lasts long and with a large  $k_{E,0}$  the process approaches the ideal Shields "puff release". The erosion constant, i.e. the characteristic time of the erosion process, has to be measured under reactor typical conditions.

In each COCOSYS calculation time step the erosion rates for wall and floor areas are calculated with AULA. The time derivation of the deposited aerosol mass in each control volume is

$$\frac{dc_{Ae,dep}}{dt} = -k_E c_{Ae,dep} + Q \quad (9)$$

- $c_{Ae,dep}$  Concentration of deposited aerosol ( $\text{kg}/\text{m}^3$ )  
 $Q$  Sources due to deposition processes (resettling, etc.),  $\text{kg}/(\text{m}^2 \text{s})$

#### IV.B First validation

At Becker Technologies, laboratory wash-down tests with an insoluble silver aerosol were performed [15]. The aerosol was deposited on steel plates, most of which were coated with GEHOPON decontamination paint. At the upper end of the differently inclined plates, water was released homogeneously by use of a special distributor. The Ag aerosol washed down was measured at the bottom end of the plate. In 14 tests the particle size, the inclination of the plate, the surface material (paint, steel) and the water flow rate were varied. The wash-down always occurred with rivulets and in no case a closed water film was observed. Because of the stable rivulets a part of the plate surface covered with the Ag aerosol remained dry.

The results showed the highest erosion rate at the beginning of the wash-down, which then decreasing exponentially with time. Small amounts of silver could be detected until the end of the tests at  $t = 15$  min. As an example the

measured results of test no. 4 are given in [15]. The Ag aerosol loading on the paint was 12.5 g/m<sup>2</sup>, the MMD of the particles was about 2 µm. The inclination of the plate was 20° and the condensate flow was 11 g/s. About 10 stable rivulets developed covering approximately 45 % of the plate surface.

In the first 130 s 23.2 % of the Ag from the area soaked by the rivulets was washed off. In the whole test which lasted 15 min 36.8 % were washed off.

With AULA the erosion process due to the rivulets was simulated. Ten rivulets with a mean width of 1.5 cm were assumed. By use of the thickness (Eq. 2) and flow velocity (Eq. 3) of the rivulets the shear velocity was calculated with Eq. 4. The critical shear velocity was calculated by the approach of Shields, Rouse and Guo (Eq. 2 to 4).

$$u_* = 1.64E-2 \text{ m/s}$$

$$u_{*,c} = 9.8E-3 \text{ m/s}$$

Since  $u_* > u_{*,c}$  the silver particles erode in test 4. The erosion rate is according to Eq. 5

$$k_E = k_{E,0} \cdot 1.8 \text{ 1/s}$$

The erosion constant  $k_{E,0} \approx 0.0205 \text{ 1/s}$  was estimated by use of some detailed results of test 4 concerning the time behaviour. Finally the mass erosion rate in the AW-3 LAB test becomes

$$k_E \approx 3.7E-2 \text{ 1/s}$$

In Fig.10 the eroded Ag masses calculated are depicted. The history of the erosion rate is in a fairly good agreement with the measurement. The erosion process lasts several minutes. For  $t > 60 \text{ s}$  the wash-down is underestimated.

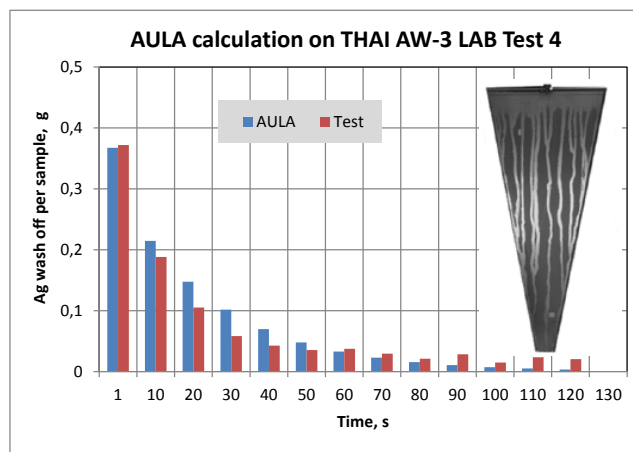
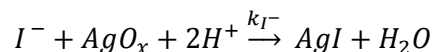
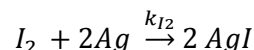


Fig.10 Measured and calculated erosion rate and rivulet flow pattern (right) in the AW-3 LAB test 4.

A systematic evaluation of the remaining 13 tests of the AW-3 LAB series will be possible when the integration of AULA into COCOSYS has been completed.

#### V) AQUEOUS IODINE/SILVER REACTION

The specific surface of the silver particles in the sump was one of the important uncertain parameters determined in the uncertainty and sensitivity study on a COCOSYS-AIM calculation on PHEBUS test FPT1 [16]. In this COCOSYS version as in most other iodine codes the specific Ag surface is considered to be constant. The iodine /silver reaction takes place at the particle surface, i.e. the kinetics of the reaction depends linearly on the specific surface of the particles.



The specific surface is the surface of all particles divided by their total mass (m<sup>2</sup>/g). For mono-disperse spherical 3 µm Ag particles it is 0.42 m<sup>2</sup>/g.

Ag particles deposited on the bottom of the sump are less efficient for the reaction with iodine than suspended particles because of the reduction of their reactive surface. When particles settle to the sump bottom the iodine/silver reaction is slowed down rapidly. During the evaluation and interpretation of the PHEBUS test FPT1 this

problem appeared already [6]. To overcome this problem the following approach is suggested.

#### V.A Reactive silver surface

The settling velocity of Ag particles in the sump water is calculated by the Stokes equation.

$$v_{\text{set}} = \frac{d_{\text{Ag}}^2 g (\rho_{\text{Ag}} - \rho_{\text{w}})}{18\eta} \quad (10)$$

$v_{\text{set}}$	Settling velocity, m/s
$d_{\text{Ag}}$	Particle diameter, m
$\rho$	Density; w water, Ag silver, kg/m <sup>3</sup>
$\eta$	Dynamic viscosity, Pa.s
$g$	Acceleration due to gravity, m/s <sup>2</sup>

With the density of compact Ag (1.E4 kg/m<sup>3</sup>) for 3  $\mu\text{m}$  particles, the settling velocity in the water is 1.35E-4 m/s. 1  $\mu\text{m}$  particles have a velocity of 1.49E-5 m/s and 10  $\mu\text{m}$  particles 1.49E-3 m/s.

In reactor containments only a small fraction of the Ag aerosol settles directly into the sump, since its surface is small compared to the total floor area. In a German Konvoi-PWR only about 3 % of the total Ag containment inventory are settled directly into the sump. Most particles are first deposited onto structures, before they are washed down into the sump. On their way they grow due to agglomeration. It is expected that the Ag particles in the reactor sump are significantly larger than in the airborne state. Appropriate measurements are not available.

The specific surface of spherical aerosol particles is

$$S_{\text{Ag}} = \frac{6}{d_{\text{p}} \cdot \rho_{\text{p}} \cdot 1E3} \quad (11)$$

$S_{\text{Ag}}$	Specific surface of Ag particles, m <sup>2</sup> /g
$d_{\text{p}}$	Particle diameter, m
$\rho_{\text{p}}$	Particle density, kg/m <sup>3</sup>

For 3  $\mu\text{m}$  Ag particles with a density of 1E4 kg/m<sup>3</sup> the specific surface is 0.2 m<sup>2</sup>/g and for 1  $\mu\text{m}$  particles 0.6 m<sup>2</sup>/g. For fluffy particles the specific surface is larger.

In a well-mixed and non-boiling reactor sump with a typical water level of 2 m an Ag aerosol of 3  $\mu\text{m}$  particles settle completely to the sump bottom within 1 day (Fig. 11). 10  $\mu\text{m}$  particles deposit within 2½ hours.

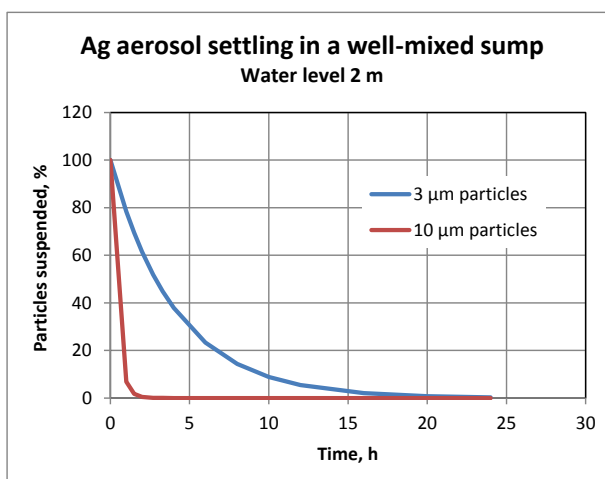


Fig. 11 Ag aerosol settling in a well-mixed reactor sump

In COCOSYS-AIM the kinetics of the I<sub>2</sub>/Ag reaction is modelled by

$$\frac{d I_2(w)}{dt} = - \frac{1}{\frac{1}{k_w} + \frac{1}{k_{28} \cdot A_{\text{Ag},\text{sus}}}} \cdot I_2(w) \cdot \frac{A_{\text{Ag},\text{tot}}}{V} \quad (12)$$

$A_{\text{Ag},\text{tot}}$	Total reactive surface of Ag particles, m <sup>2</sup>
$I_2(w)$	Aqueous concentration of I <sub>2</sub> , mol/l
$A_{\text{G},\text{sus}}$	Concentration of suspended Ag, mol/l
$k_w$	Water side I <sub>2</sub> mass transfer coefficient, m/s
$k_{28}$	I <sub>2</sub> /Ag reaction rate constant, = 0.2 m·l·mol <sup>-1</sup> ·s <sup>-1</sup>
$V$	Sump volume, m <sup>3</sup>

In the **new extended model** the total reactive surface is composed of the surfaces of the suspended and of the deposited particles.

$$A_{\text{Ag},\text{tot}} = A_{\text{Ag},\text{sus}} + A_{\text{Ag},\text{dep}} \quad (13)$$

with

$$A_{\text{Ag},\text{sus}} = A_{\text{G},\text{sus}} \cdot S_{\text{Ag}} \cdot 1000 \cdot \text{MAG} \cdot V$$

$A_{\text{Ag},\text{sus}}$	Surface of suspended Ag particles, m <sup>2</sup>
$A_{\text{Ag},\text{dep}}$	Reactive surface of deposited Ag particles, m <sup>2</sup>
$\text{MAG}$	Molecular mass of Ag, 107.87 g/mol
1000	Dimension factor in l·m <sup>-3</sup>

The reactive Ag surface of all deposited particles is the fraction  $F_{\text{Ag}}$  of the total surface of these particles, i.e. it is the part of the particle surface facing upwards. The reactive surface of all particles deposited to the bottom is

$$A_{\text{Ag},\text{sb}} = A_{\text{G},\text{dep}} \cdot A_{\text{sb}} \cdot \text{MAG} \cdot S_{\text{Ag}} \cdot F_{\text{Ag}} \quad (14)$$

$$F_{Ag} = 0.5 \quad (Default)$$

- $A_{Ag, sb}$  Total (not limited) surface area of Ag particles deposited on sump bottom,  $m^2$
- $A_{Sb}$  Sump bottom area,  $m^2$
- $AG_{dep}$  Ag concentration on sump bottom,  $mol/m^2$
- $F_{Ag}$  Ag surface fraction, i.e. the fraction of the reactive surface on the total surface of deposited Ag particles

In AIM the reactive surface is assumed to be half of the total Ag surface. Due to the package density of the particle bed and the shape of the Ag particles  $F_{Ag}$  may vary.

If the bottom is not completely covered by particles the reactive silver surface is  $A_{Ag, sb}$ . If the bottom is covered with one or several monolayers of particles the reactive surface equals the bottom area. i.e. the total reactive silver area of all deposited particles is limited to the sump bottom area.

$$\begin{aligned} A_{Ag, sb} < A_{sb}: & \quad A_{Ag, dep} = A_{Ag, sb} \\ A_{Ag, sb} \geq A_{sb}: & \quad A_{Ag, dep} = A_{sb} \end{aligned} \quad (15)$$

The sum of  $A_{Ag, dep}$  and  $A_{Ag, sus}$  is the total reactive Ag area used in the kinetic equation for the  $I_2/Ag$  reaction (Eq. 12). The procedure can also be applied to the reaction of iodide ( $I^-$ ) with  $AgOx$  particles. These are Ag particles with a  $AgOx$  shell.

### V.B Validation of the concept

In the second part of THAI test AW-3 the influence of the reactive Ag surface on the  $I_2/Ag$  reaction in the sump was investigated. At the beginning of the stagnant phase 30 g of Ag aerosol were carefully deposited on the dry sump bottom covering 1.3  $m^2$ . Afterwards the sump was filled with 500 l of water. A pH 2 was established using sulfuric acid to suppress  $I_2$  hydrolysis. Then 0.68 g of  $I_2$  was released to the water pool. The measured  $I_2/Ag$  reactions in the stagnant phase 3.1 and the well-mixed phase 3.2 are shown in Fig.12.

Within the first two hours of phase 3.1 the total iodine mass in the sump decreased and the AgI mass increased because approximately 0.5 g of Ag has been released uncontrolled, probably due to resuspension of fine Ag particles which occurred either during injection process or due to

sump water recirculation started for short time period during  $I_2$  injection. At  $t = 5.5$  h, the beginning of phase 3.2, the recirculation of the sump water was activated causing an efficient resuspension of the Ag particles from the bottom. Additionally 8.2 g of fresh Ag aerosol was released to the water. At the high Ag concentration of 0.076 g/l the remaining  $I_2$  mass of 0.08 g reacted rapidly and the  $I_2$  concentration dropped below the detection limit while the measured AgI mass reached its highest value with 0.24 g.

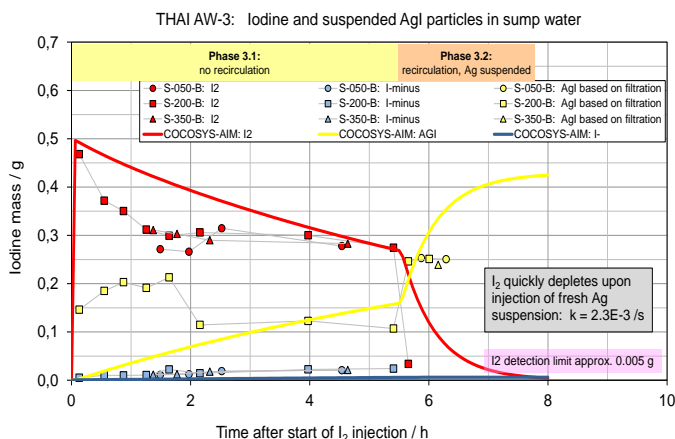


Fig.12 THAI AW-3: Measured and calculated iodine species masses in the stratified and well-mixed sump

The COCOSYS-AIM calculation on AW-3 was performed by use of the variable reactive silver surface described. The suspended Ag in phase 3.1 was taken into account.

In phase 3.2 when the maximum of silver was available, the  $I_2$  mass decreased fast and the AgI mass rose accordingly. The reaction rate constant for the  $I_2/Ag$  reaction, which is essentially the water side mass transfer coefficient  $k_w = 1.E-5$  m/s, is probably underestimated under test conditions. Additionally the AgI concentration was overestimated because the settling of the AgI particles was not considered.

Nevertheless the AW-3 test confirms clearly the reduction of the reactive Ag surface when all or a part of the particles deposit on the sump bottom. In reactor accident calculations it is necessary to take this effect into account. Without consideration the  $I_2$  concentration in the water

and gas phases as well as the iodine source term can be underestimated considerably.

## VI) CONCLUSIONS

The COCOSYS-AIM-3 model for the wash-down of iodine and aerosols was further developed in three steps and validated on THAI tests:

- water layer model;
- AULA model;
- iodine/silver model (reactive Ag surface).

The new **water layer model** for condensing conditions calculates the transfer of gaseous  $I_2$  into the water layer, the iodine chemistry within the layer and the reaction with the surface material, e.g. paint. Iodine diffusion and transport with the condensing steam are considered. The model is suitable for film and droplet condensation.

One outcome of the model application is that the iodine adsorption onto paint can be higher with a low condensation rate than with a high one. This was clearly confirmed in test Iod-24.

Another test outcome is that iodine once adsorbed by the paint will not be washed off again, i.e. only little physisorbed  $I_2$  remains on the paint. This behavior is well reproduced by the new water layer model.

As seen in an earlier interpretation of PHEBUS test FTP1 the water layer can be a considerable source of radiolytically produced  $I_2$ . This and other reactions, like the iodine/silver reaction, are regarded in the new water layer model.

The newly developed **model AULA** describes the erosion of insoluble particles by down-flowing condensate under reactor conditions. The erosion rate is calculated from aerosol properties and hydrodynamic parameters. Contrary to large particles ( $> 50 \mu\text{m}$ ) the erosion process for small, cohesive particles takes significantly longer and drops with time. The mass erosion constant, which describes the time behaviour of the process, can be obtained from tests. The THAI AW tests delivered a suitable data base. On containment floors with slight inclination the wash-off is not very efficient. Rivulet flow velocities may be too slow to initiate erosion and the rivulets leave parts of the floor dry. Therefore

an accurate wash-down simulation for insoluble aerosols like silver which are source term relevant has to be of major concern in accident analyses.

Finally the **iodine/Ag model** was improved by introducing the “reactive Ag particle surface”. It describes the loss of reactive surface area of particles settled on the sump bottom. Under reactor conditions the Ag particles settle within a few hours and consequently the iodine/silver reaction is slowed down. This effect was clearly measured in the THAI test AW-3. It was qualitatively well calculated with COCOSYS-AIM, but the  $I_2$  concentration was overestimated in the first hours of both test phases. The  $I_2/\text{Ag}$  reaction rate constant used might have been too small. This discrepancy will be investigated further.

In current COCOSYS calculations the sump is treated to be well-mixed. In a stagnant sump  $I_2$ , Ag particles and other material can be distributed inhomogeneously in the water. With the new COCOSYS module CoPool it is possible to simulate the temperature distribution and local flows in a reactor sump. It is planned to extend the module for the transport of dissolved and suspended material. Then the simulation of inhomogeneously distributed iodine species and locally occurring reactions will be possible.

In a nuclear aerosol soluble and insoluble components are well mixed forming compact particles. Leaching of soluble material distributed in the compact particles takes considerably longer than the dissolution of pure material. Moreover the dissolved material released between the particles can weaken the cohesive forces and support erosion. Therefore further wash-down tests are required with a realistic reactor typical aerosol of compact particles consisting of soluble and insoluble materials.

The good results with the improved wash-down model in COCOSYS-AIM highlight the importance of an adequate simulation of the interaction of iodine chemistry with thermal hydraulic and aerosol physics.

## ACKNOWLEDGMENTS

The work was funded by the German Federal Ministry for Economic Affairs and Energy (BMWi) in the frame of the German reactor safety research projects RS 1508, 1514 and 1532.

## NOMENCLATURE

AIM = Advanced iodine model  
 AULA = Abwaschen unlöslicher Aerosole  
 COCOSYS = Containment Code System  
 GEHOPON = Trademark of a German decontamination paint  
 THAI = Thermal Hydraulics Hydrogen Aerosol Iodine

## REFERENCES

1. B. Clément, L. Cantrel, G. Ducros, F. Funke, L. Herranz, A. Rydl, G. Weber and J.C. Wren, "State of the Art Report on Iodine Chemistry", Nuclear Energy Agency Report, NEA/CSNI/R(2007)1, (2007)
2. W. Klein-Heßling, S. Arndt, G. Weber, H. Nowack, C. Spengler, S. Schwarz "COCOSYS V 2.4 user's manual", GRS P-3/1, March 2015
3. G. Weber and F. Funke, "Description of the iodine model AIM-3 in COCOSYS", GRS report A-3508, November 2009
4. F. Funke, S. Gupta, G. Weber, G. Langrock, G. Poss, "Interaction of gaseous I<sub>2</sub> with painted surfaces and aerosols in large-scale THAI tests", OECD-NEA/NUGENIA-SARNET Workshop on the Progress in Iodine Behaviour for NPP Accident Analysis and Management, Marseille (France), March 30, April 1, 2015
5. Gupta, S., G. Langer, "Aerosol Wash-down Test (AW), Technical Report Becker Technologies 1501326-AW-QLR, Dec. 2009
6. L. Bosland, G. Weber, W. Klein-Hessling, N. Girault, and B. Clement, "Modeling and interpretation of iodine behavior in PHEBUS FPT-1 containment with ASTEC and COCOSYS codes", Nuclear Technology, Vol. 177, pp 36-62, Jan. 2012
7. R. B. Bird, W. E. Stewart, E. N. Lightfoot, "Transport Phenomena", J. Wiley Sons, New York (1960)
8. S. Hellmann, F. Funke, G.-U. Greger, A. Bleier, W. Morell, "The reaction between iodine and organic coatings under severe PWR accident conditions an experimental parameter study", OECD Workshop on the Chemistry of Iodine in Reactor Safety, PSI, Würenlingen, Switzerland, June 10 12, 1996
9. S. Gupta, F. Funke, G. Langrock, G. Weber, B. von Laufenberg, E. Schmidt, M. Freitag, G. Poss, "THAI experiments on volatility, distribution and transport behaviour of iodine and fission products in the containment", OECD-NEA/NUGENIA-SARNET Workshop on the Progress in Iodine Behaviour for NPP Accident Analysis and Management, Marseille (France), March 30, April 1, 2015
10. M. Hoehne, G. Weber, "Interpretation of the OECD THAI CsI Aerosol Wash Down Test AW by COCOSYS analyses", OECD THAI Seminar, Paris, 6 and 7 Oct., 2010
11. G. Weber, "Ein neues Abwaschmodell für unlösliche Aerosole (AULA)", GRS-TN-WEG-01/2011, Aug. 2011
12. Shields, A., "Anwendung der Ähnlichkeitsmechanik und der Turbulenzforschung auf die Geschiebebewegung", Mitt. Preuss. Versuchsanst. Wasserbau u. Schiffbau, Berlin, 26, 26 (1936)
13. Guo, J., "Hunter Rouse and Shields diagram", Advances in Hydraulics and Water Engineering, Proc. 13th IAHR-APD Congress, Vol. 2, Singapore (2002)
14. "Erosion and Sedimentation Manual", U.S. Department of the Interior, Bureau of Reclamation, Denver, Colorado (Nov. 2006)
15. B. v. Laufenberg, M. Colombet, M. Freitag, "Wash-down Test of Silver Aerosol from Stainless Steel and Painted surfaces", NUTHOS Conf., Okinawa (Japan), 14 – 19 Dec. 2014
16. G. Weber, B. Krzykacz-Hausmann, F. Funke, W. Klein-Hessling, "Uncertainty and Sensitivity Analysis on the Iodine Model in

the Containment Code COCOSYS”,  
NUTHOS-10 Conference, Okinawa, Japan,  
14-18 Dec. 2014

**Effects of constituents of seawater on formation of volatile iodine by aqueous phase radiation chemistry**

Kuniki Hata <sup>(1)\*</sup>, Kentaro Kido <sup>(1)</sup>, Yutaka Nishiyama <sup>(1)</sup>, Yu Maruyama <sup>(1)</sup>

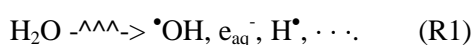
<sup>(1)</sup> Japan Atomic Energy Agency, Tokai-mura, Ibaraki, Japan

\*Corresponding author, tel: (+81) 292826778, Fax: (+81) 292825406, Email: hata.kuniki@jaea.go.jp

**Abstract** – Model calculations of radiolysis of seawater with iodide were carried out to predict effects of seawater constituents on iodine chemistry at the time of a severe accident. Through the calculations based on gamma-radiolysis of solutions at ambient temperature, it was found that the production of molecular iodine ( $I_2$ ) was promoted by the addition of seawater constituents. Especially,  $Br^-$  and  $HCO_3^-$  had a large impact on its production. The production yields of radiolytic species were affected by the addition of  $I^-$  as well. It was also shown that the pH of seawater is an important parameter to determine radiolytic conditions of iodine. These results imply the potential that the injection of seawater has significant impact on iodine source term.

## I. INTRODUCTION

Radioiodine is a hazardous fission product which could be released from fuels of nuclear reactors when a loss-of-coolant accident (LOCA) occurs. Because it could form highly-volatile species, radioiodine has been a big concern of the severe accident management. It is known that the production of volatile iodine is mainly initiated by radiolysis of coolant water. Water molecules are ionized by energy deposition of radiation, which results in the production of reactive species, such as hydroxyl radical ( $\bullet\text{OH}$ ) and hydrated electron ( $e_{\text{aq}}^-$ ).



In the coolant water, iodide ( $\text{I}^-$ ), which exists as a result of dissociation of associated chemical species such as cesium iodide (CsI), is easily oxidized by  $\bullet\text{OH}$ , and iodine atom ( $\text{I}^\bullet$ ) could be produced. Because of low stability of  $\text{I}^\bullet$ , it reacts with  $\text{I}^-$  or another  $\text{I}^\bullet$ , and eventually volatile molecular iodine ( $\text{I}_2$ ) is produced. Thus, it is quite important to understand the behavior of  $\bullet\text{OH}$  in radiolysis processes to estimate production yields of volatile iodine appropriately.

In March 2011, the severe accident occurred at the Fukushima Daiichi Nuclear Power Station (NPS) as a result of the station blackout. As an accident management measure, lots of seawater was injected into the cores and the fuel pools to cool the fuels. The concentration of chloride ( $\text{Cl}^-$ ) in the contaminated water of Unit 2 was reported to be 16,000 ppm ( $0.45 \text{ mol dm}^{-3}$ ) in July 2011.<sup>1</sup> Reactions of ions in seawater, such as  $\text{Cl}^-$  and bromide ( $\text{Br}^-$ ), with  $\bullet\text{OH}$  are generally known to be very high.<sup>2-5</sup> Because of the high concentration of  $\text{Cl}^-$  in the reactors, it is presumed that the radiolytic conditions in reactors at the Fukushima Daiichi NPS were affected by the reactions of these ions. The authors have developed a seawater radiolysis model by combining the reaction sets of seawater constituents and have provided some calculation results which show that the production of radiolytic products, such as hydrogen molecules ( $\text{H}_2$ ), are promoted by the addition of these seawater constituents as a result of the reactions of these ions with  $\bullet\text{OH}$ .<sup>6-8</sup> Because of the change

of the  $\bullet\text{OH}$  behavior in water radiolysis, iodine chemistry may be also affected if seawater is injected in reactors right after an accident occurs. However, there is little information about iodine chemistry in irradiated seawater. In this study, the authors applied a reaction set of  $\text{I}^-$  on the currently developed radiolysis model<sup>6-8</sup> and some calculations were carried out to predict effects of the constituents of seawater on oxidation of  $\text{I}^-$  in water radiolysis.

## II. CALCULATIONS

To build up the model of seawater radiolysis,  $0.5 \text{ mol dm}^{-3} \text{ Cl}^-$ ,  $8.0 \times 10^{-3} \text{ mol dm}^{-3} \text{ Br}^-$  and  $2.3 \times 10^{-3} \text{ mol dm}^{-3}$  bicarbonate ion ( $\text{HCO}_3^-$ ) were taken into account. This seawater-simulated solution is called "AQ1" in this paper. The authors have confirmed that AQ1 was equivalent to artificial seawater in terms of water radiolysis.<sup>7</sup> The other constituents, such as borate ion and sulfate ion, were ignored because of their low reactivity with radiolytic species. The interactions of microorganisms and organic compounds were also neglected in this calculation. As effects of cations contained in seawater on the radiolysis is considered to be not important, only sodium cation ( $\text{Na}^+$ ) was included in this model to maintain charge balance of the solutions. It is known that dissolved oxygen (DO) suppresses the production of  $\text{I}_2$  from irradiated water.<sup>9</sup> However, the concentration of DO generally changes with changing of the concentration of solutes in water. The concentration of DO in seawater, for example, is known to be about 5ppm, which is lower than that of fresh water, 8ppm. In this study, to focus on the effects of each seawater constituents on the iodine behavior, all calculations have carried out in deaerated conditions. The reaction sets used in this calculation were taken from the report by Elliot<sup>10</sup> for reactions of water radiolysis and the report by Kelm<sup>2</sup> for the reactions of the solute ions. To simulate the reactions of iodine, the reaction set applied in an iodine chemistry simulation tool, Kiche, was used.<sup>11</sup> Interaction of radical anions derived from halide ions,  $\text{Cl}_2^{\bullet-}$  and  $\text{Br}_2^{\bullet-}$ , reported by Ershov et al. were also taken into account.<sup>12,13</sup> Some important reactions for the production of  $\text{I}_2$  are summarized in Fig. 1 and

their rate constants are shown in TABLE I. It is known that halide ions are generally effective  $\cdot\text{OH}$  scavengers. However, the reactivity of  $\text{Cl}^-$  is relatively lower than that of  $\text{Br}^-$  at neutral pH conditions because of the high reaction rate of the back reaction of R2 as well as the low reaction rate of R3 which is dependent on pH.<sup>14,15</sup>

All the calculations were performed using FACSIMILE.<sup>16</sup> Computer calculations were designed for the “homogeneous” stage of radiolysis, which starts  $10^{-7}$  s after the energy deposition of ionizing radiation to water molecules. The primary chemical yields of radiolytic species at this point were important parameters for performing the calculations. In this study, the primary yields measured by Pucheault et al. were used for concentrated  $\text{Cl}^-$  solutions.<sup>17</sup> In their report, there is a small difference between oxidative species (i.e., dichloride radical anion ( $\text{Cl}_2^{\cdot-}$ ),  $\cdot\text{OH}$ , and hydrogen peroxide ( $\text{H}_2\text{O}_2$ )) and reductive species (i.e.,  $e_{\text{aq}}^-$ , hydrogen atom ( $\text{H}\cdot$ ), and  $\text{H}_2$ ). The authors considered this difference to be the yield of  $\text{ClOH}^{\cdot-}$ . For calculations of solutions which are free of  $\text{Cl}^-$ , the primary yields of pure water reported by Elliot was applied.<sup>10</sup> The primary yields utilized for the calculations are listed in TABLE II. If concentrations of  $\text{Cl}^-$  are high, these rate constants vary due to the ionic strength of the solution. The effect of ionic strength was programmed using the extended Debye-Hückel law. All solutions in this study were assumed to be irradiated with gamma-ray at ambient temperature. The dose rate was  $1.0 \text{ Gy s}^{-1}$ .

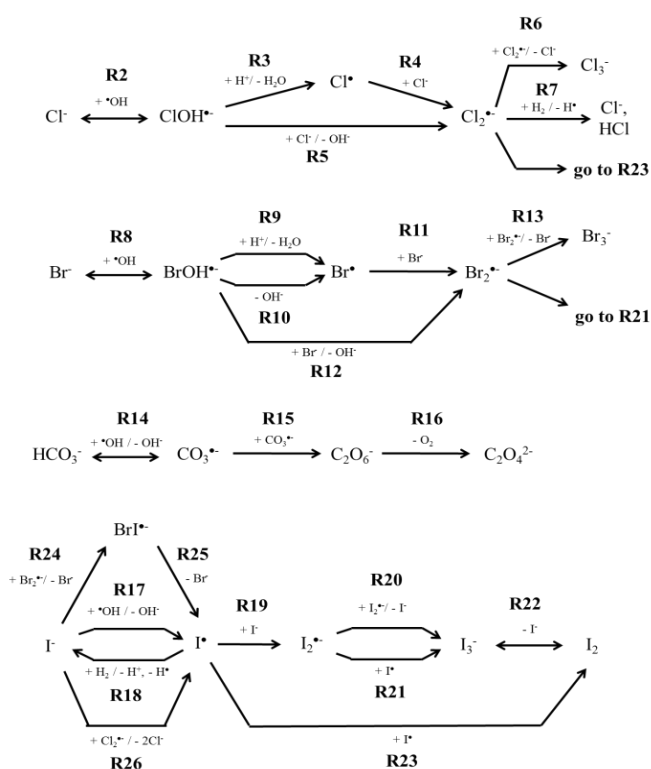


Fig. 1. Chemical reactions of ions in water radiolysis.

TABLE I. Rate constants of the chemical reactions of halide ions in water radiolysis.<sup>2,11-13</sup>

No.	Reactions	Rate constants at room temperature (dm <sup>3</sup> mol <sup>-1</sup> s <sup>-1</sup> or s <sup>-1</sup> )	
		Forward	Back
R2	Cl <sup>-</sup> + •OH ↔ ClOH•	4.3 × 10 <sup>9</sup>	6.1 × 10 <sup>9</sup>
R3	ClOH• + H <sup>+</sup> → Cl• + H <sub>2</sub> O	2.1 × 10 <sup>10</sup>	-
R4	Cl• + Cl <sup>-</sup> → Cl <sub>2</sub> •	2.1 × 10 <sup>10</sup>	-
R5	ClOH• + Cl <sup>-</sup> → Cl <sub>2</sub> • + OH <sup>-</sup>	9.0 × 10 <sup>4</sup>	-
R6	Cl <sub>2</sub> • + Cl <sub>2</sub> • → Cl <sub>3</sub> • + Cl <sup>-</sup>	7.0 × 10 <sup>9</sup>	-
R7	Cl <sub>2</sub> • + H <sub>2</sub> → Cl• + HCl + H•	4.3 × 10 <sup>5</sup>	-
R8	Br + •OH ↔ BrOH•	1.1 × 10 <sup>10</sup>	3.0 × 10 <sup>7</sup>
R9	BrOH• + H <sup>+</sup> → Br• + H <sub>2</sub> O	1.3 × 10 <sup>10</sup>	-
R10	BrOH• → Br• + OH <sup>-</sup>	4.2 × 10 <sup>6</sup>	-
R11	Br• + Br <sup>-</sup> → Br <sub>2</sub> •	1.0 × 10 <sup>10</sup>	-
R12	BrOH• + Br <sup>-</sup> → Br <sub>2</sub> • + OH <sup>-</sup>	1.9 × 10 <sup>8</sup>	-
R13	Br <sub>2</sub> • + Br <sub>2</sub> • → Br <sub>3</sub> • + Br <sup>-</sup>	3.4 × 10 <sup>9</sup>	-
R14	HCO <sub>3</sub> • + •OH → CO <sub>3</sub> • + OH <sup>-</sup>	8.5 × 10 <sup>6</sup>	-
R15	CO <sub>3</sub> • + CO <sub>3</sub> • → C <sub>2</sub> O <sub>6</sub> <sup>2-</sup>	1.4 × 10 <sup>7</sup>	-
R16	C <sub>2</sub> O <sub>6</sub> <sup>2-</sup> → C <sub>2</sub> O <sub>4</sub> <sup>2-</sup> + O <sub>2</sub>	6.5 × 10 <sup>8</sup>	-
R17	I• + •OH → I• + OH <sup>-</sup>	7.7 × 10 <sup>9</sup>	-
R18	I• + H <sub>2</sub> → I• + H• + H•	2.0 × 10 <sup>6</sup>	-
R19	I• + I• → I <sub>2</sub> •	1.2 × 10 <sup>10</sup>	-
R20	I <sub>2</sub> • + I <sub>2</sub> • → I <sub>3</sub> • + I <sup>-</sup>	4.5 × 10 <sup>9</sup>	-
R21	I <sub>2</sub> • + I• → I <sub>3</sub> •	5.0 × 10 <sup>9</sup>	-
R22	I <sub>3</sub> • ↔ I <sub>2</sub> • + I <sup>-</sup>	1.4 × 10 <sup>7</sup>	1.0 × 10 <sup>10</sup>
R23	I• + I• → I <sub>2</sub>	1.0 × 10 <sup>10</sup>	-
R24	I• + Br <sub>2</sub> • → BrI• + Br <sup>-</sup>	4.3 × 10 <sup>9</sup>	-
R25	BrI• → I• + Br <sup>-</sup>	5.7 × 10 <sup>8</sup>	-
R26	I• + Cl <sub>2</sub> • → I• + Cl• + Cl <sup>-</sup>	2.0 × 10 <sup>10</sup>	-

TABLE II. Primary yields of concentrated Cl<sup>-</sup> solutions (molecules/100 eV).<sup>16</sup>

[Cl <sup>-</sup> ] / mol dm <sup>-3</sup>	H•	e <sub>aq</sub> <sup>-</sup>	H•	H <sub>2</sub>	•OH	H <sub>2</sub> O <sub>2</sub>	-Cl•	ClOH•	-H <sub>2</sub> O	Cl <sub>2</sub> •
0	2.75	2.75	0.60	0.44	2.81	0.71	0	0	4.23	0
0.05	2.79	2.82	0.56	0.44	2.73	0.69	0.18	0.12	4.26	0.03
0.1	2.77	2.82	0.56	0.44	2.71	0.68	0.24	0.14	4.26	0.05
0.25	2.67	2.81	0.54	0.45	2.66	0.66	0.41	0.13	4.25	0.14
0.5	2.53	2.80	0.52	0.45	2.56	0.64	0.65	0.11	4.22	0.27

### III. EFFECT OF SEAWATER CONSTITUENTS ON THE PRODUCTION OF I<sub>2</sub>

To predict effects of the constituents of seawater on oxidation of I<sup>-</sup> in water radiolysis, calculations of AQ1 containing I<sup>-</sup> were conducted. Fig. 2 shows the time-dependent change of the concentration of I<sub>2</sub> and pH in water of diluted AQ1 containing 1.0 × 10<sup>-5</sup> mol dm<sup>-3</sup> I<sup>-</sup> up to 100 s. The production of I<sub>2</sub> was suppressed

by diluting these ions by less than 20 %. The pH of the solutions increased with diluting seawater constituents. This result indicates that the oxidation of I<sup>-</sup> is suppressed by the pH change or promoted by the addition of Cl<sup>-</sup>, Br<sup>-</sup>, or HCO<sub>3</sub><sup>-</sup>. According to Fig. 2 (a), I<sub>2</sub> concentration gradually reached steady-state during irradiation; however, I<sub>2</sub> is a highly volatile species. If this system faces the gas phase, the production of I<sub>2</sub> may become progress continuously.

To identify the mechanism of I<sub>2</sub> production in irradiated seawater, calculations for the solutions which did not contain these ions were carried out. The time-dependent change of the concentration of I<sub>2</sub> produced in the solutions containing 1.0 × 10<sup>-5</sup> mol dm<sup>-3</sup> of I<sup>-</sup> is shown in Fig. 3(a). The concentration of I<sub>2</sub> in the solution without Cl<sup>-</sup> was similar to that of AQ1. Because of the low reactivity of Cl<sup>-</sup> with •OH, it may not affect the oxidation of I<sup>-</sup>. On the other hand, the concentration of I<sub>2</sub> significantly decreased for the solutions without Br<sup>-</sup> or HCO<sub>3</sub><sup>-</sup>. According to the authors' previous calculations, HCO<sub>3</sub><sup>-</sup> was less important for radiolysis of seawater.<sup>6</sup> However, the calculation result in Fig. 3(a) indicates that the presence of HCO<sub>3</sub><sup>-</sup> significantly affects the oxidation of I<sup>-</sup>. Fig. 3(b) shows the time-dependent change of pH of these solutions. The pH of the solution without HCO<sub>3</sub><sup>-</sup> gradually increased and exceeded 8. The increase in pH is known to suppress the oxidation of I<sup>-</sup>.<sup>18</sup> It is considered that HCO<sub>3</sub><sup>-</sup> plays an important role to control the pH of AQ1. On the other hand, Br<sup>-</sup> affects the I<sub>2</sub> production without such a noticeable pH change. Bromide ion is considered to be one of the most important species for seawater radiolysis because of its high reaction rate with •OH.<sup>6</sup> As •OH is the most reactive reactant for I<sup>-</sup> to produce I<sub>2</sub>, it is presumed that •OH scavenging property of Br<sup>-</sup> affects the iodine behavior. Because of lower reactivity of I<sup>-</sup> than that of Br<sup>-</sup> in the calculation condition, most of •OH is thought to be scavenged by Br<sup>-</sup>, and dibromide radical anion (Br<sub>2</sub>•<sup>-</sup>) is produced. It is reported that this radical easily oxidizes I<sup>-</sup> instead of •OH (reaction R24).<sup>13</sup> As a result, a lot of I<sub>2</sub> is produced. If Br<sup>-</sup> is removed from AQ1, it is assumed that •OH can oxidize I<sup>-</sup> directly or become a water molecule through recombination reactions because of the low concentration of I<sup>-</sup>,

which results in the suppression of  $I_2$  production. To confirm this assumption, calculations of the solutions containing  $1.0 \times 10^{-3} \text{ mol dm}^{-1}$  of  $\Gamma^-$  were carried out. In this condition,  $\bullet\text{OH}$  scavenging property of  $\Gamma^-$  is equivalent to that of  $\text{Br}^-$ . The calculation results showed that the time-dependent changes of  $I_2$  concentration in AQ1 containing  $\text{Br}^-$  and AQ1 without  $\text{Br}^-$  were completely the same, indicating that  $\Gamma^-$  is oxidized by  $\text{Br}_2^{\bullet-}$  which is produced from the reaction of  $\text{Br}^-$  and  $\bullet\text{OH}$  or by  $\bullet\text{OH}$  directly before  $\bullet\text{OH}$  returns to a water molecule. These results imply that  $\text{Br}^-$  plays an important role in the oxidation of  $\Gamma^-$  when the concentration of  $\Gamma^-$  is very low.

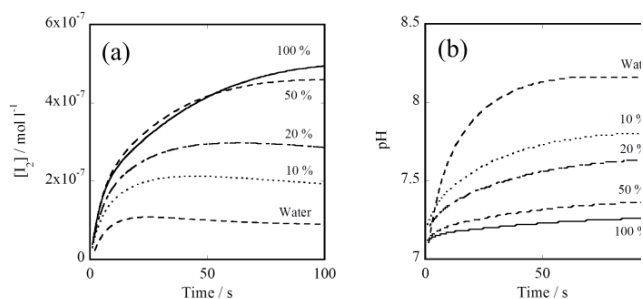


Fig. 2 Time-dependent change of (a) the concentration of  $I_2$  and (b) pH in diluted AQ1 or water containing  $1.0 \times 10^{-5} \text{ mol dm}^{-3}$   $\Gamma^-$ . The percentage means the dilution rate of AQ1.

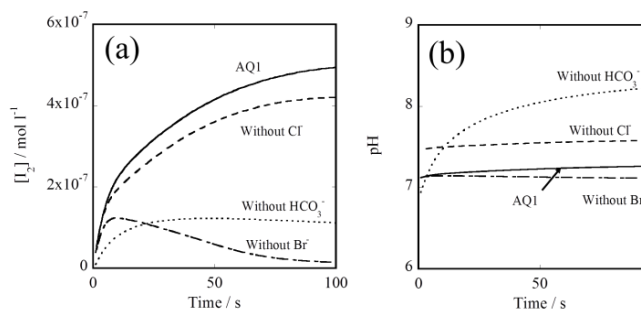


Fig. 3. Time-dependent change of (a) the concentration of  $I_2$  and (b) pH in AQ1 and the solutions which does not contain each ion containing  $1.0 \times 10^{-5} \text{ mol dm}^{-1}$  of  $\Gamma^-$ .

#### IV. EFFECT OF IODIDE ON SEAWATER RADIOLYSIS

It is known that the constituents of seawater affect the behavior of radiolytic products, such as  $\text{H}_2$ .<sup>6-8</sup> To predict the effects of iodide on the behavior of the radiolytic products, radiolysis calculations of deaerated AQ1 containing  $1.0 \times 10^{-6} - 1.0 \times 10^{-4} \text{ mol dm}^{-3}$   $\Gamma^-$  were started at pH 7. Fig. 4 shows the time-dependent change of  $\text{H}_2$  concentration during irradiation up to  $2 \times 10^4$  s. Hydrogen molecule for AQ1 in the absence of  $\Gamma^-$  was produced continuously and reached its saturating concentration ( $\sim 8 \text{ mol dm}^{-3}$ ) in  $2 \times 10^4$  s. The continuous production of  $\text{H}_2$  from irradiated seawater was reported by gamma-radiolysis experiments.<sup>19</sup> It has been considered that this  $\text{H}_2$  production is due to the  $\bullet\text{OH}$  scavenging reactions of  $\text{Cl}^-$  and  $\text{Br}^-$  because  $\bullet\text{OH}$  is an effective  $\text{H}_2$  scavenger. According to the calculation result, the production of  $\text{H}_2$  was suppressed by the addition of  $\Gamma^-$ . In the reaction set prepared for this study,  $\text{H}_2$  can be also scavenged by  $\text{Cl}_2^{\bullet-}$  and  $\text{I}^\bullet$  in the presence of the ions (reaction R7 and R18 in Fig. 1). The reaction between  $\text{H}_2$  and  $\text{Cl}_2^{\bullet-}$  was introduced by Kelm et al. to fit their calculation results to the gamma-radiolysis experimental results using autoclaves;<sup>20</sup> however, they withdrew this reaction from their reaction set later.<sup>21</sup> In either case, the concentration of  $\text{Cl}_2^{\bullet-}$  during irradiation was so low ( $< 1.0 \times 10^{-13} \text{ mol dm}^{-3}$ ) that the reaction of  $\text{Cl}_2^{\bullet-}$  cannot be an important reaction in radiolysis of AQ1. On the other hand, the concentration of  $\text{I}^\bullet$ , which is another possible  $\text{H}_2$  scavenger, was much higher ( $\sim 1.0 \times 10^{-9} \text{ mol dm}^{-3}$ ) than that of  $\text{Cl}_2^{\bullet-}$  during irradiation. The authors presumed that the suppression of  $\text{H}_2$  production in the presence of  $\Gamma^-$  was mainly due to the  $\text{H}_2$  scavenging reaction of  $\text{I}^\bullet$ . To verify the effect of this reaction on the suppression of  $\text{H}_2$  production, radiolysis calculation of AQ1 containing  $\Gamma^-$  excluding the reaction of  $\text{H}_2$  and  $\text{I}^\bullet$  was carried out. The result showed that the production rate of  $\text{H}_2$  was the same as that of AQ1 in the absence of  $\Gamma^-$ , which indicates that the reaction of  $\text{I}^\bullet$  with  $\text{H}_2$  is quite important to estimate the yield of  $\text{H}_2$  production. The rate constant of this reaction was determined to explain the experimental results of gamma-radiolysis.<sup>10</sup> Direct measurement of this reaction is thought to be important to prepare a proper

reaction set of radiolysis model for severe accidents.

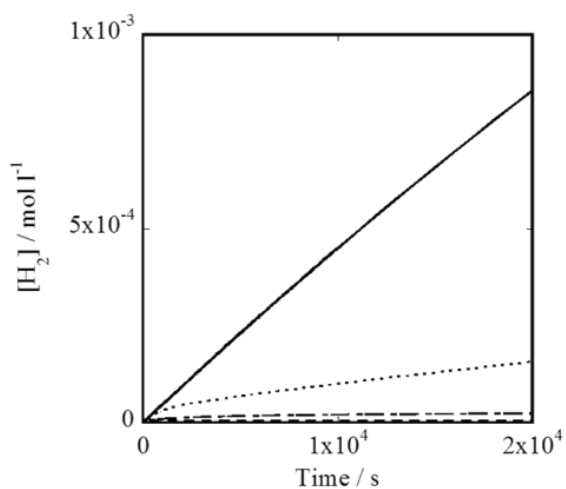


Fig. 4. Time-dependent change of the concentration of  $H_2$  produced in AQ1 containing (—) 0, (---)  $1.0 \times 10^{-6}$ , (- · - ·)  $1.0 \times 10^{-5}$ , and (·····)  $1.0 \times 10^{-4}$  mol  $dm^{-3}$   $I^-$  during irradiation.

According to the  $H_2$  concentrations in Fig. 4, the production rate of  $H_2$  increased with increasing  $I^-$  concentration. This might be due to the reaction of  $I^-$  with  $I^\bullet$ , which results in the release of  $H_2$  from scavenging reaction by  $I^\bullet$ .

#### V. EFFECT OF INITIAL pH CONDITIONS

It is known that pH is one of the most important parameters for the oxidation process of  $I^-$ . To estimate the effect of initial pH on the oxidation of  $I^-$ , radiolysis calculations of AQ1 containing  $1.0 \times 10^{-5}$  mol  $dm^{-3}$   $I^-$  at different initial pH conditions were conducted. Fig. 5 (a) shows the  $I_2$  concentration during irradiation. It was found that the production rate of  $I_2$  was decreased significantly when the initial pH was adjusted to be 9. The time-dependent change of pH is also shown in Fig. 5 (b). The pH changed quickly right after starting irradiation. The pH of the solutions adjusted its initial pH from 6 to 8 became 7.1 – 7.2. On the other hand, the pH of the solution adjusted its initial pH to 9 were slightly higher. The difference of the  $I_2$  production between the AQ1 at different initial pH is thought to be caused by the difference of

steady-state pH during irradiation. There is little experimental evidence about pH change of seawater by irradiation. Some experiments are necessary to show the validity of this calculation result.

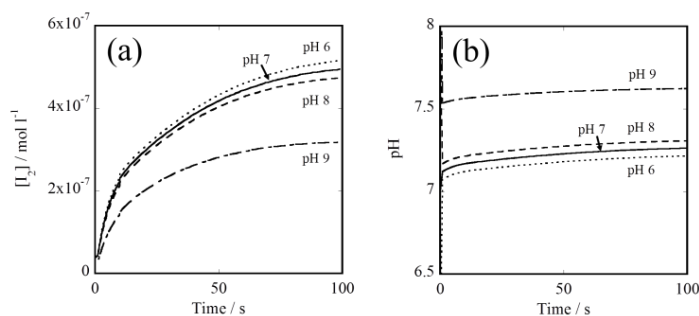


Fig. 5. Time-dependent change of (a) the concentration of  $I_2$  and (b) pH in AQ1 containing  $1.0 \times 10^{-5}$  mol  $dm^{-3}$  of  $I^-$ . The initial pH of the solution was changed from 6 to 9.

#### VI. CONCLUSION

To estimate effects of constituents of seawater on iodine chemistry during a severe accident, calculations using the model of seawater radiolysis were carried out. It was found that the production of  $I_2$  was promoted by the addition of seawater constituents. Especially,  $Br^-$  and  $HCO_3^-$  had a large impact on it. On the other hand, the production yields of radiolytic species were affected by the addition of  $I^-$ . It was also shown that the pH of seawater is an important parameter to determine radiolytic conditions of iodine. The calculation results in this study provided an important aspect of iodine chemistry in the presence of seawater. However, at the time of an accident, the other factors, such as concentrations of organic compounds and dissolved oxygen and temperature, have to be taken into account. In future, by considering effects of these factors as well as the effects of ions in seawater, the most important parameters which control the iodine behavior in irradiated seawater will be discussed to predict  $I_2$  production from a coolant which is injected seawater.

#### ACKNOWLEDGMENTS

The authors would like to express their gratitude to Professor Katsumura and Dr. Yamashita at the University of Tokyo and Dr. Muroya at Osaka

University for their support in coding the simulation model of water radiolysis.

## REFERENCES

1. TEPCO, Tokyo Electric Power Company. Situation of storing and treatment of accumulated water including highly concentrated radioactive materials at Fukushima Daiichi Nuclear Power Station (3rd Release). ([http://www.tepco.co.jp/en/press/corp-com/release/betu11\\_e/images/110713e10.pdf](http://www.tepco.co.jp/en/press/corp-com/release/betu11_e/images/110713e10.pdf)).
2. M. Kelm and E. Bohnert, "A kinetic model for the radiolysis of chloride brine, Its sensitivity against model parameters and a comparison with experiments," *FZKA 6977*, (2004).
3. S. Sunder and H. Christensen, "Gamma radiolysis of water solutions relevant to the nuclear fuel waste management program," *Nuclear Technology*, **104**, 403-417 (1993).
4. D. Zehavi and J. Rabani, "The oxidation of aqueous bromide ions by hydroxyl radicals. A pulse radiolytic Investigation," *The Journal of Physical Chemistry*, **76**, 312-319 (1972).
5. Z. Cai, X. Li, Y. Katsumura, and O. Urabe, "Radiolysis of bicarbonate and carbonate aqueous solutions: product analysis and simulation of radiolytic processes," *Nuclear Technology*, **136**, 231-240, 2001.
6. K. Hata, S. Hanawa, S. Kasahara, Y. Muroya, and Y. Katsumura, "Radiation-induced reactions of  $\text{Cl}^-$ ,  $\text{CO}_3^{2-}$ , and  $\text{Br}^-$  in seawater - Model calculation of gamma radiolysis of seawater," *Proc. of Nuclear Plant Chemistry Conference (NPC2012)*, French Nuclear Energy Society, Paris, France (2012).
7. K. Hata, S. Hanawa, S. Kasahara, T. Motooka, T. Tsukada, Y. Muroya, and Y. Katsumura, "Radiolysis calculation and gamma-ray irradiation experiment of aqueous solutions containing seawater components," *Proc. of Water Chemistry and Corrosion in Nuclear Power Plants in Asia*, National Tsing Hua University and Chung Hwa Nuclear Society, Taichung, Taiwan (2013).
8. K. Hata, S. Hanawa, S. Kasahara, T. Motooka, T. Tsukada, Y. Muroya, S. Yamashita, and Y. Katsumura, "Effects of dissolved species on radiolysis of diluted seawater," *Proc. of Nuclear Plant Chemistry Conference (NPC2014)*, Atomic Energy Society of Japan, Sapporo, Japan (2014).
9. K. Moriyama, S. Tashiro, N. Chiba, F. Hirayama, Y. Maruyama, H. Nakamura, and A. Watanabe, "Experiments on the Release of Gaseous Iodine from Gamma-Irradiated Aqueous CsI Solution and Influence of Oxygen and Methyl Isobutyl Ketone (MIBK)," *Journal of Nuclear Science and Technology*, **47**, 229-237 (2010).
10. A. J. Elliot and D. M. Bartels, "The reaction set, rate constants and g-values for the simulation of radiolysis of light water over the range 20° to 350°C based on information available in 2008", AECL EACL 153-127160-450-001 (2009).
11. K. Moriyama, Y. Maruyama, and H. Nakamura, "Kiche: A simulation tool for kinetics of iodine chemistry in the containment of light water reactors under severe accident conditions," JAEA-Data/Code 2010-034 (2011).
12. B. G. Ershov, E. Janata, and A. V. Gordeev, "Pulse radiolysis study of  $\Gamma^-$  oxidation with radical anions  $\text{Cl}_2^{\bullet-}$  in an aqueous solution," *Russian Chemical Bulletin, International Edition*, **54**, 1378-1382 (2005).
13. B. G. Ershov, E. Janata, and A. V. Gordeev, "Pulse radiolysis study of the oxidation of the  $\Gamma^-$  ions with the radical anions  $\text{Br}_2^{\bullet-}$  in an aqueous solution: formation and properties of the radical anion  $\text{BrI}^{\bullet-}$ ," *Russian Chemical Bulletin, International Edition*, **57**, 1821-1826 (2008).
14. M. Anbar and J. K. Thomas, "Pulse radiolysis studies of aqueous sodium chloride solutions," *The Journal of Physical Chemistry*, **68**, 3829-3835 (1964).
15. G. G. Jayson, B. J. Parsons, and A. J. Swallow, "Some simple, highly reactive,

- inorganic chlorine derivatives in aqueous solution,” *Journal of the Chemical Society, Faraday Transactions 1: Physical Chemistry in Condensed Phases*, **69**, 1597–1607 (1973).
16. E. M. Chance, A. R. Curtis, I. P. Jones, and C. R. Kirby, “Facsimile: A computer program for flow and chemistry simulation, and general initial value problems,” Atomic Energy Research Establishment, AERE-R 8775 (1977).
  17. J. Pucheault, C. Ferradini, R. Julien, A. Deysine, L. Gilles, and M. Moreau, “Radiolysis of concentrated solutions. 1. Pulse and  $\gamma$  radiolysis studies of direct and indirect effects in LiCl solutions,” *The Journal of Physical Chemistry*, **83**, 330-336 (1979).
  18. K. Ishigure, H. Shiraishi, and H. Okuda, “Radiation chemistry of aqueous iodine systems under nuclear reactor accident conditions,” *Radiation Physics and Chemistry*, **32**, 593-597 (1988).
  19. Y. Kumagai, A. Kimura, M. Taguchi, R. Nagaishi, I. Yamagishi, and T. Kimura, “Hydrogen production in gamma radiolysis of the mixture of mordenite and seawater,” *Journal of Nuclear Science and Technology*, **50**, 130-138 (2013).
  20. M. Kelm and E. Bohnert, “Gamma radiolysis of NaCl brine: Effect of dissolved radiolysis gases on the radiolytic yield of long-lived products,” *Journal of Nuclear Materials*, **346**, 1-4 (2005).
  21. M. Kelm, V. Metz, E. Bohnert, E. Janata, and B. Cube, “Interaction of hydrogen with radiolysis products in NaCl solution - comparing pulse radiolysis experiments with simulations,” *Radiation Physics and Chemistry*, **80**, 426-434 (2011).

## Formation and release of molecular iodine in aqueous phase chemistry during severe accident with seawater injection

Kentaro Kido(1)\*, Kuniki Hata(1), Yu Maruyama(1), Yutaka Nishiyama(1) and Harutaka Hoshi(2)

<sup>(1)</sup> Japan Atomic Energy Agency, Tokai-mura, Ibaraki, Japan, <sup>(2)</sup> Nuclear Regulation Authority, Minato-ku, Tokyo, Japan

\*Corresponding author, tel: (+81) 29-282-6159, Fax: (+81) 29-282-6147, Email: kido.kentaro@jaea.go.jp

**Abstract** – Seawater injection into the degraded core is one of the measures of accident management as it has been performed at Fukushima Daiichi nuclear power plant. The constituents in seawater deeply relates to the iodine chemistry in the water pool of the suppression chamber, which indicates that it is important to assess their effect on the source term in a severe accident. In the present study, by employing a four-component seawater (SW) model we try to simulate the time evolution of I<sub>2</sub> molecules yielded in aqueous solution based on several datasets on chemical reaction kinetics and to evaluate its fraction for the initial inventory released from aqueous solution to gas phase.

The amount of I<sub>2</sub> molecules in gas phase was in proportion to the mixing ratio of the SW model. The combination of bromide and hydrogen-carbonate anions considerably contributes to the behavior of the time evolution of I<sub>2</sub> fraction. The oxygen molecules in aqueous solution drastically reduced yielding I<sub>2</sub> molecules by catalytically consuming hydroxyl radicals, while I<sub>2</sub> molecules increased by the carbon dioxide gas involved in gas phase. The effects of both SW constituents and carbon dioxide gas are recommended to be considered in the quantitative discussion on the I<sub>2</sub> molecules released from aqueous solution

TABLE I

The gas-liquid partition constants and the mass transfer coefficients for volatile molecules used in the present study. The latter values are given in cm/s.

molecule	partition const.	10 <sup>-3</sup> mass transfer coeff.	
	all systems	system I	system II, III and IV
N <sub>2</sub>	0.0228	3.55	46.6
H <sub>2</sub>	0.0279	4.37	46.6
O <sub>2</sub>	0.0473	4.02	69.8
I <sub>2</sub>	71.3	2.49	11.7
CO <sub>2</sub>	0.85	3.43	66.1
Cl <sub>2</sub>	1.52	2.89	43.6

## I. INTRODUCTION

Radioactive iodine is a representative source term in a severe accident of nuclear power station due to the high volatility of its chemical species such as I<sub>2</sub> molecule and organic iodine (typically methyl iodide). The chemical species are yielded in aqueous solution, *e.g.*, the water pool of the suppression chamber, by reacting radioiodine compounds released from the fuels with various radicals yielded by water radiolysis. Especially, hydroxyl radicals play an important role in the chemical reactions. The amount of the iodine species strongly depends on not only the energy deposition of radiation but also the other solute molecules in the aqueous solution. For example, chloride and bromide anions, which are involved in seawater, are well-known to the scavengers of hydroxyl radical [1-4] and can not be negligible to quantify the release of iodine species.

Seawater injection into the degraded core is a measure of severe accident management in nuclear power plant. In practice, in the accident at the Fukushima Daiichi nuclear power station, seawater was injected in the degraded core to mitigate the accident consequences [5]. It is not clear that how a variety of constituents in seawater have an influence on yielding the iodine species. In order to study the effect of seawater constituents on yielding the iodine species, by using FACSIMILE software [6] a series of parametric analysis has been performed at Japan

Atomic Energy Agency (JAEA) [7-9]. The results implied that the constituents of seawater had a non-trivial impact on the I<sub>2</sub> yielding in aqueous solution. Also, by using chemical kinetics simulation software, KICHE [10], the iodine chemistry under radiation dose in pure water has been investigated. However, limited knowledge is currently available for the effect of seawater constituents on the iodine chemistry.

In the present study, based on several datasets on the kinetic information about chemical reactions among seawater constituents, we try to simulate the time profiles of their concentrations by employing a four-component seawater (SW) model aqueous solution [8]. The aqueous solution involves sodium cation, chloride, hydrogen-carbonate and bromide anions. We also try to evaluate the amount of I<sub>2</sub> molecules released from the aqueous solution to gas phase as the function of time. In addition, the effects of oxygen and carbon dioxide gases are investigated. To perform these simulations, we utilize KICHE software by updating the chemical reaction dataset and by adding datasets to treat chemical species involved in the SW model. It is noted that, different from FACSIMILE, gas phase can be treated by the interactions with aqueous solution through the gas-liquid interface in the KICHE framework. The transfer of volatile molecules yielded in aqueous solution is

described by both gas-liquid equilibrium and interfacial mass transfer.

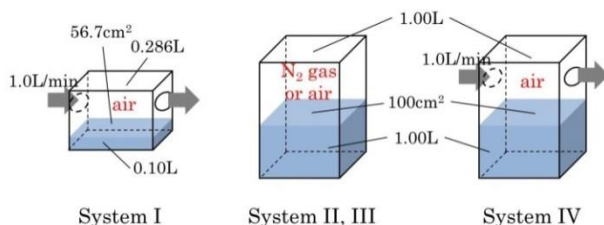


Fig. 1. The schematic pictures of system I, II, III and IV.

## II. Method and Models

### A. Systems

In this study, four-type systems consisting of gas phase and aqueous solution (system I, II, III and IV) are investigated as shown in Figure 1. The gas phase of system I (0.286 L) is filled with a realistic air ( $N_2$ : 80%,  $O_2$ : 20% and  $CO_2$ : 0.032%, total pressure is 1.0 atm) and is swept by the same gas at a constant flow rate (1.00 L/min = 0.0167 L/s). The aqueous solution (0.100L) contains  $1.00 \times 10^{-4}$  mol/L of cesium iodide and  $2.67 \times 10^{-4}$  mol/L of oxygen molecules. It is buffered by  $1.00 \times 10^{-4}$  mol/L of boric acid-sodium hydroxide. The interfacial area among gas phase and aqueous solution is 56.7 cm<sup>2</sup>. The temperature is 298.5 K. Although the temperature fluctuates from 288.0K to 298.5K in the experimental condition, in this simulation we keep the temperature constant because the reaction rates in the present dataset are obtained at 298K [1, 12-15]. The gamma-ray dose rate is set to 7.2 kGy/h (= 2.0 Gy/s) for  $1.0 \times 10^{-3}$  mol/L of  $Cl^-$  concentration whereas 6.1 kGy/h (=1.69 Gy/s) for  $1.0 \times 10^{-2}$  mol/L and  $1.0 \times 10^{-4}$  mol/L of  $Cl^-$  concentrations. The radiation is carried out for two hours from 0h. The initial pH is set to 7.0. The conditions are based on the experiments previously performed at JAEA [11].

The volume of gas phase and aqueous solution in systems II, III and IV is 1.00 L with the 100 cm<sup>2</sup> interfacial area.  $1.00 \times 10^{-5}$  mol of sodium iodide is added to each aqueous solution. In system II, the gas phase is filled by only  $N_2$  gas. In contrast, the gas phases in systems III and IV involve 20% of oxygen gas. Only system IV is swept by air with a flow rate of 1.00 L/min. The temperature

is 298.15 K. The gamma-ray dose rate is set to 3.6 kGy/h (=1.00 Gy/s). The radiation is continued for five hours from 0h. The initial pH in these three systems is set to 7.0 and total pressure is 1.0 atm.

### B. Models for chemical processes

In order to study the effect of seawater injection on the  $I_2$  molecule yielding, we employ a seawater model which consists of sodium chloride (0.500 mol/L), sodium hydrogen-carbonate ( $2.30 \times 10^{-3}$  mol/L) and sodium bromide ( $8.00 \times 10^{-4}$  mol/L). In this article, the aqueous solution is called "SW". Various mixtures of SW and pure water are used in system II, III and IV.

To simulate radiolysis occurring in aqueous solutions of the systems I, II, III and IV, the chemical reaction list published by Elliot et al. [12] was employed to express the water radiolysis. The reaction datasets were taken from Kelm et al. [1] to treat the interactions between chemical species yielded by water radiolysis and anions in the SW model aqueous solution. The parameters were used for primary yields in concentrated  $Cl^-$  solutions reported by Pucheault et al. [13]. To take the chemical reactions of iodine species into account, the reaction dataset implemented in the original KICHE software was employed. The interactions among the radical species yielded from chloride, bromide and iodide anions were simulated by the chemical reactions reported by Ershov et al. [14,15] It is quite critical to incorporate these reactions because both chloride and bromide anions can strongly scavenge hydroxyl radical which deeply relates the  $I_2$  molecule yielding. Since the effect of cations on the radiolysis is negligibly small, the sodium cations are treated to satisfy the charge neutrality of solution. In the present study, the ionic strength is not taken into account.

To realize this simulation, we utilize KICHE software by incorporating chemical reaction datasets mentioned above. Although the original KICHE can treat chloride and hydrogen-carbonate anions, the chemical reactions are very simplified. In the KICHE framework, the volatile molecules in aqueous solution can transfer to gas phase in terms of gas-liquid partition and

interfacial mass transfer [17-19]. The partition constants and mass-transfer coefficients used in the present study are summarized in Table 1. In the KICHE manual [10], readers can obtain more detailed information for their assumption and the method to calculate them.

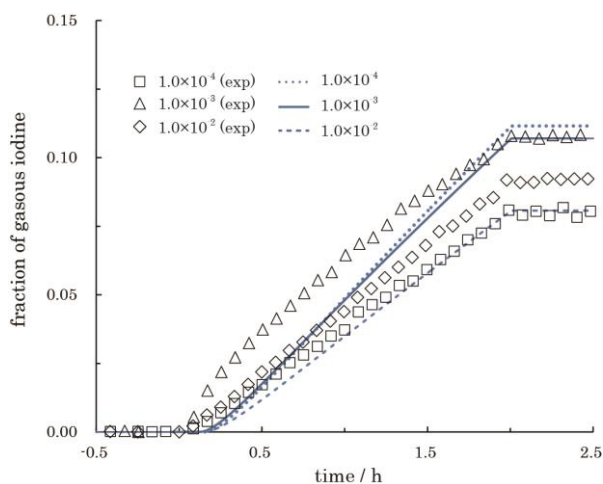


Fig. 2. Time profiles of the fraction of  $I_2$  molecules released from system I. Blue lines correspond to the simulation results. The dotted, solid and dashed lines represent  $1.00 \times 10^{-4}$  mol/L,  $1.00 \times 10^{-3}$  mol/L and  $1.00 \times 10^{-2}$  mol/L of  $Cl^-$  concentration, respectively. The experimental results are plotted by the open squares ( $1.00 \times 10^{-4}$  mol/L), triangles ( $1.00 \times 10^{-3}$  mol/L) and diamonds ( $1.00 \times 10^{-2}$  mol/L).

TABLE II

The comparison of final fractions of gaseous  $I_2$  molecules in system I. The  $Cl^-$  concentrations are given in mol/L.

$Cl^-$ conc.	this work	exptl.
$1.0 \times 10^{-4}$	0.112	0.077
$1.0 \times 10^{-3}$	0.107	0.110
$1.0 \times 10^{-2}$	0.081	0.092

### III. Results and Discussion

#### A. Benchmark test

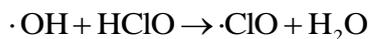
At first, using system I, we examine the validity of chemical reactions newly added to the original KICHE dataset by comparing with the small-scale fundamental experiments previously

performed at JAEA as a joint research with the former Japan Nuclear Energy Safety Organization (JNES) to investigate the influence of chloride anion on yielding  $I_2$  molecules in aqueous solution. Since the aqueous solution involves no bromide anion, the datasets of chloride and hydrogen-carbonate anions are checked.

Figure 2 shows the simulated and experimental time evolutions of the fraction of  $I_2$  molecule for the initial inventory transferred from aqueous solution in system I. As mentioned above, the radiation is cut at 2.0h. The former results are represented by the blue dotted ( $1.00 \times 10^{-4}$  mol/L of chloride anion concentration), solid ( $1.00 \times 10^{-3}$  mol/L) and dashed ( $1.00 \times 10^{-2}$  mol/L) lines. The latter one is represented by the open squares ( $1.00 \times 10^{-4}$  mol/L), triangles ( $1.00 \times 10^{-3}$  mol/L) and diamonds ( $1.00 \times 10^{-2}$  mol/L). First, let us compare the simulated time evolutions with the experimental ones. In the simulation results, the fraction is linear proportional to time and becomes small by increasing the  $Cl^-$  concentration. The trend does not appear in the experimental results. In  $1.00 \times 10^{-3}$  mol/L case (open triangles), there is a shoulder in the time profile not reproduced in the simulated one. In the other two cases (open squares and diamonds), although the fraction is in linear proportion to time, the difference does not become small from the corresponding simulation result as time evolves. Next, we discuss the final fraction at 2.5h summarized in Table 2. The simulation seems to show good agreement with the experiment except for  $1.00 \times 10^{-4}$  mol/L of  $Cl^-$  concentration in spite of the difference of time evolution due to the short radiation time (two hours). In the  $1.00 \times 10^{-4}$  mol/L case, the simulation rather overestimates the final fraction. These discrepancies among the simulation and experiment remain unclear and need further experimental information to improve the model.

Although not shown in Figure 2, we also compare the simulation results with those by the original KICHE reaction dataset. The original dataset overestimates the time evolutions for any  $Cl^-$  concentration than those by the present one. This is partially explained as follows; by the

dataset modification, a few reactions involving hydroxyl radical are newly added, for example,

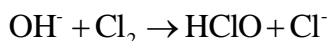


$$(\text{rate const.} = 9.0 \times 10^9 \text{ L mol}^{-1} \text{ s}^{-1}). \quad (1)$$

This reaction constructs a new pathway to scavenge hydroxyl radicals by associating with the following reactions;



$$(\text{rate const.} = 8.8 \times 10^7 \text{ L mol}^{-1} \text{ s}^{-1}) \quad (2)$$



$$(\text{rate const.} = 6.0 \times 10^8 \text{ L mol}^{-1} \text{ s}^{-1}). \quad (3)$$

Since the hydroxyl radical is needed to yield  $\text{I}_2$  molecules, the pathway contributes to reducing it.

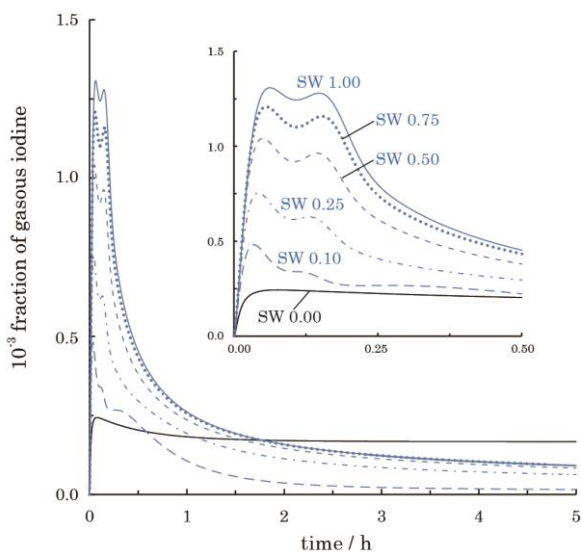


Fig. 3. The time evolutions of the fraction of  $\text{I}_2$  molecules in gas phase of system II. The black line represents the aqueous solution not mixed with SW (0%, pure water and sodium iodide). The blue solid, dotted, short-dashed, dotted-dashed, long-dashed lines correspond to 100%, 75%, 50%, 25% and 10% of SW volume fraction, respectively. The small figure is an enlarged view near 0h.

#### B. The effects of mixing SW

Figure 3 plots the time evolutions of the fraction of  $\text{I}_2$  molecules in gas phase of system II for the initial inventory and for various SW

volume fractions (100% (pure SW): blue solid line, 75%: blue dotted, 50%: blue short-dashed, 25%: blue dotted-dashed, 10%: blue long-dashed, 0% (pure water): black solid). The black line seems to be nearly flat except the low peak very near 0h, which shows that in pure water the  $\text{I}_2$  yielding reaches the equilibrium around 1h. In contrast, the blue solid line (100% SW) has the high peaks in the vicinity of 0.13h. But after the peaks, the  $\text{I}_2$  fraction exponentially decays and becomes smaller than the black line near 2h, which presents that the  $\text{I}_2$  molecules in gas phase transfer into aqueous solution by the gas-liquid partitioning due to the decrease of  $\text{I}_2$  molecules in aqueous solution. These curvatures are similar for all SW volume fractions. In addition, the  $\text{I}_2$  fraction is in proportion to the SW mixing ratio, which is consistent with the results reported by Hata et al. [20]. So, in the below let us discuss the curvatures of 100% SW.

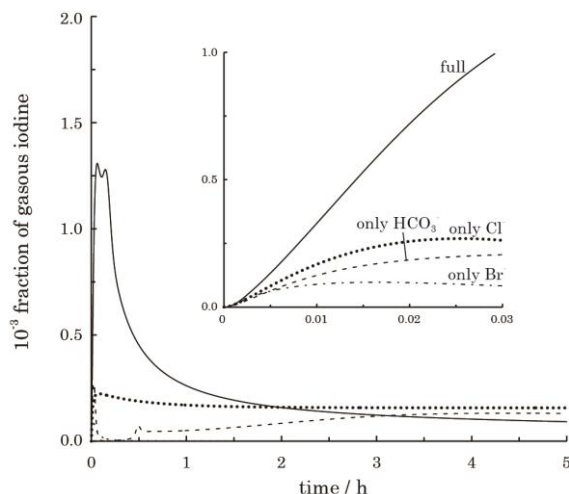


Fig. 4. The fractions of  $\text{I}_2$  molecules in gas phase of system II as the function of time. The solid, dotted, dashed and dotted-dashed lines correspond to pure SW, case A, case B and case C, respectively. The small figure is an enlarged view near 0h.

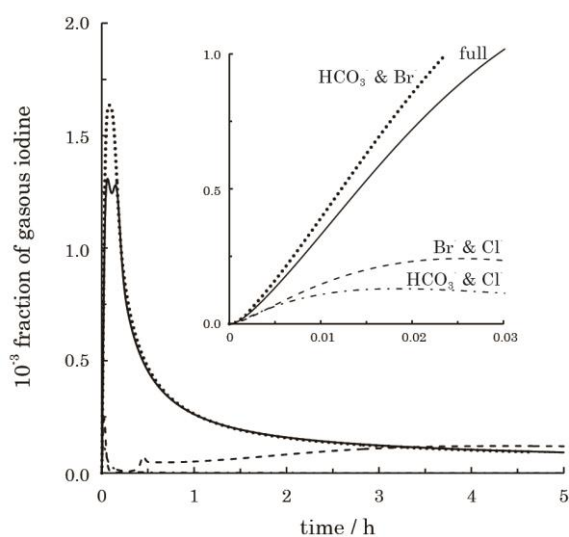


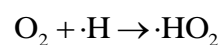
Fig. 5. The time profiles of the fraction of  $I_2$  molecules in gas phase of system II. The solid, dotted, dashed and dotted-dashed lines correspond to pure SW, case D, case E and case F, respectively. The small figure is an enlarged view near 0h.

In order to clarify the contribution of each anion involved in the SW model, we simulate three cases by removing two kinds of anion from the SW model; only chloride anion (case A), only hydrogen-carbonate anion (case B) and only bromide anion (case C). The results are shown in Figure 4. In any case, the solid line (pure SW case) is not reproduced, which presents that the curvature of pure SW model do not result from the contribution of the single anion. Furthermore, we investigate the three types of combination; bromide and hydrogen-carbonate anions (case D), chloride and bromide anions (case E) and chloride and hydrogen-carbonate anions (case F) as shown in Figure 5. The dotted line (case D) is fairly similar to the solid one (pure SW) except around the peak, which reveals that the combination of bromide and hydrogen-carbonate anions is significant for the time evolution of  $I_2$  fraction, which is consistent with the analysis by FACSIMILE reported by Hata et al. [20].

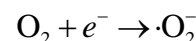
### C. The effect of oxygen gas

In pure water, the effects of oxygen and carbon dioxide gas on the  $I_2$  yielding have been well-discussed. In the present study, we investigate the effects in the SW model aqueous solution. In this section, the oxygen effect is discussed by the comparison of system II and III. Since the gas

phase consists of air in system III, oxygen molecules dissolve into aqueous solution with the saturated concentration ( $2.67 \times 10^{-4}$  mol/L) at the initial condition. Figure 6 plots the time evolutions of the  $I_2$  fraction in gas phase of system III for the initial inventory (blue and black solid lines). It is noted that the vertical axis in this figure is scaled by 1/10 of that in Figure 3, which shows that the  $I_2$  yielding decreases by oxygen molecules in aqueous solution. In the water radiolysis, the following two chemical reactions proceed much faster than system II because of oxygen molecules in aqueous solution.

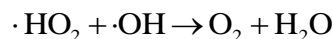


$$\text{(rate const.} = 2.00 \times 10^{10} \text{ L mol}^{-1} \text{ s}^{-1}) \quad (4)$$

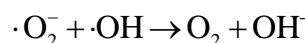


$$\text{(rate const.} = 1.94 \times 10^{10} \text{ L mol}^{-1} \text{ s}^{-1}) \quad (5)$$

The  $\cdot HO_2$  and  $\cdot O_2^-$  anion radicals consume hydroxyl radicals;



$$\text{(rate const.} = 7.10 \times 10^9 \text{ L mol}^{-1} \text{ s}^{-1}) \quad (6)$$



$$\text{(rate const.} = 9.96 \times 10^{10} \text{ L mol}^{-1} \text{ s}^{-1}). \quad (7)$$

As shown in Eqs. (4)-(7), the oxygen molecules catalytically consume hydroxyl radicals. Consequently, the chemical reaction of hydroxyl radicals with iodide anions to yield iodide radicals is strongly inhibited by the oxygen molecules. The black solid line (0% SW) is far below the blue solid one (pure SW). In the SW model aqueous solution, the chemical species yielded from  $Cl^-$ ,  $Br^-$  and  $HCO_3^-$  anions react with hydroxyl,  $\cdot HO_2$  and  $\cdot O_2^-$  anion radicals, which weakens the role of oxygen molecules as the inhibitor of yielding  $I_2$  molecules. These results are parallel with the discussion on the pure water case.

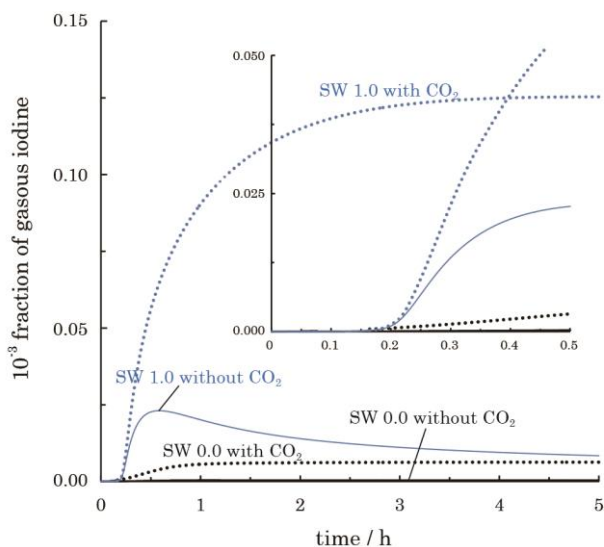


Fig. 6. The time profiles of the fraction of  $I_2$  molecules in gas phase of system III. The black solid and dotted lines correspond to 0% SW without and with carbon dioxide, respectively. The blue solid and dotted lines represent pure SW without and with carbon dioxide, respectively. The small figure is an enlarged view near 0h.

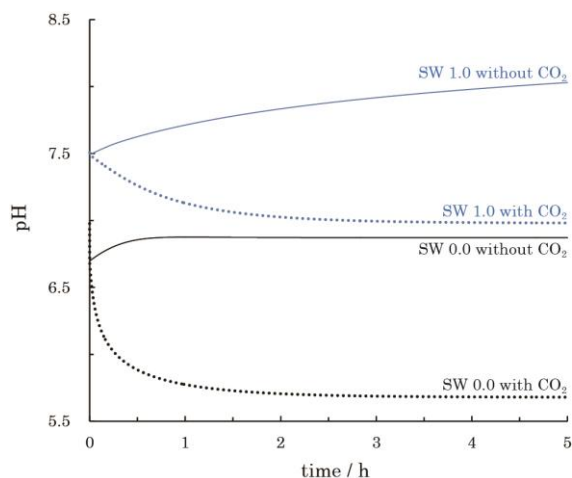
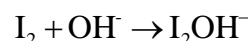


Fig. 7. The time profiles of pH of aqueous solution in system III. The black solid and dotted lines correspond to 0% SW without and with carbon dioxide, respectively. The blue solid and dotted lines represent pure SW without and with carbon dioxide, respectively.

#### D. The effect of carbon dioxide gas

Finally, we examine the influence of carbon dioxide on the  $I_2$  yielding in aqueous solution. 0.032% of the  $CO_2$  gas for total pressure is added

into the gas phase of system III. The result is shown in Figure 6 with the blue dotted line. In contrast to the oxygen effect, the carbon dioxide makes the  $I_2$  fraction increase. This is because of the pH decrease by  $CO_2$  gas dissolving into the aqueous solution. In practice, as shown in Figure 7, the pH decreases by about 0.5 units for two hours from 0h (blue dotted line) while it increases in the condition without  $CO_2$  gas (blue solid line). In a low pH condition, the chemical reaction to consume  $I_2$  molecules in aqueous solution



$$(\text{rate const.} = 1.00 \times 10^{10} \text{ L mol}^{-1} \text{ s}^{-1}) \quad (8)$$

becomes slower than a high pH condition [16]. Similar to the oxygen effect, the  $CO_2$  effect also is parallel with the investigations in pure water case.

By using system IV, the amount of  $I_2$  molecules released from the system by the sweep is investigated. Except for the sweep, the other conditions are the same as system III. Figure 8 shows the time evolutions of the fraction of  $I_2$  molecules released from the system. Similar to system III, the highest fraction is found in the case of pure SW and with  $CO_2$  gas (blue dotted line). The fractions at 5h are  $5.38 \times 10^{-5}$  (0% SW and without  $CO_2$  gas),  $8.51 \times 10^{-4}$  (0% SW and with  $CO_2$  gas),  $1.97 \times 10^{-3}$  (pure SW and without  $CO_2$  gas) and  $1.59 \times 10^{-2}$  (pure SW and with  $CO_2$  gas), respectively. This result indicates that it is critical for the quantitative evaluation of  $I_2$  gas released from aqueous solution to incorporate the effects of both seawater constituents and carbon dioxide in gas phase.

## X. SUMMARY

In this study, the  $I_2$  molecules yielded in and released from aqueous solution was investigated with a four-component seawater model to simulate an iodine chemistry in the water pool of suppression chamber when seawater was injected as a measure of accident management, based on the several kinetic datasets of chemical reactions for water radiolysis, chloride anion, bromide anion and hydrogen-carbonate anion. The software to simulate iodine chemistry in aqueous solution, KICHE, was utilized to perform the computation. Four-type systems (I, II, III and IV)

were prepared to study the effects of seawater constituents, oxygen gas and carbon dioxide gas.

In order to examine the chemical reaction datasets newly added for chloride and hydrogen-carbonate anions to the original KICHE dataset, the time evolutions of the  $I_2$  fraction for the initial inventory was simulated for three chloride anion concentrations. Although the result was compared with the experiments, the simulation did not show an agreement with the measured time evolution. The error sources to cause the discrepancy are not clear at the present.

Using system II, we investigated the effect of the constituents involved in the SW model. The  $I_2$  fraction in gas phase was in proportion to the SW mixing ratio. The time evolution for pure SW model aqueous solution had sharp and high peaks in the short range of time but became smaller than the SW 0% case by the rapidly decay after the peaks. We found that the combination of bromide and hydrogen-carbonate anions considerably contributed to its curvature. In system III, the effects of oxygen molecules dissolving into the aqueous solution were discussed, compared with the result obtained by system II. The oxygen molecules drastically reduced the  $I_2$  yielding by catalytically consuming hydroxyl radicals. On the other hand, by the carbon dioxide gas involved in air with a realistic partial pressure, the  $I_2$  molecules increased to transfer from aqueous solution. This was because of the pH decrease by  $CO_2$  dissolving into the aqueous solution. The similar trend was provided in system IV with the sweep of gas phase by air. These results indicated that the effects of the SW mixing and the dissolution of carbon dioxide gas are recommended to be considered in the quantitative discussion on the  $I_2$  molecules to transfer from aqueous solution.

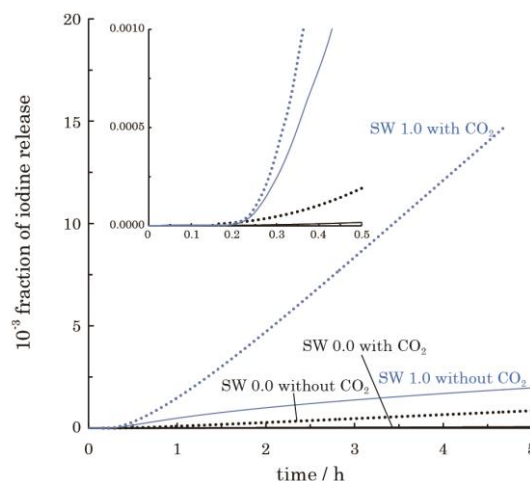


Fig. 8. The fractions of  $I_2$  molecules released from system IV as the function of time. The black solid and dotted lines correspond to 0% SW without and with carbon dioxide, respectively. The blue solid and dotted lines represent pure SW without and with carbon dioxide, respectively. The small figure is an enlarged view near 0h.

#### REFERENCES

1. M. Kelm and E. Bohnert, "A kinetic model for the radiolysis of chloride brine, Its sensitivity against model parameters and a comparison with experiments," FZKA 6977 report, 2004.
2. S. Sunder and H. Christensen, "Gamma radiolysis of water solutions relevant to the nuclear fuel waste management program," *Nuclear Technology*, **104**, 403 (1993).
3. D. Zehavi and J. Rabani, "The oxidation of aqueous bromide ions by hydroxyl radicals. A pulse radiolytic Investigation," *The Journal of Physical Chemistry*, **76**, 312 (1972).
4. Z. Cai, X. Li, Y. Katsumura, and O. Urabe, "Radiolysis of bicarbonate and carbonate aqueous solutions: product analysis and simulation of radiolytic processes," *Nuclear Technology*, **136**, 231 (2001).
5. TEPCO, Tokyo Electric Power Company. Situation of storing and treatment of accumulated water including highly concentrated radioactive materials at Fukushima Daiichi Nuclear Power Station (3rd Release). [http://www.tepco.co.jp/en/press/corp-com/release/betu11\\_e/images/110713e10.pdf](http://www.tepco.co.jp/en/press/corp-com/release/betu11_e/images/110713e10.pdf).

6. E. M. Chance, A. R. Curtis, I. P. Jones, and C. R. Kirby, "Facsimile: A computer program for flow and chemistry simulation, and general initial value problems," Atomic Energy Research Establishment, AERE-R 8775 (1977).
7. K. Hata, S. Hanawa, S. Kasahara, Y. Muroya, and Y. Katsumura, "Radiation-induced reactions of  $\text{Cl}^-$ ,  $\text{CO}_3^{2-}$ , and  $\text{Br}^-$  in seawater - Model calculation of gamma radiolysis of seawater," *Proceedings of Nuclear Plant Chemistry Conference (NPC2012)*, Paris, France (2012).
8. K. Hata, S. Hanawa, S. Kasahara, T. Motooka, T. Tsukada, Y. Muroya, and Y. Katsumura, "Radiolysis calculation and gamma-ray irradiation experiment of aqueous solutions containing seawater components," *Proceedings of Water Chemistry and Corrosion in Nuclear Power Plants in Asia*, Taichung, Taiwan (2013).
9. K. Hata, S. Hanawa, S. Kasahara, T. Motooka, T. Tsukada, Y. Muroya, S. Yamashita, and Y. Katsumura, "Effects of dissolved species on radiolysis of diluted seawater," *Proceedings of Nuclear Plant Chemistry Conference (NPC2014)*, Sapporo, Japan (2014).
10. K. Moriyama, Y. Maruyama, and H. Nakamura, "Kiche: A simulation tool for kinetics of iodine chemistry in the containment of light water reactors under severe accident conditions," *IAEA-Data/Code*, 2010-034 (2011).
11. K. Moriyama, S. Tashiro, N. Chiba, F. Hirayama, Y. Maruyama, H. Nakamura, and A. Watanabe, "Experiments on the Release of Gaseous Iodine from Gamma-Irradiated Aqueous CsI Solution and Influence of Oxygen and Methyl Isobutyl Ketone (MIBK)," *Journal of Nuclear Science and Technology*, **47**, 229 (2010).
12. A. J. Elliot and D. M. Bartels, "The reaction set, rate constants and g-values for the simulation of radiolysis of light water over the range 20° to 350°C based on information available in 2008", AECL EACL, 153-127160-450-001 (2009).
13. J. Pucheault, C. Ferradini, R. Julien, A. Deysine, L. Gilles, and M. Moreau, "Radiolysis of concentrated solutions. 1. Pulse and  $\gamma$  radiolysis studies of direct and indirect effects in LiCl solutions," *The Journal of Physical Chemistry*, **83**, 330 (1979).
14. B. G. Ershov, E. Janata, and A. V. Gordeev, "Pulse radiolysis study of  $\Gamma^-$  oxidation with radical anions  $\text{Cl}_2^{\bullet-}$  in an aqueous solution," *Russian Chemical Bulletin, International Edition*, **54**, 1378 (2005).
15. B. G. Ershov, E. Janata, and A. V. Gordeev, "Pulse radiolysis study of the oxidation of the  $\Gamma^-$  ions with the radical anions  $\text{Br}_2^{\bullet-}$  in an aqueous solution: formation and properties of the radical anion  $\text{BrI}^{\bullet-}$ ," *Russian Chemical Bulletin, International Edition*, **57**, 1821 (2008).
16. K. Ishigure, H. Shiraishi, and H. Okuda, "Radiation chemistry of aqueous iodine systems under nuclear reactor accident conditions," *Radiation Physics and Chemistry*, **32**, 593 (1988).
17. J. Ball et al. "ISP 41 containment iodine computer code exercise based on a Radioiodine Test Facility (RTF) experiment," NEA/CSNI/R(2000)6, vol.1-2, NEA (2000).
18. J. Ball et al. "ISP-41-follow-up exercise (phase 2): iodine code comparison exercise against CAIMAN and RTF experiments," NEA/CSNI/R(2004)16, NEA (2004).
19. B. Clement, C. Marchand, H.J. Allelein, and G. Weber., "Lessons learnt concerning iodine chemistry ISP-41, ISP-46," *EUROSAFE 2003, Seminar 2* (<http://www.eurosafe-forum.org/>) (2003).
20. K. Hata, K. Kido, Y. Nishiyama, Y. Maruyama, "Effects of constituents of seawater on formation of volatile iodine by aqueous phase radiation chemistry", *Proceedings of the International OECD/NEA-NUGENIA/SARNET Workshop on the Progress in Iodine Behaviour for NPP Accident Analysis and Management*, 2-2, Marseille, France (2015).

**Session 3: organic iodide formation and partitioning, chemistry and interactions with aerosols, droplets and surfaces in the gas phase**

**Chalmers - Project on volatile organic iodine species behavior and retention under severe nuclear accident conditions in LWRs**

*S. Tietze<sup>1\*</sup>, M. R.StJ. Forema<sup>1</sup> and C. Ekberg<sup>1</sup>*

*<sup>(1)</sup> Nuclear Chemistry, Chalmers University of Technology, Goeteborg (SE)*

*\*Corresponding author, Email:Tietze-Sabrina@gmx.de*

**Abstract** – *At Chalmers University of Technology extensive experimental studies on the volatile iodine source term, particularly with a focus on the chemistry of organic iodides have been performed between 2009 and 2015. The formation, partitioning behavior between gaseous and aqueous phase, the gaseous and aqueous phase radiolysis, the hydrolysis, the sorption behavior on painted surfaces, as well as possibilities to remove volatile iodine species in dry, solid filter beds and wet-filter systems have been investigated under conditions relevant during severe nuclear accidents in light water reactors.*

## I. INTRODUCTION

Within in a 5 year research project the impact of organic iodides on the volatile iodine source term was studied and compared to other volatile iodine species at the Nuclear Chemistry Department at Chalmers University of Technology.

The formation of organic iodides from different sources of organic materials such as cable plastics, paint films and pump oil was investigated both qualitatively and quantitatively under a series of severe nuclear accident relevant conditions. Different organic iodides were identified to be released in significant high amounts and were furthermore investigated towards their partitioning behavior in the containment, as well as their interactions with containment surface materials. The different chemical pathways resulted in the formation of new iodine species that were found to be as well partially volatile or re-volatilizable and therefore be able to (re)enter the volatile iodine cycle. Varying containment conditions in both gaseous and aqueous phase (pH, T, impurities, dose and dose rate), pyrolysis products, and radiolysis products as well as other fission products such as Cs and Ru, and the use of sea water for cooling were taken into consideration. Attempts have been made to model the pathways of organic iodides in the containment (e.g. OIPHA-1 and OIPHA-2 model) to predict the impact of organic iodides on the volatile iodine source term. Different currently used solid absorber and wet-scrubber filter systems have been tested for their ability to retain the identified organic iodides and iodine model substances, and alternative approaches have been investigated. A main focus of the project was on the effects of epoxy paint films and their ageing behavior on the iodine speciation, interactions and retention. The obtained results were used for the development of modified paint formulations for paint coatings that could act as passive iodine traps inside the containment by permanently retaining significant amounts of gaseous or aqueous iodine species. The potential release of iodine into the environment is a remaining concern in severe nuclear accident management. Elemental iodine can be well retained in the

traditionally used filter systems such as charcoal filter and the wet-scrubber filter systems containing a 0.015 M alkaline sodium thiosulfate solution. However, the retention of organic iodides is assumed and in some case also determined to be significant lower for methyl iodide. The knowledge obtained about the radiolysis and hydrolysis behavior of also organic iodides other than methyl iodide was used to investigate suitable filter materials to retain organic iodides in solid-filter beds and in wet-scrubber filter systems.

## II. RESULTS AND DISCUSSION

This publication contains an overview of the results obtained. Some of the results have been already published in scientific journals, other data are still in progress to be published. Particularly quantitative results will be reported in the corresponding journal publications.

### FORMATION OF ORGANIC IODIDES

The formation of organic iodides was investigated from mainly epoxy paint films, but also for cable plastics and pump oil that could leak into the containment in case of a pipe break. Therefore, a large material study of these organic materials was performed [1]. The composition, as well as the thermal and radiolytic degradation behavior of common materials used in Swedish nuclear power plants such as Teknopox Aqua VA epoxy paint and chlorine rich CSPE and PVC cable plastics was determined using analytical methods like TGA, (pyro)-GC-MS and residual solvent analysis. The release of the main solvents and plasticizer were studied and investigated further. To determine the components and the groups that form organic iodides the cured paint, the single identified components and synthesized surrogates of the resin were mixed with elemental iodine and exposed to gamma irradiation. It was found that not only methyl iodide was formed but also a range of other, longer chained organic iodides. It was found that the bisphenol-A based resin itself formed only very low amounts of methyl iodide and at doses higher than 1 MGy some aromatic organic iodides were formed (Fig. 1). The paint solvents such as texanol ester alcohol and benzyl

alcohol, however, caused the formation of a variety of organic iodides [2]. The most dominating ones are shown in Fig. 2. With increasing dose the yield of methyl iodide formation was found to decrease, whereas the fraction of longer chained organic iodides increased. The same experiments were repeated with alpha radiation using tributyl borate as alpha radiation source. The neutron activation was performed at Berkeley University. The higher LET radiation caused the formation of higher yields of longer chained organic iodides.

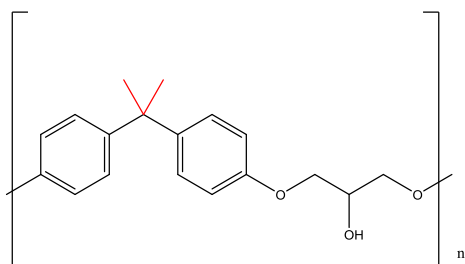


Fig. 1. MeI formation from the two methyl groups associated with the aromatic rings of the bisphenol-A unit in the bisphenol-A based resin of Teknopox Aqua VA epoxy paint.

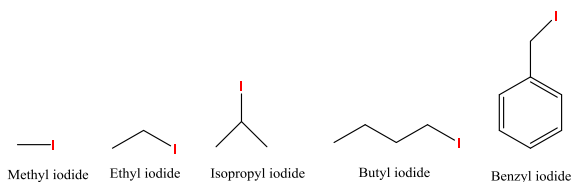


Fig. 2. Variety of organic iodides formed from Teknopox Aqua VA epoxy paint and elemental iodine in presence of gamma irradiation.

The yield of organic iodide formation dropped significantly when the paint films were thermally aged for short periods (less than a week) at temperatures above 100 °C. From the studies it was concluded that the yield of organic iodide formation can be reduced by a change of the solvent profile to more radiation resistant components such as aromatic components with less side chains or components with little branching. Different types of alternative resins were synthesized and it was found that a bisphenol-Z or a vegetable oil based resin resulted in a significantly lower methyl iodide yield (Fig. 3) [3, 4].

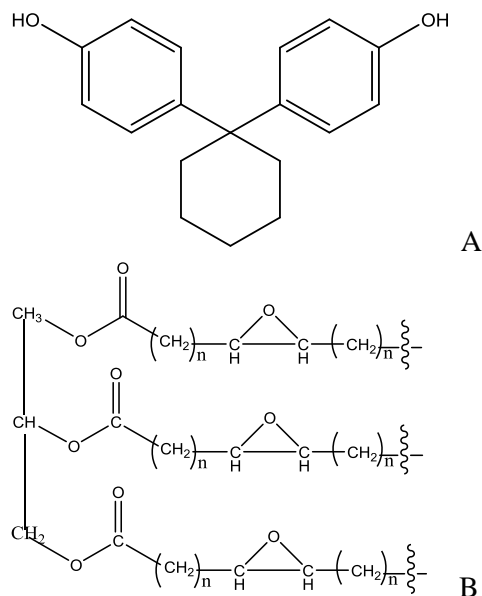


Fig. 3. A) Bisphenol-Z based resin B) Vegetable oil based resin

Another way to reduce the formation of organic iodides in the containment that was investigated was the addition of an additive that can react with elemental iodine but does not rerelease it under accident conditions. Aromatic additives that were linked with an amine that can furthermore react with the resin before the paint is cured with the hardener were found to be suitable. After 1 month heating at 100 °C approx. 50 % more elemental iodine were retained by adding 1 w % of the anthracene containing additive (Fig. 4) [3].

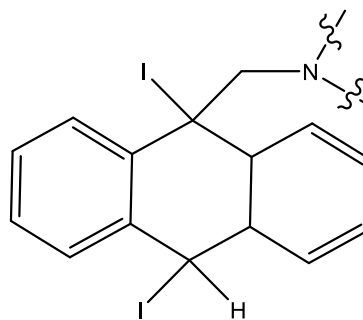
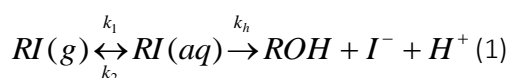


Fig. 4. Retention of elemental iodine in an anthracene modified bisphenol-A resin

## PARTITIONING BEHAVIOUR OF ORGANIC IODIDES

The partitioning behavior of the organic iodides that were identified in the irradiation studies of the paint films with iodine was studied using I-131 labelled species. Synthesis methods were developed to generate impurity free I-131 labelled organic iodides [5]. The mass transfer behavior of gaseous I-131 labeled organic iodides was studied using the FOMICAG facility which is a self-build small scale apparatus simulating a Swedish BWR containment [6]. The experimental data are evaluated with a newly developed mathematical model (OIPHA) that allows to determine the partitioning coefficient for organic iodides for every gas/liquid ratio and known interface area. The model and experimental method are described elsewhere [6, 7].



$$K_D = \frac{2RI_{g,0}k_1 + RI_{aq,0}(k_1 - k_2 - k_h) + RI_{aq,0}\sqrt{-4k_1k_h + (k_1 + k_2 + k_h)^2}}{2RI_{aq,0}k_2 + RI_{g,0}(-k_1 + k_2 + k_h) + RI_{g,0}\sqrt{-4k_1k_h + (k_1 + k_2 + k_h)^2}} \quad (2)$$

The main result found was that longer chained organic iodides and aromatic organic iodides persist longer in gaseous phase than methyl iodide which is important for the filtration of containment air [3]. At low pH and for increasing temperatures the mass transfer rates were found to increase for all studied organic iodides.

## RADIOLYSIS BEHAVIOUR OF ORGANIC IODIDES IN AQUEOUS AND GASEOUS PHASE

Radiolysis studies of organic iodides were performed in both gaseous and aqueous phase. In aqueous phase it was found that in presence of irradiation immediately elemental iodine was formed in aqueous phase that partitions back into the gaseous phase independent of the pH and composition of the aqueous phase. It was also found that the conversion rate into elemental iodine is dependent on the hydrolysis rate of the organic iodide. Hydrolysis studies showed that not only the chain length and therefore the

hydrophobic character determines the rate of the hydrolysis. Particularly, branched organic iodides that preferably undergo  $S_N1$  reactions other than linear, non-branched organic iodides such as methyl iodide, and therefore hydrolyses much quicker (Fig. 5) [3, 8].

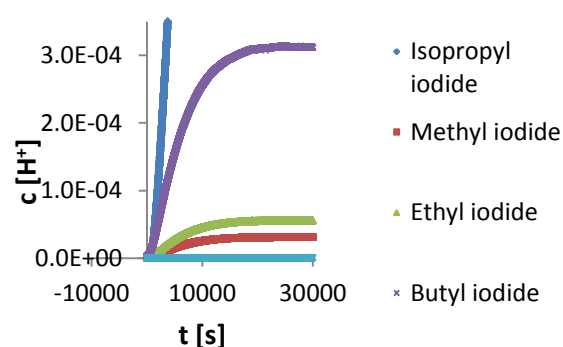


Fig. 5. Hydrolysis of organic iodides in distilled water

The high ionic strength and the higher activity coefficient in sea water or chlorine release from cable plastics was found to accelerate the hydrolysis [3,9].

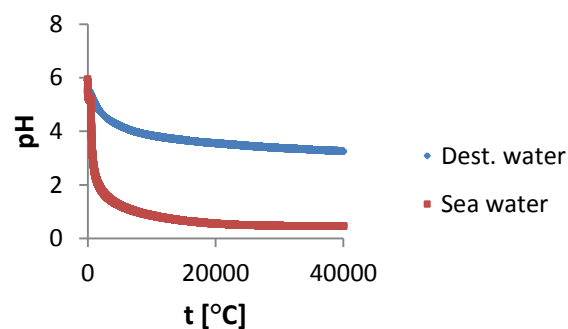


Fig. 6. Hydrolysis of EtI in sea water and distilled water (40 °C)

The replacement of distilled water with sea water was found to increase the rate of elemental iodine formation from all the organic iodine compounds tested (Fig. 7, Table 1) [3]. In distilled water hydroxyl radicals remove a hydrogen from  $sp^3$  hybridized organic iodides. In chlorine rich media large amounts of dichloride radicals are also formed, which chloride ions reduce iodide ions to form elemental iodine [8].

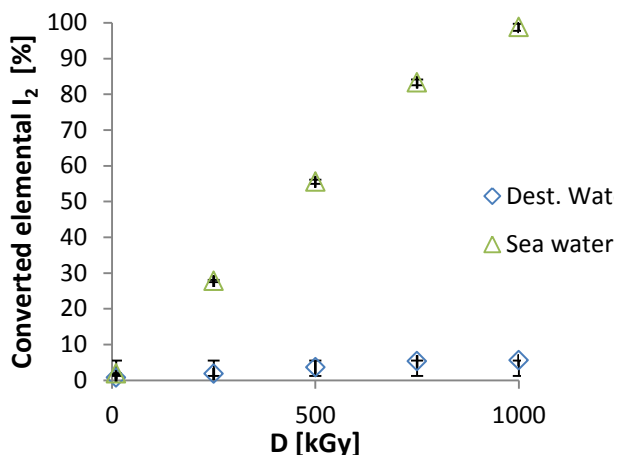


Fig. 7. Radiolytic conversion of methyl iodide into elemental iodine (10 kGy/h, 21 °C)

Table 1: Radiolytic conversion of aqueous iodine species (%) into elemental iodine (dose rate 10 kGy/h, 43 °C)

Medium	Distilled water	Sea water				
Dose [kGy]	50	200	500	50	200	500
Iodide	0.5 ± 0.1	3.7 ± 0.4	8.5 ± 0.1	0.9 ± 0.3	28.6 ± 0.6	75.1 ± 1.4
Methyl iodide	16.5 ± 0.8	28.6 ± 0.5	35.1 ± 0.9	22.9 ± 0.1	35.7 ± 0.4	77.0 ± 9.1
Ethyl iodide	9.2 ± 0.3	19.8 ± 0.4	21.2 ± 0.8	15.3 ± 0.1	24.3 ± 0.2	32.7 ± 0.8
Isopropyl iodide	22.4 ± 0.8	37.3 ± 0.2	77.1 ± 1.7	40.2 ± 0.3	42.5 ± 0.8	94.5 ± 5.2
Benzyl iodide	34.1 ± 0.4	54.6 ± 0.1	64.2 ± 2.1	45.2 ± 0.6	57.8 ± 1.3	77.3 ± 4.7
Butyl iodide	16.9 ± 0.8	27.0 ± 0.1	32.0 ± 0.4	37.5 ± 0.4	47.8 ± 1.3	54.3 ± 2.1
Allyl iodide	23.4 ± 0.4	42.2 ± 0.9	46.3 ± 0.5	93.7 ± 7.2	96.2 ± 6.1	99.3 ± 3.5
Chloriodomethane	32.5 ± 0.7	81.7 ± 1.2	97.7 ± 7.1	61.9 ± 0.7	85.7 ± 4.7	99.5 ± 6.4
Diiodomethane	8.6 ± 0.3	21.1 ± 1.0	37.2 ± 0.7	15.9 ± 1.9	22.7 ± 0.7	51.0 ± 2.4
Bromiodomethane	12.5 ± 0.1	22.6 ± 1.0	31.7 ± 0.3	19.9 ± 2.3	28.4 ± 0.6	78.8 ± 2.8
Iodo-anisole	27.3 ± 0.4	41.73 ± 0.3	66.1 ± 0.2	31.0 ± 1.0	47.7 ± 0.7	71.2 ± 3.3
HI	16.3 ± 0.3	22.1 ± 0.2	74.8 ± 0.3	18.1 ± 0.4	25.8 ± 0.5	91.3 ± 4.6

The radiolysis in gaseous phase showed that the yield of elemental iodine formation is highest from methyl iodide, whereas longer chained organic iodides form with an increasing dose an increasingly larger fraction of other organic iodides (Fig. 8) [3]. The formation of elemental iodine was also found to be proportional to the dose and dose rate (Fig. 9) [3].

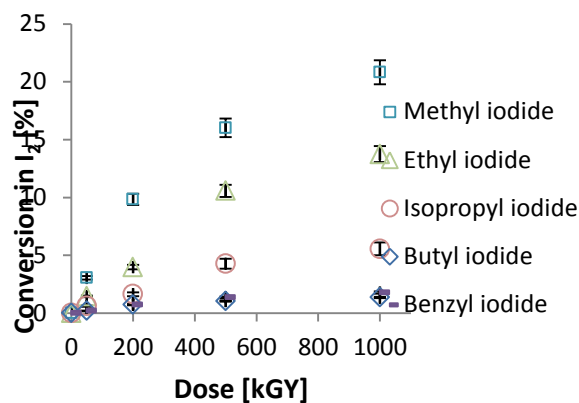


Fig. 8. Gamma radiolysis of organic iodides at 10 kGy/h at circa 43 - 45 °C

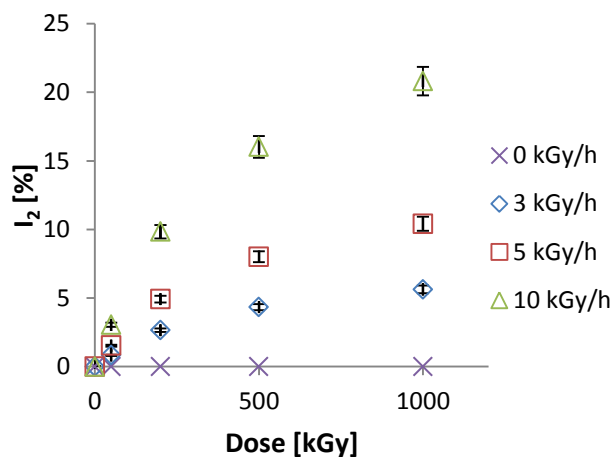


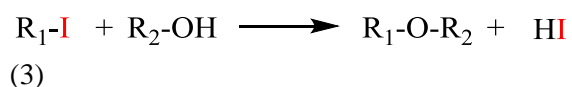
Fig. 9. Gamma radiolysis of methyl iodide at different dose rates at circa 43 - 45 °C

The data obtained for the speciation change of organic iodides in both aqueous and gaseous phase by hydrolysis and radiolysis are implemented in the OIPHA model to obtain more accurate partitioning coefficients for organic iodides to determine their gaseous fraction in the containment that could possibly enter the filter systems.

#### SORPTION BEHAVIOUR OF ORGANIC IODIDES ON PAINT FILMS IN GASEOUS AND AQUEOUS PHASE

<sup>13</sup>C-NMR studies revealed that methyl iodide and other alkyl iodides are able to be retained in Teknopox Aqua VA™ epoxy paint by the reaction of the methyl group (alkyl group) with

alcohol groups (-OH) forming esters, Eq. (3).



As found for the formation of organic iodides the retention of organic iodides was significantly reduced in a paint film that was thermally aged (1 month at 100 °C reduced by ca. 38 %). It was proven to be due to the loss of solvents (Table 2) [3,4]. A comparison made between the pure poly-bisphenol-A epichlorohydrin resin and a cured but non-aged Teknopox Aqua VA™ paint confirmed that the presence of solvents increases the reactivity of paint with methyl iodide.

Table 2. MeI exposed resin and paint

A (I-131) [%]	Resin	Paint
After exposure	20.3 ± 0.3	78.8 ± 3.9
20 h, 150 °C	43.1 ± 0.6	71.7 ± 6.6

In the thermally aged paint films a greater fraction of the original adsorbed organic iodide persisted in the matrix. These paint films also showed a higher re-vaporisation rate which was identified to be due to the higher fraction of physisorption of the organic iodides [3,4]. The same phenomena was observed in aqueous phase or on wet surfaces. The sorption rate was much lower into the paint film and the leaching rate from the paint film was found to be significantly higher [3,4]. The leaching rate and re-vaporisation rates were also accelerated in presence of either aqueous or gaseous chlorine species [3,4].

The effects of surface sorption, re-vaporisation and leaching on paint films is to be implemented in the OIPHA-III model.

#### RETENTION OF ORGANIC IODIDES IN SOLID FILTER BEDS

Solid absorbers have been mainly investigated for their ability to retain particulate matter, elemental iodine and methyl iodide [10]. The retention of organic iodides on activated charcoal filters requires that a nucleophilic substitution occurs, while elemental iodine can also be reliably retained in non-impregnated charcoals by the formation of charge transfer complexes

with the aromatic carbon rings [11]. As observed in the hydrolysis studies for different groups of organic iodides the selectivity of the filters can vary between different organic iodides. An initial study of the selectivity of a 10 % loaded DABCO charcoal confirmed that more than 50 % less isopropyl iodide was retained than methyl iodide (Table 3) [3]. Pre-irradiation of the absorber with 1 MGy additionally revealed that the DABCO lost its ability to retain the organic iodides after irradiation, whereas the non-impregnated charcoal showed the same ability as before irradiation (Table 3) [3]. It is assumed that due to the gamma irradiation some of the DABCO evaporated out of the pores of the charcoal. The aromatic compound benzyl iodide could not be retained on any of the studied absorber with more than 1 %.

Table 3. Retention of organic iodides on DABCO impregnated charcoal

[%]	MeI	Isopropyl-I
Charcoal non(irr)	5.1 ± 1.2	2.0 ± 0.3
10 % DABCO	14.3 ± 0.4	10.4 ± 0.3
Irr: 10 % DABCO	8.0 ± 2.4	5.2 ± 3.1

Experiments with a silver-loaded zeolite and a silver loaded SAMMS (silica) revealed that the silica had a *circa* 30 % higher ability to retain isopropyl iodide but a 60 % higher retainability of methyl iodide than ordinary charcoal [3]. The retention of both organic iodides was similar (Table 4). Both of them showed to be more radiation stable than the DABCO loaded charcoal and therefore to be more suitable for the organic iodide retention. However, the reactivity of the silver loaded SAMMS reduced when being exposed to gamma irradiation due to the mixed inorganic-organic composition whereas the zeolite is purely inorganic and therefore more irradiation resistant.

Table 4. Retention of organic iodides on silver-loaded solid absorber

%	MeI	Isopropyl I
Ag-loaded zeolite	65.7 ± 0.1	34.3 ± 0.1
Ag loaded SAMMS	66.5 ± 0.3	33.3 ± 0.3
Pre-irradiated zeolite	64.3 ± 0.1	33.9 ± 0.1
Pre-irradiated SAMMS	60.2 ± 4.2	29.5 ± 3.9

A retention higher than 65 % could not be obtained for any of the organic iodides and benzyl iodide was not retained with more than 1 % [3]. Chlorine and iodine bearing species such as chloriodomethane were retained with a similar efficiency as isopropyl iodide [3]. The retention on solid absorber materials is often dependent on many parameters (humidity, temperature, flow, loading, impurities) that are difficult to be controlled in case of an accident scenario. Therefore it was concluded that the most reliable retention could be obtained with a wet-scrubber filter system.

#### RETENTION OF ORGANIC IODIDES IN WET-FILTER SYSTEMS

The wet-scrubber filter system in current use in Sweden is of today to be operated with a 0.015 M sodium thiosulfate solution. It has been shown in both real scale tests and in lab scale experiments that gaseous organic iodides like methyl iodide are only slowly removed. In the FOMICAG facility several hours were required until all gaseous methyl iodide was removed ( $21.5 \pm 0.5$  °C) from the nearly steady gaseous phase. The polar nature of the aqueous medium and the short residence time of the incoming gas stream containing the volatile organic iodine species in the industrial scale scrubber were identified as reasons for the app. 20 times lower retention of methyl iodide with the current scrubber design [3,12]. Altering the inorganic scrubber solution with a few  $\mu\text{l}$  of tributyl, trihexyl or trioctyl phosphine let to an instant reduction of the gaseous organic iodide activity, even in the not-well mixed FOMICAG facility. The measurement interval in the FOMICAG facility was 10 seconds. Within less than 1 minute the gaseous activity of all studied organic iodides was removed (Fig. 10) [3,12]. In shaking experiments and flow through studies simulating the conditions in a Venturi scrubber all studied organic iodides were instantly removed [12,3]. The approach has been patented in collaboration with Westinghouse (Sweden) [13] and is currently studied on industrial scale by Westinghouse in Sweden.

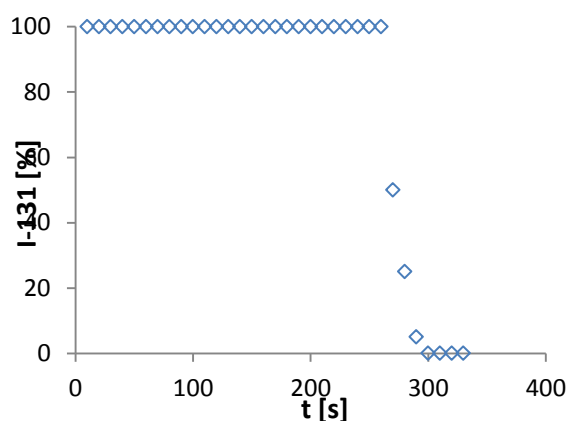


Fig. 10. Removal of gaseous methyl iodide ( $2 \cdot 10^{-2}$  mol) from air in the FOMICAG facility by a tributyl phosphine added at 260 seconds.

It has been calculated that after a scram in the end of a life-cycle of a Swedish BWR up to 20 g of organic iodine and 620 g of elemental iodine could enter the containment [3, 12]. Cesium iodide and other inorganic iodine species entering the scrubber can be ignored as they will decompose in aqueous phase. If the assumption is made that both the elemental iodine and the organic iodides pass unchanged through the containment into the scrubber-tank then the small amount of organic iodine (expressed as methyl iodide, 20 g (0.14 mol)) produced in the reactor will only require 34.5 ml of tributyl phosphine. If the scrubber was to be operated without the thiosulfate solution a small amount of additional tributyl phosphine (605 ml) would be required to convert the elemental iodine into inorganic iodide ions. Depending on the scrubber design it might be difficult to obtain the required mixing with such a small amount of the phosphine. The optimum organic to aqueous ratio and other parameters need to be investigated for the scrubber design specific conditions.

As the iodine is not chemically bonded to the organic additive, the system, similarly to the current system, will still depend on the aqueous-phase pH. However, possible revolatilisation of elemental iodine as a result of an acidification will be prevented as long as enough organic iodide or thiosulfate if added is available. The chemical reactivity of the trialkyl phosphines was proven to be independent on the pH of the aqueous solution or impurities in aqueous solution [3,12]. The main disadvantage of the

scrubbing approach is the oxygen sensitivity of trialkyl phosphines [3,12]. It is therefore proposed to use this solution for inert systems or systems with predictable oxygen content.

#### OTHER PROJECTS ON THE VOLATILE IODINE SOURCE TERM

The sorption and reevaporation behavior of iodine oxide aerosols and caesium iodide and their impact on the volatile iodine source term were studied in collaboration with VTT (Finland) [14, 15].

The effects of the sorption of ruthenium tetroxide on surface materials on the volatile iodine source term are studied in collaboration with Mr. Ivan Kajan at Chalmers University of Technology.

The effect of other impurities on the sorption behaviour of iodine species but also the effect of the leaching of organics out of paint films on the nitric acid formation have been investigated.

The behaviour of Gehopon epoxy paint used in the THAI facility is compared to the behavior of the paint films studied at Chalmers within a collaboration with GRS (Germany).

### III. SUMMARY OF SELECTED RESULTS AND CONCLUSIONS

It was found that a range of organic iodides can be formed from the organic materials present in the containment. Paint solvents and plasticizers were identified to determine the yield and variety of organic iodide formation from modern bisphenol-A based paints. The thermal age of the paints was identified to be the dominating parameter determining organic iodide formation. Aged paint films showed a greatly reduced ability to form organic iodides but after 20 years of ageing under real reactor conditions still relevant amounts of paint solvents that generated organic iodides were detected on paint disks from the Barsebäck nuclear power plant in Sweden. Due to the great variety of paint products, non-regulated cycles of paint film exchanges in nuclear plant, the varying organic

inventory in each containment and the additionally greatly varying conditions in different accident scenarios make a general prediction of the gaseous organic iodide fraction difficult.

The sides in the molecules causing the formation of organic iodides were identified. As a result proposals are made to modify currently-used paint products to either reduce the formation of aliphatic organic iodides or to increase the irreversible retention of elemental iodine in the paint film by adding an accident-conditions-resistant additive. The chemical behaviour of organic iodides in the containment was identified to be also very dependent on the structure of the organic iodide and not only on the conditions in the containment. This affects greatly the choice of filter materials to retain organic iodides in nuclear power plants. Chlorine species were identified to be important for decomposition of organic iodides and the volatile elemental iodine yield. Addition of trialkyl or triaryl phosphines was identified to be an instant, efficient and cheap approach to retain any alkyl iodides in wet-scrubber filter systems independent of radiation, impurities, other fission products, pH and temperature in the filter solution.

The release of hydrochloric acid and the use of sea water for emergency cooling were proven to affect both the formation and retention of organic iodides and to favour the formation of gaseous elemental iodine from organic iodides. The majority of the chlorine inventory of cable plastics was proven to be sealed in acid scavengers and will not enter the containment unless the scavenger comes into contact with water. Irradiation of cables showed to cause hydrochloric acid releases to start at lower temperatures (< 300 °C) and in higher amounts. In order to simplify the iodine chemistry halogen containing materials should be exchanged for halogen free, highly crosslinked and irradiation stable plastics.

#### REFERENCES

1. S. Tietze, M.R.StJ. Foreman, C.H. Ekberg, B.E. van Dongen, Identification of the chemical inventory of different paint types

- applied in nuclear facilities, *Journal of Radioanalytical and Nuclear Chemistry*, 3, pp. 1981-1999 (2013).
2. S. Tietze, M.R.StJ. Foreman, C.H. Ekberg, Formation of organic iodides from containment paint ingredients caused by gamma irradiation, *Journal of Nuclear Science and Technology*, 50(7), pp. 689-694 (2013).
  3. S.Tietze, The chemistry of organic iodides under severe nuclear accident conditions in LWRs, Dissertation, Chalmers University of Technology (SE), ISBN 978-7597-158-2 (2015).
  4. S. Tietze, M.R.StJ. Foreman, C.H. Ekberg, F. Davis, P. Wormald, Degradation studies of bisphenol-A based epoxy paints under severe nuclear accident conditions, Manuscript (2015).
  5. S. Tietze, M.R.StJ. Foreman, C.H. Ekberg, Synthesis of I-131 labeled iodine species relevant during severe nuclear accidents in light water reactors, *Radiochimica Acta*, 101(10), pp. 675–680 (2013).
  6. H. Glänneskog, J.-O. Liljenzin, L. Sihver, G. Skarnemark, A. Ödegaard-Jensen, Interactions of I<sub>2</sub> and CH<sub>3</sub>I with reactive metals under BWR severe-accident conditions, *Nuclear Engineering and Design*, 227, pp. 323-329 (2004).
  7. S. Tietze, M. Lindgren, S. Holgersson, C. Ekberg, OIPHA-I and II Model – Mathematical models to describe the partitioning and hydrolysis behavior of organic iodides between gaseous and aqueous phases, Iodine Workshop, Marseille (2015).
  8. R.T. Morrison, R.N. Boyd, *Organic Chemistry*, 5th edition, Allyn and Bacon Inc., 1987.
  9. S. Tietze, M.R.StJ. Foreman, B.E. van Dongen, C.H. Ekberg, The impact of cable materials on the iodine chemistry during severe nuclear accidents in LWRs, Manuscript (2015).
  10. IAEA, IAEA Safety Standards Series, Design of Reactor Containment Systems for Nuclear Power Plants, Safety Guide No. NS-G-1.10, 2004.
  11. S. Kothai, Charge Transfer Complexes of Iodine with Aromatic Hydrocarbons, *Journal of Applied Chemical Research*, 11, pp. 24-33 (2009).
  12. S. Tietze, M.R.StJ. Foreman, C.H. Ekberg, The use of trialkyl phosphines as novel wet-scrubber filter additives to enhance the decontamination factor for organic iodides from vented containment gas streams, Manuscript (2015).
  13. Patent on a novel wet-scrubber solution to reduce the release of organic iodides in case of a containment venting, Registration number: 1451118-2 (2014, Sweden) Inventors: S. Tietze, M.R.StJ. Foreman, C. Ekberg (Chalmers University of Technology) Patented with: Westinghouse Electric Sweden.
  14. S. Tietze, T. Kärkelä, C. Ekberg, A. Auvinen, U. Tapper, J. Jokiniemi, Adsorption and revaporisation studies of thin iodine oxide and CsI aerosol deposits from containment surface materials in LWRs, NKS-R, NKS-285, ISBN 978-87-7893-360-7 (2013).
  15. S. Tietze, T. Kärkelä, M.R.StJ. Foreman, C. Ekberg, A. Auvinen, U. Tapper, S. Lamminmäki, J. Jokiniemi, Adsorption and revaporisation studies on iodine oxide aerosols deposited on containment surface materials in LWRs, NKS-R, NKS- 272, ISBN 978-87-7893-345-4 (2012).

**OIPHA-I AND II MODEL - MATHEMATICAL MODELS TO DESCRIBE THE  
PARTITIONING AND HYDROLYSIS BEHAVIOR OF ORGANIC IODIDES BETWEEN  
GASEOUS AND AQUEOUS PHASES**

*S. Tietze<sup>1\*</sup>, M. Lindgren<sup>2</sup>, S.Holgersson<sup>1</sup> and C. Ekberg<sup>1</sup>*

*(1) Nuclear Chemistry, Chalmers University of Technology, Goeteborg (SE)*

*(2) Energy and Environment, Chalmers University of Technology, Goeteborg (SE)*

*\*Corresponding author, Email:Tietze-Sabrina@gmx.de*

**Abstract** – *Models to determine the gaseous fraction of organic iodides under severe nuclear accident conditions are under development. The **O**rganic **i**odide **p**artitioning and **h**ydrolysis **a**nalysis models (OIPHA) are based on experimental studies that investigate the partitioning behavior of organic iodides between gas and aqueous phase considering the effects of temperature, pH, impurities (e.g. chlorine species), radiolysis, hydrolysis and sorption phenomena on paint films for any LWR containment.*

## I. INTRODUCTION

Due to a limit amount of data describing the behavior of organic iodides under severe nuclear accident conditions in LWR's in safety codes like MAAP, mathematical models were developed to determine the partitioning coefficient of gaseous organic iodides such as methyl iodide. The OIPHA-I and -II Models (Organic iodide partitioning and hydrolysis analysis models) are based on experimental studies of the partitioning and the hydrolysis behavior of organic iodides for any liquid-gas phase systems with known gas phase volume, aqueous phase volume and interface area. The OIPHA-I model allows to determine the kinetic parameters of the partitioning and hydrolysis reactions of organic iodides which are required for the determination of the partitioning coefficient for varying pH and temperature. The effects of gamma irradiation on the iodine speciation and on the partitioning coefficient have been taken into consideration in the OIPHA-II model. The models are verified with experimental data determined with the FOMICAG (Facility for Online Measurements of I-131 Concentrations between an Aqueous and Gaseous phase) facility [1], a small-scale BWR containment set-up, at Chalmers University of Technology, as well as in solvent extraction experiments and ion selective electrode measurements. I-131 labelled organic iodide model substances (methyl-, ethyl-, isopropyl-, butyl-, benzyl-, allyl iodide, chloriodomethane and iodo-anisol) were synthesized for the studies.

## II. EXPERIMENTAL

Paragraph text here. I-131 labelled organic iodides (methyl-, ethyl-, isopropyl-, butyl-, benzyl-, allyl iodide, chloriodomethane and iodo-anisol) in their liquid form for the studies were synthesized as described in [2].

## OIPHA-I studies

The majority of the experimental data used for the description of the mass transfer of organic iodides from gaseous phase to aqueous phase and their hydrolysis in absence of irradiation were performed in the FOMICAG facility (Fig. 1) [1]. Organic iodides have a high vapor pressure and can therefore easily be converted from their liquid form into their gaseous form by placing the desired liquid amount into a round bottom flask. The flask was then sealed with a septum. After about 1 h at room temperature ( $21.5 \pm 0.5$  °C) the liquid partitioned into the gaseous phase and could be transferred using a gas-tight glass syringe. The gas saturated with the organic iodide was then injected through another septum into the gas phase of the FOMICAG facility (Fig. 1). The change of the gaseous I-131 activity in gaseous and aqueous phase was determined with two sodium iodide detectors that were placed in the gaseous and aqueous phase of the facility. The effects of temperature ( $21.5 \pm 0.5$  °C to 250 °C (gas phase)), pH (2 – 12) and impurities on the mass transfer between gaseous and aqueous phase were studied.

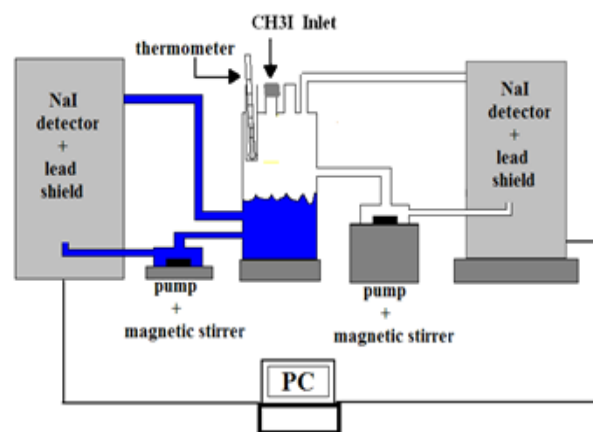


Fig.1. Diagram of the FOMICAG facility illustrating the injection of gaseous methyl iodide

## OIPHA-II studies

Due to the measurement with sodium iodide detectors in the FOMICAG facility the change of the speciation of the organic iodides could not be determined. Therefore, further batch studies using e.g. solvent extraction experiments were required to separate the aqueous species formed as a result of the hydrolysis. In these studies also the effect of irradiation and paint could be determined.

A majority of the studies was performed in glass flasks as small as 20 ml with varying gas/liquid ratio. For these studies typically less than 50  $\mu\text{l}$  of the I-131 labelled organic iodide were added in liquid form. For studies involving gamma irradiation the flasks were irradiated in a gamma irradiator with a dose rate between 20 kGy/h and 3 kGy/h at Chalmers University of Technology.

The speciation of the radioactive iodine in the bulk was determined with a two-step solvent extraction procedure (Fig. 2). 1 ml water samples were extracted with

octane (1 ml) in a 3.5 ml glass shaking vial. The extraction was performed with a shaking machine (IKA Vibrex VSR basic) to which a custom made sample holder was attached using a shaking time of 1 minutes at 1500 rpm. It was assumed that all organic iodine compounds (RI) and elemental iodine ( $\text{I}_2$ ) were partitioned into the octane layer, while all ionic inorganic iodine compounds remained in the aqueous layer ( $\text{I}^-$ ). Samples of the organic layer bearing the organic iodides and the aqueous phase bearing the ionic inorganic iodine species were subject to liquid scintillation. The octane layer (0.5 ml) was subjected to a second extraction with a 1 M KI solution (0.5 ml) which converted all elemental iodine present in the organic phase (visible as a pink colour of the organic layer) into triiodide ions ( $\text{I}_3^-$ ) leaving the organic iodides in the organic phase. Aliquots of each phase were again evaluated by LSC.

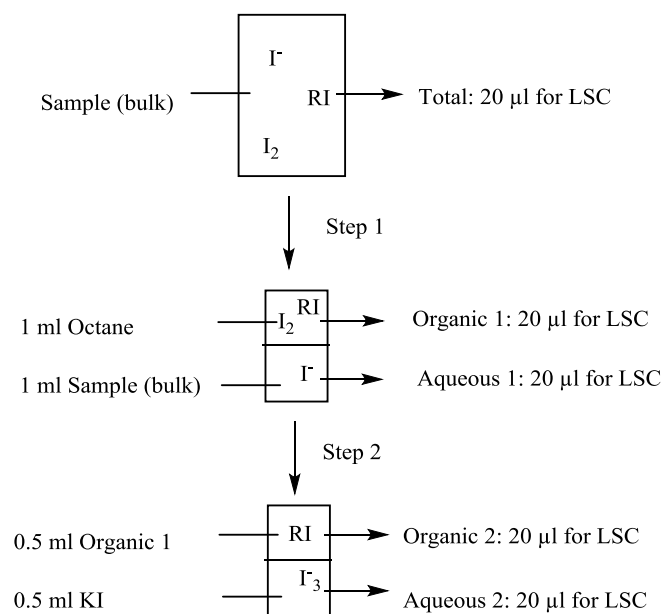


Fig. 2. Schematic of the solvent extraction procedure to separate aqueous iodine species

The hydrolysis of organic iodides was studied also with non-radioactive methods using online measurements with an iodide selective and pH electrode (Titrand, Metrohm).

## III. MODEL DEVELOPMENT

### OIPHA-I

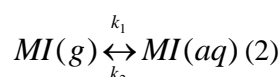
The ratio of a chemical substance between two phases at equilibrium can be described by the partitioning coefficient  $K_D$  (Eq. 1). The partitioning coefficient helps to make an estimate of the fraction of organic iodides that will remain in gaseous phase and that could possibly be released into the environment. The model is based on two key reactions of gaseous organic iodides:

- 1) the partitioning behavior/mass transfer between the containment gas phase and aqueous phase (Eq. 2) and
  - 2) the hydrolysis of the organic iodides in the water pool (Eq. 3).
- The effects of radiolysis and sorption effects on surface materials have been neglected at this stage.

The partitioning coefficient of methyl iodide (MI) (Eq. 1) and similar structured organic

iodides (RI) between a gaseous and aqueous phase can be described by the ratio of the amount in moles of methyl iodide in aqueous phase ( $MI_{aq}$ ) relative to the amount of methyl iodide available in gaseous phase ( $MI_g$ ), (Eq.1). It is assumed that an equilibrium saturation of the gas phase in the aqueous phase is obtained prior.

$$K_D = \frac{MI_{aq}}{MI_g} \quad (1)$$

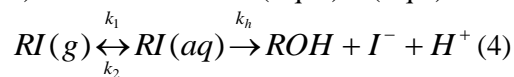


In aqueous phase dissolved methyl iodide ( $MI_{aq}$ ) undergoes furthermore hydrolysis (Eq. 3) leading to the formation of iodide ions ( $I^-$ ) which are defined as the main inorganic, ionic, immobilized iodine species for the model.



$k_1$ ,  $k_2$  are temperature dependent kinetic rate constants and  $k_h$  is the hydrolysis rate constant. MOH is the amount of methanol in moles which is formed from the hydrolysis of methyl iodide and the remaining proton ( $H^+$ ) is contributing to an acidification of the water pools. The formation of elemental iodine becomes relevant for acidic conditions ( $pH < 4$ ) and has been neglected for the studied pH range of  $4 < pH < 10$ .

Based on the chemical reactions representing the behavior of gaseous organic iodides  $RI(g)$  in the containment the differential equations for the reaction rates of the involved iodine species (Eq. 4) can be formulated (Eq. 5) – (Eq.7).



$$\frac{dRI_g}{dt} = k_2 RI_{aq} - k_1 RI_g \quad (5)$$

$$\frac{dRI_{aq}}{dt} = k_1 RI_g - k_h RI_{aq} - k_2 RI_{aq} \quad (6)$$

$$\frac{dI_{aq}^-}{dt} = k_h RI_{aq} \quad (7)$$

By solving the set of differential equations Eq. (5)-(7) expressions for the time (t) dependent change of the amounts of  $RI_g$ ,  $RI_{aq}$  and  $I_{aq}^-$  in moles for a aqueous-gas phase system with known aqueous and gaseous phase volume and

interface area can be obtained, Eq. (8)-(10).  $RI_{aq,0}$ ,  $RI_{g,0}$  and  $I_{aq,0}$  are start values at a start time  $t = 0$ . These equations were used for the analysis of experimental data which were obtained in experimental studies.

$$RI_g(t) = RI_{g,0} e^{-k_1 t} + \frac{RI_{aq,0}(-e^{-Xt} + e^{-Zt})k_2}{X - Z} + \frac{RI_{g,0}k_1((-X+Z)e^{-k_1 t} + e^{-Zt}(X-k_1) + e^{-Xt}(-Z+k_1))k_2}{(X-Z)(Z-k_1)(-X+k_1)} \quad (8)$$

$$RI_{aq}(t) = \frac{RI_{aq,0}(Xe^{-Xt} - Ze^{-Zt}) + RI_{g,0}(-e^{-Xt} + e^{-Zt})k_1 + RI_{aq,0}(-e^{-Xt} + e^{-Xt})k_1}{X - Z} \quad (9)$$

$$I_{aq}^-(t) = I_{aq,0}^- + \frac{RI_{aq,0}(-e^{-Xt} + e^{-Zt})k_h}{X - Z} - \frac{(-X + Z - Ze^{-Xt} + Xe^{-Zt})(RI_{g,0}k_1k_h + RI_{aq,0}k_1k_h)}{X(X - Z)Z} \quad (10)$$

$$X = \frac{\frac{1}{2}(k_1 + k_2 + k_h) - \sqrt{k_1k_2 - k_1(k_2 + k_h) + \frac{1}{4}(k_1 + k_2 + k_h)^2}}{1} \quad (11)$$

$$Z = \frac{\frac{1}{2}(k_1 + k_2 + k_h) + \sqrt{k_1k_2 - k_1(k_2 + k_h) + \frac{1}{4}(k_1 + k_2 + k_h)^2}}{1} \quad (12)$$

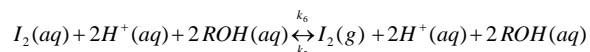
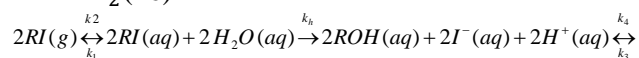
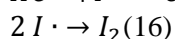
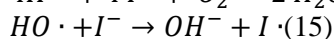
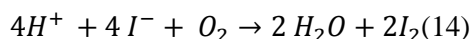
The set of differential equations Eq. (5)-(7) was transformed and solved in Laplace space. Equations (8)-(10) were obtained by transforming the solutions to real space. From the equations Eq. (8) and Eq. (9) an expression for  $t \rightarrow \infty$ ,  $K_D$  (13) could be obtained using Eq. (1).

$$K_D = \frac{2RI_{g,0}k_1 + RI_{aq,0}(k_1 - k_2 - k_h) + RI_{aq,0}\sqrt{-4k_1k_h + (k_1 + k_2 + k_h)^2}}{2RI_{aq,0}k_2 + RI_{g,0}(-k_1 + k_2 + k_h) + RI_{g,0}\sqrt{-4k_1k_h + (k_1 + k_2 + k_h)^2}} \quad (13)$$

The constants  $k_1$ ,  $k_2$  and  $k_h$  that are required to satisfy equation Eq. (13) can be obtained from the fitting of experimental data of at least one of the three iodine species involved in the model Eq. (8, 9, 10). The fitting was performed using the fit function in Wolfram Mathematica 10.1 which is using the method of least square.

### OIPHA-II

For acidic pH's (Eq. 14) and under the presence of gamma irradiation (Eq. 15-16) the formation of elemental iodine was observed, see Eq. (17), and is currently to be implemented in the model.



(17)

## III. RESULTS AND DISCUSSION

This section contains only selected data. Some of the experimental data are published in Ref. 3. The quantitative assessment of the experimental data is still in progress and will be published by the authors in 2015/16 in scientific journals.

### OIPHA-I

The studies in the FOMICAG facility revealed that organic iodides have a different fast mass transfer behaviour to the aqueous phase. The studies showed that longer chained and aromatic organic iodides persist longer in gaseous phase than shorter chained ones (Fig. 3).

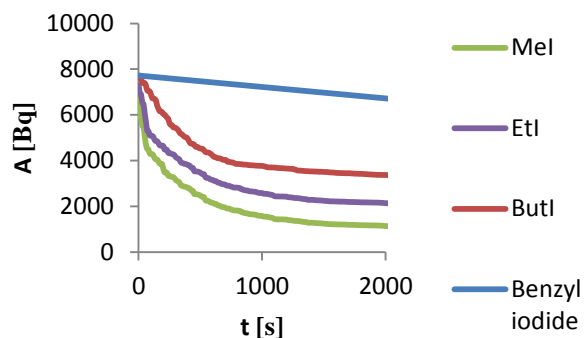


Fig.3. Partitioning behavior of organic iodides from gaseous phase (air) into aqueous phase ( $21 \pm 0.5$  °C)

The mass transfer rate increased with increasing temperature for all the studied organic iodides (Figure 4).

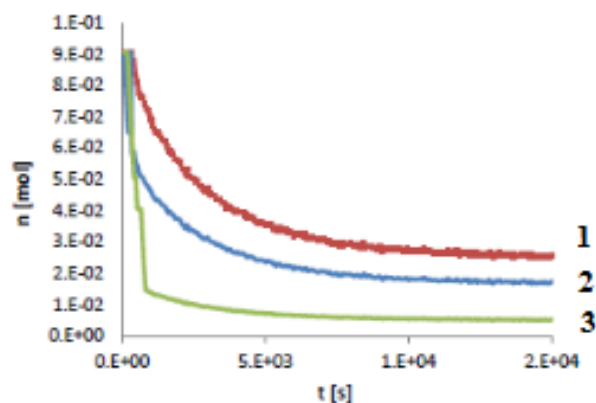


Fig. 4. Partitioning behavior of methyl iodide from gaseous phase (air) into aqueous phase 1 ( $21 \pm 0.5$  °C), 2 ( $40 \pm 0.5$  °C), 3 ( $70 \pm 0.5$  °C).

The partitioning coefficient for the organic iodides was determined in dependence of pH and temperature. Fig. 5 shows the comparison of  $K_D$  for methyl iodide determined with the OIPHA-I model in comparison to temperature dependent correlations reported in the literature [4]. For other organic iodides no such data are reported.

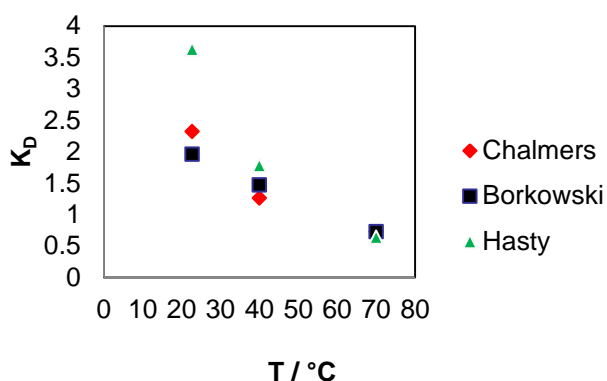


Fig. 5.  $K_D$  for MeI obtained with OIPHA-I in comparison to correlations reported in the literature [4]

### OIPHA-II

The hydrolysis studies showed that in agreement with the mass transfer between the gaseous and aqueous phase the kind of organic iodide matters. The hydrolysis of the different organic iodides was found to be not only governed by the solubility and the chain length but also by the structure of the organic molecules, the presence of chlorine impurities, as well as pH, temperature and irradiation.

In isopropyl iodide the iodine is bonded to a branched alkyl chain. Isopropyl iodide despite the fact that it is more hydrophobic than methyl iodide (and thus less soluble in water) was shown to hydrolyze more quickly in the aqueous phase than methyl iodide (Fig. 6). Branching at the carbon bearing the iodine causes a steric hindrance of the  $S_N2$  reaction [5]. This branching favors  $S_N1$  reaction which is only dependent on the isopropyl iodide concentration. Benzyl iodide was expected to hydrolyse much quicker than the other organic iodides due to the aromatic ring. However, in this case the low solubility of the aromatic iodide in the aqueous solution is the dominating factor.

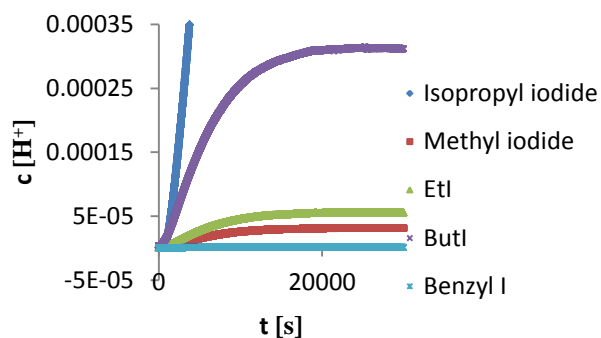


Fig. 6. Hydrolysis of organic iodides in distilled water

It can be concluded that the secondary and tertiary alkyl iodides will be much easier washed down (removed from air) by containment sprays and trapped in aqueous scrubber solutions than either primary alkyl iodides or aryl iodides.

Hydrolysis studies of ethyl iodide in salt water and distilled water showed an accelerated hydrolysis behavior of it in salt water (Fig. 7). As a pH change was observed a simple halogen exchange reaction between iodide ions bonded to the organic iodide and chloride ions in the water phase can be excluded. The high ionic strength of sea water due to the chloride ions is assumed to accelerate the hydrolysis.

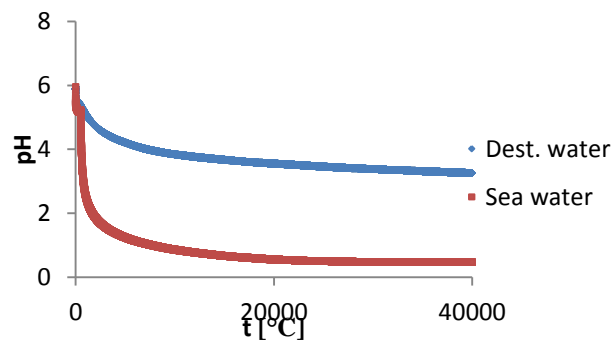


Fig. 7. Hydrolysis of EtI in sea water and distilled water (40 °C)

When gamma irradiation was present during the hydrolysis a rapid formation of elemental iodine was observed independent of the pH of the solution and the presence of chlorine.

The dissolution of the organic methyl iodide showed to be the rate controlling step and appeared therefore to increase instead to decrease (Fig. 8). As the aqueous methyl iodide (MeI(aq)) decreased it can be concluded that the conversion into inorganic iodide is a faster reaction. The

kinetics of the radiolytic oxidation of the iodide ions was found to be a faster step than the hydrolysis as the elemental iodine showed to rapidly increase whereas the iodide ion concentration remained low and nearly stable. As this was observed it was concluded that in aqueous phase the organic iodides are not directly converted into elemental iodine. It is assumed that OH<sup>•</sup> radicals which are formed in the radiolysis of water attack the organic iodide and form organic iodide radicals that decomposes into a iodine radical and an aldehyde. The aldehyde can be readily reduced to a primary alcohol, whereas the iodine radicals can recombine to form elemental iodine.

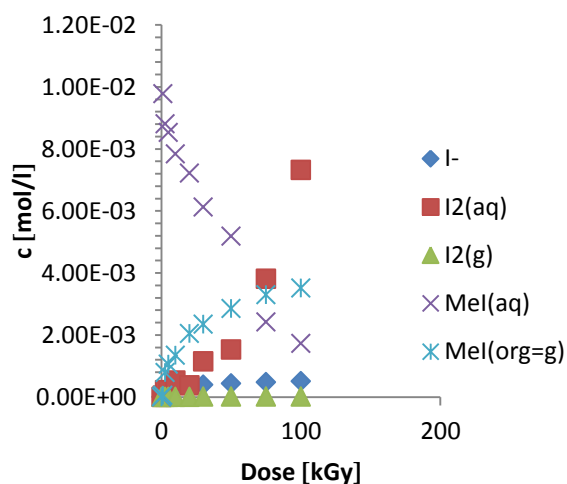
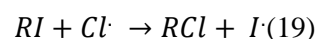
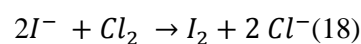


Fig. 8. Radiolysis of methyl iodide in distilled water (10<sup>-2</sup> mol/l MeI, 10 kGy/h)

The chlorine content of the water pools showed to have an additional impact on the iodine chemistry when gamma irradiation was present (Fig. 9). It is not easily possible to predict how large a chlorine release into the containment water pools will occur from chlorinated cable plastics. The majority of the chlorine release is to be expected when a total decomposition of the organic coatings of cable rich in chlorine such as PVC or CSPE's occurs and the inorganic chlorides are exposed to water. The length and

type of cable present in different containments will vary a lot as will the conditions the cables are exposed to. Salt water has been considered as worst case scenario when all water would be replaced with sea water. It was found that in the chloride rich water the conversion rate from methyl iodide into elemental iodine was increased (Fig. 9). Similar results were observed when iodide ions were the iodine source present in aqueous phase. This suggests that the radiolysis of organic iodides is altered by chloride ions. One possibility is the formation of elemental iodine by the reaction of elemental chlorine with iodide anions (Eq. 18). Another phenomenon which could cause the higher conversion of methyl iodide into elemental iodine is a halogen exchange reaction (Finkelstein reaction) of chlorine radicals with the organic iodide which will eject an iodine radical that can recombine to form elemental iodine, (Eq. 19).



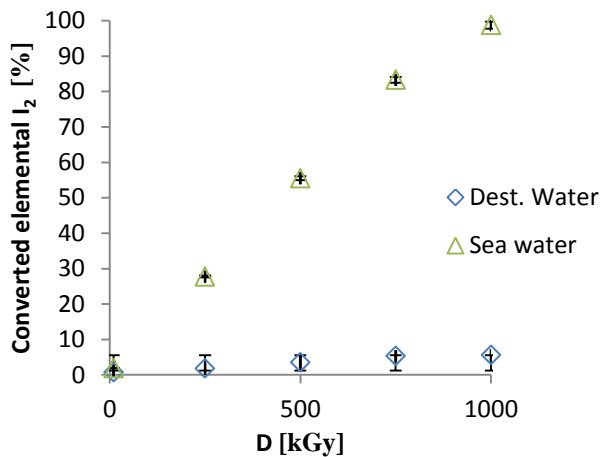


Fig. 9. Radiolysis of methyl iodide in distilled and sea water ( $10^{-2}$  mol/l MeI, 10 kGy/h, 43 °C) into elemental iodine

#### IV. FUTURE WORK

Experimental data are currently evaluated to determine the required kinetic parameters to be able to more reliably estimate the volatile iodine source term. The OIPHA-III model will discuss furthermore the effects of radiolysis in gaseous phase and the sorption behavior of iodine species on painted surfaces. The radiolysis studies in gaseous phase showed that longer chained organic iodides form a lower yield of elemental iodine than methyl iodide but an with chain length increasing yield of other organic iodides and other inorganic iodine species such as iodine oxide aerosols (Fig. 10).

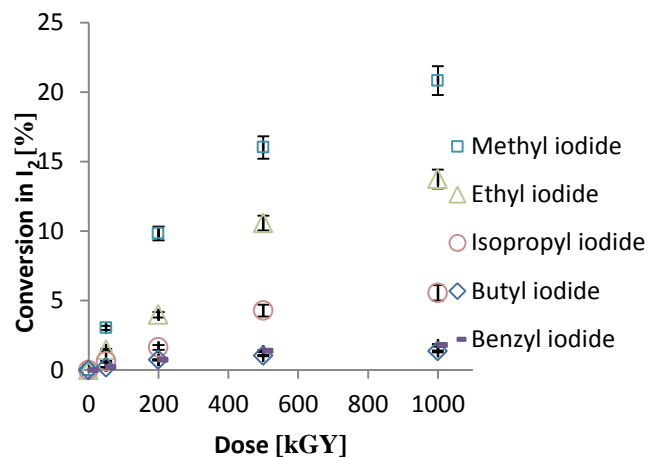


Fig. 10. Radiolytic conversion of organic iodides into elemental iodine (dose rate 10 kGy/h)

#### REFERENCES

1. H. Glänneskog, J.-O. Liljenzin, L. Sihver, G. Skarnemark, A. Ödegaard-Jensen, Interactions of  $I_2$  and  $CH_3I$  with reactive metals under BWR severe-accident conditions, *Nuclear Engineering and Design*, 227, pp. 323-329 (2004).
2. S. Tietze, M.R.StJ. Foreman, C.H. Ekberg, Synthesis of I-131 labeled iodine species relevant during severe nuclear accidents in light water reactors, *Radiochimica Acta*, 101(10), pp. 675-680 (2013).
3. S.Tietze, The chemistry of organic iodides under severe nuclear accident conditions in LWRs, Dissertation, Chalmers University of Technology (SE), ISBN 978-7597-158-2 (2015).
4. R. Borkowski, Untersuchungen zum Chemischen Verhalten des Methyliodides bei schweren Störfällen in Druckwasserreaktoren, Dissertation, KfK 3969 (1985).
5. R.T. Morrison, R.N. Boyd, *Organic Chemistry*, 5th edition, Allyn and Bacon Inc., (1987).

## THE RADIOLYSIS OF GASEOUS METHYL IODIDE IN AIR

G M N Baston(1), S R Bowskill(2), S Dickinson(3)\*, H E Sims(2)

<sup>(1)</sup>AMEC, Harwell, UK <sup>(2)</sup>National Nuclear Laboratory, Harwell, UK.

\*Corresponding author, tel: (+44)7894 598707, Email: shirley.dickinson@nnl.co.uk

**Abstract** – Organic iodides, exemplified by  $\text{CH}_3\text{I}$ , are among the most volatile forms of iodine and therefore important when considering the behaviour of radioiodine in reactor faults. In many small- and large-scale tests, low-molecular weight organic iodide has been determined to be the dominant form of gaseous iodine, particularly when measures have been taken to minimise the concentrations of volatile inorganic iodine, for example by the use of elevated pH in aqueous solutions. In order to predict the behaviour of  $\text{CH}_3\text{I}$  in PWR containment under fault conditions it is necessary to know both its formation and destruction rates.

The mechanism of  $\text{CH}_3\text{I}$  formation is uncertain, but it probably occurs on containment surfaces and in the aqueous phase. The formation rates at surfaces and in solution have been measured by a number of workers, generating extensive data for use in model development. Decomposition can occur via several mechanisms, however in a PWR containment the majority of  $\text{CH}_3\text{I}$  is expected to be found in the gaseous phase due to its low partition coefficient and the large gas to liquid volume ratio. Gas-phase radiolysis therefore needs to be considered as one of the potentially important decomposition routes.

This paper describes experimental measurements of the radiolytic destruction of  $\text{CH}_3\text{I}$  in moist air which were carried out as part of the EC 5<sup>th</sup> Framework Project on Iodine Chemistry and Mitigation Mechanisms (ICHEMM) and have not previously been published in the open literature. In the only previous reported study, the experimental conditions were limited to radiolysis in dry air and low temperature. The main objective of our work was to extend the measurements to more accident-relevant conditions of high temperature and steam atmospheres, and to study other possible sensitivities.

Experimental and analytical techniques were developed to measure radiolytic decomposition as a function of concentration of  $\text{CH}_3\text{I}$ , concentration of  $\text{O}_2$ , surface area to gas volume ratio, temperature, liquid water volume, dose-rate and surface area to gas volume ratio. Experiments were carried out with  $\text{C}_2\text{H}_5\text{I}$  to compare decomposition with  $\text{CH}_3\text{I}$ .

The decomposition rates measured in this study are of a similar magnitude to those in previously reported work conducted at very low water vapour concentrations. No significant effect of temperature was observed, but increasing the concentration of  $\text{O}_2$ , the surface area to gas volume and the water vapour concentration all decreased the decomposition rate. The decomposition showed a square-root dependence on dose-rate. The rate of decomposition of  $\text{C}_2\text{H}_5\text{I}$  is found to be similar to that of  $\text{CH}_3\text{I}$ .

Overall, no significant sensitivities have been observed and the rates measured can be applied to containment models and the prediction of organic iodide behaviour in reactor faults.

## I. INTRODUCTION

Organic iodine, in particular methyl iodide ( $\text{CH}_3\text{I}$ ), is one of the most volatile forms of iodine and so is important when considering the behaviour of radioiodine in reactor faults. In many small- and large-scale tests it has been found to be the dominant form of gaseous iodine, particularly when measures have been taken to minimise the volatile inorganic iodine concentration, for example by the use of elevated pH in aqueous solutions. The formation route of  $\text{CH}_3\text{I}$  is uncertain but is thought to occur on containment surfaces and in the aqueous phase. Its presence as the major gaseous form is probably partly associated with its lower reactivity with surfaces.

Formation rates of organic iodine have been measured from surfaces and from solution by many workers, although no widely accepted mechanism is available. There are several potential decomposition routes. In aqueous solution  $\text{CH}_3\text{I}$  can be hydrolysed by thermal reactions and/or radiolytically decomposed by reaction with the hydrated electron or hydrogen atom. However, because of its low partition coefficient and the large gas to liquid ratio in a PWR containment, the majority of  $\text{CH}_3\text{I}$  will be in the gas phase where in the presence of a relatively high dose-rate from fission product Xe and Kr, radiolysis may be an important decomposition route for  $\text{CH}_3\text{I}$ .

In the only previous reported study of the radiolytic decomposition of  $\text{CH}_3\text{I}$  in air, Tang and Castleman<sup>1</sup> measured the gas phase decomposition of  $\text{CH}_3\text{I}$  as a function of its concentration in a dry air atmosphere at room temperature. Other data from the same authors in moist air are included in a review by Postma<sup>2</sup>. Containment conditions would be rather different with temperatures of up to approximately  $100^\circ\text{C}$  and saturated steam, so it is important to ascertain the decomposition rate of  $\text{CH}_3\text{I}$  under these conditions.

This paper describes an experimental study of the radiolysis of gaseous  $\text{CH}_3\text{I}$ , conducted as a part of the EC 5<sup>th</sup> Framework project ICHEMM

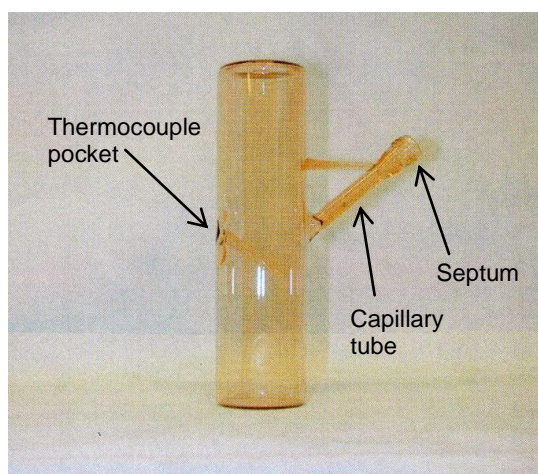
(Iodine Chemistry and Mitigation Mechanisms). In this work, the decomposition of  $\text{CH}_3\text{I}$  in moist air has been measured as a function of concentration, temperature, gas composition, moisture content and surface area to gas volume ratio in order to obtain data under a range of relevant conditions.

## II. METHODS

### *Irradiation Vessel Design*

To examine the effect of varying conditions on the radiolytic destruction of  $\text{CH}_3\text{I}$ , an irradiation vessel and sampling system were developed to give reproducible and reliable results.

The basic vessel design is shown in Fig. 8. A reusable glass irradiation cell was attached to a capillary tube. A septum on the end of the capillary tube, which was as remote as possible from the high dose-rate region of the irradiation cell, was used to inject samples of  $\text{CH}_3\text{I}$  into the



vessel and to collect samples for analysis.

Fig. 8. Vessel 2, upon which the other vessel designs are based.

Various modifications to the basic vessel design were made to allow for different vessel surface areas and volumes. In total, four designs were used in this work, see

Table III. Vessel 1 was used only for low temperature ( $\sim 30^{\circ}\text{C}$ ) experiments and did not

require a thermocouple pocket.

**TABLE III**

Irradiation Vessel Design Parameters

Design	Volume ( $\text{cm}^3$ )	Surface Area ( $\text{cm}^2$ )	S:V ratio ( $\text{cm}^{-1}$ )
Vessel 1	100	150	1.5
Vessel 2	100	150	1.5
Vessel 3	100	380	3.8
Vessel 4	650	455	0.7

#### *Radiolysis Experiments*

Vessel irradiations were performed at Harwell Laboratory using a Co-60 gamma source to measure the effects of a range of variables on the radiolysis of  $\text{CH}_3\text{I}$ :

- TABLE III)
- Dose-rate (5.5, 71, 560  $\text{Gy hr}^{-1}$ )
- Addition of  $\text{C}_2\text{H}_5\text{I}$  instead of  $\text{CH}_3\text{I}$

For experiments conducted at low temperature the temperature was uncontrolled and is estimated to be approximately  $30^{\circ}\text{C}$ .

#### *Filling the flasks*

A dilute solution of  $\text{CH}_3\text{I}$  ( $\sim 0.01 \text{ mol dm}^{-3}$ ) was prepared by dissolution in  $\text{H}_2\text{O}$ . The irradiation vessel was heated if required, and when at the correct temperature, was sealed with the septum. If an oxygen atmosphere was required, the vessel was flushed with the gas, using two hypodermic needles as inlet and outlet, inserted through the septum. A  $5 \mu\text{l}$  or  $500 \mu\text{l}$  volume of  $\text{CH}_3\text{I}$  solution was injected into the vessel, which was then placed into the irradiation chamber. Samples were removed periodically using a gas syringe and analysed by gas chromatography. A few tests were done without irradiation to determine the

- Initial  $\text{CH}_3\text{I}$  concentration ( $6 \times 10^{-7}$  to  $3 \times 10^{-9} \text{ mol dm}^{-3}$ )
- Liquid water injected ( $5 \mu\text{l}$  and  $500 \mu\text{l}$ )
- Temperature ( $\sim 30^{\circ}\text{C}$  and  $80^{\circ}\text{C}$ )
- Atmosphere (air,  $\text{O}_2$ , 1%  $\text{O}_2$  in  $\text{N}_2$ ,  $\text{N}_2$  and  $\text{N}_2\text{O}$ )
- Vessel surface area and volume (rate of thermal decomposition or leakage from the vessel).

For tests conducted under “dry” conditions the irradiation vessels were dried overnight at  $80^{\circ}\text{C}$  and then fitted with the septum. The irradiation vessels were then purged via syringe needles inserted through the septa with air that was dried by flowing through a tube filled with silica gel. In order to inject a relatively dry sample of  $\text{CH}_3\text{I}$ , liquid  $\text{CH}_3\text{I}$  was equilibrated with the gas volume in a glass vial with a septum and an aliquot of gas withdrawn into a syringe. This gas sample was diluted in a similar manner before  $100 \mu\text{l}$  was added to the irradiation vessel.

#### *SAMPLE ADDITION AND ANALYSIS*

The  $\text{CH}_3\text{I}$  concentration was measured by injecting a  $100 \mu\text{l}$  sample of  $\text{CH}_3\text{I}$ /air into the gas chromatograph. The GC used was a Pye Unicam model 4550 with a SGE BP5-1.0 column and an electron capture detector.

#### *Surface sorption experiments*

A single experiment was set up to measure the amount of iodine deposited onto the vessel walls after decomposition of  $\text{CH}_3\text{I}$ . 50  $\mu\text{l}$  of methyl iodide solution was injected into the glass vessel, to give  $1.6 \times 10^{-7}$  mol  $\text{dm}^{-3}$  methyl iodide in air. The vessel was irradiated for 2.5 hours at  $\sim 30^\circ\text{C}$  at a dose rate of  $496 \text{ kGy hr}^{-1}$ , by which time the concentration of methyl iodide had fallen to 51% of its original value. The vessel was then flushed with nitrogen and the outlet gas passed through a solution of  $10^{-3}$  molar NaOH, and the outlet pipe was rinsed with  $10^{-3}$  molar NaOH into the trap solution. A sample of the gas from the vessel was then analysed to ensure that all oxygen and methyl iodide had been removed, before washing the walls of the irradiation vessel with  $10^{-3}$  molar sodium hydroxide. The two sodium hydroxide solutions (purge gas trap and wall wash), plus a blank solution, were analysed for iodine by ICP-MS.

#### *Dosimetry*

Dosimetry was by the Fricke method<sup>3</sup>. Correction was made to the doses to allow for the slightly lower electron density of the gas compared with that of liquid water.

### **III. Results and discussion**

The change in methyl iodide,  $\text{CH}_3\text{I}$ , concentration during  $\gamma$  irradiation has been measured for a wide range of conditions, generating data that can be applied to the behaviour of volatile iodine in reactor containments. In all of the tests, with the exception of those conducted in a nitrogen atmosphere, the concentration of  $\text{CH}_3\text{I}$  decreased exponentially with increasing dose according to the decay equation:

$$C = C_0 e^{-kD} \quad (1)$$

where  $C$  and  $C_0$  are the concentration of  $\text{CH}_3\text{I}$  at a absorbed dose ( $D$ ) and at zero dose respectively.

For each experiment, the decomposition rate constant,  $k$ , has been calculated. The experimental rate constants from tests conducted under an air atmosphere are summarised in

Fig. 9. Control tests without gamma irradiation showed no evidence of thermal decomposition or leakage of methyl iodide from the vessels.

In the following sections data are normalized to the percentage of  $\text{CH}_3\text{I}$  remaining and plotted on semilogarithmic coordinates as a function of total dose (Gy) absorbed by the atmosphere unless otherwise stated.

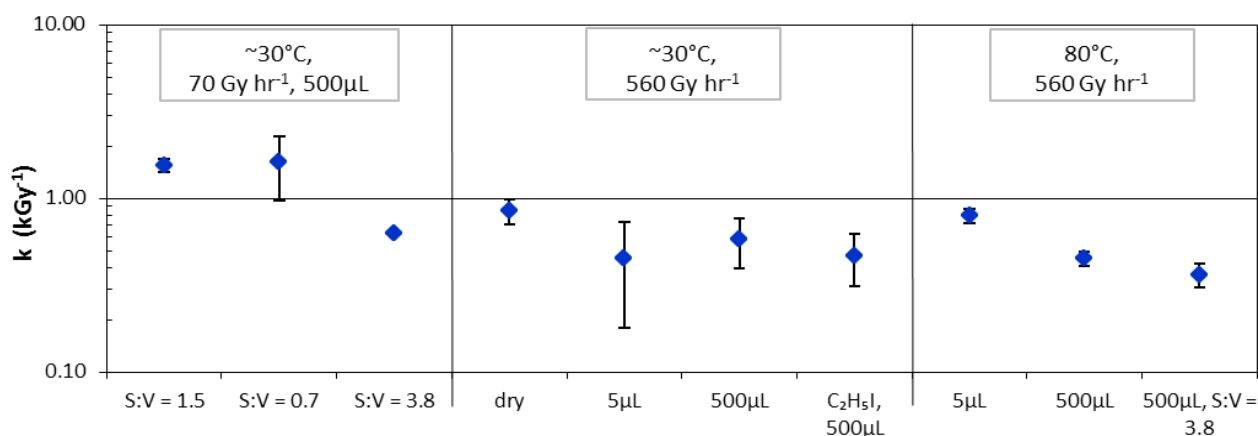


Fig. 9. Summary of the decomposition rate constants of methyl iodide,  $k$ , for experiments conducted in an air atmosphere under a range of conditions. The irradiation conditions altered are temperature ( $^{\circ}\text{C}$ ), dose rate ( $\text{kGy hr}^{-1}$ ), water added to the system ( $\mu\text{l}$ ) and surface area to volume ratio (S:V). One set of experiments was conducted with ethyl iodide ( $\text{C}_2\text{H}_5\text{I}$ ) instead of  $\text{CH}_3\text{I}$ . Error bars give one standard deviation between replicates.

#### *Effect of liquid water at $\sim 30^{\circ}\text{C}$*

Experiments were conducted in an air atmosphere, and 5  $\mu\text{l}$  or 500  $\mu\text{l}$  of water was introduced with the injected  $\text{CH}_3\text{I}$  to examine the effects of water on radiolysis. The saturation pressure of water at  $\sim 30^{\circ}\text{C}$  is 4.2 kPa which equates to about 3 mg of water in 100 ml. Therefore a small amount of liquid water would have been present even in the tests with 5  $\mu\text{l}$  injected. There was a large degree of scatter on results from duplicate experiments, although the individual data points for each experiment generally lie close to an exponential trend-line (Fig. 3). The mean decomposition rates in the tests with 5 and 500  $\mu\text{l}$  water were 0.45 and 0.58  $\text{kGy}^{-1}$  respectively, with relative standard deviations of 60% and 30%. Within the uncertainties, therefore, no effect of liquid water can be determined at  $\sim 30^{\circ}\text{C}$ .

Two experiments were conducted under “dry” conditions. These gave decomposition rates of approximately 0.85  $\text{kGy}^{-1}$ , at the upper end of those measured in the presence of liquid water. However, in view of the large scatter in the data it is difficult to conclude on whether the difference is significant; it is clear, however, that

there is not a large effect of the addition of water to the system.

It can be seen from the exponential trend line plotted in Fig. 3 that the results of these tests agree reasonably well with those of Tang and Castleman<sup>2</sup>. In the current work, the water concentration at  $\sim 30^{\circ}\text{C}$  is  $\sim 10^{-3}$  moles  $\text{dm}^{-3}$ , a factor of ca. 5 more than the maximum used by Tang and Castleman for decomposition of  $\text{CH}_3\text{I}$  in air containing water vapour. They observed a factor of 2-3 decrease in decomposition rate when the  $\text{H}_2\text{O}$  concentration was decreased from  $2.1 \times 10^{-4}$  moles  $\text{dm}^{-3}$  to  $3.7 \times 10^{-7}$  moles  $\text{dm}^{-3}$ . However their result at the lowest water vapour concentration is not consistent with their data for dry  $\text{CH}_3\text{I}$ , which gave a higher rate of decomposition than with water addition.

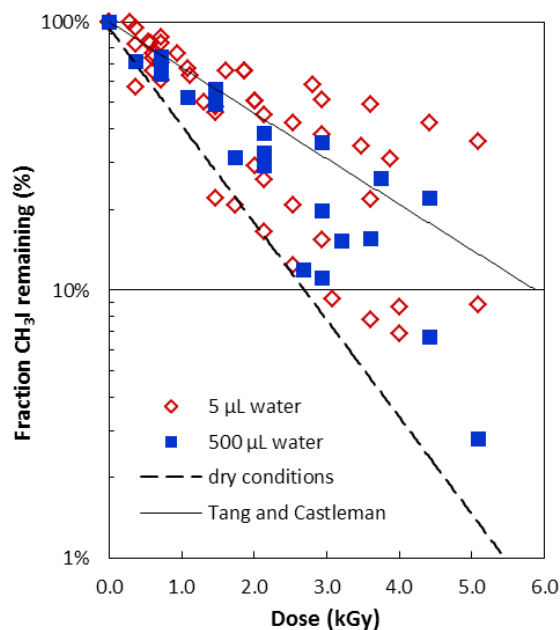


Fig. 10. The decomposition of  $\text{CH}_3\text{I}$  during  $\gamma$  irradiation in air at  $\sim 30^\circ\text{C}$  with the addition of  $5\ \mu\text{L}$  ( $\diamond$ ) or  $500\ \mu\text{L}$  of water, ( $\blacksquare$ ). The average rate of methyl iodide decomposition under 'dry' conditions is plotted as a solid line. The average rate of change seen in the Tang and Castleman experiments in moist air<sup>1</sup> is plotted as a dotted line

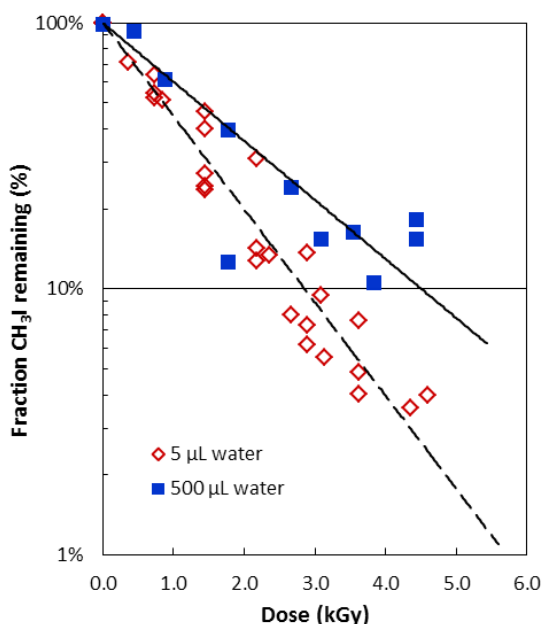


Fig. 11. The decomposition of  $\text{CH}_3\text{I}$  during  $\gamma$  irradiation in air at  $80^\circ\text{C}$  with the addition of  $5\ \mu\text{L}$  ( $\diamond$ ) or  $500\ \mu\text{L}$  ( $\blacksquare$ ) of water. The trend lines show the average decomposition rate for the two experimental conditions.

#### *Effect of liquid water at $80^\circ\text{C}$*

The effect of liquid water at higher temperature is shown in Fig. 4. The saturated vapour pressure of water at  $80^\circ\text{C}$  is about 47 kPa, corresponding to a steam concentration of  $1.6 \times 10^{-2}\ \text{mol dm}^{-3}$ , so in the  $500\ \mu\text{L}$  tests about 30 mg of water would have vaporised in the  $100\ \text{cm}^3$  vessel. In the  $5\ \mu\text{L}$  tests, all the water would have evaporated giving a steam concentration of  $\sim 3 \times 10^{-3}\ \text{mol dm}^{-3}$ .

The results indicate that the decomposition rate with  $500\ \mu\text{L}$  of water in the vessel was about 50% lower than with  $5\ \mu\text{L}$  ( $0.45$  compared with  $0.79\ \text{kGy}^{-1}$ ). The tests with the higher water volume gave similar decomposition rates to those measured at  $\sim 30^\circ\text{C}$ , supporting the observation made in the previous section that the presence of liquid water may have more effect than the temperature. However, it can again be seen that the effect is quite small.

#### *Effect of temperature*

All experiments were conducted at either  $\sim 30$  or  $80^\circ\text{C}$ . The decomposition rate at  $80^\circ\text{C}$  with  $5\ \mu\text{L}$  water initially added was  $0.79\ \text{kGy}^{-1}$ , about twice as high as in comparable tests at  $\sim 30^\circ\text{C}$ . Reproducibility was much better in the higher-temperature tests; the relative standard deviation was less than 10% even though the initial concentrations of  $\text{CH}_3\text{I}$  ranged from  $10^{-8}$  to  $5 \times 10^{-7}\ \text{mol dm}^{-3}$ .

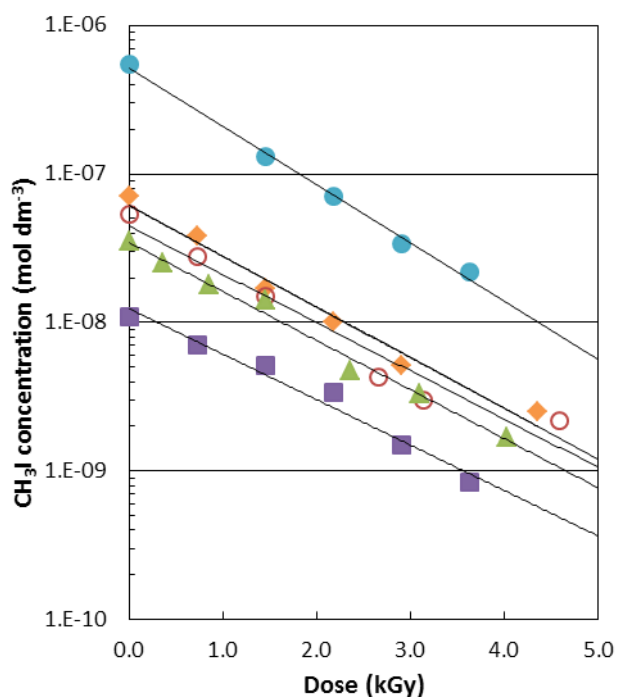


Fig. 12. The decomposition of  $\text{CH}_3\text{I}$  during  $\gamma$  irradiation in air at  $80^\circ\text{C}$  with the addition of  $5\ \mu\text{l}$  water from different starting concentrations. Exponential trend lines are fitted to each individual experiment.  $\text{CH}_3\text{I}$  remaining is given in  $\text{mol}\cdot\text{dm}^{-3}$ .

It should be noted that in these  $80^\circ\text{C}$  tests, all the injected water would have evaporated. It is therefore difficult to conclude whether the apparent rate increase is due to the higher temperature or the lack of liquid water, since the rate at  $80^\circ\text{C}$  is close to the “dry” rate measured at  $\sim 30^\circ\text{C}$ . However, it is clear that the decomposition rate is not strongly temperature dependent.

Unfortunately it is not possible to study some effects independently in this system, for example increasing the temperature increases the water vapour concentration because  $\text{CH}_3\text{I}$  is injected as aqueous solution as discussed. Similarly, at  $80^\circ\text{C}$ , introducing liquid water also increased the water vapour concentration.

#### *Effect of initial methyl iodide concentration*

The effect of the initial  $\text{CH}_3\text{I}$  concentration on radiolysis was studied at  $80^\circ\text{C}$  as the results were more reproducible at this temperature (Fig. 5). The decomposition was first order over the range

studied ( $10^{-8}$  to  $6\times 10^{-7}$   $\text{mol}\ \text{dm}^{-3}$   $\text{CH}_3\text{I}$ ). There may be a slight trend towards a faster rate at higher initial concentration, but this result is not significant within the uncertainties. In their work in dry conditions, Tang and Castleman<sup>2</sup> found no effect of initial  $\text{CH}_3\text{I}$  concentration at levels studied in the current work.

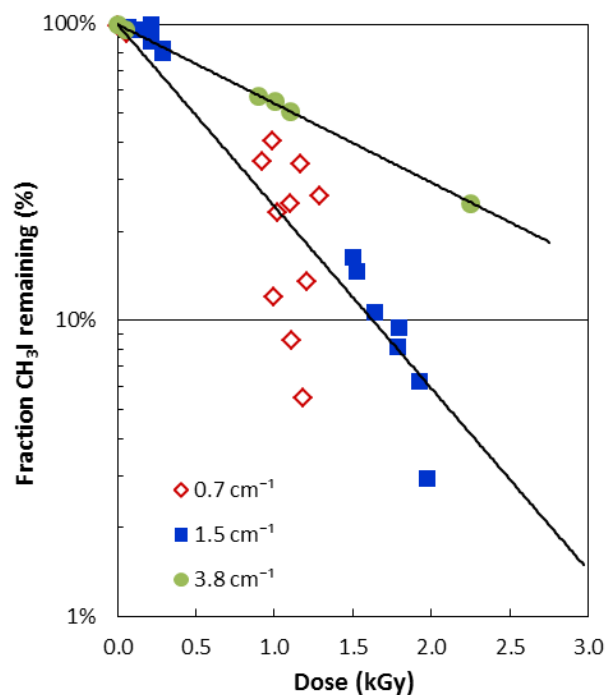


Fig. 13. The decomposition of  $\text{CH}_3\text{I}$  during  $\gamma$  irradiation in air at  $80^\circ\text{C}$  with the addition of  $5\ \mu\text{l}$  water in vessels of varying surface area to volume ratios ( $\text{cm}^{-1}$ ). Trend lines are fitted to the data from vessels S/V of  $1.5\ \text{cm}^{-1}$  and  $3.8\ \text{cm}^{-1}$ .

#### *Effect of surface area to volume ratio*

Two experiments were carried out using a vessel with increased surface area at  $80^\circ\text{C}$  (Vessel 3, Table I). In Fig. 6 these results are compared with those of the standard vessel (Vessel 2, Table I) under the same conditions. Increasing the surface area of the glass vessel by a factor of 2.5 reduced the decomposition rate by about half.

It was not possible to decrease the surface area to volume (S/V) ratio in the high dose-rate position of the irradiation facility, so experiments with larger volume vessels were carried out in the lower dose position where more space was available. For these experiments the vessel used previously for high dose-rates was used along

with a larger volume vessel (Vessel 4, Table I). At the lowest S/V ratio the decomposition rates are, on average, the same as those for the intermediate S/V ratio although there is considerable scatter in the results. At the highest S/V ratio there is again a decrease in the decomposition rate by about a factor of 3 (see Fig. 6).

The effect of increasing surface area was to decrease decomposition at both high and low dose-rates, indicating losses of reactants at surfaces. Surfaces have been found to be important in other gas phase studies particularly involving measurements of radiolysis products from water vapour.

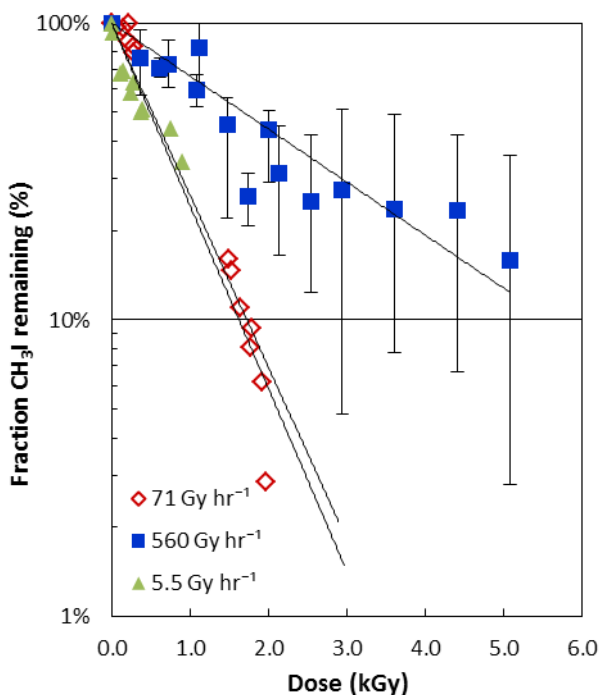


Fig. 14. The decomposition of  $\text{CH}_3\text{I}$  during  $\gamma$  irradiation, at a high, low or very low dose rate, in air at  $\sim 30^\circ\text{C}$ . The high dose rate ( $560 \text{ kGy hr}^{-1}$ ) data is averaged over various adsorbed dose points. Error bars give the range of the results to demonstrate the large amount of scatter. Exponential trend lines are fitted to each experimental condition.

The presence of liquid water appears to have a similar effect to that of increasing the surface area, and this may be associated with dissolution of reactants.

### Effect of Dose-rate

The effect of reducing the dose-rate is shown in Fig. 7. Results show that reducing the dose-rate by a factor of 8 (from  $560$  to  $71 \text{ Gy hr}^{-1}$ ) only decreases the decomposition rate (expressed as a function of time) by a factor of approximately 3. In terms of dose, therefore, the decomposition rate increased from  $0.58$  to  $1.54 \text{ kGy}^{-1}$  when the dose rate was decreased from  $560$  to  $71 \text{ Gy hr}^{-1}$ .

Such dose-rate effects are often observed in radiation chemical systems as a result of second order reactions. Decreasing the dose rate decreases the concentrations of radical species, making them more likely to encounter other reactants (e.g.,  $\text{CH}_3\text{I}$ ) than each other.

Decreasing the dose rate again to  $5.5 \text{ Gy hr}^{-1}$  gave no further change in the rate of decomposition. It appears that there is a change in the dose dependency of decomposition at very low doses, which cannot be satisfactorily explained.

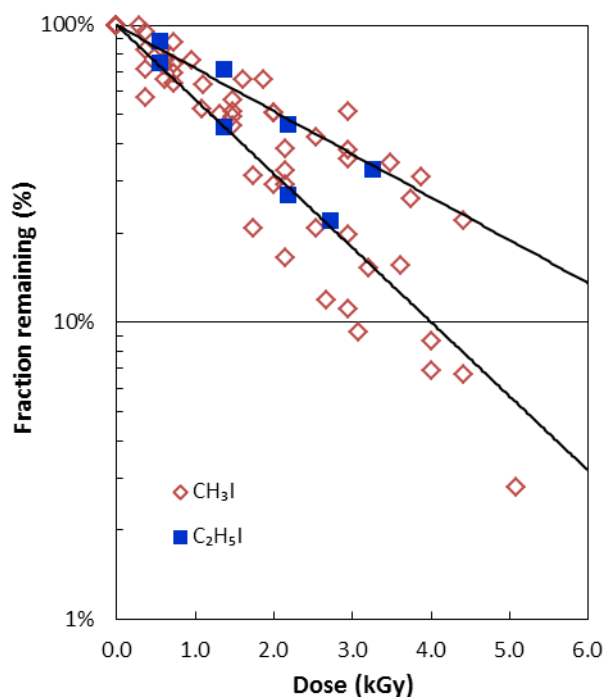


Fig. 15. The decomposition of  $\text{C}_2\text{H}_5\text{I}$  (■) compared with decomposition of  $\text{CH}_3\text{I}$  (◇) during  $\gamma$  irradiation in air at  $\sim 30^\circ\text{C}$ . Trend lines are fitted to the data from  $\text{C}_2\text{H}_5\text{I}$  decompositions.

### Decomposition of C<sub>2</sub>H<sub>5</sub>I

All work described so far has been carried out with CH<sub>3</sub>I, however, the reactions of I with organic materials found in containment could produce a range of volatile organic iodides, such as C<sub>2</sub>H<sub>5</sub>I. Two tests therefore were carried out to establish whether the decomposition rate of C<sub>2</sub>H<sub>5</sub>I was significantly different to that of CH<sub>3</sub>I. Fig. 8 shows that the decomposition of C<sub>2</sub>H<sub>5</sub>I is within the experimental scatter of the CH<sub>3</sub>I results. This suggests that the decomposition mechanisms are similar in both cases and are probably similar for all aliphatic organic iodides.

### Post irradiation reactions

To examine and detect any post-irradiation reactions, a sample of CH<sub>3</sub>I was irradiated for 3.5 hours; irradiation was then stopped and the CH<sub>3</sub>I concentration was repeatedly sampled. After the 3.5 hours of irradiation, only ~10% of the initial CH<sub>3</sub>I remained. No further decrease was observed suggesting that no post-irradiation reactions occurred (Fig.9). This indicates that stable air radiolysis products such as HNO<sub>3</sub>, HNO<sub>2</sub>, NO<sub>x</sub> and O<sub>3</sub> do not react significantly with CH<sub>3</sub>I in the quantities produced at this dose.

The absence of any post-irradiation reactions is contrary to a note in the paper by Tang and Castleman<sup>2</sup>. In this work the residual CH<sub>3</sub>I concentration was quite low which could be an important factor as could the relative dose-rate. The dose-rate used by Tang was probably a factor of 10 greater than that used in this work.

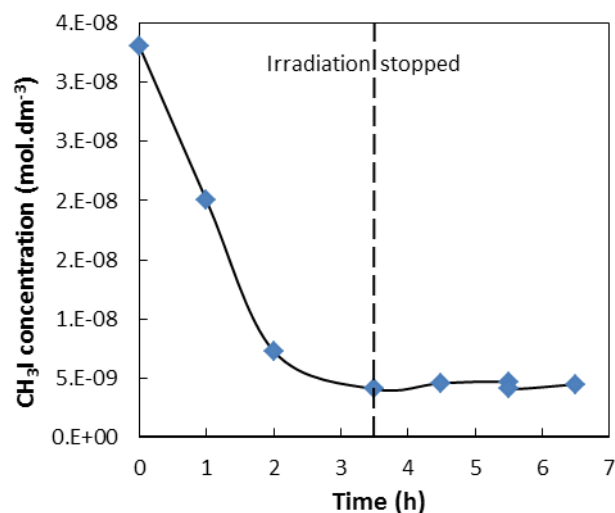


Fig. 16. The decomposition of CH<sub>3</sub>I during  $\gamma$  irradiation at a dose rate of 560 Gy hr<sup>-1</sup> in air at ~30°C with the addition of 5  $\mu$ l water before irradiation was stopped at 3.5 hours.

### Different Atmospheres

A number of experiments were conducted under atmospheres other than air to give information on possible reaction mechanisms of CH<sub>3</sub>I decomposition and to obtain data relevant to inerted atmospheres used in some reactor containments. The decomposition rate constants for these experiments are summarised in Fig. 10.

### Effect of pure oxygen atmosphere

With experiments at 20°C, there was difficulty obtaining reproducible results and no difference between results in air and oxygen atmospheres could be seen. The average rate constant was 0.86 kGy<sup>-1</sup> compared with 0.45 kGy<sup>-1</sup> for comparable tests in air, but again, the relative standard deviation was high (~40%). At 80°C the reproducibility of results was better (Fig. 11) and the mean decomposition rate was 0.58 kGy<sup>-1</sup> compared with 0.79 kGy<sup>-1</sup> for the same conditions in air.

### Effect of N<sub>2</sub>O

One of the main initiating reactions for CH<sub>3</sub>I decomposition is thought to involve the electron:



In two experiments  $N_2O$  was used on the basis that it also undergoes dissociative electron capture and may compete with  $CH_3I$  for  $e^-$  and help confirm the mechanism.

However, this was not entirely successful since the rate constant of  $N_2O$  with  $e^-$  is not sufficiently high to compete effectively. Also, the radiation chemistry of  $N_2O$  is very different to  $N_2/O_2$  so comparing the decomposition behaviour in the two gases is not straightforward. The decomposition rate constant did decrease, the average value for two experiments was  $0.56 \text{ kGy}^{-1}$  compared with dry air where  $k_{\text{ave}} = 0.85 \text{ kGy}^{-1}$  (see Fig. 10).

moist 1%  $O_2$  was even faster with  $k_{\text{ave}} = 8.30 \text{ kGy}^{-1}$ . Results are shown in Fig. 11.

The increase in  $CH_3I$  decomposition rate with decreasing  $O_2$  is consistent with a mechanism in which the main reactant for  $CH_3I$  is the electron. Competition between  $O_2$  and  $CH_3I$  for  $e^-$  would result in the observed behaviour.

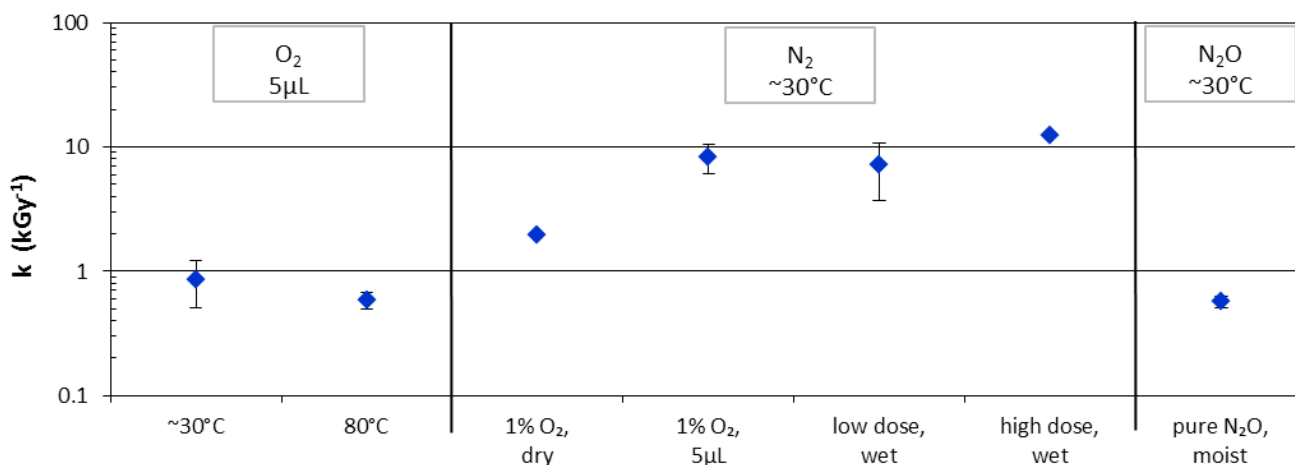


Fig. 17. Summary of the decomposition rate constants of methyl iodide,  $k$ , for experiments conducted in  $O_2$ ,  $N_2O$ , 1%  $O_2$  in  $N_2$  &  $N_2$  atmospheres in a range of conditions. The irradiation conditions altered are temperature ( $^\circ\text{C}$ ), dose rate (high or low) and water added to the system (dry or moist conditions). Error bars give one standard deviation

#### Effect of 1% $O_2$

There were two reasons for measuring the effect of low  $O_2$  concentrations: (i) BWR reactor containments operate with a nitrogen inerted atmosphere which by definition is low in  $O_2$  and (ii) to provide further information to help understand the decomposition mechanisms

The decomposition rate constant,  $k$ , for a dry 1%  $O_2$  atmosphere was  $1.9 \text{ kGy}^{-1}$ . Decomposition in

#### Effect of pure $N_2$

Tests in pure  $N_2$  completed the range of  $O_2/N_2$  atmosphere experiments. The decomposition rate was too fast to measure accurately at the high dose-rate and rather scattered and non-exponential at the low dose-rate. The calculated rate constants are included in Fig. 10 for completeness. At the low dose-rate one

experiment gave a decomposition rate constant of  $7.20 \text{ kGy}^{-1}$ , consistent with the lack of competition for  $e^-$ .

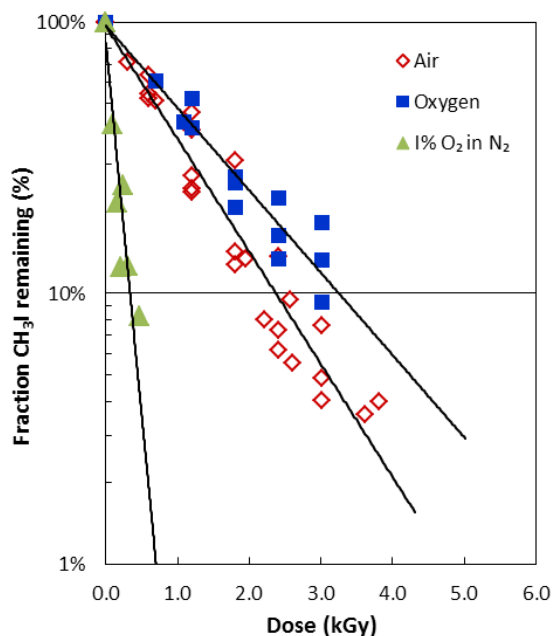


Fig. 11. The decomposition of  $\text{CH}_3\text{I}$  during  $\gamma$  irradiation in air at  $80^\circ\text{C}$  with an oxygen (■), air (◇) or 1%  $\text{O}_2$  in  $\text{N}_2$  (▲) atmosphere. Trend lines are fitted to each data set.

One reason for the scatter could be residual  $\text{O}_2$  in the sample although the GC measurement suggests this was not large.

#### *Deposition of iodine onto surfaces after decomposition of $\text{CH}_3\text{I}$*

As noted above, a single test was carried out to determine the fate of iodine after radiolytic decomposition of methyl iodide gas and the iodine distribution after irradiation was calculated. After irradiation 51% of the iodine remained as  $\text{CH}_3\text{I}$ , but only 19% found on the vessel walls. No iodine (<1%) was measured in the NaOH trap, on the purge line from the vessel. Although there is uncertainty in accounting for the 30% of iodine not recovered, it is thought most likely to be due to experimental errors and/or losses during the experiment, rather than the iodine being in a gaseous form that was not trapped by the sodium hydroxide.

#### *Experimental Scatter*

In this work there was considerable scatter as mentioned several times above. Tang and Castleman<sup>1</sup> reported data which appear to vary by  $\pm 20\%$ . In the text they noted that in low concentration experiments the impurity level often interfered with the radiolytic decomposition of  $\text{CH}_3\text{I}$ . In this work described here, no particularly stringent measures were taken to exclude impurities; glassware was washed with pure water but not annealed at  $500^\circ\text{C}$  and vacuum degassed as carried out in the work of Tang and Castleman<sup>2</sup>. It seems likely that surface or airborne impurities are responsible for the scatter. This scatter has restricted the amount of mechanistic information that is possible to derive from the results but does suggest that they are rather more applicable to reactor containment.

#### IV. CONCLUSION

The radiolytic decomposition of  $\text{CH}_3\text{I}$  has been measured as a function of concentration of  $\text{CH}_3\text{I}$ , concentration of  $\text{O}_2$ , surface area to gas volume ratio, temperature, liquid water volume, dose-rate and surface area to gas volume ratio.

Experiments have also been carried out with  $\text{C}_2\text{H}_5\text{I}$  to compare with  $\text{CH}_3\text{I}$ .

The decomposition rates measured here are of a similar magnitude to those in the only previously reported work at very low water vapour concentrations. There is no significant effect of temperature, but increasing the concentration of  $\text{O}_2$ , the surface area to gas volume and the water vapour concentration all decrease the decomposition rate. The decomposition showed a square-root dependence on dose-rate. The rate of decomposition of  $\text{C}_2\text{H}_5\text{I}$  is similar to that of  $\text{CH}_3\text{I}$ . Overall, no significant sensitivities have been observed and rates measured here can be applied to containment situations.

The results of these experiments have been used to develop a mechanistic model of  $\text{CH}_3\text{I}$  decomposition and this is described in a separate paper [4].

### ACKNOWLEDGMENTS

This work was originally conducted as part of the 5<sup>th</sup> Framework ICHEMM project, which was jointly financed by the European Commission.

### NOMENCLATURE

D = absorbed dose

GC = Gas Chromatograph

ICHEMM = Iodine Chemistry and Mitigation Mechanisms

ICP-MS = Inductively Coupled Plasma Mass Spectrometry

PWR = Pressurised Water Reactor

S:V = Surface Area to Volume Ratio

### REFERENCES

1. I. N. Tang and A. W. Castleman, "Kinetics of  $\gamma$ -Induced Decomposition of Methyl

Iodide in Air," *Journal of Physical Chemistry*, 74, 22, 3933-3939, (1970).

2. I. N. Tang and A. W. Castleman BNL-12854, Figure given and referenced in A. K. Postma and R. W. Zavadoski, WASH-1233, 1972, but does not appear in the accessed copy of BNL-12854.
3. Standard Test Method for Absorbed Gamma Radiation Dose in the Fricke Dosimeter. American Society of Testing and Materials, Designation: D 1671 – 72, 682-685 (1972).
4. S. Dickinson, S. Bowskill, H. E. Sims, "The IODAIR model for radiolysis of gaseous iodine species in air: data comparisons and predictions", This conference, Paper 3.4.

## THE IODAIR MODEL FOR RADIOLYSIS OF GASEOUS IODINE SPECIES IN AIR: DATA COMPARISONS AND PREDICTIONS

*S Dickinson\*, S Bowskill, H E Sims*

<sup>(1)</sup> *National Nuclear Laboratory, Harwell, Didcot, Oxon, OX11 0QT, UK*

*\*Corresponding author, tel: (+44) 7894 598707, Email: shirley.dickinson@nnl.co.uk*

**Abstract** – *This paper describes the mechanistic IODAIR model which was developed to predict and interpret the behaviour of gaseous iodine species in irradiated moist air. The model predictions are compared with experimental measurements of I<sub>2</sub> radiolysis, including the PARIS tests, and with data from experimental studies of CH<sub>3</sub>I radiolysis carried out at Harwell as well as later measurements from the OECD Behaviour of Iodine Programme (BIP). The Harwell experiments on CH<sub>3</sub>I radiolysis are described in a companion paper.*

*The model predicts that the radiolytic destruction of both I<sub>2</sub> and CH<sub>3</sub>I results in the formation of various intermediate gaseous species, the most abundant being HI and IONO<sub>2</sub> under the conditions of the experiments modelled. Formation of the final solid oxide products occurs via reactions involving the minor intermediate species IO, I<sub>2</sub>O<sub>2</sub> and IO<sub>2</sub>, and there is considerable uncertainty in some of the rates and mechanisms of these reactions. The model gives good agreement with experimental measurements of gaseous I<sub>2</sub> decomposition during irradiation at relatively high starting concentrations. However, at lower concentrations the extent of decomposition is overestimated, and it is possible that back-reactions are important.*

*The model also gives good agreement with measurements of the radiolytic destruction of CH<sub>3</sub>I in air, and reproduces the observed increase in rate at low O<sub>2</sub> concentrations. Mechanisms are proposed to account for the experimentally-observed dose rate dependence, which changes from linear at  $\geq 500$  Gy hr<sup>-1</sup> to a square-root dependence at lower dose rates, and for the effect of humidity.*

*Model calculations to investigate the potential importance of CH<sub>3</sub>I formation by homogeneous gas-phase reactions of I<sub>2</sub> and CH<sub>4</sub> are also presented.*

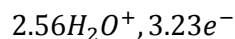
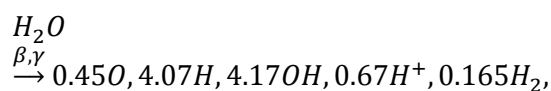
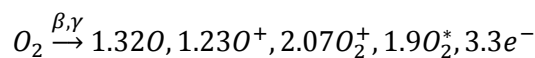
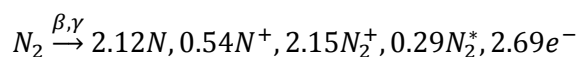
## I. INTRODUCTION

Iodine has a complex chemistry which determines its chemical form and, consequently, its volatility in the containment. In reducing conditions, iodine would be released from the fuel predominantly as CsI or other metal iodides, which are involatile at containment temperatures and would normally dissolve in blowdown or reflood water. Radiolytic oxidation is the main mechanism for oxidation of iodide in solution to volatile forms such as I<sub>2</sub>. I<sub>2</sub> can react with surfaces in the containment, leading to its retention but also to the potential formation of volatile organic forms [1]. Once these species are released into the containment atmosphere they will be subject to radiolytic reactions which result in the conversion of the gaseous species into involatile iodine oxides, which may deposit on surfaces or re-dissolve in water pools. The concentrations of volatile species in the atmosphere will therefore be determined by the balance between their formation and destruction reactions.

The current paper describes the mechanistic IODAIR model which was developed to predict and interpret the behaviour of gaseous iodine species in irradiated moist air. The model predictions are compared with experimental measurements of I<sub>2</sub> radiolysis, and with data from experimental studies of CH<sub>3</sub>I radiolysis carried out at Harwell [2] as well as later measurements from the OECD Behaviour of Iodine Programme (BIP) [3].

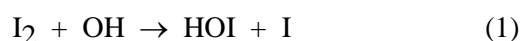
## II. DESCRIPTION OF THE IODAIR MODEL

Kinetic models of the chemistry of iodine species in moist air in a radiation field have been assembled by Sagert [4] and Aubert [5], and there are many similarities with the model presented here. The basis of these models is a set of reactions describing the production and interaction of ionic and radical species produced by the irradiation of N<sub>2</sub>, O<sub>2</sub> and H<sub>2</sub>O gases. The interaction of radiation with the molecular species produces ions, electrons and excited radical species. In the H<sub>2</sub>O-air system, the primary reactions are:

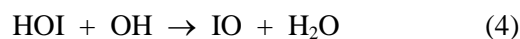


The figures given above are the G-values for production of the species in units of molec./100eV absorbed by the appropriate gaseous component, taken from Busi et al. [6]. The interactions of these primary products result in the accumulation of ozone, HNO<sub>2</sub>, HNO<sub>3</sub> and smaller amounts of N<sub>2</sub>O. Other N-O and O-H species are also predicted to be formed with low, constant concentrations. Experimental measurements of the major products can be used to validate the predictions of mechanistic models of air radiolysis; however, it is debatable how much of an insight such measurements can give into the rate of oxidation of gaseous iodine species if the dominant reactions mainly involve short-lived intermediate species rather than the stable products.

Reactions of gaseous iodine species were added to an air/steam radiolysis model to produce the IODAIR model, which was used to simulate the experiments discussed in Section III. These calculations showed that I<sub>2</sub> reacts initially with OH, O and H radicals to form intermediate species:



HOI and HI are oxidised by OH:



HOI and I can also form the intermediate INO<sub>2</sub>



which re-forms I<sub>2</sub>:



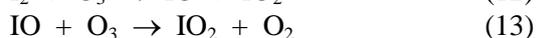
IO reacts with NO:



and reversibly with  $\text{NO}_2$  to form an  $\text{IONO}_2$  intermediate



The above reactions would result in the almost complete conversion of  $\text{I}_2$  to  $\text{IONO}_2$ . Iodine oxides (such as  $\text{I}_2\text{O}_5$  or  $\text{I}_4\text{O}_9$ ) are produced by a relatively minor route involving  $\text{IO}_2$ , which is produced by the reactions of  $\text{I}_2$  and IO with  $\text{O}_3$ :



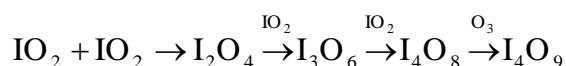
However, the reaction rate for  $\text{IO} + \text{O}_3$  given by Larin et al. [7] is quite low and IODAIR predicts that the main pathway is as proposed by Bloss et al. [8]:



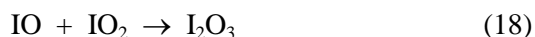
There are two possible isomers of the  $\text{I}_2\text{O}_2$  intermediate, with different decomposition routes:



$\text{IO}_2$  is assumed to dimerise to  $\text{I}_2\text{O}_4$  and other oxide aerosols:



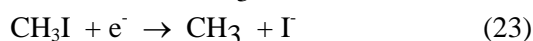
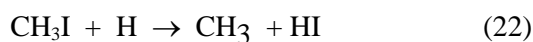
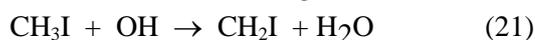
$\text{IO}_2$  also reacts with IO:



and this presumably undergoes polymerisation and/or oxidation to produce the final products.

The above scheme implies that the reaction of  $\text{O}_3$  with  $\text{I}_2$  does not have an important influence on the rate of  $\text{I}_2$  removal, and in fact the calculated rate of  $\text{I}_2$  destruction is not significantly changed if this reaction is removed from the model. The main role of ozone in this reaction scheme is in the production of more highly oxidised products than could be formed by polymerisation of IO and  $\text{IO}_2$ .

The decomposition of  $\text{CH}_3\text{I}$  can be initiated by several reactions:



The reaction rates used in the model for these were taken from the NIST compilation [9] and the electron reaction rate is the average of several values tabulated by Burns et al. [10]. Modelling studies indicate that electron reaction is dominant, and the decomposition rate observed in air can be reasonably well reproduced by this reaction alone. The reaction leads to first-order decomposition in air at low  $\text{CH}_3\text{I}$  concentration because the majority of the electrons are consumed by reaction with  $\text{O}_2$  (see equation (33) below), and this is consistent with the higher decomposition rate observed in 1%  $\text{O}_2/\text{N}_2$  atmosphere compared with air. Aubert [5] suggested that the reaction of  $\text{CH}_3\text{I}$  with N atoms was at least as important as with electrons, although the products of this reaction have not been identified. This mechanism would also give rise to first order kinetics at low  $\text{CH}_3\text{I}$  concentrations since atomic N also reacts rapidly with  $\text{O}_2$ .

Kinetic data have been reported [11] for



However, including this in the model was found to give very fast decomposition rates, possibly because  $\text{NO}_3$  is overestimated. In the reported work,  $\text{NO}_3$  was generated by reaction of NO with  $\text{CH}_3$  radicals and it was concluded that the asymmetric form (O-N-O-O) would be dominant. In the radiolysis of air, the main formation reaction for  $\text{NO}_3$  is



which has been estimated to give only 3% of  $\text{NO}_3$  in the asymmetric form [12]. As it is not clear that the reported rate constant for reaction (24) is applicable to this system, and its inclusion leads to considerable overestimation of the  $\text{CH}_3\text{I}$  decomposition rate, this reaction has been excluded from the model.

No reaction between  $\text{CH}_3\text{I}$  and  $\text{O}_3$  was included in the kinetic model as no reported rate constant was found for such a reaction. It has been shown

that iodine oxide particulate is not formed when  $\text{CH}_3\text{I}$  and  $\text{O}_3$  are combined in the absence of UV radiation, confirming that direct reaction with ozone is not a significant mechanism for the formation of solid iodine oxides [13].

The I ions produced by the reaction of  $\text{CH}_3\text{I}$  with electrons would be rapidly neutralised to I atoms by positive ions such as  $\text{N}^+$ . Reaction of two I atoms to produce  $\text{I}_2$  is only predicted at high  $\text{CH}_3\text{I}$  concentrations, as observed by Tang and Castleman [14]; at lower concentrations the I atoms are more likely to react with the products of air radiolysis so the reaction mechanism and products will be similar to those for  $\text{I}_2$  oxidation.

### III. COMPARISON WITH EXPERIMENTAL DATA ON $\text{I}_2$ DECOMPOSITION

#### (A) Funke tests.

Funke et al. [15] reported measurements of  $\text{I}_2$  destruction by air radiolysis in air and steam/air atmospheres, at dose rates of 1.9 and 20  $\text{kGy hr}^{-1}$  and temperatures of 25, 80 and 130°C. The  $\text{I}_2$  remaining after irradiation was measured by washing the irradiation vessel with an organic solvent which was then analysed photometrically.

The predictions of the IODAIR model are compared with these results in the following figures. Fig. 1 shows the effect of dose rate and steam concentration at 25°C. The “dry air” and “steam/air” calculations assumed  $\text{H}_2\text{O}$  fractions of  $2 \times 10^{-5}$  (~0.1% RH) and 0.02 (~80% RH) respectively. The experimental results show that there is no significant effect of dose rate or steam concentration on the  $\text{I}_2$  decomposition rate, and the calculations reproduce this behaviour and the measured decomposition rates quite well.

Fig. 2 shows the effect of  $\text{I}_2$  concentration at 80°C and 130°C. The measured decomposition rates increase with decreasing initial  $\text{I}_2$  concentration, and again this behaviour is reproduced by the model.

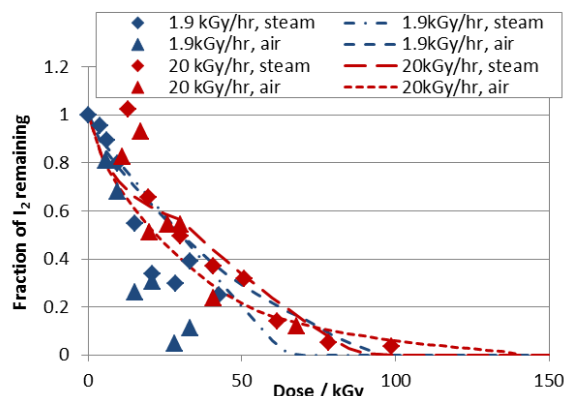
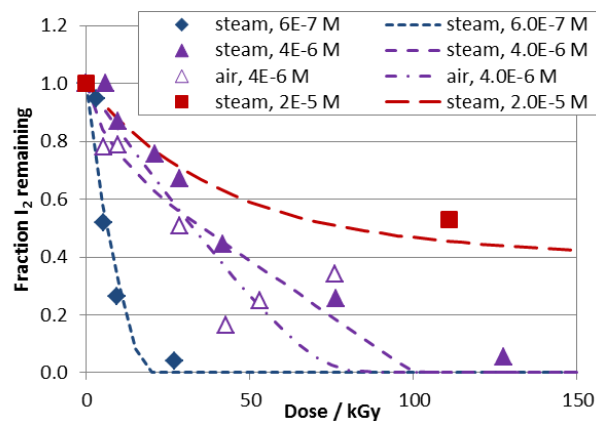
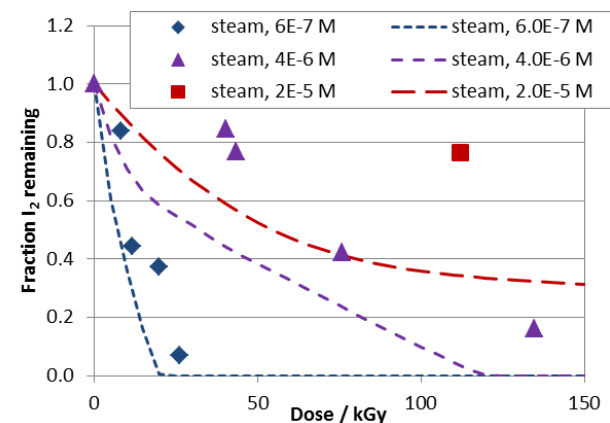


Fig. 1. Comparison of IODAIR model with data from Funke et al. [15] for experiments at 25°C with an initial  $\text{I}_2$  concentration of  $4 \times 10^{-6} \text{ mol dm}^{-3}$ . The points are experimental data and the lines are IODAIR calculations.



(a) 80°C



(b) 130°C

Fig. 2. Comparison of IODAIR model with data from Funke et al. [15] for experiments at different  $\text{I}_2$  concentrations. The points are experimental data and the lines are IODAIR calculations.

The effect of temperature on the decomposition rate was small, showing, if anything, a decrease in rate with increased temperature. The model overestimates the decomposition somewhat at 130°C.

(B) I<sub>2</sub> decomposition: PARIS tests.

The radiolytic oxidation of I<sub>2</sub> at lower initial concentrations was studied in the PARIS programme [16,17]. In these tests, gas mixtures (air, O<sub>2</sub> or H<sub>2</sub> + 30% steam) containing between 2.5x10<sup>-9</sup> and 7.5x10<sup>-7</sup> mol dm<sup>-3</sup> I<sub>2</sub> were irradiated at 80°C and about 1 kGy hr<sup>-1</sup> for ~1 hour or ~15 hours. CCl<sub>4</sub> and water were injected into the vessel at the end of the test to extract the water- and organic-soluble iodine fractions, which were

assumed to be oxidised iodine and unreacted I<sub>2</sub> respectively. The results show that the extent of radiolytic oxidation after ~ 1 kGy decreased with increasing iodine concentration. For a given initial I<sub>2</sub> concentration, the degree of oxidation was generally higher in O<sub>2</sub>/steam, and lower in H<sub>2</sub>/steam, than in air/steam atmospheres. Complete oxidation occurred in most tests after ~15 kGy, except at the highest concentrations (>10<sup>-7</sup> mol dm<sup>-3</sup>) and in some tests with H<sub>2</sub> where the results were rather inconsistent.

The IODAIR model reproduced the observed trends in these tests, but generally overpredicted the extent of I<sub>2</sub> destruction occurring after a dose of ~1 kGy as shown in Table I.

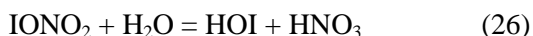
TABLE I

Comparison of IODAIR model with PARIS test results

Test ref	Gas	[I <sub>2</sub> ] <sub>init</sub> mol/dm <sup>3</sup>	Fraction remaining after ~1 kGy		
			I <sub>2</sub> (exp)	I <sub>2</sub> (calc)	I <sub>other</sub> (calc)
6V21	air	3.1E-09	44%	0%	32% IONO <sub>2</sub>
8V1 <sup>†</sup>	air	1.1E-08	72%	0%	26% IONO <sub>2</sub>
4V25	air	6.1E-08	87%	31%	48% IONO <sub>2</sub>
4V24	air	6.1E-08	90%	31%	48% IONO <sub>2</sub>
11T13	O <sub>2</sub>	2.5E-09	7%	0%	30% HOI
6V17	O <sub>2</sub>	7.2E-09	20%		
6V16	O <sub>2</sub>	7.2E-09	6%		
6V26	O <sub>2</sub>	9.8E-09	7%	0%	16% HOI
3V18	O <sub>2</sub>	1.6E-08	70%		
3V19	O <sub>2</sub>	1.9E-08	69%	0%	17% HOI
4V13	H <sub>2</sub>	2.6E-08	93%	9%	80% HI
4V14	H <sub>2</sub>	2.6E-08	91%		
4V15	H <sub>2</sub>	2.6E-08	89%		

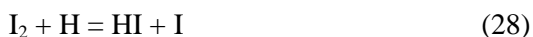
<sup>†</sup> The iodine mass balance was very low (35%) in this test so results are subject to considerable uncertainty

For initial  $I_2$  concentrations below  $2 \times 10^{-8}$  mol  $dm^{-3}$ , the model predicts complete removal of  $I_2$  after less than 1 kGy dose in either steam/air or steam/ $O_2$ , in contrast to the test results. However, a significant fraction of the iodine is calculated to form  $IONO_2$  (in steam/air) or  $HOI$  (in steam/ $O_2$ ). These products would be expected initially to dissolve in the aqueous phase during the extraction procedure, but could then hydrolyse and/or disproportionate to liberate  $I_2$ :

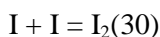


It is possible, therefore, that the measured  $I_2$  fraction also includes some intermediate species.

In the  $H_2$  atmosphere, the model predicts that the  $I_2$  is rapidly converted to  $HI$ :



which reacts with further  $H$  atoms to re-form  $I_2$ :



This results in a steady state  $HI/I_2$  ratio of about 10 for the conditions studied here.  $I_2$  oxidation by  $OH$  radicals (reaction (2)) produced from radiolysis of steam is largely suppressed by the reaction



so oxidation occurs more slowly by  $O$  atoms (reactions (2) and (14)). The large difference between the model and experimental results cannot be readily accounted for by possible changes in the product speciation during the extraction procedure.

After  $\sim 15$  kGy irradiation, practically no  $I_2$  remained in the tests in  $O_2$  atmosphere, whereas in  $H_2$  the remaining fraction ranged from 9 – 90% with no apparent correlation with the initial concentration. The model predicts complete oxidation at this dose in both cases. In air, the amount of  $I_2$  remaining appears to correlate roughly with the initial concentration above  $10^{-8}$  mol  $dm^{-3}$ , as shown in Fig. 3. This also shows the calculated concentrations of  $I_2$  and ( $I_2 + IONO_2$ ), which show a similar trend.

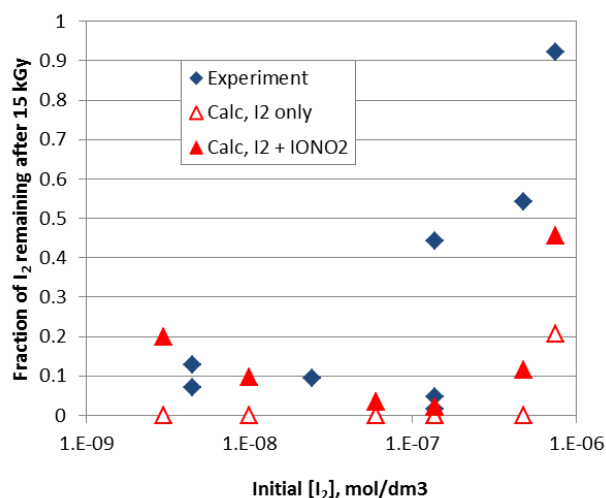


Fig. 3. Comparison of IODAIR model with data from PARIS tests in steam/air after 15 kGy irradiation.

It can also be seen that the highest  $I_2$  concentrations in the PARIS tests,  $\sim 5 \times 10^{-7}$  and  $7 \times 10^{-7}$ , are similar to the lowest concentration used in Funke's tests, in which 20% of the  $I_2$  remained after 15 kGy irradiation under similar conditions (Fig. 2(b)). This could provide support for the suggestion that other species are included in the  $I_2$  measurements.

#### IV. COMPARISON WITH EXPERIMENTAL DATA ON $CH_3I$ DECOMPOSITION

##### (A) Harwell tests.

Experimental measurements of  $CH_3I$  radiolysis are reported in a companion paper [2]. These studies looked at the effect of a number of variables, including  $CH_3I$  concentration, atmosphere, dose rate and humidity. The predictions of the model are compared with the experimental results in the following sections. In the tests discussed below, the irradiation vessel contained a small amount of liquid water, unless stated otherwise, so the bulk gas would have been saturated in  $H_2O$ .

##### *Effect of initial methyl iodide concentration*

The experiments showed that the decomposition of  $CH_3I$  was first order over the range of initial concentrations studied ( $\sim 10^{-8} - 5 \times 10^{-7}$  mol  $dm^{-3}$ ). The calculations reproduce the observed behaviour as shown in Fig. 4.

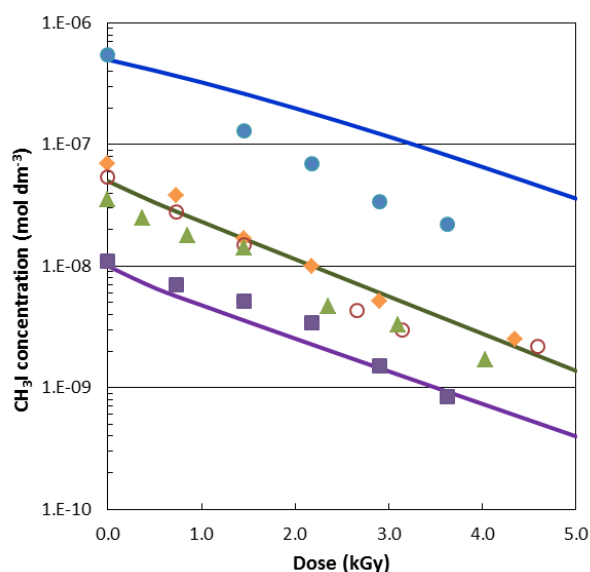
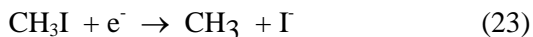
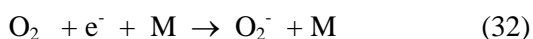


Fig. 4. Comparison of IODAIR model with data from  $\text{CH}_3\text{I}$  radiolysis tests at  $80^\circ\text{C}$ : effect of initial  $\text{CH}_3\text{I}$  concentration. The points are experimental data and the lines are IODAIR calculations.

The first order behaviour is consistent with the dominant removal reaction in air being



This is in competition with the reaction between electrons and  $\text{O}_2$ :



where M is a third body in the termolecular reaction. Although reaction (23) is much faster than (32), the concentration of  $\text{CH}_3\text{I}$  is much lower than that of  $\text{O}_2$  so most of the electrons are removed by (32). The removal rate of  $\text{CH}_3\text{I}$  by reaction (23) is therefore given by:

$$\frac{d[\text{CH}_3\text{I}]}{dt} = \frac{k_{23}[\text{CH}_3\text{I}]}{k_{32}[\text{O}_2][\text{M}]} DG_{e^-} = k_{eff}[\text{CH}_3\text{I}] \quad (33)$$

Where  $k_{23}$  and  $k_{32}$  are the rate constants of reactions (23) and (32),  $D$  is the dose rate,  $G_{e^-}$  is the electron production rate and  $k_{eff}$  is an effective first-order decomposition rate which depends on  $[\text{O}_2]$  (and on the identity of the third body M as discussed below). Equation (33) only applies if  $k_{32}[\text{O}_2][\text{M}] \gg k_{23}[\text{CH}_3\text{I}]$ ; at higher  $[\text{CH}_3\text{I}]$  or lower  $[\text{O}_2]$  it becomes

$$\frac{d[\text{CH}_3\text{I}]}{dt} = \frac{k_{23}[\text{CH}_3\text{I}]}{k_{32}[\text{O}_2][\text{M}] + k_{23}[\text{CH}_3\text{I}]} DG_{e^-} \quad (34)$$

so the decomposition would no longer be first order.

#### Effect of atmosphere

Tests were conducted in air,  $\text{O}_2$  and 1%  $\text{O}_2/\text{N}_2$  and the results are compared with the IODAIR calculations in Fig. 5.

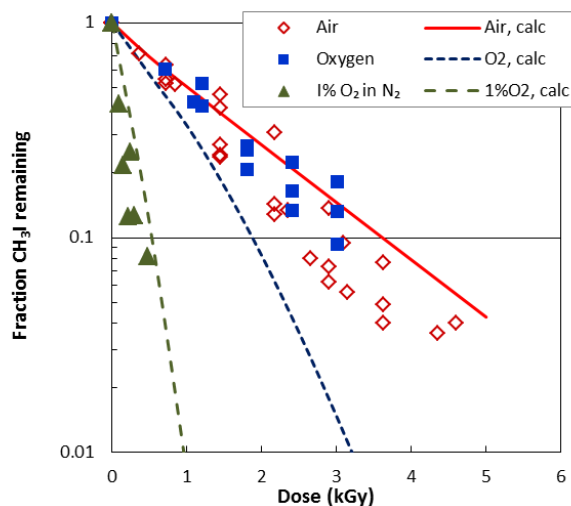


Fig. 5. Comparison of IODAIR model with data from  $\text{CH}_3\text{I}$  radiolysis tests at  $80^\circ\text{C}$ : effect of atmosphere. The points are experimental data and the lines are IODAIR calculations.

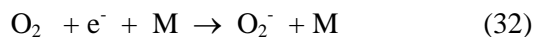
The experiments at  $80^\circ\text{C}$  show a slight decrease in the decomposition rate in  $\text{O}_2$  compared with air, whereas the model predicts about a factor of 2 increase. The dominant removal reaction in  $\text{O}_2$  is with OH radicals (reaction (21)) as the electrons react mainly with oxygen. The discrepancy suggests that there may be other reactions of OH that are missing from the model; however, these conditions are of limited interest here so this was not pursued. At low  $\text{O}_2$  concentration the  $\text{CH}_3\text{I}$  decomposition rate increased, and this is consistent with the behaviour discussed above (equation (33)).

#### Effect of dose rate

Experiments at 560, 71 and 5  $\text{Gy hr}^{-1}$  showed that the  $\text{CH}_3\text{I}$  decomposition rate is proportional to the square root of the dose rate. This is not consistent with the behaviour reported by Tang and Castleman, who found that the decomposition rate was directly proportional to the dose rate over the range 0.35 to 12  $\text{kGy hr}^{-1}$ . This apparent change in the dose rate dependence of the decomposition rate suggests that there

could be two main reactants for  $\text{CH}_3\text{I}$  whose concentrations change differently with dose rate.

Primary radiolysis products such as  $\text{OH}$ ,  $\text{O}$  and  $\text{e}^-$  are produced at a rate that is directly proportional to the dose rate. The main reactions of  $\text{O}$  and  $\text{e}^-$  are with bulk gaseous components:



so the steady-state concentrations, and hence the rate of reaction with  $\text{CH}_3\text{I}$ , will also be proportional to the dose rate.  $\text{OH}$  radicals react mainly with N-O species that accumulate with dose, so the reaction of  $\text{CH}_3\text{I}$  with  $\text{OH}$  could give rise to the observed dose rate effect; however, this reaction only makes a very minor contribution to the overall decomposition at  $25^\circ\text{C}$ .

It has not been possible to unequivocally identify the reactant(s) responsible for the dose rate effect, but one possibility is the  $\text{NO}_3^-$  ion. A number of possible mechanisms have been considered, and the one that appears the most thermodynamically favourable is



A rate constant of  $10^8 \text{ mol}^{-1} \text{ dm}^3 \text{ s}^{-1}$  for this reaction produces the dose rate effect shown in Fig. 6.

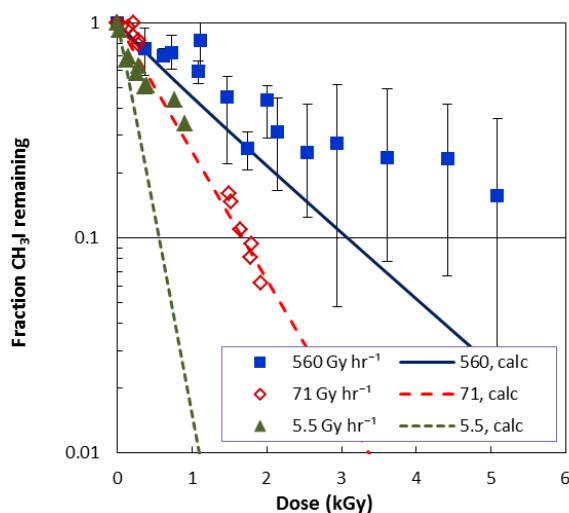


Fig. 6. Comparison of IODAIR model with data from  $\text{CH}_3\text{I}$  radiolysis tests at  $20^\circ\text{C}$ : effect of dose rate. The points are experimental data and the lines are IODAIR calculations.

The model overestimates the decomposition rate at the very low dose rate, which may indicate that the value of  $k_{36}$  is too high or that other effects (e.g. with surfaces or impurities) become more important under these conditions.

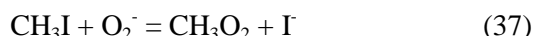
#### *Effect of temperature and humidity*

In most of the experiments described in [2],  $\text{CH}_3\text{I}$  was introduced as an aqueous solution. The volume of solution was either 5 or 500  $\mu\text{l}$ , which meant that at  $25^\circ\text{C}$  liquid water was present in all the tests. At  $80^\circ\text{C}$ , 5  $\mu\text{l}$  of water would have completely evaporated giving about 7%  $\text{H}_2\text{O}$  in the gas phase; with 500  $\mu\text{l}$ , the saturated vapour pressure corresponds to about 47%  $\text{H}_2\text{O}$  and some liquid water would have remained.

There are a number of ways in which the water concentration can affect the  $\text{CH}_3\text{I}$  decomposition rate. Firstly, decreasing  $[\text{H}_2\text{O}]$  decreases the concentration of  $\text{OH}$  radicals, but this has a small effect as reaction (21) is only a minor pathway for decomposition.

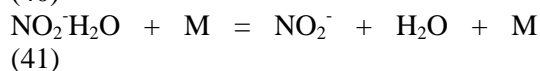
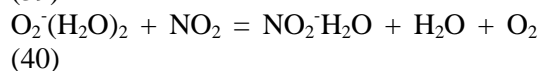
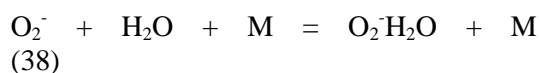
At relatively high  $[\text{H}_2\text{O}]$ , there is a third body effect on the  $\text{O}_2 + \text{e}^-$  reaction (32); the rate constants for this reaction with  $\text{M} = \text{O}_2$ ,  $\text{N}_2$  and  $\text{H}_2\text{O}$  are  $7.2 \times 10^{11}$ ,  $3.1 \times 10^{10}$  and  $5 \times 10^{12} \text{ mol}^{-2} \text{ dm}^6 \text{ s}^{-1}$  respectively [18]. The overall rate in dry air is therefore  $1.7 \times 10^{11} \text{ mol}^{-2} \text{ dm}^6 \text{ s}^{-1}$  so a few percent of  $\text{H}_2\text{O}$  would increase the reaction rate and therefore decrease the  $\text{CH}_3\text{I}$  decomposition rate according to equation (33). However, for  $\text{H}_2\text{O}$  fractions below about 0.5% the effect on this reaction will be insignificant.

Another mechanism is therefore needed to account for the effect of humidity at much lower concentrations. Tang and Castleman observed a factor of 2-3 decrease in the  $\text{CH}_3\text{I}$  decomposition rate when  $[\text{H}_2\text{O}]$  was decreased from  $2.1 \times 10^{-7} \text{ moles cm}^{-3}$  to  $3.7 \times 10^{-10} \text{ moles cm}^{-3}$  [13]. This suggests that  $\text{H}_2\text{O}$  competes with  $\text{CH}_3\text{I}$  for another reactive species. One possibility is the  $\text{O}_2^-$  ion formed in reaction (32). This could react with  $\text{CH}_3\text{I}$ :



No kinetic data were found for reaction (37) but the rate constants for the analogous reactions of  $\text{CH}_3\text{Cl}$  and  $\text{CH}_3\text{Br}$  are  $4.5 \times 10^{11}$  and  $7.8 \times 10^{11} \text{ mol}^{-1} \text{ dm}^3 \text{ s}^{-1}$  respectively [19] so it is reasonable to estimate a value of  $10^{12}$  for reaction 37.

At high  $\text{H}_2\text{O}$  concentrations, most of the  $\text{O}_2^-$  is removed by clustering reactions with  $\text{H}_2\text{O}$ :



At low  $[\text{H}_2\text{O}]$ , these reactions will be less important so more  $\text{O}_2^-$  will be available to react with  $\text{CH}_3\text{I}$  by reaction (37).

The experimental data show that decomposition at  $80^\circ\text{C}$  is faster at lower  $[\text{H}_2\text{O}]$ , and this is consistent with the mechanisms discussed above. The model gives the same qualitative behaviour but the effect is less pronounced than observed, as shown in Fig. 7.

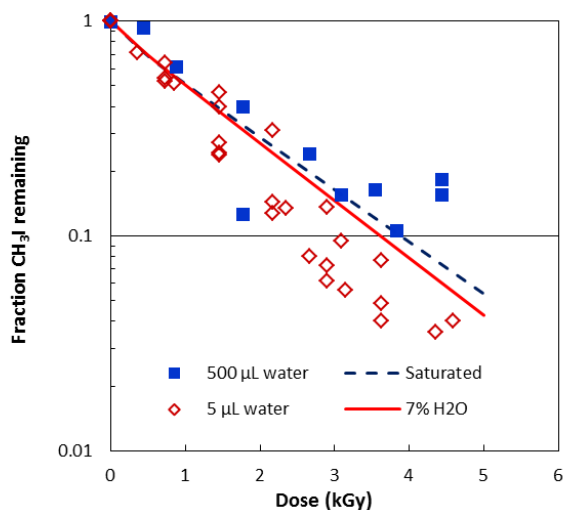


Fig. 7. Comparison of IODAIR model with data from  $\text{CH}_3\text{I}$  radiolysis tests at  $80^\circ\text{C}$ : effect of humidity. The points are experimental data and the lines are IODAIR calculations.

A similar tendency towards increasing decomposition rate at lower humidity is shown by the “dry” test at  $25^\circ\text{C}$  in which  $\text{CH}_3\text{I}$  was injected as a gas rather than in aqueous solution. This is also reproduced by the model as shown in Fig. 8.

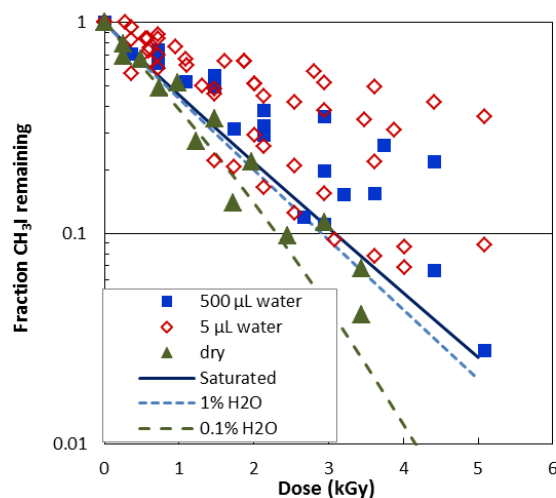


Fig. 8. Comparison of IODAIR model with data from  $\text{CH}_3\text{I}$  radiolysis tests at  $20^\circ\text{C}$ : effect of humidity. The points are experimental data and the lines are IODAIR calculations.

Although the model somewhat under-predicts the effect of changing  $[\text{H}_2\text{O}]$  at  $80^\circ\text{C}$ , it does reflect the experimental observation that humidity has a relatively minor effect on  $\text{CH}_3\text{I}$  decomposition. There may be other effects associated with the presence of liquid water that are not taken into account in the model.

The model predicts that reaction (37) makes an increasing contribution to the  $\text{CH}_3\text{I}$  decomposition rate at  $\text{H}_2\text{O}$  concentrations below about 0.1%, as shown in Fig. 8.

Comparison of Fig. 7 and 8 also shows that changing the temperature from 25 to  $80^\circ\text{C}$  has a small effect on the measured decomposition rate, although the large scatter in the low temperature tests makes this difficult to quantify. This low sensitivity to the temperature is also apparent in the model results.

#### (B) BIP tests.

The OECD Behaviour of Iodine Project (BIP) investigated the adsorption of iodine adsorbed onto painted surfaces and the subsequent production of organic iodides under irradiation [3]. Because the irradiation tests were carried out in a closed system over many hours, the measured  $\text{CH}_3\text{I}$  concentrations reflected the balance between the production and decomposition processes. A quantitative understanding of the decomposition reactions is

therefore necessary to determine the long-term release behaviour.

Some of the tests showed that the  $\text{CH}_3\text{I}$  concentration gradually increased at long irradiation times, suggesting either that the production rate was increasing or the decomposition rate decreasing. A possible mechanism for the latter is the reaction between  $\text{e}^-$  and  $\text{HNO}_3$



which has a rate constant of  $\sim 3 \times 10^{13} \text{ dm}^3 \text{ mol}^{-1} \text{ s}^{-1}$  [20]. As  $\text{HNO}_3$  builds up due to irradiation, this reaction could compete with reaction (23) and thus decrease the  $\text{CH}_3\text{I}$  decomposition rate. There are only a limited number of reactants that would have this effect since, as equation (34) shows, the product of the rate constant and reactant concentration would have to be comparable to  $k_{32}[\text{O}_2][\text{M}]$  to significantly affect the  $\text{CH}_3\text{I}$  decomposition rate.

The effect of irradiation time (or accumulated dose) on the  $\text{CH}_3\text{I}$  decomposition rate was investigated by the BIP team with tests similar to those described above, except that once the initial charge of  $\text{CH}_3\text{I}$  was exhausted, additional injections were made without opening the vessel. The results showed that the destruction rate was not significantly changed by the buildup of radiolysis products. The IODAIR model results are compared with the experimental behaviour in Fig. 9. In this calculation, the model was tuned slightly (by removing the  $\text{CH}_3\text{I} + \text{NO}_3^-$  reaction (36) and setting the  $\text{H}_2\text{O}$  concentration to 0.1%) to give good agreement with the results from the first injection. It can be seen that the effect of reaction (42) is small over the duration of the test, but agreement is slightly better at long irradiation times if reaction (32) is not included. The most likely explanation for this behaviour is that  $\text{HNO}_3$  does not build up in the gas phase, as assumed by the model, but is lost to surfaces. Another implication of this comparison is that the rate of reaction (36) is lower than suggested in the data shown in Fig. 6, since this reaction would lead to an increase in the decomposition rate at long irradiation times which is not consistent with the experimental observations.

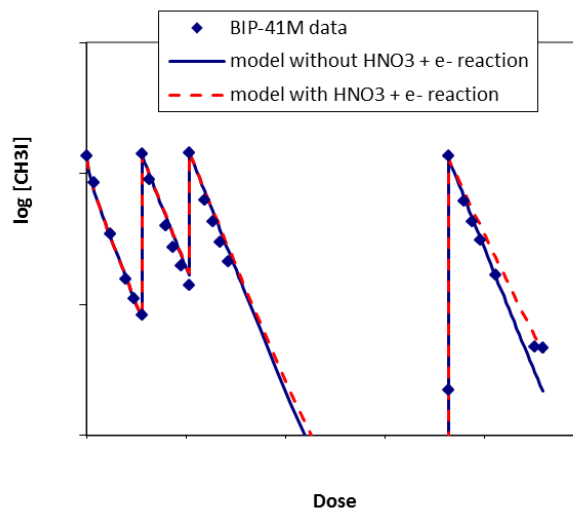


Fig. 9. Comparison of IODAIR model with data from BIP tests with multiple  $\text{CH}_3\text{I}$  injections

(Data are proprietary to the BIP partners so are shown without axis markings)

The decomposition rates measured in the BIP tests were similar to those in the AEAT tests, and the data showed much less scatter. This could be due to the fact that the irradiation vessel was baked at  $500^\circ\text{C}$  before the tests, which would have minimised the amounts of impurities. Also, the  $\text{CH}_3\text{I}$  was introduced as a gas so there would have been no liquid water present, though no particular means were taken to dry the air within the vessel.

## V. COMPARISON WITH EXPERIMENTAL DATA ON $\text{CH}_3\text{I}$ FORMATION

Experimental measurements of  $\text{CH}_3\text{I}$  formation from irradiated  $\text{I}_2 - \text{CH}_4$  mixtures were reported by Bartonicek et al. [21]. They found that when moist air containing  $10^{-8} \text{ mol dm}^{-3} \text{ I}_2$  and  $10^{-3} \text{ mol dm}^{-3} \text{ CH}_4$  was irradiated at  $0.05 \text{ Gy s}^{-1}$ , the  $\text{CH}_3\text{I}$  concentration increased to about  $10^{-9} \text{ mol dm}^{-3}$  (i.e. about 5% of the total iodine) after a dose of 20 kGy, after which the  $\text{CH}_3\text{I}$  concentration slowly decreased. Less  $\text{CH}_3\text{I}$  was observed in Ar, up to a maximum of  $\sim 1\%$  of the iodine.

The IODAIR model is unable to duplicate the findings of these tests, and predicts only a very small concentration of  $\text{CH}_3\text{I}$  ( $\sim 10^{-18} \text{ mol dm}^{-3}$ ). The model contains reactions leading to the formation of  $\text{CH}_3\text{I}$  such as:



where the  $\text{CH}_3$  radicals are produced by reactions such as



However, the dominant reaction of  $\text{CH}_3$  in air is:



which has a rate constant of about  $7 \times 10^9 \text{ dm}^3 \text{ mol}^{-1} \text{ s}^{-1}$  at 298 K. The rate constant of reaction (42) is similar,  $3.5 \times 10^9 \text{ dm}^3 \text{ mol}^{-1} \text{ s}^{-1}$ , but the  $\text{O}_2$  concentration is much higher than that of  $\text{I}_2$  (about  $8 \times 10^{-3} \text{ mol dm}^{-3}$  at 298 K) so the fraction of  $\text{CH}_3$  radicals that would react with  $\text{I}_2$  in the conditions of Bartonicek's experiments is about  $6 \times 10^{-7}$ . The model predicts that the total  $\text{CH}_3$  formation rate is about  $4 \times 10^{-9} \text{ mol dm}^{-3} \text{ s}^{-1}$  at a dose rate of  $0.05 \text{ Gy s}^{-1}$ , so the formation rate of  $\text{CH}_3\text{I}$  by reaction (42) would be  $2.5 \times 10^{-15} \text{ mol dm}^{-3} \text{ s}^{-1}$  giving a concentration of  $2.5 \times 10^{-12} \text{ mol dm}^{-3}$  after 20 kGy (neglecting any decomposition reactions). The reported concentration of  $\sim 10^{-9}$  is a factor of 400 higher than this. The  $\text{CH}_3\text{I}$  concentration calculated by the model is even lower than given by this simplified calculation, because other effects such as  $\text{CH}_3\text{I}$  decomposition are also taken into account.

A search of the NIST database has not revealed any plausible mechanism by which  $\text{CH}_3\text{O}_2$  would react directly with  $\text{I}_2$  to form  $\text{CH}_3\text{I}$ , or generate any other species that would be expected to do so. The main  $\text{CH}_3$ -containing product in the model is methanol,  $\text{CH}_3\text{OH}$ , although ultimately complete oxidation to  $\text{CO}_2$  would be expected to occur. It is therefore difficult to reconcile the experimental observations with the expected reactions in this system. A possible explanation is that the radiolysis products are able to react at surfaces to produce methyl iodide, and any future studies of this system should be designed to take this into account.

## VI. DISCUSSION

The IODAIR gives good agreement with the  $\text{I}_2$  removal rates measured by Funke et al. [15] at relatively high  $\text{I}_2$  concentrations. However, it does not predict the apparent shift towards first-order kinetics at low concentrations shown by the PARIS data [16,17], and so overestimates the

degree of radiolytic oxidation of gaseous  $\text{I}_2$  at concentrations below  $10^{-6} \text{ mol dm}^{-3}$ . The reason for this is not known, but one explanation could be that other reaction products were included in the analysis of  $\text{I}_2$  in these tests. Another possibility is that decomposition of the oxide product occurs, possibly due to hydrolysis reactions on the vessel surfaces, resulting in a low but constant  $\text{I}_2$  concentration at long irradiation times.

The model also gives reasonable agreement with experimental measurements of  $\text{CH}_3\text{I}$  decomposition, and successfully reproduces the effects of changing  $\text{CH}_3\text{I}$  and oxygen concentrations. Reactions have been postulated that explain the observed dependences on dose rate and humidity, but the rate constants used are not based on independent kinetic measurements and so there are large uncertainties associated with these parts of the model. In particular, comparison with the BIP results suggests that the rate constant used for the reaction of  $\text{CH}_3\text{I}$  with  $\text{NO}_3^-$ , which is postulated to explain the non-linear effect of dose rate, is probably too high as it would lead to a change in the decomposition rate at long irradiation times which is not observed experimentally.

One area where the model has not been successful is in reproducing the results of experiments showing significant production of  $\text{CH}_3\text{I}$  from the gas-phase reaction of  $\text{CH}_4$  and  $\text{I}_2$  under irradiation. It is difficult to rationalise this observation with the expected reactions of methane in irradiated air; the same conclusion was reached by Sagert in an earlier modelling study [4]. It is possible that surface reactions between the radiolysis products play an important role. Further experimental work would be required to confirm and explain these observations.

## VII. CONCLUSION

The IODAIR model has been shown to give reasonable agreements with experimental measurements of  $\text{CH}_3\text{I}$  and  $\text{I}_2$  radiolysis. Although there are some discrepancies between the test data and model predictions that remain unexplained, the use of a mechanistic model leads to a better understanding of the important processes, and highlights the main uncertainties

that could be addressed in future experimental programmes.

#### ACKNOWLEDGMENTS

The IODAIR model was originally developed as part of the 5<sup>th</sup> Framework ICHMM project, which was jointly financed by the European Commission.

#### REFERENCES

1. L. BOSLAND et al., “Iodine–paint interactions during nuclear reactor severe accidents”, *Annals of Nuclear Energy* 74, p. 184, (2014).
2. G. M. N. BASTON et al., “The radiolysis of gaseous methyl iodide in air”, This conference, Paper 3-3, (2015).
3. G. A. GLOWA, C. J. MOORE and D. BOULIANNE, “The main outcomes of the OECD Behaviour of Iodine project”, This conference, Paper 1-6, (2015).
4. N. H. SAGERT, “Radiolysis of iodine in moist air: A computer study”, *Proc. 2<sup>nd</sup> CSNI Workshop on Iodine Chemistry in Reactor Safety*, Toronto, Canada, 2-3 June 1988, AECL-9923 (CSNI-149), p. 235, (1989).
5. F. AUBERT, « Destruction par Radiolyse Gamma de l’Iodure de Methyl en Faible Concentration dans l’Air Humide », Thèse de Doctorat de l’Université d’Aix-Marseille III, (2002).
6. F. BUSI et al., “Radiation treatment of combustion gases: formulation and test of a reaction model”, *Radiat. Phys. Chem.*, 25(1-3), p. 47, (1985).
7. I. K. LARIN et al., “Measurements of rate constants for the reaction of iodine monoxide with ozone”, *Kinet. Catal.*, 40 (4), p. 435, (1999).
8. W. J. BLOSS et al., “Kinetics and products of the IO self-reaction”, *J. Phys. Chem. A*, 105, p. 7840, (2001).
9. J. A. MANION et al., NIST Chemical Kinetics Database, NIST Standard Reference Database 17, Version 7.0 (Web Version), Release 1.6.8, Data version 2013.03, National Institute of Standards and Technology, Gaithersburg, Maryland, 20899-8320. Web address: <http://kinetics.nist.gov/NIST>.
10. S. J. BURNS, J. M. MATTHEWS and D. L. MCFADDEN, “Rate coefficients for dissociative electron attachment by halomethane compounds between 300 and 800 K”, *J. Phys. Chem.*, 100, p. 19436, (1996).
11. T. JOHNSTON and J. HEICKLEN, “Photolysis of methyl iodide in the presence of nitric oxide”, *J. Phys. Chem.*, p. 70, 3088, (1966).
12. R. A. COX and G. B. COKER, “Kinetics of the reaction of nitrogen dioxide with ozone”, *J. Atmospheric Chem.* 1, p. 53, (1983).
13. S. DICKINSON et al. “Experimental and modelling studies of iodine oxide formation and aerosol behaviour relevant to nuclear reactor accidents”, *Annals of Nucl. Energ.* 74, 200-207 (2014).
14. I. N. TANG and A. W. CASTLEMAN Jr., “Kinetics of  $\gamma$ -induced decomposition of methyl iodide in air”, *J. Phys. Chem.*, 74(22), p. 3933, (1970).
15. F. FUNKE, P. ZEH and S. HELLMANN, “Radiolytic Oxidation of Molecular Iodine in the Containment Atmosphere”, *Iodine Aspects of Severe Accident Management*, Vantaa, Finland, May 1999, NEA/CSNI/R(99)7, p. 79, (1999).
16. L. BOSLAND et al., “PARIS project: Radiolytic oxidation of molecular iodine in containment during a nuclear reactor severe accident. Part 1. Formation and destruction of air radiolysis products-Experimental results and modelling”, *Nucl. Eng. Des.*, 238 (12), p. 3542, (2008).
17. L. BOSLAND et al., “PARIS project: Radiolytic oxidation of molecular iodine in

- containment during a nuclear reactor severe accident: Part 2: Formation and destruction of iodine oxides compounds under irradiation – experimental results modelling”, Nucl. Eng. Des., 241 (9), p. 4026, (2011).
18. H. SHIMAMORI and Y. HATANO, “Thermal electron attachment to O<sub>2</sub> in the presence of various compounds as studied by a microwave cavity technique combined with pulse radiolysis”, Chem. Phys., 21, p. 187, (1977).
  19. Y. IKEZOE, et al., Gas phase ion-molecule reaction rate constants through 1986, Ion Reaction Research Group of the Mass Spectrometry Society of Japan, (1986).
  20. F. C. FEHSENFELD and C. J. HOWARD, “The ion chemistry of HNO<sub>3</sub> and NO<sub>2</sub>”, Bull. Am. Phys. Soc., 20, p. 239, (1975).
  21. B. W. BARTONICEK and A. HABERSBERGEROVA, “Investigation of the formation possibilities of alkyl iodides in nuclear power plants”, Radiat. Phys. Chem., 28 (5/6), p. 591, (1986).

## INTERACTION OF GASEOUS I<sub>2</sub> WITH PAINTED SURFACES AND AEROSOLS IN LARGE-SCALE THAI TESTS

F. Funke(1)\*, S. Gupta(2), G. Weber(3), G. Langrock(1), G. Poss(2)

<sup>(1)</sup> AREVA GmbH, Erlangen, Germany, <sup>(2)</sup> Becker Technologies GmbH, Eschborn, Germany,

<sup>(3)</sup> Gesellschaft für Anlagen- und Reaktorsicherheit mbH, Garching, Germany, "

\*Corresponding author, Tel: (+49)90097681, Fax: (+49)90097312, Email: Friedhelm.Funke@areva.com

**Abstract** – Deposition of gaseous molecular iodine (I<sub>2</sub>) onto dry or wet surfaces in nuclear power plant containments during severe accidents represents an important sink to reduce iodine volatility. Decontamination paint, covering large surface areas of walls and floors, is well-known to provide the necessary high reactivity towards I<sub>2</sub>. Aerosols, with their high specific surface of small particles, can significantly increase the I<sub>2</sub> deposition surface area. Models to predict the I<sub>2</sub> depletion from atmospheres by interaction with painted surfaces are available. These are commonly based on results obtained from small-scale tests including volumes of only up to about 0.3 m<sup>3</sup>. Up to now no models have been included in severe accident containment codes to quantify the I<sub>2</sub> depletion by adsorption onto aerosols. The 60 m<sup>3</sup> vessel of the THAI test facility is used to bridge the differing scales of laboratory tests and containment dimensions. At the same time coupled effects such as I<sub>2</sub>/aerosol interaction and iodine deposition in aerosol form have been studied in the large-scale THAI facility.

The reaction of gaseous I<sub>2</sub> with painted surfaces was addressed in a number of THAI tests (Iod-15, Iod-17, Iod-20, Iod-21, Iod-24, Iod-27A, Iod-28, and Iod-30). An empirical deposition / desorption model was developed and included in COCOSYS/AIM-3, but it still needs more refinements: (1) paint is only a German epoxy paint, and there is no connection to compare its behaviour versus iodine with the effects of other paints, (2) ageing of paint is not explicitly scaled but always referring to 15 years, (3) ageing procedure is different from other experimental programs and a deeper analysis of this issue including connecting tests is necessary, (4) modeling of relative humidity and temperature effect on chemisorption are to be developed, (5) the partitioning between physisorbed and chemisorbed iodine on paint is to be checked and adapted to the high fraction of chemisorbed iodine measured. This issue could entrain the necessity of further tests in the laboratory-scale.

The reaction of gaseous I<sub>2</sub> with wet painted surfaces was studied with tests Iod-21 and Iod-24 and the expected phenomena of I<sub>2</sub> deposition and wash-off were quantified. A new water-film-based model, which explicitly considers detailed condensation rate, and which considers the iodine chemistry in the water film, was designed and preliminary adjusted to THAI test Iod-24. More analytical and validation work is necessary for optimisation.

The two THAI tests on the I<sub>2</sub>/aerosol reactions (Iod-25, Iod-26) are providing the effect of I<sub>2</sub> removal from containment atmospheres by interaction with containment aerosol, the reactive silver (Ag) aerosol providing a high reactivity, and the inert tin oxide (SnO<sub>2</sub>) a low reactivity under the given boundary conditions of the tests. The I<sub>2</sub> chemisorption reaction with the Ag particle surface is as high as for the higher range of I<sub>2</sub>/paint reactions, as evident from comparison of large-scale THAI tests and associated laboratory-scale tests. Real mixed aerosol in the containment can be expected to exhibit I<sub>2</sub> removal rates between the bounding cases "reactive Ag" and "inert SnO<sub>2</sub>". If source term analyses reveal a significant effect of the I<sub>2</sub>/aerosol interaction in the containment, the actual surface reactivity of an aerosol defined by the thermochemical phases available to gaseous I<sub>2</sub> lays between the bounding cases "reactive Ag" and "inert SnO<sub>2</sub>". Additional tests using a more realistic aerosol (e.g. from simulated core melts) could turn out necessary, as well as the study of an effect of steam.

## I. INTRODUCTION

Deposition of gaseous molecular iodine ( $I_2$ ) onto dry or wet surfaces in nuclear power plant containments during severe accidents represents an important sink to reduce iodine volatility. Decontamination paint, covering large surface areas of walls and floors, is well-known to provide the necessary high reactivity towards  $I_2$ . Aerosols, with their high specific surface of small particles, can significantly increase the  $I_2$  deposition surface area. Models to predict the  $I_2$  depletion from atmospheres by interaction with painted surfaces are available. These are commonly based on results obtained from small-scale tests including volumes of only up to about  $0.3 \text{ m}^3$ . No models are included in severe accident containment codes to quantify the  $I_2$  depletion by adsorption onto aerosols. The  $60 \text{ m}^3$  vessel of the THAI test facility bridges the differing scales of laboratory tests and containment dimensions. At the same time coupled effects such as  $I_2$  / aerosol interaction and iodine deposition in aerosol form can be studied in the large-scale THAI facility. This paper presents test results and conclusions on the interaction of  $I_2$  with dry or wet paint and with suspended aerosol from a number of THAI tests performed during different THAI projects funded by the German Federal Ministry for Economic Affairs and Energy or within the NEA THAI-2 project. Results on the  $I_2$  / aerosol interaction from supporting laboratory tests are included.

## II. EXPERIMENTAL

### Test set-up

The THAI facility and the THAI vessel are described in detail in paper 1.4 of this Workshop.

The painted surfaces relevant for the  $I_2$  / paint interaction studies discussed in this paper were provided as deposition coupons (about  $10 - 20 \text{ m}^2$ ), by mounting differently sized painted plates and / or painted bodies into the THAI vessel. Compartments are established in the THAI vessel using steel internals (plates, inner cylinder). Some painted surfaces were locally monitored online for iodine uptake, some of them were recovered after the end of a test to measure the final iodine uptake. Some of the painted bodies can be heated or cooled by separate inner steam or water circuits to increase

the surface temperature or force wall condensation, respectively.

### Iodine instrumentation

A sketch of a typical iodine and aerosol instrumentation relevant to this paper is shown in Fig. 1, as it was in detail relevant to the tests Iod-25 and Iod-26. Numbers and positions of the instrumentations are partly adapted in the other tests of this paper according to the specific objectives.

The injection of the gaseous  $I_2$ , radio-labelled with I-123, into the THAI vessel atmosphere was performed using carrier gas, usually air. The  $I_2$  injection amounts were between 0.3 and 2.4 g. The preparation of the labelled  $I_2$  was always using 1 GBq I-123. The resulting  $I_2$  concentrations are clearly higher than in a severe accident containment but more reliably to measure, as (i) artefacts from conceivable background reactions are suppressed and as (ii) supporting chemical measurements are possible on the required trace levels.

Gaseous  $I_2$  concentrations were measured by six gas scrubbers distributed over the whole vessel. Additionally, in tests where different gas-borne iodine species can occur, two Maypack filter stations at different heights were discriminating iodine in aerosol form, gaseous  $I_2$ , and organic iodide. In such tests, the interpretation of the gas scrubbers results requires special attention, as gas scrubbers also trap iodine in aerosol form and potentially some organic iodide.

The evolution of iodine surface depositions were monitored by scintillation detectors focused on deposition coupons mounted in front of glass windows. The total accumulated iodine loadings were additionally measured in some tests by recovering a number of deposition coupons at the end of a test.

An irradiation source has never been available in THAI, so there is no relevant dose rate, and the thermally induced production of organic iodides is only on a very small or negligible level.

### Aerosol instrumentation and material

Aerosol mass concentrations were measured by 4 different filter stations. Continuous monitoring of aerosol mass concentrations was performed using

a photometer measuring the extinction of laser light. The particle size distribution was measured with a low-pressure cascade impactor. The aerosol particle deposition was measured gravimetrically from recovered aerosol coupons.

The Ag powder was provided by the company CHEMPUR, Karlsruhe, Germany. According to manufacturer, particle sizes were 0.7 - 1.2  $\mu\text{m}$  and the measured specific surface area was 2.5  $\text{m}^2/\text{g}$ . Sauter mean diameters and the calculated specific surface area of the  $\text{SnO}_2$  aerosol particles were 0.62 - 0.74  $\mu\text{m}$  and 1.3  $\text{m}^2/\text{g}$ , respectively, assuming spherical particles with a density of 6950  $\text{kg}/\text{m}^3$ . SEM images were taken from a number of filter loadings or deposition coupon loadings, partly including an EDX analysis providing elemental mass ratios.

#### Painted surfaces: material and ageing

The epoxy-type decontamination paint GEHOPON from GEHOLIT & WIEMER GmbH, Graben-Neudorf, Germany, which was used in several German reactor containments, was also used in all THAI tests with painted surfaces. The painted coupons were produced before each test by painting one coat of metal primer (GEHOPON E24) and typically two finishing coats (GEHOPON EW 10, colour RAL 1013), to obtain a total thickness of the coating of 150 - 200  $\mu\text{m}$  after drying in ambient conditions.

Artificial ageing of the painted surfaces was always performed by heating the painted coupons for 21 hours at 160  $^\circ\text{C}$  or 24 hours at 155  $^\circ\text{C}$ . According to [DIN 2578] and Siemens data underlying the  $\text{I}_2$ /paint tests in [Hellmann 1996], the Arrhenius-type expression  $t_1 / t_2 = \exp\{8816 \cdot (1/T_1 - 1/T_2)\}$  was used to correlate simulated ageing and artificial heating temperatures ( $T_1$ ,  $T_2$  in Kelvin,  $T_1=303$  K) with artificial and simulated ageing times ( $t_1$ ,  $t_2$ ). For the above THAI ageing conditions, a simulated ageing at plant operation conditions of 15 years is thus estimated. The norm [DIN 2578] is aiming at optical, mechanical and electrical properties, but not on chemical properties, so the simulated age can only be considered as an estimate.

Advantages of always performing this same ageing procedure with the same paint material is that (1) all THAI  $\text{I}_2$  / paint tests can directly be compared to each other, and that (2) the  $\text{I}_2$  / paint tests from THAI can directly be compared to earlier laboratory-scale tests [Hellmann 1996]. It was concluded in [Hellmann 1996] that the  $\text{I}_2$  deposition kinetics on paint did not depend on ageing, whether ageing was for 20 weeks at ambient conditions or artificially heated to simulate 10 years (1000 hours at 80  $^\circ\text{C}$ , 24 hours at 125  $^\circ\text{C}$ , using the above equation). However, this conclusion was based upon comparing only two tests, and these two tests were run in condensing conditions at 160  $^\circ\text{C}$ , so that simultaneous iodine wash-off by the condensate flow was strongly interfering with persistent iodine deposition and could have masked an effect of ageing on  $\text{I}_2$  deposition onto dry paint.

After mounting into the THAI vessel, the painted surfaces are washed together with the whole vessel before a THAI iodine test by condensing steam from subsequent steam injections for cleaning purposes.

The above estimation of a simulated age only considers thermal ageing of paint in dry air and does not consider the effect radiation or humidity in containment, during normal operation and during severe accidents, for which no model is available.

The described pre-treatment of the paint applied in THAI tests adds to the several different pre-treatments applied in other relevant projects world-wide, see e.g. [Bosland 2014]. As the iodine / paint reactions are also depending on the pre-treatment procedure, a model to include the effect of pre-treatment on iodine / paint interaction would be desirable to enable comparison of the different experimental projects with differing pre-treatments.

#### Test procedure

An iodine test in THAI is usually initiated by injecting radio-labelled gaseous  $\text{I}_2$  into the dome part of the THAI vessel within a few minutes. In the single-compartment tests atmospheric convection leads to homogeneous  $\text{I}_2$  mixing within < 15 min. During a first test phase, typically lasting a couple of hours or even longer, iodine deposition on the walls and the mounted

deposition coupons is taking place while thermal-hydraulic boundary condition are kept constant. In further test phases, one or more boundary condition(s) are changed and the iodine measurements are continued to measure the impact of the different boundary conditions on the iodine behaviour. Such changes typically include e.g. increase / decrease of temperature, increase / decrease of relative humidity, switching on condensation of steam, and injection of aerosol. In the multi-compartment tests the atmospheric mixing conditions within the vessel were changed additionally.

Vessel pressures are typically between 1.2 and 2 bar, mainly depending on steam injection, and they usually change during the tests and the different tests phases. Even in tests without steam a slight over-pressure is nearly always used for a convenient operation of the iodine sampling instrumentation.

#### Test matrix

Table 1 summarises all I<sub>2</sub> / paint and I<sub>2</sub> / aerosol interaction tests in THAI.

### III. REACTION OF GASEOUS I<sub>2</sub> WITH DRY PAINTED SURFACES

#### Experimental phenomena

The general I<sub>2</sub> behaviour after injection is the spreading and dilution of the initial, concentrated I<sub>2</sub> cloud by transport with the atmospheric flows inside the vessel. Homogeneously mixed I<sub>2</sub> is typically achieved within less than 15 min in single-compartment tests. In parallel and during the further test periods, the I<sub>2</sub> is deposited onto surfaces, which decreases the atmospheric I<sub>2</sub> concentration. In the absence of painted surfaces, the large steel wall surfaces alone are removing a fraction of the gaseous I<sub>2</sub>, depending on relative humidity and temperature. The persistent gaseous I<sub>2</sub> concentration is due to the equilibration between I<sub>2</sub> desorption from the steel walls and the I<sub>2</sub> chemisorption onto paint.

The test Iod-17 is exemplarily discussed to demonstrate the additional phenomena introduced by painted surfaces (10.3 m<sup>2</sup>). Fig. 2 shows that the gaseous I<sub>2</sub> is decreased by

2 orders of magnitude within the first 4 - 5 hours. The 116 m<sup>2</sup> of stainless steel in this test alone would decrease the gaseous I<sub>2</sub> only by much less than one order of magnitude. The I<sub>2</sub> / paint interaction is therefore significantly influencing the I<sub>2</sub> behaviour in the steel vessel during test Iod-17.

During the transition phase, where temperature was increased from 75°C up to 120°C by heating of the vessel walls, the decrease of the gaseous I<sub>2</sub> concentrations stops (Fig. 2). Even a small, temporary increase of gaseous I<sub>2</sub> at 8-10 hours could have occurred. Obviously, I<sub>2</sub> desorption from steel surfaces and deposition on painted surfaces is taking place. Accordingly, a relatively constant level of gaseous I<sub>2</sub> is present in the gas phase during the I<sub>2</sub> relocation between steel and painted surfaces.

The evolution of iodine deposits on a painted coupon is shown in Fig. 3. During the first 5 hours, I<sub>2</sub> is accumulating quickly and approaches a saturation level. During the 120°C phase, there is a very slight increase of the iodine loading, and this is explained by the I<sub>2</sub> desorbed from the heated steel surfaces. Obviously, I<sub>2</sub> is relocated from steel to paint.

The online monitored painted coupon was temporarily heated up twice, at 2.5 h and at 10.5 h up, to about 130°C. No desorption is observed, and this indicates that the iodine on the paint is mainly efficiently bound, i.e. chemisorbed, in contrast to being weakly physisorbed.

The specific iodine loading on recovered paint coupons at the end of the test is almost the same as for the non-recovered, online-monitored deposition coupon (52 mg/m<sup>2</sup>, uncertainty of factor 2 possible based upon long-term experience in THAI). A set of smaller painted coupons had a specific iodine loading of 82 mg/m<sup>2</sup> (std. dev. ~ 19 %), a set of larger painted coupons was at 70 mg/m<sup>2</sup> (std. dev. ~ 16 %). The loadings on neighbouring recovered steel coupons were 1.7 (small coupons) and 0.6 mg/m<sup>2</sup> (large coupons), at std. dev.'s ~ 36 and 26 %. Although local effects can introduce significant uncertainties on the detailed iodine loadings, the paint is more efficient in

bounding  $I_2$  than steel by factors of 50-100 in the conditions of test Iod-17.

Gaseous organic iodide concentrations, obtained from Maypack filters, are generally low. Thermal production of volatile organic iodide on iodine-loaded painted surfaces is only weak and generally does not influence the analyses and assessments of the iodine behaviour in the THAI tests.

### Modelling

As the stainless steel walls of the THAI vessel (steel 1.4571, ~AISI 316Ti) represents an  $I_2$  deposition area in the range of 100 - 160 m<sup>2</sup> (depending on use of internal structures, 116 m<sup>2</sup> in Iod-17), the  $I_2$ /steel interaction is always significantly influencing the  $I_2$  behaviour. An  $I_2$ /steel interaction model was therefore developed based on a number of THAI tests with only steel surfaces. The model enables to numerically discriminate the  $I_2$ /steel effect in tests to study the  $I_2$ /paint or  $I_2$ /aerosol interaction. The  $I_2$ /steel model considers two steps, (i) physisorption of  $I_2$ , and (ii) conversion of physisorbed  $I_2$  into chemisorbed iodine ("FeI<sub>2</sub>"), going back to a concept described in [Wren 2001] and included in AIM-3 [Weber 2012]. The chemisorption step is strongly depending on the relative humidity, so that it is essential in analyses of THAI tests with gaseous  $I_2$  to precisely know the relative humidity, either from humidity sensors and / or from steam mass balances.

An  $I_2$ /paint deposition / desorption model was developed according to the  $I_2$ /steel model and based upon the single-compartment tests Iod-15, Iod-17, and Iod-20 with generally similar  $I_2$  phenomena (Fig. 4). It consists of two steps, according to the concept of the  $I_2$ /THAI steel model in AIM-3. The first step is physisorption of  $I_2$  onto dry paint. The second step is the conversion of deposited  $I_2$  on the paint into chemisorbed iodine on paint. The release of  $I_2$  from paint back into the gas phase is only possible through desorption of physisorbed  $I_2$ . The release of chemisorbed iodine from paint into the gas phase is possible in AIM-3, but requires the formation of volatile organic iodide, induced thermally or by radiation. Organic iodide is almost of low importance in THAI tests, as

there is no radiation and as thermal organic iodide production is relatively weak.

In the model of  $I_2$ /paint interaction physisorption is depending on temperature but not yet chemisorption. It does not depend on relative humidity, unlike the  $I_2$ /steel model, because no effect of relative humidity was detected in the underlying THAI older tests performed in a significant but narrow band of relative humidity, and because more recent NEA BIP results on  $I_2$ /paint deposition depending on relative humidity as well as Iod-27A, in which relative humidity was only < 1 %, did not yet exist. The solid line in Fig. 2 represents the results of an AIM-3 calculation including both, the  $I_2$ /steel and the  $I_2$ /paint deposition model. Whereas the gaseous  $I_2$  concentrations from an  $I_2$ /paint test without desorption phase, Iod-15 (no Figure), where reproduced very well, the model is not fully satisfactory during the transition phase and hot phase in test Iod-17: during the heat-up measured gaseous  $I_2$  seems to be slightly underestimated, and during the hot phase  $I_2$  is overestimated. Reasons are probably non-optimal rate constants for  $I_2$  desorption from steel and/or paint, and non-optimal rate constants for conversion of physisorbed  $I_2$  into chemisorbed iodine on the paint.

The later THAI test Iod-27A, a multi-compartment test with  $I_2$  injection into the dome compartment and the painted surfaces mounted only in lower compartments, was performed in air without any steam. The multi-compartment issue is discussed in Gupta's paper 1.4 of this Workshop. The  $I_2$ /paint interaction in Iod-27A is of relevance as the effect on iodine behaviour was surprisingly small. Fig. 5 displays the specific iodine loading on paint and steel coupons in test Iod-27A, and it reveals surprisingly low iodine loading on the paint. Further THAI multi-compartment tests including painted surfaces, high relative humidity, and aerosol, Iod-28 and Iod-30, have recently been performed, also with a focus on the low effect of paint in the very dry Iod-27A.

To establish a comparison of all  $I_2$ /paint tests with dry paint, so-called distribution coefficients ( $K_D$ ) were derived from all relevant THAI tests.  $K_D$  is defined as the ratio of the specific iodine loading on paint at the end of a test or the end of

a representative test phase ("final loading"), and the corresponding, representative I<sub>2</sub> gas phase concentration. The derived K<sub>D</sub> values (Fig. 6) lie fully within the broad range of values from older laboratory-scale tests for different paints and different ageing, as compiled in [Sims 1997]. The K<sub>D</sub> values from THAI tests are increasing with relative humidity, namely by a factor of about 25 when increasing from nearly zero to nearly 80 % relative humidity. This goes along with the increase of the deposition rate constant for I<sub>2</sub> onto Ripolin epoxy paint as recently measured in the NEA BIP project for other paint types. It is noted, without specific figure, that K<sub>D</sub> does not depend on temperature in the studied range from 60 to 100°C.

The multi-compartment tests Iod-27A and Iod-28 included helium to support dissolution of atmospheric stratification and as a tracer for atmospheric mixing in the tests, at concentration levels of 12-13 % in the mixed test phases. It was speculated whether helium would hinder I<sub>2</sub> deposition by intrusion into the paint where it could then block further I<sub>2</sub> adsorption. Helium was not used in the multi-compartment test Iod-30, and Fig. 6 suggests that there is no such helium effect.

It will be necessary to include the dependency of the I<sub>2</sub> deposition onto paint on relative humidity into the AIM-3 model. Additional laboratory-scale tests, including the parameters age and type of ageing, type of paint, and temperature would be helpful. Whether relative humidity or steam concentration is a relevant parameter for the I<sub>2</sub> adsorption on paint, is currently discussed but not concluded in BIP.

Current GRS plant calculations with AIM-3 reveal surprisingly high fractions of physisorbed I<sub>2</sub> on paint and, as a consequence, desorption of I<sub>2</sub> is rather strong so that very high iodine amounts in the containment atmosphere are resulting. With a modified model more analyses will be necessary on this issue, also considering the length of adsorption phase in BIP (up to 70 hours at constant I<sub>2</sub> level) being much longer than in THAI tests (significant but quickly decreasing I<sub>2</sub> concentrations only during the first few hours). The longer adsorption phase should even more favour the fraction of chemisorbed iodine on the paint.

#### IV. INTERACTION OF GASEOUS I<sub>2</sub> WITH WET PAINTED SURFACE

##### Experimental phenomena

THAI tests in condensing conditions and producing wet wall surfaces showed that there is no closed water film on the paint, but that small local and short-lived rivulets are formed at changing locations. Upon flowing downwards and integrated over a time period of hours, the whole painted surface can be considered to be washed off by the condensate. Besides gaseous I<sub>2</sub> deposition on paint as in dry conditions, a fraction of the I<sub>2</sub> is penetrating into a water layer on the paint before interacting with the paint. The downward flow of the condensate can transport I<sub>2</sub> in the water film directly into a sump without I<sub>2</sub> having reacted with the paint. I<sub>2</sub>, initially deposited on the paint surface, can be washed off by the condensate flow. Reaction of I<sub>2</sub> with paint components and I<sub>2</sub> hydrolysis can produce iodide, which is also washed off and transported into a sump.

THAI test Iod-24 was run to measure the effect of wet painted surfaces (7.4 m<sup>2</sup>) on the removal of gaseous I<sub>2</sub> and on the iodine wash-off into a sump. The painted surfaces were provided in the form of two large deposition bodies with 3.7 m<sup>2</sup> each, which were cooled from the inside by a separate cooling circuit to establish condensation rates at the painted surface representative for PWR containments. Cooling power for the painted bodies, steam injection, and heating of the vessel were operated such that all other surfaces remained dry besides the paint. One painted body was run at a low condensation rate of 0.13 g/(m<sup>2</sup>·s), and the other at a high condensation 1.2 g/(m<sup>2</sup>·s). I<sub>2</sub> was injected into the phase of condensing conditions, and the iodine deposition and wash-off was measured for 13.5 hours at constant condensation rates, followed by a subsequent dry-out phase. The gas temperature was 100°C, the relative humidity 90 %.

At the end of the test, 19 % of the injected I<sub>2</sub> was found in the sump, from I<sub>2</sub> wash-off from cool steel tubes required for the cooling circuit of the painted bodies, and from I<sub>2</sub> mass transfer at the gas/liquid interface. Another 24 % was on the vessel steel surfaces. The non-washed iodine

deposition on both paints was 25 %, and the iodine wash-off was 23 % from the paint with the higher condensation rate, and 9 % from the paint with the lower condensation rate.

Iodine concentrations in the condensate are shown in Fig. 7. With a small delay caused by the condensate transport to the sampling station, the decreasing iodine concentrations in the condensates are qualitatively going along with the decreasing iodine concentrations in the atmosphere (see Fig. 8). The iodine concentration in the condensate with the higher rate is a factor 0.25 lower than in the condensate with the lower rate. Qualitatively, this is understood as a consequence of the higher iodine dilution at the higher condensation rate. The iodine wash-off rates and the integrated amounts of iodine wash-off are higher by factors of about 2 at the higher condensation rate.

There was almost no  $I_2$  in the condensate, as measured by UV/VIS. Obviously, conversion of  $I_2$  into other iodine species took place, either during the test itself or in the time between samplings and their analyses. The pH of the condensate was 4.5 to 5 during the whole test Iod-24. Gaseous  $I_2$  decreased by two orders of magnitude within the first 6 hours.

#### Modeling

The interaction of gaseous  $I_2$  with painted surfaces in condensing conditions is modeled in AIM-3.  $I_2$  physisorption and conversion into chemisorbed iodine are similar to the dry case. Iodine wash-off in the form of  $I_2$  or iodide are additional phenomena. The model is based upon laboratory-scale tests [Hellmann 1996] and representative for experimental condensation rates at 0.4 to 0.44 g/(m<sup>2</sup>·s) at T = 160°C. The condensation rate is no explicit parameter in the model. The  $I_2$  fraction washed off immediately after deposition is fixed at 68 % (Iod-24 at low condensation rate 38 %, at high condensation rate 69 %).

Due to the short-comings of the AIM-3 model, a more detailed model was developed at GRS in the course of the preparation of test Iod-24, using a film-based approach. The water film in each zone is simulated by a flat water pool, through which the condensate is flowing. Iodine chemistry is similar to that in the sump. The

thickness of the water film is provided by the user. The iodine sump chemistry in AIM-3 is applied to the water film, including the iodine reactions with immersed painted surfaces. Gaseous  $I_2$  depositing onto paint needs to first penetrate the water film by the known interfacial mass transfer at the gas/liquid interface before reacting with the immersed paint. The pH value of the water film is required as an input.

Fig. 7 compares model calculations of iodine concentrations in the condensates using a water film thickness of 65 µm. High (upper) and low (lower) condensation rate at the two painted bodies are considered. Fig. 8 compares equivalent  $I_2$  model concentrations with measured data in the gas phase. Additional parameters variations, not shown here, indicate the potential of the model for further optimisation. The accumulated iodine loading on the painted surfaces is also reasonably reproduced by the model. Test Iod-21 with wet painted surfaces in the 2nd test phase is providing more data for further model development, these analyses have not yet been performed.

#### V. REACTION OF GASEOUS $I_2$ WITH AEROSOLS

The reaction of gaseous  $I_2$  with aerosols was studied in the THAI tests Iod-25 and Iod-26. Both tests were run at about 70°C and in air atmosphere without steam. These tests were supported by laboratory-scale tests to study the  $I_2$  adsorption / desorption behaviour of various materials in various boundary conditions.

In Iod-25, tin oxide (SnO<sub>2</sub>) aerosol was injected to provide a non-reactive, inert aerosol, where gaseous  $I_2$  should only be influenced by weak physisorption onto the particles. In Iod-26, silver (Ag) aerosol was injected to provide a reactive aerosol, where gaseous  $I_2$  should be chemisorbed, i.e. bound as AgI, on the surface of the particles.

Both tests Iod-25 and Iod-26 were essentially run identically: the first test phase was to inject  $I_2$  and to measure the small effect of  $I_2$  depletion by the steel walls. In the second test phase, a puff release of aerosol was performed to achieve a high and representative aerosol concentration, which is depleting in the course of this test

phase. In a third test phase, aerosol was injected continuously, to keep the aerosol concentration on a constant level. The aerosol mass concentrations showed similar evolutions, the Ag aerosol is shown in Fig. 9.

Gas scrubbers 1, 4, 5, and 6 measured the total airborne iodine, i.e. potentially gaseous  $I_2$  plus aerosol-bound iodine. Gas scrubbers 2 and 3 were equipped with aerosol pre-filters, so they were measuring always only  $I_2$ .

Upon injecting  $SnO_2$  aerosol in Iod-25, an accelerated iodine removal from the vessel atmosphere takes place (Fig. 10). However, the injection of Ag in Iod-26 is clearly more efficient in removing gas-borne iodine (Fig. 11). The fast and complete decrease of the gaseous  $I_2$  concentrations in the Ag test is demonstrated by the results of gas scrubbers 2 and 3.

Maypack measurements also show that Ag aerosol was efficiently trapping the gaseous  $I_2$  within a few minutes, and that iodine was in an aerosol form for the rest of the test. In contrast, during the whole  $SnO_2$  test, gaseous  $I_2$  remained the predominant iodine species, and iodine in the aerosol form was only on a percent level.

The specific iodine loadings on the different aerosol materials were visualised by monitoring iodine deposition on local deposition coupons covered by  $SnO_2$  powder or covered by an Ag foil, although these material forms may not be fully representative of the surface area of an aerosol. The  $I_2$  loading on the  $SnO_2$  coupon was very similar to the  $I_2$  loading on steel. The iodine loading on Ag foil was higher than on steel by more than two orders of magnitude at the end of the test (Fig. 12).

Whereas the  $I_2$  removal from the vessel atmosphere in the Ag test is governed by the settling rate of the Ag/AgI particles, the  $I_2$  removal by  $SnO_2$  aerosol is strongly influenced by  $I_2$  desorption from  $SnO_2$  surfaces. This also includes desorption from  $I_2$ -loaded  $SnO_2$  particles that had already been deposited at the bottom. The net difference of the  $I_2$  removal efficiency in the two THAI tests is about a factor of 4, as obtained from comparing Fig. 10 and Fig. 11.

A future detailed kinetic analysis of the iodine decreases by deposition onto settling aerosols

needs to consider that the injected aerosol was poly-disperse in both cases,  $SnO_2$  and Ag. The log-normal size distribution had a geometric standard deviation of 2.0 respectively 1.8. The larger particles are settling faster than the smaller ones, but the smaller, more persistent particles are providing the larger surface area and thus a larger iodine adsorption. Consequently, the removal of trapped iodine from the vessel atmosphere by settling is somewhat slower than the overall aerosol settling.

Laboratory-scale tests were performed in support of the THAI tests Iod-25 and Iod-26, to study the effects of a limited number of conceivable chemical parameters. Temperatures and relative humidity were also varied. Radio-labelled  $I_2$  was passed over thin powder layers of several materials, which circumvents the difficulty of providing suspended particles in these simple chemistry tests. The accumulating iodine adsorption on the powder was monitored for typically 2 - 3 hours. Thereafter, the  $I_2$  was eliminated from the carrier gas flow and desorption phases were thus performed for some additional hours. The relative humidity at the point of the powder was mostly at a percent level, resulting purely from passing nitrogen as a carrier gas over an aqueous  $I_2$  source. The iodine loading decreased from Ag powder (same powder as in Iod-26), cesium iodide (CsI) crystals and iron (Fe) chips down to  $SnO_2$  powder, iodine on  $SnO_2$  even remained below the detection limit. No iodine desorption from Ag and Fe was measured, indicating strong chemisorption. Adsorption was fast in the beginning and then slowed down to apparently achieve saturation of the iodine loading. No temperature dependency (80°C - 140°C) was measured for the initial adsorption rate in the  $I_2$  interaction with Ag. The specific iodine loading on Ag particles increases with the  $I_2$  concentration.

Fig. 13 shows  $K_D$  values obtained from the laboratory tests, together with the range of  $K_D$  values from the THAI tests with paint (see Fig. 6). The Ag reactivity at 80 - 93°C is at the upper range of paint reactivity from THAI tests. For the Ag reactivity, a small influence of relative humidity as well as on temperature cannot be excluded. For the  $SnO_2$  powder, no

iodine loading was measured, corresponding to its expected inert character. Iron (Fe) powder is less reactive than Ag powder by at least one order of magnitude, and the iodine loading on Fe clearly decreases with temperature. The CsI reactivity at 80°C is surprisingly high. At 140°C, iodine loadings are generally lower than at the lower temperatures.

## VI. CONCLUSION

The reaction of gaseous I<sub>2</sub> with painted surfaces was addressed in a number of THAI tests (Iod-15, Iod-17, Iod-20, Iod-21, Iod-24, Iod-27A, Iod-28, and Iod-30). The experimental work was accompanied by analytical work to specify the tests, to improve existing models, and to develop new models.

For I<sub>2</sub> reaction with dry surfaces in THAI, an empirical deposition / desorption model was developed, but it still needs more refinements: (1) paint used is a German epoxy paint, and there is no connection to compare its behaviour versus iodine with the effects of other paints, (2) ageing of paint is not explicitly scaled but always referring to 15 years, (3) ageing procedure is different from other experimental programs and a deeper analysis of this issue including connecting tests is necessary, (4) modeling of the effects of relative humidity and temperature on the chemisorption reaction is to be developed, (5) the partitioning between physisorbed and chemisorbed iodine on paint is adapted to produce the correct high fraction of chemisorbed iodine, this issue could entrain the necessity of further tests in the laboratory-scale.

The on-going international development of a mechanistic iodine/paint model could provide answers to the above issues from the empirical model. However, this work including also a consistent release model for organic iodide is far from being completed. Nevertheless, semi-empirical models will still be required by accident codes for plant applications.

The reaction of gaseous I<sub>2</sub> with wet painted surfaces is qualitatively providing the expected phenomena, but a new model was designed and preliminary adjusted to THAI test Iod-24. More

analytical work is necessary for optimisation, including e.g. the wet phase of THAI test Iod-21.

The two THAI tests on the I<sub>2</sub> / aerosol reactions (Iod-25, Iod-26) are providing the effect of I<sub>2</sub> removal from containment atmospheres by interaction with containment aerosol, the reactive Ag aerosol providing the maximum reactivity, and the inert SnO<sub>2</sub> the minimum reactivity under the given boundary conditions of the tests. The I<sub>2</sub> reaction with the Ag particle surface is as high as for the higher range of I<sub>2</sub> / paint reactions, as evident from comparison of large-scale and laboratory-scale tests in THAI. Real containment aerosol mixed of different materials can be expected to exhibit I<sub>2</sub> removal rates between the investigated bounding cases "reactive Ag" and "inert SnO<sub>2</sub>". If source term analyses reveal a significant effect of the I<sub>2</sub> / aerosol interaction in the containment, the actual surface reactivity of an aerosol defined by the thermochemical phases available to gaseous I<sub>2</sub> needs to be interpolated between the bounding cases "reactive Ag" and "inert SnO<sub>2</sub>". Additional tests using a more realistic aerosol (e.g. from simulated core melts) could turn out necessary, as well as the study of an effect of steam.

## ACKNOWLEDGMENTS

The THAI tests reported in this document were funded by the German Federal Ministry for Economic Affairs and Energy (BMWi) in the frame of the reactor safety research projects 150 1272, 150 1325, 150 1361, 150 1420, and 150 1455.

The THAI tests Iod-25, Iod-26, and the associated lab-scale tests were additionally funded by the partners of the OECD THAI-2 project (2011-2014).

## NOMENCLATURE

AIM-3: Advanced Iodine Model [Weber 2009]

COCOSYS: Containment Code System  
[Klein-Heßling 2013]

THAI: Thermal Hydraulics, Hydrogen,  
Aerosols, Iodine.

## REFERENCES

[Bosland 2014]: L. BOSLAND et al., "Iodine-paint interactions during nuclear reactor severe accidents", *Annals of Nuclear Energy*, **74**, 184–199 (2014).

[DIN 2578]: "Kunststoffe: Bestimmung der Temperatur-Zeit-Grenzen bei langanhaltender Wärmeeinwirkung", European standard EN ISO 2578 : 1998 corresponding to German standard DIN EN ISO 2578, October 1998.

[Hellmann 1996]: S. HELLMANN et al., "The reaction between iodine and organic coatings under severe PWR accident conditions. An experimental parameter study", *Proc. of the 4th OECD/CSNI Workshop on the Chemistry of Iodine in Reactor Safety*, p.345 - 365, PSI, Würenlingen, Switzerland (1996)

[Klein-Heßling 2013]: W. KLEIN-HESSLING et al., "COCOSYS V 2.4 user's manual", Revision 0, GRS, April 2013

[Sims 1997]: H. E. SIMS et al., "Iodine behavior in containment - the reaction of iodine with surfaces", EPRI report ACEX TR-B-06, Draft (1997)

[Weber 2009]: G. WEBER et al., "Description of the iodine model AIM-3 in COCOSYS", GRS report A-3508, November 2009

[Weber 2012]: G. WEBER et al., "Thermal-hydraulic-iodine chemistry coupling: Insights gained from the SARNET benchmark on the THAI experiments Iod-11 and Iod-12", *Nuclear Engineering and Design*, **265**, 95–107 (2013).

[Wren 2001]: J. C. WREN et al., "Kinetics of gaseous iodine uptake onto stainless steel during iodine-assisted corrosion," *Nuclear Technology*, **133**, 33–49 (2001).

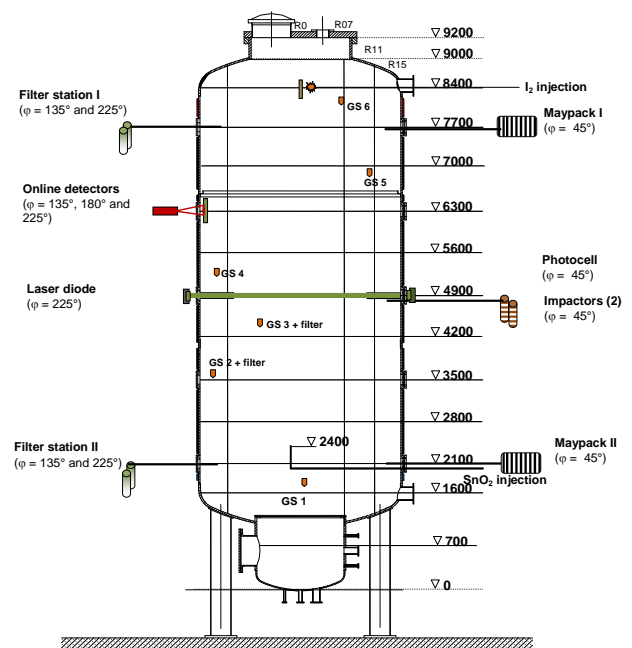


Fig. 1. Sketch of the iodine and aerosol instrumentation in the THAI tests on  $I_2$  reaction with paint and aerosols.

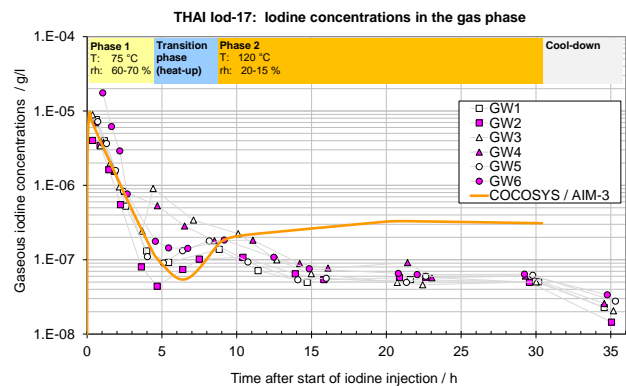


Fig. 2. THAI test Iod-17: Gaseous iodine concentrations in  $I_2$  tests with dry painted surfaces.

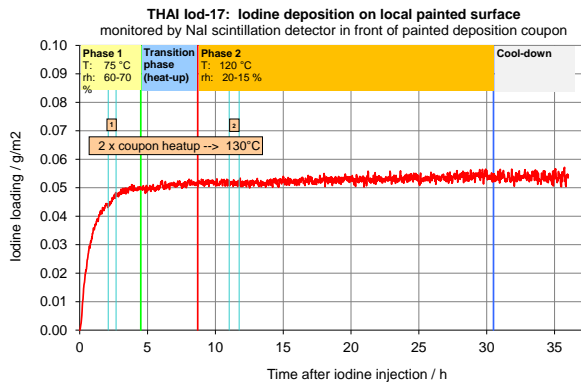


Fig. 3. THAI test Iod-17: Specific iodine loading on local painted surface.

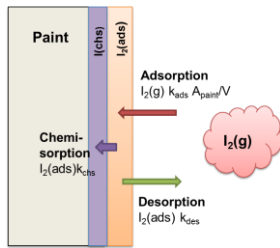


Fig. 4. Two-step model of gaseous I<sub>2</sub> reaction with dry painted surfaces as realised in AIM-3.

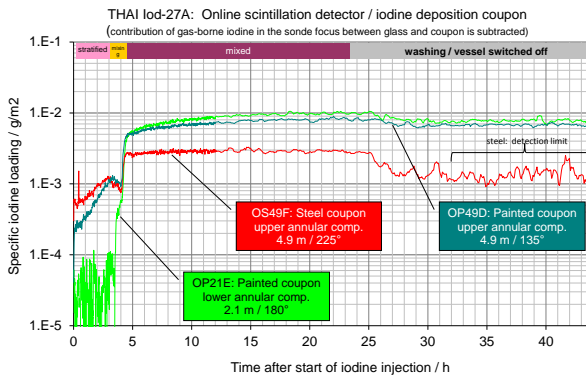


Fig. 5. THAI test Iod-27A: specific iodine loading on painted coupons and steel coupon.

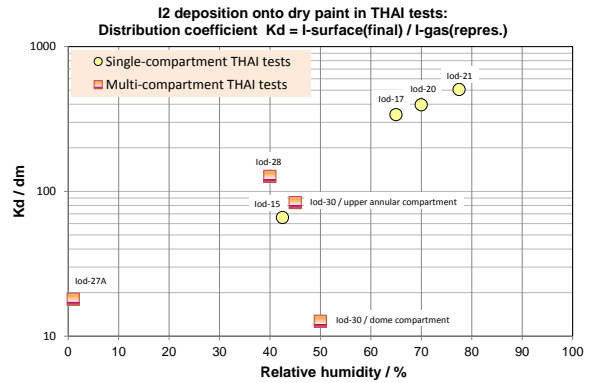


Fig. 6: Distribution coefficients for gaseous I<sub>2</sub> interaction with dry painted surfaces in THAI tests.

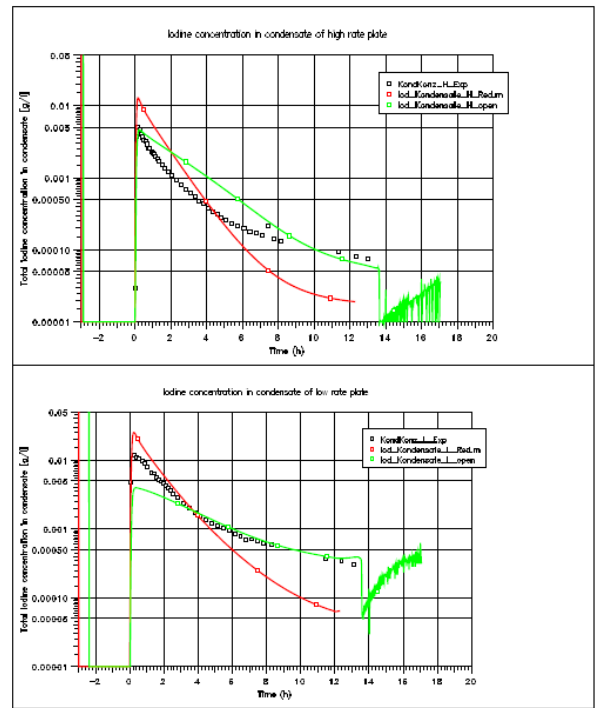


Fig. 7: Test Iod-24: Iodine concentrations in the wall condensates of the painted bodies with high (upper) and low (lower) condensation rate.

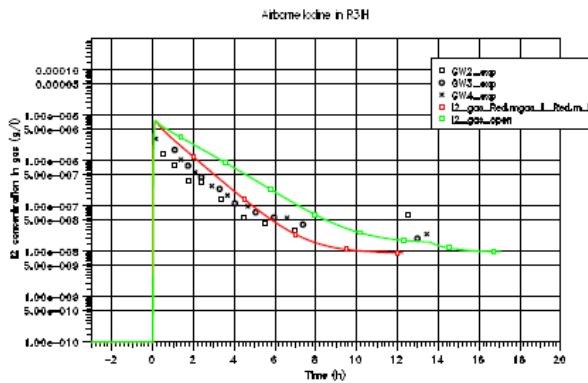


Fig. 8: Test Iod-24: Iodine concentrations in the gas phase (only gas scrubbers 2, 3, and 4), only the first 13.5 hours of are considered.

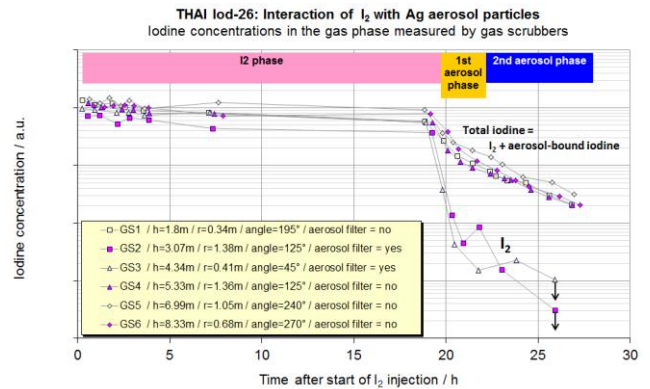


Fig. 11. THAI test Iod-26: Decrease of gas-borne iodine by chemisorption of I<sub>2</sub> onto settling Ag particles.

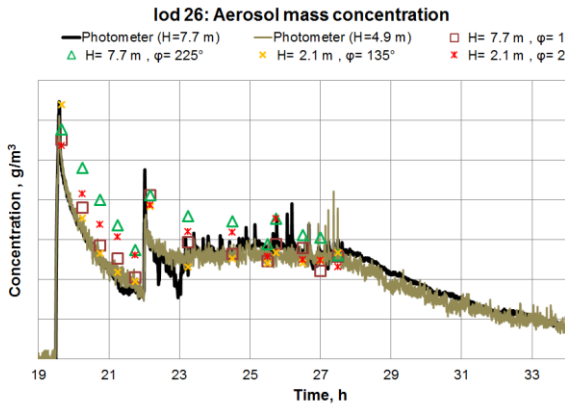


Fig 9. THAI test Iod-26: Ag aerosol mass concentrations.

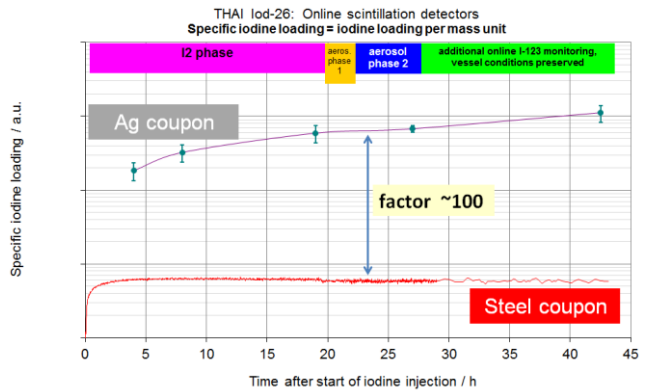


Fig. 12. THAI test Iod-26: specific iodine loading on Ag foil and steel coupon.

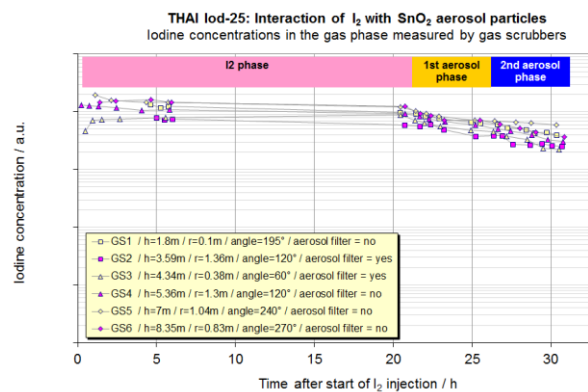


Fig. 10. THAI test Iod-25: Decrease of gas-borne iodine by physisorption of I<sub>2</sub> onto settling SnO<sub>2</sub> particles.

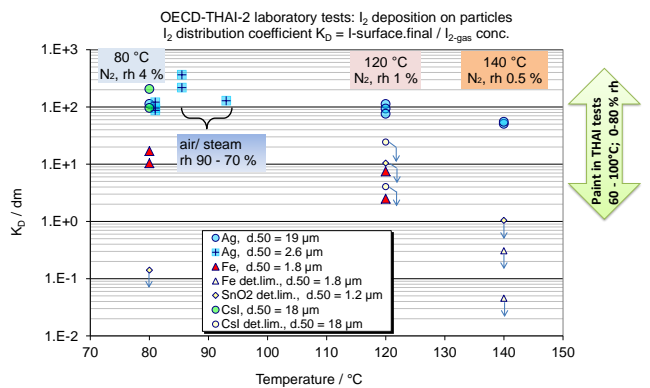


Fig. 13. Distribution coefficients for interaction of gaseous I<sub>2</sub> with dry deposited aerosol particles in laboratory tests.

TABLE I

Test matrix on THAI test to study I<sub>2</sub> interactions with dry and wet paint, and with aerosol.

Test	Gas temp. / °C	Rel. humid. / %	Painted surface state / m <sup>2</sup>	Cond. rate paint / g/(m <sup>2</sup> s)	Aerosol
Iod-15	100	40-45	dry, 20	-	-
Iod-17	75 120	70 20-15	dry, 10.3	-	-
Iod-20	100 130	70 30	dry, 11.3	-	-
Iod-21	100	not eval.	dry, 9 wet, 9	- 0.15	-
Iod-27A	60	< 1	dry, 10.4	-	-
Iod-28	60	40	dry, 10.4	-	-
Iod-30	85 80	45 45	dry, 10.4 dry, 10.4	-	Ag
Iod-24	100	90	wet, 7.4	0.13 / 1.2	-
Iod-25	70	air, no steam	-	-	SnO <sub>2</sub>
Iod-26	70	air, no steam	-	-	Ag

## EFFECT OF WATER-DROPLET SIZES ON THE MIGRATION OF VOLATILE I<sub>2</sub> AND CH<sub>3</sub>I

*Hee-Jung Im(1)\*, Jei-Won Yeon(1), Jin-Ho Song(2)*

*(1) Nuclear Chemistry Research Division, Korea Atomic Energy Research Institute,  
150 Deokjin-dong, Yuseong-gu, Daejeon 305-353, Republic of Korea*

*(2) Severe Accident & PHWR Safety Research Division, Korea Atomic Energy Research Institute,  
150 Deokjin-dong, Yuseong-gu, Daejeon 305-353, Republic of Korea*

*\*Corresponding author, tel: (+82) 428684740, Fax: (+82) 428688148, Email: imhj@kaeri.re.kr*

**Abstract** – Volatile iodine and organic iodide are commonly known to move in gaseous or several types of aerosol forms. Therefore, to study how iodine-related aerosols are formed and behave in the containment of a nuclear power plant and further in the environment, a lab-scale set-up including an I<sub>2</sub> (or CH<sub>3</sub>I) gas generator, a water droplet generator, and an aerosol collector was installed as a single system with steady control. Experimental findings on the migration of I<sub>2</sub> and CH<sub>3</sub>I on water droplets of different sizes are reported using two different analysis methods: a quantitative analysis based on UV-vis and GC-MS. In addition, Ag nanoparticle-embedded blank and ligand-anchored silica gels were synthesized for the future adsorption-property studies of iodine species to investigate the chemical behaviors of iodine from water droplets–air flow.

## I. INTRODUCTION

Iodine is a relatively high fission-yield product and volatile nuclide of nuclear fuel [1]. It can readily interact with steam and water droplets in a nuclear reactor, and the contaminated iodine aerosols formed can be exhausted into the atmosphere during emergency venting or after nuclear power plant damage [2]. The aerosols released can further interact both homogeneously and heterogeneously with tropospheric particulate matter, such as smoke, sea salts, or cloud droplets.

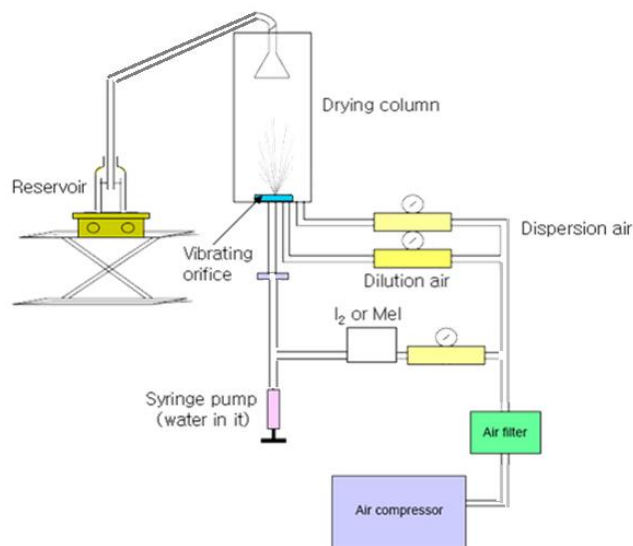
The following experiments were originally planned to look at the effect of water-aerosol sizes on the migration of volatile  $I_2$  and  $CH_3I$  that may occur during an accident in the nuclear reactor containment. The results may also be helpful for an understanding of not only iodine wash-out behavior by water spray but also the  $I_2$  and  $CH_3I$  transfer during an SGTR (Steam Generator Tube Rupture). During such an SGTR accident, the  $I_2$  and  $CH_3I$  are transferred from the primary coolant (liquid phase) into the second system (which contains the two phases) [3].

Since the contaminated iodine aerosols can be easily released into the environment and accumulated in the human body owing to its high volatility, an evaluation of the behavior of the iodine aerosols and a stabilization and determination technique of the aerosols are essential. Therefore, we also synthesized a new sorbent for future studies. Ag metal is as effective as  $Ag^+$  in combining with various iodine species, and inorganic-organic hybrid silica gels are readily mixable, not only in aqueous or organic solutions, but also with gaseous molecules. Thus, Ag nanoparticle-embedded inorganic-organic hybrid silica gels can be good sorbents to adsorb a variety of iodine species in various media. These materials can be used further for the study of chemical behaviors of the iodine and iodide species and stabilizing them.

## II. DESCRIPTION OF EXPERIMENT

The methods used to generate volatile iodine species (such as  $I_2$  and  $CH_3I$ ) that are typically determined in contaminated exhaust air were properly chosen, and water droplets with constant particle sizes were generated and evaporated using the Model 3450 Vibrating Orifice Aerosol Generator (TSI Incorporated, USA) [4]. Each experiment was performed at room temperature, and the approximate inlet iodine mass and volume were controlled to be 0.0254 g of solid  $I_2$  or 0.7 mL of liquid  $CH_3I$ . The generated volatile gases went through a cylindrical water jet with water together and then spread out to certain sizes of water aerosol based on a periodic disturbance of a controlled frequency, to look into their migration from water droplets–air flow [5].

To absorb transferred volatile wet  $I_2$ , a pure water filled bottle and a 0.1 M sodium hydroxide solution filled bottle were composed into a flow type experimental apparatus, as shown in Scheme 1 and Figure 1. However, volatile  $CH_3I$ , unlike  $I_2$ , is not absorbed well by a liquid phase such as a NaOH solution, and thus a Tenax tube, which is filled with a solid sorbent, was used to adsorb transferred volatile wet  $CH_3I$  directly using a mini pump.



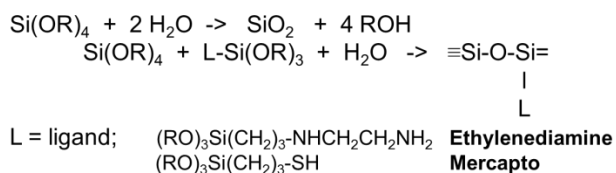
Scheme 1. Schematic diagram of lab scale for a behavioral study of volatile  $I_2$  from water droplets-air flow.



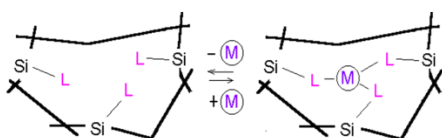
Fig. 1. Photo of lab scale set-up for a behavioral study of volatile I<sub>2</sub> from water droplets-air flow.

Ultraviolet-visible (UV-vis) spectroscopy and gas chromatography-mass spectroscopy (GC-MS) methods were adopted to analyze the transferred I<sub>2</sub> and CH<sub>3</sub>I qualitatively and quantitatively.

As mentioned in the introduction, the sorbents [6] were designed and synthesized in our laboratory for the localization of volatile iodine aerosols [7]. For the preparation of Ag nanoparticle-embedded inorganic-organic hybrid gels, ligands of ethylenediamine (NH<sub>2</sub>CH<sub>2</sub>CH<sub>2</sub>NH-, TMSen) and mercapto (HS-) functionalized three-dimensional porous SiO<sub>2</sub> sol-gels were first synthesized through hydrolysis and condensation reactions [8], and Ag nanoparticles were then embedded into the TMSen- and mercapto-anchored silica gels each, through electron-beam (e-beam) irradiation. The whole process mentioned above is briefly shown in scheme 2.



M = Ag



Scheme 2

### III. RESULTS AND DISCUSSION

“The vibrating orifice monodisperse aerosol generator is based on the instability and break-up of a cylindrical liquid jet. A cylindrical liquid jet broke up into droplets by mechanical disturbances. When these mechanical disturbances were generated at a constant frequency and with sufficient amplitude on a liquid jet of constant velocity, the jet broke up into equal sized droplets [9].” Thus, 0, 38, 42, and 48 μm sizes of water droplets could be generated when 0, 80, 60, and 40 kHz frequencies were applied at a nominal operating condition (20 μm orifice diameter, 20 cm<sup>3</sup> syringe capacity, 8.2 x 10<sup>-4</sup> cm/s syringe pump run speed, and 0.139 cm<sup>3</sup>/min liquid feed rate). The formed monodisperse water droplets were well dispersed with 15 x 100 cm<sup>3</sup>/min air and diluted 40 L/min air before a significant coagulation occurs. Gases of I<sub>2</sub> and CH<sub>3</sub>I were generated at about 60°C and 4°C respectively, and then led to a cylindrical water jet with a volumetric flowrate of 5cc/min (Figure 2).

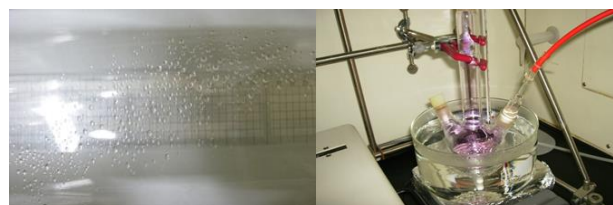
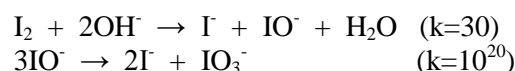


Fig. 2. Monodisperse (48 μm size) water droplets produced by an aerosol generator (left photo) and volatile I<sub>2</sub> produced from solid I<sub>2</sub> by temperature controlling and air flowing (right photo).

The concentrations of I<sup>-</sup>, I<sub>2</sub>, I<sub>3</sub><sup>-</sup>, and CH<sub>3</sub>I in an aqueous phase can be calculated from the absorbancies at 226, 460, 288 (or 350), and 250 nm of obtained UV-vis spectra respectively. Based on the following equations,



the concentrations of transferred volatile wet I<sub>2</sub> can be calculated from the absorbance of I<sup>-</sup> at

226 nm when the 0.1 M NaOH solution is an absorbing liquid.

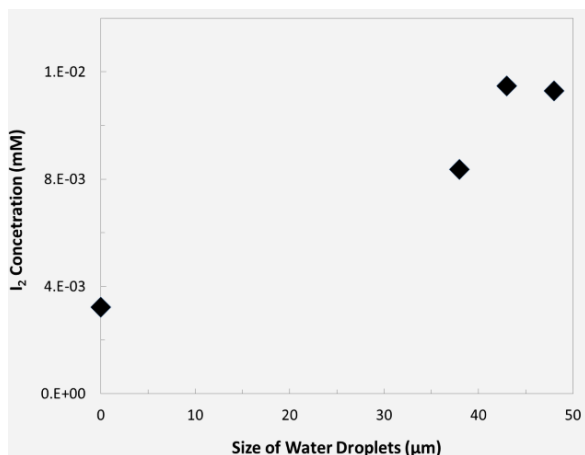


Fig. 3. Relationship between transferred volatile I<sub>2</sub> concentrations and water droplet sizes when each of the approximate inlet iodine concentration was 0.0254 g of solid I<sub>2</sub>.

As shown in Figure 3, the amount of transferred volatile iodine was strongly influenced by the existence of water. However, small changes in water-droplet sizes did not influence the transfer of volatile iodine much compared to the case of I<sub>2</sub>, but a larger amount of I<sub>2</sub> was transferred with a bigger sized water droplet than a smaller one when the same amount of water was applied. Similar results were also obtained for volatile CH<sub>3</sub>I transfer in the case of size changes in the water droplets. Hydrolysis reaction rates of I<sub>2</sub> and CH<sub>3</sub>I with water are very slow in comparison with physical weathering and physical dissolution, and they are only slightly soluble in water. Thus, smaller sized (higher surface areas) water droplets did not help the transfer of the volatile wet I<sub>2</sub> and CH<sub>3</sub>I.

In the case of our synthesized sorbents, the addition of ligands yielded a larger average pore size than the absence of any ligand. Moreover, the TMSen ligand led to looser structures and better access of the Ag nanoparticles to the TMSen-anchored gel. As a result, more Ag nanoparticles were introduced into the TMSen-anchored gel. The preparation and

characterization of Ag nanoparticle-embedded blank and ligand-anchored silica gels will be discussed in detail during the IODE workshop. The color of the blank and ligand-anchored gels, **1-3**, changed from colorless to a brownish color in gels **4-6** after e-beam irradiation in a AgNO<sub>3</sub> solution, as shown in Figure 4. The ICP-AES results of the remaining Ag concentrations in each AgNO<sub>3</sub> aqueous phase after the e-beam irradiation of gels **1-3** were as follows: The starting Ag concentration of 516.5 (± 0.5) μg/mL in the solution was significantly decreased to 18.35 (± 0.15), 0.91 (± 0.01), and 3.645 (± 0.025) μg/mL, respectively. Around 4.618, 4.780, and 4.755 mmol of Ag were embedded into each 10 g of a blank gel, and TMSen- and mercapto-anchored gels. Upon immersing the blank and TMSen- and mercapto-anchored gels into the AgNO<sub>3</sub> solutions, Ag-nanoparticle suspensions, which were reduced as Ag metals from Ag<sup>+</sup> of AgNO<sub>3</sub> by e-beam irradiation were spontaneously adsorbed into these gels owing to a strong covalent bonding between the silver and ligands of ethylenediamine and thiol groups, or pores produced in three-dimensional structures.



Fig. 4. Photo of blank and TMSen- and mercapto-anchored gels **1-3**, and Ag nanoparticle-embedded blank and TMSen- and mercapto-anchored gels **4-6** (180 – 600 μm sizes).

#### IV. CONCLUSION

The generated volatile iodine gases have been introduced into the water droplets-air flow to look into aerosol related behavior, and several spectroscopic methods were applied for a quantitative look. In addition, Ag nanoparticles were successfully embedded into blank and TMSen- and mercapto-anchored gels through e-beam irradiation. These Ag nanoparticle-

embedded blank and ligand-anchored gels are ready for the adsorption-property studies of iodine species to investigate the chemical behaviors of iodine from water droplets–air flow, and to define the chemically stable condition of the products in it.

#### ACKNOWLEDGMENTS

This work was supported by the Nuclear Research and Development program of the National Research Foundation of Korea (NRF) grant funded by the Korea government (MSIP).

#### REFERENCES

1. B. Clément, L. Cantrel, G. Ducros, F. Funke, L. Herranz, A. Rydl, G. Weber, and C. Wren, *State of the Art Report on Iodine Chemistry*, Report NEA/CSNI, no. R1 (2007).
2. H.-J. Allelein, A. Auvinen, J. Ball, S. Guntay, L. E. Herranz, A. Hidaka, A. V. Jones, M. Kissane, D. Powers, and G. Weber, *State of the Art Report on Nuclear Aerosols*, Report NEA/CSNI, no. R5 (2009).
3. A. Cartonnet, *Contribution à l'étude de rejet à l'environnement de l'iode radioactif lors d'une séquence accidentelle de type RTGV*, Doctor Thesis, University of Lille & the IRSN (2013).
4. Instruction Manual, *Model 3450 Vibrating Orifice Aerosol Generator*, P/N 1933450, Revision L (TSI, October 2002).
5. G. Brenn and U. Lackermeier, "Drop formation from a vibrating orifice generator driven by modulated electrical signals", *Phys. Fluids*, **9**, 3658 (1997).
6. H.-J. Im, B. C. Lee, and J.-W. Yeon, "Preparation and characterization of Ag nanoparticle-embedded blank and ligand-anchored silica gels", *J. Nanosci. Nanotechnol.* **13**, 7643 (2013).
7. D. R. Haefner and T. J. Tranter, *Methods of gas phase capture of iodine from fuel reprocessing off-gas: A literature survey*, Report INL/EXT-07-12299 (2007).
8. H.-J. Im, Y. Yang, L. R. Allain, C. E. Barnes, S. Dai, and Z. Xue, "Functionalized sol-gels for selective copper(II) separation", *Environ. Sci. Technol.* **34**, 2209 (2000).
9. R. N. Berglund and B. Y. H. Liu, "Generation of Monodisperse Aerosol Standards", *Environ. Sci. Technol.* **7**, 147 (1973).



**Session 4: filtered containment venting systems**

## WESTINGHOUSE MOLECULAR SIEVE TECHNOLOGY

*Dr. Anders Andrén(1)\*, Dr. Ralf Obenland(2)*

*(1) Westinghouse Electric Sweden AB, Engineering Equipment & Major Projects, 721 63 Västerås, Sweden,*

*(2) Westinghouse Electric Germany GmbH, 68167 Mannheim, Germany*

*\*Corresponding author, tel: (+46) 732367765, Fax: (+46) 21414190, Email:andrenal@westinghouse.com*

**Abstract** – *In case of severe accident conditions such as core melt-down, there may be a need to release pressure from the containment to the atmosphere to ensure containment integrity. To minimize the radioactive release to the environment during the venting process, Filtered Containment Venting Systems (FCVS) are generally back-fitted to nuclear power plants. Beside of radioactive aerosols, the vented gas flow typically contains gaseous iodine, elemental as well as organic, that need to be efficiently removed before the gas is released to the atmosphere. Westinghouse offers dry and wet FCVS. Dry FCVS consist of a metal fiber filter for the removal of radioactive aerosols and a molecular sieve (MS) for filtering gaseous iodine, whereas wet FCVS use scrubber systems to remove aerosols and elemental iodine. As organic iodine removal capability of scrubber systems is generally limited, Westinghouse developed and filed a patent for a special MS, supplementing wet scrubbers, in order to meet modern organic iodine retention requirements.*

*Westinghouse molecular sieve designs are flexible such that they can meet plant-specific conditions including design and operating pressure and temperature, amount and composition of gas and radioactive contents, available installation location and required decontamination efficiency (DF). The filters are designed for small pressure losses and may easily be back-fitted to existing containment filtered vent systems*

*After an introduction into the various venting filters of Westinghouse and an outline of the need for iodine filtering, the Westinghouse MS technology is described in some more detail but also the limitation of traditional wet scrubber systems based on thiosulphate to filter organic iodine.*

## I. INTRODUCTION

Following a severe accident in a nuclear power plant the need to preserve containment integrity may require venting to the atmosphere. The vent gases typically contain, besides steam, aerosols and gases of various compositions. To prevent radioactive releases to the environment the venting lines may be equipped with filters. These Filtered Containment Venting Systems (FCVS) are typically designed to retain a certain fraction of an aerosol size distribution, and to retain elemental and organic iodine.

Westinghouse currently proposes two different FCVS products; a wet scrubber system commonly referred to as “SVEN” (Safety VENTing system) and a dry filter system, commonly referred to as “DFM” (Dry Filter Method). The offering of a select choice of products allows for an adjustment to the specific constraints and needs of each nuclear power station

### Wet FCVS of Westinghouse - SVEN

The SVEN wet scrubber system is based on a combination of wet scrubbing and sintered metal fibre filter separation technique [1]. Aerosol filtering and retention of gaseous elemental and organic iodine is in SVEN performed in five consecutive steps, see Figure 1.

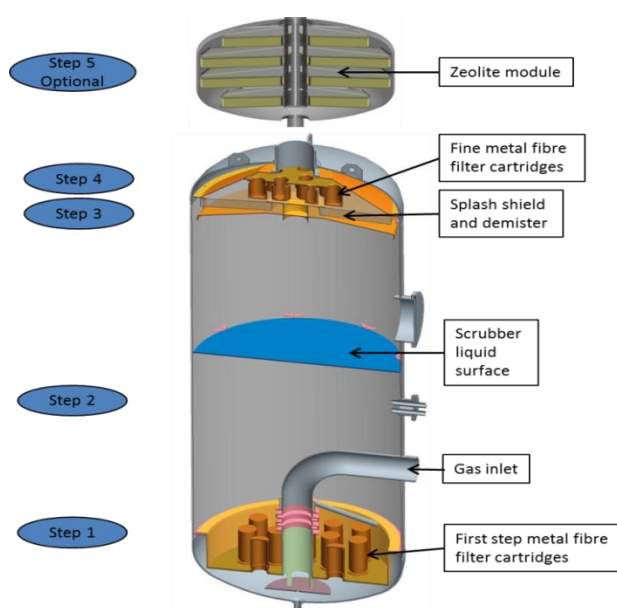


Fig. 1. Principle of the Westinghouse SVEN filtered containment venting system.

The venting flow is first routed through a set of sintered metal fibre filter cartridges submerged in a scrubber liquid inside a pressure vessel. The venting flow forces the liquid out from the manifold and the cartridges. The majority of aerosols (>99%) in the vent flow are removed by the submerged filter media as the vent flow flows from the inside of the cartridges to the outside through the filter media. The venting flow then pass a liquid volume where the large interfacial area between gas and liquid lead to scrubbing of the gas flow from aerosols. The scrubber liquid consists of sodium thiosulphate ( $\text{Na}_2\text{S}_2\text{O}_3$ ) and sodium hydroxide ( $\text{NaOH}$ ) dissolved in demineralized water. During this bubbling phase elemental iodine is removed by a very fast chemical reaction with thiosulphate solution. Sodium hydroxide ( $\text{NaOH}$ ) is used as a buffer to provide a sufficiently high pH level. Stand-by pH level is defined by the severe accident scenarios defined for the actual plant installation and depends on amount and nature of acidic materials such as e.g. chlorine in the vent stream. A detailed chemical analysis is made that ensures a pH level above 7 during venting in order to prevent re-volatilization of iodine. Above the scrubber liquid, a splash shield and a demister to remove moisture from the vent flow are installed. The demister prevents release of aerosols due to re-suspension when aerosols encapsulated in liquid droplets follow the gas flow from the scrubbing volume. A DF for aerosols >1,000 is obtained by these first three steps, but the vent flow exiting the scrubber may still contain small amounts of fine aerosol particles. A second set of HEPA rated metal fibre filters is therefore provided in the upper part of the SVEN tank, designed to capture a smaller load of log-normal size distribution aerosols with MMD  $0.3 \mu\text{m}$  and a geometric standard deviation of 2.

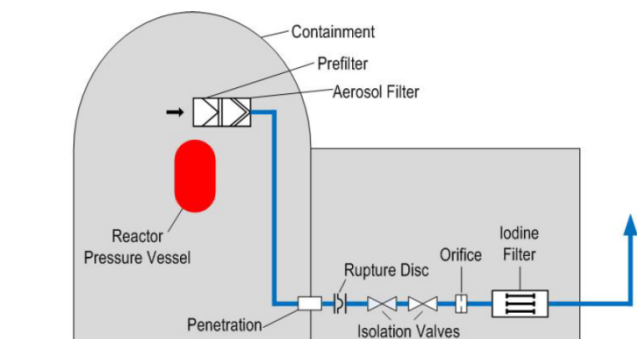
Typical aerosol retention efficiencies obtained in extensive testing of the integrated system are higher than 99.99 % (DF > 10,000) [1]. Typical elemental iodine retention efficiencies are larger than 99.9 % [1]. Organic iodine retention in the bubbling phase is moderate, about 50% (DF $\approx$ 2). The gas exiting from the SVEN tank may therefore contain small amounts of organic

iodine. To achieve a specified guaranteed DF for organic iodine, respectively total gaseous iodine, an optional molecular sieve, consisting of beds of silver doped zeolite beads through which the vent flow is routed, is provided. Zeolite is a micro porous ceramic material with a high inner porosity. The filtering principle inside the zeolite filter is based on the chemical reaction between iodine (both, elemental and organic) and the silver doping, which is called chemical sorption. The molecular sieve beds are placed in a separate housing downstream of the SVEN tank and provide the fifth and last filtration step of the SVEN system. The SVEN system molecular sieve is tailored to the chosen DF, typically 50, based on the conditions of the specific installation.

### Dry FCVS of Westinghouse - DFM

The DFM system consists of a series of modular filter stages, see Figure 2 [2].

Fig. 2. Principle of the Westinghouse DFM filtered containment venting system.



For aerosol filtering and gaseous iodine retention, two different types of filters are applied. In a first step, aerosols are filtered from the venting gas flow using a specially designed deep bed metal fibre filter. The deep bed fibre filter consists of a multistage design containing metal fibres which decrease in diameter over the depth of the filter. The metal fibres in the initial filter stages have relatively large diameters whereas the later filter stages are composed of smaller metal fibres. Most of the aerosol mass load is retained within the first filter stages, while the last aerosol filter stages achieve the overall high filtering efficiency. The metal fibre filter

contained in the DFM system has participated in the internationally sponsored Advanced Containment Experiments (ACE) [3]. Main objective of the ACE tests was the investigation of the performance of different containment venting filtration devices. For this, the efficiency for removal of fission product aerosols which might be potentially released during a postulated severe reactor accident was measured for eight filtration systems utilizing the same aerosols, carrier gas, and test protocol. Among others an aerosol mixture consisted of CsI, CsOH, and MnO was utilized. The ACE tests demonstrate an excellent performance of the DFM aerosol filter with decontamination factors up to 3,000,000 for Cs. In addition, when considering the overall test results of all three elements (Cs, I, and Mn) the DFM aerosol filter showed the best performance of the investigated venting filtration systems.

In the second step, located downstream of the aerosol filter, gaseous iodine (both elemental and organic) is retained in a molecular sieve. The molecular sieve contains a silver-doped zeolite. In order to optimize the retention efficiency for gaseous iodine, the venting gas flow is expanded in a fully passive manner to eliminate the humidity of the steam and superheat the venting gas before entering the iodine filter. Typically designed decontamination factors for the iodine filter of the DFM are 1,000 for elemental iodine and 50 for organic iodine. The depth of the zeolite bed can be designed to achieve higher or lower DF for gaseous iodine as required by the customer.

Due to the modular design, different configurations of a DFM system are possible. Aerosol and iodine filter modules can be installed separately but also in combined filter housings, according to plant specific requirements and available space inside the plant. In addition, several relatively small filter modules can be installed inside the containment (see e.g. Figure 2), providing especially the incomparable advantage among others that filtered radioactive particles always remain inside the containment. Inside and outside containment configurations had been installed already more than 20 years ago in Germany. To meet increased decay heat removal capability, which is typically the case for other nuclear

power plants worldwide, additional cooling tube modules have been added in recent installations. The application of the DFM to several plant designs is described in [4,5].

## II. IODINE FILTRATION NEEDS

In terms of requirements relating to ultimate releases to the environment, there are no internationally standardized regulatory requirements for severe accidents and venting system performance.

This implies that appropriate requirements for the DF must be derived from severe accident analysis by codes like MAAP or MELCOR. In addition, considering the differing filtration efficiencies for the different forms of iodine, various combinations of DF for aerosols, elemental and organic iodine may be possible in order to meet the overall release limit. There is no stringent reason to impose the same DF requirement on different chemical forms of a fission product when these are present in different fractions.

NUREG-1465 [6] is widely used as a generic approximation for source term to containment. According to [6] about 95 % of the iodine will be present in form of aerosols (CsI). The remaining 5 % are present in gaseous form. NRC Regulatory Guide RG 1.183 [7], which is based on NUREG-1465, suggests that 97 % of these 5 % (4.85 % of total iodine) are present in form of elemental iodine and 3 % (0.15 % of total iodine) are present in form of organic iodine.

Since NUREG-1465 had been written, the behavior of iodine in the reactor system and in the containment has been investigated in more detail. Aspects such as the complexity of surface reactions, the mass transfer of gaseous iodine species between aqueous and gas phase and radiolytic oxidation leading to formation of solid oxide products have been investigated within the SARNET cooperation. An overview of some of these results can be found in [8]. The complex interaction between iodine and paint used inside the containment, especially in connection with irradiation, was studied in the EPICUR, NROI and BIP [9] programs. The results, besides providing input to modelling efforts, shows that the interactions are very complex and time

varying such that the partitioning between elemental and organic suggested in [7] may be underestimating the organic iodine fraction. The large scale PHEBUS experiments support this observation and show the presence of volatile organic iodides in the containment atmosphere as well as the importance of interactions with different types of surfaces for the distribution of iodine in the containment [10]. Together with results from the THAI test facility on iodine oxides aerosol formation it is clear that the composition of the containment atmosphere following a potential severe accident may be strongly time dependent. Predictions of iodine species concentration are therefore still linked to large uncertainties. From an industrial perspective this means that the FCVS design must be robust and able provide filtration efficiency margin. In practice that higher decontamination factors than previously used for gaseous and especially for organic iodine may need to be considered.

## III. WET SCRUBBER IODINE FILTRATION

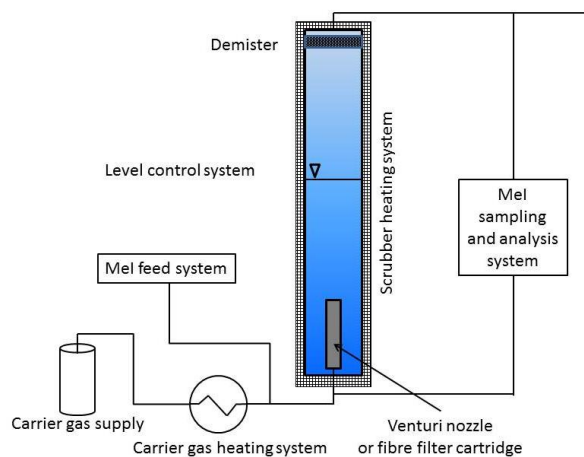
Gases vented from containment may contain both elemental iodine and to a lesser extent organic iodides. When the first FCVS were designed and installed in the 1980's, following the Three Mile Island accident, there were no requirements on retention of organic iodides [2]. Wet scrubber systems therefore utilized a scrubber liquid consisting of sodium thiosulphate ( $\text{Na}_2\text{S}_2\text{O}_3$ ) and sodium hydroxide (NaOH) dissolved in de-mineralized water. The elemental iodine is in this scrubber liquid removed by a very fast chemical reaction with the thiosulphate solution. Iodide ions created in the reactions are soluble in water. This technology were used both by ABB Atom (nowadays Westinghouse) in their Filtra-MVSS system and by KWU (nowadays Areva) in their wet scrubber system.

The purpose of the sodium hydroxide is to create a buffer that maintains the pH level above 7 during venting. This is necessary to prevent re-volatilization of iodine as acidic materials in the vent stream, typically hydrochloric acid formed from pyrolysis or irradiation of cable isolations, paint films, etc., are captured in the scrubber.

Wet scrubber retention efficiency for elemental gaseous iodine in a sodium thiosulphate based scrubber liquid is excellent. Retention efficiency primarily depends on the generated gas-to-liquid interface area and the residence time for the gas in the scrubber. Quoted retention efficiencies [2] are typically better than 99.9%, corresponding to a DF of 1,000, or better. Retention efficiency measurements are typically based on highly accurate gas chromatography-mass spectrometry techniques. Variations in obtained values are due more to repeatability of test conditions during large scale testing (temperature, pressure, flow rates, etc.), than to concentration analysis errors. Quoted DF values are generally therefore lower bounds with significantly better values obtained in individual cases.

With an increased focus on creation of organic iodides in the containment during a severe accident, e.g [8], has followed new requirements on FCVS systems ability to filter also organic iodides. Traditional alkaline scrubbers are known to retain very little of organic iodides [11, 12]. It has however been unclear as to which extent the sodium thiosulphate based scrubber liquid will retain organic iodides. To determine retention of organic iodide in the commonly used sodium thiosulphate based wet scrubber technology, Westinghouse has performed prototype scale testing [13, 14]. Two test rigs, A and B, were erected to determine organic iodide retention. The general layout of the test rigs are depicted in Figure 3.

Fig. 3. General layout of wet scrubber iodine retention test rig.



A full height scrubber equipped with either a venturi nozzle or a fibre filter cartridge was kept heated and pressurized at pre-set temperature and pressure. Nitrogen was used as carrier gas and heated to the required test point temperature. Methyl iodide (MeI) was used as trace gas to determine retention efficiency. Flow rates of carrier gas, MeI feed, and sample flows were used to control the experiments. Samples representative of upstream and downstream conditions were taken through sampling lines connecting close to the inlet and outlet of the scrubber.

Test rig A used an aqueous solution of NaI, containing the radiotracer isotope 1-131, and dimethyl sulphate that was mixed to produce radioactive MeI. Dosage of MeI was made by continuously bubbling nitrogen gas through the liquid in a cylinder. The volatile MeI was carried by the nitrogen flow and debouched into the main flow gas stream. Sampled flows were dried and routed through carbon filters which were then analyzed for MeI content.

Test rig B used a nebulizer to atomize liquid MeI into a vaporization chamber in which the MeI was mixed with the carrier gas.

Several tests were made covering typical pressure, temperature and pH operating conditions. The ranges covered where 1.1 bar(a) < pressure < 5.3 bar(a), 73°C < liquid

temperature  $< 129^{\circ}\text{C}$ ,  $10.5 < \text{pH} < 13.4$ . Figure 4 shows retention efficiency in percent as function of scrubber liquid temperature. It is clear that retention is low, of the order of 15%-70%, with no clear trend with temperature. As shown in Figure 5 the data show no trend with pH either. Data point symbols indicates corresponding points in Figures 4 and 5. The average retention is found to be 36% corresponding to a DF equal to 1.6.

It is clear from these tests that the traditional sodium thiosulphate based wet scrubber technology provides limited retention of organic iodine. In order to meet modern organic iodine retention requirements Westinghouse have therefore developed an iodine filter product line based on molecular sieve technology for supplementing the scrubber system.

Fig. 4. Prototypic scale testing of organic iodide retention in sodium thiosulphate based wet scrubbers as function of scrubber liquid temperature.

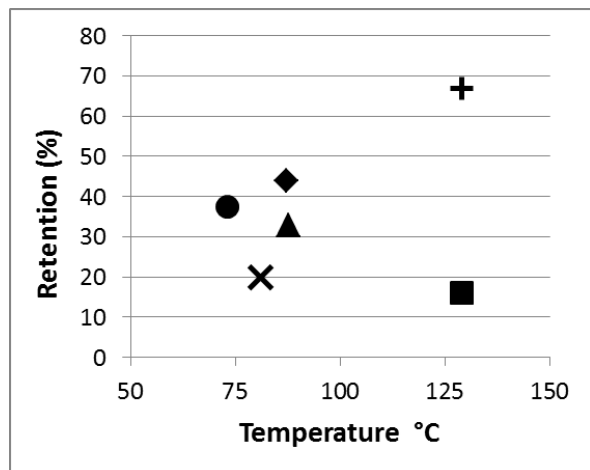
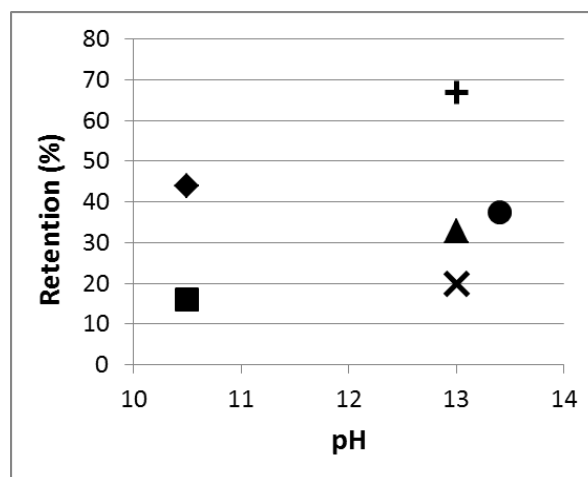


Fig. 5. Prototypic scale testing of organic iodide retention in sodium thiosulphate based wet scrubbers as function of scrubber liquid pH.



#### IV. WESTINGHOUSE MOLECULAR SIEVE TECHNOLOGY

Westinghouse provides two alternative designs for the molecular sieve: “cylindrical type”, see Figure 6, and “box type”, see Figure 7, designs. The cylindrical design was developed to supplement a wet scrubber system especially regarding modern organic iodine retention requirements and can be designed for high pressure (up to 10 bar). The box type has been already installed in the past as part of the DFM system and is therefore applied for near atmospheric pressure. Compared to the cylindrical type, where only small amounts of organic iodine exiting the SVEN scrubber remain to be filtered, the box type design can be adjusted by the means of passive cooling tubes (see Figure 7) to cope with high decay heat.

Both the cylindrical design MS and the box design MS use the same working principle for filtering of gaseous iodine, which is the use of silver doped zeolites to clean the gas from elemental and organic iodine.

Fig. 6. Cylindrical Molecular Sieve. The red arrows symbolize the gas containing organic iodine and the green arrows symbolize the cleaned gas, ready to exit to the atmosphere.

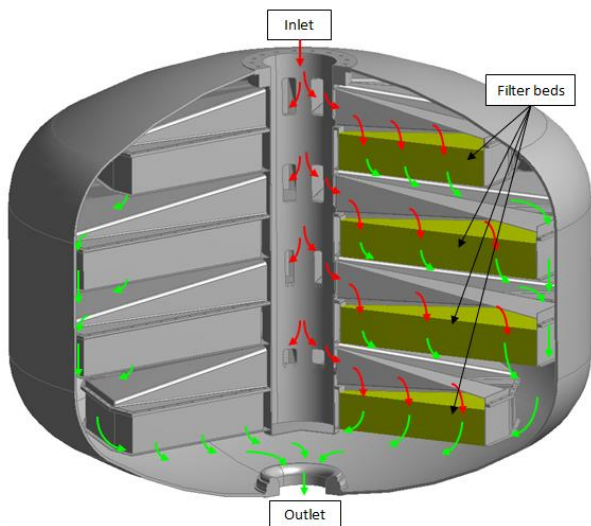
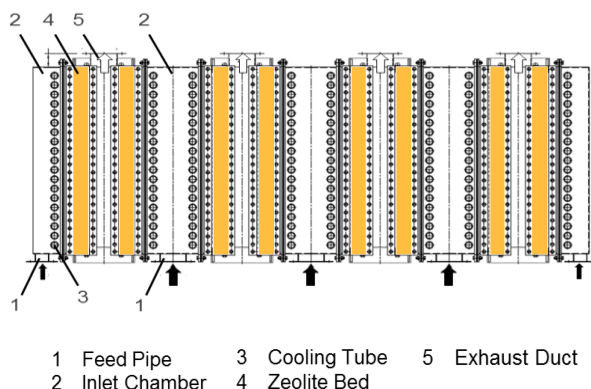


Fig. 7. Box Type Molecular Sieve.



The zeolite is a micro porous ceramic material with a high inner porosity doped with added silver. In a chemical reaction between iodine and silver, silver iodide (AgI) is formed.

The zeolites are commonly made of a synthetic crystalline aluminosilicate zeolite X type. This zeolite type is sensitive to moisture. The filter efficiency for gaseous elemental and organic iodine therefore depends both, on the residence time of the gas inside the zeolite bed and on the distance of the gas temperature to the dew point of the steam contained in the gas mixture. The venting gas is expanded in a fully passive manner by a pressure reducing expansion orifice,

leading to an increase in dew point distance and superheated steam. At higher containment pressure, a larger dew point distance can be achieved. At lower vent pressure, the distance to dew point will go down and hence the apparent efficiency of the iodine filter will be reduced. This effect is, however, compensated by the lower flow rates at lower containment pressure and the resulting longer residence times of the gas molecules inside the filter bed. Hence, the efficiency of the iodine filter remains constant and can be guaranteed over the full range of flow and pressure of the venting cycle.

In the MS the gas is evenly distributed and passes through zeolite beds. In the cylindrical type design (Figure 6), vent flow is maintained downward through the zeolite bed whereas, in the box type design (Figure 7), a horizontal flow is maintained through the zeolite beds. In the cylindrical design, gas flow is evenly distributed by the inlet distribution pipe openings and the flow path shapes. Multiple techniques are used in the box design MS to provide even distribution of gas flow to the parallel filter modules and to the single filter beds.

Significant performance improvements with respect to structural stability, weight and hydrophobic behavior, of doped zeolites have been obtained in recent years. Westinghouse cooperates with the leading zeolite vendors to assure optimal selection of zeolite type for each installation. Several qualification tests are done in order to qualify a specific zeolite batch to be used. The zeolite material is tested at various air/steam mixtures, and at various superheating values (distance from dew point) to determine retention efficiencies for various residence times. In addition, the zeolite material is exposed to harsh steam, radiation and high temperature conditions and then the efficiency is measured again to assure minimal performance degradation. The dew point distance is selected to be representative for the conditions at the specific nuclear power plant. Further improvement of iodine filtering could be achieved by the use of next generation zeolite materials, providing very good filter performance also under saturated conditions.

Typically designed decontamination factors for the iodine filter are 1,000 for elemental iodine

and 50 for organic iodine. The depth of the zeolite bed can be designed to achieve higher or lower DF if required.

Experience from MS installations has shown no degradation of the zeolite material over time when nitrogen cover gas is used to maintain the zeolite material in a dry atmosphere.

## V. CONCLUSIONS

Following the Fukushima Daiichi accident the awareness of the importance of filtered containment venting as a part of plant defense in-depth increased. Therefore, the installation or the enhancement of a FCVS has become a requirement in more and more countries worldwide. New research results are in addition indicating a larger than previously assumed presence of organic iodine compounds in the vented gases: To maintain a high level of safety and protection to the environment in case of a severe accident Westinghouse have therefore refined its filtration technologies to meet modern requirements.

With the molecular sieve designs, which can be designed to meet any gaseous iodine retention requirements, integrated in a passive self-regulating filter system design, Westinghouse is well positioned with its portfolio of FCVS, meeting also requirements for organic iodine filtering, for which especially wet scrubber systems based on thiosulphate solutions showed up in latest tests to be limited to a decontamination factor in the order of 2.

## NOMENCLATURE

DF = Decontamination factor

DFM = Dry Filter Method

FCVS = Filtered Containment Venting System

HEPA = High Efficiency Particulate Arresting

MeI = Methyl Iodide

MS = Molecular Sieve

SVEN = Safety VENTing system

## REFERENCES

1. P-O. Nilsson, "*SVEN Filtered Containment Venting System, Design and Testing*", Westinghouse Electric Sweden AB, Report SEB 14-040, rev 1, Proprietary, 2014.
2. "*Status Report on Filtered Containment Venting*," Nuclear Safety, NEA/CSNI/R(2014)7, July 2014.
3. I. Wall, M. Merilo, "Containment Filtration Systems Tests - Advanced Containment Experiments (ACE) Project Summary Report," Electric Power Research Institute (EPRI), February 1992.
4. C. Hartmann, M. Bauer, J.C. Adams, "*Experience from the application of the Dry Filtered Method for Filtered Containment Venting to several plant designs*" Proceedings of the 33<sup>rd</sup> NACC, June 22-24 2014, St. Lois, MO.
5. C. Hartmann, M. Bauer, H. Ulrich, "*Experience from the Application of the Dry Filtered Method for Filtered Containment Venting to Several Plant Designs*" atw - International Journal for Nuclear Power- Issue 8/9 2014.
6. L. Soffer, S. B. Burson, C. M. Ferrell, R. Y. Lee, J. N. Ridgely, "Accident Source Terms for Light-Water Nuclear Power Plants" NUREG-1465, 1995.
7. U.S. Nuclear Regulatory Commission, "Alternative radiological source terms for evaluating design basis accidents at nuclear power reactors", Regulatory Guide 1.183, July 2000.
8. S. Dickinson, A. Auvinen, L. Bosland, G. Glowa, D. Powers, B. Teisseire, S. Tietze, "*Iodine Chemistry in Nuclear Reactor Accident Conditions: Recent Studies and Hypotheses*", NPC Sapporo, 2104.
9. Glenn A. Glowa, Chris J. Moore, Joanne M. Ball, "*The main outcomes of the OECD Behaviour of Iodine (BIP) Project*", Annals of Nuclear Energy 61, pp. 179–189, 2013.

10. B. Simondi-Teisseire, N. Girault, F. Payot, B. Clément, “*Iodine behaviour in the containment in Phébus FP tests*”, *Annals of Nuclear Energy* 61, pp. 157–169, 2013.
11. D. R. Haefner, T. J. Tranter, “*Methods of Gas Phase Capture of Iodine from Fuel Reprocessing Off-Gas: A Literature Survey*”, Idaho National Laboratory, INL/EXT-07-12299, February 2007.
12. P. Paviet-Hartmann, W. Kerlin, S. Bakhtiar, “*Treatment of Gaseous Effluents Issued from Recycling – A Review of the Current Practices and Prospective Improvements*”, Idaho National Laboratory, INL/CON-10-19961 PREPRINT, November 2010.
13. S. Kristensson, “*FILTRA-MVSS removal of methyl iodine at different pH and thiosulfate concentration*” Westinghouse Electric Sweden AB, Memorandum SEB 14-070, rev 0, Proprietary, 2014.
14. S. Kristensson, “*SVEN pilot plant Iodine – description*”, Westinghouse Electric Sweden AB, Report SEB 14-119, rev 0, Proprietary, 2014.

## IMPROVED IODINE RETENTION AT FILTERED CONTAINMENT VENTING

P. Zeh\*, S. Buhlmann, A. Stahl, N. Losch  
AREVA GmbH, Erlangen / Offenbach, Germany

\*Corresponding P. Zeh, Tel: (+49) 913190097690, Fax: (+49) 913190097312,  
Email: peter.zeh@areva.com

**Abstract** - During a severe accident in a NPP the containment pressure can exceed the allowable maximum pressure. To avoid uncontrollable cracking of the containment shell, pressure relief is necessary. To perform this AREVA developed and qualified a Filtered Containment Venting System (FCVS) already 25 years ago. It contains a venturi scrubber whose scrubbing liquid has high potential for chemisorption of iodine compounds followed by a subsequent droplet separator and a metal fiber filter unit. The performance of the system has been verified to remove aerosols and iodine with very high decontamination factors. Since once the aerosol and iodine release has been significantly reduced by an above described filtered venting system, the release of organic iodine becomes a leading contributor to the radiological consequences, that still remain, but on a much lower level as compared to without a filtered venting system

Therefore, long before the Fukushima accident AREVA in 2009 decided to improve its qualified Filtered Containment Venting System (FCVS), composed of a venturi scrubber followed by a subsequent droplet separator and a metal fiber filter unit. Aim was to improve the comparatively limited retention capability of organic iodide species of the AREVA FCVS to values of above 98 % by adding an additional filtering unit, focused on organic iodide retention, to the existing design.

Development tests were performed at a lab-scale scrubber test facility, called “VESPER<sup>34</sup>” which allows testing retention of elemental and organic iodine species under flow conditions at temperatures up to 200°C and up to 10 bar. This VESPER<sup>34</sup> test facility simulates the FCVS conditions at a lab scale in a vessel of 9 l containing 3 l scrubbing liquid followed by variable filtering units downstream. A variable steam / air-flow is purged through a venturi nozzle into a scrubbing liquid containing a solution of sodium hydroxide and sodium thiosulfate for iodine retention and stabilization. Methyl iodide (MeI) was used as test substance for investigating retention of organic iodine compounds, since MeI shows the lowest retention compared to all other species of organic iodine. This MeI was traced with I-131 and injected continuously into the gas flow upstream the venturi scrubber. The retention of MeI was improved by adding an additional molecular sieve filtering unit downstream the venturi scrubber. In parametric studies, the best adsorption material was selected and operational conditions were optimized.

After the design phase, qualification tests were performed at the large scale test facility at AREVA Karlstein. Here a filtered venting system of original height with a reduced flow cross section of approx. 1:10 was used for qualification tests. In this filtered venting system an additional molecular sieve filter section was implemented downstream the metal fiber filter unit. Parametric tests were performed between 1 to 8 bar at a temperature range from 110°C to 160°C. As test substance unlabeled MeI was injected continuously into the gas flow upstream the venturi scrubber. The qualification tests verified good organic iodine retention under all operating conditions. The MeI-retention was above, mostly far above, 98%.

The large scale test results are used to design the additional sorbents stage for the requested application. The dimensions of the sorbents stage can be adjusted to meet the customer request regarding the DF for organic iodine. This form of qualification ensures reliable and verified performance values by excluding relevant scaling errors from lab scale to industrial application. The performed lab scale tests complete the qualification of used sorbents material for severe-accident conditions.

### I. INTRODUCTION

During a severe accident scenario in a NPP the containment pressure can exceed the allowable

maximum pressure. To avoid uncontrollable cracking of the containment shell pressure relief is necessary. In order to minimize radionuclide release to the environment due to containment pressure reduction via venting, filtered venting systems have been designed, internationally qualified and implemented in many NPP's. Main focus was given to the reliable and efficient aerosol retention. In addition also efficient iodine retention was requested, as this element has significant activity content in nuclear fuel in combination with high volatility and radiotoxicity. Therefore, efforts are made to reduce the radionuclide emission of iodine in the off-gas during venting.

In 2014 the state-of-the-art-report of NEA on FCVS [1] was updated with the collaboration of AREVA. This is one of the good opportunities AREVA uses to challenge the products on market requests. Currently several new topics are more or less intensively discussed as sub-micron aerosols  $IO_x$ ,  $RuO_4$  and organic iodine. The latter one is discussed in the paper on hand.

State-of-the-art containment wet venting scrubbing liquids use a solution of sodium hydroxide and sodium thiosulfate in order to wash out volatile iodine species. Under severe accident conditions such volatile iodine species are aerosol bound iodide as well as gaseous compounds of elemental iodine, hydrogen iodide and organic iodide species. With alkaline thiosulfate solution high retention efficiencies for aerosol bound iodide as well as elemental iodine and hydrogen iodide are achieved.

Since once the aerosol and iodine release has been significantly reduced by an above described filtered venting system, the release of organic iodine becomes a leading contributor to the radiological consequences, that still remain, but on a much lower level as compared to without a filtered venting system

Therefore, long before the Fukushima accident AREVA in 2009 decided to improve its qualified Filtered Containment Venting System (FCVS), composed of a venturi scrubber followed by a subsequent droplet separator and a metal fiber filter unit. Aim was to improve the comparatively limited retention capability of

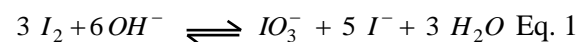
organic iodide species of the AREVA FCVS to values of above 98% by adding an additional filtering unit, focused on organic iodide retention, to the existing design.

For system development and design numerous tests at a lab-scale test facility were performed, followed by qualification tests at a large scale test facility of original height. The AREVA test facilities capable of testing behavior of different iodine species under venting conditions are described and qualification results are given.

## II. IODINE CHEMISTRY IN WET VENTING SYSTEMS

Iodine in the containment atmosphere under severe accident conditions is expected to be present in various species whose species composition and distribution changes over time [1]. The iodine species entering a filtered venting system reflect the species distribution of iodine in the containment at a given time.

Especially at first venting, a substantial part of iodine is expected to be aerosol bound. Possible aerosol species of iodine are CsI, AgI or  $IO_x$ . Iodine oxides ( $IO_x$ ), which are expected to form small size aerosols (micro aerosols), are issue of further research [3]. Such species can be captured very efficiently in any liquid of a venturi scrubber. But alkaline conditions are necessary to avoid reformation of elemental iodine from dissolved CsI under radiolytic conditions [1, 3]. Equilibrium of reversible disproportionation / conproportionation reaction of elemental iodine (Eq. 1) is under alkaline conditions almost quantitatively on the disproportionation side of the ionic species ( $IO_3^-$  and  $I^-$ ). High pH ensures that the formation of elemental iodine, the first step for revolatilization, is hindered.



Further on the presence of thiosulfate ( $S_2O_3^{2-}$ ) as reducing agent prohibits the radiolytic oxidation of I therefore  $IO_3^-$  cannot exist.

Besides aerosol bound iodine there are various volatile iodine species present in the vented gas, first of all elemental iodine ( $I_2$ ) followed by HI

and unknown organic iodide species. Such species are formed in the containment by interaction of iodine with organic material [5]. Due to its high volatility, gaseous organic iodide is often dominated by methyl iodide [6].

To assure the retention of volatile iodine species chemical additives are necessary to assure high decontamination factors of vented steam and gas from the containment. Therefore sodium hydroxide and sodium thiosulfate are added to the scrubbing solution allowing chemisorption of HI and elemental iodine with very high retention factors. Thiosulfate works in that process as reducing agent, transforming elemental iodine to iodide (I<sup>-</sup>). In parallel NaOH itself supports in principle the destruction of volatile I<sub>2</sub> by producing non-volatile iodide I<sup>-</sup> and iodate IO<sub>3</sub><sup>-</sup> according the disproportionation reaction of Eq. 1. HI, an acidic gas is captured by NaOH due to a neutralization reaction. By this the emission of these species (I<sub>2</sub>, HI) can be lowered by several orders of magnitude.

Organic iodide compounds will react in the scrubbing solution with OH<sup>-</sup> and S<sub>2</sub>O<sub>3</sub><sup>2-</sup> by nucleophilic displacement reactions [7]. Exemplarily given for methyl iodide, the dominant representative of organic iodide compounds, the decomposition reactions are given in Equation 2 and 3.



Kinetic of methyl iodide decomposition reactions are not fast enough to achieve complete conversion under representative venting conditions. Due to limited residence time of venting gas the retention of organic iodide is limited.

The overall retention efficiency of iodine compounds strongly depends on those iodine compounds of low retention. This can be clarified by the following equations. The overall retention  $R_I$  is given by:

$$R_I = 1 - \frac{\sum A_{I_x,out}}{\sum A_{I_x,in}} \quad \text{Eq. 4}$$

with:

$$\sum A_{I_x,in}$$

the sum of activity (in Bq) of all iodine species  $x$  entering the filtered venting system and

$$\sum A_{I_x,out}$$

the sum of activity (in Bq) of all iodine species  $x$  leaving the filtered venting system.

The iodine fraction leaving the filtered venting system strongly depends on the species of iodine compound and the individual decontamination factor achieved for this species ( $DF_{I_x}$ ). There are different retentions expected for iodine aerosols, elemental iodine, hydrogen iodide and organic iodide. In theory for each species ( $I_x$ ) the activity release can be calculated using equation 5. Practically the activity fraction of different iodine species is not known in detail and usually only three fractions are distinguished (aerosol bound, inorganic volatile and organic volatile iodide).

$$A_{I_x,out} = A_{I_x,in} \cdot \frac{1}{DF_{I_x}} \quad \text{Eq. 5}$$

In case the decontamination factor of one species is much lower than all others there is a risk that this species dominates the overall release. This is illustrated from following thought-experiment where three species at different arbitrary concentrations and decontamination factors are defined and the species of lowest concentration has at the same time the lowest decontamination factors. In such a case the release can be dominated by the species of lowest concentration (see Table I). In example of Table 1 species A gives 90% of the total release even when its fraction was only 0.9% in the gas entering the filter system.

The fraction of organic iodide species is usually minor compared to the fractions of aerosol bound or volatile inorganic iodine but it shows the lowest retention in filtered venting systems. This

was the motivation to further improve the AREVA Filtered Containment Venting System.

TABLE I

Thought-experiment, showing the dependence of release from decontamination factor of species

Species	entering activity (arbitrary unit)	arbitrary DF	released activity (arbitrary unit)
A	1	10	0.1
B	10	1000	0.01
C	100	100000	0.001

### III. EXPERIMENTAL FACILITIES FOR TESTING IODINE BEHAVIOUR UNDER VENTING CONDITIONS

For testing the behavior of iodine species under venting conditions AREVA has two test facilities of different size, a lab scale test facility called VESPER<sup>34</sup> and a large scale test facility called JAVA.

The lab scale test facility VESPER<sup>34</sup> is located in the AREVA radiochemistry laboratories in Erlangen, Germany. This test facility simulates the FCVS conditions in a vessel of 9 l containing 3 l scrubbing liquid followed by variable filtering units downstream. A variable steam / air-flow is purged through a venturi nozzle into a scrubbing liquid containing a solution of sodium hydroxide and sodium thiosulfate for iodine retention and stabilization. Different iodine species such as elemental iodine or organic iodide compounds are added to the flow, and their retention at variable parameters is tested. Usually the iodine species are labeled with radioactive tracers of I-123 or I-131. With this the retention behavior of iodine compounds can be easily followed at concentration ranges of  $10^{-9}$  to  $10^{-12}$  mol/l.

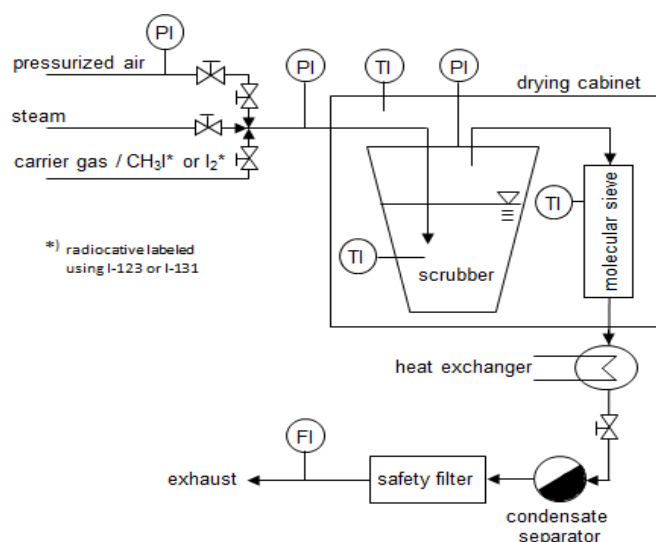
The schematic set-up of the VESPER<sup>34</sup> test facility is given in figure 1. Retention tests can be performed under flow conditions at temperatures up to 200°C and up to 10 bar. The operable parameter range is given in Table II. Typical containment venting conditions of temperature, pressure, flow velocity and iodine concentration can be tested over a wide range with this facility.

TABLE II

### Operable parameter range of VESPER<sup>34</sup> test facility

Parameter	Operable range
Temperature	RT – 200°C
Pressure (abs.)	1 -10 bar
Mass flow steam	0.01 – 1.1 g/s
Mass flow gas (air)	0.01 – 1.3 g/s
concentration of iodine compound	variable, usually in the range of $10^{-8}$ to $10^{-9}$ mol/l
Gas / steam composition	any gas / steam composition possible at any mixing ratio

Fig. 1. Schematic set-up of the VESPER<sup>34</sup> test facility with submerged injection nozzle.



The large scale test facility JAVA is located in Areva's Technical Center in Karlstein, Germany. The test facility is especially erected for the testing of FCVS and includes dedicated instrumentation and process control. It includes three different filtration stages, a Venturi scrubber, a metal fiber filter (dry stage) and an adsorption filtration stage including a passive superheating device. The scrubbing liquid of the wet venting stage of the venturi scrubber has a high potential for chemisorption of iodine compounds and retention of aerosols. The subsequent droplet separator and metal fiber filter unit prevents the carry-over of droplets and gives high retention for remaining fine aerosols.

To this filtered venting system additionally an adsorption filtration stage downstream the metal fiber filter unit was implemented, which is capable of absorbing and immobilizing organic iodide compounds.

This JAVA test facility is scaled up to the FCVS original height of 8 m with a reduced flow cross section of 1:10. Since the single process sections are integrated in the original scale, very representative results can be produced. This test facility allows retention tests at flow velocities and gas residence times similar to realistic (calculated) venting scenarios. The operable parameter range is given in Table III. Due to its modular design the test facility enables the testing of single or combined process steps under various test conditions. Numerous tests were performed at this JAVA test facility to qualify the AREVA FCVS system under representative conditions. Retention of aerosols, elemental and organic iodide as well as thermo hydraulic performance were tested. In figure 2 a picture of the test facility is given.

Fig. 2. Image of JAVA test facility.



TABLE III

Operable parameter range of JAVA test facility

Parameter	Operable range
Temperature	RT – 200°C
Pressure (abs.)	1 -11 bar
Mass flow	0.05 – 1.5 kg/s
concentration of iodine compound	variable, usually in the range of $10^{-7}$ to $10^{-9}$ mol/l
Gas / steam composition	any air / steam composition possible at any mixing ratio

#### IV. QUALIFICATION TESTS FOR IMPROVED FILTERED CONTAINMENT VENTING SYSTEM

Developing tests were performed at the VESPER<sup>34</sup> test facility. Methyl iodide (MeI) was used as test substance for investigating retention of organic iodide compounds. Due to its highest partial pressure (544 hPa at 20°C) of organic iodide compounds it is regarded to cover this group of compounds conservatively. For lab-scale tests MeI was traced with I-131 and injected continuously into the gas flow upstream the venturi scrubber. The retention of MeI was improved by adding an additional molecular sieve filtering unit downstream the venturi scrubber. In parametric studies different adsorption materials were tested and operation conditions were optimized. . These data were used for a new design of filtered venting system. Finally one material was selected for further more extensive qualification which was found the optimum regarding retention performance, long-life and stability under the predictable operating conditions.

After the design phase, qualification tests were performed at the JAVA test facility at AREVA Karlstein, at a filtered venting test facility in approx. 1:10 scale of flow cross section and original in height. Parametric tests were performed between 1 and 8 bar in a temperature range from 110°C to 160°C. The mass flow of steam and gas was around 1 kg/s, which is roughly 10% of the expected mass flow of calculated venting scenarios.

As test substance, unlabeled commercially available MeI (methyl iodide) was injected

continuously into the air / steam flow upstream the venturi scrubber at a constant mass flow. This was performed by injecting with a high pressure pump a defined mass flow of liquid MeI into an evaporator unit where MeI is evaporated instantaneously and flushed with a nitrogen carrier gas into the main air / steam flow. The decision for unlabeled CH<sub>3</sub>I was made by balancing between advantages and drawbacks. The decision required amongst others to develop the measuring and injection technology and to check the influence of CH<sub>3</sub>I concentration.

At the same time fractions of the gas flow of steam and air were sampled up- and downstream the filtering unit of venting system. MeI content in the gas sample is filtered by absorption on charcoal. Later on methyl iodide is extracted quantitatively from the collected charcoal samples and converted to iodide (I<sup>-</sup>). The iodine content in the extraction solution was analyzed by ICP-MS (Inductive Coupled Plasma Mass Spectrometry). From iodine concentration, mass of extraction solution and the portion of sampled gas (referred to the main flow), the formed methyl iodide concentration in the main gas flow can be calculated. Similar to Eq. 4 the retention can be estimated from methyl iodide concentration up- and downstream of the filtered venting system.

From 2012 to 2014 more than 50 tests of methyl iodide retention were performed at variable pressure, temperature and mass flow conditions. These qualification tests verified that the improved FCVS gives, besides the already verified high retention of aerosols and inorganic volatile iodine (I<sub>2</sub>), also very good retention of organic iodide compounds. Under all operating conditions the MeI-retention was above, mostly far above, 98%. In addition the adsorption filtration section also improves the retention of inorganic volatile iodine as such species are also bound with high efficiency on the used adsorbent.

The large scale test results are used to design the additional sorbents stage for the requested application in detail. The dimensions of the sorbents stage can be adjusted to meet the customer request regarding the DF for organic

iodide. Thereby the qualification tests ensure most reliable verified performance values by excluding relevant scaling errors from lab scale to industrial application which could easily result in an overestimation of retention efficiency by order(s) of magnitude. The performed lab scale tests complete the qualification of used sorbents material for severe accident conditions.

TABLE IV

Methyl iodine retention at different boundary conditions

Pressure* (bar <sub>abs.</sub> )	Temperature ** (°C)	Steam (wt.%)	DF
7.2	139	70	256
5.0	118	50	195
1.5	105	90	53

\* upstream FCVS

\*\* inside sorbent section

## V. CONCLUSION

Retention of iodine in a filtered containment wet venting system was improved by focusing on the retention of organic iodide. Such species have much lower retention in a venturi scrubber than aerosol bound or inorganic volatile iodine. By implementing an additional adsorption filtration section with a passive superheating device it was possible to improve the overall retention of iodine species.

Development tests were performed at the VESPER<sup>34</sup> test facility where the best adsorption material could be selected and operation conditions optimized during parametric studies. After the design phase, qualification tests were performed at the large scale JAVA test facility at AREVA Karlstein, a filtered venting system of original height. The large scale test results are used to design the additional sorbents stage for the requested application. Based on the found relationships, the dimensions of the sorbents stage can be adjusted to meet the requirement of different authorities or customer request regarding the DF for organic iodine. Thereby the qualification ensures reliable and verified performance values by excluding relevant scaling errors from lab scale to industrial application. The performed lab scale tests complete the

qualification of used sorbents material for severe accident conditions.

Under all operating conditions the MeI-retention was above, mostly far above, 98% for the used sorbents section dimensions. In addition the adsorption filtration section also improves the retention of inorganic volatile iodine as such species are also bound with high efficiency on the used adsorbent.

#### ACKNOWLEDGMENTS

The authors would like to thank all the team members for their commitment.

#### NOMENCLATURE

FCVS = Filtered Containment Venting System

MeI = methyl iodide

#### REFERENCES

1. Jacquemain, D., et al. "Status report on filtered containment venting", OECD / NEA report, NEA/CSNI/R (2014)7
2. Girault, N., Dickinson, S., et al. "Iodine behaviour under LWR accident conditions: Lessons learnt from analyses of the first two Phebus FP tests." Nuclear Engineering and Design 236(12): 1293-1308 (2006).
3. Dickinson, S., et al. "Experimental and modelling studies of iodine oxide formation and aerosol behaviour relevant to nuclear reactor accidents" Annals of Nuclear Energy 74 (2014) 200–207
4. Girault, N., Fiche, C., et al. "Towards a better understanding of iodine chemistry in RCS of nuclear reactors." Nuclear Engineering and Design 239 (2009) 1162-1170.
5. Wren, J.C. , Ball, J.M., Glowa, G.A. , "The interaction of iodine with organic material in containment", Nucl. Technol. 125 (1999) 337-362
6. Marchand, C., "Production d'iodes organiques a partir des surfaces peintes de l'enceinte de confinement d'un reacteur a eau pressurisee en situation accidentelle", IPSN Note technique DPEA I SEAC/97-04, October 1997
7. E.A. Moelwyn-Hughes, "The kinetic of certain reactions between methyl halides and anions in water", Proc. Roy. Soc. (London), Vol. 196, 540ff (1949)

## DESIGN ON THE PERFORMANCE TEST OF FILTERED CONTAINMENT VENTING SYSTEM

Kwang Soon Ha(1)\*, Jaehoon Jung(1), Sang Mo An(1), Hwan Yeol Kim(1), Jinho Song(1)

<sup>(1)</sup> Korea Atomic Energy Research Institute, Daejeon, Korea

\*Corresponding author, tel: (+82) 428688653, Fax: (+82) 428688256, Email:tomo@kaeri.re.kr

**Abstract** –A scaling analysis method is proposed for the design of a test loop for the qualification of the performance of a Filtered Containment Venting System (FCVS). FCVS is employed in the nuclear power plant to maintain the integrity of the containment by releasing the mixture of steam and fission products from the reactor containment to the outside. During the release, fission products in the form of aerosol and gas are filtered to avoid substantial release of radioactive material into the environment. An integral test facility is designed to verify the performance of a proposed FCVS. The proposed FCVS system consists of pool venturi scrubber, cyclone separator, particulate filter, and molecular sieve filter. A scaling method was developed to design a reduced scale FCVS test facility. Tests to quantify the performance of the FCVS include a thermal-hydraulic test, aerosol removal test, elemental iodine removal test, organic iodine removal test, re-suspension of aerosol test, re-volatilization of iodine test, and dynamic test under a high-pressure gas ejection from the containment. The scaling method was designed to reproduce the same fundamental phenomena in the scaled down test facility as the prototype.

## I. INTRODUCTION

In the case of a severe accident like the Fukushima accident [1], the melted core material (corium) can be relocated to the lower plenum of the reactor pressure vessel. If the reactor vessel is breached the molten corium will be discharged into the containment environment.

The defense in depth approach is used to prevent significant release of radioactive material outside the containment. In the case of a LWR (Light Water Reactor), there are 4 step physical barriers. The first barrier is a fuel pellet that can contain fission gas and all radioactive materials. The second barrier is fuel cladding enclosing the fuel pellets. During a severe accident, first and second barriers are breached, and then the reactor vessel and containment can prevent the release of radioactive material as third and fourth barriers.

The discharge of corium would lead to substantial releases of fission products in the form of aerosols and gases, which are simultaneously released with steam and non-condensable gases such as hydrogen. The hydrogen is generated during the oxidation of zircaloy in the core material while non-condensable gases are generated due to corium concrete interaction.

During the severe accident pressure inside the containment can increase substantially, and the integrity of the containment may be threatened. In the Fukushima accident the last barrier is breached, which led to a significant release of radioactive material to the environment and contamination of huge area including sea, soil, and rivers. A prolonged station black out (SBO) due to earthquake and tsunami caused loss of four barriers discussed above.

Therefore, a use of additional system like FCVS is considered in many countries to provide additional barrier [2] to maintain the containment integrity even during the prolonged SBO.

FCVS (Filtered Containment Venting System) is employed to maintain the integrity of the containment by releasing the high-temperature and pressure gas from the containment to outside through a pipe line while capturing and scrubbing radioactive gases and aerosols.

The FCVS should decrease the pressure inside the containment by releasing steam and non-condensable gases to maintain the integrity of the containment during severe accident. In addition, the performance of the filtration should be considered in the FCVS design so that radioactive materials such as cesium and radioactive aerosol are not released outside the environment. In addition, the FCVS was designed to operate passively. Accordingly, the FCVS immediately copes with increasing the pressure inside the containment and prevents the failure of the containment. At this time, the flow rate of the discharge gas is changed according to the sliding pressure inside the containment to make a continuous operation in the wide pressure range. In addition, the FCVS does not need off-site power because of the passive operation. For this reason, the FCVS can operate in perfect working order to maintain the integrity of the containment during a long SBO such as the accident in the Fukushima nuclear power plant. Furthermore, the FCVS was designed to prepare for an earthquake.

However, still there is a risk of early containment failure due to a steam explosion, direct containment heating, or hydrogen explosion. Also, the bypass sequence such as steam generator tube rupture or interfacing system LOCA cannot be mitigated by an installation of FCVS. Additional provisions have to be made to mitigate the consequences of bypass sequences.

Korea has 23 reactors (19 PWR, 4 PHWR) on 4 sites (Hanbit (6), Hanul (6), Kori (6), Wolsong (1 PWR, 4 PHWR)) providing about 30% of its electricity. Fukushima accidents triggered a discussion on the need to protect from a containment failure by an over pressurization and mitigate an uncontrolled release of activity into the environment.

In the Wolsong-1 PHWR unit, the installation of the first FCVS (High Speed Sliding Pressure Venturi (HSSPV) type) was completed at the end of 2012 (during the preparation to acquire approval for a continued operation after a 30 year operation). The remaining 22 Korean NPP units (19 PWR, 3 PHWR) are planned to be equipped with FCVS, and an open tender is being prepared. Korea is now developing a new FCVS for the light water reactors as a depressurization

system of the containments under a severe accident.

To verify the performance of FCVS, tests [2] were performed in the scaled test facilities such as ACE and JAVA. A new FCVS test facility was designed and is under construction. The FCVS test facility consists of a test vessel, thermal-hydraulic, and aerosol/iodine generation and measurement parts. .

In the same manner, an integral test facility is designed to verify the performance of a proposed FCVS. The proposed FCVS system consists of pool venturi scrubber, cyclone separator, particulate filter, and molecular sieve filter.

In this paper, a scaling method is discussed for a design of a reduced scale FCVS test facility. Tests to quantify the performance of the FCVS include a thermal-hydraulic test, aerosol removal test, elemental iodine removal test, organic iodine removal test, re-suspension of aerosol test, re-volatilization of iodine test, and dynamic test under a high-pressure gas ejection from the containment. The scaling method was developed to reproduce the same fundamental phenomena in the scaled down test facility as the prototype.

## II. DESIGN FEATURES OF A FCVS

General design features of current FCVSs are summarized in Table I. Current major suppliers on FCVSs are AREVA, Westinghouse, and IMI in Switzerland [2].

Korea is now developing a domestic FCVS for light water reactors as a depressurization system of the containments. As shown in Fig. 1, the Korean CFVS consists of the four main components. The venturi scrubber including the pool, droplet or particle separator, metallic fiber filter (MFF), and molecular sieve are main components of the CFVS.

During the severe accident, if the pressure inside the containment reaches desired set point, the vent valve pipe will be opened by the operator or the operation of the rupture disk. Then, the radioactive gas mixture which consists of steam, gases, and aerosols are discharged to the filtration tank filled with water through the vent pipe.

Table I Comparison of current FCVS systems

Supplier	AREVA	Westinghouse DFM	Westinghouse FILTRA-MVSS	IMI
Filtration process	Venturi scrubber, metal fiber filter, chemical retention of iodine, Molecular sieve tested	Metal fiber filter, Molecular sieve	Venturi scrubber, metal fibre filter, chemical retention of iodine	Sparger assemblies, co-current scrubber, recirculation zone, droplet separator, chemical retention of iodines
Max. design pressure	10bar(g)	6bar(g)	6bar(g)	6bar(g)
Max. design Temperature	200°C	550°C	70~150°C	128°C
Max. design flow rate	4~6kg/s	3~4.5kg/s	0.1~13kg/s	13.8kg/s
Reference plant	1000MWe PWR	German PWR	MARK II	GE BWR
Qualification test	ACE/JAVA	ACE, without molecular sieve	ACE, venturi only	PSI

The species for the fission product, sizes, and event sequences leading to the release of radioactive gases are discussed in reference 3. While the mixture gas passes the venturi nozzle, a swarm of droplets coming through the hole in the throat of the nozzle is supplied to the mixture gas. During this process, impaction occurs between the gas and the droplet due to a velocity difference, therefore the radioactive materials are removed from the gas.

The mixture gas including the aerosols will pass through a pool of water. While the gases pass through the pool in the form of bubbles, scrubbing process occurs. It will result in a scrubbing of gas such as elemental iodine and aerosols. Scrubbing of gas is by a mass diffusion process, while scrubbing of aerosols is driven by the inertial impaction and settling in the gas bubbles. The gas bubble dynamics and thermal

hydraulic condition of pool are dominant factors affecting the decontamination [4, 5].

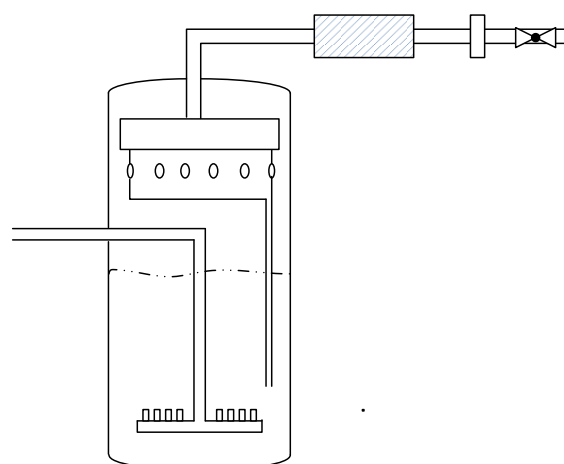


Fig.1. Conceptual Design of proposed CFVS system

Most of the radioactive aerosol and iodine are removed in the venturi scrubber, however the gas passing the pool still includes tiny aerosol and entrained water droplets. In the cyclone, the heavy particles and hygroscopic moisture of gas are removed by centrifugal force. As shown in the Figure 1, a number of cyclones are contained in a closed space like a box while the inlet of cyclone is exposed to the gas space such that the mixture gas containing the water droplet and aerosols could pass through the cyclones. The box has several holes for the cyclone inlet. The exit of cyclone is contained in the closed space, at the bottom of which a drain line is connected deep into the pool such that the droplets would drain into the lower part of the water pool. Addition of chemicals is known to augment the scrubbing process for the elemental and organic iodine gases.

In next stage, the metallic fiber filter into removes very tiny aerosols and droplets whose size is less than 2  $\mu\text{m}$ . The metallic fiber filter can be the pre-filter and the aerosol filter. The pre-filter consisted of the metallic fiber with a thickness of 6 – 10 $\mu\text{m}$  is installed in front of the

aerosol filter. The aerosol filter installed after the pre-filter consists of the metallic fiber with a thickness of 2 – 8 $\mu\text{m}$  in order to remove the tiny particles. The thickness of the metallic fiber is a parameter affecting the efficiency of the capturing performance; the performance is better as the thickness is thinner.

The molecular sieve box is located outside the CFVS vessel to remove the organic iodine. The gas passing the metallic fiber filter goes to the molecular sieve in order to remove the iodine. The molecular sieve plays a role in filtering organic iodine. The molecular sieve consists of the synthetic zeolite, silver zeolite is used so that the radioactive iodine is removed in the high temperature process. There are a lot of uniform tiny holes, therefore the gas coming from the molecular sieve will pass the holes to remove the iodine.

Finally an orifice and valve is installed after the exit of the molecular sieve. The location of orifice has to be optimized as it will change the volumetric flow into the molecular sieve, which would affect the amount of molecular sieve, which is quite expensive as it contains Ag.

Table II Local phenomena and scaling parameters

Components	Local Phenomena	Scaling parameters
Pool scrubber	Submerged Jet mixing Pool circulation Separation of aerosols-iodine Iodine absorption Entrainment	Jet Reynolds number, Nozzle diameter, Pool height and gas/liquid density ratio Iodine/aerosol density ratio, concentration flux Contact Surface area Pool height, gas velocity
Droplet separator	Droplet impact –breakup Re-entrainment	Entrained droplet and gas velocity Gas velocity at separator, flow path
Dry aerosol filter	Particle Capture	Filter pore size and flow path

### III. DESIGN OF A REDUCED SCALE TEST FACILITY

As described in the previous chapter, the key components of the FCVSs are a pool scrubbing chamber, droplet separator such as a cyclone, and dry aerosol filtration system. Each of these has

various phenomena associated with them. These local phenomena associated with each of these components are summarized in Table II. Also in this table the pertaining scaling parameters with each of the local phenomenon are listed. The major scaling parameters for designing a test

facility are a gas residence time and pressure drop.

### III.1. Scaling principle and design requirement

Based on the discussions in previous sections, scaling principle and design requirement for the integral test facility to simulate the performance of prototypic FCVS is provided. It is divided into source term, system performance, and local phenomena at the components including pool, venturi, cyclone, and Metal Fiber Filter.

The scaling principle for the source term and FCVS system performance is briefly summarized in Table III. The scaling principle is developed to preserve the important integral phenomena and decontamination principle in the prototype be preserved in the scale-down test facility.

The next step is to preserve the local phenomena in each components of FCVS system, which are discussed below.

### III.2. Venturi with Self priming mode

A schematic of venturi nozzle is shown in Fig 2. The venturi nozzle is located at the lower part of

the suppression tank, which has deep water pool. The venturi scrubber is operated in self priming mode such that water is injected from the pool through the holes located in the throat section of venturi. The pressure difference between the pool and inside the throat section of the nozzle drives the liquid inflow. The size of dispersed liquid droplet in the throat section depends on the size and number of holes, pressure difference, gas velocity, and thermos-physical properties of liquid.

Below is a discussion on the requirement on venturi dimensions and gas flow rate to enable self-priming mode of operation.

The pressure drop due to skin friction in a converging nozzle is calculated as below;

$$\Delta P_c = \int \left(\frac{f}{D}\right) \frac{1}{2} \rho v^2 dl \quad (1)$$

$$\dot{m} = \rho v (\pi D^2)/4 = \text{constant}. \quad (2)$$

The pressure drop is calculated as;

Table III Scaling Principle for the source term and FCVS system performance

	Prototype FCVS	Scaling Principle	Scaled Model
Source term	Discharge of steam and non-condensable gases with aerosols	Use the same fluid and/or similar non-toxic fluid	Use Steam, nitrogen, air, and aerosols
Early venting	Radioactive gas (noble, elemental and organic iodine), aerosols (lognormal, 3 $\mu\text{m}$ AMMD)	Preserve type and size Use of non-radioactive material	Gas (elemental and organic iodine), Particles 3 $\mu\text{m}$ AMMD (in-soluble particles such as $\text{SiO}_2$ )
Late venting	Penetrating small aerosols (0.5 $\mu\text{m}$ AMMD)	Preserve type and size Use of non-radioactive material	Particles at smaller size (in-soluble particles such as $\text{SiO}_2$ , 0.5 $\mu\text{m}$ AMMD)
Aerosol density	Typical Concentration in the containment (10 g /m <sup>3</sup> N, m <sup>3</sup> N means the volume at 0°C, 1 bar)	Preserve the typical density	Low density could be used, if measurement accuracy for the decontamination is warranted
System	Discharge of a mixture of steam and non-condensable gas from the containment at FCVS opening pressure, where aerosols are contained	Preserve thermal-hydraulic conditions  Maintain the range of mass flux	Full pressure  Reduce scale in flow area (1/N) Preserve the mass flux

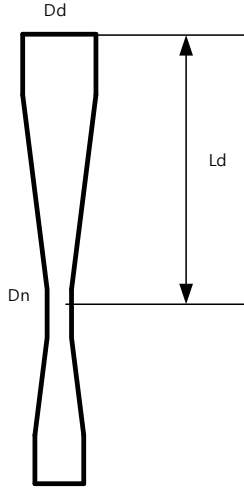


Fig.2. Schematic of venturi nozzle

$$\Delta P_c = 8f\dot{m}^2/(\rho\pi^2)L_i(D_n^2 + D_i^2)(D_n + D_i)/(D_n^4 D_i^4). \quad (3)$$

The pressure drop at the diffuser section can be calculated in a similar manner;

$$\Delta P_d = 8f\dot{m}^2/(\rho\pi^2)L_d(D_n^2 + D_d^2)(D_n + D_d)/(D_n^4 D_d^4). \quad (4)$$

However, this is a crude approximation. In reality, due to the injection of liquid into through the holes in the nozzle section, there will be a flow of two phase mixture of gas and liquid droplet. It will increase the pressure drop in the diffuser. So, the above equation should be modified as;

$$\Delta P_d = \Phi 8f\dot{m}^2/\rho\pi^2 L_d(D_n^2 + D_d^2)(D_n + D_d)/(D_n^4 D_d^4) \quad (5)$$

where  $\Phi$  is a two-phase multiplier to incorporate the effect of droplet gas mixture flow.

The pressure in the nozzle is calculated as;

$$P_i + \frac{1}{2}\rho v_i^2 - \Delta P_c = P_n + \frac{1}{2}\rho v_n^2. \quad (6)$$

The pressure in the diffuser is calculated as

$$P_n + \frac{1}{2}\rho v_n^2 - \Delta P_d = P_d + \frac{1}{2}\rho v_d^2. \quad (7)$$

At the exit of the diffuser, the gas flow will be discharged to the pool with the total pressure of  $P_d + 1/2\rho v_d^2$ , which will be static equilibrium with the pool of water. Pressure drop balance near venturi nozzle, for the liquid injection through the holes in the nozzle section, the pressure drop in the diffuser should be smaller than the hydrostatic head. To maintain the higher hydrostatic head the pool of liquid near the venturi should be maintained as liquid. The pressure at the nozzle inside the venturi is calculated as ;

$$P_n = P_d + \frac{1}{2}\rho v_d^2 + \Delta P_d - \frac{1}{2}\rho v_n^2. \quad (8)$$

The pressure in the pool outside the nozzle is calculated as ;

$$P_{no} = P_d + \frac{1}{2}\rho v_d^2 + \rho_p g L_d. \quad (9)$$

There is an assumption that the gas steam is in mechanical equilibrium with pool of water just at the exit of the diffuser. It is reasonable because the density of gas is much smaller than the liquid. Since the pressure inside the nozzle should be less than that the pool at the same elevation, we obtain the equation below;

$$\Delta P_d - \frac{1}{2}\rho v_n^2 < \rho_p g L_d. \quad (10)$$

From the expression,  $\dot{m} = \rho v_n (\pi D_n^2)/4$ ,

$$\Phi f/L_d(D_n^2 + D_d^2)(D_n + D_d)/D_d^4 - 1 < D_n^4 (\rho\pi^2 \rho_p g L_d)/(8\dot{m}^2) \quad (11)$$

$$\Phi f D_d/L_d(\zeta^2 + 1)(\zeta + 1) - 1 < (\rho_p g L_d)/(1/2\rho v_n^2) \quad (12)$$

, where  $\zeta = D_n/D_d$ .

It tells that the kinetic energy at the nozzle should be much smaller than the hydrostatic head to have a wide range of operation. As the fraction of droplet increases, we have bigger pressure drop in the diffuser section due to two phase mixture.

Also, if we have bigger nozzle velocity it is better in terms of droplet break up, but it reduces

the range of operation. So, there is a range of optimal operation, which has to be determined experimentally. By installing cooling fins at the outer surface of the FCVS tank is recommended to have subcooled water pool at least at the bottom of the tank to enable water injection into the nozzle section to enable self-priming mode of operation.

Lehner [6] indicated that the separation efficiency depends on the inlet gas velocity, and particle diameter and number of injection nozzles. Therefore, range of operation should be determined in a separate component test.

### III.3. Pool Scrubbing Phenomena

A brief discussion on the pool scrubbing phenomena is provide below to understand fundamental physics which influence the design of pool. Most information is taken from Reference 7.

Vapor scrubbing model on the removal of volatile gas like iodine is described in equation (13).

$$SF = 1 - \exp[-3k_2t_B/R_B] \quad (13)$$

In equation (13),  $k_2$  is overall mass transfer coefficient for vapor,  $t_B$  rise time of bubble,  $R_B$  radius of bubble.

Particle scrubbing mechanisms within a gas bubble are categorized in an inertial impaction for particles bigger than 0.5  $\mu\text{m}$  due to circulation of gas in a bubble, diffusion due to Brownian motion for small particles 0.1  $\mu\text{m}$ , and sedimentation for big particles larger than 1.0  $\mu\text{m}$ . If Brownian motion can be neglected, the scrubbing factor is expressed as ;

$$SF = 1 - \exp[-653.33t_B\rho_p r_p^2/(\mu_G R_B)] \quad (14)$$

, where  $\rho_p$  particle density,  $\mu_G$  viscosity of gas,  $r_p$  particle radius in cgs unit.

Decontamination factor is the ratio of initial ( $N_0$ ) to final amount ( $N_1$ ) of fission product after the scrubbing. It can be represented by equation (15),

where  $\lambda$  is the removal rate coefficient for a fixed and defined volume  $V$  of carrier gas.

$$DF = N_0/N_1 = \exp(\lambda t) \quad (15)$$

Results of previous experimental program [6] related to the pool scrubbing suggested that the pool depth, pool thermal-hydraulic condition and injector configuration is the major parameters affecting the decontamination factor. Therefore, maintaining the same pool height, the same unit cell injector with multi nozzles, and unit-cell thermal inertia will preserve the pool scrubbing phenomena for the particles and iodine vapor.

Pool scrubbing performance can be preserved by the unit cell of pool scrubber section to consider venturi to venturi interaction can be simulated. Also it is required to preserve pressure drop between each component while maintaining the same inlet velocity and K-factors.

### III.4. Droplet separator - Cyclone

Cyclone separators are gas cleaning devices that utilize the centrifugal force created by a spinning gas stream to separate particles from a gas. A standard tangential inlet vertical reverse flow cyclone separator is shown in Fig. 3.

The gas flow is forced to follow the curved geometry of the cyclone while the inertia of particles in the flow causes them to move toward the outer wall, where they collide and are collected. The gas stream may execute several complete turns as it flows from one end of the device to the other.

Correlations for typical pressure drop across the cyclone and cut off diameter can be found from Altmeyer et; el.[8] and Dirgo and Leith [9]. The pressure drop can be expressed as below;

$$\Delta P = 0.003\rho(16Q_0^2)/(abD_e^2) \quad (16)$$

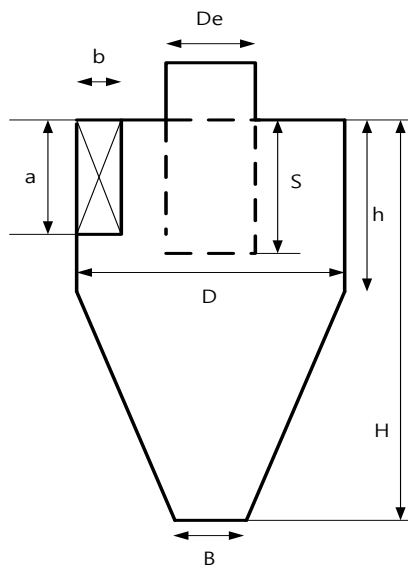
, where  $Q_0$  is inlet volumetric flow rate in  $\text{m}^3/\text{s}$ . And cut size diameter is given by;

$$d_{pc}^2 = (9\mu Dab)/[4\pi N_t Q_o(\rho_p - \rho)] \quad (17)$$

$$N_t = V_{ab}(0.1079 - 0.00077V_{ab} + 1.924 \times 10^{-6}V_{ab}^2) \quad (18)$$

where  $V_{ab} = Q_o/(ab)$ .

Fig.3. Typical cyclone dimension



It is shown that the pressure drop and cut off diameter is a strong function of volumetric flow rate. If we reduce the volumetric flow rate the pressure drop will decrease in a quadratic manner while the cut off diameter is inversely proportional. If we reduce the volumetric flow rate 1/4, the pressure drop will be 1/16. And the cutoff diameter will increase about 2 times.

As the number of cyclone is expected to be smaller than N, the mass flux to the cyclone at the reduced scale facility will be lower than prototype. Then the collection efficiency will be lower and the pressure drop will also be lower than the prototype. In terms of decontamination, this is conservative.

However, if we go with single nozzle the inlet velocity is small such that centrifugal force is

less than the gravity. So, the test with single nozzle has to go with reduced scale cyclone. However, as the performance of cyclone is non-linear a separate effect test is required to compare the performance of full scale cyclone and scaled cyclone.

If we go with multi nozzle such as three nozzles, the centrifugal force is greater than the gravity. Use of one full scaled cyclone is justified as it will give us a conservative result in terms of collection efficiency and cut off diameter.

If we use a prototype cyclone in a reduced scale, the inlet velocity of the cyclone will decrease if the scaling ratio M is bigger than the number of cyclone  $N_c$ .

Please note that if we want to the inlet velocity for the scaled down cyclone, the ratios of (ab) between the prototype and scaled model should be ;

$$(ab)_{experiment}/(ab)_{prototype} = N_c/M \quad (19)$$

If  $N_t$  and  $V_{ab}$  is maintained, then cutoff diameter can be maintained with the same D between the prototype and scaled facility. If the cyclone diameter decreases, it will result in a smaller cut off diameter, which is not conservative. And equation (16) indicates that the pressure drop will change with ratio of  $(Q_o/D_c)^2$ . So, the pressure drop will decrease in a scaled facility.

### III.5. Summary of Scaling Principle

A brief summary of scaling principle is described in Table IV. Prototypic venturi nozzles, cyclone, metal fiber filter and molecular sieves are used to maintain the local phenomena. The number and size of component is adjusted to preserve system performance at a reduced scale.

Separate Test for aerosols and iodine are considered. Mixture gas without steam could be conservative in terms of decontamination. Effect of steam could be simulated by a nearly saturated pool.

It is noted that the test facility is designed to be operated at full pressure and full temperature using the same fluid. So, there will be no scaling distortion in terms of material property. Also it is noted that the test facility is designed to have the same height as the prototype FCVS such that residence time of gases in the pool is maintained.

By scaling the mass flow rate to have the same mass flux, flow velocity is preserved. Also, the same fluid level in the pool would maintain the same thermal inertia of the fluid. How the local phenomena is preserved was already discussed.

Table IV. Summary of Scaling Principle for the Test Facility

	Parameter	CFVS	Test facility	Remarks
Decay heat	Decay heat from the FPs	Accumulate in the pool and MFF	Heating of MFF may be required	Decay heat from the FP particles has to be evaluated
System	Diameter	$D_p$	$D_p/M^{1/2}$	M is scaling ratio
	Height	$H_p$	$H_p$	Full height
	Design Pressure	$P_d$	$P_d$	Full pressure
	Design Temperature	$T_d$	$T_d$	Water subcooled and nearly saturated
	Flow rate	$Q_o$ or $\dot{m}_p$	$Q_o/M, \dot{m}_p/M$	
	Inlet dia./ Outlet dia.	$D_{ip}, D_{op}$	$D_{ip}/M^{1/2}, D_{op}/M^{1/2}$	System K factor has to be maintained
Scrubber	No. of Nozzle	$N_s$	$N_s/M$	Use of multiples of prototypic venturi
	Water Pool Height	$H_{pool}$	$H_{pool}$	
Droplet separator	Volumetric flow	$Q_o$	$Q_o/M$	Use a prototypic cyclone could be an option, $M > N_{ds}$ is conservative
	Inlet velocity	$Q_o / (A_{ds} \times N_{ds})$	$(Q_o/M) / A_{ds}$	
MFF	Height×Width×Depth×EA	$H_{mf} \times W_{mf} \times D_{mf} \times N_{mf}$	$H_{mf} \times D_{mf} \times (W_{mf} \times N_{mf}/M)$	Adjust number of MFF and width
Molecular Sieve	Height×Width×Depth×EA	$H_{ms} \times W_{ms} \times D_{ms} \times N_{ms}$	$H_{ms} \times D_{ms} \times (W_{ms} \times N_{ms})/M$	Adjust number of MS and width

#### IV. TEST CATEGORY FOR PERFORMANCE TEST

The following test category need to be performed to verify the performance of the FCVS. A brief summary of test and measurement requirement is described in Table V.

**Thermal hydraulic test:** An investigation into the thermal hydraulic phenomena in the FCVS will be performed. To measure the pressure drop at each component within the operating pressure range of the FCVS, at least two cases, which are high/low inlet pressure conditions, will be performed using 100% saturated steam. In addition, a test to observe the non-condensable gas effect in the scrubber pool will be performed, using the steam/nitrogen or steam/air gas.

**Dynamic test under high pressure gas discharge from containment:** During a severe accident, if the pressure inside the containment is reached at the specific opening value, the vent pipe will be opened and high-pressure gas will release into the FCVS. Through a dynamic test, it will be confirmed that the components in the FCVS are functioning normally during the transient process. It also needs some time to reach normal operation from a start-up. Thus, the measuring parameters are the change of the scrubber pool height, the pressure at each component, and the time to reach the normal

operation condition from a start-up. The non-condensable gas effect will be investigated.

**Aerosol removal test:** In a high inlet pressure condition, the collection efficiency of the scrubber and cyclone increases while the efficiency of the metal fiber filter and molecular sieve decreases. In contrast, the collection efficiency of the scrubber and cyclone decreases while the efficiency of the metal fiber filter and molecular sieve increases in the low inlet pressure condition. Thus, an aerosol removal test will be performed under the same conditions as a thermal hydraulic test. The decontamination factor (DF) of the FCVS is measured. To simulate the most severe case, a test will be conducted at a maximum aerosol concentration condition (less than  $10\text{g}/\text{m}^3$ ). Non-soluble particles such as  $\text{SiO}_2$  will be used. Furthermore, because it is hard to remove a  $0.5\text{-}\mu\text{m}$  particle, one aerosol removal test using small particles (near  $0.5\mu\text{m}$ ) will be conducted.

**Re-suspension of aerosol test:** As a change of the vessel temperature and pressure, the particles are re-suspended from the scrubber pool and surface of the component. In this test, it will be confirmed that the re-suspension of aerosol is removed in the FCVS. Most of this test will be conducted after an aerosol removal test.

Table V. Summary Test and Measurement requirement

	Design Requirement and Measurement requirement
Extended operation	<ul style="list-style-type: none"> <li>▪ Since the pool has to be heated up to the saturated condition, the duration of the test has to be estimated.</li> <li>▪ During the heat up process, the steam has to be discharged either to the ambient or to the suppression pool</li> <li>▪ The aerosols at the exit of the FCVS should be collected and should not be discharged to the ambient.</li> <li>▪ The duration of the test at saturated pool condition should be estimated to determine the size of the suppression tank. It could be in the range of hours.</li> <li>▪ Extended operation for the re-suspension test would require more hours for the operation</li> <li>▪ The test with iodine would require closed loop operation for the safety reason. However, closed loop system would result in a very big facility like cooling tower</li> </ul>
Re-suspension/ re-entrainment of aerosols from the pool	<ul style="list-style-type: none"> <li>▪ Extended operation of aerosol test approaching the maximum particle density in the pool</li> <li>▪ Measure DF just before MFF</li> <li>▪ Monitor Liquid droplet entrainment and removal by cyclone</li> </ul>
Retention of Iodine	<ul style="list-style-type: none"> <li>▪ Iodine gas concentration at inlet and exit of CFVS at given pool height, temperature, pH, and mixture velocity</li> <li>▪ Contaminated pool water should be treated carefully for the safety</li> <li>▪ Iodine concentration at the exit of the CFVS should be monitored, if it is above the safety level the test has to be terminated</li> <li>▪ The pipe should be coated to minimize iodine deposit on the piping.</li> </ul>

**Elemental iodine removal test:** As either the water content of radioactive gas increases or the velocity of gas increases, the collection efficiency of the molecular sieve decreases. For this reason, an iodine removal test will be conducted in a high inlet pressure with 100% steam. To simulate the most severe case, a test will be conducted at the maximum elemental concentration condition. Although the remove efficiency of iodine in a scrubber pool is dependent on the PH, this effect will not be observed in this performance test.

**Organic iodine removal test:** This test will be conducted according to the similar procedures to the elemental iodine removal test.

**Re-volatilization of iodine test:** As the change of the vessel temperature and the pressure, the

iodine is re-volatilized from the scrubber pool and the surface of the component. In this test, it will be confirmed that the re-volatilization of elemental/organic iodine is removed in the FCVS. Most of this test will be performed after an elemental/organic iodine removal test.

#### V. PROPOSED DESIGN IMPROVEMENTS

In addition to the need for the increase in decontamination of organic iodine, there are issues related to the performance of the system as the prolonged operation of FCVS, like more than 72 hours, are required after the advent of the Fukushima accident, where power recovery to the site took several days [1]. Some of the issues are already pointed out in Reference 2. In this section design improvements are suggested to solve outstanding issues.

### V.1. Collection efficiency of venture-scrubber

The collection efficiency of venture scrubber is a strong function of liquid inlet flow into the nozzle. During the prolonged operation of the FCVS, the fission product aerosols are accumulated in the lower part of the scrubbing pool. The decay heat from the fission product aerosols will heat up the liquid such that the lower part of the pool could be heated up until reaching the saturated condition. If the liquid in the lower part of the scrubbing pool becomes two phase liquid, the liquid inflow into the venture nozzle will decrease significantly due to increase in pressure drop through the nozzle holes and increase in void fraction. This would certainly result in a significant decrease in collection efficiency.

By providing a cooling fin on the surface of the tank and locating the lower part of the pool in a cavity where liquid can be flooded, the above issue can be minimized. The cooling provided by the boiling of the flooded water would maintain the temperature of the lower part of the liquid pool below saturation temperature. Then the performance of venture scrubber will not be deteriorated during long term operation. Conceptual picture of the proposed solution is shown in Fig. 4.

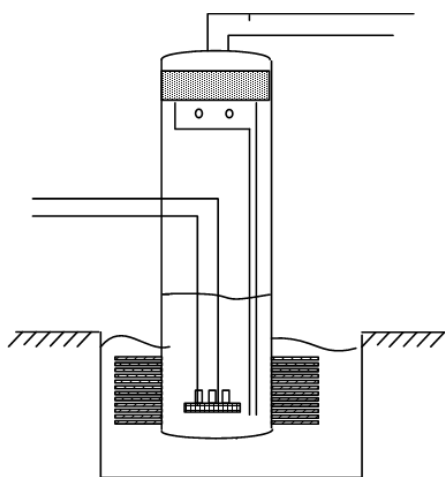


Fig.4. Cooling of scrubbing vessel

### V.2. Retention of gaseous iodine in a liquid pool

Retention of Iodine gas in the liquid pool is the major contributor for the gaseous iodine removal

in the FCVS system. The retention of Iodine in the liquid pool is highly affected by the pH of the liquid pool. Maintaining high pH helps to retain the iodine in the pool. However, the gamma radiation coming from the fission product tends to reduce the pH of the pool such that the iodine retention in the liquid pool is deteriorated while the fission product aerosols are accumulated in the liquid pool. To solve this problem it is suggested that separate tank be used for the removal of fission product aerosol and iodine retention [6, 10]. In the first tank the fission product aerosols be removed. Then in the second tank gaseous iodine is removed by pool scrubbing. As most of the fission product aerosols are removed in the first tank, the pH of the liquid in the second tank would not change. There will be no deterioration of gaseous iodine removal. Conceptual picture of proposed design is shown in Fig. 5.

### V.3. Provision for the bypass scenarios

Though the containment integrity is maintained, there are event sequences which would result in a bypass scenario such as steam generator tube rupture [11]. To mitigate these sequences it is suggested that the steam generator be flooded, which would result in a significant decontamination of fission product due to water scrubbing. However, the release to the environment in a long term cannot be avoided, because the atmospheric dump valve (ADV) of steam generator has to be opened to prevent steam generator overflow due to continuous leakage from the primary side of the reactor. This direct release to the environment has to be mitigated. Another usage of FCVS can be considered to handle this issue. It is suggested that the exit of ADV be connected to the FCVS to prevent direct release of radioactive material. Then there could be technical challenges. The design pressure and capacity of FCVS has to be increased to accommodate release from the steam generator.

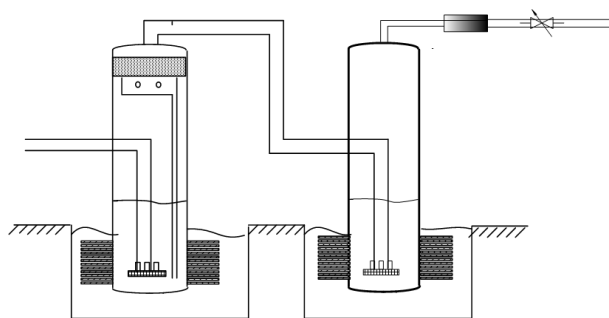


Fig.5. Proposed two tanks solution

## VI. CONCLUSION

An integral test facility at reduced scale is designed to verify the performance of a newly developed FCVS. A scaling principle is proposed where integral system behavior and local phenomena is preserved. A full pressure, temperature and full height test facility is developed. A test and measurement requirement is also developed for thermal-hydraulic test, aerosol removal and iodine gas removal test. Finally design improvements are proposed to solve the deficiencies of the current generation of FCVS.

## ACKNOWLEDGMENTS

This work was supported by the Korea Institute of Energy Technology Evaluation and Planning (KETEP) grant funded by the Korean government (Ministry of Trade, Industry, and Energy) (No. 20131510101700).

## REFERENCES

1. Report of Japanese Government to the IAEA Ministerial Conference on Nuclear Safety - The Accident at TEPCO's Fukushima Nuclear Power Stations -, June 2011, Nuclear Emergency Response Headquarters, Government of Japan.
2. Committee on the Safety of Nuclear Installations, "Status Report on Filtered Containment Venting", NEA/CSNI/R(2014)7, July 2014.
3. Committee on the Safety of Nuclear Installations, "Status-of-the-art Report on Nuclear Aerosols", NEA/CSNI/R(2009)5, Dec. 2009.

4. P. C. Pwczarski and K. W. Burk, "SPARC-90: A Code for Calculating Fission Product Capture in Suppression Pools", NUREG/CR-5765, Oct. 1991.
5. M. E. Berzal, et al., "State-of-the-art Review on Fission Products Aerosol Pool Scrubbing under Severe Accident Conditions", EUR Report 16241, 1995.
6. M. Lehner, "Aerosol Separation Efficiency of a Venturi Scrubber Working in Self-Priming Mode", Aerosol Science and Technology, Vol. 28, No.5, pp. 389-402, 1998.
7. M. Escudero Berzal, M.J. Marcos Crespo, M. Swiderska-Kowalczyk, M. Martin Espigares, J. Lopez Jimenez ISSN 1018-5593, State of the art review on fission products aerosol pool scrubbing under severe accident conditions, Report EUR 16241, 1995
8. S. Altmeyer, V. Mathieu, S. Jullemier, P. Contal, N. Midoux, S. Rode, J.-P. Leclerc, "Comparison of different models of cyclone prediction performance for various operating conditions using a general software", Chemical Engineering and Processing 43, pp. 511-522, 2004.
9. John Dirgo, David Leith, "Cyclone Collection Efficiency: Comparison of Experimental Results with Theoretical Predictions", Aerosol Science and Technology, 4:4, pp. 401-415, 1985.
10. Sang-Hyuk Jung, Jei-Won Yeon, Sue Young Hong, Yong Kang, Kyuseok Song, "The Oxidation Behavior of Iodide Ion under Gamma Irradiation Conditions", Nuclear Science and Engineering, 2015, in press
11. Y. Liao, S. Guentay, "Potential steam generator tube rupture in the presence of severe accident thermal challenge and tube flaws due to foreign object wear", Nuclear Engineering and Design, Vol.239, pp.1128-1135, 2009.

## THERMAL HYDRAULIC EFFECT ON IODINE IN THE FILTERED CONTAINMENT VENTING SYSTEM

Young Su Na(1)\*, Kwang Soon Ha(1), Sungil Kim(1), Jin Ho Song(1), and Song-Won Cho(2)

<sup>(1)</sup> Korea Atomic Energy Research Institute, Korea, <sup>(2)</sup> NSE, Korea

\*Corresponding author, tel: (+82) 42-868-8522, Email:ysna@kaeri.re.kr

**Abstract** – *The effect of thermal hydraulic conditions on iodine scrubbing in a FCVS (Filtered Containment Venting System) was estimated in this study. The decontamination factor of metal iodide aerosols especially cesium iodide (CsI), on a scrubbing solution in the FCVS was calculated by the MELCOR computer code, where SBO in the OPR 1000 was simulated and the FCVS operates when the pressure in the containment building approaches 5 bars. The dimensions of a cylindrical vessel for the FCVS are 3 m in diameter and 6.5 m height and a vessel includes a scrubbing solution of 21 tons. The decontamination factor increased rapidly as soon as the FCVS operated at 33 hours after the start of SBO. When the temperature of a scrubbing solution nearly reached its saturation temperature, the decontamination factor started to decrease. Steam condensation in a scrubbing solution can occur in the early FCVS operation, and a scrubbing solution is then constantly evaporates owing to the consecutive steam supply with high temperature from the containment building. The variation of the decontamination factor during the accident progress process can be determined by both the steam condensation and pool evaporation in the FCVS.*

## I. INTRODUCTION

The FCVS (Filtered Containment Venting System) has the main objectives of both the depressurization in the containment building and the decontamination of fission products generated under a severe accident. One of the commercial FCVS consists of a cylindrical pressure vessel including a scrubbing solution and filters (Ref. 1). A FCVS vessel can be installed on the outside of the containment building, and is connected with the containment through a venting pipe closed under normal conditions. When the pressure in the containment building approaches a setting value, which should be below the failure pressure of the containment, a venting pipe opens to operate the FCVS. The amount of steam and gas mixtures generated in the containment building under a severe accident can be released into the FCVS through a venting pipe, where the exit nozzles of a pipe are submerged into a scrubbing solution in the FCVS vessel. Non-condensable gases and fine aerosols can pass a scrubbing solution. They are released into the atmosphere, and they then enter the filters in the FCVS vessel. The decontaminated gases are finally discharged from the FCVS to the outside environment, and the pressure in the containment building decreases.

Previous studies (Refs. 2 and 3) calculated the thermal hydraulic variations in the FCVS vessel during a long operating time of over 24 hours using the MELCOR computer code. It was observed that a scrubbing solution in the FCVS vessel was constantly evaporating owing to high-temperature steam released continuously from the containment building. A scrubbing solution in the FCVS vessel was completely evaporated at about 31 hours after the FCVS operation. Pool evaporation in the FCVS vessel can negatively affect the decontamination feature of the FCVS because it reduces the scrubbing depth for fission products in an aerosol form. This study carefully evaluated the decontamination factor of metal iodide aerosols especially cesium iodide (CsI), on a scrubbing solution in the FCVS under thermal hydraulic variations during FCVS operation.

## II. METHODS

The MELCOR computer code simulated that one of the severe accident scenarios, an SBO (Station Blackout), occurred in a target nuclear power plant, an OPR 1000. The reactor type is a PWR (Pressurized Water Reactor) with a thermal power of 2,815 MWt. It is assumed that the FCVS (Filtered Containment Venting System) operates when the pressure in the containment building reaches 5 bars. This study applied the same MELCOR input file and the modeling of the FCVS used in the previous studies (Refs. 2 and 3). In the summary of the FCVS modeling, a cylindrical vessel for the FCVS has a 3 m diameter and 6.5 m height, and it includes a scrubbing solution of 21 tons, i.e., the pool depth is 3 m. The inlet of the FCVS vessel is connected with the containment dome through a venting pipe with a 25 cm diameter, where the control volume hydrodynamics (CVH) and flow path (FL) packages in the MELCOR computer code were used (Ref. 4). The exit of a venting pipe is submerged into a scrubbing solution in the FCVS vessel, and is located 2 m below the surface of a pool. A venting pipe includes a multi-hole sparger, which is defined in the radionuclide (RN) package (Ref. 4). The outlet of the FCVS vessel is linked to the outside environment through an exhaust pipe with a 25 cm diameter, where aerosol filters on this flow path (Refs. 2 and 3) were removed to estimate the decontamination factor on a scrubbing solution.

The decontamination factor of a cesium iodide (CsI) aerosol on a scrubbing solution in the FCVS is defined by the ratio of the input mass of CsI aerosol to its output mass. The MELCOR computer code can calculate the mass of the CsI aerosol in the atmosphere and a pool in the FCVS vessel and the outside environment. The input mass of CsI aerosol into a scrubbing solution in the FCVS is the sum of CsI aerosol mass in a pool in the FCVS vessel and the output mass of CsI aerosol from a scrubbing solution, where the output mass can be estimated by CsI aerosol mass in the FCVS vessel atmosphere plus that in the outside environment.

### III. RESULTS AND DISCUSSION

To assess the thermal hydraulic effect on cesium iodide (CsI) aerosol scrubbing in the FCVS (Filtered Containment Venting System), the variation of aerosol mass during the accident progress process was calculated by the MELCOR computer code.

Figure 1 shows the accumulated mass of CsI aerosol in a scrubbing solution in the FCVS vessel, where the aerosol mass deposited on the heat structure, i.e. a FCVS vessel wall, was not included. As soon as the FCVS operates at 33 hours after the start of SBO, the CsI aerosol mass increases continuously until 59 hours. The increment rate of the aerosol mass in Fig. 1 eventually slows. The accumulated mass of the CsI aerosol in a scrubbing solution is unvaried from 59 hours to 64 hours in Fig. 1. This indicates that the mass released from the containment building into a scrubbing solution in the FCVS is identical to the mass discharged from a pool into the atmosphere in the FCVS vessel, i.e., there is no scrubbing of CsI aerosol in a pool in the FCVS vessel. In addition, the elevation of the pool level in the FCVS vessel at 59 hours decreased by that of the venting pipe exit, which was initially submerged into a scrubbing solution in the FCVS vessel, i.e., the distance to the scrub aerosol became zero (Refs. 2 and 3). The accumulated mass of CsI aerosol in a scrubbing solution falls sharply at 64 hours in Fig. 1 because a pool in the FCVS vessel was completely evaporated at that time (Refs. 2 and 3), i.e., no aerosol particles remain in the scrubbing solution.

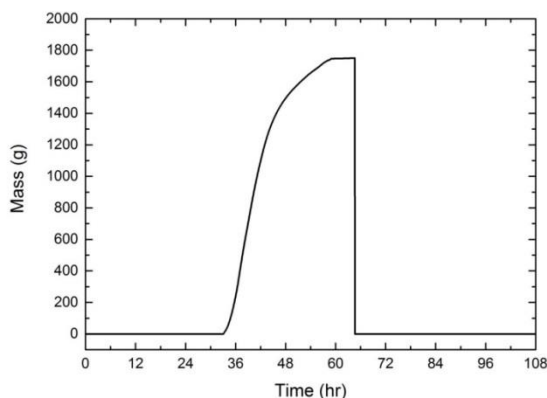


Fig. 18. Accumulated mass of CsI aerosol in a pool in the FCVS vessel.

Figure 2 shows the accumulated mass of CsI aerosol in the FCVS vessel atmosphere. It was observed that there are no CsI aerosols in the atmosphere in the FCVS vessel from the start of the FCVS operation to about 59 hours. It can be explained by a thorough scrubbing of CsI aerosol in a pool below the atmosphere in the FCVS vessel until 59 hours in Fig. 1. The accumulated mass of CsI aerosol in the FCVS vessel atmosphere increases from 59 hours to 72 hours in Fig. 2, where the elevation of a scrubbing solution approached the venting pipe exit at 59 hours, and a pool was completely evaporated at 64 hours (Refs. 2 and 3). The first peak of the accumulated mass at 64 hours in Fig. 2 can occur because the remaining CsI aerosol in a pool can be released suddenly into the atmosphere in the FCVS vessel. The accumulated mass of CsI aerosol reaches the maximum value at 72 hours, and then decreases in Fig. 2. This can be caused by the reduction of CsI aerosol generation in the containment building under a severe accident at 72 hours in Fig. 3, which shows the accumulated mass of CsI aerosol in the atmosphere in the containment building dome.

Figure 4 shows the accumulated mass of CsI aerosol in the outside environment, where the aerosol mass deposited on the heat structure, i.e., the environment wall, was not included. CsI aerosol mass discharged from the FCVS to the outside environment through the exhaust pipe starts to increase at 59 hours. When the pool depth to scrub aerosol in the FCVS becomes zero at 59 hours (Refs. 2 and 3), CsI aerosol appears in the atmosphere above a scrubbing solution in Fig. 2, as well as in the outside environment in Fig. 4. The accumulated mass of CsI aerosol increases from 59 hours to 90 hours in Fig. 4, where the amount of CsI aerosol generated in the containment building under a severe accident reduces near 90 hours in Fig. 3. The accumulated mass of CsI aerosol in the outside environment is kept from 90 hours because the amount of CsI aerosol discharged from the containment building is constantly decreasing, and it finally becomes zero, which is shown in Fig. 3.

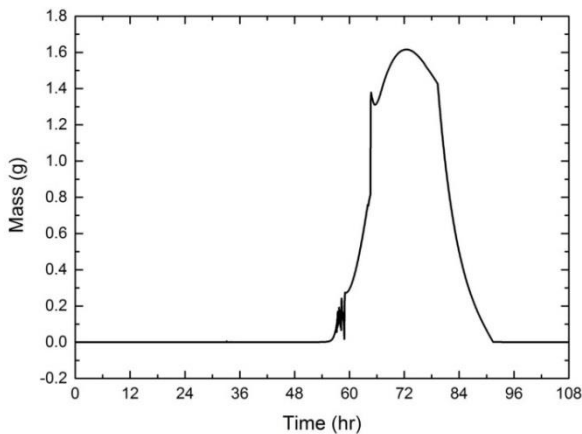


Fig. 19. Accumulated mass of CsI aerosol in the FCVS vessel atmosphere.

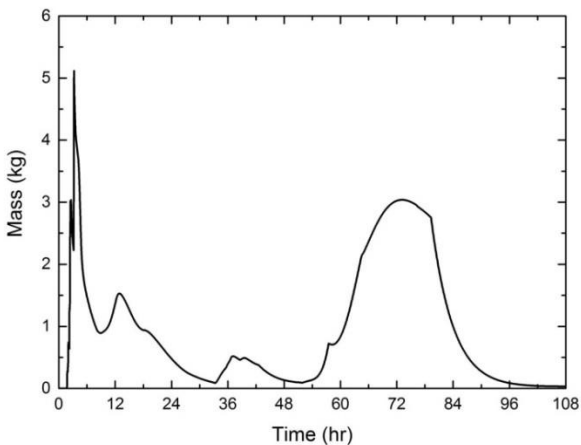


Fig. 20. Accumulated mass of CsI aerosol in the containment atmosphere.

Figure 5 shows the input and output of the accumulated CsI aerosol mass on a scrubbing solution in the FCVS in the left axis, where the input indicates the accumulated mass of CsI aerosol released from the containment building to a scrubbing solution, and the output presents the accumulated mass of CsI aerosol discharged from a scrubbing solution in the FCVS. In addition, the right axis of Fig. 5 shows the decontamination factor of CsI aerosol on a scrubbing solution in the FCVS. The output mass is the sum of accumulated mass of CsI aerosol in the FCVS vessel atmosphere in Fig 2, and that in the outside environment in Fig 4. The input mass can be calculated by the accumulated mass of CsI aerosol in a scrubbing solution in Fig. 1 plus the output mass in Fig. 5. To estimate the

decontamination factor of CsI aerosol on a scrubbing solution in the FCVS, the input mass was divided by the output mass. The input mass increases continuously from 33 hours to 64 hours, where the FCVS operation started at 33 hours, and a scrubbing solution was completely evaporated at 64 hours (Refs. 2 and 3). As soon as the pool level approaches the bottom of the FCVS vessel at 64 hours, the inlet mass falls sharply, and its variation then follows the accumulated mass of CsI aerosol in the outside environment in Fig. 4. The output mass in Fig. 5 also depends on the accumulated mass of CsI aerosol in the outside environment in Fig. 4, where the amount of the accumulated mass of CsI aerosol in the atmosphere in the FCVS vessel in Fig. 2 is relatively too small. The output mass in Fig. 5 starts to increase when the pool level is reduced by the level of a venting pipe exit initially submerged in a scrubbing solution in the FCVS vessel. The accumulated output mass is unvaried from about 90 hours because the amount of CsI aerosol mass generation in the containment building under a severe accident is constantly decreasing from 72 hours in Fig. 3.

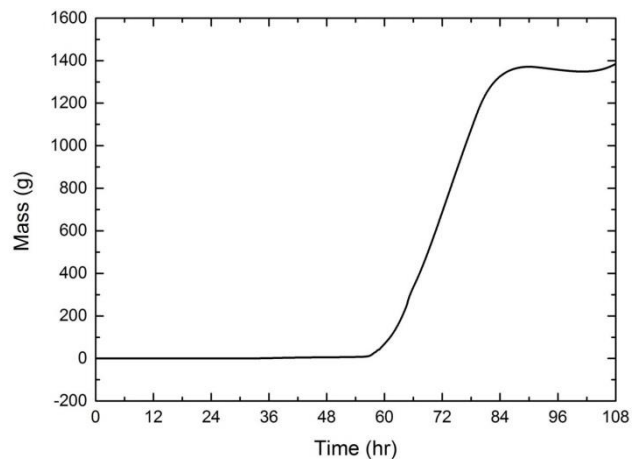


Fig. 21. Accumulated mass of CsI aerosol in the outside environment.

The decontamination factor of CsI aerosol on a scrubbing solution in the FCVS presented in the right axis of Fig. 5 starts to dramatically increase at 33 hours as soon as the FCVS operates. It peaks at 50 hours, where the pool temperature in the FCVS vessel reached its saturation temperature at that time (Refs. 2 and 3), and it

then decreases sharply by unity, i.e., no scrubbing of CsI aerosol in a pool in the FCVS, at 64 hours, where a scrubbing solution was completely evaporated at 64 hours (Refs. 2 and 3). In the early FCVS operation, the condensation of high-temperature steam released from the containment building to a room-temperature scrubbing solution in the FCVS vessel occurs due to the temperature difference. Steam condensation can enhance the ability to capture particles in a scrubbing solution. In addition, aerosol particles can stay longer in a scrubbing solution because steam condensation increased the pool level (Refs. 2 and 3). Opposite the steam condensation in the early FCVS operation, the evaporation of a scrubbing solution took place owing to a consecutive supply of high-temperature steam from the containment building (Refs. 2 and 3). The evaporation negatively affects the particle scrubbing in a FCVS pool, where the pool level was continuously decreased from 36 hours to 64 hours (Refs. 2 and 3). In addition, the scrubbing depth also decreases during the pool evaporation, i.e. the time for particles staying in a scrubbing solution becomes short. The decontamination factor of CsI aerosol on a scrubbing solution can be finally dependent of the thermal hydraulic conditions in the FCVS vessel.

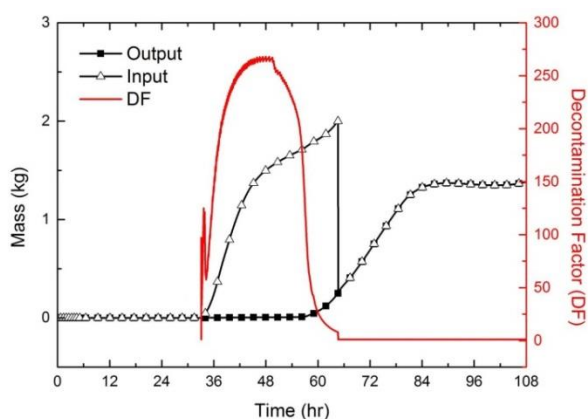


Fig. 22. Decontamination factor calculated by input and output of CsI aerosol mass on scrubbing solution.

#### IV. CONCLUSION

This study estimated the decontamination factor of metal iodide aerosols, especially cesium iodide (CsI), on a scrubbing solution in the FCVS (Filtered Containment Venting System). The MELCOR computer code simulated that an SBO (Station Blackout) occurred in the OPR 1000, where the FCVS operates when the pressure in the containment building approaches 5 bars. The FCVS consists of a cylindrical vessel with a 3 m diameter and 6.5 m height, and it includes a scrubbing solution of 21 tons. Accumulated mass of CsI aerosol was calculated in a scrubbing solution and the atmosphere in the FCVS vessel and the outside environment. The variations of CsI aerosol mass during a severe accident progress can be affected by the thermal hydraulic conditions in the FCVS. The CsI aerosol was released into a scrubbing solution in the FCVS as soon as the FCVS operated at 33 hours after the start of an SBO, and it increased by 59 hours. The scrubbing solution was constantly evaporating because of the amount of high-temperature steam released from the containment building to a pool in the FCVS vessel. The pool level in the FCVS vessel decreased by the elevation of the exit of a venting pipe, which was initially submerged in a pool, and a scrubbing solution was then completely evaporated at 64 hours.

The decontamination factor of CsI aerosol on a scrubbing solution in the FCVS vessel can be determined by the thermal hydraulic conditions. In the early FCVS operation, the decontamination factor of CsI aerosol rapidly increased owing to steam condensation in a scrubbing solution. When the temperature of the scrubbing solution approached its saturation temperature, the decontamination factor of CsI aerosol started to decrease because of pool evaporation in the FCVS. Particle capture in a scrubbing solution can be affected by both the steam condensation in a scrubbing solution in the early FCVS operation and the pool evaporation owing to a consecutive supply of high-temperature steam from the containment building. In this study, it is clearly observed that the decontamination factor of CsI aerosol on a scrubbing solution can be dependent on the thermal-hydraulic conditions in the FCVS.

It is necessary to add a pool chemistry model to estimate the gas phase iodine which was not considered in this study. We are developing an analysis tool to assess the performance of the FCVS, i.e., depressurization and decontamination, where the MELCOR computer code can calculate the behaviour of the fission product under a severe accident, as well as thermal hydraulic conditions. The sensitivity analysis is required to enhance the reliability of calculation results. Further studies on an operating procedure of the CFVS and the interaction among safety systems can contribute to improve a strategy for severe accident management.

#### ACKNOWLEDGMENTS

This work was supported by the National Research Foundation of Korea (NRF) grant funded by the Korea government (Ministry of Science, ICT, and Future Planning) (No. NRF-2012M2A8A4025893).

#### REFERENCES

1. AREVA's presentation to US Nuclear Regulatory Commission, "Filtered Containment Venting Systems: General

Overview and Applicability to CANDU Plnats," ML12206A266 (2012).

2. YOUNG SU NA, KWANG SOON HA, REA-JOON PARK, JONG-HWA PARK, and SONG-WON CHO, "Thermal hydraulic issues of containment filtered venting system for a long operating time," *Nuclear Engineering and Technology*, **46**, 6, 1-6 (2014).
3. YOUNG SU NA, KWANG SOON HA, RAE-JOON PARK, JONG-HWA PARK, and SONG-WON CHO, "Design of containment filtered venting system for depressurization in containment under severe accidents," *Proc. of ICAPP 2014*, Charlotte, USA (2014).
4. R. O. Gauntt et al., "MELCOR Computer Code Manuals Vol. 1: Primer and Users Guide Version 1.8.6 September 2005", SAND 2005-5713, Sandia National Laboratories, USA (2005).

## INVESTIGATION OF IODINE RETENTION IN A FILTERED CONTAINMENT VENTING SYSTEM IN THE VEFITA TEST PROGRAM

*D. Suckow(1)\*, M. Furrer(1), J. Yang(1), B. Jäckel(1), T.Lind(1)*

*<sup>(1)</sup> Paul Scherrer Institute, Villigen-PSI, Switzerland*

*\*Corresponding author, tel: (41)563104145, Fax: (+41)3104481, detlef.suckow@psi.ch*

**Abstract** – *An extensive experimental and analytical program has been conducted to study the iodine chemistry for both molecular iodine and organic iodide (i.e. methyl iodide) in aqueous solutions. Based on these investigations a novel chemical process was established which uses a phase transfer catalyst (Aliquat336<sup>®</sup>) as a co-additive to sodium thiosulfate widely used in water pools of filtered containment venting systems (FCVS). Experiments under a variety of conditions have shown the process effectively decomposes volatile gaseous organic iodide into non-volatile iodide ions and effectively hinders their revolatilization by radiolytic oxidation. First experiments in a dynamic system of a small lab-scale liquid scrubber column demonstrate promising decontamination factors for methyl iodide. It is foreseen to apply the process in a commercial FCVS. To assess the retention for gaseous iodine species under anticipated severe accident flow conditions a full height, reduced diameter model of a FCVS was erected and measurement techniques developed to measure molecular and methyl iodide concentrations at the inlet and outlet side of the test facility. Planned experiments are presented to determine the decontamination factors for both iodine species. An outlook to accompanying analytical and experimental work is given to model the two-phase flow hydrodynamics in water pools of FCVS.*

## I. INTRODUCTION

Modern filtered containment venting systems (FCVS) can considerably reduce the leakage of radioactive materials to the environment. In many countries the implementation of FCVS's is under discussion to mitigate fission product release not only in the short-term but also in the long-term view. In severe accidents elemental and organic iodides are the main gaseous iodine species in the containment atmosphere. Release of the gaseous species in sufficient quantities from containment filter systems generates a risk for public health.

Experimental programmes have confirmed the existence of gaseous organic iodide in the long-term in even higher concentrations than for gaseous molecular iodine ( $I_2$ ), [1]. Methyl iodide ( $CH_3I$ ) is probably the most dominant volatile organic iodide compound in relevant accident conditions. Its reaction with surfaces and the removal by i.e. containment filters and scrubbers is less efficient in comparison to molecular iodine.

In the recent years an experimental and analytical research program has been conducted at the Paul Scherrer Institute (PSI) to develop a process leading to a fast, comprehensive and reliable retention of volatile iodine species in aqueous solutions, i.e. in the water pool of a scrubber type FCVS.

A summary of the PSI work on the iodine chemistry since 2002 in the presence of impurities and additives in aqueous solutions under the influence of different conditions including radiation is presented in a separate paper in this publication [2].

The result of this extensive work is a novel established process to fast decompose volatile iodine species into non-volatile ions in aqueous solution. The process has been tested in small lab-scale under different boundary conditions including the influence of radiation, pH, temperature and impurities.

In this paper the novel process and the main experimental findings are presented together with

the VEFITA (**V**enting **F**ilter **A**ssessment) test program which aims to experimentally determine the enhanced retention of organic iodide species using this process in a representative, scaled model of a technical scrubber type FCVS under prototypical thermal-hydraulic flow conditions. Tests are planned with elemental iodine or with organic iodide loaded carrier gas consisting of pure non-condensable gas, pure steam and of typical mixtures of non-condensable gas/steam.

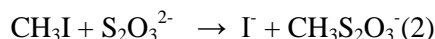
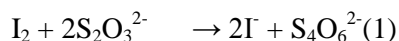
## II. THE NOVEL PROCESS

The objective of the PSI research and development program was to establish a process for a fast and effective decomposition of gaseous methyl iodide and to reduce iodine volatility to a minimum or, ideally, to hinder it completely. Research since the 1970s ([3]) has suggested that sodium thiosulfate  $Na_2S_2O_3$  (THS) dissolved in spray water would increase the decomposition of molecular iodine and organic iodide. It was also concluded that the  $CH_3I$  decomposition rate is not high enough to reduce gaseous iodine activity in the containment using THS in the aqueous solution in spray droplets. Additionally, the use of a high pH in water pools was suggested to retain the iodide formed as a non-volatile product of gaseous  $CH_3I$  decomposition or  $I_2$  hydrolysis. To enable a fast and complete  $CH_3I$  decomposition in an aqueous solution a chemical reagent (additive) should be sufficiently thermally and radiolytically stable, must enhance and not suppress the thermal and radiolytic decomposition of  $CH_3I$ , be usable in a wide pH range, in the presence of impurities in the aqueous solution and at anticipated boundary conditions of a scrubber type FCVS. Ideally the additive should help to bind iodide, thus suppressing its subsequent thermal and radiolytic oxidation to volatile elemental Iodine.

In the development program PSI found a second additive to act as a co-additive to the widely used THS to increase sufficiently high the  $CH_3I$  decomposition rate, a quaternary long chain ammonium salt, Aliquat336<sup>®</sup>. It contains a mixture of C8 (octyl) and C10 (decyl) chains with C8 predominating. Aliquat336<sup>®</sup> (ALI) is a commercial reagent [4], which is successfully applied in nuclear technological processes, such

as spent fuel reprocessing and other metallurgical processes for metal extraction. The high stability to ionizing radiation was demonstrated by the spent fuel reprocessing industry.

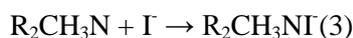
The removal process of volatile gaseous iodine species from gas bubbles in an aqueous solution takes place by the nucleophilic reduction of elemental iodine and organic iodides with THS, Eq.(1) and Eq.(2).



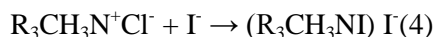
While the first reaction is fast and effective, the second reaction needs to be accelerated. Aliquat336<sup>®</sup> has a dual function.

Aliquat336<sup>®</sup> functions as a phase transfer catalyst by clustering both reactants, i.e. THS ions and the CH<sub>3</sub>I molecules get together to accelerate their interaction. Thus the decomposition of CH<sub>3</sub>I is enhanced.

In addition Aliquat336<sup>®</sup> contains an inorganic anion (chloride) which can act as an ion exchange for iodide ions and thus preventing their radiolytic oxidation into I<sub>2</sub>. In this way the CH<sub>3</sub>I decomposition product iodide can be bound. The ion exchange takes place as a concurrent reaction to the nucleophilic reduction by a covalent reaction with an exchange of iodide ion for the chloride ion to form a tertiary amine Eq.(3) and quaternary long chain ammonium salt Eq.(4).



and



This novel process developed at PSI was successfully patented ([5]) and is foreseen to be applied in a commercial FCVS ([6], [7]).

Many experiments were conducted to achieve an optimum mixture of THS and Aliquat336<sup>®</sup> under a wide range of conditions, such as temperature, pH, interference from co-existing ions, thermal and radiation ageing. In the

experiments the radiotracer technique was applied using the iodine isotope <sup>131</sup>I to label methyl iodide (CH<sub>3</sub><sup>131</sup>I) and to track CH<sub>3</sub>I decomposition and its products. An overall mass balance was performed for each test by determining the deposited activity in the different components of the test setup which could usually be closed by an uncertainty of typically ±15%. This technique provided sufficient sensitivity to detect near complete decomposition. Tests were performed in small lab scale reaction vessel typically of a few cm<sup>3</sup> in volume. The pH in the different test solutions were usually buffered using boric acid and sodium borate mixtures, or by adding sodium hydroxide to boric acid solutions. The main findings are presented in the following sections.

Maximum decomposition rates for CH<sub>3</sub>I were obtained for specific THS and Aliquat336<sup>®</sup> concentrations in aqueous solutions, subject to the patent. Figure 1 shows the CH<sub>3</sub>I decomposition rate at 22°C and pH 9 versus Aliquat336<sup>®</sup> aqueous concentrations for different THS concentrations. Aliquat336<sup>®</sup> becomes effective once the concentration is higher than about 1.10<sup>-5</sup> mol/dm<sup>3</sup>. The data confirm the effectiveness of Aliquat336<sup>®</sup> even when the CH<sub>3</sub>I initial concentration is increased 15 times and the optimized THS concentration remain unchanged. The rates for Aliquat336<sup>®</sup>-free reaction solutions are shown in the log-scale diagram at a fictive concentration of 10<sup>-7</sup> mol/dm<sup>3</sup>. Low concentrations of Aliquat336<sup>®</sup> (< 2.10<sup>-5</sup> mol/dm<sup>3</sup>) do have only a small beneficial effect. The effect is pronounced for ratios of THS:Aliquat336<sup>®</sup> of about 10:1.

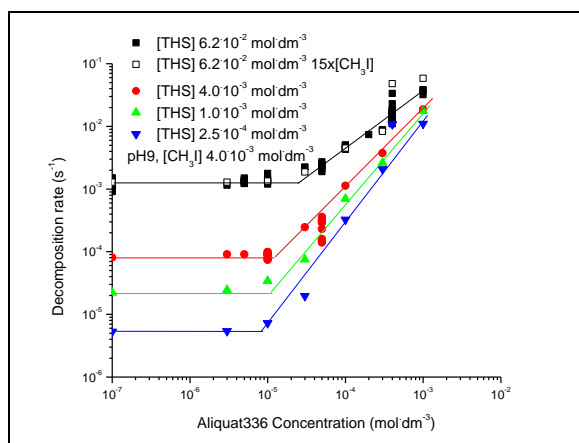


Fig. 1.  $\text{CH}_3\text{I}$  decomposition rates vs. Aliquat336 and THS concentrations.

Figure 2 presents the influence of pH of the solution on the decomposition rate of  $\text{CH}_3\text{I}$  in the presence or absence of Aliquat336<sup>®</sup> at the optimized THS concentration of  $6.2 \cdot 10^{-2} \text{ mol/dm}^3$  at a temperature of  $22^\circ\text{C}$ . Different  $\text{CH}_3\text{I}$  concentrations were tested. The significantly enhanced  $\text{CH}_3\text{I}$  decomposition rate in the presence of Aliquat336<sup>®</sup> is apparent and is nearly 2 orders of magnitudes higher than with THS only. The rate is independent of the pH in the range of 4 to 14 and is even effective at strong acidic conditions. The slower decomposition rate for  $\text{pH} < 4$  may be due to Aliquat336<sup>®</sup> decomposition or net yet known effects in more acidic solutions.

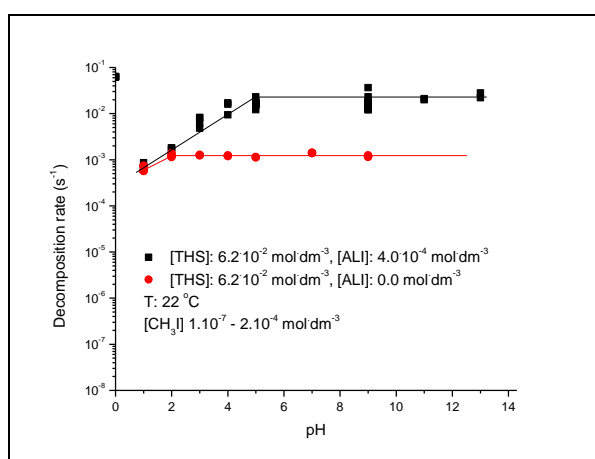


Fig. 2.  $\text{CH}_3\text{I}$  decomposition rates vs. pH, with THS, w/w/o Aliquat336<sup>®</sup>.

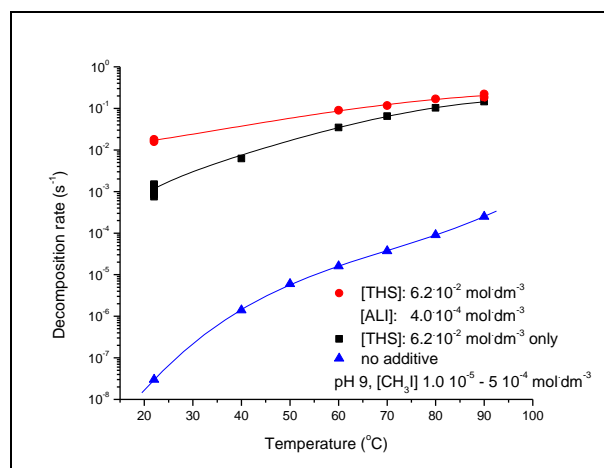


Fig. 3.  $\text{CH}_3\text{I}$  decomposition rates vs. temperature w/w/o THS and w/w/o Aliquat336<sup>®</sup> at pH 9.

Decomposition rates for  $\text{CH}_3\text{I}$  are temperature dependent. The decomposition rates at temperatures between  $22^\circ\text{C}$  and  $90^\circ\text{C}$  obtained for pH 9 buffered solutions are shown in Figure 3 for mixtures of Aliquat336<sup>®</sup> and THS, for THS only and are compared to additive-free  $\text{CH}_3\text{I}$  solutions. The additives clearly bring a rate increase of several orders of magnitude, although the decomposition rates had increased more slowly with temperature than without additives. The addition of Aliquat336<sup>®</sup> to the THS solution increased the rate for low temperatures by a factor of about 10 but the rate increase at higher temperatures is smaller, apart from the higher hydrolysis rates.

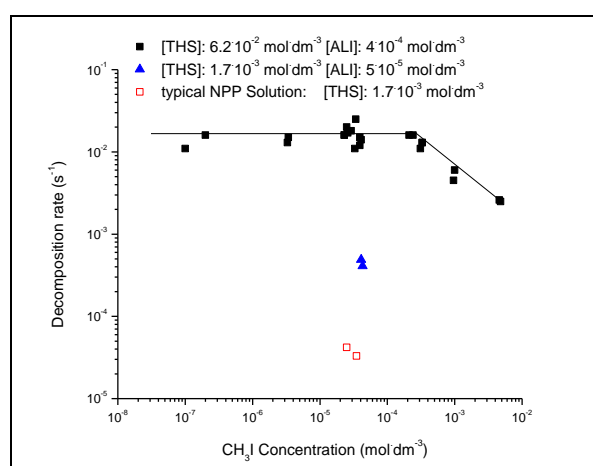


Fig. 4.  $\text{CH}_3\text{I}$  decomposition rates vs.  $\text{CH}_3\text{I}$  concentration at pH 9 and room temperature, w/w/o Aliquat336<sup>®</sup>.

The measured decompositions rates at 22°C and pH 9 as a function of the initial  $\text{CH}_3\text{I}$  concentration derived for the optimum concentrations of THS and Aliquat336® in the solution is presented in Figure 4. For comparison the decomposition rate obtained for a typical scrubber solution in a FCVS of a nuclear power plant using THS only with a concentration of  $1.7 \cdot 10^{-3} \text{ mol/dm}^3$  is shown. By adding Aliquat336® at an aqueous concentration of  $5 \cdot 10^{-5} \text{ mol/dm}^3$  an increase of the rate by one order of magnitude can already be achieved. Using a further increase of the concentrations of THS and Aliquat336® to the optimal values of  $6.2 \cdot 10^{-2} \text{ mol/dm}^3$  and  $4 \cdot 10^{-4} \text{ mol/dm}^3$ , respectively, an overall enhancement in the decomposition rates of 2 to 3 orders of magnitudes compared to a typical scrubber solution can be achieved.

Separate experiments were performed to confirm the effectiveness of Aliquat336® to bind iodide ions as a result of the exchange of I for Cl in the quaternary ammonium compound including irradiation conditions. The fixation ability of Aliquat336® for  $\text{I}_2$  is demonstrated in Figure 5, which shows the  $\text{I}_2$  release fraction versus time from a solution where only  $\text{I}_2$  or  $\text{I}^-$  and  $\text{I}^-$  ions are present. The tests were performed at 22°C and pH 5 under un-irradiated conditions. The solution was sparged with Argon gas for a certain time. In the presence of Aliquat336® the release of  $\text{I}_2$  was greatly reduced. This gives an insight into the effect of Aliquat336® in hindering the radiolytic oxidation of iodide ions to form volatile  $\text{I}_2$ .

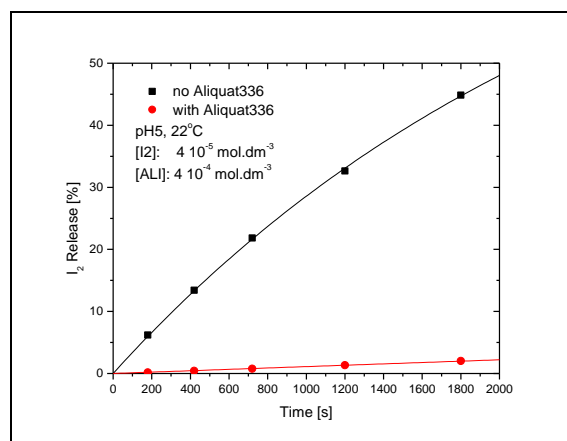


Fig. 5. Influence of Aliquat336® on  $\text{I}_2$  fraction released vs. sparging time at 22°C and pH 5.

### III. BASIC EXPERIMENT

To obtain an estimate of the potential decontamination factor (DF) in a scrubber type filter system containing the optimized THS and Aliquat336® aqueous solution mixture several small-scale laboratory tests in a column type scrubber were performed. The DF is defined as the ratio of the mass of a species at the inlet of a system to the one at the outlet. The test setup consists of two different vessels. Table I provides the main dimensions and experimental conditions.

Total Height	m	2.0
Sparger Submergence	m	0.035 - 1.40
Liquid volume	l	0.2 - 0.8
Pressure, inlet	bar(abs)	1.0 - 1.2
Pressure, test section	bar(abs)	ambient
Gas temperature, inlet	°C	22
Water temperature	°C	22 - 80
Argon gas flow rate	$l_n/\text{min}$	0.052 - 0.103

Table I. Column scrubber dimensions and boundary conditions.

The first vessel (donor vessel) contained an aqueous solution of liquid  $\text{CH}_3\text{I}$  labelled with  $^{131}\text{I}$ , without any additives and with a gas phase above the liquid. The second vessel (scrubber column) was filled with an aqueous solution of the decomposing substances for  $\text{CH}_3\text{I}$  retention. Both vessels were connected by a flexible small PTFE (Polytetrafluoroethylene) tube as shown in Figure 6a. As scrubber a 2 m long glass tube with a heating jacket was used to perform tests at different liquid temperatures. At the bottom of

each vessel a gas discharge unit (frit) was installed producing small gas bubbles in the size range of 1-2 mm. A gas flow of Argon at room temperature, controlled by an electronic mass flow controller, was used to sparge the  $\text{CH}_3\text{I}$  from the donor vessel into the scrubber column. The remaining  $\text{CH}_3\text{I}$  released into the gas stream leaving the scrubber column was trapped in activated charcoal (ACC) filter impregnated by tri-ethylene-diamine (TEDA) placed at the outlet. Dedicated experiments were previously conducted to determine the liquid  $\text{CH}_3\text{I}$  transfer rate from the aqueous solution in the donor vessel into gas bubbles. Before and after the tests samples were taken from the solutions in the donor and scrubber vessel using a specific handling procedure. The samples and the ACC-filters were measured with a NaI  $\gamma$ -ray detector and analyzed to achieve a complete mass balance.

Tests were performed at temperatures of the aqueous solution in the scrubber column from 22°C to 80°C. The required pH in the scrubber solution was buffered and obtained using boric acid ( $\text{H}_3\text{BO}_3$ ) and sodium hydroxide (NaOH) mixtures. Different solution heights were involved in the scrubber, which determine together with the bubble diameters the bubble residence time. The residence time was estimated to be between 5 s up to 35 s depending on the conditions used. A bubble diameter reduction from 1-2 mm to less than 1 mm was observed when either pure water (Figure 6a) or a mixture of THS and Aliquat336<sup>®</sup> (Figure 6b) was used, respectively. The reduction in bubble size diameter is due to the lower surface tension in the presence of Aliquat336<sup>®</sup>.

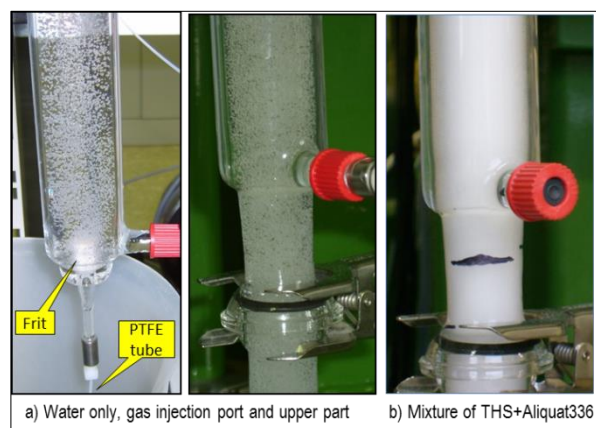


Fig. 6. View of bubbles in column scrubber at different conditions.

Figure 7 shows the measured decontamination factors  $DF^*$  normalized by the height of the scrubber solution as a function of the scrubber liquid temperature. A strong influence of the temperature on the decomposition of methyl iodide was found. The decontamination factor at room temperature varied from 3 to 19 and depended on the water height in the scrubber and whether THS was used alone or a mixture of THS and Aliquat336<sup>®</sup>. The solution with Aliquat336<sup>®</sup> at the derived optimum concentrations showed an increase in the  $DF^*$  by a factor of about two at the different temperatures. Without the additives (pure water) no decontamination took place. The  $DF^*$  was about 2600 when using the additive mixture at 75 °C. This value is about 150 times higher than at room temperature.

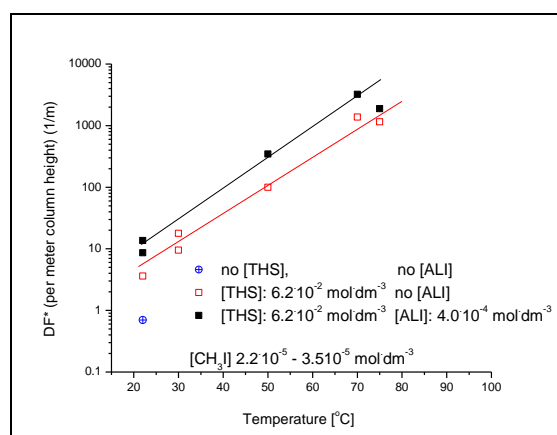


Fig. 7. Normalized decontamination factor  $DF^*$  vs. temperature in a column scrubber, w/o Aliquat336<sup>®</sup>, w/w THS.

These experiments provided first results on the sub-mergence and temperature dependent decontamination factor of a dynamic scrubber system, where a mass transfer of methyl iodide from the gas phase through rising bubbles in a liquid column into the liquid phase took place. The bubble size directly influences the total interfacial area of mass transfer of the gas species for scrubbing. Another important aspect was the quite low terminal rise velocity of the very small bubbles causing an enhanced transfer time for the gas species in the liquid and thus promoting high decontamination factor.

#### IV. APPLICATION IN FCVS

In the dynamic system of a technical scrubber type FCVS the flow conditions in the aqueous solution are much more complex than in the experiments performed at lab-scale. The species transfer rate from the gaseous phase (bubbles) into the liquid phase depends on the heat and mass transfer properties, which are dominated by the bubble hydrodynamics. The main controlling parameters are the gas bubble size (interfacial area), the bubble residence time and the thermodynamic properties of the gas mixture and steam content, which is especially important if steam condensation takes place. In addition the liquid temperature and surfactants in the liquid, affecting the gas and liquid side of the bubble surface for heat and mass transfer rates.

At PSI the analytical and experimental program VEFITA is conducted to study the iodine retention behavior for both elemental and organic iodide species in a large scale technical wet filter system. Tests will investigate the anticipated enhancement in iodine retention using the novel process under prototypical thermal-hydraulic flow conditions of a FCVS, but in the absence of radiation.

The test facilities used in this investigation are based on a commercial FCVS developed by the IMI-Nuclear CCI AG, Switzerland, schematically shown in Figure 8.

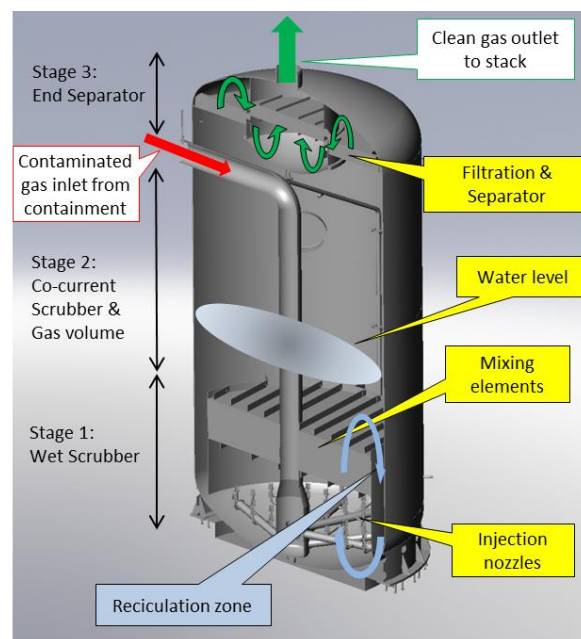


Fig. 8. Schematic view of the industrial FCVS system of IMI- Nuclear (CCI AG), Switzerland.

The filter ([8], [9]) consists of a stainless steel vessel comprised of a wet scrubber section with a gas injection assembly, an inner riser column with specific internal structures (structured mixing elements) to disintegrate gas bubbles into smaller ones to enhance the interphase mass transfer. The lower wet scrubber section is followed by a gas space and an end separator section with several stages to remove droplets and fine moisture from the cleaned gas stream leaving the filter to the stack. The filter has a height of about 9 m, a diameter of about 3.5 m and a liquid volume typically of about 30 m<sup>3</sup>.

In the wet scrubber section the gas sparger assembly is composed of a large number of special designed injection nozzles, where the size and number is depending on the required flow rate to depressurize the containment. The scrubbing water is doped normally with THS and either with sodium hydroxide (NaOH) or with sodium carbonate (Na<sub>2</sub>CO<sub>3</sub>) at certain aqueous concentrations for pH control.

#### ***1:1 full height FCVS test facility VEFITA***

The retention of iodine and organic iodide will be performed in the new established

VEFITA test facility, which is a scaled-down, full height, reduced diameter mock-up of the CCI FCVS, Figure 9.

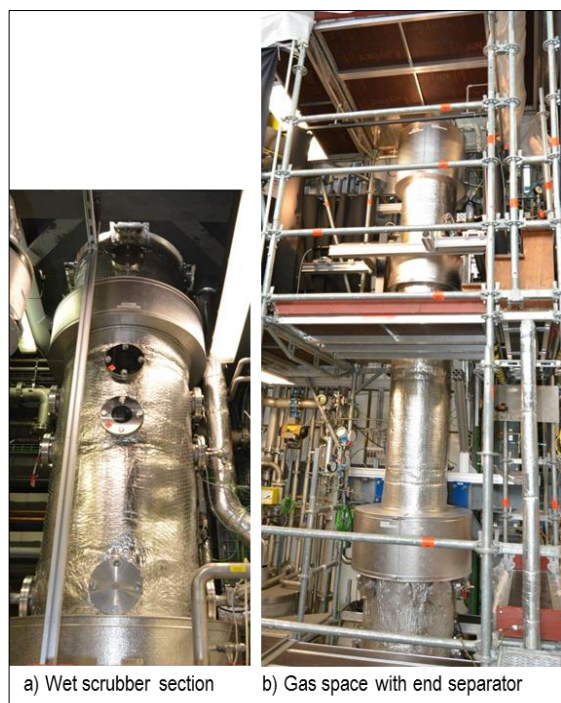


Fig. 9. The 1:1 height, reduced diameter scale FCVS facility VEFITA to determine aerosol,  $I_2$  and  $CH_3I$  retention; a) lower part wet scrubber, b) upper part droplet and end separator sections.

Table II VEFITA facility dimensions and operating conditions.

Total Height	m	12
Inner Diameter	m	0.58 / 0.40
Cross sectional flow area, wet scrubber section	m <sup>2</sup>	0.266
Number of injection nozzles	-	1
Sparger (nozzle) submergence	m	2.0 - 3.5
End separator section	-	Yes
Pressure, inlet	bar(abs)	1.3 - 9.5
Pressure, test section	bar(abs)	1.0 - 4.5
Gas temperature, inlet	°C	35 - 200
Water temperature	°C	35 - 140
Nitrogen flow rate, max.	kg/h	1200
Steam flow rate, max.	kg/h	250
Steam mass fraction	%	0 - 100

To preserve the thermal-hydraulic behaviour and phenomena of the industrial FCVS, VEFITA has all the internal structures, including one prototypical injection nozzle, the water pool with the inner riser column and mixing elements, the gas space and the three stages of the end separator. These three stages are arranged in series after each other to allow access for measurement systems and probe sampling. The full height of the test facility enables similar gas residence times and velocities as in the real scale FCVS. Table II provides the main geometrical dimensions together with the achievable experimental boundary conditions. The water submergence of the nozzle can be varied up to 3.5 m. The maximum operation pressure in front of the nozzle is 9.5 bar and the temperature is 200°C. The test section can be operated from ambient pressure up to 4.5 bar by a pressure control system in order to simulate pressure losses due to long pipe works downstream of the gas outlet of a real FCVS. By pressurizing the gas space tests with elevated water saturation temperatures up to 140°C can be performed, depending on the gas mixture used.

The test facility schematically shown in Figure 10 is intensively instrumented to measure the fluid, gas and wall temperatures, the absolute, gauge and differential pressures along the test section and the flow rates at the inlet and outlet of the test section. The collapsed water level and the water level swell are monitored online by differential pressure probes and by a special guided radar probe, respectively. The pH of the scrubber solution is determined on-line during the test by a pH electrode device. The inlet and outlet piping as well as the whole test section can be trace heated to compensate for heat losses, to prevent steam condensation and to reduce iodine losses at cold walls.

Gaseous molecular iodine is generated by dissolving solid iodine crystal in a certain amount of ethanol. The liquid solution is fed by an electronic controlled dosing pump to a two-fluid spray nozzle attached to a heated evaporation chamber where the solution is atomized by a hot nitrogen flow into extremely fine droplets. The liquid ethanol evaporates and gaseous molecular iodine is formed and injected



Molecular iodine will be sampled to liquid gas scrubber columns with a coolant jacket and analyzed by iodide ion selective electrodes (ISE) in continuous and batch sampling mode. Several gas scrubber columns will be operated in parallel and in series during the test providing multiple data points.

Methyl iodide is characterized on-line with highly sensitive UV photo ionization detectors (PID) installed in special gas sampling trains. The sample gas is mixed with a flow of hot nitrogen directed to a condenser where the gas is cooled down to the maximum operating temperature of 50°C of the PID sensor. Thereby any steam present in the sample is removed and the added nitrogen is used to keep the partial pressure of CH<sub>3</sub>I in the sample gas flow low enough so that no condensation of CH<sub>3</sub>I can take place. Parallel to the PID measurements gas samples are taken to a second type of sampling where the gas sample is mixed with nitrogen and directed to a condenser where any steam present is condensed and collected in a liquid trap. The residual gas with the contained CH<sub>3</sub>I is bubbled through two liquid gas scrubbers arranged in series and operated with toluene. The condensed steam sample and the two samples from the toluene scrubbers are analyzed off-line using a gas chromatography/mass spectrometer (GC/MS). This method can detect CH<sub>3</sub>I concentrations down to ppb level. In addition to the PID and GC/MS method a continuous gas sample flow is directed from the inlet and outlet of the test section to a mass spectrometer (MS).

### ***Tests in VEFITA***

In VEFITA a series of thermal-hydraulic experiments have been performed to characterize the pressure and temperature behavior and the water inventory behavior due to heat-up, steam condensation and evaporation as a function of the gas composition of the venting gas with respect to the mass fractions of non-condensable (NC) gas and steam. The pressures in the inlet piping upstream of the injection nozzle were between 1.3 and 9.5 bar at mass flow rates up to 1200 kg/h and temperatures of the gas between 35°C and 165°C, respectively. The water pool temperatures were between ambient up to

saturation (boiling) in case of pure steam tests. Different sizes of injection nozzles were tested. In a series of tests special attention was focused on the two-phase mixture level-swell of the scrubber solution, which is of particular interest to the design and operation of the filter system. The gas composition of the venting gas (mass fraction of NC gas and steam), the water pool temperature and the pressure in the gas space of the filter (ambient up to 4 bar) were varied. The level-swell gave insights into the gas hold-up and the residence time of the gas bubbles, [10].

In the experimental iodine test program tests are foreseen either with elemental iodine or with organic iodide loaded carrier gas consisting of pure NC gas (Nitrogen), pure steam and of mixtures of NC gas/steam at different steam mass fractions. To investigate the effect of the novel process tests with and without Aliquat336<sup>®</sup> will be done with aqueous concentrations of THS and Aliquat336<sup>®</sup> defined by the novel process. In all tests an initial pH of 11 (given at 25°C) will be used by adding NaOH to the scrubber solution of de-ionized water.

Based on analyzed containment venting scenarios for the CCI FCVS some representative and some for the filter performance challenging test conditions have been selected for the experiments in VEFITA. For a given injection nozzle size and nominal mass flow rate the gas mixture inlet pressure and temperature will be about 3.5 - 4 bar and 165°C, respectively. The gas space above the wet scrubber section is at ambient pressure and the water temperature will range from ambient to 90°C and to saturation temperature (boiling) in case of pure steam injection. A nominal water level of about 3.1 m above the injection nozzle will be used. All tests are planned at stationary conditions and with iodine injection phases lasting 4-5 hours to collect an appropriate number of I<sub>2</sub> and CH<sub>3</sub>I samples at the inlet and especially at the outlet, respectively. Thermal-hydraulic (T - H) pretests without iodine feeding at the selected test conditions are used for detailed test planning. The following iodine retention tests are planned, Table III.

test type	T <sub>water</sub>	H <sub>water</sub>	gas comp.	T <sub>gas</sub>	flow rate	ALI
T-H	low high	nominal	NC NC+steam	nominal	nominal	w/o w
CH <sub>3</sub> I	low		NC		nominal	w/o w
CH <sub>3</sub> I	close to T <sub>sat</sub>		NC+steam		nominal	w/o w
CH <sub>3</sub> I mult. cycles	high		NC+steam		Cy1: high Cy2: low	w
I <sub>2</sub>	close to T <sub>sat</sub>		NC+steam		nominal	w

Table III. Main tests planned in VEFITA.

- CH<sub>3</sub>I retention at nominal flow rate and lowest feasible water temperature of about 35°C using only NC gas at nominal gas temperature of 165°C. One test run will be performed without and a second test with the co-additive Aliquat336<sup>®</sup> (ALI). These conditions will provide a relative lower limit of the DF for organic iodide at nominal flow rate and at the most challenging conditions when the water pool is cold, a condition present during start of the first venting cycle in a FCVS, and no credit can be given for the enhancing effect of steam condensation to the mass transfer of the gaseous phase to the liquid phase. The level swell will have a relative maximum.

- CH<sub>3</sub>I retention at a water temperature close to saturation of approximately 90°C using a gas mixture of NC gas and steam. Tests with and without Aliquat336<sup>®</sup> will be carried out. These tests will give the DF when steam condensation takes place in the presence of NC gases with complex two-phase hydrodynamic behavior. The high pool temperature will cause steaming and influence the water inventory by water evaporation into the NC gas leaving the test section.

- In severe accident management procedures multiple venting cycles are also foreseen, with an intermediate stand-by without flow for several hours. A CH<sub>3</sub>I retention test with two venting cycles with a stand-by time of 10 h will study the behaviour of the chemical additives (THS and Aliquat336<sup>®</sup>) in the scrubber water during restart. The inlet gas mixture will be composed of NC gas and steam with a high steam mass fraction.

In the two venting cycles high and low mass flow rates corresponding to high and low inlet pressures will be used.

- I<sub>2</sub> retention at a water temperature close to saturation of approximately 90°C using an inlet gas mixture of NC gas and steam at the nominal flow rate and temperature. The scrubber water will be doped with both additives.

In addition tests are under discussion to study the effect of a reduced water level above the injection nozzle on the DF and the retention behavior if pure steam is injected where the water pool is at boiling conditions.

#### *Pre-test facility mini-VEFITA*

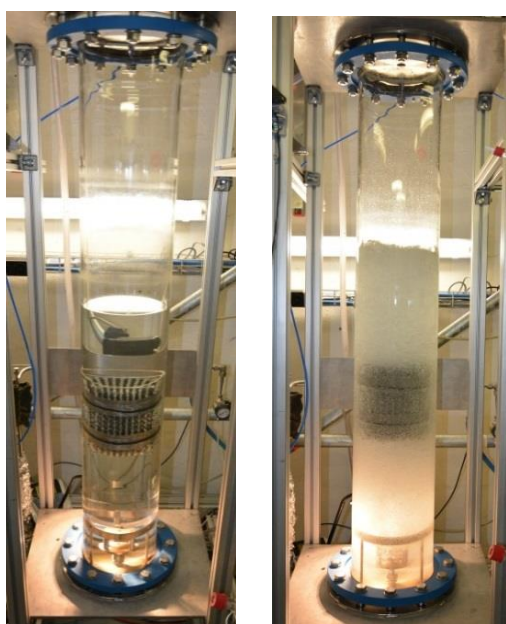
In a small pre-test facility, mini-VEFITA (Figure 11), with a further reduced height and volume and without the upper end separator sections of VEFITA, dedicated experiments have been started to evaluate the measurement techniques foreseen for the measurement of I<sub>2</sub> and CH<sub>3</sub>I, which will be implemented in VEFITA.

The geometrical dimensions and boundary conditions are given in Table IV. The test section is not a scaled-down representation of the real FCVS but mainly used for demonstration purpose and instrument testing.

Total Height	m	1.5
Inner Diameter	m	0.2
Cross sectional flow area	m <sup>2</sup>	0.0314
Number of injection nozzles		1
Sparger (nozzle) submergence	m	0.8 - 1.2
Pressure, inlet	bar(abs)	1.0 - 2.0
End separator section		No
Pressure, test section	bar(abs)	atmosphere
Gas temperature, inlet	°C	35 - 100
Water temperature	°C	20 - 80°C
Nitrogen flow rate	l <sub>n</sub> /min	100 - 300
Steam flow rate	kg/h	0 - 5
Steam mass fraction	%	0 - 100

Table IV. Mini-VEFITA pre-test facility dimensions and operating conditions.

The test section consists of a borosilicate glass tube of 0.2 m in diameter, a height of 1.5 m and an inner acrylic glass riser holding only one structured mixing element layer in contrast to the taller three layer arrangement used in the full height VEFITA test facility. At the bottom an injection nozzle assembly similar to the ones used in the VEFITA (FCVS) is installed. The water level above the injection nozzle can be varied from 0.8 m to about 1.2 m. The gas outlet is at the top. Nitrogen as well as steam and mixtures of both can be used at limited flow rates.



a) Stagnant                      b) With gas injection

Fig. 11. Small scale pre-test facility Mini-VEFITA, a) stagnant and b) with gas flow and level swelling.

Figure 11b demonstrates the flow behaviour in the scrubber at a gas flow rate of 200 l<sub>n</sub>/min causing a water level swell of about 0.1 m. Several bubble sizes can be observed ranging from a few mm to about 20-30 mm, which are quite different to the observed nearly constant bubble sizes of 1-2 mm in the lab-scale scrubber column tests (Figure 6). Directly at the injection nozzle big gas globules are formed. At the impaction plates of the nozzle the bubbles break-down to smaller ones which are further disintegrated when rising in the riser and passing through the mixing element. Some small gas bubbles are even trapped in the recirculation

zone formed by the annulus between the inner riser and the outer glass tube.

The test section will be used for short lasting tests of about 30 minutes to perform parametric studies on a relative basis not providing absolute values of the DF with respect to the full height model. Different effects will be studied such as the effect of the water, the relative change in retention of I<sub>2</sub> and CH<sub>3</sub>I with and without Aliquat336<sup>®</sup> and the influence of different steam mass fractions in the gas mixture.

## V. FURTHER WORK

Although the processes of iodine transfer from the gas phase to the bulk liquid are relatively well described in existing iodine codes mainly representing the sump of a PWR, the complex hydrodynamic characteristics in water pools are either not included in the codes or only in a very rudimentary approach. In a further step an experimental investigation is considered to better characterize the two-phase-flow hydrodynamics in pools under turbulent to churn-turbulent flow conditions typically found in FCVS or wetwells and coupling the hydrodynamics with existing gaseous iodine mass transfer models. The experiments are foreseen to be conducted in the TRISTAN test facility of PSI, [11]. TRISTAN consists of a large square water pool (0.5 m x 0.5 m) with an overall height of 6.2 m, with transparent side walls allowing access for optical measurement devices. The facility is operated under ambient conditions. NC gas can be injected at ambient temperatures through exchangeable injection devices up to high flow rates (max. 450 kg/h). The water level inside the pool can be controlled and adjusted. The characterization of the bubble-hydrodynamics (i.e. bubble size distribution, interfacial area, bubble velocity, etc.) is measured by a wire-mesh-sensor (WMS). The WMS technique is essentially based on the differences of the electrical conductivity of a dispersed and continuous phase, detected by two planes of wire grids placed in the flow in a short distance from each other. The grids act as electrodes, while one plane acts as a transmitting and the other as the receiving plane. It is planned to use the WMS or another suitable technique to describe the mass

transfer and retention of gaseous iodine using a gas phase simulant.

The experimental work is accompanied with code simulations. The very complex two-phase flow behavior in the wet scrubber section of the FCVS is challenging to code models. The thermal-hydraulic data of the VEFITA facility are used for the assessment of system codes such as RELAP5/Mod3.3-p3 and TRACE/V5.0-p2. Models are developed for the facility and experiment transients are simulated, [10].

## VI. CONCLUSIONS

The retention of gaseous organic iodides in wet scrubber type filtered containment venting filters using only chemical additives typically present in the water pools, i.e. sodium thiosulfate and sodium hydroxide or sodium carbonate is limited even at high water temperatures. In an extensive research and development program a novel process was established to suppress the release of gaseous iodine species from aqueous solutions. The process enables not only the fast and efficient decomposition of organic iodides into non-volatile iodide ions but also a fixation of iodide ions so that their radiolytic and thermal oxidation is suppressed. Experimental investigations have demonstrated the effectiveness of the process under a broad range of pH, temperature, organic iodide (CH<sub>3</sub>I) concentrations, dose and in the presence of impurities. Optimized aqueous concentrations of the additives used in the process have been identified. First tests in the dynamic system of a lab-scale scrubber column in which volatile CH<sub>3</sub>I is transferred from the gas phase into the aqueous phase during sparging have shown the potential of the process for FCVS application.

To study the application of the novel process in a technical FCVS a full height, reduced diameter test facility with all internal components was erected, in which retention tests for both molecular iodine and methyl iodide will be performed under prototypical conditions present during containment venting scenarios. A set of experiments is planned to assess the effectiveness of the chemical additives on the retention under complex two-phase flow conditions. A new experimental and analytical project will study the bubble hydrodynamics in

FCVS type water pools to better model the mass transfer process of gaseous iodine from the gas phase into the liquid phase.

## ACKNOWLEDGMENTS

A large fraction of the work on the novel iodine process was carried by R. Cripps, H. Bruchertseifer and S. Guntay who have already retired. Their work is gratefully acknowledged. Without the support of the PSI hot laboratory the experimental programme using radiotracer would not have been possible. The VEFITA test facility was erected in collaboration with IMI-Nuclear (CCI AG) which provided specific internal structures of the test section. SwissNuclear, the Nuclear Energy Section of swisselectric (Switzerland) supports financially the ongoing experimental programme in the large-scale test facility.

## NOMENCLATURE

ACC = Activated Charcoal

ALI = Aliquat336<sup>®</sup>

DF = Decontamination Factor

DF\* = Decontamination Factor per meter length

FCVS = Filtered Containment Venting System

GC/MS = Gas Chromatography / Mass Spectrometer

ISE = Ion Selective Electrodes

NC = non-condensable

PID = Photo Ionization Detector

PWR = Pressurized Water Reactor

PTFE = Polytetrafluoroethylene

TEDA = Tri-ethylene-diamine

THS = Sodium Thiosulfate (Na<sub>2</sub>S<sub>2</sub>O<sub>3</sub>)

TRISTAN = Tube Rupture In Steam generator multi-phase flow investigations

VEFITA = Venting Filter Assessment

WMS = Wire Mesh Sensor

## REFERENCES

1. B. Clément et al., "LWR severe accident simulation: synthesis of the results and interpretation of the first Phébus FP experiment FPT0", *Nuclear Engineering and Design*, Vol. 226, p. 5-82, (2003).

2. T. Lind, B. Jaeckel, S. Guntay, "A summary of the PSI Investigations on Iodine Chemistry in the Presence of Impurities and Additives," *OECD-NUGENIA/ SAR-NET workshop on "Progress in Iodine Behaviour for NPP Accident Analysis and Management"*, Marseille, March 30 - April 1, (2015).
3. L.F. Parsly, "Chemical and physical properties of methyl iodide and its occurrence under reactor accident conditions (A summary and annotated bibliography)", ORNL-NSIC-82, (1971).
4. BASF, "Aliquat336, Technical information", *TI/EVH 0125/4e*, (2013).
5. H. Bruchertseifer, S. Guntay, "Fast Reduction of Iodine Species to Iodide", United States Patent, Patent No. US 8,142,665 B2, March 27, (2012).
6. S. Guntay, H. Bruchertseifer, H. Venz, F. Wallimann, B. Jaeckel, "A Novel Process for Efficient Retention of Volatile Iodine Species in Aqueous Solutions during Reactor Accidents", *NEA Workshop on the Implementation of Severe Accident Management Measures (ISAMM)*, Oct.26-28, Paul Scherrer Institute PSI, Villigen, Switzerland, (2009).
7. H. Bruchertseifer, R. Cripps, S. Guntay, B. Jäckel, "Experiments on the retention of the fission product iodine in nuclear reactor accidents", *Scientific Report Volume IV: Nuclear Energy and Safety*, Paul Scherrer Institut, ISSN 1423-7334, Switzerland (2004).
8. D. Grob, "Filtered Containment Venting System", *NRC Public Meeting*, Rockville MD, September 4, USA (2012).
9. D. Jacquemain et al. "OECD/NEA/CSNI Status Report on Filtered Containment Venting", *NEA/CSNI/ R(2014)7, Appendix 3*, (2014).
10. J. Yang, D. Suckow, H.-M. Prasser, M. Furrer, T. Lind, "Assessment of RELAP5/TRACE against VEFITA Thermal-Hydraulic Level Swell Tests", *Proceedings of the International Congress on Advances in Nuclear Power Plants (ICAPP)*, paper No. 14154, Charlotte, April 6-9, USA (2014)
11. T. Betschart, D. Suckow, V. Brankhov, H.-M. Prasser, "High resolution two-phase flow structure investigations under pool scrubbing conditions", *Proceedings International Topical Meeting on Nuclear Thermal-Hydraulics (NURETH)*, paper NURETH15-191, Pisa, Italy, May 12-17, (2013)

## THE EUROPEAN PASSAM PROJECT ON ATMOSPHERIC SOURCE TERM MITIGATION: HALF-WAY PROGRESS AND MAIN RESULTS

T. Albiol(1), L. Herranz(2), E. Riera(3), S. Guieu(4), T. Lind(5), S. Morandi(6),  
T. Kärkelä(7), N. Losch(8), B. Azambre(9)

<sup>(1)</sup>IRSN, Centre de Cadarache, BP3, 13115 Saint Paul les Durance Cedex, France (thierry.albiol@irsn.fr)

<sup>(2)</sup>CIEMAT, Avda. de la Complutense, 40, Madrid 28040, Spain

<sup>(3)</sup>CSIC, Serrano 144, Madrid 28006, Spain

<sup>(4)</sup>EDF, 12 - 14 avenue Dutriévoz, 69628 Villeurbanne Cedex, France

<sup>(5)</sup>PSI, 5232 Villigen, Switzerland

<sup>(6)</sup>RSE, via Rubattino 54, 20134 Milano, Italy

<sup>(7)</sup>VTT, BI7, Biologinkuja 7, P.O. Box 1000, FI-02044 VTT, Finland

<sup>(8)</sup>AREVA GmbH, Kaiserleistrasse 29, 63067 Offenbach, Germany

<sup>(9)</sup>Université de Lorraine - LCPA2MC – Institut Jean Barriol – Rue Demange, 57500 Saint Avold, France

**Abstract** - The PASSAM (Passive and Active Systems on Severe Accident source term Mitigation) project has been launched in the frame of the 7<sup>th</sup> framework programme of the European Commission. Coordinated by IRSN, this four year project (2013 – 2016) involves nine partners from six countries having a strong experience on severe accidents: IRSN, EDF and university of Lorraine (France); CIEMAT and CSIC (Spain); PSI (Switzerland); RSE (Italy); VTT (Finland) and AREVA GmbH (Germany).

It is mainly of an R&D experimental nature, aiming at studying phenomena that, under severe accident conditions, might have the potential for reducing radioactive atmospheric releases to the environment. Improvements of existing source term mitigation devices (pool scrubbing systems; sand bed filters plus metallic pre-filters), as well as innovative systems which may achieve larger source term attenuation (Acoustic agglomeration systems; High pressure spray agglomeration systems; Electric filtration systems; Improved zeolite filtration systems; Combined Filtration Systems) are studied.

After two years, the current status of the project is as follows. A state-of-the-art report has been completed, allowing a precise definition of the experimental test matrices in direct link with the identified gaps of knowledge. The experimental work is in progress and in some domains (e.g. pool hydrodynamics, use of zeolites for iodine trapping, combined wet and dry filtrations systems, etc...) major results have already been obtained. We can also quote the organization of an open workshop mainly targeted to R&D organizations, to National Safety Authorities and their Technical Support Organizations, to utilities and to vendors, held on February 26<sup>th</sup>, 2014 in Madrid. A second workshop will be organized at the end of the project, in December 2016.

Simple models and/or correlations will result from in-depth analysis of PASSAM experimental results. Once implemented in severe accident analysis codes, these models should allow enhancing the capability of modelling Severe Accident Management measures and developing improved guidelines.

The project's final outcomes will constitute a valuable database which may be strategic for helping the utilities and regulators in assessing the performance of the existing source term mitigation systems, evaluating potential improvements of the systems and developing severe accident management measures.

**Keywords:** nuclear, safety, accident, mitigation, FCVS, PASSAM

## I. INTRODUCTION

After the Fukushima-1 accident one of the main concerns of the nuclear industry has been the search for improved atmospheric source term mitigation systems. The motivation underneath stems from two major evidences: venting of the containment building might be an essential accident management measure in order to prevent the loss of its mechanical integrity, but this containment venting might result in substantial radioactive releases if no efficient source term mitigation system is implemented. Many countries have recently considered the implementation of Filtered Containment Venting Systems (FCVS) as a mean to further enhance their Nuclear Power Plants (NPPs) safety; while some others, like Sweden, Switzerland, Finland, Germany and France, had already adopted that measure in their NPPs.

The renewed interest for FCVS has pushed new international activities, like writing a status report by the working group on the Analysis and Management of Accidents of the CSNI (Committee on the Safety of Nuclear Installations) of the OECD-NEA [1], or launching the European Commission (EC) project on “Passive and Active Systems on Severe Accident source term Mitigation” (PASSAM) [2].

This paper gives an overview of the objectives, work structure, current status and main results of the PASSAM project two years after its starting date.

## II. PASSAM OBJECTIVES

The industrial FCVS are essentially based on two approaches: “dry” and “wet” systems. In dry systems, large trapping surfaces are provided either by gravel or sand beds, or by metal fibers or by molecular sieves. In wet systems, trapping occurs in a liquid (water plus additives) pool as a consequence of several removal mechanisms the efficiency of which depends mainly on thermal-hydraulic conditions. These systems can be enhanced by including venturi scrubbers: water droplets injected in the gas stream capture

aerosol particles and make them more easily trapped by solid filters or liquid pools).

These systems, some of which are installed on NPPs, have been well characterized as regards aerosol retention efficiency, but to a far lesser extent as regards volatile iodine retention. In this context the Advanced Containments Experiment (ACE) can be considered as the largest international test programme [3]. Since then, the potential high contribution of gaseous organic iodine to the radioactive release in case of a loss of the containment building leak-tightness has been evidenced. Additional tests have been performed on FCVS, and improvements of the systems have been proposed for organic iodide retention in water pools. Nevertheless the research on this specific aspect needs to be complemented. A lack of knowledge also appears clearly for organic iodine retention in dry systems. Finally, gaps may also remain in the investigation of systems performance that have not been properly addressed, either because evolution of anticipated working conditions and/or because of new insights coming from recent research on fission product behaviour. Hence, some specific experiments could provide meaningful insights into the systems performance that could result in an optimization of their working conditions.

In parallel, several alternative and innovative approaches are appearing in the literature or are even already proposed by some vendors. Electric filtration systems are already widely used in industry, out of the nuclear field, for separation of particles, for instance, from flue gases of coal-fired power plants or from product gases in iron manufacturing or in cleaning indoor air applications. There are also a number of proposed solutions based on molecular sieves (improved zeolites, metallic organic filters, etc...) that are widely used as filter in many industrial processes. Many kinds of zeolite exist; the key point would be to find the more efficient zeolite for iodine species in severe accident relevant conditions. Another promising innovative solution consists of the combination of wet and dry filter systems. Besides, as it is well known that, generally speaking, the filtration systems are less efficient for aerosol

particles of some tenths of microns, some systems are being developed, aiming at agglomerating aerosol particles in order to get bigger particles which will be better filtered. Implementing such a device upstream of the filtration system would overcome the decrease of filtration efficiency of sub-micron particles.

Another subject which has poorly been studied is the long term behaviour of the trapped fission products (i.e., potential for re-vaporisation and/or re-entrainment of radioactive material) due to surrounding conditions relevant to an accident and more especially, due to continuous irradiation, coupled to continuous flow-rate (if the venting system remains open), temperature, humidity, etc... Indeed the re-entrainment of trapped aerosols was tested in different small scale facilities and, at larger scale, in the international ACE programme where the aerosol loaded filters (dry and wet filters) were operated with clean gas and the aerosol concentrations of the gas downstream of the filters were measured. Nevertheless, no data on long term re-vaporisation under irradiation, both for aerosols and for gaseous iodine forms, could be found in the open literature.

In this context, the PASSAM project has been built to explore potential enhancements of existing source term mitigation devices and check the ability of innovative systems to achieve even larger source term attenuations. Heavily relying on experiments, the PASSAM project aims at providing new data on the capability and reliability of a number of systems related to FCVS: pool scrubbing systems, sand bed filters plus metallic prefilters, acoustic agglomerators, high pressure sprays, electrostatic precipitators, improved zeolites and combination of wet and dry systems. Nonetheless, the scope of some of the ongoing research - as fission products and aerosol retention in water ponds - goes beyond FCVS and might be applied for accident situation other than containment venting.

The main outputs of the project will be:

- a relevant extension of the current database on these existing or innovative mitigation systems,

- a deeper understanding of the phenomena underlying their performance and models/correlations that allow modelling<sup>6</sup> of the systems in accident-analysis codes, e.g., ASTEC [4],
- an estimation of the order of magnitude for source term reduction for each filtration system and suggestions for improved filtration systems<sup>7</sup>.

### III. PASSAM WORK STRUCTURE

The PASSAM project launched under 7<sup>th</sup> framework programme of EURATOM has started in January 2013. Participated by 9 organizations (IRSN, EdF and University of Lorraine, France; CIEMAT and CSIC, Spain; PSI, Switzerland; RSE, Italy; VTT, Finland; and AREVA GmbH, Germany) and coordinated by IRSN, the project involves nearly 400 person-month and the associated cost is estimated to be more than 5 M€. Fig.1 shows a map of EU-PASSAM partners across Europe.

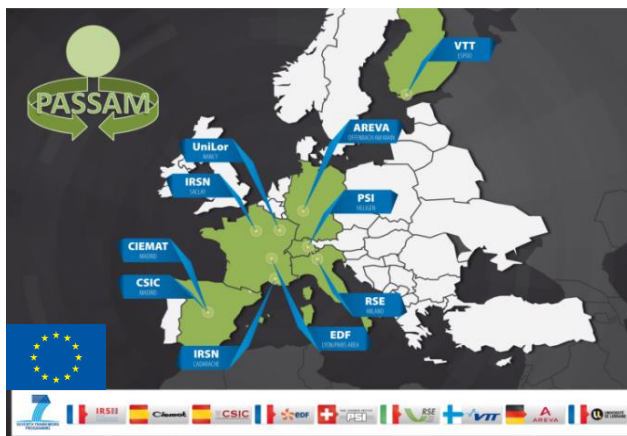


Fig. 1. The PASSAM partnership

The PASSAM project is organized into 5 Work Packages (WP) that are described next:

<sup>6</sup> The implementation of models in Severe Accident codes is out of the scope of PASSAM.

<sup>7</sup> Note that the hydrogen risk within the FCVS, which has to be taken into account, is not studied in PASSAM which focuses more on the retention of aerosols and gaseous iodine and on their potential release at mid or long term.

- WP1:(MANAG) Project Management (leader: IRSN). Project scientific, administrative and financial coordination, quality management included.
- WP2:(THEOR) State of the art and modelling (leader: CIEMAT). Analytical work supporting both test matrices definition and development of models and/or correlations from the experimental results.
- WP3:(EXIST) Existing filtration systems (leader: PSI). Two types of devices will be experimentally studied: pool scrubbers (WP3.1) and sand bed filters - plus metallic pre-filters(WP3.2).
- WP4:(INNOV) Innovative filtration systems (leader: VTT). Experimental campaigns will be conducted on devices that might enhance mitigation of source term, either through pre-agglomeration of the radioactive load that would reach the filter stage (acoustic agglomerators (WP4.1) and high pressure sprays(WP4.2)) or alternative filter systems (electric precipitators (WP4.3), improved zeolites (WP4.4) and combination of wet and dry filters(WP4.5)).
- WP5:(DKS) Dissemination of knowledge and synthesis (leader: IRSN). Matters concerning PASSAM visibility, the communication of its results and the sharing of the experience gained.

#### IV. PASSAM CURRENT STATUS

The experimental nature of the project and the final outcomes foreseen, make its planning to be rather linear as a whole, with three conceptual project phases:

- set-up of technical and organizational bases;
- execution of experimental campaigns;
- project wrap-up.

The first phase included a literature survey on the existing and innovative systems to be experimentally studied in the project [5]. This survey confirmed, with more details, the anticipated gaps of knowledge and so it allowed to optimize the test matrices for each

experimental work-package [6, 7]. It ended up with an open workshop held in Madrid (Spain) in February 2014 [8].

The experimental phase, which constitutes the largest part of the PASSAM activities, is presently ongoing and will last up to mid-2016. It will result with the development of robust and sound databases for each system tested. The main results already obtained are presented in the next section of this paper.

The last phase will focus on managing the project output in the best way so that nuclear community can easily benefit from the research conducted. In particular a final PASSAM workshop will be organized by end 2016 and the final synthesis report of the project will be available in open literature.

Fig. 2 illustrates how the project development is related to specific activities considered within the various work-packages and their interaction.

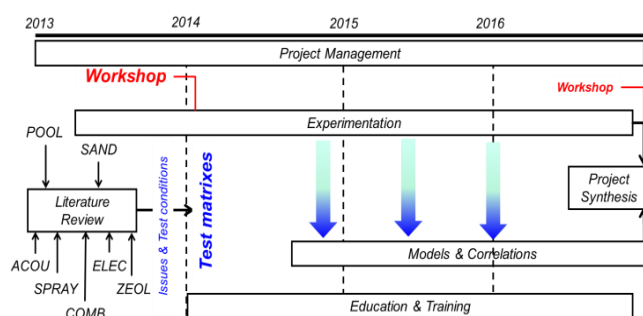


Fig. 2. PASSAM Timing and major activities

#### V. PASSAM MAIN EXPERIMENTAL RESULTS

##### WP3.1: Experimental studies of pool scrubbing systems (leader PSI)

Removal of contaminating particles and/or vapours from a carrier gas when passing through an aqueous pond is known as pool scrubbing. Most pool scrubbing investigation dates back to 80's and 90's of last century [9].

In the last 20 years, there have been few specific studies focused on hot pools [10] and jet regime [11]. These experimental campaigns, however, were limited in their scope. More recently, some

additional information on pool scrubbing of aerosols has been gained through the ARTIST projects [12, 13], in which the most distinctive element was the presence of submerged surfaces representing the secondary side of a steam generator.

The gathered database allowed drawing some insights into pool scrubbing but there are still significant weaknesses: lack of systematic analysis of the parameters influencing pool scrubbing (i.e., submergence, particle size, steam content, etc.); no experimental tracking of variables like bubble size and shape; conditions hardly addressed in the past, as jet injection or in-pool gas rise under churn-turbulent regime; few experiments on scrubbing of fission products vapors. No less important, since the experimental programs were performed, some information has been lost throughout the years.

There are a good number of studies concerning bubble hydrodynamics out of the nuclear safety community. However, they mostly address conditions far from those anticipated in severe accidents. Anyway, the existing significant information will be brought on-board, so that it is taken into account during results discussion and modelling.

As a consequence, the following issues are investigated in PASSAM:

- *Pool scrubbing of aerosols in the jet injection regime (CIEMAT)*. The experimental phase, involving SiO<sub>2</sub> particles, is planned from April to October 2016.
- *Pool scrubbing of aerosols in the presence of additives in the water, simultaneous determination of aerosol scrubbing efficiency and pool two-phase flow hydrodynamics (RSE)*. Preliminary experiments on bubble studies are ongoing up to May 2015. In parallel the first experiments involving SiO<sub>2</sub> aerosols have started and the whole experimental set should be completed by mid-2016.
- *Pool hydrodynamics under churn-turbulent two-phase flow representative of the steam generator tube rupture (SGTR) conditions when the tube rupture is submerged (PSI)*. Many experiments were performed in the Tristan facility in 2013 and 2014. A specific wire mesh sensor technology for measurement of 3D flow patterns and void fractions was successfully developed, complemented by application of imaging techniques for very small bubbles. Clear differences were observed between different flow regimes and channel geometries. The highly three dimensional nature of the flow was clearly visible. Large gas agglomerates were evidenced next to small bubbles. Large spreading of bubble sizes throughout the channel was observed and bubble shapes could be reconstructed. A so-called “Gradient Methods” was implemented for determining interfacial area and for estimating the velocity of the gas phase. New experimental data were collected for bundle and large square channel geometries. These data are used for the validation of 3D hydrodynamic models and improvement / development of the pool scrubbing models regarding pool hydrodynamics. New experience was gained in understanding the phenomenology of two-phase flows. More details can be found in [14].
- *Mid/Long term behaviour of iodine in the water pools under irradiation (IRSN)*. The first two tests have been performed in December 2014 and March 2015 using the IRSN EPICUR facility. The results are still being analysed, but under the experimental (severe) conditions, a significant release of iodine from the “scrubber solution” was observed for the first test. An additional test is scheduled in 2015.
- *Retention of organic iodine in the pool, including in the presence of scrubbing additives and submerged structures (AREVA)*. Experiments at laboratory scale (VESPER34 facility) were performed on the influence of scrubbing liquid composition, of mixing elements and of temperature. The additives often used in commercial scrubbers are NaOH for pH control and Na<sub>2</sub>S<sub>2</sub>O<sub>3</sub> as primary reactant. The CH<sub>3</sub>I retention performance could not be further enhanced by increasing the sodium thiosulfate concentration. Yet the CH<sub>3</sub>I retention performance in the scrubber could be moderately increased by: Aliquat 336

(quaternary ammonium salt serving as phase transfer catalyst); mixing elements (increase of residence time and of metallic surface); increased temperature. However, if Aliquat scrubbing liquid is used, the retention performance is not further increased by mixing elements nor by increased temperature (a reduction of  $\text{CH}_3\text{I}$  retention was even observed above  $110^\circ\text{C}$ ). It was not possible to reach high  $\text{CH}_3\text{I}$  retention performance with the studied parameters (additive concentrations, geometries ...), under the conditions used in the tests. The application of sliding pressure to AREVA's FCVS (scrubber is operated close to containment pressure) results already in increased pool temperatures and thus the potential of  $\text{CH}_3\text{I}$  retention is seen as maxed out. So AREVA's conclusion is that alternative filtration methods (e.g. dry filtration) are necessary to reach a qualitative step towards high  $\text{CH}_3\text{I}$  retention (see PASSAM WP4.5).

### WP3.2: Experimental studies of sand bed filters plus metallic pre-filters (leader IRSN)

Sand bed filters were decided to be implemented on the French PWRs (Fig. 3) in the early 90's of last century. Their initial design was based on a set of boundary conditions: containment pressure and temperature of 5 bar and  $140^\circ\text{C}$ , respectively; gas flow rate through the FCVS line of 3.5 kg/s; gas mixture composed of air (33%), steam (29%),  $\text{CO}_2$  (33%) and CO (5%) ( $\text{H}_2$  risk was addressed later on); aerosol concentration of  $0.1 \text{ g/m}^3$  with an Aerodynamic Mass median Diameter (AMMD) of  $5 \mu\text{m}$ . The initial objective consisted of obtaining a Decontamination Factor (DF) of 10 for aerosol particles. The system was tested at two different scales: PITEAS and FUCHIA [15]. The PITEAS-filtration program enabled to determine the characteristics of the filter material as well as its domain of use, and check its ability to meet the filtering efficiency criterion under accident conditions. The full-scale FUCHIA program validated the thermo-hydraulic and filtering behaviour of the filtered venting line (without pre-filtration)

Then, it was decided to add a metallic pre-filter upstream of the sand filter, in the containment building.

According to the experiments performed, the DF attributed to the sand bed plus metallic pre-filter system is:

- 1000 for aerosol particles (metallic pre-filter DF assumed to be 10),
- 10 for inorganic gaseous iodine, 1 for organic gaseous iodine (no test done).

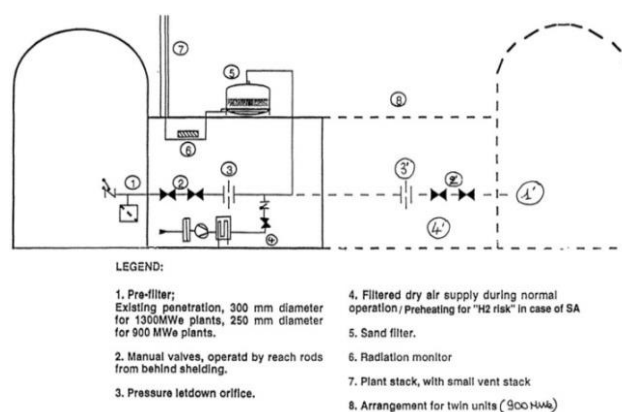


Fig. 3. Sketch of the French FCVS (from [15])

Despite the qualification of the system, two domains appeared not (or not enough) to be covered and are presently investigated in the PASSAM project:

- *Filtration efficiency of gaseous molecular and organic iodides* (IRSN). First laboratory scale experiments recently performed showed no trapping of gaseous molecular iodine ( $\text{I}_2$ ) in the tested conditions on pure sand. A dedicated iodomethane Gas Chromatography analysis method was largely improved and allows now to reach extremely low detection limit for  $\text{CH}_3\text{I}$  (10 ppt) without pre-concentration. Next experiments planned in 2015 and 2016 will focus on  $\text{I}_2$  retention on sand filter system in more representative conditions and on  $\text{I}_2$  and  $\text{CH}_3\text{I}$  retention by metallic prefilters.
- *Mid/Long term stability of filtered fission products, in particular iodine, under severe accident conditions (temperature, flow-rate, pressure, humidity, irradiation)* (IRSN). The corresponding experiments are foreseen in 2015 and 2016 using the IRSN EPICUR facility.

WP4.1: Experimental studies of acoustic agglomeration systems (leader CIEMAT – main contributor CSIC)

Enhancement of particle agglomeration would have the potential of enhancing mitigation. On one side, agglomeration of sub-micron particles in the containment building would result in larger particles that would be much faster depleted by sedimentation (settling velocity is proportional to aerodynamic diameter squared). On the other side, if the agglomeration is done in the venting line to a wet/dry containment filter, the performance of the filtration devices would be improved by enlarging particles, since the efficiency of those systems show a minimum in the range of 0.1 to 0.3 microns.

Acoustic agglomeration (AA) was first experimentally investigated in the 30's of last century and has been extensively studied over many years to understand its basic mechanisms. Its practical applications came a little later in the late 40's with the development of powerful air-jet sound generators. Since then a broad research of potential applications have been investigated [16, 17, 18, 19]. The development of acoustic high-intense chambers as pre-conditioners of filters was specifically tested in some of these works. These studies found out optimum working conditions as regards exposure times; particle concentrations and distributions in the agglomeration chamber. As for the ultrasonic field optimization in nuclear severe accident conditions, it is known to be largely dependent on particle size (micron/sub-micron) and humidity while no degradation should be expected under high pressure and temperature environments.

Therefore, the main challenge for a potential application of AA in nuclear severe accident conditions will consist of checking the system performance under the anticipated working conditions during a severe accident. In the PASSAM frame, preliminary tests have been carried out in 2014 with an Acoustic Agglomerator (21 KHz, 300W/unit) developed by CSIC and implemented in the CIEMAT PECA facility. They allowed setting up the test protocol. The experimental phase in the PECA facility is ongoing since November 2014 and planned up to May 2015.

WP4.2: Experimental studies of high pressure spray agglomeration systems (leader RSE)

High pressure sprays have been used in multiple industrial applications [20], including NPPs (High Pressure Core Spray System of BWR/5 and BWR/6). This type of sprays works between 50 and 200 bar and can generate droplets smaller than 100  $\mu\text{m}$  at velocities near 100 m/s. Under these conditions, in addition to clean-up and cool atmospheres, they can also foster growth of submicron particles [21]. However, few studies have addressed this potential capability and most investigation on sprays performance has been conducted for low pressure sprays [22]. Therefore, high pressure sprays application as an agglomerator in the pre-filter stage of a FCVS would require addressing generic studies:

- Determination of the agglomeration efficiency as a function of injection pressure and droplet size and velocity.
- Enhancement of agglomeration efficiency by adding water additives and/or by droplet charging.

These studies are planned in the frame of PASSAM. The RSE SCRUPOS facility has been set-up and preliminary tests have been carried out for checking the good performance of the instrumentation. The experimental phase in the SCRUPOS facility is foreseen up to mid-2016.

WP4.3: Experimental studies of electrostatic precipitators (leader VTT)

Potential of electric filtration systems were discovered early 19<sup>th</sup> century, when corona discharge was found to remove particles from gas streams. Today many types of these filters exist including electrostatic precipitators (ESP), air ionizers and ion wind devices. Typically they are very efficient filtration systems with minimal resistance to the gas flow. They are applied for reduction of many industrial emissions, including coal and oil fired power plants, salt cake collection from black liquor boilers in pulp mills, and catalyst collection from fluidized bed catalytic cracker units in oil refineries

An ESP removes aerosols from gas flow due to forces induced by strong electric fields [23]. In case particles do not get high enough charge for their collection, a pre-charging water mist can be

sprayed to enhance particle charging: This system is called Wet ESP (WESP). The operation temperature of a typical WESP at atmospheric pressure is limited to 90 °C and the pressure drop through the system is small. The reported energy requirement for the filtration of 1 m<sup>3</sup> of gas by ESP varies from 10<sup>-5</sup> to 10<sup>-3</sup> kW.h. The atomization of water is probably the main power drain of WESP. In case of the atomization of small droplets, it is approximately 400-800 W for a gas flow-rate of 1 m<sup>3</sup>/s.

Typical collection efficiency of a WESP for particles is between 99 to 99.9 %. Nonetheless, collection efficiency can be increased by maximizing the strength of the electric field [24] and the residence time within the precipitator. Other factors affecting efficiency are dust resistivity, gas temperature, chemical composition (of the dust and of the gas flow), and particle size distribution. WESP performance has been hardly tested for gaseous iodine, although preliminary tests were conducted on gaseous iodine filtration by VTT in 2011. In this case higher efficiency might be reached by adding an oxidation stage (ozone generator) that turns gaseous iodine species into iodine oxide particles.

Application of WESP under the foreseen conditions of a nuclear severe accident poses two major challenges:

- Conditions still not explored, like radiation and high temperatures (>90°C), and pressures (>1 bar).
- Filtration of iodine volatile species including organic iodides.

The status of the PASSAM experiments on this domain is as follows. The facility has been set-up and preliminary tests have started in April 2014 using WESP at room conditions. Experimental phase in more representative conditions began recently using TiO<sub>2</sub> aerosols and showing a strong decrease of the trapping efficiency for voltages below 15 kV (negative). Preliminary retention tests for gaseous and particulate iodine have also been conducted.

#### WP4.4: Experimental studies of improved zeolites (leader IRSN – main contributor UniLor)

Zeolites are crystalline materials containing pores of molecular size (5-12 Å). They are composed of [SiO<sub>4</sub>]<sup>4-</sup> and [AlO<sub>4</sub>]<sup>5-</sup> tetrahedra linked by oxygen atoms. The substitution of the Si<sup>4+</sup> by Al<sup>3+</sup> leads to a negative charge, which is compensated by the presence of a metallic (M) cation of n valence (M<sub>x/n</sub> [AlO<sub>2</sub>]<sub>x</sub> [SiO<sub>2</sub>]<sub>y</sub> · zH<sub>2</sub>O, where y/x should be higher than 1; i.e., more Si than Al tetrahedral). Several zeolites families are presently being used for different industrial processes: Mordenite, Ferrierite, Faujasite and others. A number of studies have been conducted to assess the zeolites capability for iodine retention [25, 26, 27, 28] and among all the metallic cations tested (Cd, Pb, Na, Cu ...), for iodine trapping, silver seems to give the best results for potential nuclear applications. Two types of silver-containing solids have been successfully tested for iodine trapping: silver mordenite (AgZ) and silver faujasite (AgX). The trapping mechanism seems to involve chemical redox reactions with some embedded Ag species, which results in the formation of a stable insoluble iodine AgI precipitate.

Investigation has given insights into the iodine capture by zeolites: structural and chemical features of zeolites heavily affect trapping; the Faujasite Ag-X adsorbents showed high decontamination factors (DF) for both molecular iodine and organic iodides, but their efficiency depends on steam and nitrous oxides presence; in Mordenite I<sub>2</sub> chemisorption is enhanced if metallic silver is present [29]; high humidity affects negatively organic iodide trapping; silver zeolites are robust and withstand harsh temperature, humidity and radiation conditions.

In spite of all the knowledge gathered concerning iodine trapping in zeolites, little information is available concerning impacts of zeolite structure and cation loading as well as the persistence of high iodine DF under oxidizing conditions resulting from radiation.

More precisely, the experiments in the frame of the PASSAM project are focused on:

- the optimization of the nature of the zeolite in order to avoid poisoning effects and to obtain high iodine DFs;

- the definition of optimal active sites for the trapping of iodine and organic iodides (deeper understanding of the trapping mechanisms);
- providing extensive and sound data on the effect of expected severe accident working conditions including influence of chemical effects (steam and gas contaminants) and potential irradiation effects on iodine trapping capacity.

The experimental programme started in 2013 and is foreseen up to 2016. The main results acquired up to now by the French University of Lorraine are as follows:

- Up to 20 metal-exchanged zeolites were prepared and characterized.
- Adsorption tests of CH<sub>3</sub>I in gaseous phase under different conditions were performed. About the trapping efficiency, silver zeolites lead to the best adsorption performances in the absence of contaminants and the experiments are now oriented to a better assessment of the effects of structure and silver incorporation method. About the trapping stability, the formation of a highly stable AgI phase was evidenced as well as less stable products.

#### WP4.5: Experimental studies of “combined” filtration systems (leader AREVA)

The AREVA FCVS is based on an extensive series of laboratory tests and further large-scale investigations. As a result, a combined retention process was selected, consisting of complementary wet scrubbing and particulate filtering. The AREVA FCVS standard comprises a venturi scrubber unit consisting of a venturi section (wet section), a combined droplet separator and metal fibre filter section (dry section) combined with a throttling orifice for a sliding pressure process. By the entrainment and dispersion of the scrubbing liquid, large reaction surfaces are created in the venturi nozzles which result in an additional effective sorption of gaseous iodine. For optimum iodine retention, the scrubbing liquid is conditioned with caustic soda and other additives.

The AREVA FCVS provides already retention efficiencies higher than 99.99% for aerosols

(even those smaller than 0.5 µm) and higher than 99.5% for I<sub>2</sub>. Despite this performance, as it is reminded in the PASSAM objectives section (Section II), there are studies [30] which indicate that a significant generation of organic iodine in the containment atmosphere might occur during a severe accident. Consequently the AREVA FCVS Plus (Fig. 4) was developed by supplementing the existing AREVA FCVS Standard with a sorbent (zeolite) section as a third retention stage with combined passive superheating [31].

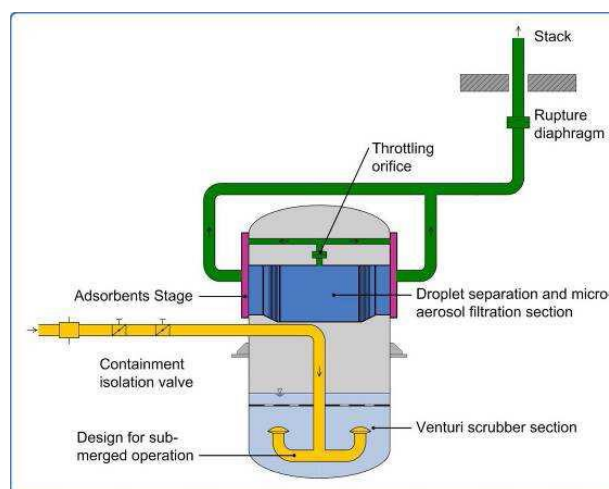


Fig. 4. AREVA High Speed Sliding Pressure Venting<sup>Plus</sup>

In link with the PASSAM project, the AREVA experimental programme on this “FCVS PLUS” combined system was completed in 2013. The main results on organic iodine retention as stated by AREVA are:

- Retention efficiency of zeolite depends upon many parameters: sorbent material, geometry / flow dynamics, superheating / relative humidity, heat repartition, residence time, gas composition, flow velocities, etc.
- Extensive large-scale test campaigns were conducted at the JAVA PLUS test facility. The performed JAVA PLUS tests verified that this combined filter is able to reach the target DF, e.g. superior to 50 for organic iodine (more than 98% retention).
- The studied parameters allowed to develop a model in order to customize the DF for organic iodine by appropriate design of the

sorbent stage for the requested operating range.

The performed test campaign results in a fully qualified combined filter design of this “FCVS PLUS”.

## VI. CONCLUSION

The four year (2013-2016) European PASSAM project devoted to mitigation of atmospheric source term is being conducted as initially planned. After two years of operation, the experimental work is in progress and in some domains (e.g. pool hydrodynamics, use of zeolites for iodine trapping, combined wet and dry filtrations systems) major results have already been obtained

Thanks to the PASSAM project, databases on existing or innovative mitigation systems will be extended. Among the various topics studied, three of them may be quoted for their potential direct impact on severe accident management: gaseous iodine retention (molecular and organic iodine), hydrodynamics for scrubbers, and long term stability of trapped compounds in the various systems.

It is expected to get a deeper understanding of the phenomena underlying the performance of these mitigation systems, and to be able to propose simple models or correlations which should be easy to implement in accident analysis codes, like ASTEC.

Orders of magnitude for source term reduction for each mitigation system studied, including on the long term, in accident conditions, as well as general advantages and drawbacks of all these systems (efficiencies, passive behaviour, robustness, long term retention, etc...) is being assessed. It should allow to give hints for improved filtration systems.

The main technical outcomes of the project will be documented in a final synthesis report and presented in a final workshop to be held in Paris area by end 2016. Finally, all the public documents of the project are uploaded on line on a dedicated web site at <https://gforge.irsn.fr/gf/project/passam/>.

## ACKNOWLEDGMENTS

The authors thank the European Atomic Energy Community (Euratom) for showing a strong

interest in the PASSAM Project, and for funding it in the frame of the 7<sup>th</sup> framework programme FP7/2007-2013 under grant agreement n° 323217.

## REFERENCES

1. D. JACQUEMAIN, S. GUENTAY, S. BASU, M. SONNENKALB, L. LEBEL, H. J. ALLELEIN, B. LIEBANA MARTINEZ, B. ECKARDT and L. AMMIRABILE, *OECD/NEA/CSNI Status Report on Filtered Containment Venting*, NEA/CSNI/R(2014)7.
2. T. ALBIOL, L. E. HERRANZ, E. RIERA, S. GUIEU, T. LIND, G. MANZINI, A. AUVINEN and N. LOSCH, “New studies on passive and active systems towards enhanced severe accident source term mitigation – The PASSAM Project”, *Eurosafe Forum* Bruxelles, Belgium, November 5-6, 2012.
3. H. J. ALLELEIN, A. AUVINEN, J. BALL, S. GUENTAY, L. E. HERRANZ, A. HIDAKA, A. JONES, M. KISSANE, D. POWERS and G. WEBER, *State-of-the-art on nuclear aerosols (pages 248-255)*, OECD/NEA/CSNI/R(2009)5.
4. P. CHATELARD, S. ARNDT, B. ATANASOVA, G. BANDINI, A. BLEYER, T. BRAHLER, M. BUCK, I. KLJENAK and B. KUJAL, “Overview of the ASTEC V2.0 and V2.0-rev1 validation”, *5<sup>th</sup> European Review Meeting on Severe Accident Research (ERMSAR 2012)*, Cologne, Germany, March 21-23, 2012.
5. L. E. HERRANZ, T. LIND, K. DIESCHBOURG, E. RIERA, S. MORANDI, P. RANTANEN, M. CHEBBI and N. LOSCH, *PASSAM “State-of-the-art report” - Technical Bases for Experimentation on Source Term Mitigation Systems*, PASSAM-THEOR-T04 [D2.1], (2013), <https://gforge.irsn.fr/gf/project/passam/docman/?action=DocmanFileEdit&id=5627>
6. L. E. HERRANZ, T. LIND, C. MUN, E. RIERA, S. MORANDI, P. RANTANEN, B. AZAMBRE and N. LOSCH, *PASSAM Experimental Tests Matrixes*, PASSAM-THEOR-T06 [D2.2], (2014),

- <https://gforge.irsn.fr/gf/project/passam/docman/?action=DocmanFileEdit&id=5948>
7. L. E. HERRANZ, T. LIND, K. DIESCHBOURG, E. RIERA, S. MORANDI, P. RANTANEN, M. CHEBBI, and N. LOSCH, “Technical Bases for Experimentation on Source Term Mitigation: The EU-PASSAM Project”, *Proceedings of the 10<sup>th</sup> International Topical Meeting on Nuclear Thermal-Hydraulics, Operation and Safety (NUTHOS-10)*, Okinawa, Japan, December 14-18, 2014.
  8. PASSAM 1st Workshop on source term mitigation of severe accidents, Madrid (Spain), February 26<sup>th</sup>, 2014, <https://gforge.irsn.fr/gf/project/passam/docman/?subdir=2135>
  9. L. E. HERRANZ, R. DELGADO, T. BERSCHART, T. LIND and S. MORANDI, “Remaining issues on pool scrubbing: Major drivers for experimentation within the EU-PASSAM project”, *Proceedings of ICAPP '14*, Charlotte, USA, April 6-9, 2014.
  10. A. DEHBI, D. SUCKOW and S. GUENTAY, “Aerosol retention in low-subcooling pools under realistic accident conditions”, *Nuclear Engineering and Design*, **203**, 229–241 (2001).
  11. L. E. HERRANZ, V. PEYRES, J. POLO, M. J. ESCUDERO, M. ESPIGARES and J. LÓPEZ JIMÉNEZ, “Experimental and analytical study on Pool Scrubbing under jet injection regime”, *Nuclear technology*, **120**, 95–109 (1997).
  12. S. GUENTAY, “ARTIST: introduction and first results”, *Nuclear Engineering and Design*, **231**, 109–120 (2004).
  13. T. LIND, A. DEHBI and S. GUENTAY, “Aerosol retention in the flooded steam generator bundle during SGTR”. *Nuclear Engineering and Design*, **241**, 357–365 (2011).
  14. T. TH. BETSCHART, T. LIND, D. SUCKOW, V. BRANKOV AND E. H.-M. PRASSER, “Two-phase flow hydrodynamics characterization for understanding the aerosol retention in liquid pools”, *7<sup>th</sup> European Review Meeting on Severe Accident Research (ERMSAR 2015)*, Marseille (France), March 24-26, 2015.
  15. S. GUIEU, “Prevention of Delayed Containment Failure: the Sand-Bed Filter. Characteristics and Role in Severe Accident Management”, *Proceedings of the OECD/SAMI Workshop on the implementation of severe accident management measures*, NEA/CSNI/R(2001)20, PSI Report Nr. 01-15 (2001).
  16. E. RIERA, L. ELVIRA, I. GONZÁLEZ, J. J. RODRÍGUEZ, R. MUÑOZ and J. L. DORRONSORO, “Investigation of the influence of humidity on the ultrasonic agglomeration of submicron particles in diesel exhausts”, *Ultrasonics*, **Vol. 41**, p. 277-281 (2003).
  17. E. RIERA, J. A. GALLEGU-JUÁREZ and T. J. MASON, “Airborne ultrasound for the precipitation of smokes and powders and the destruction of foams”, *Ultrasonics Sonochemistry*, **Vol. 13**, p. 107-116 (2006).
  18. J. MAGILL, S. PICKERING, S. FOURCAUDOT, J. A. GALLEGU-JUÁREZ, E. RIERA and G. RODRIGUEZ, “Acoustic aerosol scavenging”, *Journal of Nuclear Materials*, **Vol. 166**, p. 208-213 (1989).
  19. J. MAGILL, P. CAPERÁN, J. SOMERS, K. RICHTER, S. FOURCAUDOT, P. BARRAUX, P. LAJARGE, J. A. GALLEGU-JUÁREZ, E. RIERA, G. RODRIGUEZ and N. SEYFERT, “Characteristics of an electro-acoustic precipitator (EAP)”, *Journal of Aerosol Science*, **Vol. 23 Suppl. 1**, S803-S806 (1992).
  20. A. B. CECALA, A. D. O'BRIEN, J. SCHALL, J. F. COLINET, W. R. FOX, R. J. FRANTA, J. JOY, W. R. REED, P. W. REESER, J. R. ROUNDS and M. J. SCHULTZ, *Dust Control Handbook for Industrial Minerals Mining and Processing*, RI 9689 (2012). <http://www.cdc.gov/niosh/mining/UserFiles/works/pdfs/2012-112.pdf>
  21. T. CHUEN-JINN, L. CHIA-HUNG, W. YU-MIN, H. CHENG-HSIUNG, L. SHOU-NAN, W. ZONG-XUE and W. FENG-CAI, “An Efficient Venturi Scrubber System to Remove Submicron

- Particles in Exhaust Gas”, *Journal of Air & Waste Management Association*, **Vol. 55**, p. 319–325 (2005).
22. D. A. POWERS and S. B. BURSON, “A Simplified Model of Aerosol Removal by Containment Sprays”, **NUREG/CR-5966**, SAND92-268 (1993).
  23. C. RIEHLE, *Applied electrostatic precipitation*, Chapter 3, p 25-88, “Basic and theoretical operation of ESP’s”, Edited by K.R. PARKER, Chapman & Hall, London, UK (1997).
  24. J. CHANG, Y. DONG, Z. WANG, P. WANG, P. CHEN and C. MAN, “Removal of sulphuric acid aerosol in a wet electrostatic precipitator with single terylene or polypropylene collection electrodes”, *Journal of Aerosol Science*, **Vol. 42**, p. 544–554 (2011).
  25. D. T. PENCE, F.A. DUCE and W. J. MAECK., “A Study of the Adsorption properties of metal zeolites for airborne iodine species”, *Proceeding of the 11<sup>th</sup> AEC Air Cleaning Conference*, Richland (WA, USA), August 31 – September 3, 1970.  
[http://rsearch.hitechsvc.com/nuclearsafety/qa/hep\\_a/nureg\\_11Vol2/session5b.pdf](http://rsearch.hitechsvc.com/nuclearsafety/qa/hep_a/nureg_11Vol2/session5b.pdf)
  26. H. G. DILLMANN, H. PASLER AND J. G. WILHELM, “Filtered venting for German power reactors”, *Nuclear technology*, **Vol. 92**, p. 40-49 (1990).
  27. B.S. CHOI, G.I. PARK, J. H. KIM, J. W. LEE and S. K. RYU, “Adsorption equilibrium and dynamics of methyl iodide in a silver ion-exchanged zeolite column at high temperatures”, *Adsorption*, **Vol. 7**, p. 91-103 (2001).
  28. B.S. CHOI, G.I. PARK, J. W. LEE, H. Y. YANG and S. K. RYU, “Performance test of silver ion-exchanged zeolite for the removal of gaseous radioactive methyl iodide at high temperature condition”, *Journal of Radioanalytical and Nuclear Chemistry*, **Vol. 256**, p. 19-26 (2003).
  29. K. W. CHAPMAN, P. J. CHUPAS and T. M. NENOFF, “Radioactive iodine capture in silver-containing mordernites through nanoscale silver iodide formation”, *Journal of American Chemistry Society*, **Vol. 132**, p. 8897-8899 (2010).
  30. B. CLÉMENT, L. CANTREL, G. DUCROS, F. FUNKE, L. E. HERRANZ, A. RYDL, G. WEBER and C. WREN, *State of the art report on iodine chemistry*, NEA/CSNI/R(2007)1.
  31. N. LOSCH, S. BUHLMANN and C. HUTTERER, “High speed sliding pressure venting PLUS (AREVA’s FCVS with enhanced organic iodine retention) design principles and qualification of severe accident equipment”, *Nuclear Plant Chemistry Conference*, SFEN, Paris (France), September 24 – 28, 2012.



**Session 5: recent developments in iodine chemistry modelling in severe accidents and applications to source term and radiological consequences evaluations**

## IODINE CHEMISTRY IN DESIGN BASIS FAULTS

A Zodiates(1)\*, S Dickinson(2)

<sup>(1)</sup> EDF Energy, Barnwood, Gloucester, UK, <sup>(2)</sup> National Nuclear Laboratory, Harwell, UK

\*Corresponding author, tel: (+44) 1452653915, [tasos.zodiates@edf-energy.com](mailto:tasos.zodiates@edf-energy.com)

### **Abstract.**

*Iodine is the dominant contributor to off-site doses in Design Basis Faults (DBFs) in Pressurised Water Reactors. The volatile nature of iodine makes the assessment of iodine release very complicated.*

*This paper considers the range of conditions and the potential iodine release pathways applicable to typical design basis faults, and identifies the iodine chemistry parameters that need to be known in order to carry out an assessment of the iodine release. The paper also identifies potential gaps in our understanding of iodine chemistry parameters which may be addressed by a future experimental programme.*

## I. INTRODUCTION

The Sizewell B safety case probabilistic safety assessment (PSA) considers in detail the Design Basis (Accidents) Faults (DBFs). The reactor event tree analysis and the consideration of hazards and radwaste faults resulted in the order of ~5000 DBFs. The DBFs were grouped into ~1000 Limiting DBFs (LDBFs) based on the event tree endpoints and the scope and description of the initiating faults. A further grouping process based on the fault characteristics and the radiological aspects of the faults (source term, release path, retention mechanisms), resulted in ~200 Bounding LDBFs (BLDBFs).

Detail radiological consequences assessments including all nuclides were carried out for representative BLDBFs. These assessments showed that iodine is the dominant contributor to the off-site doses. Therefore, the radiological consequences assessments of the BLDBFs, with a few exceptions, were carried out based on iodine consideration only.

This paper considers the range of conditions and the potential iodine release pathways applicable to typical design basis faults, and identifies the iodine chemistry parameters that need to be known in order to carry out an assessment of the iodine release. These are identified by considering a typical auxiliary building Loss Of Coolant Accident (LOCA); for example, leakage through a Residual Heat Removal System (RHRS) valve or pump in an RHRS pump room.

The paper also identifies potential gaps in our understanding of iodine chemistry parameters which may be addressed by a future experimental programme.

## II. OVERVIEW OF AUXILIARY BUILDING LOCA

Some parts of the primary circuit systems are located in the auxiliary building adjacent to the reactor building. Loss of coolant from leaks in these systems can result in airborne activity in the auxiliary building followed by a release to the external atmosphere via the ventilation systems or direct leakage. A general description of the fault is as follows:

- i) Primary coolant discharges through the breach at a pressure and temperature dependent on the system affected and the status of the reactor. Depending on the system, the fault can occur during reactor operation, during normal shutdown, following a primary circuit fault with fuel failures or during long-term post fault cooling operations.
- ii) The water jet discharging from the leak point fragments to form a droplet distribution suspended in the room atmosphere, an aerosol, and may also partially flash to form steam.
- iii) On detection of a release of activity into the auxiliary building, the emergency exhaust systems (containing iodine filters) are switched into operation.
- iv) Operator action isolates the leaking coolant system, although a discharge continues until the isolated pipe is empty.

In the auxiliary building LOCA the relevant parameters span the following typical ranges:

- Water leak rate: 0.5 – 60 kg/s
- T of discharging water: 70 – 200 °C
- P of discharging water: 6 – 155 bar a
- T of droplets/room atmosphere/sump water: 70–100°C
- pH = 4.6 or 8
- D = few mGy/hr to few tens Gy/hr
- Iodine concentration =  $10^{-6}$  –  $10^{-11}$  moles/kg

## III. IODINE RELEASE PATHWAYS

Iodine in a water solution exists in two forms in terms of volatility: volatile (e.g. I<sub>2</sub>) which can escape from solution and involatile (e.g. iodide or iodate) that remains in solution. If the conditions in the solution are constant or evolve only slowly, the volatile and involatile forms will reach a steady state depending on dose rate and the pH and temperature of the water solution.

The volatile iodine that escapes from the water may accumulate in the room atmosphere. Depending on the physical processes taking place, i.e. room ventilation rate, the iodine concentration in the gas side and the volatile iodine concentration in the water may reach an equilibrium.

Figure 1 illustrates the various iodine processes and release pathways considered in an auxiliary building LOCA.

There are no significant retention mechanisms for volatile iodine released into the room atmosphere and all volatile iodine is taken to be

discharged from the room via the ventilation system where iodine retention may be claimed on charcoal filters should they be available in the ventilation system. The water loading on the filters and the resultant reduction in filtration efficiency is taken into account.

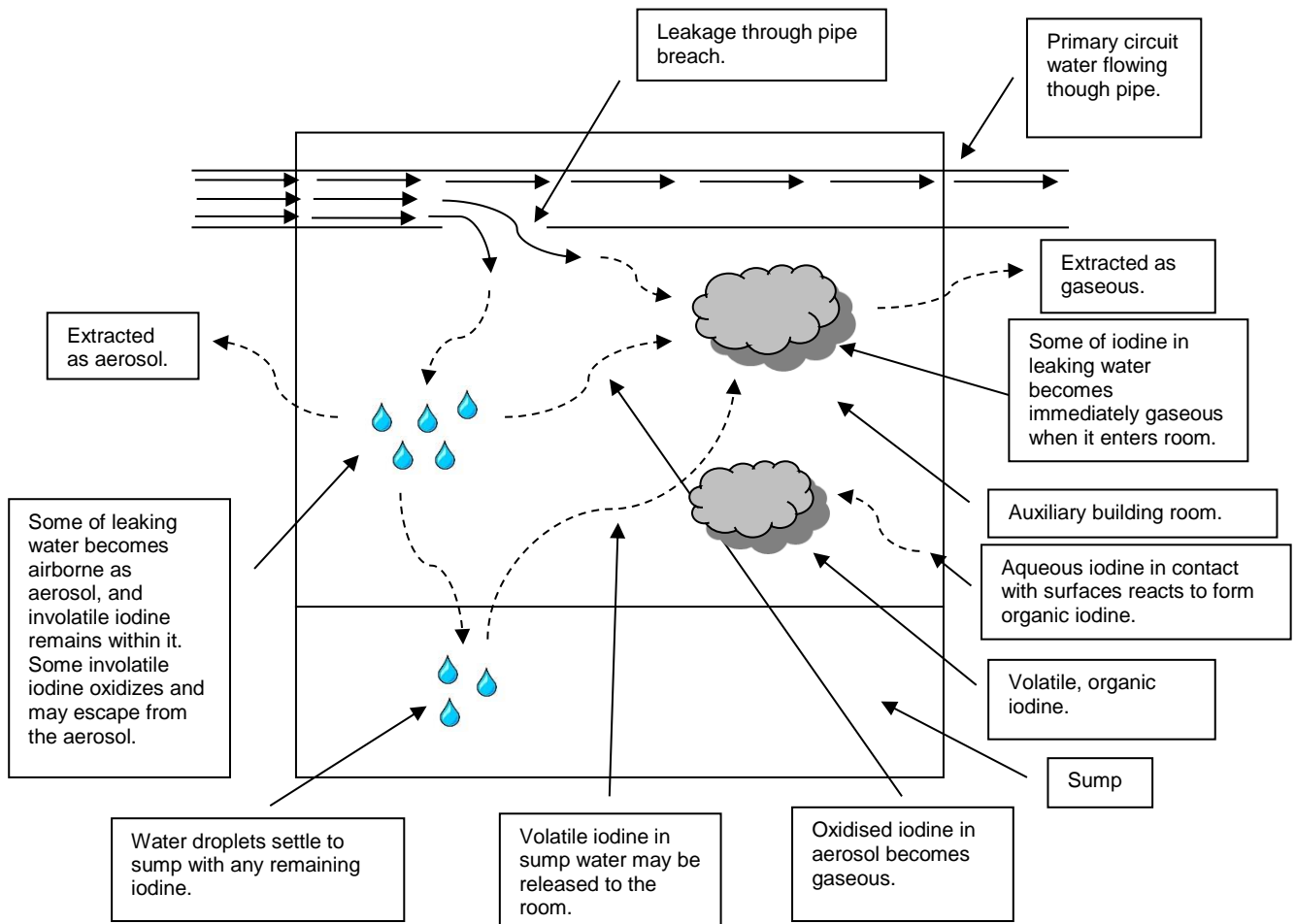


Fig 1: Iodine Processes in an Auxiliary Building LOC

The iodine release pathways are:

- i) 'gaseous from primary'
- ii) 'extracted as dissolved in droplets'
- iii) 'gaseous from droplets'
- iv) 'partitioned from sump'
- v) 'organic from surfaces'

In order to make the assessment manageable it is necessary to use simplified iodine models and this, by nature, tends to lead to a conservative assessment which can be easier to support and justify in the absence of consistent experimental data.

These pathways are discussed in the sections below.

#### IV. GASEOUS FROM PRIMARY

Oxidation of iodine to form volatile  $I_2$  or  $I$  occurs in the radiation fields of the primary circuit. Other potentially volatile iodine species, such as HOI, are also formed but this has a much higher partition coefficient than the other forms, particularly atomic  $I$ , so is considered to be less significant. The equilibrium **volatile iodine fraction**,  $F_{vol}$ , depends on the water pH and temperature and is derived in a conservative way from experimental results at high doserates [1].

The volatile fraction is considered for two pH ranges: 'buffered'  $pH > 7$ , and 'unbuffered'  $pH < 7$ .

The temperature range covered by the experimental results is 25 to 140 °C.

All the volatile iodine in the water discharging through the leak is conservatively assumed to be released into the room atmosphere and extracted by the room ventilation.

#### V. EXTRACTED AS DISSOLVED IN DROPLETS

The water jet discharging into the room from the leak, fragments into droplets of various sizes depending on the water temperature and system pressure. The larger size droplets fall out of the room atmosphere faster, and are collected in the room sump or floor pool. The fine droplets remain airborne for longer.

The room ventilation flow will carry out with it airborne droplets and any iodine that is present in the droplets. The iodine concentration in the droplets depends on:

- a) the iodine that remained in the droplets after the volatile iodine has been released at the point of discharge, see IV above, and
- b) on the rate of formation of volatile iodine in the droplets and its rate of release from the droplets, see VI below.

Therefore, the iodine release from the room as 'extracted as droplets' depends on the initial droplet size distribution, the droplet settling processes, the ventilation rate and the iodine droplet concentration (which may have been modified by release of volatiles as in (a) above)..

#### VI. GASEOUS FROM DROPLETS

The droplets produced at the moment the water is discharged into the room contain involatile iodine only as it is assumed that all volatile iodine partitions from the water at that moment. However, in the presence of the radiation field in the room, volatile iodine is produced in the droplets.

Given the small size of the droplets and the large area to volume ratio of the fine droplets remaining airborne, it is conservatively assumed that the volatile iodine partitions out of the droplets as it is produced. This is likely to overestimate the release from the droplets, particularly if the discharged water contains pH control chemicals.

The volatile iodine fractional production rate is dependent upon the iodine '**G value**' and it is assumed to be proportional to the doserate and independent of the iodine concentration and the water pH. The '**G value**' was determined from experimental results at relatively high dose rates,  $> 100$  Gy/hr, and concentrations,  $> 10^{-5}$  mol/kg.

The airborne doserate in the room depends on the total activity in the discharging water which is fault dependent and can be as low as a few mGy/hr. The iodine concentration also can vary by orders of magnitude. Extrapolation of the experimentally-observed behaviour over such a

wide range of conditions is not straightforward, as discussed below in Section IX.

It would be beneficial in the modelling of these faults to extend the experimental data to lower doserates and a wider range of iodine concentrations.

## VII. PARTITIONED FROM SUMP

As the water discharges through the leak the vast majority settles to the room floor and sump very quickly. Volatile iodine will build up in the water and be available to escape from the water into the room atmosphere. Retention of iodine on the surfaces of the sump walls and room floor or submerged equipment is conservatively ignored. Although deposition on sump surfaces is a potential source of volatile organic iodine, the assumptions made in calculating the organic iodine production are sufficiently conservative that this additional source does not need to be considered.

In the auxiliary building LOCA calculations the following simplifying assumptions are made:

- the volatile iodine concentration in the water is always at its equilibrium value,  $F_{vol}$ , for the conditions;
- the gaseous side iodine concentration in the room atmosphere, which can slow down the release from the water, is neglected.

The first assumption can be very conservative if the volatile iodine production rate is less than the volatile iodine release rate, which may be the case at low doserates. Thus, there is a need to extend the range of experimental results to low doserates as identified in the previous section.

The iodine release rate from the sump is determined by mass transfer and is evaluated from the following equation, using values of  $A$  and  $V$  appropriate to the sump as a whole:

$$\frac{d[I_{total}]_{aq}}{dt} \approx \frac{-K_t A}{V_w IPC} [I_{total}]_{aq}.$$

where:

$[I_{total}]_{aq}$  = total iodine concentration in the water (Bq)

$K_t$  = overall iodine mass transfer coefficient (m/s)

$A$  = water/gaseous interface area ( $m^2$ )

$V$  = water volume ( $m^3$ )

**IPC = overall Iodine Partition Coefficient** =  $R / F_{vol}$

$F_{vol}$  = iodine volatile fraction

**R = iodine partition coefficient**

Consideration is given to the release of both inorganic iodine and organic iodine from the sump.

The complexity in the assessment arises in the identification of appropriate values for IPC and  $K_t$ . IPC depends on the volatile iodine species,  $I_2$ ,  $I$  or organic iodine, and can also depend on water temperature, pH and doserates.  $K_t$  depends (among other things) on the volatile iodine species, the geometry of the water volume and the room air flow convection patterns.

For buffered solutions,  $pH > 7$ , IPC is calculated based on the doserate. For un-buffered solutions,  $pH < 7$ , IPC is calculated conservatively from the expression  $R/F_{vol}$  on the assumption that  $I_2$  is the volatile species, or for low iodine concentrations by a value that bounds the available experimental results.

Additional experimental data for low iodine concentrations,  $< 10^{-8}$  mol/dm<sup>3</sup>, and lower doserates, 0.01 – 10 Gy/hr, may be useful in removing conservatism in the interpretation of the experimental results.

## VIII. ORGANIC FROM SURFACES

An additional pathway for releasing iodine to the room atmosphere is the formation of organic iodine through surface reactions of iodine in solution deposited on the room surfaces which are not under water.

The organic iodine formation rate, as a fraction of the iodine activity on the surfaces, is given by:

$$k_{orgI} = (K + K_r D) \frac{A}{V_l}$$

where:

$K / K_r$  = thermal and radiolytic production rates,

$D$  = dose rate

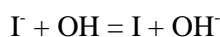
$A/V_1$  = water area to volume ratio of the surface water film taken to be 0.1mm.

The thermal and radiolytic production rates are based on experimental measurements of methyl iodine production from painted surfaces loaded with iodine [2]. The values used in the assessments have been periodically checked against more recent data from the EPICUR [3] and BIP [4] programmes to ensure that the assessment methods remain conservative. Although some differences have arisen between the new data and those used in the assessments, these are not very large and, particularly given the as-yet unexplained variations between different data sets, a change to the values used is not merited. Also, the more recent studies have been directed towards severe accident conditions where the surface concentrations may be orders of magnitude higher than those expected in some design basis faults.

#### IX. VOLATILE IODINE PRODUCTION AT LOW CONCENTRATION AND DOSE RATE

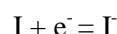
Parts of the assessment described above require a production rate for volatile iodine in irradiated solution. The formula currently used is based on measurements in irradiated solutions using iodine concentrations up to  $10^{-4}$  mol dm<sup>-3</sup> and dose rates of 0.1 to 1 kGy hr<sup>-1</sup>. Whilst these are appropriate to severe accidents, the values for design basis faults can be very much lower. Although it is usually conservative to assume that behaviour observed in experiments will apply under much less severe conditions, this may not be the case here.

The initial reaction in the radiolytic production of volatile iodine species (I<sub>2</sub> or atomic iodine) from I<sup>-</sup> ions in irradiated water involves the hydroxyl radical:



If it is assumed that every OH radical produced in the irradiation of water reacts to convert an iodide ion into volatile form then the production rate of volatile iodine will be equal to the G value of OH radicals, which is approximately  $3 \times 10^{-7}$  mol dm<sup>-3</sup> Gy<sup>-1</sup> at 70°C. This is the upper limit for the volatile iodine production rate. However, if the dose rate is sufficiently high

there will be other radical reactions which remove volatile iodine e.g.



or which compete for OH radicals and reduce the formation rate of I atoms. The net result is that the production rate of volatile iodine becomes much less than the OH radical production rate at high dose rates. At very low dose rates, however, the concentration of other reactive species is very low so the volatile iodine production rate may approach its limiting value.

The production rate of volatile iodine has not been measured at dose rates below about 100 Gy hr<sup>-1</sup> so the range of validity of the formula used in the DBF assessments is unknown. The iodine radiation chemistry model INSPECT [5] predicts that it is valid at dose rates above 1 Gy hr<sup>-1</sup> but at lower dose rates the limiting value applies (Fig. 2).

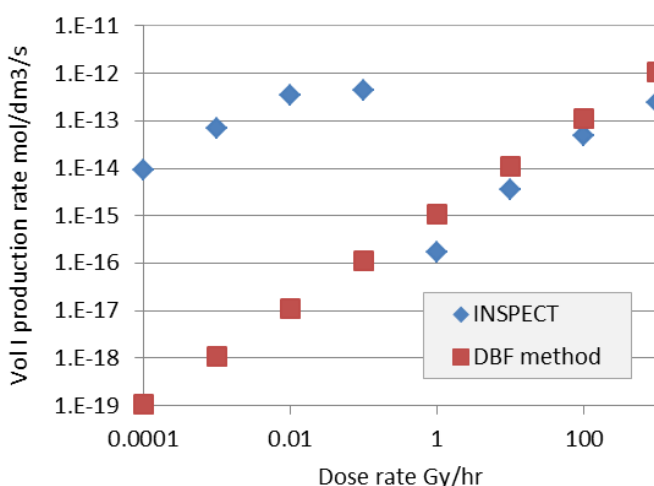


Fig 2. Production rate of volatile iodine in  $10^{-8}$  mol dm<sup>-3</sup> I<sup>-</sup> solution: comparison of INSPECT predictions with the DBF assessment method.

Although INSPECT is a mechanistic model which uses a large number of chemical rate constants to simulate the iodine behaviour, it is not validated at such low dose rates and its predictions should therefore be treated with some caution. Experimental data at low dose rates would be very helpful in validating the model prediction and improving the assessment methods.

## X. SUMMARY

Iodine is the dominant contributor to off-site doses in Design Basis Faults (DBF) in Pressurised Water Reactors. The volatile nature of iodine makes the assessment of iodine release very complicated.

This paper uses the example of auxiliary building LOCA to identify the range of conditions and the potential iodine release pathways applicable to typical design basis faults. It also identifies the iodine chemistry parameters that need to be known in order to carry out an assessment of the iodine release. Suitable values for the iodine chemistry parameters need to be specified to cover the whole range of conditions that exist in typical faults. These values are derived based on experimental results. In general, the experimental data tend to cover the range of temperatures up to below 100°C and some extends to about 140°C. Temperatures in many design basis accidents exceed this range and it is worth considering extending the experimental temperature range to beyond 140°C.

The paper also identifies that there are potential gaps in our understanding of iodine chemistry parameters that are relevant to the conditions of low doserates and very low iodine concentrations. It is worth considering whether these conditions can be the subject of future research.

## NOMENCLATURE

PSA = Probabilistic Safety Assessment

DBF = Design Basis Fault

LDBF = Limiting Design Basis Fault

BLDBF = Bounding Limiting Design Basis Fault

LOCA = Loss of Coolant Accident

RHRS = Residual Heat Removal System

IPC = Iodine Partition Coefficient

## REFERENCES

1. W. G. BURNS et al, "Iodine chemistry in nuclear reactor environments", Water Chemistry of Nuclear Reactor Systems 5, p. 281, BNES, (1989)
2. A. M. DEANE, "Volatile organic iodine formation by surface processes", Proc. 3<sup>rd</sup> CSNI Workshop on Iodine Chemistry in Reactor Safety. p181, NEA/CSNI/R(91)15 (1992)..
3. J. COLOMBANI et al., "Experimental study of organic iodide formation from painted surfaces in the containment atmosphere during a severe accident", ICAPP-2011, Nice. France, 2-5 May 2011..
4. G. A. GLOWA, C. J. MOORE and D. BOULIANNE, "The main outcomes of the OECD Behaviour of Iodine project", This conference, (2015).
5. S. DICKINSON and H. E. SIMS, "Development of the INSPECT Model for the Prediction of Iodine Volatility from Irradiated Solutions", Nuclear Technology 129, p374, 2000.

## **IODINE BEHAVIOUR IN THE CIRCUIT AND CONTAINMENT: MODELLING IMPROVEMENTS IN THE LAST DECADE AND REMAINING UNCERTAINTIES**

L. Bosland<sup>(1)\*</sup>, L. Cantrel<sup>(1)</sup>

<sup>(1)</sup> Institut de Radioprotection et de Sûreté Nucléaire, Saint-Paul Lez Durance, France

\*Corresponding author, Tel: (+33)4.42.19.94.46, loic.bosland@irsn.fr

### **Abstract**

*Within the past decade, international experimental programmes were performed in the area of iodine behaviour in the Reactor Coolant system (RCS) and containment during a severe accident (SA) in a Nuclear Power Plant (NPP). The objectives were to better understand involved physico-chemical processes and develop relevant models in SA codes like ASTEC which are used to estimate Source Term (i.e., radioactive releases to the environment). Significant progresses have been made in the modelling of the iodine behaviour in the RCS and the containment. This article provides a synthesis of the progresses made in the last decade, what has been understood from the experimental data and which models have been developed, validated and implemented in the ASTEC code. Significant progresses have been made on understanding and modelling of key processes for iodine behaviour which gives more confidence on iodine Source Term (ST) assessments and which highlights remaining major source of uncertainties for such assessments. These uncertainties mostly concern processes that have been recently identified as potential important contributors to the releases at mid-term, notably for some NPPs in conjunction with the use of Emergency Containment Filtered Venting Systems (EFCVS). These processes are discussed and are the subject of on-going R&D programmes (e.g., OECD-STEM, ANR-MIRE, EC-PASSAM) and future R&D initiatives (e.g., OECD-STEM2, OECD-BIP3, OECD-THAI3) in the ST field.*

## I. INTRODUCTION

Iodine behaviour during a nuclear reactor severe accident has been investigated within the past decade through several international experimental programs that have significantly contributed to develop the knowledge in this field. These include the PHEBUS-FP integral tests [1-4] and more analytical programs such as ISTP [5], PARIS [6, 7], OECD-STEM [8], OECD-THAI [9, 10] and OECD-BIP [11, 12] programs which were focused on iodine behaviour either in the Reactor Coolant System (RCS) [13-15] or in the gaseous phase of the containment [6, 7, 9-12, 16, 17] (the liquid phase iodine chemistry was mostly investigated between 1994 and 2005 [18]).

For the RCS, the kinetics of the I-O-H system, the influence of fission products (Cs, Mo) and Boron (B) on iodine transport has been investigated. Concerning the potential impact of the control rod material (Ag, In, Cd), the studies are ongoing at IRSN. In the containment, most of the efforts have been put on iodine interaction with Epoxy paint under irradiation [16, 17, 19-21], iodine oxides (IOx) formation [6, 7, 9, 22-24] and radiolytic decomposition [7, 12, 25], iodine interaction with steel [26, 27] and iodine adsorption on aerosols [10]. For each phenomena investigated at the experimental level, a significant effort has also been put on the interpretation of the data in order to model each phenomenon with the objective to implement these new models in the ASTEC severe accident code (jointly developed by GRS and IRSN) [28-30]. This paper recaps in Section II the progress made for iodine modeling in the RCS whereas section III synthesizes the progress made at IRSN for gaseous iodine chemistry modeling in the containment for about 10 years. Section IV identifies new containment phenomena whose influence on iodine volatility might be significant and needs to be studied.

## II. IODINE CHEMISTRY IN THE RCS

One unexpected result coming from PHEBUS-FP tests is that a significant gaseous iodine amount enters in the containment from the circuit during the fuel bundle degradation [31]. In FPT0, FPT1 and FPT2, this gaseous fraction reaches

few percents of the i.b.i (initial bundle inventory) whereas in FPT3, it is up to 30% of the i.b.i (and representing 90% of the iodine entering in the containment). The understanding of this result has been pursued through the ISTP-CHIP program, whose objective was to investigate the iodine transport through the RCS. Semi-global experiments [13] as well as more analytical ones [14, 32] were carried out to study the influence of the most relevant elements on iodine speciation (gaseous or particulate forms) at the break. These experimental efforts have been coupled with the development of theoretical chemistry methodologies which allow us getting more fundamental data as thermodynamic properties [33, 34] and rate constants for elementary reactions [35].

For the “iodine system”, a kinetic reaction scheme was developed [36] and validated on a wide range of experimental conditions either in pure steam atmosphere or in hydrogen atmosphere. It appears that for temperature below  $\sim 1000$  K, in oxidizing conditions, the system cannot be considered to be at chemical equilibrium whereas in reducing conditions, the kinetics are faster and very close to the equilibrium even at low temperatures.

In presence of cesium (and without any other element), the formation of CsI is very fast because the reaction  $\text{CsOH} + \text{HI} \rightleftharpoons \text{CsI} + \text{H}_2\text{O}$  is barrier-less. As there is an excess of Cs with respect to I, CsI is formed without any possible existence of gaseous iodine.

If Mo is added to the Cs-I system, the reactivity completely changes because Mo has a high chemical affinity with Cs and forms some cesium molybdates [15] ( $\text{Cs}_x\text{MoO}_y$  compounds) but in practice  $\text{Cs}_2\text{MoO}_4$  is the most stable gaseous molybdates. For a steam atmosphere, up to 80% of gaseous iodine is transported in a thermal gradient tube with an outlet temperature of  $150^\circ\text{C}$  with a low fraction under aerosol form. The gaseous iodine flow is mainly composed of molecular iodine ( $\sim 2/3$ ); the remaining iodine fraction can be reasonably attributed to HI or HOI. The Mo aerosol forms are  $\text{Cs}_x\text{MoO}_y$  and  $\text{MoO}_3$ . In hydrogen atmosphere,  $\text{Cs}_x\text{MoO}_y$  cannot be formed and the results obtained regarding the iodine speciation are similar to those without Mo, i.e. the formation of CsI aerosols dominates.

If Boron is added to the Cs-I system, with steam, gaseous iodine is promoted but in a lower extent than for the Mo case, due to the formation of  $\text{CsBO}_2$ .

For control rod material, Ag and Cd are expected to be reactive with respect to iodine and to prevent the formation of gaseous iodine along the RCS. An IRSN experimental program is ongoing to check this. A preliminary result obtained with the Cd-Cs-I-Mo- $\text{H}_2\text{O}$  gaseous system seems to be a bit surprising as the amount of  $\text{CdI}_2$  formed is lower than expected.

From a qualitative point of view, the trends are summarized in Table 4.

**Table 4: influence of elements on iodine speciation at the RCS cold-leg break**

System	Oxidant gaseous conditions	Reducing gaseous conditions
Iodine	Not in equilibrium	Tend to equilibrium
Iodine + cesium	Tend to equilibrium, CsI formation	
Iodine + cesium + boron [13, 37]	Not in equilibrium for $\text{BCsO}_2$ formation	
	$\text{CsI} + \text{I}_2$ formation	CsI formation
Iodine + cesium + Mo [15]	Tend to equilibrium for $\text{Cs}_2\text{MoO}_4$ formation	
	$\text{I}_2 + \text{HI}$ formation	CsI formation
Iodine + cesium + Mo + Cd	$\text{CdI}_2$ not in equilibrium, to be confirmed by additional tests	

From a modelling point of view, these data have led us to implement a kinetic I-O-H scheme in ASTEC and also complete/review the thermodynamic database (for example,  $\text{CdMoO}_4$  was missing whereas it has been experimentally observed).

Another point is the possible release of gaseous iodine resulting from remobilization of some metallic iodides deposits onto RCS walls that can lead to gaseous delayed releases inside the containment. Analytical tests performed in the frame of the French MIRE project [38] will be performed in a near future to check and quantify this phenomenon.

At the end of 2017, the improvements expected are to:

- get a good understanding and modelling of the influence of the control rod materials onto the iodine transport;
- better model possible revaporization from metal iodides deposited along the RCS.

### III. IODINE CHEMISTRY IN THE CONTAINMENT

#### III.1. Iodine interaction with paint

The equilibrium between iodine adsorption and radiolytic release by Epoxy type paint (commonly used in most of the reactors) has been identified as a main phenomenon contributing to iodine volatility. Some studies have been performed with immersed and dry paints in the 1990'. For the gaseous phase, different experimental conditions have been studied by separate teams and have led to a significant scattering of the data. The uncertainties on the optimized kinetics constants are thus important [39, 40] and this has been an obstacle to the development of a relevant model that would fit more accurately the whole set of data. EPICUR irradiation facility has been set up in 2004 to provide the possibility to measure on-line gaseous organic and inorganic iodine species at the same time after being desorbed from paints under irradiation. Some tests were conducted within the ISTP [5] and STEM [8] projects with the objective to evaluate the release rate of organic and inorganic iodine from Epoxy paint under irradiation and for different conditions (temperature, dose rate, dose, humidity and iodine loading on the paint). The whole set of data has led to the development of a new iodine-paint model [41] in ASTEC. It was applied to different test cases and especially to PHEBUS FPT-3 test for which more than 90% of the

iodine entered in the containment under a gaseous inorganic form (and representing 386 mg) [4] whereas iodine multi-component aerosols mass settling on dry containment surfaces is not significant (4 mg). Under irradiation, it has been shown in the OECD-STEM program [8, 25] that CsI aerosols are not stable under irradiation and lead to the production of volatile iodine. The fate of deposited multi-components iodine aerosols in PHEBUS is not well known and a significant uncertainty exists on their influence on iodine volatility for FPT-0/1/2 tests as their deposited mass is more important than in FPT-3. FPT-3 test is thus an interesting test to identify to what extent the new iodine-paint interaction model modifies our understanding of iodine volatility as the decomposition of deposited multi-component iodine aerosols coming from the RCS is not expected to have a significant influence.

To perform this calculation, the dose rate (DR) has been estimated all along the test with the activities detected by the gamma-counters in the gaseous phase and in the sump.

A stand-alone calculation was then performed with the ASTEC/IODE module. Fig. 23 and Fig. 24 show the comparison between the gaseous inorganic and organic iodine data with the ASTEC modeling.

The initial inorganic iodine concentration peak is well modelled with the injection of 386 mg of I<sub>2</sub> from the circuit. Its evolution in the long term is underestimated up to one order of magnitude even if the tendency is well caught. The initial organic iodine peak is quite well reproduced with the new iodine-paint interaction model until the end of the aerosol phase (~ 35.000 sec) whereas the long term concentration is also underestimated by one to two orders of magnitudes.

As significant discrepancies appear after the aerosol phase for both volatile species, it was checked if the uncertainties on the DR estimation and the experimental data could explain those discrepancies. The uncertainty on the DR is estimated to be close to a factor 2. Setting up a higher (x 2) or lower DR (x 0.5) does not change

the conclusions as both calculated iodine concentrations remain significantly outside the experimental uncertainty margins that are estimated to be close to ± 30-50 % for inorganic iodine and ± 40-100 % for organic iodide (the calculation of these uncertainties is not detailed in this paper). It means that other phenomena govern iodine volatility in the long term.

Two phenomena have been identified as eventually contributing to iodine volatility in PHEBUS tests:

- Iodine aerosols radiolytic decomposition: iodine aerosol (IO<sub>x</sub> and multi-components aerosols) might be partly unstable under irradiation and might contribute to re-volatilize gaseous I<sub>2</sub>.
- The radiolytic conversion of I<sub>2</sub> into CH<sub>3</sub>I: this reaction was reported to happen as volatile organics (CH<sub>3</sub>R compounds type) create °CH<sub>3</sub> radicals under irradiation that quickly reacts with gaseous O<sub>2</sub> and I<sub>2</sub>.

Both phenomena are explained in more details in the next two sections. Their influence on iodine volatility has also been checked.

### III.2. Iodine oxides formation and radiolytic decomposition

Considering the formation of iodine oxides compounds (IO<sub>x</sub>) gained in importance within the past decade. Air radiolysis leads to the formation of air radiolytic products (ARP) like NO<sub>2</sub>, O<sub>3</sub> or HNO<sub>3</sub> [6] that can oxidize iodine and lead to IO<sub>x</sub> particles that sediment onto surfaces [7, 22]. From PARIS tests [6, 7], a radiolytic model of IO<sub>x</sub> formation-destruction was set up in ASTEC (I).



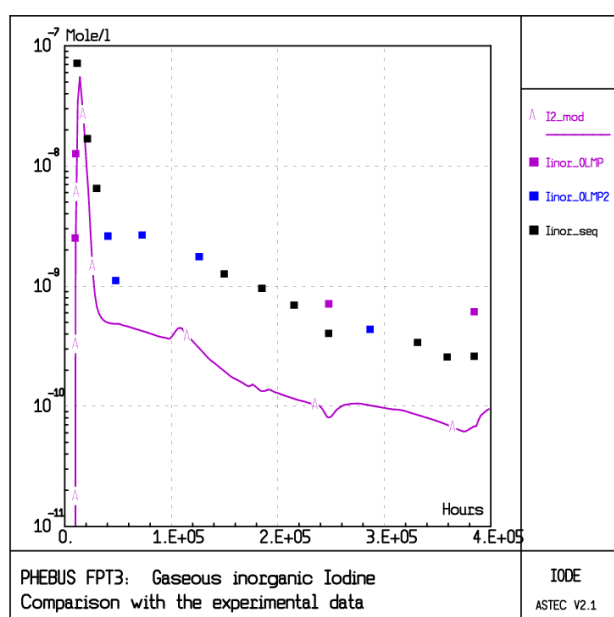


**Fig. 23. Gaseous inorganic iodine concentration in FPT3 containment with the new iodine-paint model**

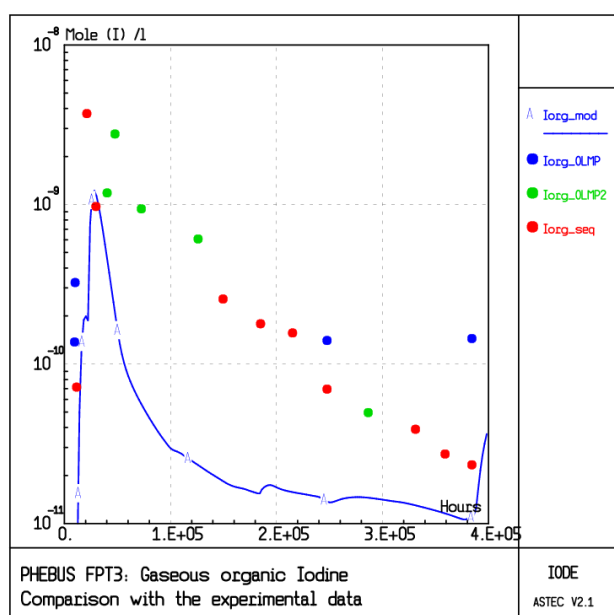


**Fig. 24. Gaseous organic iodide concentration in FPT3 containment with the new iodine-paint model**

More studies have been launched since and were summarized recently [12, 42, 43] in order to better understand IOx composition and behaviour under irradiation and thermal conditions. IOx are small aerosol particles ( $< 1 \mu\text{m}$ ), whose composition is not well known as several

anhydrous forms were detected like  $\text{I}_2\text{O}_5$ ,  $\text{I}_4\text{O}_9$  or hydrated forms like  $\text{I}_2\text{O}_5 \cdot \text{HIO}_3$  (or  $\text{HI}_3\text{O}_8$ ) that might lead to the formation of  $\text{HIO}_3$  at high humidity [44].

More studies are still being conducted to get a better estimation of their size, composition and behaviour under different conditions within the objective to better consider their behaviour in the severe accident codes. The main recent progress that has been implemented in ASTEC V2.1 is to consider IOx as aerosols (possibly agglomerating with other kind of aerosols) as they used to be considered as a volatile species before. This leads to the possibility of interaction and condensation with other aerosols, especially in the short term of an accident when they settle down.

A more complete understanding of their radiolytic and thermal stability once deposited on the containment dry surfaces is also needed as i/ OECD-STEM project results [8] have shown that IOx partly decompose under irradiation and ii/ VTT has shown that volatile iodine is released from IOx uptake of water from humid air and heat [43]. This is planned to be further addressed in the OECD STEM2 project [45].

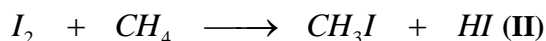
Another uncertainty that remains about IOx is their filtration efficiency by filtered containment venting system (FCVS) as their size was found to be under  $1 \mu\text{m}$  [42]. Some studies are being performed within PASSAM project [46] to evaluate the sand filters IOx trapping efficiency installed on French PWRs as well as their radiolytic stability in the sand filter (radioactive aerosols trapped in the sand filter would deliver a significant local irradiation field that might lead to IOx and iodine aerosols decomposition into volatile iodine, which would increase the iodine Source Term).

Finally, the Fukushima accident has highlighted some modifications of iodine speciation (gas - particle) in the environment during its transport in the atmosphere. The influence of photolysis, atmospheric conditions and the presence of pollutants are suspected to play a significant influence on iodine speciation. Some work is being performed at IRSN to quantify those

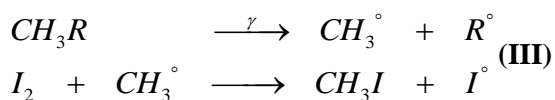
atmospheric modifications that are crucial for the iodine ST estimation [47].

### III.3. Radiolytic gaseous conversion of I<sub>2</sub> into CH<sub>3</sub>I

The reaction between methane (CH<sub>4</sub>) (and more generally volatile organics CH<sub>3</sub>R) and I<sub>2</sub> (II) has been discussed several times and the knowledge on this reaction has been summarized several times [40, 48, 49]:



CH<sub>3</sub>R concentration is at least that of methane in the atmosphere (3.10<sup>-8</sup> mol.L<sup>-1</sup>) and could reach 1.10<sup>-6</sup> mol.L<sup>-1</sup> [48]. However, no relevant model has ever been published. It is known that the forward thermal reaction is not likely at representative containment temperature (T < 200 °C) as it would start to be significant for T > ~ 400 °C. At representative containment temperatures, the radiolytic reaction would take place instead with the following mechanism (III) [40, 48, 49]:



I° radical formed would then contribute to the formation of gaseous iodine oxides. Most of the experiments performed in this area have led to a result expressed in terms of conversion percentage so that no kinetics data were ever published before Bartonicek [50] obtained some data in representative conditions. From these data, a model was set up (Eq. 1) that was assumed to follow an order one on each reactant and recently implemented in the ASTEC V2.1 code.

$$\frac{d[CH_3I]}{dt} = k \cdot DR \cdot [CH_3R] \cdot [I_2] \quad \text{(Eq. 1)}$$

DR: dose rate (Gy.s<sup>-1</sup>)

k: radiolytic reaction kinetics (L.Mol<sup>-1</sup>.Gy<sup>-1</sup>)

Nevertheless, this model needs to be completed as the temperature, humidity, dose, dose rate and reactants concentration might influence the reaction kinetics. Their effect have thus to be checked and quantified. This is planned to be addressed in the OECD BIP3 project [51].

### III.4. Influence of IOx decomposition and CH<sub>3</sub>R reaction with I<sub>2</sub> under irradiation on the modeling

A simple model of radiolytic decomposition of IOx deposited on dry surfaces has been set up to check how IOx decomposition into I<sub>2</sub> could influence iodine volatility in PHEBUS FPT-3 test. Fig. 25 and Fig. 26 show how the containment iodine volatility modeling is modified for PHEBUS FPT-3 when we consider these 2 reactions (developed in section III.2. and III.3.). It leads to a better estimation of inorganic and organic iodine for FPT-3. The agreement is better for both species, with some remaining discrepancies that cannot be explained by the uncertainty on the multi-components iodine aerosols radiolytic stability as their mass is not significant. A possible explanation resides in the degradation of IOx by carbon monoxide (CO) that is produced in significant amount by FPT-3 fuel bundle degradation (containing B<sub>4</sub>C control rod), further detailed in section IV.2.

However, for FPT-0, FPT-1 and FPT-2, the inorganic iodine is still underestimated after the aerosol phase by one order of magnitude when we consider these 2 phenomena. In these tests, IOx aerosols are one type of iodine aerosols being formed in the containment. They co-exist with multi-component iodine aerosols that come from the circuit, enter in the containment, agglomerate and settle down in the dry surface and the sump. Their composition is more complex as they involve different fission products and structure materials [1-3]. As CsI aerosols were found to be unstable under irradiation in OECD-STEM project [25], an estimation of the radiolytic decomposition kinetics of these multi-component aerosols was made. It could range between one to two orders of magnitude lower than IOx decomposition kinetics to model accurately the inorganic iodine concentrations. Consequently, these deposited multi-component aerosols could be the main

source of inorganic iodine in the long term. For organic iodides,  $\text{CH}_3\text{I}$  concentrations could mostly depend on  $\text{I}_2$  concentration via reactions of mechanism (III) that might be the main source of organic iodides whereas, in the short term, paint would contribute more.

As the main gaseous iodine source in the long term could take its origin in the multi-component aerosols decomposition, the determination of their radiolytic decomposition kinetics is of crucial importance in order to complete the modeling in ASTEC also for iodine Source Term estimation.

Other reactions have been updated or developed in ASTEC V2.1 recently. They are detailed in the next two sections.

### III.5. $\text{I}_2$ interaction with steel

Until recently,  $\text{I}_2$ -steel interaction model has been treated in a simple way with a physical adsorption and desorption reaction [52]. However, some updates on the mechanisms have been published, highlighting the fact that some iodine is definitively trapped on the steel under an oxidized form (IV) [53].



It considers two reversible steps leading to the adsorption of iodine under  $\text{I}_2$  and  $\text{FeI}_2$  forms. Then, an irreversible step leads to the chemical trapping of an oxidized species ( $\text{FeI}_2\text{O}$ ).

The kinetics model has thus been recently updated in ASTEC, based on GRS work [54] and is now available in the ASTEC V2.1 version which will better model iodine interaction with steel surfaces. It does not change our interpretation and understanding of iodine volatility in PHEBUS test as paint surfaces play a more important role on iodine volatility than steel.

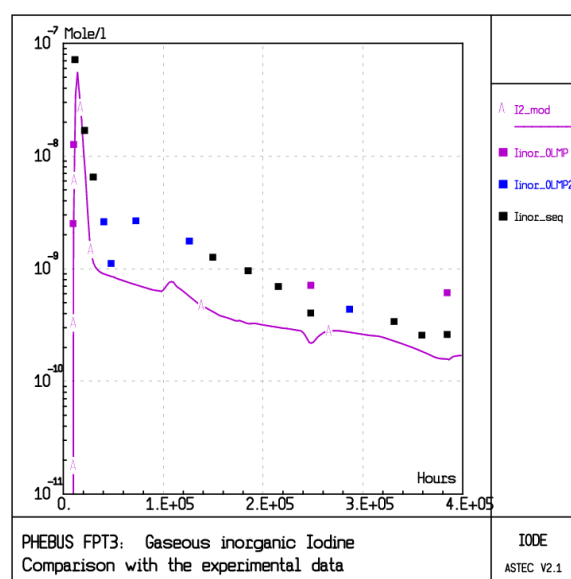


**Fig. 25. Gaseous inorganic iodine concentration in FPT3 containment considering IOx radiolytic decomposition and  $\text{I}_2$  radiolytic conversion into  $\text{CH}_3\text{I}$**

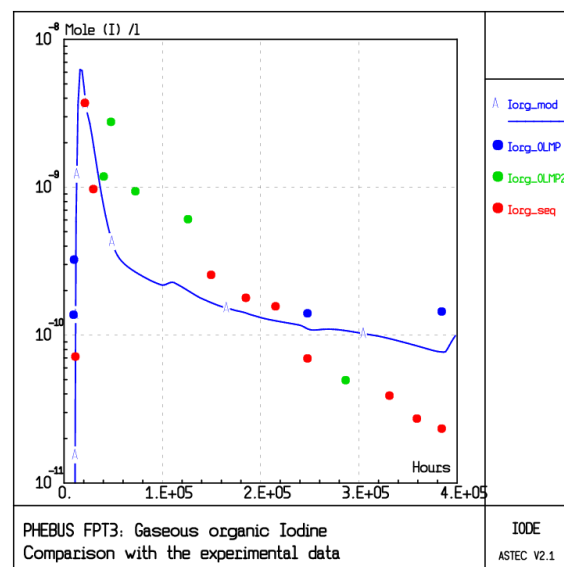
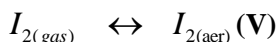


**Fig. 26. Gaseous organic iodide concentration in FPT3 containment considering IOx radiolytic decomposition and  $\text{I}_2$  radiolytic conversion into  $\text{CH}_3\text{I}$**

### III.6. I<sub>2</sub> adsorption on aerosols

Recently, THAI 2 tests were performed (as part of the OECD-THAI 2 program) with silver aerosols (considered to be one of the most reactive aerosols towards I<sub>2</sub>) and tin oxide (SnO<sub>2</sub>) (expected to be chemically inert). They have shown that I<sub>2</sub> adsorbs faster on silver (by chemisorption) than on tin oxide aerosols (by physisorption) [10] in suspension. During the short term of a severe accident, aerosols sediment and might contribute to lower I<sub>2</sub> volatility if I<sub>2</sub> adsorption on aerosols competes significantly with others gaseous phenomena like iodine adsorption on paint or IO<sub>x</sub> formation. In order to evaluate how important this could be for iodine volatility (especially in the short term) a simple model (V) of I<sub>2</sub> adsorption-desorption on aerosols has been developed in the ASTEC V2.1 version.



It will help evaluating if this phenomenon might affect iodine volatility in the short term when aerosols settle down and if we need to get more experimental data in this field. Preliminary evaluations performed for the most probable accident sequences have shown that iodine adsorption on aerosols do not affect significantly iodine ST. Nevertheless, uncertainties remain about the iodine adsorption kinetics on representative multi-component aerosols that has not yet been studied due to experimental limitations in producing such kind of multi-component aerosols.

The next section deals with containment phenomena that have been identified as eventually having a significant influence on iodine volatility but whose quantification need to be completed.

IV. Other containment phenomena whose influence on iodine volatility needs to be quantified

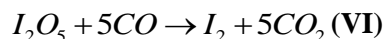
#### IV.1. Paint ageing

Most of power plants are now between 20 and 40 years old and materials ageing raises some

questions, in particular for their influence on iodine volatility. For paints, natural ageing in normal operating conditions as well as their ageing during the accident (under irradiation, high temperature and humidity) might influence iodine adsorption and/or release kinetics so that iodine volatility could be modified. Aleksandrov [55] has shown that pre-irradiating an Epoxy paint between 0.1 kGy and 1 MGy before adsorbing iodine leads to an I<sub>2</sub> adsorption kinetics that is decreased by one order of magnitude. Glowa has found the same tendency for iodine adsorption on pre-irradiated coupons at ~1 Gy.s<sup>-1</sup> for 160h [11] and that this pre-irradiation phase favors CH<sub>3</sub>I release kinetics under irradiation [12]. In case of a severe accident, the cumulated dose absorbed by the paint is expected to reach 1 to 10 MGy (the upper value being the dose recommended by three standards [56-59] in such a case). This raises the question about how paint ageing (in normal operating conditions followed by irradiating conditions) might influence iodine volatility and Source Term. In the forthcoming OECD STEM2-BIP3 program [45, 51], some tests are planned in this field to complete our understanding and eventually adapt our models in the ASTEC code.

#### IV.2. Iodine oxides decomposition by carbon monoxide (CO)

Various authors have reported iodine pentoxide (I<sub>2</sub>O<sub>5</sub>) decomposition by carbon monoxide [60, 61] as being complete at ambient temperature (VI).



Other organic compounds (like benzene, propane, butane...) also react with iodine pentoxide. Nevertheless, the reaction with CO might play a significant influence on iodine volatility as carbon monoxide might be formed in significant amount in the containment by:

- the B<sub>4</sub>C control rods or plates (present in numerous NPPs) degradation in the bundle (like in FPT3 for which the CO concentration in the containment could have reached 6.10<sup>-5</sup> mol.L<sup>-1</sup> i.e. at least 3 orders of

- magnitude over the iodine volatile concentration)
- the molten corium-concrete interactions in the containment.

It is not clear whether the iodine oxides formed inside the containment are pure  $I_2O_5$  or a mix between hydrated forms and non-hydrated forms (as mentioned in section III.2) and if those hydrated forms would also react with CO. CO might also be converted to  $CO_2$  under irradiation so that its concentration would decrease along the transient. The influence of this reaction on iodine volatility has thus to be estimated.

## V. CONCLUSION

Within the past 10 years, significant progresses have been made in the modeling of iodine volatility in the RCS and the gaseous phase in the containment.

In the RCS, chemical understanding of iodine transport has been improved with PHEBUS-FP tests as well as ISTP CHIP tests. The iodine phenomenology in the RCS appears to be much more complex than expected two decades ago with the simple “CsI” assumption i.e iodine being transported as CsI aerosols in the RCS. A mechanistic modeling is needed to take into account the large range of conditions that can be encountered in various scenario of severe accident.

The first improvements were made considering kinetics of the “iodine system” and in extending/refining the thermodynamic database in ASTEC with new element. Some complementary models have to be developed to cover the influence of structure materials and other fission products. The possible remobilizations of FP deposits have also to be modeled, considering chemical transformation onto RCS surfaces.

In the containment, significant progresses have been made as the modeling of five phenomena has been recently updated or added in ASTEC code. They are listed below:

- A new model of iodine ( $I_2$  and  $CH_3I$ ) interaction with paint under irradiation has been set up

- A model of iodine oxides aerosols formation and radiolytic decomposition has been developed
- A preliminary model of gaseous conversion of  $I_2$  into  $CH_3I$  through volatile organic compounds has been created
- The model of  $I_2$  interaction with steel has been refined
- The adsorption of  $I_2$  on aerosols has been modelled

They have helped in the research of the remaining uncertainties in iodine volatility estimation and iodine ST estimations. Those uncertainties are listed below:

- Paint ageing: their ageing in normal operation and/or during the course of an accident (with beta and gamma rays) could change the paint capacity to trap iodine which could lead to a higher iodine volatility
- Iodine oxides radiolytic decomposition: more parameters need to be investigated to consider their influence in the modeling (temperature, humidity, presence of CO etc)
- More generally, the radiolytic oxidation of multi-component iodine aerosols, or at least others metallic iodide aerosols than CsI, need to be checked to evaluate how much volatile iodine could be released under irradiation from deposited iodine aerosols on dry surfaces. Iodine adsorption on those aerosols is also of interest
- The gaseous radiolytic conversion of  $I_2$  into  $CH_3I$  through volatile organic components has been highlighted and need to be completed with the influence of more parameters like the humidity, dose rate, dose and temperature
- Filtered containment venting system (FCVS) efficiency: it is currently being studied in the European PASSAM project [46] and French MIRE program [37] with the objectives to estimate their efficiency under irradiation and better evaluate the iodine and ruthenium gaseous Source Term
- In-containment delayed releases: iodine remobilization can come from boiling sump or thermal and mechanical loading effects resulting from transient phenomena on FP deposited onto inner walls (such as  $H_2$  combustion, thermal radiation from passive autolytic recombiners and large steam

- production during corium flooding (in and ex-vessel)). Their influence has to be checked
- The modification of the iodine speciation in the environment that has been highlighted by the Fukushima accident. Iodine transport and its reactivity in the atmosphere under the photolysis and atmospheric conditions with presence of pollutants [47] is being currently studied in order to better evaluate its speciation in the environment.

Those phenomena are listed in **Table 5** with the objectives to orientate the research programs in this field, fill in the remaining gaps by setting up/refining relevant models and gain confidence in ST computations.

#### ACKNOWLEDGMENTS

Authors acknowledge the partners of the PHEBUS-FP, ISTEP, NUGENIA-SARNET, OECD-THAI and THAI2, OECD-BIP and BIP2 and OECD-STEM programs whose results have largely contributed to increase our understanding and develop relevant models of iodine behaviour in the RCS and containment.

#### NOMENCLATURE

ASTEC: Accident Source Term Evaluation Code

BIP: Behaviour of Iodine Project

CHIP: Iodine Chemistry in the Primary cooling system

FCVS: Filtered Containment Venting System

FP: fission Product

ISTEP: International Source Term Project

MIRE : MITigation des Rejets à l'Environnement

OECD : Organization for Economic Co-operation and Development

PARIS: Program on Air Radiolytic, Iodine adsorption on Surfaces

PASSAM: Passive and Active Systems on Severe Accident source term Mitigation

PWR: Pressurized Water Reactor

RCS: Reactor Coolant System

ST: Source Term

STEM: Source Term Evaluation and Mitigation

THAI: Thermal-hydraulics, hydrogen, Aerosols and Iodine

#### **Table 5: Phenomena whose influence on iodine ST needs to be completed**

Phenomena	Justification	Project name
<b>In RCS</b>		
Iodine transport in the RCS	Progress with CHIP – more data expected on the influence of Ag, In and Cd	IRSN project
Delayed FP releases from RCS deposits	Scarce data	MIRE [38]
<b>In containment</b>		
Paint ageing	Literature review + BIP-BIP2 data	OECD STEM2-BIP3 [45, 51]
Iodine oxides decomposition $IOx \xrightarrow{\gamma} I_2$	STEM & BIP2 data	
Radiolytic decomposition of iodine multi-component aerosols $I_{aer} \xrightarrow{\gamma} I_2$	STEM data	
Gaseous homogeneous $CH_3I$ radiolytic production $0.5I_2 + CH_3R \xrightarrow{\gamma} CH_3I$	Literature review & STEM data	
Effect of CO on IOx decomposition $IOx + CO \longrightarrow 0.5I_2$	Literature review	
FCVS efficiency	Literature review + Fukushima accident have reinforced the need for consolidating existing systems	
Iodine remobilization from boiling sump	Need to study the influence of hydrodynamics coupled with chemistry	Partly addressed in OECD-THAI3
Iodine remobilization from dynamic loadings on walls	Influence of thermal and mechanical loadings on iodine revolatilization	Partly addressed in OECD-THAI3
<b>In atmosphere (outside the containment)</b>		
Iodine reactivity in the environment	Modification of the iodine speciation in the atmosphere after Fukushima accident	IRSN project [47]

## REFERENCES

- [1]. N. Hanniet and G. Repetto, "FPT-0 final report", *CEA/IPSN/DRS/SEA/PEPF - Report PHEBUS PHPF IP/99/423*, (1999).
- [2]. D. Jacquemain, S. Bourdon, *and al.*, "FPT-1 final report", *CEA/IPSN/DRS/SEA/PEPF - rapport SEA 1/100 - Report PHEBUS FP IP/00/479*, (2000).
- [3]. A. C. Gregoire, P. March, *and al.*, "FPT-2 final report", *IRSN/DPAM/DIR 2008 - 272 - Report PHEBUS-FP IP/08/579*, (2008).
- [4]. F. Payot, T. Haste, *and al.*, "FPT-3 final report", *DPAM/DIR-2010-148 - PF IP/10/587*, (2010).
- [5]. B. Clement and R. Zeyen, "The Phebus Fission Product and Source Term International Programmes", *Nuclear Energy for New Europe, Bled, Slovenia, September 5-8*, (2005).
- [6]. L. Bosland, F. Funke, *and al.*, "PARIS project: Radiolytic oxidation of molecular iodine in containment during a nuclear reactor severe accident. Part 1. Formation and destruction of air radiolysis products- Experimental results and modelling", *Nucl. Eng. Des.*, 238, (12), p. 3542-3550, (2008).
- [7]. L. Bosland, F. Funke, *and al.*, "PARIS project: Radiolytic oxidation of molecular iodine in containment during a nuclear reactor severe accident: Part 2: Formation and destruction of iodine oxides compounds under irradiation – experimental results modelling", *Nucl. Eng. Des.*, 241, (9), p. 4026-4044, (2011).
- [8]. B. Clement and B. Simondi-Teisseire, "STEM: An IRSN project on source term evaluation and mitigation", *Transactions of the American Nuclear Society - 2010 ANS Annual Meeting; Las Vegas, NV, U.S.; November 7-11th*, 103, 475-476, (2010).

- [9]. F. Funke, G. Langrock, *and al.*, "Iodine oxides in large-scale THAI tests", *Nucl. Eng. & Des.*, 245, p. 206-222, (2012).
- [10]. F. Funke, S. Gupta, *and al.*, "Interaction of gaseous I<sub>2</sub> with painted surfaces and aerosols in large-scale THAI tests", *Proc. of the Int. OECD-NEA/NUGENIA-SARNET Workshop on the Prog. in Iodine Behaviour for NPP Acc. Anal. and Manag. - March 30, April 1 - Marseille (France)*, (2015).
- [11]. G. Glowa, C. J. Moore, *and al.*, "The main outcomes of the OECD Behaviour of Iodine (BIP) Project", *Annals of Nuclear Energy*, 61, p. 179-189, (2013).
- [12]. G. Glowa, C. J. Moore, *and al.*, "The main outcomes of the OECD Behaviour of Iodine Project", *Proc. of the Int. OECD-NEA/NUGENIA-SARNET Workshop on the Prog. in Iodine Behaviour for NPP Acc. Anal. and Manag. - March 30, April 1 - Marseille (France)*, (2015).
- [13]. A. C. Gregoire and H. Mutelle, "Experimental Study of the [B, CS, I, O, H] and [MO, CS, I, O, H] Systems in the Primary Circuit of a Pwr in Conditions Representative of a Severe Accident", *21th International Conference Nuclear Energy for New Europe, Ljubljana, Slovenia, September 5-7*, (2012).
- [14]. M. Gouello, H. Mutelle, *and al.*, "Analysis of the iodine gas phase produced by interaction of CsI and MoO<sub>3</sub> vapours in flowing steam", *Nucl. Eng. & Des.*, 263, p. 462-472, (2013).
- [15]. A. C. Gregoire, J. Kalilainen, *and al.*, "Studies on the role of molybdenum on iodine transport in the RCS in nuclear severe accident conditions", *Annals of Nuclear Energy*, 78, p. 117-129, (2015).
- [16]. S. Guilbert, L. Bosland, *and al.*, "Formation of organic iodide in the containment in case of a severe accident", *Transactions of the American Nuclear Society, Annual Meeting, June, 08 - 12 Anaheim, United States*, 98, 291-292, (2008).
- [17]. J. Colombani, "Experimental study of organic iodide volatilization from painted surfaces present in the containment during a severe accident", *ERMSAR 2013, Avignon, October 2-4*, (2013).
- [18]. B. Clement, L. Cantrel, *and al.*, "State of the art report on iodine chemistry", *OECD-NEA-CSNI-R(2007)1*, (2007).
- [19]. L. Cantrel, S. Guilbert, *and al.*, "Radiolytic oxidation of iodide in the containment : current status", *Session 5, ERMSAR 2005, Aix-en-Provence*, (2005).
- [20]. A. Auvinen, L. Bosland, *and al.*, "Iodine-paint interaction", *6th European Review Meeting on Severe Accident Research (ERMSAR), Avignon (France), October 02-04*, (2013).
- [21]. L. Bosland, S. Dickinson, *and al.*, "Iodine-Paint Interactions during Nuclear Reactor Severe Accidents", *Annals of Nuclear Energy*, 74, p. 184-199, (2014).
- [22]. F. Funke, P. Zeh, *and al.*, "Radiolytic oxidation of molecular iodine in the containment atmosphere", *OECD Workshop on Iodine Aspects of Severe Accident Management, Vantaa, Finland, May 18-20*, 79-89, (1999).
- [23]. S. Zhang, R. Strekowski, *and al.*, "Formation of iodine oxide particles from the photooxidation of CH<sub>3</sub>I in the presence of O<sub>3</sub> and humidity under the conditions of a major nuclear power plant accident", *Poster, 22nd International Symposium on Gas Kinetics, June 17th-22th, Boulder, CO, USA*, (2012).
- [24]. A. Auvinen, Y. Ammar, *and al.*, "Experimental and modelling studies of iodine oxide formation and aerosol behaviour relevant to nuclear reactor accidents", *6th European Review Meeting*

- on Severe Accident Research (ERMSAR), Avignon (France), October 02-04, (2013).
- [25]. J. Colombani, "Main Outcomes of the IRSN Experimental Programs Performed on Iodine Chemistry in Severe Accident Conditions", *Proc. of the Int. OECD-NEA/NUGENIA-SARNET Workshop on the Prog. in Iodine Behaviour for NPP Acc. Anal. and Manag. - March 30, April 1 - Marseille (France)*, (2015).
- [26]. G. Weber, L. Bosland, *and al.*, "ASTEC, COCOSYS, and LIRIC Interpretation of the Iodine Behavior in the Large-Scale THAI Test Iod-9", *Journal of Engineering for Gas Turbines and Power*, 132, (11), p. (2010).
- [27]. G. Weber, L. Herranz, *and al.*, "SARNET2 WP8 benchmark on THAI multi-compartment iodine tests - Results for test Iod-11", *ERMSAR 2012, Cologne, Germany, March 21-23*, (2012).
- [28]. J. P. Van Dorsselaere, P. Chatelard, *and al.*, "Validation Status of the ASTEC Integral Code for Severe Accident Simulation", *Nucl. Tech.*, 170, (3), p. 397-415, (2010).
- [29]. L. Cantrel, F. Cousin, *and al.*, "ASTECV2 severe accident integral code: Fission product modelling and validation", *Nucl. Eng. & Des.*, 272, p. 195-206, (2014).
- [30]. P. Chatelard, N. Reinke, *and al.*, "ASTEC V2 severe accident integral code main features, current V2.0 modelling status, perspectives", *Nucl. Eng. & Des.*, 272, p. 119-135, (2014).
- [31]. T. Haste, F. Payot, *and al.*, "Transport and deposition in the Phébus FP circuit", *Annals of Nuclear Energy*, 61, p. 102-121, (2013).
- [32]. Y. G. Delicat, "Etude la réactivité de l'iode transporté dans un mélange H<sub>2</sub>/H<sub>2</sub>O en conditions de combustion dans des flammes basse pression pré-mélangées", *University of Lille 1 - France*, (2012).
- [33]. M. Badawi, B. Xerri, *and al.*, "Molecular structures and thermodynamic properties of 12 gaseous cesium-containing species of nuclear safety interest: Cs<sub>2</sub>, CsH, CsO, Cs<sub>2</sub>O, CsX, and Cs<sub>2</sub>X<sub>2</sub> (X = OH, Cl, Br, and I)", *J. Nucl. Mat.*, 420, p. 452-462, (2012).
- [34]. R. Vandeputte, F. Louis, *and al.*, "Thermochemistry of Cs<sub>x</sub>ByO<sub>z</sub> type of compounds", *Theory and Applications of Computational Chemistry (TACC), 2-7 Septembre 2012, Pavia (Italie)*, (2012).
- [35]. S. Canneaux, B. Xerri, *and al.*, "A theoretical study of gas-phase reactions of iodine atoms with H<sub>2</sub>, H<sub>2</sub>O, HI and OH", *J. Phys. Chem. A* 114, (34), p. 9270-9288, (2010).
- [36]. B. Xerri, S. Canneaux, *and al.*, "Ab initio calculations and iodine kinetic modeling in the reactor coolant system of a pressurized water reactor in case of severe nuclear accident", *Computational and Theoretical Chemistry*, 990, p. 194-208, (2012).
- [37]. M. Gouello, H. Mutelle, *and al.*, "Chemistry of Iodine and Aerosol Composition in the Primary Circuit of a Nuclear Power Plant", *21st International Conference - Nuclear Energy for New Europe (NENE), 5-7 September*, (2012).
- [38]. L. Cantrel, L. Herranz, *and al.*, "Overview of ongoing and planned R&D works on delayed releases and FCVS efficiencies", *ICAPP (International Congress on Advances in nuclear Power Plants) 2015 conference, May 03-06, Nice, France*, (2015).
- [39]. F. Funke, "Data analysis and modelling of organic iodide production at painted surfaces", *OECD Workshop on Iodine Aspects of Severe Accident Management, Vantaa, Finland, May 18-20*, 151-168, (1999).
- [40]. S. Dickinson, H. E. Sims, *and al.*, "Organic iodine chemistry", *Nucl. Eng. and Design*, 209, p. 193-200, (2001).

- [41]. L. Bosland and J. Colombani, "Study of iodine releases from Epoxy and Polyurethane paints under irradiation and development of a new model of iodine-Epoxy paint interactions for PWR severe accident applications", *To be submitted in 2015*, p. ( ).
- [42]. S. Dickinson, A. Auvinen, *and al.*, "Experimental and modelling studies of iodine oxide formation and aerosol behaviour relevant to nuclear reactor accidents", *Annals of Nuclear Energy*, 74, p. 200-207, (2014).
- [43]. S. Tietze, M. R. Foreman, *and al.*, "Adsorption and revaporisation studies of thin iodine oxide and CsI aerosol deposits from containment surface materials in LWRs", *NKS-285 - ISBN 978-87-7893-360-7*, (2013).
- [44]. B. K. Little, S. B. Emery, *and al.*, "Physicochemical characterization of Iodine(V) oxide, Part 1: hydration rates", *Propellants Explos. Pyrotech.*, p. (article in press).
- [45]. C. Mun, L. Bosland, *and al.*, "OECD-STEM Project and its Follow-up STEM2", *Proc. of the Int. OECD-NEA/NUGENIA-SARNET Workshop on the Prog. in Iodine Behaviour for NPP Acc. Anal. and Manag. - March 30, April 1 - Marseille (France)*, (2015).
- [46]. T. Albiol, "The European PASSAM Project on Atmospheric Source Term Mitigation: Half-Way Progress and Main Results", *Proc. of the Int. OECD-NEA/NUGENIA-SARNET Workshop on the Prog. in Iodine Behaviour for NPP Acc. Anal. and Manag. - March 30, April 1 - Marseille (France)*, (2015).
- [47]. J. Trincal, F. Cousin, *and al.*, "In What Extent the Iodine Reactivity in the Atmosphere Can Impact the Radiological Consequences", *Proc. of the Int. OECD-NEA/NUGENIA-SARNET Workshop on the Prog. in Iodine Behaviour for NPP Acc. Anal. and Manag. - March 30, April 1 - Marseille (France)*, (2015).
- [48]. A. M. Deane, "Organic iodide chemistry relevant to nuclear reactors: a review", *AERE-R-12359*, (1988).
- [49]. L. F. Parsly, "Chemical and Physical Properties of Methyl Iodide and its Occurrence under Reactor Accident Conditions", *ORNL-NSIC-82*, (1971).
- [50]. B. Bartonicek and A. Habersbergerova, "Formation of methyl iodide by ionizing radiation", *4th working meeting on Radiation Interaction, Leipzig*, 491-495, (1987).
- [51]. P. A. Yakabuskie, C. J. Moore, *and al.*, "The Behaviour of Iodine Project: a Proposal for BIP3", *Proc. of the Int. OECD-NEA/NUGENIA-SARNET Workshop on the Prog. in Iodine Behaviour for NPP Acc. Anal. and Manag. - March 30, April 1 - Marseille (France)*, (2015).
- [52]. L. Bosland, L. Cantrel, *and al.*, "Modelling of iodine radiochemistry in the ASTEC severe accident code: description and application to FPT-2 PHEBUS test", *Nucl. Tech.*, 171, (1), p. 88-107, (2010).
- [53]. J. C. Wren and G. A. Glowa, "Kinetics of gaseous iodine uptake onto stainless steel during iodine-assisted corrosion", *Nucl. Tech.*, 133, (1), p. 33-49, (2001).
- [54]. G. Weber and F. Funke, "Description of the iodine model AIM-3 in COCOSYS", *GRS - A - 3508*, (2009).
- [55]. A. B. Aleksandrov, N. I. Ampelogova, *and al.*, "The effect of physicochemical conditions on the absorption of molecular iodine by protective varnish and paint coatings during accidents at a nuclear power station with a VVER-640 reactor", *Therm. Eng.*, 42, (12), p. 991-996, (1995).
- [56]. Astm, "D4082-10 - Standard Test Method for Effects of Gamma Radiation on Coatings for Use in Nuclear Power Plants", (2010).

- [57]. Afnor, "Peintures pour l'industrie nucléaire: essai de tenue aux rayonnements ionisants (réacteur à eau sous pression)", *AFNOR NF T 30-903 - ISSN 0335-3931*, (1988).
- [58]. N. D. Norm, "Coating materials - Methods for testing the resistance of coatings to ionizing radiation in nuclear plants", *DIN 53781:2003-07*, (2003).
- [59]. C. D. Watson, J. C. Griess, *and al.*, "Protective coatings (paints) for PWR and BWR reactor containment facilities", *Nucl. Tech.*, 10, p. 538-545, (1971).
- [60]. C. M. Stevens and L. Krout, "Method for the determination of the concentration and of the carbon and oxygen isotopic composition of atmospheric carbon monoxide", *Int. J. Mass Spect. & Ion Phys.*, 8, p. 265-275, (1972).
- [61]. H. J. Kavanaugh, J. W. Dahlby, *and al.*, "The gravimetric determination of carbon in uranium-plutonium carbide materials", *LA-7981 - Los Alamos Scientific Laboratory*, (1980).

## HETEROGENEOUS CHEMISTRY IN REACTOR ACCIDENTS

*Michael Salay\*, Richard Lee, and Dana Powers  
U. S. Nuclear Regulatory Commission,  
Rockville, Maryland, USA*

*\*Corresponding author, tel: (+1) 301-415-2408, Fax: (+1) 301-415-6671, Email:Michael.Salay@nrc.gov*

**Abstract** – *The effects of heterogeneous chemistry on reactor accident behavior are discussed. Heterogeneous chemistry is one of the three elements of the Nuclear Regulatory Commission's approach to modeling containment chemistry. The other elements are gas-phase chemistry and liquid phase chemistry. Heterogeneous chemistry is typically not considered when predicting fission product behavior although it can influence fission product behavior and the release of fission products to the environment. Gas-solid, gas-liquid, and liquid-solid heterogeneous chemistry are reviewed with examples provided for each. These examples focus primarily on iodine interactions or phenomena that affect the prediction of iodine behavior. Particular attention is given to the influence of heterogeneous chemistry on containment modeling.*

## I. INTRODUCTION

Experiments in the Phébus-FP program have put a premium on garnering a better understanding of the chemistry of fission products in reactor containments following severe reactor accidents [Jacquemain, *et al.*, 1999]. Prior to the conduct of these experiments, the behaviors of various fission products released to the containments were treated simply. Noble gas fission products (xenon and krypton) were thought to have no significant chemistry aside from very modest solubility in water. Most other radionuclides released to containment were thought to be in the form of aerosol particles that could settle or be removed using engineered safety systems such as sprays and suppression pools. Iodine was viewed as the exceptional fission product that could be released to containment either as vapor or as aerosol particles. Mitigation of the inventory of iodine in aerosol form available for release to the environment could be done using the same engineered safety systems and natural processes as were applied to other radionuclides in aerosol form. Mitigation of iodine in vapor form focused on solvating the iodine in strongly basic solutions [Soffer, *et al.*, 1995].

The Phébus-FP experiments showed, however, that a residual, essentially steady-state, amount of iodine vapor could persist in the containment atmosphere for days despite temperatures or pH of sump waters. Much of the attentions to account for the experimental observations have focused on the heterogeneous interactions of iodine with epoxy paints on surfaces within the reactor containments. It has been known for decades that paint can absorb molecular iodine [Rosenburg *et al.*, 1969]. The salient finding of separate effects tests is that iodine absorbed by paint can desorb as either molecular iodine ( $I_2$ ) or organic iodide (nominally  $CH_3I$ ) vapor under irradiation [Guilbert, *et al.*, 2007]. Furthermore, paint can absorb molecular iodine from irradiated solutions of iodide ion. Finally, it has been observed that both molecular iodine and organic iodide vapors in the containment atmosphere can be converted to exceptionally fine particles of iodine oxide ( $IO_x$ ) during irradiation [Dickinson, *et al.*, 2014]. These results cast some doubt about regulatory schemes that envisage nominal

fractions of released iodide in the containment atmosphere as particulate material or as vapor. Clearly, experimental results show that there can be interchanges between particulate and vapor iodine. Furthermore, iodine trapping by basic solutions in containment sumps may be ineffective if iodine interacts preferentially with surfaces in the containment.

The impetus to better understand the chemistry of fission products in reactor containments following reactor accidents has grown as a result of the accidents at the Fukushima Dai-ichi sites in Japan. The recovery and decommissioning of the three damaged plants at this site are complicated by the presence of high concentrations of contaminated water in the containment. Radiation fields produced by the radionuclides in the reactor containments and the reactor buildings must be reduced substantially before major manual recovery operations can begin. Water cycling through purification systems as well as natural radioactive decay have reduced the fields, but the reduction has not been enough for recovery to begin. Indeed, it appears that there are continuing sources of contamination of the water inventories in the damaged reactors. More effective cleanup will be needed that will necessarily involve more than just the purification of water. Surface cleansing may also be required.

In support of its systems-level accident analysis model, MELCOR, the U.S. Nuclear Regulatory Commission has undertaken an effort to better understand radionuclide chemistry in reactor containments following severe reactor accidents. This effort is not restricted to understanding the chemistry of iodine, but iodine is an important focus. The effort also seeks to understand the radiological implications of the use of emergency coolants such as seawater used during the Fukushima accidents.

Chemistry of interest includes aqueous-phase chemistry, gas-phase chemistry, and heterogeneous chemistry. The aqueous-phase chemistry of iodine has been investigated for decades within the reactor safety community [Clément, *et al.*, 2007]. There now exists an understanding of aqueous-phase chemistry

adequate for the safe regulation of nuclear power plants. The gas-phase chemistry of iodine has been studied extensively over the last decade within the atmospheric sciences community [Vogt, *et al.*, 1999]. It appears that the understanding is sufficient that it can be adapted to the needs for safe regulation of commercial nuclear power plants. Heterogeneous chemistry has not received as much attention, though ever more is being learned about the heterogeneous interactions of iodine with paint [Bosland, *et al.*, 2014]. The rest of this paper identifies some pertinent aspects of heterogeneous chemistry and provides some examples that merit consideration in the design of computer models for prediction of severe reactor accident processes.

## II. HETEROGENEOUS CHEMISTRY

Heterogeneous chemistry of interest for the analysis of reactor accidents includes gas-solid interactions, gas-liquid interactions, and liquid-solid interactions. Within the general category of gas-solid interactions are processes such as vapor condensation or reactions with structural surfaces and with the surfaces of aerosol particles [Beard *et al.*, 1999]. For the most part, these processes are expected to be complete in the reactor coolant system prior to the escape of fission products to the reactor containment. Most vapor-solid interactions of fission products are, then, outside the scope of this paper. The exception is the interaction of iodine vapor with painted surfaces within containment that has been the topic of so much recent study [Bosland *et al.*, 2014]. The understanding of this interaction of iodine with paint is not complete even for engineering purposes. The topic is excluded here from further consideration only because it merits a more complete discussion other authors can give it.

The interaction of fission product vapors with liquid water is fundamental to many of the important engineered safety systems for mitigation of iodine release from reactor containments to the environment. Vapor interactions can occur with water pools, water films, and water droplets. Iodine absorption in water pools kept basic with sodium phosphate buffers has been an important, passive, safety strategy for many nuclear power plants. This

strategy has been under some debate because of precipitates formed by phosphate ions during design basis accidents that can clog screens used to protect intakes for water circulated through the reactor coolant system. Vapor-liquid interactions also arise in decontamination of bubbles sparged through steam suppression pools and in decontamination of containment atmospheres by sprays.

The interaction of iodine vapors with water surfaces is primarily an issue of mass transfer both in the aqueous phase and in the gas phase. Mass transfer considerations also affect the prediction of liquid acidification by nitric acid generated by radiolysis of the reactor containment atmosphere or by hydrochloric acid generated by radiolysis or pyrolysis of cable insulations such as chlorosulfonated polyethylene. Water acidification can affect the propensity for iodine to be retained in liquid water. In the third section of this paper, some considerations of the mass transport of solutes to and within liquid water are presented.

The interaction of contaminated liquids with solid surfaces in the reactor containment is a multi-faceted topic. Of current interest in connection with the recovery from the Fukushima accident is the leaching of fission products from reactor fuel exposed to water. Fuel may be exposed to water in the reactor coolant system or in the containment if core debris was able to penetrate the reactor vessel as is thought to be the case in Unit 1. Fuel leaching by water has been a topic of considerable interest within the community addressing the issues of radioactive waste disposal. A considerable and rather sophisticated understanding of the leaching processes has been developed within this context. It will be of considerable interest to see if this understanding of leaching for waste disposal can be adapted adequately for the purposes of reactor accident analysis and for recovery of the damaged Fukushima reactors. Leaching is not discussed further here.

Recovery from severe reactor accidents can take a rather long time. Decontamination of the damaged reactor at Three Mile Island took nearly a decade. It is anticipated that recovery of the

damaged reactors at the Fukushima site may take at least as long. The long-term exposure of the reactor coolant system and the containment boundary to contaminated water raises the issue of corrosion. Corrosion over long periods can compromise the containment boundary and the continued cooling of the damaged reactor fuel. Corrosion products can affect the operability of the system for the post-accident cooling of core debris by both obstructing the flow of coolant or by coating heat transfer surfaces. The corrosion products may augment the load of solid contaminants in coolant waters brought on by other heterogeneous chemical processes in the containment including the corrosion and leaching of concrete.

Corrosion *per se* is not discussed here. What is of interest is the adsorption of dissolved fission products on corrosion products. To be sure, contaminated corrosion products and other precipitates in water may have to be removed prior to major decontamination of the Fukushima reactors. Removal of these corrosion products and precipitates may be challenging relative to the removal or purification of containment waters. Indeed, contamination of the precipitates may well frustrate and delay efforts to purify containment water. It is, then, useful to have some appreciation of the radionuclide contamination of suspended and deposited solids in the containment. Some aspects of this issue are discussed further in later sections of this paper.

### III. GAS-LIQUID MASS TRANSFER

Consider a fission product vapor with water solubility characterized by Henry's Law:

$$P_{int} = Hc_{int}$$

where:

$$P_{int} = \text{interfacial partial pressure of the soluble vapor (bar)}$$

$$c_{int} = \text{interfacial concentration of solute (moles/m}^3\text{)}$$

$$H = \text{Henry's law 'constant' (bar - m}^3\text{/mole)}$$

The mass flux of vapor to the interface,  $N_{gas}$ , is given by:

$$N_{gas} = \frac{k_g}{RT} [P_{bulk} - P_{int}]$$

where:

$$k_g = \text{gas phase mass transfer coefficient (m/s)}$$

$$= D_g / \delta_g$$

$$D_g = \text{gas phase diffusion coefficient (m}^2\text{/s)}$$

$$\delta_g = \text{gas phase film thickness (m)}$$

$$R = \text{gas constant (8.3144621x10}^{-5}\text{ bar - m}^3\text{/K)}$$

$$T = \text{absolute temperature (K)}$$

$$P_{bulk} = \text{partial pressure of the soluble vapor in the bulk gas phase (bar)}$$

$$N_g = \text{vapor flux (moles/m}^2\text{ - s)}$$

The mass flux of solute away from the interface into the bulk aqueous phase,  $N_{liq}$ , is given by:

$$N_{liq} = k_{liq} [c_{int} - c_o]$$

where:

$$k_{liq} = \text{liquid - phase mass transport coefficient (m/s)}$$

$$= D_{liq} / \delta_{liq}$$

$$D_{liq} = \text{liquid phase diffusion coefficient (m}^2\text{/s)}$$

$$\delta_{liq} = \text{liquid phase film thickness (m)}$$

$$c_o = \text{concentration of solute in the bulk liquid phase (moles/m}^3\text{)}$$

$$N_{liq} = \text{solute flux in liquid phase (moles/m}^2\text{ - s)}$$

Within the reactor safety community, it has been common to solve this mass transport problem using the so-called "two film" model [Weber, *et al.*, 1992]. A quasi-steady state is assumed. Fluxes to the gas-liquid interface and away from the interface are equated and:

$$N_{gas} = N_{liq} = N = \frac{P_{bulk} - P_o}{\left[ \frac{RT}{k_m} + \frac{H}{k_{liq}} \right]}$$

where  $P_o = Hc_o$ . Introduced in 1924 by Lewis and Whitman [1924] and re-derived many times, the two-film model has typically adequate

flexibility to account for observations in particular experiments. It has been abandoned, however, by the chemical engineering community because it has been found that results derived from experiments of one type do not transfer accurately to other circumstances. Instead, the surface-renewal model of Higbie [1935] where:

$$N_{liq} = 2 [c_{int} - c_o] \sqrt{\frac{D_{liq}}{\pi t_e}} = k_{liq} [c_{int} - c_o]$$

$t_e = \text{time of surface renewal (s)}$

or Dankwerts' [1951] penetration model where:

$$N_{liq} = [c_{int} - c_o] \sqrt{D_{liq} s} = k_{liq} [c_{int} - c_o]$$

$s = \text{parameter for probability density of surface renewal (s}^{-1}\text{)}$

have been adopted. More complicated models with additional parameterization exist [See for example Seo and Lee, 1988]. These modeling differences are significant especially when a simulant is used in place of iodine vapor for parameterization of the model. This is especially true when correlations are used to derive mass transport coefficients based on a gas other than the fission product vapor of interest.

The chemical engineering and oceanographic communities have been developing correlations for mass transport coefficients pertinent to the analysis of vapor absorption in water during reactor accidents. Some that may be pertinent include:

**Laminar flow over a shallow pool of water** [Cuest, *et al.*, 1999]:

$$\frac{Lk_{liq}}{D_{liq}} = \frac{2}{\sqrt{\pi}} \left( 1 - 0.35 \left( \frac{\varphi}{Re_H} \right)^{1/3} \right) \sqrt{\varphi Sc Re_H}$$

where:

$L = \text{length of pool (m)}$

$H = \text{depth of pool (m)}$

$\varphi = L/H$

$$Re_H = \frac{\rho_{liq} H U_s}{\mu_{liq}}$$

$\rho_{liq} = \text{liquid density (kg/m}^3\text{)}$

$\mu_{liq} = \text{liquid viscosity (Pa} \cdot \text{s)}$

$$Sc = \frac{\mu_{liq}}{\rho_{liq} D_{liq}}$$

$U_s = 0.03 U^\infty = \text{shear velocity (m/s)}$

$U^\infty =$

$\text{gas velocity far from liquid surface (m/s)}$

**Water pool agitated by falling raindrops:**

$$k_{liq} = \begin{cases} 0.00135 M_f & 0 < M_f < 0.0111 \text{ kg/m} \cdot \text{s}^2 \\ 0.00035 (M_f)^{0.7} & 0.0111 < M_f \end{cases}$$

where:

$$M_f = \rho_{liq} \dot{Q} v_{drop}$$

$\dot{Q}$

$= \text{volumetric droplet flux (m}^3 \text{ droplets per m}^2 \text{ exposed water surface per second)}$

$v_{drop} =$

$\text{impact velocity of droplet on pool surface (m/s)}$

An extended discussion of terminal velocities of falling water droplets is provided by Clift, Grace, and Weber [1978].

**Falling wavy liquid films in turbulent flow** [Banerjee, Scott and Rhodes, 1968]:

$$k_{liq} = 0.00293 Re^{0.933} \sqrt{D_{liq}}$$

An alternative, more complicated, formulation proposed by Won and Mills [1982] is:

$$\frac{k_{liq}}{D_{liq}} \left( \frac{\mu_{liq}^2}{g \rho_{liq}^2} \right)^{1/3} = 6.97 \times 10^{-9} \frac{Re^m Sc^\beta}{\sqrt{Ka}}$$

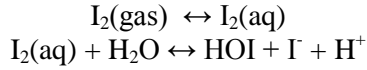
$g = \text{acceleration due to gravity} = 9.80665 \text{ m/s}^2$

$$m = 3.49 Ka^{0.0675}$$

$$\beta = 1 - \frac{0.137}{Ka^{0.055}}$$

$$Ka = \frac{\mu_{liq}^4 g}{\rho_{liq} \sigma_{liq}^3}$$

The problem of using simulant solutes to deduce the behavior of iodine mentioned briefly above extends to the treatment of diffusion in the liquid phase. Molecular iodine is not inert in water. A rapid reaction in solution is:



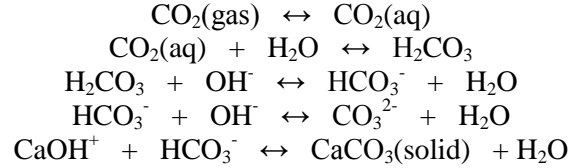
Consequently, the diffusion of the uncharged species  $I_2$  and HOI is affected by the ionic diffusion produced by reaction with water. The complication of ion diffusion does not arise in studies with oxygen as a simulant and can be suppressed when carbon dioxide is used as a simulant. Methods such as those discussed by Wiens and Leaist [1986] must be adapted to account for the electrochemical potential of the ions and to deduce effective diffusion coefficients for the uncharged species particularly for water films on surfaces in containment that are neither borated nor treated with buffer or other indifferent electrolyte.

Complications also arise in gas phase diffusion when water vapor is either evaporating from or condensing on water surfaces which will nearly always be the case during reactor accidents. The flux of evaporating or condensing water can retard or enhance solute transport to water pools or films. The coupling between diffusion of the solute and the water vapor in an immobile background gas (air or nitrogen) requires the use of Stefan-Maxwell formulations of the diffusion equation rather than the Fickian formulation, which requires determination of many more diffusion coefficients, or, more crudely, simple binary diffusion.

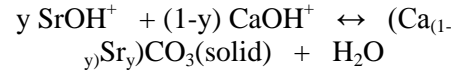
#### IV. CO-PRECIPITATION OF CALCIUM CARBONATE AND FISSION PRODUCTS

If water pools come into contact with concrete within the reactor containment, the water will leach the concrete and become saturated in calcium ion. Emergency coolant water from natural sources such as seawater may already be saturated in calcium ion. Additives to the coolant such as borate or phosphate buffer may precipitate calcium from the solution. The potential effects of these flocculent precipitates will be discussed in the next section of this paper. Once the additives have been exhausted, there can be continued dissolution of calcium ion from the concrete. This calcium ion can be

precipitated by reaction with carbon dioxide dissolved from the containment atmosphere:



It is not uncommon for calcium carbonate to precipitate initially as aragonite and transform into calcite [Morse, *et al.*, 1997]. This precipitation is of great interest in both oceanography and geology, so it has been much studied. Among the findings of these studies is that there can be the co-precipitation of strontium carbonate:



This implies that calcium carbonate crusts that typically form near the interface between the gas phase and the saturated water phase in reactor containments can be contaminated with radioactive isotopes of strontium and barium. Experimental investigations show that the partitioning of strontium and barium ions between the precipitating aragonite and the fluid in a closed system follows the so-called Doerner-Hoskins relationship [Gaetani and Cohen, 2006]:

$$\begin{aligned} \ln \left( 1 + \frac{m_{\text{Sr}}(\text{solid})}{m_{\text{Sr}}(\text{fluid})} \right) \\ = K_{DH}^{\text{Sr}} \ln \left( 1 + \frac{m_{\text{Ca}}(\text{solid})}{m_{\text{Ca}}(\text{fluid})} \right) \end{aligned}$$

where:

$$\begin{aligned} m_C(\text{phase}) &= \text{moles cation } C = \\ &\text{Ca}^{2+}, \text{Sr}^{2+} \text{ or } \text{Ba}^{2+} \text{ in phase} = \\ &\text{solid or fluid} \\ K_{DH}^C &= \\ \text{Doerner - Hoskins constant for cation } C &= \\ &\text{Sr}^{2+} \text{ or } \text{Ba}^{2+} \text{ in aragonite} \end{aligned}$$

Gaetani and Cohen found:

$$\begin{aligned} \ln K_{DH}^{\text{Sr}} &= \frac{605 \pm 47}{T(K)} - 1.89 \pm 0.15 \\ \ln K_{DH}^{\text{Ba}} &= \frac{2913 \pm 154}{T(K)} - 9.0 \pm 0.5 \end{aligned}$$

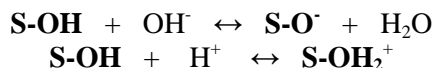
Hexavalent uranium and, presumably, rare earth ions can partition into the precipitating calcium carbonate crystals [Gabitov, *et al.*, 2008].

Depending on the level of contamination, it may be necessary to remove calcium carbonate encrustations near water-atmosphere interfaces within the Fukushima reactor containments and buildings prior to the start of intensive remediation.

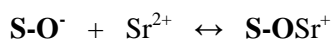
#### V. ADSORPTION OF FISSION PRODUCT IONS ON SURFACES

The current understanding of the aqueous chemistries of fission products is based on experimental and analytic results for relatively dilute and simple aqueous mixtures. Typically, only buffers such as borate have been included in the solutions. Waters in reactor containments will not be so simple. Many species will exist in solution. But, as noted above, there will also be suspended solids coming from precipitation reactions and corrosion products. The sumps at Three Mile Island were a milky white from suspended corrosion products of aluminum – mostly  $\text{Al}(\text{OH})_3$  and  $\gamma\text{-AlO}(\text{OH})$  – as well as zinc corrosion products. Over a longer term, corrosion products of iron will contribute to the complexity of aqueous solutions in containment.

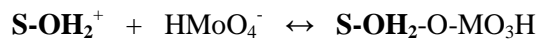
Typically, oxides suspended in solution are surface active. The activity can be understood in terms of surface hydroxides. Let **S-OH** denote a surface species such as iron ion or aluminum ion on a suspended solid with an associated hydroxide group pointed into the aqueous phase. The hydroxide species can protonate or deprotonate depending on both the nature of the solid and the ambient pH of the solution:



Dissolved fission product ions can adsorb on these surface sites and contaminate the suspended solids with radionuclides. The more highly charged the solute the more likely it is to adsorb. Cations such as  $\text{Cs}^+$  and  $\text{Sr}^{2+}$  adsorb under basic conditions when the surface hydroxides are deprotonated:



and, consequently, negatively charged anions such as molybdate [Goldberg, *et al.*, 1996] and iodate [Machesky, *et al.*, 1989] can adsorb under acidic conditions when the surface hydroxides are protonated:



In the case of flocculent, calcium phosphate precipitates suspended in solution, adsorbed molybdate anion may be incorporated into the precipitate as a phospho-molybdate species. Iodate adsorption can distort via the iodine mass balance equation the equilibria in solution that lead to the formation of aqueous molecular iodine.

Suspended solids are not the only possible sites of fission product ion adsorption from solution. The so-called “green rusts” formed by corrosion of mild steel can adsorb ions. These surface layers are nominally ferrous hydroxide, but can incorporate other ionic species such as chloride, carbonate and sulfate to form different structures. Depending on the ambient conditions, outer layers can be converted to ferric and ferric-ferrous species such as goethite, ( $\alpha\text{-FeO}(\text{OH})$ ), and magnetite, ( $\text{Fe}_3\text{O}_4$ ). Surface hydroxides on these species can be protonated or deprotonated to form sites for ion adsorption.

There are well developed models for the prediction of ion adsorption on surfaces exposed to aqueous solutions [See for examples: Bousse, *et al.*, 1983; Hiemstra, *et al.*, 1989]. These models are all highly empirical and require data for the particular solids and conditions. Among the most studied solids are goethite, which can be produced by corrosion of mild steel in the post accident environment, and aluminum hydroxide, which can be produced by aluminum corrosion [See for example: Hingston, *et al.*, 1972]. Experimental data do tend to be scattered perhaps because of unmodeled peculiarities of the solids.

Aqueous solutions expected to be present in reactor containments following reactor accidents will be chemically complicated and include both radioactive and nonradioactive solutes – all of which can compete for adsorption sites on suspended solids or corrosion products exposed

to the solution. Rather detailed chemical speciation models will be needed to predict the extent of radionuclide contamination of the suspended solids and the surface materials by ion adsorption. Some iteration between models and data may be required to obtain reliable predictions.

## VI. CONCLUSIONS

Heterogeneous chemistry involving the interactions of species across phase boundaries must be considered along with aqueous-phase and gas-phase chemistry to model fission product behavior in reactor accidents. Heterogeneous chemistry must also be considered in the cleanup and remediation of reactor facilities following accidents. Example considerations are the coprecipitation of radionuclides with non-radioactive materials such as calcium carbonate and the adsorption of ions on solids suspended in solutions or deposited on surfaces within the reactor.

## REFERENCES

1. S. Banerjee, D.S. Scott, and E. Rhodes, "Mass Transfer to Falling Wavy Liquid Films in Turbulent Flow", *Industrial and Engineering Chemistry – Fundamentals*, **7**, 22-27, (1968).
2. A.B. Beard, C.G. Benson, and B.R. Bowsher, "Fission product vapour-aerosol interactions in containment: simulant fuel studies", AEEW-R-2449, UKAEA Atomic Energy Establishment, Winfrith, UK, 1999.
3. L. Bousse, N.F. De Rooij, and P. Bergveld, "The Influence of Counter-ion Adsorption on the  $\psi_0$ /pH Characteristics of Insulator Surfaces", *Surface Science*, **135**, 479-496, (1983).
4. L. Bosland, S. Dickinson, G.A. Glowa, L.E. Herranz, H.C. Kim, D.A. Powers, M. Salay, and S. Tietze, "Iodine-paint interactions during nuclear reactor severe accidents", *Annals of Nuclear Energy*, **74**, 184-199, (2014).
5. B. Clément, L. Cantrel, G. Ducros, F. Funke, L. Herranz, A. Rydl, G. Weber, and C. Wren, *State of the Art Report on Iodine Chemistry*, NEA-CSNI-R-2007-01, Nuclear Energy Agency, Paris, France, 2007.
6. R. Clift, J.R. Grace, and M.E. Weber, *Bubbles, Drops, and Particles*, Academic Press, New York, 1978.
7. Cuesta, F.X. Grau, F. Giralt, and Y. Cohen, "Air-water mass transfer of organics from shallow ponds under laminar recirculation", *International Journal of Heat and Mass transfer*, **42**, 165-179, (1999).
8. P.V. Danckwerts, "Significance of liquid film coefficients in gas absorption", *Industrial and Engineering Chemistry*, **43**, 1460-1467, (1951).
9. S. Dickinson, A. Auvinen, Y. Ammar, L. Bosland, B. Clément, F. Funke, G. Glowa, T. Kärkelä, S. Tietze, G. Weber, and S. Zhang, "Experimental and modeling studies of iodine oxide formation and aerosol behavior relevant to nuclear reactor accidents", *Annals of Nuclear Energy*, **74**, 200-207, (2014).
10. R.I. Gabitov, G.A. Gaetani, E.B. Watson, A.L. Cohen, and H.L. Ehrlich, "Experimental determination of growth rate effect on  $U^{6+}$  and  $Mg^{2+}$  partitioning between aragonite and fluid at elevated  $U^{6+}$  concentration", *Geochimica et Cosmochimica Acta*, **72**, 4058-4068, (2008).
11. G.A. Gaetani and A.L. Cohen, "Element partitioning during precipitation of aragonite from seawater: A framework for understanding paleoproxies", *Geochimica et Cosmochimica Acta*, **70**, 4617-4634, (2006).
12. S. Goldberg, H.S. Forster, and C.L. Godfrey, "Molybdenum Adsorption on Oxides, Clay Minerals, and Soils", *Soil Science Society of America Journal*, **60**, 425-432, (1996).
13. S. Guilbert, C. Gomez, L. Martinet, K. Boucault, and A.-L. Imbert, "S2-6-3 Epicur Test Report", DPAM-SEREA-2007-148, ISTP N° 46, Institut de Radioprotection et de Sûreté Nucléaire, Cadarache, France, 2007.

14. T. Hiemstra, W.H. Van Riemsdijk, and G.H. Bolt, "Multisite Proton Adsorption Modeling at the Solid/Solution Interface of (Hydr)oxides: A New Approach", *J. Colloid and Interface Science*, **133**, 91-104, (1989).
15. R. Higbie, "The rate of absorption of a pure gas into a still liquid during short periods of exposure", *Transactions American Institute of Chemical Engineers*, **35**, 365-388, (1935).
16. F.J. Hingston, A.M. Posner and J.P. Quirk, "Anion adsorption by Goethite and Gibbsite 1. The Role of the Proton in Determining Adsorption Envelopes", *Journal of Soil Science*, **23**, 177-192, (1972).
17. D. Jacquemain, N. Hanniet, C. Poletiko, R. Cripps, C. Wren, D. Powers, Y. Drossinos, and F. Funke, "An Overview of the Iodine Behaviour in the Two First Phebus Tests FPT-0 and FPT-1", *Proceedings of the OECD Workshop on Iodine Aspects of Severe Accident Management*, Vantaa, Finland, 1999.
18. W.K. Lewis and W.G. Whitman, "Principles of Gas Absorption", *Industrial and Engineering Chemistry*, **16**, 1215 -1220, (1924).
19. M.L. Machesky, B.L. Bischoff, and M.A. Anderson, "Calorimetric Investigation of Anion Adsorption onto Goethite", *Environmental Science and Technology*, **23**, 580-587, (1989).
20. J.W. Morse, Q. Wang, and M.Y. Tsio, "Influences of temperature and Mg:Ca ratio on CaCO<sub>3</sub> precipitates from seawater", *Geology*, **25**, 85-87, (1997).
21. H.S. Rosenburg, J.M. Genco, and D.L. Morrison, *Fission-Product Deposition and its Enhancement Under Reactor Accident Conditions: Deposition on Containment-System Surfaces*, BMI-1865, Battelle Memorial Institute, Columbus, Ohio, 1969.
22. Y.G. Seo and W.K. Lee, "Single-eddy model for random surface renewal", *Chemical Engineering Science*, **43**, 1395-1402, (1988).
23. L. Soffer, S.B. Burson, C.M. Ferrell, R.Y. Lee, and J.N. Ridgely, *Accident Source Terms for Light-water Nuclear Power Plants*, NUREG-1465, U.S. Nuclear Regulatory Commission, Washington, DC, USA, 1995.
24. R. Vogt, R. Sander, R. von Glasow, and P.J. Crutzen, "Iodine Chemistry and its Role in Halogen Activation and Ozone Loss in the Marine Boundary Layer: A Model Study", *J. Atmospheric Chemistry*, **32**, 375-395, (1999).
25. C.F. Weber, E.C. Beahm, and T.S. Kress, *Models of Iodine Behavior in Reactor Containments*, ORNL/TM-12202, Oak Ridge National Laboratory, Oak Ridge, TN, USA, 1992.
26. B. Wiens and D. Leaist, "Multicomponent diffusion of double salts. Sodium hydrogen sulphate in aqueous solution", *J. Chemical Society, Faraday Transactions 1*, **82**, 247-253, (1986).
27. Y.S. Won and A.F. Mills, "Correlation of the Effects of Viscosity and Surface Tension on Gas Absorption Rates into Freely Falling Turbulent Liquid Films", *International Journal of Heat and Mass Transfer*, **25**, 223, (1982).

## APPLICATION OF THE COCOSYS IODINE CHEMISTRY MODEL AIM-3 TO PWR CONTAINMENT ANALYSES USING NEW VALIDATION RESULTS FROM RTF AND CAIMAN EXPERIMENTS

A. Danilevich<sup>(1)</sup>, P. Levi<sup>(1)</sup>, F. Funke<sup>(1)</sup>, M. Bendiab<sup>(1)</sup>, H. Dimmelmeier<sup>(1)\*</sup>

<sup>(1)</sup> AREVA GmbH, Erlangen, Germany, Germany

\*Corresponding author, Tel: (+49)913190095035, Fax: (+49)913190097507, Email: harald.dimmelmeier@areva.com

**Abstract** – In the severe accident containment code COCOSYS, the module AIM is used for modeling iodine chemistry to predict a best-estimate radiological source term. In the current version AIM-3, 70 chemical and physical processes are calculated for 26 iodine species and 8 other chemical species. The iodine transport between compartments by gas and water flows is considered as well according to the results provided by the thermo-hydraulics module in COCOSYS.

In contrast to the previous version AIM-2, AIM-3 utilizes new validation data from large-scale experiments performed for instance in the THAI and PHEBUS facilities. A particular focus is the iodine deposition on surfaces (including the reaction with paint that can form organic iodine compounds) and possible re-suspension processes as well as iodine-silver reactions in sumps. This has also led to the modification of certain reaction parameters and even the structure of underlying kinetic equations.

In order to quantify and analyze the difference between AIM-2 and AIM-3, and to extend the validation basis for AIM-3, the experiments ACE/RTF 3b (performed in Whiteshell, Canada) and CAIMAN 2001/03 (performed in Cadarache, France) that were calculated with AIM-2 were recently repeated by AREVA with AIM-3. By modifying some default parameters in AIM-3 for the iodine reaction with paint to account for the specific properties of the paints used in the experiments, we were able to acquire very good agreement of the COCOSYS calculations with the experimental results.

Finally, calculations of the iodine behavior in the containment during a typical severe accident scenario in a generic pressurized water reactor were performed with AIM-3 using both the original and the new parameter selection to assess the impact of the different AIM parameters on the relative distribution of the different iodine species and the radiological source term.

## I. INTRODUCTION

In the severe-accident containment code COCOSYS, the module AIM is used for modelling iodine chemistry for predicting a best-estimate radiological source term. In the current version AIM-3, 70 chemical and physical processes are calculated for 26 iodine species and 8 other chemical species. Chemical and physical reactions between iodine species as well as between iodine and other chemical species are modelled by AIM. Furthermore, interfacial mass transfer between the gas phase and the sump is considered. Intercompartment iodine transport by gas and water flows is considered as well according to the results provided by the thermo-hydraulics module in COCOSYS.

In contrast to the previous version AIM-2, AIM-3 utilizes new validation data from large-scale experiments performed for instance in the THAI and PHEBUS facilities. A particular focus is the iodine deposition on surfaces (including the reaction with paint that can form organic iodine compounds) and possible re-suspension processes as well as iodine-silver reactions in sumps. This has also led to the modification of certain reaction parameters and even the structure of underlying kinetic equations.

In order to quantify and analyse the difference between AIM-2 and AIM-3, and to extend the validation basis for AIM-3, the experiments ACE/RTF 3b (performed in Whiteshell, Canada) and CAIMAN 2001/03 (performed in Cadarache, France) that were calculated with AIM-2, were recently repeated by AREVA with AIM-3.

In this paper, a comparison of AIM-2 and AIM-3 results with the experiment is outlined. Moreover, the difference between the AIM-3 results and the experimental values is addressed: The results of a parameter variation study of the iodine reaction with painted surfaces are presented. Key iodine-paint reactions which affect the iodine concentration in the sump and the gas phase are identified both for the CAIMAN and the ACE/RTF experiment.

## II. ACE/RTF 3b EXPERIMENT

The experiment ACE/RTF 3b was conducted in the Canadian Radioiodine Test Facility (RTF) in Whiteshell. The experimental steel container has a total volume of 386 l, of which the sump takes up 35 l. The walls of the container are completely painted with epoxy decontamination paint. The surface area between the gas phase and the painted walls amounts to 2.4 m<sup>2</sup> and the surface area of the immersed painted surfaces is 0.6 m<sup>2</sup>. The interfacial area between the sump and the atmosphere is 0.41 m<sup>2</sup>. The temperature of the sump is kept constant throughout the experiment at 60°C and the temperature of the gas phase at 53°C. The experiment was conducted at a constant pressure of 1 bar. At the start of the experiment, a CsI solution is injected into the sump to reach an initial iodine concentration of  $1.3 \times 10^{-5}$  mol/l. In order to achieve and maintain homogeneous concentrations, both the gas phase and the sump are continuously mixed through recirculation loops at rates of 3 l/min for the sump and 23 l/min for the gas phase. 73 h after initiation of the experiment the pH value of the sump is changed from 5.7 to 9.0 by injecting LiOH. Throughout the course of the experiment both the sump and the gas phase are subject to a constant radiation dose rate of 2 kGy/h.

### II.1 COMPARISON BETWEEN EXPERIMENT AND AIM-2/AIM-3 CALCULATIONS

Concentrations of iodine compounds in the sump and in the gas phase were measured in the experiment and can be compared with calculation results. In Fig. 1 through Fig. 3 one can see the total concentration of iodine compounds in the sump, the total concentration of iodine compounds in the gas phase and the concentration of organic iodine in the gas phase, respectively. In addition to the iodine sources in Fig. 1 through Fig. 3, iodine is deposited on the painted surfaces in the sump and in the atmosphere. Furthermore, iodine oxides are present in the atmosphere. No separate experimental values are available for iodine oxide. However, in the total concentration of all iodine compounds in the gas phase, Fig. 2, both

the experimental values and the numerical results include iodine oxides.

As shown in Fig. 1, the COCOSYS calculations with both AIM-3 and AIM-2 over-estimate the total amount of iodine in the sump, AIM-3 being closer to the experimental values. In Fig. 2 AIM-2 provides a slightly better overall prediction of the total amount of iodine in the gas phase. On the other hand, AIM-2 under-estimates the experimental values for organic iodine compounds in the atmosphere (see Fig. 3). Here AIM-3 is more precise than AIM-2. As a reason for the over-prediction of the sump iodine concentration by both versions of AIM, it was considered that different paints were used for the validation of the AIM paint reaction constants and in the ACE/RTF 3b experiment.

## II.2 AIM-3 PARAMETER STUDY

It was assumed that the main difference between experiment and simulations stems from a wrong set of constants for iodine reactions with paint in the sump and in the gas phase. These reactions include deposition and re-suspension of  $I_2$  and  $\Gamma$  on the painted surfaces in the sump and in the gas phase, transformation between chemisorbed and physisorbed  $\Gamma$  in the sump and between chemisorbed and physisorbed  $I_2$  in the gas phase, as well as thermal and radiolytic formation of organic iodine compounds from iodine species on painted surfaces. In order to estimate the influence of these reactions on the total amount of iodine in the sump and in the gas phase, a step-by-step variation of the corresponding reaction constants over several orders of magnitude in both directions from the respective default values was performed. The reaction constants for different types of reactions were varied independently such that cross-dependencies could be excluded.

As a result the amount of iodine-paint reactions which have a significant impact (within the boundary conditions of the experimental setup) on the total amount of iodine in the sump and in the atmosphere could be reduced to a single reaction pair:

- Reaction 37, which describes the deposition of  $\Gamma$  on the immersed painted surfaces.
- Reaction 19, which is the reverse to the reaction 37 and corresponds to the re-suspension of  $\Gamma$  in the sump.

The reactions 19 and 37 which govern the deposition of  $\Gamma$  on paint and the re-suspension from paint were adapted to laboratory tests using painted epoxy surfaces, see 2 for details. Apart from the adsorption / desorption steps 37 / 19 considered to describe fast physisorption, the model also includes a chemisorption step occurring at the paint, where physisorbed iodine is slowly converted into a chemisorbed iodine species (reactions 79 / 80. and 76 / 77). The rate constants of the corresponding overall I- / paint model include a complex dependence of the reaction constants on the parameters temperature, pH, age of the paint, etc. It is important to point out that the model was adapted to experiments where GEHOPON epoxy paint was used. Therefore iodine reactions with different types of paints (as e.g. employed in the RTF and CAIMAN experiments) could lead to other reaction constants of paint-iodine reactions. Therefore the finding that reactions 19 and 37 turn out to have significant impact on the numerical values is in agreement with the expectations, since most of the iodine is contained as  $\Gamma$  in the sump or as  $\Gamma$  adsorbed on paint in the sump, and an inappropriate modeling of the corresponding reaction constants would cause to a noticeable inaccuracy in the iodine concentrations. The age of the paint in the AIM simulation was assumed to be 5 years. The age of the paint also affects the reaction constants for reaction 19 and 37 and can be another source for systematic errors. The age of the paint cannot be set below 5 years in the implemented iodine model.

When considering the total amount of iodine in the sump and in the atmosphere, other iodine-paint reactions turned out to play a minor or no role at all in the framework of the ACE/RTF 3b experimental conditions. By adjusting reactions 19 and 37 it is possible to change the amount of iodine deposited on immersed painted walls and consequently the total amount of iodine in the sump. The reaction constants for reaction 19 and

37 were fine-tuned such that numerical results for the total amount of iodine compounds in the sump are in good agreement with the experiment, see Fig. 4. As a result of increasing the amount of  $\Gamma$  adsorbed on the paint in the sump, adjusting reactions 19 and 37 leads to a reduced amount of iodine available in the sump for interfacial transfer to the gas phase. The change of the aqueous phase parameters does not largely affect the good agreements of gaseous iodine concentrations, as seen in Fig. 5 and Fig. 6. Overall, adjusting reactions 19 and 37 leads to a good agreement of experiment and simulation for the iodine concentrations in the sump and in the atmosphere, which are both crucial for the radiological source term in containment applications.

After the variation of reactions 19 and 37 an additional calculation was performed, in which the reaction constant for the radiolytic formation of  $I_2$  from  $\Gamma$  in the sump (reaction 20 in AIM-3) was enhanced by a factor of 20. This calculation was carried out with the newly modified constants for reactions 19 and 37. This additional variation was performed in order to bring the changes to the reaction constants in consistency between the ACE/RTF 3b and CAIMAN 2001/03 calculations. In the CAIMAN 2001/03 simulations, adjusting reaction 20 is crucial for properly balancing the total amount of iodine in the gas phase (see Section III for a detailed discussion). Enhancing reaction 20 leads to an increased rate of formation of molecular iodine  $I_2$  from  $\Gamma$  in the sump. As a result, the volatile  $I_2$  is being transferred from the sump to the gas phase, increasing the total iodine concentration in the atmosphere and in turn reducing the iodine concentrations in the sump. Thus, reaction 20 can be used as an adjusting mechanism for balancing iodine between the sump and the atmosphere.

The results of the additional calculation are presented in Fig. 4 through Fig. 6. In contrast to the CAIMAN 2001/03 experiment (see Section III), enhancing reaction 20 by a factor of 20 for ACE/RTF 3b calculations does not lead to a significant change in the total iodine concentrations in the sump or the atmosphere. One possible reason for this insensitivity is that in the ACE/RTF 3b calculation  $I_2$ , which is

created in the sump and transported to the gas phase, is being adsorbed on the painted surface in the gas phase via the fast physisorption reaction. Therefore no changes in the iodine concentrations in the gas phase are observed after increasing the radiolytic  $I_2$  formation. In contrast to RTF, in CAIMAN there is much less painted surface available in the gas phase – most of the surface area is steel. The corresponding chemisorption of  $I_2$  on steel is slower than the physisorption reaction on paint. Consequently, a significant change in the iodine concentration in the gas phase can be observed when  $I_2$  is being transported from the sump. Also, suppressing the thermal formation of organic iodine from iodine adsorbed on painted surfaces in the gas phase (reaction 14 in AIM-3), which is done as a variation in the calculation of the CAIMAN 2001/03 experiment, has only little effect on the ACE/RTF 3b calculation and is thus not discussed here.

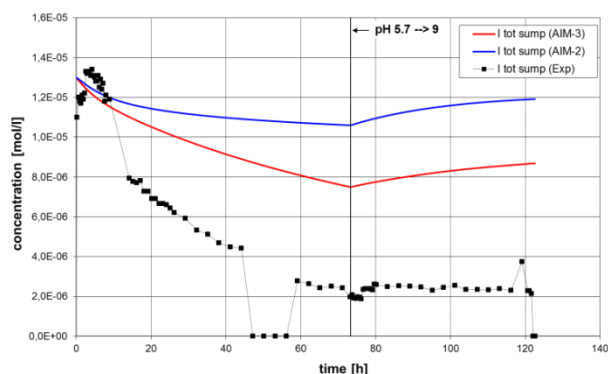


Fig. 1. ACE/RTF 3b. Total amount of iodine compounds in the sump. Comparison between AIM-2/AIM-3 calculations and the experimental values. Both AIM-2 and AIM-3 severely over-estimate the total amount of iodine in the sump.

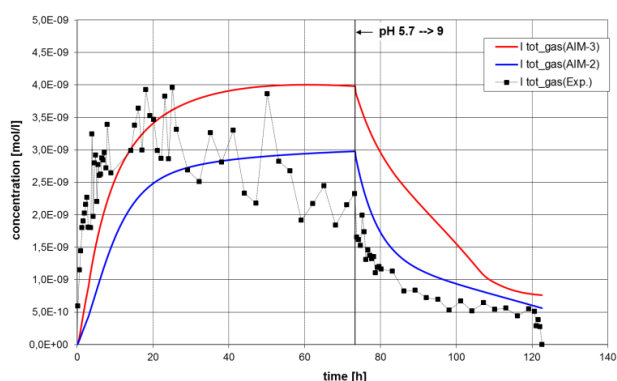


Fig. 2. ACE/RTF 3b. Total amount of iodine-containing compounds in the gas phase. Comparison between AIM-2/AIM-3 calculations and the experimental values. Both numerical calculations lie within an acceptable range around the experimental values. The AIM-3 model seems to over-estimate the total amount of iodine in the gas phase.

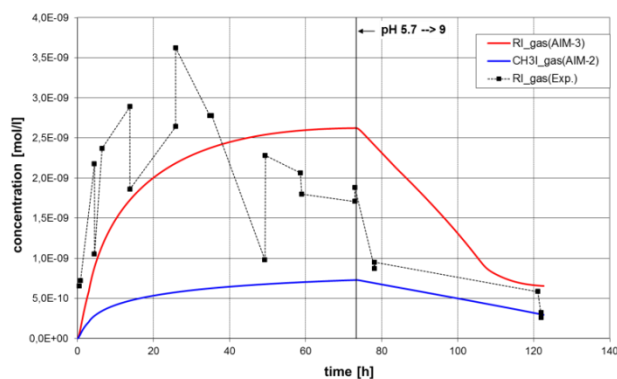


Fig. 3. ACE/RTF 3b. Concentration of organic iodine in the gas phase. Comparison between AIM-2/AIM-3 calculations and the experimental values. In contrast to the AIM-3 results, the AIM-2 calculations seem to under-predict the concentration of organic iodine compounds in the gas phase.

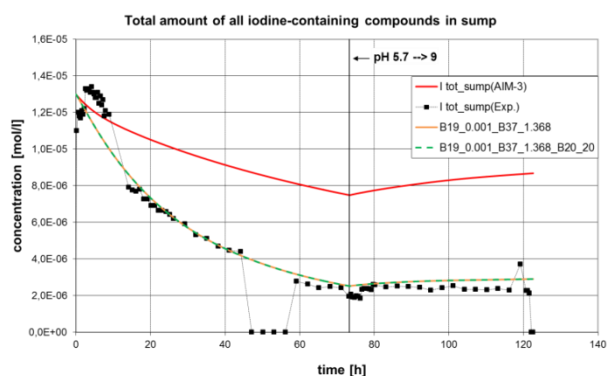


Fig. 4. ACE/RTF 3b. Total amount of iodine compounds in sump. The red line represents the original AIM-3 results, which significantly over-predict the experimental concentration. The solid orange line corresponds to a modified AIM-3 calculation with the reaction constant for

reaction 37 (adsorption of  $\Gamma^-$  on immersed painted surfaces) enhanced by a factor of 1.368 and the reaction constant for the reverse reaction 37 (re-suspension of  $\Gamma^-$  from immersed painted surfaces to the sump) reduced by a factor of 1000. Apparently the modified AIM-3 calculation was brought into very good agreement with the experimental values. The four experimental values in the time range around 50 h are close to zero due to a measurement error, they are plotted but not considered for the comparison between experiment and simulation. In addition to the variation of reactions 19 and 37, an additional calculation was performed where the reaction constant for the radiolytic formation of  $I_2$  from  $\Gamma^-$  in the sump (reaction 20) was enhanced by a factor of 20 (on top of the modified constants for reactions 19 and 37). This variation was performed in order to bring the changes for the ACE/RTF simulation in consistency with the variations of the CAIMAN 2001/03 simulations. In the CAIMAN 2001/03 simulations reaction 20 is crucial for balancing the total amount of iodine in the gas phase (see Section III for a detailed discussion). The results of this variation are represented by the dashed green curve.

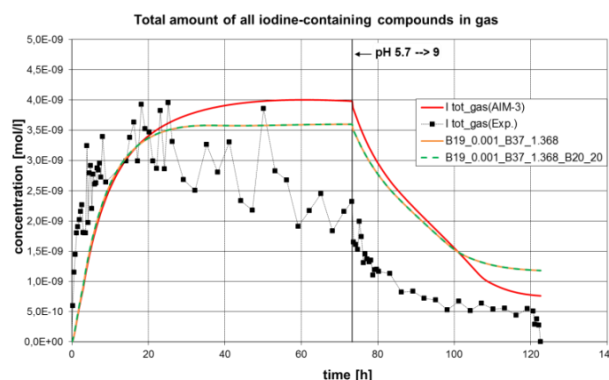


Fig. 5. ACE/RTF 3b. Total amount of iodine-containing compounds in the gas phase. The red line represents the original AIM-3 results. The solid orange line corresponds to the modified AIM-3 calculation as described in Fig. 5. Apparently the modified AIM-3 calculation is in good agreement with the experimental values. The dashed green curve presents results for the additional variation of reaction 20 as also described in Fig. 5.

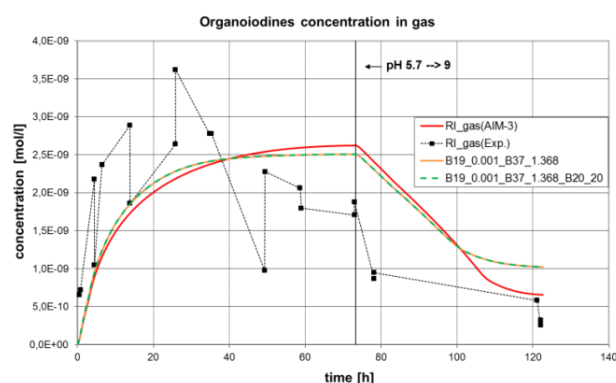


Fig. 6. ACE/RTF 3b. Concentration of organic iodine compounds in the gas phase. The red line represents the original AIM-3 results. The solid orange line corresponds to the modified AIM-3 calculation as described in Fig. 5. Apparently both AIM-3 calculations are in very good agreement with the experimental values. The dashed green curve presents results for the additional variation of reaction 20 as also described in Fig. 5.

### III. CAIMAN 2001/03 EXPERIMENT

The experimental setup of the CAIMAN 2001/03 experiment features several qualitative similarities to the ACE/RTF 3b experiment. The experimental steel container has the total volume of 300 l, of which the sump takes up 3.3 l. The sump is connected to the atmosphere through a narrow bottleneck. The interfacial surface area is only 0.0013 m<sup>2</sup> and therefore significantly smaller than in ACE/RTF 3b. In contrast to ACE/RTF 3b, painted coupons are placed on the steel surfaces in the atmosphere and in the sump (instead of having a completely painted surface as it is the case in ACE/RTF 3b). The total painted surface area in the gas phase is 0.018 m<sup>2</sup>, while with 1.9 m<sup>2</sup> the total surface area between the steel walls and the gas phase is much larger. The total painted immersed surface area is 0.0082 m<sup>2</sup> and the total immersed steel surface area is 0.014 m<sup>2</sup>. The pressure is set to 1.6 bar absolute pressure by injecting nitrogen at 20°C before initiating the experiment. After adjusting the pressure, the container is isolated against particle exchange with the environment throughout the course of the experiment. The temperature is adjusted by heating the walls in three phases:

- $T = 130^{\circ}\text{C}$ ,  $p = 4.91$  bar (absolute) for  $t < 42.5$  h.

- $T = 110^{\circ}\text{C}$ ,  $p = 3.52$  bar (absolute) for  $47$  h  $< t < 68$  h.
- $T = 90^{\circ}\text{C}$ ,  $p = 2.68$  bar (absolute) for  $72$  h  $< t < 161$  h.

The radiation source is located in the sump such that the radiation dose rate is 5 kGy/h in the sump and 5 Gy/h in the atmosphere. Due to technical difficulties, the experiment was not subjected to radiation for  $4.5$  h  $< t < 19.5$  h. At the initiation of the experiment, CsI is dissolved in the sump, resulting in the initial iodine concentration of  $2.92 \times 10^{-5}$  mol/l. Throughout the experiment homogeneous concentrations are maintained by mixing gas phase and sump through separate recirculation loops at rates of 150 l/h and 30 l/h, respectively.

The concentrations of I<sub>2</sub> and organic iodine compounds were measured in the gas phase. Furthermore, the amount of iodine absorbed on paint coupons in the gas phase was measured as well. In the sump the total concentration of all iodine compounds was measured. In addition to these measured concentrations, iodine is adsorbed on steel walls in the sump and in the gas phase and can be present as iodine oxides in the gas phase, although the concentration of iodine oxides is expected to be very low due to the low radiation dose rate in the gas phase. These additional concentrations were not measured during the experiment and therefore cannot be compared with numerical values. It should be pointed out that the experimental measurements of the total iodine concentration in the sump, see Fig. 7 and Fig. 11, are subject to a systematic error: for  $t > 42$  h the total concentration of iodine compounds in the sump exceeds the total initial amount of iodine which was dissolved in the sump at the beginning of the experiment. Therefore only experimental data from the initial phase  $t < 42$  h are used for the comparison of iodine in the sump between experiment and simulation.

#### III.1 COMPARISON BETWEEN EXPERIMENT AND AIM-2/AIM-3 CALCULATIONS

Experimental results are compared with AIM-2 and unmodified AIM-3 calculations in

Fig. 7 through Fig. 10. In all four cases AIM-2 provides better results than AIM-3. AIM-3 systematically under-predicts the experimental values. In the case of the  $I_2$  concentration in the gas phase and the amount of iodine adsorbed on paint in the gas volume the difference between AIM-3 and the experiment is several orders of magnitude. In contrast to AIM-3, AIM-2 is in good agreement with the experimental values. Similar to the ACE/RTF 3b experiment, the paint used in the CAIMAN experiments was different from the paint used for the validation of the AIM paint reaction constants. Therefore it can again be assumed that the difference between experiment and AIM-3 stems from inappropriate reaction constants for iodine-paint reactions implemented in AIM-3. The postulated consequence would be that an unrealistic amount of iodine is adsorbed on the immersed painted surfaces, therefore leading to an under-prediction of all other iodine concentrations.

In the time interval between 5 h and 20 h after the initiation of the experiment, where the radiation source in the experiment was not operational, it can be expected that the strong discrepancy between the experimental data and the AIM-3 results (of around 2 to 8 orders of magnitude for amount of iodine adsorbed on the paint and  $I_2$  in the gas phase) is not only caused by variations in the paint type, but points to deficiencies of the AIM-3 reaction set.

### III.2 AIM-3 PARAMETER STUDY

In order to test this hypothesis the influence of iodine-paint reactions on the total amount of iodine in the sump and in the gas phase was tested. A step-by-step variation of the corresponding reaction constants over several orders of magnitude in both directions from the respective default values was performed. The reaction constants for different types of reactions were varied independently such that cross-dependencies could be excluded.

As a result, again most of the iodine-paint reactions were found to have no significant impact on the iodine concentrations in the sump and in the atmosphere. In a similar manner to the ACE/RTF 3b simulations, the reactions 19 and

37, which govern the deposition and re-suspension of  $I^-$  on immersed painted surfaces, were found to have an influence on the balance between the total amount of iodine in the sump and the amount of iodine adsorbed on the painted walls. The reaction constants for reactions 37 and 19 were fine-tuned such that the total amount of iodine in the sump is in good agreement with the experimental values. As a result, the deposition rate of  $I^-$  on the immersed surfaces was reduced by 50% and the re-suspension was enhanced by a factor 10 (see Fig. 11). It is interesting to note that the reaction constants for reactions 19 and 37 for the CAIMAN 2001/03 experiment have to be adjusted in the opposite direction than the adjustments for the ACE/RTF 3b simulations as described in Section II. The AIM-3 paint reactions constants were modelled on the experimental basis of German THAI experiments. The corresponding model for reaction 19 and 37 incorporates dependencies on temperature, pH and age of the paint. Consequently, the supposed reason for the different adjustments of reactions 19 and 37 between RTF and CAIMAN simulations is the fact that three different types of paint and different pre-conditioning of the paint were used.

In addition, removing reaction 14, which corresponds to thermal formation of organic iodine from physisorbed  $I_2$  in the gas phase, was found to improve the numerical results towards the experimental values at the time before 20 h, where the gap between original AIM-3 results and the experiment is exceptionally large (compare the solid and dashed red curves in Fig. 12 and Fig. 14). Most likely, AIM-3 with default parameters strongly underestimates chemisorption of iodine on the paint. This process is currently modeled to be preceded by previous physisorption, but chemisorption needs to be accelerated independently from the physisorption process. The deactivation of reaction 14 closes the normally rather effective reaction channel for desorption of physisorbed iodine, thereby artificially retaining iodine on the paint which in reality should remain bound as chemisorbed iodine on paint.

Even after adjusting the thermal formation of organic iodine from adsorbed  $I_2$  in the gas phase

(reaction 14) and balancing the iodine in the sump via reactions 19 and 37, the simulation still under-predicts the experimental iodine concentrations in the gas phase by about 1 to 2 orders of magnitude, as seen in the green curve in Fig. 12 through Fig. 14. Since all other paint reactions were ruled out to have any significant impact, the only remaining way to adjust the concentrations in the gas phase was by balancing the iodine concentration between sump and gas phase. Two possible ways to achieve this goal were identified: Increasing radiolytic formation of  $I_2$  in the sump or increasing the interfacial mass transfer between the sump and the gas phase. By increasing the radiolytic formation of  $I_2$  from  $I^-$  in the sump, which is governed by reaction 20 in AIM-3, the much more volatile  $I_2$  is being transferred to the gas phase, thus effectively balancing the total amount of iodine between sump and atmosphere. Since reaction 20 in AIM-3 is still subject to an inherent uncertainty, it was decided to adjust the radiolytic formation of  $I_2$  in the sump via reaction 20 in order to balance iodine between the sump and the gas phase. Reaction 20 was enhanced by a factor of 20 such that the AIM-3 iodine concentrations in the gas phase were brought in agreement with the experimental results (see Fig. 12 through Fig. 14).

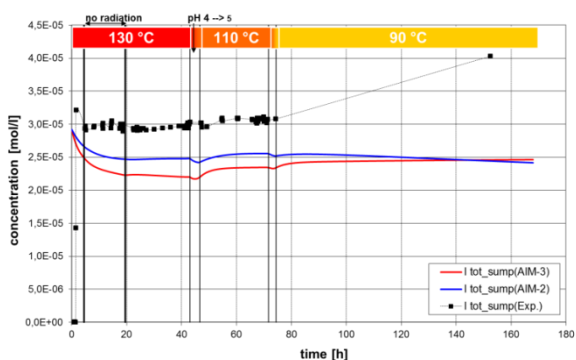


Fig. 7. CAIMAN 2001/03. Total amount of iodine-containing compounds in the sump. The experimental values in the time period  $t > 42$  h are not used for the comparison between experiment and simulation (for details see the main text). Both AIM-2 and AIM-3 results under-predict the experimental values.

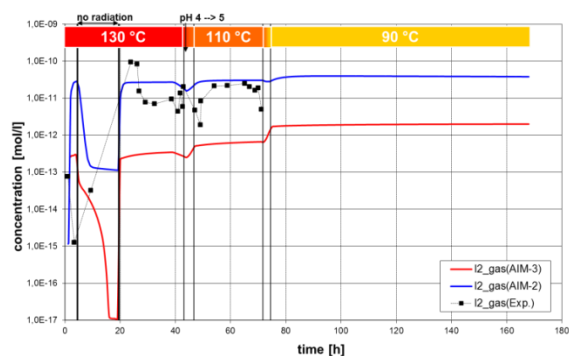


Fig. 8. CAIMAN 2001/03. Total amount of  $I_2$  in the gas phase. In contrast to AIM-2 (blue line), AIM-3 (red line) severely under-predicts the experimental values. In particular, around  $t = 20$  h the difference is around 4 to 5 orders of magnitude.

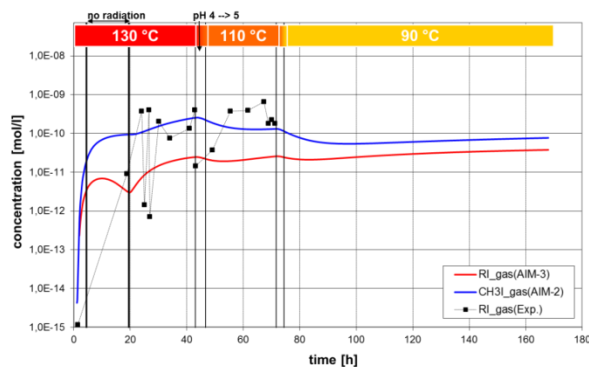


Fig. 9. CAIMAN 2001/03. Total amount of organic iodine compounds in the gas phase. On the logarithmic scale, both AIM-2 and AIM-3 are in agreement with the experiment.

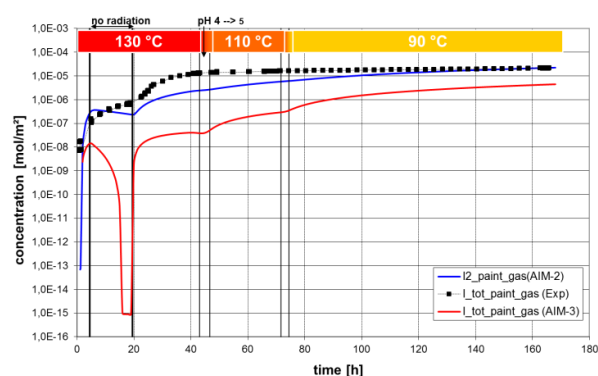


Fig. 10. CAIMAN 2001/03. Total amount of iodine adsorbed on paint in the gas phase. On the logarithmic scale, AIM-2 is in good agreement with the experiment. In contrast concentration values calculated by AIM-3 under-predict the experiment by several orders of magnitude. In particular around  $t = 20$  h the difference is around 8 orders of magnitude.

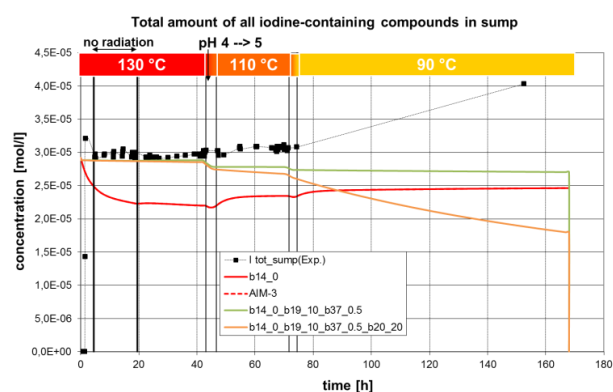


Fig. 11. CAIMAN 2001/03. Total amount of iodine-containing compounds in the sump. The experimental values for  $t > 42$  h exceed the maximum possible iodine concentration of  $2.92 \times 10^{-5}$  mol/l and therefore are not used for comparison between experiment and model. The original AIM-3 calculation (dashed red line, almost identical with the solid red line) is almost identical to the AIM-3 calculation with disabled reaction 14 (solid red line, corresponds to disabled reaction 14, i.e. disabled formation of organic iodine from  $I_2$  adsorbed on paint in the gas phase). Both red lines under-predict the experimental values. After additionally adjusting the iodine adsorption behavior in the sump via reaction 19 and 37, the experimental data are reproduced sufficiently well (solid green line). Additionally enhancing the radiolytic  $I_2$  formation in the sump via reaction 20 (orange line) does not lead to a significant change in the total sump iodine concentration in the time interval  $0 \text{ h} < t < 42 \text{ h}$ .

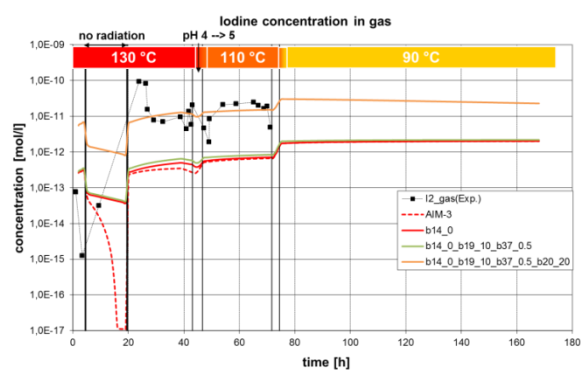


Fig. 12. CAIMAN 2001/03. Total amount of  $I_2$  in the gas phase. The original AIM-3 calculations (dashed red line) significantly under-predict the experiment. Disabling the thermal formation of organic iodine from adsorbed iodine in the gas phase (reaction 14, solid red line) leads to significantly increased concentration around  $t = 20$  h as compared to the original AIM-3 results. However, adjusting iodine adsorption and re-suspension in the sump does not significantly affect the iodine concentration in the gas phase (solid green line, corresponds to adjustment of reactions 14, 19 and 37, as described in Section III). Finally, enhancing radiolytic  $I_2$  formation from  $I^-$  in the sump (reaction 20) by a factor of 20 leads to an increased transport of the volatile  $I_2$  to the atmosphere (solid orange line). Therefore the

under-prediction of the experiment by the original AIM-3 calculation is corrected by this adjustment.

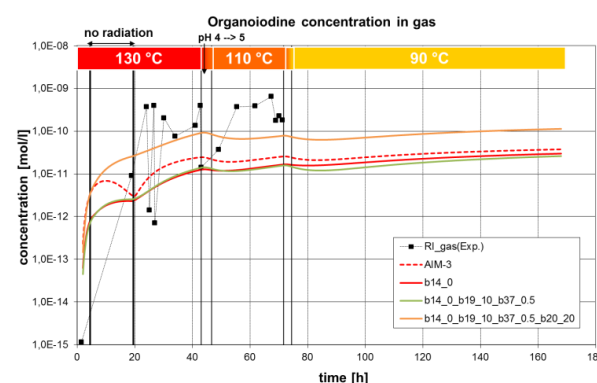


Fig. 13. CAIMAN 2001/03. Total amount of organic iodine compounds in the gas phase. The dashed red line represents the original AIM-3 calculation, while the solid red line corresponds to AIM-3 with disabled reaction 14, see Section III. The solid green line corresponds to the AIM-3 calculation with disabled reaction 14 and adjusted reactions 19 and 37. Increasing the radiolytic formation of  $I_2$  in the sump via reaction 20 (orange line, corresponds to disabled reaction 14, adjusted reactions 19, 37 and enhanced reaction 20) leads to a better agreement between experiment and AIM-3.

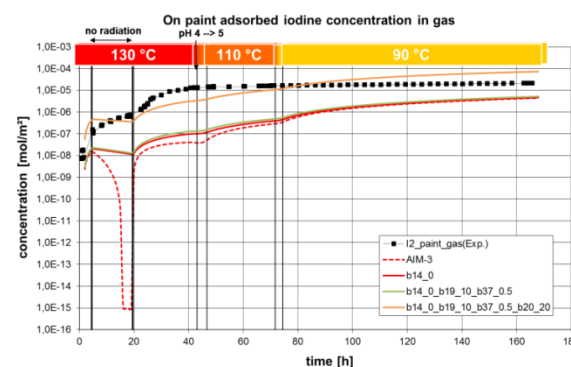


Fig. 14. CAIMAN 2001/03. Total amount of iodine adsorbed on paint in the gas phase. The AIM-3 calculations with disabled thermal formation of organic iodine on painted surfaces, i.e. disabled reaction 14 (solid red line), yield a significant improvement of the original AIM-3 results (dashed red line) around  $t = 20$  h. The falling slope of the solid red line at  $15 \text{ h} < t < 20 \text{ h}$  (no radiation, no thermal formation of organic iodine from physisorbed iodine) can be attributed to re-suspension of physisorbed iodine ( $I_2$ ) from the painted surfaces to the gas phase. As expected, additionally adjusting adsorption and re-suspension of iodine in the sump via reactions 19 and 37 (green line) does not influence the amount of iodine adsorbed on the painted surfaces in the gas phase. However, increasing the radiolytic formation of  $I_2$  in the sump leads to increased  $I_2$  deposition on the painted surfaces in the atmosphere (orange line, corresponds to modified reactions 14, 19, 37 and 20, as described in Section III).

#### IV. COCOSYS SIMULATION OF A SEVERE ACCIDENT WITH ADJUSTED PARAMETERS FOR AIM-3

The AIM-3 paint reaction parameters have to be adjusted in different ways to reproduce the experimental results for the simulation of the ACE/RTF 3b and CAIMAN 2001/03 experiments. In order to estimate the impact of these parameter changes on a containment simulation and the corresponding radiological source term, a COCOSYS simulation of a typical severe accident sequence was carried out. As the basic scenario a loss-of-offsite-power accident in a generic pressurized water reactor was selected. In the course of the accident a core meltdown and the corresponding release of mass and energy into the containment occurs. Consequently the containment is contaminated with fission products, among others iodine. As a result of the leakage from the primary circuit and the accident mitigation measures, water is injected into the containment which leads to deposition of fission products in the sump in the lower levels of the containment. COCOSYS/AIM-3 simulates the iodine chemistry in the containment sump and the atmosphere and couples the chemical reactions to the thermo-hydraulic mass and energy transfer inside the containment.

In order to estimate the difference between an AIM-3 calculation with original paint reaction parameters and two calculations with paint reaction parameters adjusted to match the ACE/RTF 3b and CAIMAN 2001/03 experiments, the total mass of iodine in the containment sump and the total mass of iodine in the containment atmosphere are compared between the three cases. The results can be seen in Fig. 15 through Fig. 17. Fig. 17 is a magnification of Fig. 16 with respect to the vertical axis to allow a better assessment of the differences in the time period after 10 h, i.e. after the initial fission product deposition phase when the relative differences are most pronounced. Note that in this severe accident scenario the start of core oxidation is at about 3 h 30 min, and the reactor pressure vessel fails at about 8 h 40 min, which means that during the in-vessel phase of

the accident no significant differences in the iodine chemistry are observed.

During the first part of the ex-vessel phase, however, the differences in the total mass of iodine compounds in the sump between the three AIM-3 parameter sets can be as high as 20% (see Fig. 15). In the simulations of the ACE/RTF 3b experiment, modifying the paint reaction parameters resulted in sump iodine concentration changes by a factor of 4 (see Fig. 4), whereas in the simulation of the CAIMAN 2001/03 experiment the maximal changes amounted to approximately 40% (see Fig. 11). The variations in the containment simulation are thus not as pronounced as in the experiment, which is for two possible reasons: a) the experimental setups feature temperature and pH conditions which do not necessarily closely match those during the accident and b) the impact of the iodine-paint reactions is more limited in the containment simulation due to geometrical reasons, since the relative influence of surface reactions on volumetric concentrations is reduced as the total considered volume grows and therefore the surface-to-volume ratio shrinks.

It is interesting to note that when the set of parameters used to match the CAIMAN 2001/03 experiment is applied in the containment simulation, the total amount of iodine compounds in the sump decreases compared to the original AIM-3 set of parameters (see Fig. 15). This is in contrast to the behavior in the calculations of the CAIMAN 2001/03 experiment itself, where the modifications in AIM-3 lead to an effect in the opposite direction (see Fig. 11). This is probably caused by the different initial and boundary conditions (geometrical scales, ratio of sump and gas phase volumes, surface-to-volume ratio, iodine concentrations, temperature, pH value, level of radiation, etc.) and the fact that not only the reaction constants of the paint reactions but also of other reactions were adjusted.

The maximum change in the total mass of iodine in the containment atmosphere amounts to approximately 30% (see Fig. 17). In the ACE/RTF simulations the change was approximately between 10% at  $t = 60$  h and 50%

at  $t = 120$  h, see Fig. 5, while modifying paint reaction constants and radiolytic  $I_2$  formation in the CAIMAN 2001/03 simulation resulted in changes of the atmospheric iodine concentrations over several orders of magnitude (see Fig. 12 and Fig. 13).

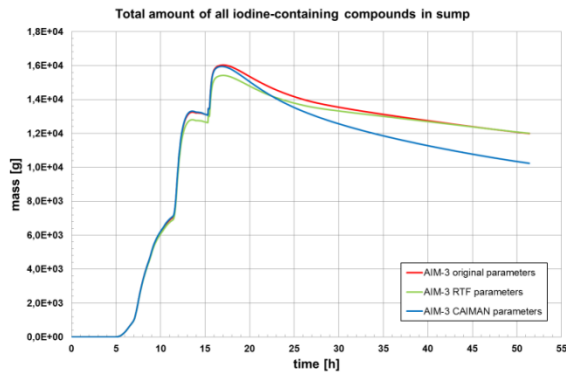


Fig. 15. Accident simulation with COCOSYS/AIM-3. Total amount of iodine compounds in the containment sump. Comparison between the original AIM-3 calculation (red line), AIM-3 with reaction parameters as adjusted for the RTF experiment (green line, see Section II) and the CAIMAN experiment (blue line, see Section III).

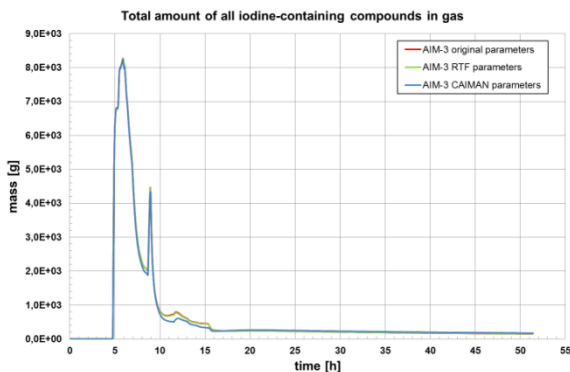


Fig. 16. Accident simulation with COCOSYS/AIM-3. Total amount of iodine compounds in the containment atmosphere. Comparison between the original AIM-3 calculations (red line), AIM-3 with reaction parameters as adjusted for the RTF experiment (green line, see Section II) and the CAIMAN experiment (blue line, see Section III).

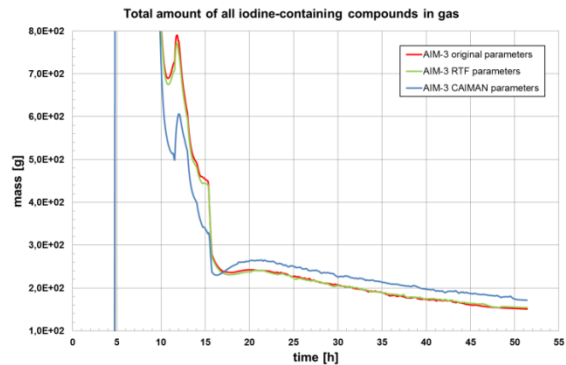


Fig. 17. Accident simulation with COCOSYS/AIM-3. Total amount of iodine compounds in the containment atmosphere. Comparison between the original AIM-3 calculations (red line), AIM-3 with reaction parameters as adjusted for the RTF experiment (green line, see Section II) and the CAIMAN experiment (blue line, see Section III).

## V. CONCLUSION

The differences between AIM-2 and AIM-3 were studied on the basis of experimental measurements of iodine behavior in the ACE/RTF 3b and CAIMAN 2001/03 experiments. For ACE/RTF 3b, AIM-3 with default parameters provides better results for the total amount of iodine in the sump and the concentrations of organic iodines in the gas phase, while AIM-2 predicts the overall iodine concentration in the gas phase more precisely. For the CAIMAN 2001/03 experiment AIM-2 yields better prediction of all experimentally measured concentrations than AIM-3 with default parameters. As a hypothesis for this behavior it was assumed that the reaction constants for iodine-paint reactions in AIM-3 have to be re-evaluated due to different types of paints used in the experiments. In order to test this hypothesis, for both experiments parameter studies were carried out with AIM-3 in order to investigate the influence of iodine-paint reactions on the total amount of iodine in the sump and the atmosphere and the corresponding radiological source term in containment applications.

For both experiments deposition and re-suspension of  $I^-$  on immersed painted surfaces (reactions 19 and 37 in AIM-3) were identified as the main mechanisms for balancing the total amount of iodine in the sump. Fine-tuning of the corresponding reaction constants was performed to bring the simulation values in agreement with

the experiment. The reaction constants had to be adjusted in opposite directions from the AIM-3 default values for ACE/RTF 3b and CAIMAN 2001/03. This result is interpreted to stem from the fact that three different types of paint were used in RTF, CAIMAN and previous AIM validation experiments.

In addition to iodine adsorption and re-suspension, radiolytic  $I_2$  formation from  $I^-$  in the sump (reaction 20 in AIM-3) was identified to be an important mechanism for balancing iodine between the sump and the atmosphere. By adjusting the corresponding reaction constant the amount of iodine species in the gas phase could be brought in agreement between the CAIMAN 2001/03 experimental values and the corresponding AIM-3 simulation. Applying the same modifications to the ACE/RTF 3b simulation did not lead to significant changes in the already good results for the iodine concentrations in the sump or the atmosphere. A possible explanation for this is that in the ACE/RTF 3b calculation  $I_2$  that is created in the sump and transported to the gas phase is rapidly being adsorbed on the painted surface in the gas phase via the fast physisorption reaction, which is also not significantly affected by increasing the radiolytic  $I_2$  formation. In contrast to RTF, in CAIMAN there is much less painted surface in the gas phase available for such fast physisorption, as most of the surface area is steel. The corresponding chemisorption of  $I_2$  on steel is a much slower process, and thus stronger radiolytic  $I_2$  formation can considerably increase the iodine concentrations in the gas phase.

For the CAIMAN 2001/03 experiment, adjusting the thermal formation of organic iodine from iodine adsorbed on painted surfaces in the gas phase (reaction 14 in AIM-3) was proven to have a significant influence on the overall amount of iodine in the gas phase at high temperatures. The corresponding reaction constant was set to zero in order to achieve the best agreement between experiment and simulation. For the ACE/RTF 3b experiment, reaction 14 was tested within the parameter study and was found to have no significant impact (under the boundary conditions given by the experiment) on the iodine concentrations in the

atmosphere and in the sump. This is not surprising as the suppression of this reaction only had an effect during the non-irradiated period of the CAIMAN 2001/03 experiment. However, no additional sensitivity analysis for reaction 14 was performed for the ACE/RTF 3b calculation after applying the modified set of reaction parameters for reactions 19, 37 and 20.

All other iodine-paint reactions implemented in AIM-3 were found to have no significant impact on the total amount of iodine species in the sump or the atmosphere.

Summarizing, paint reaction constants apparently have to be precisely adjusted in AIM depending on which type of paint is being simulated with COCOSYS. With manually adjusted paint reaction constants, AIM-3 outperforms AIM-2 when comparing simulations and experiments.

Additionally a COCOSYS analysis of a typical severe accident scenario in a generic containment was carried out with three different sets of reaction parameters, as used in the original AIM-3 model, in the ACE/RTF 3b simulation and in the CAIMAN 2001/03 simulation. In order to estimate the impact of the adjustments on the radiological source term, iodine concentrations in the containment sump and in the containment atmosphere were compared between the three cases. As expected, the impact of the variations is less pronounced in the containment simulation than in the experiments. However, still differences in the source-term-relevant concentrations of about 20% to 30% in the ex-vessel phase were observed between the three sets of reaction parameters. These effects must be set in relation to other possible uncertainties that affect the radiological source term during a severe accident. Additional studies could be used to estimate an exact (or at least a conservative) set of reaction parameters for the most common types of decontamination paint.

#### ACKNOWLEDGMENTS

The simulations reported in this document were funded by the German Federal Ministry of

Economics (BMWi) in the frame of the project “*Analyses of the impact of containment typical phenomena on fission product distribution*”, project number 1501457.

#### NOMENCLATURE

- AIM-3 = Advanced Iodine Model [Weber 2009]
- CsI = Caesium iodide
- COCOSYS = Containment Code System [Klein-Heßling 2009]
- Iodine = term used without specifically considering the iodine species; depending on the type of measurement in specific boundary conditions, it may represent the sum of several or of all iodine species
- I<sub>2</sub> = Molecular iodine; the term is used if this species is known, or if it is to be discriminated from other iodine species (i.e. iodine in aerosol form, organic iodide)

- THAI = Thermal Hydraulics, Hydrogen, Aerosols, Iodine experimental facility

#### REFERENCES

1. [Bauer2007]: M. BAUER et al., "Validierung des Iod-Modells von COCOSYS", AREVA Report NGPS4/2005/de/0004 Rev. A, 2007
2. [Weber 2009]: G. WEBER et al., "Description of the iodine model AIM-3 in COCOSYS", GRS report A-3508, Gesellschaft für Anlagen- und Reaktorsicherheit (GRS) mbH, Schwertnergasse 1, Cologne, 2009
3. [Klein-Heßling 2013]: W. KLEIN-HESSLING et al., "COCOSYS V 2.4 user's manual", Gesellschaft für Anlagen- und Reaktorsicherheit (GRS) mbH, Schwertnergasse 1, Cologne, 2013

## **IODINE SOURCE TERM COMPUTATIONS WITH ASTEC, LINK WITH PSA2-TOOLS AND FAST RUNNING SOURCE TERM TOOLS FOR EMERGENCY ORGANISATION**

*K. Chevalier-Jabet \* (1), F. Cousin(1), L. Bosland (1), L. Cantrel (1), V. Créach (1), S. Fougerolle(1), J. Denis(1), E. Veilly(1)*

*<sup>(1)</sup> Institut de Radioprotection et de Sécurité Nucléaire (IRSN), Saint Paul Lez Durance, 13115, France,  
\*Corresponding author, tel: (+33) 42199364, Email:karine.chevalier-jabet@irsn.fr*

**Abstract** – *Severe accident (SA) phenomenology related to iodine release to the environment has been closely investigated at IRSN over the last decades, by conducting semi-integral or analytical experimental programs like PHEBUS FP, ISTP (CHIP, EPICUR) and OECD/STEM and contributing to others such as OECD/BIP and THAI. These programs have led to the improvement of knowledge and modelling of iodine behavior in the reactor coolant system and the containment during a SA at a nuclear power plant (NPP). Computational tools developed at IRSN for source term (ST) assessment have benefited from these improvements.*

*Three kinds of codes are developed and used at IRSN for different purposes:*

- The Accident Source Term Evaluation Code, ASTEC, is a dedicated tool used to simulate and predict accident evolution from the initiating event to the releases to the environment with a detailed modelling of the accident phenomenology tackling the coupling between various processes. The accuracy of the prediction depends on the status of knowledge and uncertainties of the involved processes;*
- The fast running code MER is developed in order to get a rapid assessment of releases for Level 2 Probabilistic Safety Assessment. MER provides the associated iodine release for a large number and variety of accident situations, with a reasonable accuracy;*
- In the field of emergency response, the fast running tool PERSAN provides a relative conservative assessment of the releases to the atmosphere, also for a wide range of conceivable situations.*

*The short calculation times needed for MER and PERSAN to achieve an evaluation of a release are obtained by imposing some features of the accident progression scenario, evaluated aside, and by using a simplified modeling. After a presentation of these three source term assessment tools, the article explains the implemented methodology at IRSN to build suitable models for each of the three applications. Simplifications are driven by the final need of realism or conservatism, using uncertainty modeling when necessary. Calculation examples are given for MER and PERSAN.*

## I. INTRODUCTION: PRESENTATION OF THE TECHNICAL CONTEXT

In case of severe nuclear accident, the estimation, at a given time of the amount and nature of the radioactivity released to the environment, named “source term” (ST) hereafter in this paper, is a key issue in several ways : emergency center staff elaborate recommendations related to sanitary measures (evacuation of the public for example) for decision makers ; considering safety assessment, for a given plant, an estimation of the source term associated to a large variety of situations, given their frequency, gives an overview of the risk associated to the plant. These estimations are based on the use of a set of calculation tools, each of them providing a more or less approximated description of the accident processes and integrating to some extent four decades of research and development but without necessarily be at the state of the art.

The Accident Source Term Evaluation Code [1,2] (ASTEC), jointly developed by Institut de Radioprotection et de Sûreté Nucléaire (IRSN) and Gesellschaft für Anlagen und Reaktorsicherheit mbH (GRS), aims at simulating an entire Severe Accident sequence on a nuclear power plant from the initiating event to the release of radioactive substances to the environment. Historically, ASTEC has been designed for several purposes: the first one is the validation and the capitalization of the comprehension of the severe accidental phenomenology, leading to predictability at the reactor scale. It is an integral code, as it takes into account in a unified framework a large part of the severe nuclear accident phenomenology, ensuring that the interactions between the various phenomenological aspects are taken into account. It is a multi-purpose code, as it is used at IRSN directly for safety assessment, support to Level 2 Probabilistic Safety Assessment (L2PSA) development, contribution to emergency preparedness, or source term assessment. Considering source term assessment, as ASTEC capitalizes the last Research and Development results on SA topics, the ASTEC source term calculations can be seen as representative of the state of the art.

In some situations time is a limiting factor for source term assessment, and choices have to be made regarding the way phenomenology is taken into account: in L2PSA, a large number of situations are to be quantitatively assessed. IRSN, acting as a Technical Safety Organization for the French Nuclear Safety Authority, is developing L2 PSAs, using its own self-developed probabilistic tools. MER tool is developed in support to PSA and is dedicated to fast ST computation and it is extended (MERCOR) to also calculate radiological consequences. These tools can be run from KANT, the IRSN probabilistic Accident Progression Event Tree (APET) development and quantification tool. In that case, the assessment of the associated consequences of each given accidental sequence of the several thousands of sequences of the whole L2PSA lead to a hierarchized vision of the overall plant severe accident related risk : it leads to rank the contribution to the global risk of all the initiating events or containment failure modes, using various risk metrics; it allows hierarchical representation of the plant safety as well as a comprehensive analysis of certain scenarios, such as the impact of iodine chemistry and aerosols release uncertainties on emergency planning. A validation/comparison of MER/ASTEC results on a limited number of accident scenarios is currently ongoing, and is part of the MER qualification process.

In the case of management of nuclear/radiological emergency situations, one of the fundamental roles of IRSN is technical support for French public authorities; for that matter, the assessment of the situation of the impacted nuclear facility and its possible evolutions in term of accident progression and radiological consequences to the public and the environment is performed. The main IRSN expertise outputs are a diagnostic and prognostics of the plant status, including source terms and the associated radiological consequences, i.e. doses to the public. In that context, source term simulations are repeatedly performed over time as and when comprehension of the accident progresses.

For these two last tools, simplification assumptions are made:

- physical models are simpler or less complete,
- a decoupling is performed between the physical models: from the source term assessment point of view, some phenomenological aspects (degradation thermo-hydraulics, ...) can indeed be seen as boundary conditions for the fission products behavior and transport part, no feedback being taken into account from the latter aspects to the first ones on a first order approximation basis. This decoupling process is associated to a prior assessment of the boundary conditions, which are given as input data to these source term tools;
- the plant geometry is simplified (compared to an ASTEC representative plant input deck), which is legitimate if the decoupling assumption validity is correct.

This paper gives a more detailed insight of each of the three previously mentioned source term tools, starting with ASTEC. An example of source term preliminary assessment using the newly developed version 2.1 of the code (to be released in April 2015) for a 900MW PWR is presented.

The L2PSA MER code system is described afterwards, with its validation process; an example of MER results based on a PWR900 example is given afterwards.

The emergency source term assessment tool and its use in Fukushima crisis context is described in a third part.

## II. ASTEC

ASTEC has been designed to perform SA calculations for various light water plant types; plant applications were for instance performed for PWR-900, PWR-1300, KONVOI-1300, VVER-440, VVER-1000, and EPR. New developments are currently under progress within the CESAM FP7 project to also deal with BWRs. Regarding ST assessment with ASTEC, the whole accidental phenomenology is involved; each part of the addressed severe accident phenomenology is handled via a dedicated module, which can work either in a stand-alone mode as well as coupled to the other modules (see figure 1). Each module has been validated

through comparison with experimental results; they are presented afterwards, although the validation experimental base is not presented in detail for severe accident progression modules (details in this field are available in [1]).

As previously mentioned, some modules can be considered as providing boundary conditions evaluation modules: they refer to thermal hydraulics, fuel and vessel degradation, basemat erosion, residual power calculation, and are related to the accident progression. Others are directly involved in the modeling of radioactive elements release, transport, and chemical behavior. The description of the version 2.1 of ASTEC, to be released in April 2015, is detailed hereafter.

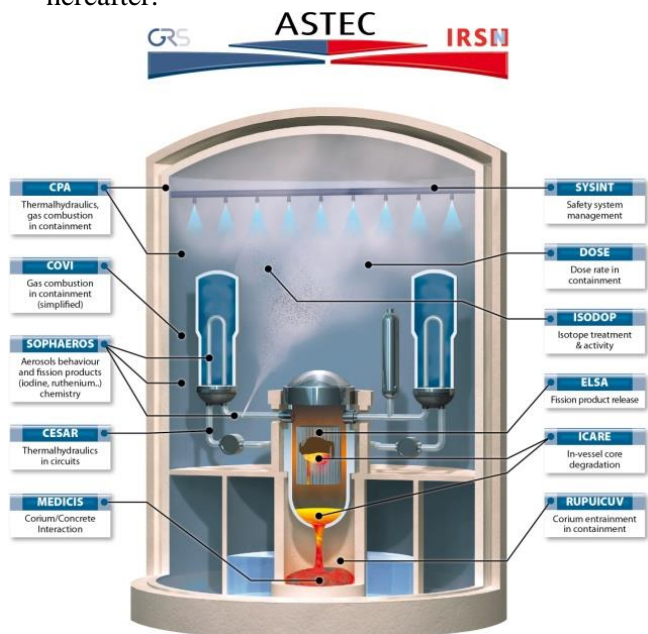


Fig. 1. ASTEC code organization scheme

### II.1 Severe accident progression modules

CESAR [3] module simulates the thermal-hydraulics in the reactor vessel, the primary and the secondary circuit. The CESAR diphasic thermal-hydraulics modeling is based on 1D modeling (allowing cross flows) using control volumes, and takes into account water, steam, and non-condensable gases (hydrogen, helium, nitrogen, argon and oxygen). Thermal non-equilibrium is considered between phases, with the possibility of sub-cooled liquid and superheated steam; a mechanical non-equilibrium

between phases is considered too, with the possibility of counter-current as well as stratified flows. Specific swollen water level volumes are used to model large two-phase domains such as pressurizer. Hydro-accumulators, pumps, valves, breaks, pressurizer spray and heater systems are modeled specifically.

CPA [4] module simulates thermal-hydraulics (including related hydrogen combustion pressure build up) in the containment. The discretization through a lumped-parameter approach (0D zones connected by junctions and surrounded by walls) simulates multiple compartments with possible leakages, filtered or not, to the environment or to other buildings. CPA calculates gases and water distribution, temperature field, pressure build-up, local heat and mass transfer to walls (free and forced convection, radiation, condensation), 1D heat conduction in structures, as well as gas (hydrogen and carbon monoxide) combustion. Equilibrium model or non-equilibrium model can be used in the various compartments. Mass transfer between zones is described separately for gas and liquid flows by momentum equations accounting for the height differences between zone centres. Engineered safety systems such as passive auto-catalytic recombiners (PAR) of different types, containment sprays, have been modeled.

ICARE[5] module describes in-vessel early and late degradation phases phenomena. It is based on a control volume modeling. For early phase degradation, ICARE enables the simulations of mechanical as well as chemical aspects of degradation: ballooning, creep and burst of zircaloy fuel rod claddings, creep of control rod stainless steel claddings for the mechanical part. As far as chemistry is concerned, oxidation of zircaloy or stainless steel by steam, dissolution of  $UO_2$  by solid and liquid Zr, dissolution of Zr by liquid Silver-Indium-Cadmium alloy, dissolution of Zr by solid steel, oxidation, degradation and release of  $B_4C$  control rods, oxidation/dissolution of relocating and relocated U-O-Zr magmas, oxidation of solid debris particles.

Material melting, 2D movement of magmas, debris formation and vertical collapse, molten

pool formation, corium slump into the lower plenum are also modeled, including corium jet fragmentation on contact with water.

In the lower plenum, a 2D meshing of the vessel lower head wall, combined with a 0D approach within the plenum volume accounting for 3 stratified liquid corium layers (light metallic layer, oxide pool, heavy metallic layer) and 2 possible debris layers.

At vessel lower head rupture, melt-through or mechanical failure (plastic or creep rupture) is modeled, accounting for the corium and water loading on the lower head wall and also for the possible vessel wall partial melting.

MEDICIS [6] module simulates Molten-Core-Concrete Interaction (MCCI) after vessel rupture and corium slump in the cavity, using a lumped-parameter 0D approach with averaged corium layers. It models concrete ablation, corium oxidation and release of steam and non-condensable gases ( $H_2$ ,  $CO$ ,  $CO_2$ ) into the containment. Corium remaining in the cavity interacts with concrete interfaces. Either a well-mixed oxide/metal pool configuration or pool stratification into separate oxide and metal layers can be assumed; the possible switch between homogeneous and stratified pools is evaluated through criteria using the superficial gas velocity, and density differences between oxide and metal. In both cases the possibility of an upper crust formation is taken into account. Element speciation, thermodynamic data as liquidus temperatures or enthalpies, thermo-physical properties as density, viscosity are taken into account and assessed via the Material Data Bank of ASTEC.

Between the pool bulk and the concrete interface, a convective zone and a possible conductive zone described as a crust and a slag layer are modeled as the corium/concrete interface; the energy exchange between the corium and the containment involve radiative heat transfer, as well as gas production.

For EPR plants, special modeling has been performed to account for corium pouring kinetics from the cavity towards the core-catcher; the evaluation of the melt spreading capability

allows to evaluate the spreading radius and, thus the spreading duration of corium, the thickness of the spread corium and of the spread solidified part, and finally the duration for corium to reach the trigger and the time for the beginning of corium quenching by water injection above corium.

ISODOP module, if provided an initial fuel inventory, simulates radioactive isotopes decay and its associated power production, in different zones of the reactor or containment. The assessment is based on the JEFF (Joint Evaluated Fission and Fusion) database [7], including about 3800 isotopes.

## II.2 Fission products related modules

ELSA [8,9] simulates the release of fission products (FP) and structural materials from the degraded core. It is tightly coupled with the ICARE module.

Considering actinides and fission products, a classification based on volatility has been elaborated and associated to a limiting process modeling: the volatile, the semi-volatile and the low-volatile elements.

The release of volatile elements (noble gases, Iodine, Cesium, Tellurium for example) is assumed to be related to solid-state diffusion through grains of  $\text{UO}_2$  fuel matrix, taking into account fuel oxidation and grain-size distribution. Tellurium trapping in the cladding, depending on the temperature and on the degree of cladding oxidation is modeled. At fuel melting, remaining volatile species located in the liquid part of the fuel are supposed to be instantaneously released.

The release of semi-volatile fission products, among which notable elements such are ruthenium, molybdenum, strontium, barium are included, is assumed to be related to evaporation and mass transfer processes at the interface of carrier gas/solid matrix. Species like ruthenium are, according to this modeling, slightly released in reducing conditions and largely released when the fuel oxygen potential is high.

Low-volatile species include actinides and other notable species such as technetium. Their release is based on the  $\text{UO}_2$  volatilization as  $\text{UO}_3$  species.

This classification and associated modeling is used either for early degradation fuel rod configuration, but also for debris bed configuration, the difference lying mostly in some macroscopic properties such as surface to volume ratios.

Considering the molten corium pool configuration, given the high-temperature conditions, the chemical equilibrium is assumed in the magma so that the release is governed by mass transfer and evaporation processes from the free surface. Central to the modeling is the calculation of the vapor pressures of the elements in the molten pool, a non-ideal solution chemistry assumption being made for phase distribution.

TEST	Description
MCE-1, HCE2-CF2, HCE2-CM2 HCE3 [30,29]	CANDU UO <sub>2</sub> fuel fragment, low burn up (except for HCE2-LM2) max. temperature 1623-2273 K Air, Ar/(H <sub>2</sub> or O <sub>2</sub> ), steam
HEVA [11-14]	Short re-irradiated cladded PWR fuel rod 36.7 GWj/tU max. temperature 2070-2370 K steam/H <sub>2</sub> , except HEVA6 in H <sub>2</sub>
VERCORS, VERCORS HT and RT [16]	Cladded re-irradiated PWR fuel rod, 37 to 55 GWj/tU max. temperature 2130-3170 K Steam, steam + H <sub>2</sub>
ORNL HI or VI [17,26]	Cladded PWR fuel rod 10 to 47 GWj/tU max. temperature 1675-2720 steam, H <sub>2</sub> or H <sub>2</sub> / steam
WP2-2/1 [27]	Cladded PWR fuel rod, ceramic melt 57 GWj/tU 2928 K Inert atmosphere
EMAIC [28]	cladded SIC control rod + tube guide Steam or steam + H <sub>2</sub>
FPT1 to 3 [9]	Cladded re -irradiated PWR fuel rod max. temperature 2450-2650 K Integral test
FPT4 [9]	Debris bed of PWR fuel rods + clad max. temperature 3273 K Integral test

Table 1 Experimental validation base of ELSA  
module

Finally, for Silver Indium Cadmium (SIC) elements and steel materials, release is described by evaporation and mass transfer processes: silver, indium, cadmium are released from degraded SIC control rods at the control rod failure. It is followed by the release from free surface of the control rod and its molten alloys

during their candling along the rod external surface. Iron, nickel, chromium are released during the candling of steel materials, using the same type of modeling.

ELSA models have been tested on an experimental database involving about forty tests (Table 1), analytical or integral, including different types of configurations, from fuel fragments up to debris beds or molten pools. The database will be extended in a near future to the CEA VERDON tests including MOX fuels. Considering fuel degradation and fission products release, the influence of fuel type, burn-up, thermal conditions and carrier gas composition was assessed. In a large number of cases, the fuel was re-irradiated in order to follow short lived fission products.

SOPHAEROS [10] module simulates the transport of vapours and aerosols in the reactor coolant system and in the containment, approximated to control volumes, accounting for the chemical reactions in vapour or liquid phase, and aerosol physics. Using five physical states (suspended vapours, suspended aerosols, vapour condensed on walls, deposited aerosols, sorbed vapours), SOPHAEROS is based either on a mechanistic or a semi-empirical approach to model the main aerosol and liquid or vapour-phase phenomena.

Considering aerosol phenomena, agglomeration, gravitational, brownian diffusion, turbulent diffusion are modeled. For deposition mechanisms, eddy impaction, sedimentation, thermophoresis, diffusiophoresis, impaction in bends, or flow contraction can be simulated. Revaporisation, mechanical resuspension are taken into account, based either on the "Force Balance" model or on the "rock and roll" one. At last, a dedicated pool scrubbing model accounts for the retention of aerosols in the secondary side of flooded steam generators for Steam Generator Tube Rupture scenarios.

Liquid or vapour-phase phenomena take into account chemisorption of vapours on walls,

homogeneous or heterogeneous nucleation, condensation/revaporisation on/from aerosols and walls. For chemical reactions, two different assumptions may be taken into account: gas equilibrium chemistry, assessed through the Material Data Bank, or kinetics chemistry, which might not be neglected compared to transport phenomena when concentrations or temperatures are too low ; this might indeed be the case in the primary circuit, and influence the gaseous iodine mass fraction at the break, which is an unexpected result of PHEBUS-FP programme, especially the FPT3 experiment involving boron

carbide control rods : a gaseous iodine fraction of 30%/c.i. was observed at the Reactor Coolant System (RCS) break. It was afterwards considered that iodine chemistry in the RCS may potentially be affected by other elements like Cs, Ag, In, or Cd, Mo, B and this led to separate effects tests : CHIP programme focused on iodine interactions with caesium, molybdenum and boron, confirming the possibility of significant gaseous iodine mass fraction at the RCS break. The effect of SIC is being investigated in the ongoing CHIP+ program conducted at IRSN.

	Experiments	phenomena
Aerosol physics	TUBA	Thermophoresis, diffusiophoresis
	DEPAT	Eddy impaction, resuspension in turbulent flow
	LACE	Eddy impaction, bend impaction
	TRANSAT	Settling, eddy impaction, bend impaction
	STORM	Thermophoresis, eddy impaction, mechanical resuspension
	ADPFF	Settling, eddy impaction, bend impaction
Vapour	DEVAP	Condensation and chemisorption
	AERODEVAP	Heterogeneous nucleation, condensation and vapour-aerosol interaction
	FALCON	Chemistry, condensation and vapour-aerosol interaction
	REVAP-ASSESS	Revaporisation
	CHIP	Kinetics of Cs-I-O-H system in RCS
Iodine Chemistry in containment	CAIMAN	Mass transfer phenomena
	ACE PHEBUS RTF	Liquid and gaseous chemistries and mass transfer phenomena
	Radiolysis tests	Liquid chemistry (oxidation of I <sup>-</sup> )
	EPICUR	Gaseous chemistry (Org-I formation)
	PARIS	Gaseous chemistry (I <sub>2</sub> oxidation)
	SISYPHE	Mass transfer phenomena (liquid-sump)
	BIP	Gaseous chemistry (Org-I formation)
	PhD academic studies	Liquid and gaseous chemistries, mass transfer
	CARAIDAS	Iodine removal by spray
	European projects of the 4th and 5th FwP	Liquid and gaseous chemistries
	Literature data	Liquid and gaseous chemistries
Integral	VERCORS [16]	Overall phenomenology
	HCE [30]	
	Phébus.FP	

Table 2 Experimental Validation base of SOPAHEROS

Considering ruthenium behaviour, OECD STEM/START (Study of the TrAnsport of RuThenium in the primary circuit) experimental programme shall supplement the validation database.

In ASTEC v2.1 version, the former IODE [31,32] module reactions have been integrated as a part of SOPHAEROS module, and therefore one single solver is used for iodine chemistry in RCS and in containment; SOPHAEROS enables the simulation of all iodine species in containment, aerosol or gaseous ones, as well as ruthenium behaviour.

Iodine modelling in containment involves about 40 phenomenological models focused on the predominant chemical reactions in the sump, in gaseous phase, and mass transfer reactions at the liquid-sump interface or at the surfaces. The kinetics of the chemical transformations of iodine in the reactor containment building take into account three kinds of processes: thermal reactions, radiolytic reactions and mass transfer processes. The iodine species involved in the reactions in the containment are  $I_2$ ,  $CH_3I$ ,  $I$ ,  $IO_3^-$ ,  $HOI$ ,  $AgI$  and  $I_2O_5$ . Other relevant species, like  $Ag$  (from in-core control rods),  $Ag_2O$  ( $Ag$  oxidised in the containment),  $CH_3R$  (organics),  $R$  (organic radicals),  $O_2$  and  $O_3$  are also taken into account. For the ruthenium compounds in the containment chemistry, species are gaseous  $RuO_4$  and aerosol  $RuO_2$ .

Considering mass transfer, exchanges between sump and gaseous phase for diffusion/convection processes are modeled, as well as the effect of steam condensation on the walls and on the sump surface. Transfer of non-volatile iodine oxides towards the sump are also accounted for.

The effect of spray on molecular iodine is modeled through mass transfer between gaseous phase and droplet, interfacial equilibrium at the droplet surface and liquid mass transfers inside the droplet being assumed; chemical reactions in the bulk liquid are also taken into account. The module computes kinetics of the overall gaseous iodine removal process during the droplet fall down and the output information is the rate of

capture of  $I_2$  for each compartment (for  $CH_3I$  the removal is supposed to be negligible).

At last, adsorption/desorption of molecular iodine on painted, steel and concrete walls, is modeled.

Chemical reactivity in the liquid phase (i.e. sumps) is taken into account through a number of reactions listed hereafter:

- hydrolysis of molecular iodine  $I_2$ ,
- $HOI$  dissociation/disproportionation,
- Oxidation of  $I^-$  by the oxygen dissolved in the sump water,
- radiolytic oxidation of  $I^-$  into  $I_2$  in the sump, where oxidation depends on the production rate of  $OH$  radicals, and where  $I_2$  reduction is temperature, pH and  $[I^-]$  dependent,
- reduction of iodates by radiolysis into molecular iodine,
- silver iodide ( $AgI$ ) formation by heterogeneous reactions (both  $Ag_2O/I^-$  and  $Ag/I_2$  reactions are considered, the reaction of  $Ag_2O$  with  $I^-$  depending on the solubility of  $Ag_2O$  and  $AgI$ ),
- formation of organic iodide  $RI$  by homogeneous reaction in the liquid phase with the Taylor's homogeneous model: solvents are released from paint in liquid phase, then oxidised under radiation to form organic acids, and finally  $RI$  are formed by interaction between  $I_2$  and solvents or sub-products,
- decomposition of organic iodides in the liquid phase, according to two possible destruction processes (either radiolysis or hydrolysis).

The gaseous phase chemical reactivity has been improved in the last version of ASTEC, by taking into account latest results of the EPICUR programme as follows :

- Ozone ( $O_3$ ) formation, considered as a surrogate of the air radiolysis products,
- organic iodide formation, either by a homogeneous model or by a heterogeneous model linked to iodine adsorption onto paint. It consists of a 3 sites adsorption surface from which organic and inorganic iodine are released under irradiation (Figure 2),
- oxidation of molecular iodine into iodine oxides (simplest form iodate) by air radiolysis

- products.- Decomposition of iodine oxides into organic iodides,
- radiolytic oxidation of organic iodine into iodine oxides (simplest form iodate),
- Decomposition of iodine oxides into organic iodides.

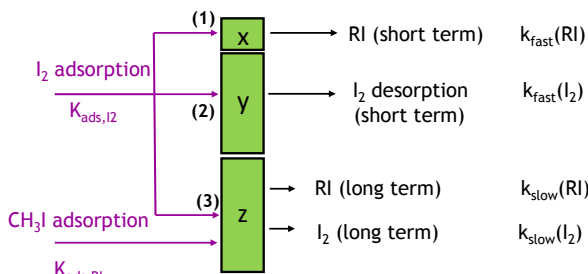


Fig. 2. ASTEC 2.1 modeling of organic iodine production in gaseous phase

Regarding ruthenium, the main modeled reactions are:

- Decomposition in bulk phase (dry and moist air) of the ruthenium tetroxide  $RuO_4(g)$  coming from the RCS into ruthenium deposits,
- ruthenium ozonation (reaction between ruthenium deposits and ozone).
- oxidation of ruthenium deposit due to the action of air radiolytic products (revolatilisation from  $RuO_2$  surface deposits producing  $RuO_4(g)$  at low temperature).

DOSE module was designed to supply dose rates for gaseous radiolytic reactions. This module allows evaluating the dose rate in bulk gaseous phase for each zone of the containment, as well as the inner wall dose rate.

### II.3 An example source term calculation using ASTEC

The hereafter described sequence is one of the first ST sequences calculated using ASTEC version 2.1. It is a PWR 900 MW sequence (see Table 3 for scenario description), the initiator is a 12"LOCA on the cold leg of the pressurizer loop. Containment spray system is unavailable, as well as safety injections systems when switching to recirculation mode.

time	event
0 s	12" break opening on cold leg
0,2 s	Reactor shutdown
3,5 s	HP Injection on containment high pressure criterion
3,8 s	Primary pumps shutdown on high containment pressure and low pressurizer pressure criterion
1 min 07 s	Injection by water tanks
1 h 21 min	Loss of injection when switching to recirculation
2 h 09 min	Clad burst
2 h 13 min	Material structure release
2 h 16 min	First corium slump
5 h 04 min	Vessel rupture ; MCCI onset
3 d 07 h	Containment venting system activation
11 d	Basemat rupture

Table 3 : PWR 900 LOCA sequence description

Reactor automatic shutdown occurs at 0.2 s on low primary flow criterion, which triggers turbine insulation. Steam generators normal feedwater circuit is then isolated at 2.2 s on high water level criterion. In the containment, the pressure build up triggers safety injection at 3.5 s, itself triggering in turn the onset of safety steam generators feedwater circuit. Primary pumps stop at 3.8 s on high pressure level in containment and low pressure level in primary circuit. The accumulators discharge starts at 1 min 07 s when primary circuit pressure reaches 42 bars, and are isolated when primary pressure passes below 15 bars. Safety injection is lost at 1 h 21 s when asking recirculation on low water level criterion reached in water tank.

	Sand bed filter efficiency with pre-filtering	Sand bed filter efficiency
Aerosols	99,9%	99,0%
$I_2$	90,0%	90,0%
$CH_3I$	0.	0.
$I_2O_5$	90,0%	90,0%

Table 4: assumed filtration efficiencies for iodine species

Fission products and structural material are released in a short period of time near 2 h 13 min

(Table 3); the available silver is entirely released in the primary circuit, 988.28 kg being released to the containment; considering iodine, 16.70 kg are released from the core, among which about 43% deposits on the cold legs, under CsI, Cs<sub>2</sub>I<sub>2</sub>, I<sub>3</sub>La, INi forms. The iodine release to the containment amounts to 9,5 kg, 2% of the total being under gaseous form.

The first corium slump in the reactor vessel occurs at 2 h 16min, and the vessel breaks down at 5 h 04min. 65 tons of corium slump down in the reactor pit. Secondary slumps occurring over two hours duration period lead to a final total amount of 140 t of corium in the reactor cavity. The reactor pit being made of limestone iron reinforced concrete, the gas emission tend to swirl and homogenize the corium, and therefore radial and axial ablation have the same kinetics.

The MCCI induced gas production tend to accelerate pressure build up in containment, leading to containment venting system activation (CVS) at 3d 7h on the reach of high pressure criterion in the dome (Figure 4). At this time, the iodine species in the containment atmosphere are gaseous species, the aerosols being entirely deposited (Figure 5 and 6). In sumps the pH is 5.0 because no soda is injected, and the temperature is high (~400 K) because of the absence of recirculation cooling in the considered scenario. Therefore, after CVS activation, when pressure starts to decrease, evaporation conditions in sumps are met, and iodine is transferred to the containment atmosphere; the sand bed filter is supposedly inefficient for organic iodine, and an efficiency of 90% for molecular iodine and oxides is assumed (Table 4). In these conditions, the overall iodine release to the environment through the FCVS is ~0.15g, leading to a global iodine mass release of 0.19 g considering direct leaks (Figure 7).

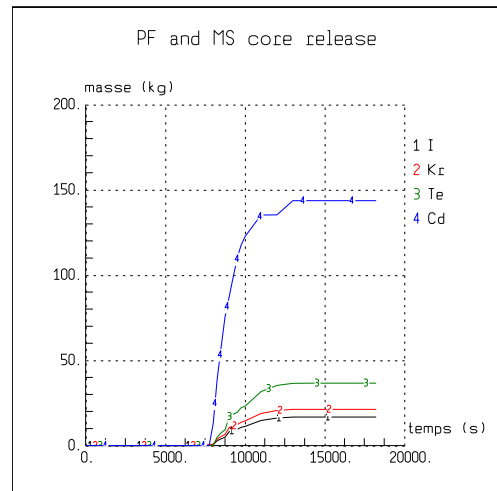


Fig. 3. Iodine release from core

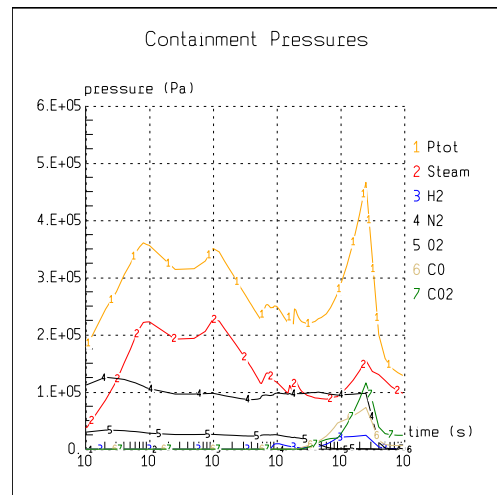


Fig. 4. Pressure in containment

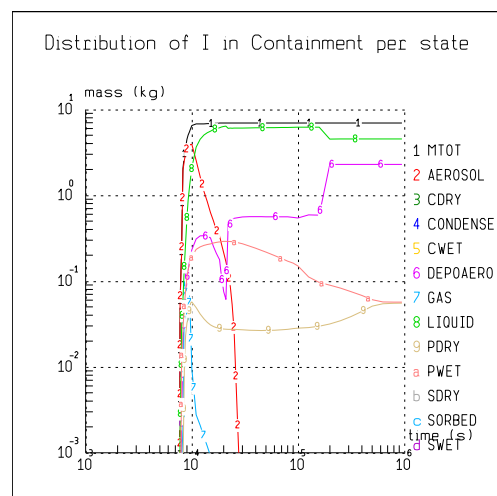


Fig. 5. Iodine distribution in containment

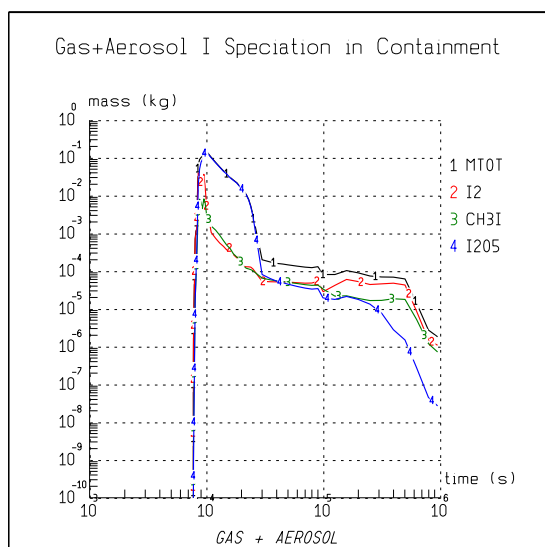


Fig. 6. Iodine speciation in containment gaseous phase

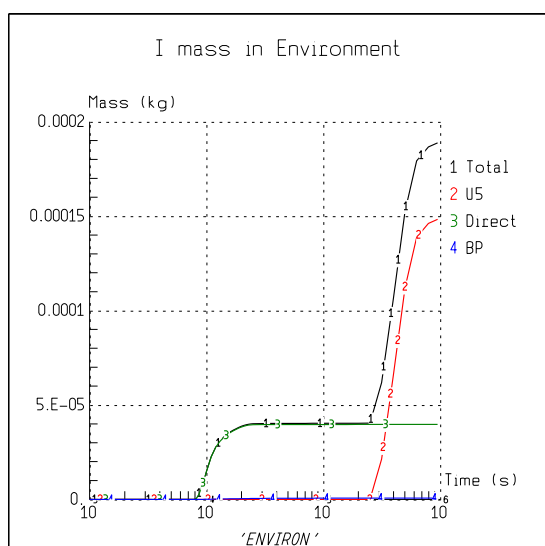


Fig. 7. Iodine release to environment (U5 = through FCVS, direct = direct leaks)

This simulation is a preliminary one with the recent release of ASTEC v2.1. It has been performed with best estimate modeling using most recent research and development data. The order of magnitude of remaining iodine related uncertainties is ongoing and their influence will be evaluated in the future for an entire accidental sequence, using the IRSN uncertainties propagation tool, SUNSET.

### III. LEVEL 2 PROBABILISTIC SAFETY ASSESSMENT: MER

#### III.1. Presentation

The risks reduction obtained by improved or new accident prevention and mitigation measures is assessed at IRSN using Level 2 PSA by comparing the situation before and after taking into account safety improvements, notably in terms of reduction of radiological consequences. The MER code [33,34] for environmental releases estimation is fast-running with a precision fitted to the purpose.

MER takes into account the boundary conditions elaborated by the APET and its associated support calculations, summarized in Table 5.

For a given sequence, MER can produce some detailed post-processing. Last years have been devoted to the achievement of a realistic modeling of nuclear accident consequences and to enhancement of legibility, for acceptance in decision making process. That includes the extension of the traditional radioactive release assessment to the evaluation of radiological consequences, based on MERCOR module.

There are two MER models at IRSN, one for the 900 MWe French PWR and the other for the 1300 MWe French PWR, a model for EPR being planned for the future. The 1300 MWe PWR model includes recent results from the IRSN R&D on ST modeling, notably those of the ISTP and STEM programs. The 1300 MWe version includes a modeling of double containment and more detailed modeling for the chemical species.

MER is based on the resolution of mass conservation equations, allowing the description of different kind of phenomena such as mechanical phenomena like the deposition, or chemical phenomena like radiolysis reactions.

According to the importance of the different phenomena on ST, several approaches can be used to construct these models for MER:

- a first approach consists in integrating the complex models and simplifying the calculation of some non-preponderant physical parameters of the models; the

identification of non-preponderant physical parameters can be performed by different methods like experimental designs or expert judgments;

- a second approach consists in integrating directly R&D program results; to illustrate this approach, in case of SGTR accident, MER evaluates the retention in the primary and secondary circuits thanks to ARTIST results;
- an approach consists in designing a mathematic correlation based on a particular assessment; for example, MER uses a correlation for modeling the aerosol behavior based on ASTEC support studies for reactor cases. The aerosol behavior within the containment building is subjected to different phenomena like agglomeration and deposition; it is not possible to evaluate simply the particle size evolution to model the agglomeration. This is the reason why we use a correlation for the evaluation of deposition coefficient which englobes all the deposition processes; the last approach consists in integrating a model based on engineer judgment because of a lack of knowledge. This approach allows the evaluation of the

importance of the phenomenon through a risk or consequence assessment.

The simplified models related to FP behavior are:

- the in-vessel release of fission products;
- the fission products retention in the primary and secondary circuits;
- aerosols resuspension mechanisms inside the primary system;
- ex-vessel release of fission products: release of aerosols from a boiling sump, release during molten corium-concrete interaction, aerosols resuspension mechanisms inside the containment building (in case of hydrogen combustion, in-vessel steam explosion, reflooding);
- the behaviour of the aerosols within the containment building: agglomeration and deposition, aerosol depletion by spray;
- ruthenium and iodine chemistry.

APET Phase	RC variable	Range
In-Vessel core degradation	CHRS availability	Yes/ partially/ No
	Containment break size	0.065 cm <sup>2</sup> to total failure
	Delay before containment failure	No failure At the beginning of the phase At the end of the phase
	Delay before vessel break	From 1 hour to 16 hours
	RCS fission products retention	Yes/no
	Core reflooding	Yes/no
	Energetic phenomena in RCS	Yes/no
	Average primary pressure	From 3 to 80 bar
	SGTR	No SGTR, SGTR with empty SG 1 or 2 tube(s) 10 tubes Induced SGTR
	Leakage by containment isolation failure ( $\alpha$ mode)	0.065 cm <sup>2</sup> to 50 cm <sup>2</sup>
	Venting system functioning	yes/partially/no
	Filtration type	Iodine filters High efficiency filters No filtering
	V-LOCA	Yes/no
	Energetic phenomena in containment	No energetic phenomenon ex-vessel steam explosion hydrogen combustion
Vessel rupture	Containment break size	0.065 cm <sup>2</sup> to total failure
	vessel rupture mode	No rupture Non energetic rupture Steam explosion
Ex-vessel phase	CHRS availability	Yes/ partially/ No
	Containment break size	0.065 cm <sup>2</sup> to total failure
	Leakage by containment isolation failure ( $\beta$ mode)	0.065 cm <sup>2</sup> to 50 cm <sup>2</sup>
	First containment failure mode	No failure, H <sub>2</sub> /CO combustion, U5 filter (FCVS), Containment slow pressurization Failure of containment isolation valves
	Energetic phenomena in containment	hydrogen combustion, ex-vessel steam explosion,
	Delay before containment failure	0 hours to up to 30 days
	Venting system functioning	yes/partially/no
	Filtration type	Iodine filters High efficiency filters No filtering

Table 5 accident progression variables

The modelling of iodine behaviour in MER takes into account the following issues:

- the fraction of gaseous iodine released from the RCS;
- the iodine oxides (IO<sub>x</sub>) formation and destruction in the gaseous phase by the reactions between I<sub>2</sub> or organic iodine with air radiolysis products;
- the iodine adsorption/desorption onto paints in gaseous phase;
- the production of organic iodine in the atmospheric part of the containment from iodine adsorbed onto paints;
- destruction of organic iodides in the gaseous phase;

- the radiolytic oxidation of iodide ions into molecular iodine (I<sub>2</sub>) in the liquid phase;
- the iodine adsorption onto paints in liquid phase;
- I<sub>2</sub> formation by metallic iodine reaction into the recombiner.
- the formation of AgI by reaction with iodide ions and molecular iodine (I<sub>2</sub>)

The modeling of ruthenium is based on:

- the release in case of degraded fuel contact with air,
- the release into the containment building in gaseous form (ruthenium tetroxide),
- the adsorption and desorption of gaseous ruthenium on metal and painted surfaces,
- the re-volatilisation of ruthenium deposited on the surfaces, under irradiation and ozone action,
- the re-volatilisation of ruthenium trapped in the liquid phase under irradiation and ozone action.

In a L2 PSA, the gaseous form of ruthenium (ruthenium tetroxide) is considered as a non-filtered species.

The following species are taken into account:

- noble gases;
- volatile aerosols;
- semi volatile aerosols;
- ruthenium aerosols;
- ruthenium oxide (RuO<sub>2</sub>);
- ruthenium tetroxide (RuO<sub>4</sub>);
- iodine aerosols (aerosols containing I such as CsI);
- molecular iodine I<sub>2</sub>;
- organic iodine ICH<sub>3</sub>;
- iodine oxide IO<sub>x</sub>,
- iodide ion, molecular iodine I<sub>2</sub>, AgI and organic reactive compounds contained in the paint in sumps.

The outputs of the assessment are the following:

- environmental release (mass or activity) for each fission products group, for each phase of the accident and each release pathway;
- suspended activity/mass in the buildings;
- fission products deposits in the buildings;

- fission products retained mass in the filters of ventilation systems;
- dose equivalent and thyroid dose at given points (in the axis of the plume) versus time (corresponding to total release and each pathways);
- deposited activities 2 weeks from the beginning of the accident, among which <sup>137</sup>Cs deposited activity (corresponding to total release and each pathways);
- data linked to emergency preparedness: the time when counter-measure levels are reached. At a given time, the geographical extent of each countermeasure;
- the calculation of the INES level of the accidental sequence.

L2 PSA allows the risk assessment by integrating uncertainties. These uncertainties are related to modeling error, lack of knowledge about physical phenomena, or scenario uncertainties. In L2 PSA, the uncertain parameters can be gathered in four groups:

- concerning the accidental scenario (mainly the containment break size for certain types of containment failures, the duration of in-vessel core degradation phase and molten corium concrete interaction phase, etc.);
- concerning the aerosol behavior (mainly releases from fuel, retention in circuits, fraction of wall-deposited aerosols that subsequently undergo resuspension, etc.);
- concerning the iodine behavior (mainly the fraction of gaseous iodine released at the RCS break, the iodine adsorption/desorption onto paints in gaseous phase, the production of organic iodide from paints etc.);
- concerning the ruthenium behavior (mainly releases from fuel, retention in circuits, etc.).

The evaluation of their impact is assessed using a probabilistic Monte Carlo method based on Latin Hypercube Sampling. For each of these numerical results, statistical distribution percentiles are evaluated: 5%, 50%, and 95%. The average value is also calculated.

### III.2. Validation process

The MER validation process includes three steps. To illustrate the validation process, the iodine

behavior into the containment (liquid and gas phases) is given thereafter.

Before performing an ASTEC/MER comparison for different sequences, the unitary validation of MER models is realized first by comparison with ASTEC models and a specific assessment. The unitary validation corresponds to a comparison of the results of a chemical model only in the liquid or gaseous phase. Figure 8 illustrates this step by presenting the comparison of the radiolytic oxidation of iodide into molecular iodine between MER and ASTEC.

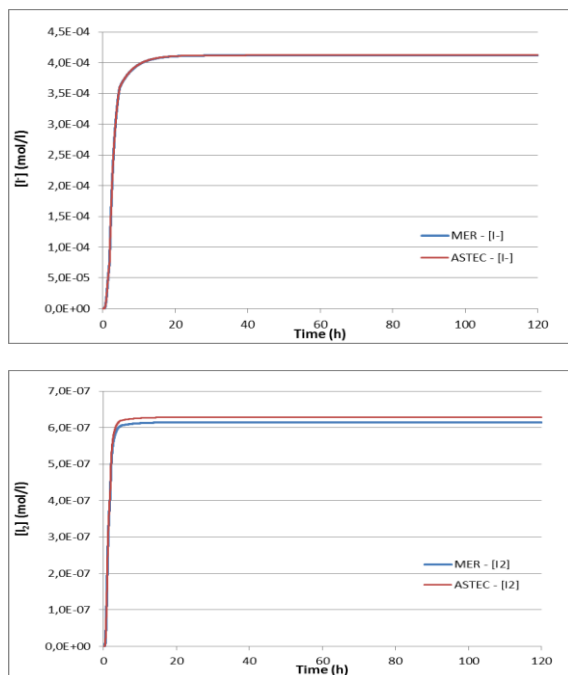


Figure 8: radiolytic oxidation of iodide into molecular iodine, unitary validation

After comparing each elementary reaction, an overall validation is performed for each phase (gas and liquid). The MER model considers a limited number of reactions representative of the main reactions occurring in the liquid phase. Figure 9 illustrates the impact of these simplifications.

As mentioned before, the last stage of MER validation process uses ASTEC code for different accident categories (LOCA, SGTR, blackout situation etc.). The validation consists in comparing the ST kinetics and amplitude in terms of released activities and masses as shown in Figure 10. It is thus necessary to compare the

behavior of fission products in the containment, in particular the different iodine species, as illustrated by Figure 11.

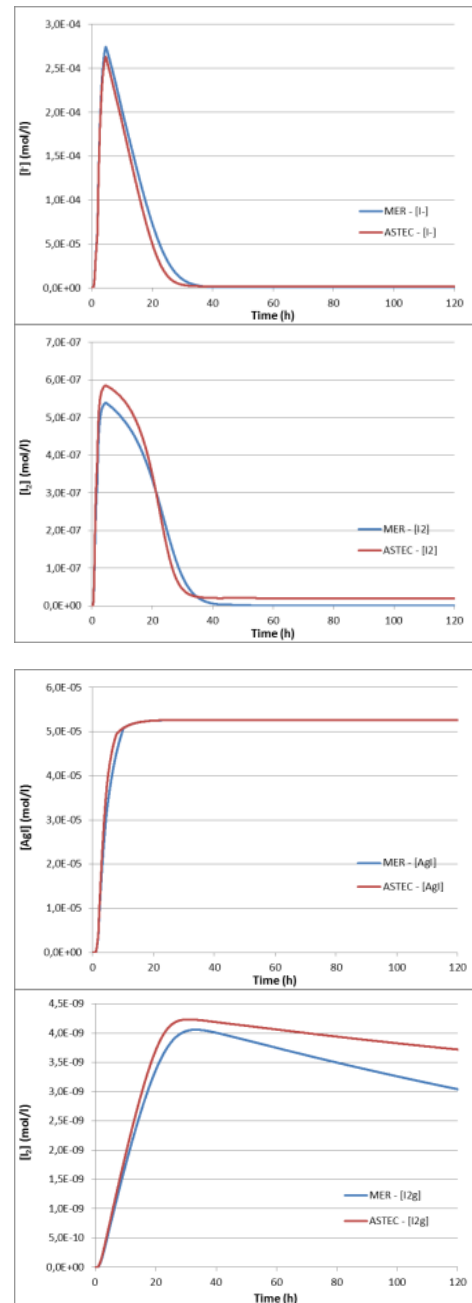


Figure 9: iodine behaviour in liquid phase - overall validation

The validation of iodine behaviour can be detailed with the comparison of chemical reaction kinetics allowing the identification of preponderant reactions.

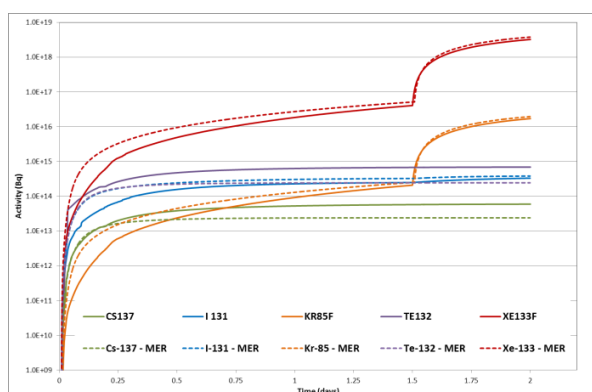


Figure 10: ASTEC/MER comparison: elements and isotopes activities.

Finally, after performing the validation with ASTEC, a comparison can be realized with PERSAN, although model assumptions are different. MER performs realistic calculation with uncertainties evaluation which corresponds to the R&D knowledge, while PERSAN performs more consolidated and conservative calculation. The 95 percentile of MER calculations could be compared to the PERSAN result while the median could be compared to the ASTEC calculation.

### III.2 An example source term calculation using MER

To illustrate an example of MER use, we have chosen to present the results of the French 900 MWe PWR PSA level 2 study. Figure 12 details the global risk of the French 900 MWe PWR. For this, the release into environment, the radiological consequences and the INES level were calculated with MER.

At this step, for this study, around one thousand scenarios of release are found, associated with an environmental release for each phase of the accident and with radiological consequences.

## IV. EMERGENCY SOURCE TERM ASSESSMENT: PERSAN

### IV.1. Presentation

For the technical emergency center staff a suite named Software for Emergency Situations and Assessment Methodology, SESAME, has been

developed and is operationally used to meet the needs of the emergency responder experts. Each tool of the SESAME suite is devoted to one specific field of expertise. Among these 8 specific tools, two thermo-hydraulic softwares are devoted to the determination of the break size and the delay before the core may be uncovered. The information given by these tools is then used as input for the two different ST calculation tools, one devoted to Steam Generator Tube Rupture (SGTR) situations the other made for Loss of Coolant Accident situations (LOCA).

The fast-running Program for Evaluation of Release during a Severe Accident on a Nuclear reactor, PERSAN, assesses the releases to the atmosphere for LOCA situations. This operational software has been designed and developed to be used by experts during emergency situations. One of the main constrain which has been imposed throughout the conception and the development of the software is a very short computing time; in order to be able to assess iteratively some key parameters of the plant during the diagnosis stage of the expertise. Furthermore, some sensitivity studies are also needed to estimate the influence of some uncertainties on the atmospheric releases (i.e. equipment availability), require that the software to run rapidly. The computing time of PERSAN is lower than one minute to calculate 24 hours of release. The accident progression and physical phenomena occurred in the reactor does not change the computing time.

Getting reliable information on the plant condition is complex and uncertain during the development of the accident. Consequently, the lack of information must not prevent the estimation of STs. The Fukushima accident confirms this point where evaluations of radiological consequences were mandatory to protect the surrounding population but also to give the world a general understanding of the developing situation. Moreover, limiting the number of hypothesis as input of expertise emergency response software is a paramount concept to insure a proper expertise process.

The main input assumptions in PERSAN code are: buildings leak rates, fuel damage,

containment pressure evolution, long term availability of containment spray system and of ventilations systems in the auxiliary buildings. The measured buildings leak rates obtained during containment building tests are used as default input assumptions. STs calculated by PERSAN are realistic but are believed to be conservative in term of quantities released or chemical form produced in regards with the radiological consequences. The uncertainties which still exist on many physical phenomena arising during a core melt require, for emergency response, to use a conservative approach for the selection of model parameters as, for example, for the release rate of some chemical element in primary circuit.

The PERSAN models are based on fission products mass balances. The FP concentration in suspension in each building depends of the mass emitted in the building, the mass deposit and the building leak rate. Several correlations are used for the aerosols deposition. These correlations depend mainly on the building type, the mass in suspension and the thermohydraulic conditions. The deposition laws in containment building vary during FP emission, after the emission, with the use of spray system and during concrete interaction with melt core. Especially, the molecular iodine is deposited in the containment building on painted wall and by the containment spray system. All deposition correlations have been calculated with an ASTEC module. The validation has been realized with ASTEC with a large representative sample of accident scenarios.

The current iodine chemistry model in liquid and gaseous phases has been developed by IRSN R&D and emergency experts few years ago.

In the gaseous phase, a part of the molecular iodine is adsorbed by painted walls. The adsorption rate is given by empiric formula which depends of wall temperature. The production of organic iodine by paints is simplified. The molecular iodine adsorbed by paints is immediately transformed into organic iodine on the basis of a conversion coefficient.

The iodine behaviour in the liquid phase is more complex. The sumps of containment building are

an important source of molecular iodine for French 1300 MWe and 1450 MWe PWRs. The iodine aerosols emitted in the building are deposited on walls, sumps, etc. The deposition repartition between all elements in buildings is hard to determine and requires a detailed modeling. PERSAN uses a simplified modeling which insures an upper bound evaluation of the ST. The deposition model considers that all iodine aerosols are deposited in sumps.

The liquid phase model is based on ASTEC model. The amount of molecular iodine release by sumps depends of the liquid volume, the pH, the temperature, the silver concentration and the dose rate. All these parameters, except the silver concentration, are to be set before the start the ST calculation. The silver emission from control rods is not modeled in PERSAN. A representative silver concentration is imposed in the model.

In the case of 900 MWe French PWR, the silver concentration in sumps is considered sufficiently high to trap all iodide. No molecular iodine is released from sumps for this power plant in PERSAN.

The recent research advances on iodine chemistry in containment building already present in ASTEC and MER codes are not yet integrated in PERSAN. This work is under progress. The integration of a new model in crisis tools follows a lengthy validation process and requires secure and well established results from R&D. Indeed, the ST evaluations from PERSAN are used to make recommendations to the French public authorities relative to the population protection during an emergency situation based on calculated doses to the public. The government uses also the calculated protected doses from different type of accident to define preparedness strategies and the management of a severe nuclear accident in France. Thus, the impact of any new model of a process related to ST released into the atmosphere must be carefully evaluated in term of impact on the radiological consequences and on the population protection strategies.

The last produced research on iodine chemistry [32]] showed a large production of oxide iodine in containment building. This specie was not considered in previous models. Uncertainties associated to this new model must be listed as well as the parameters not reachable in emergency situation.

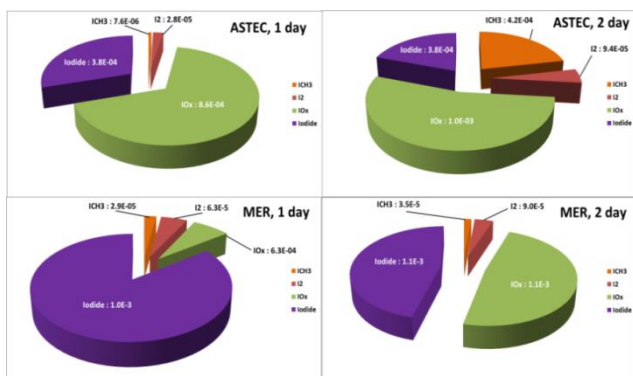


Figure 11: ASTEC/MER comparison: iodine mass speciation at 1 day and 2 days (kg).

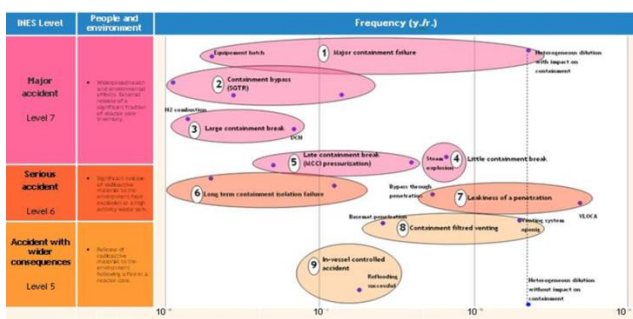


Figure 12: Overall results (IRSN L2 PSA 900 MWe PWR) – Frequency-Consequence diagram – Ines Scale

Afterwards, a simplified modeling shall be developed in accordance with the uncertainties identified and the constraints for an operational use. The model must be validated with ASTEC comparisons. In parallel, a study must be done on thyroid dose associated to this specie (actually no dose coefficient is known for this chemical form). Finally, the consequences of this new iodine chemical model must be studied and

analyzed before to being implemented for the ST calculation in emergency situation.

Concerning iodine chemistry in the reactor building, results of the PHEBUS program have been taken into account for the modeling of the release rate of molecular iodine in the primary circuit. The uncertainty on this parameter is important. Therefore, in order to be reasonably conservative, 25% has been added to the maximum experimental measured rate. The rest of iodine is emitted in aerosol form.

The fission products retention in the primary circuit is an input hypothesis and can be modified by the containment expert. Nevertheless, the localization of the break during an emergency response being difficult, this retention rate is set to zero by default, which is equivalent to setting a default location of the break on the hot leg, ensuring conservatism.

The realization of all these steps requires time and explains the modeling difference between PERSAN and ASTEC on iodine model.

#### IV.2. An example of use: the Fukushima accident source term assessment

During the Fukushima accident, several evaluations of radiological consequences have been realized by IRSN technical emergency centre with STs provided by PERSAN. These calculations require the evolution of the release over the time. Around 40 STs have been calculated during the first two weeks of activity of the IRSN technical emergency center, from March, 11. An example of Fukushima ST published on 18 March 2011 is represented in figure 13. The calculation starts on 11 March 2011 and finishes on 24 March 2011. Each peak corresponds to a containment depressurization which occurred on the damaged reactors.

### V. CONCLUSION

This paper presented various source term assessment tools used at IRSN on different purposes: from the validation of phenomenology comprehension and capitalization, ASTEC is an

integrated tool used for predictive calculations, representative of the knowledge status at a given time.

Fast running tool MER, based on a fitted to purpose precision modeling provides the ability to produce a global insight regarding severe accident related probabilistic safety assessment. The MER validation is based partly on ASTEC/MER comparison.

Finally, conservative modeling for emergency fast source term assessment tool PERSAN, and the cautious incorporation of research and development results provides French public authorities a relevant decision making tool.

For ASTEC and MER, possible uncertainties have to be considered. These are currently under re-assessment at IRSN, for instance integrating the results of R&D programs like OCDE STEM program. Models related to iodine behavior in sumps are now considered mature; a reasonably conservative model, based on remaining uncertainties, can therefore be elaborated for fast running tool PERSAN.

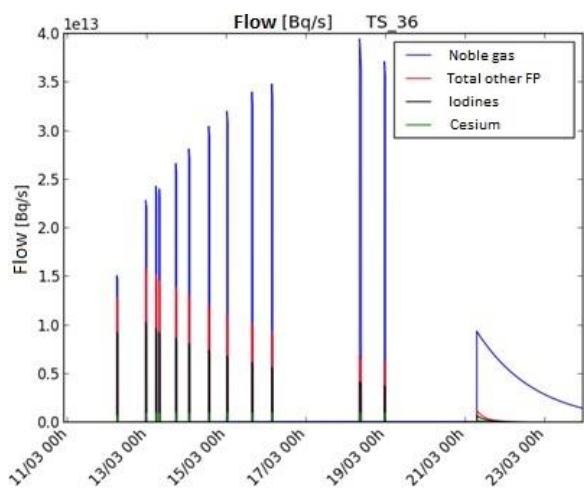


Figure 13 : Source term calculated by PERSAN fast running code during Fukushima accident

NOMENCLATURE

APET	Accident Progression Event Tree
ASTEC	Accident Source Term Evaluation Code
CHRS	Containment Heat Removal System
CVS	Containment Venting System

EPR	European Pressurized water Reactor
FP	Fission product
GRS	Gesellschaft für Anlagen und Reaktorsicherheit mbH
INES	International Nuclear Event Scale
IRSN	Institut de Radioprotection et de Sûreté Nucléaire
L2 PSA	Level 2 Probabilistic Safety Assessment
LOCA	LOss of Coolant Accident
MCCI	Molten-Core-Concrete Interaction
PERSA N	Program for Evaluation of Release during a Severe Accident on a Nuclear reactor
PWR	Pressurized Water Reactor
RCS	Reactor Coolant System
SESAM E	Software for Emergency Situations & Assessment Methodology named
SGTR	Steam Generator Tube Rupture
ST	Source Term
SIC	Silver Indium Cadmium
VVER	Vodo-Vodianoi Energueticheski Reaktor

REFERENCES

1. P. CHATELARD, S. ARNDT, B. ATANASOVA, G. BANDINI, A. BLEYER, T. BRÄHLER, M. BUCK, I. KLJENAK, B. KUJAL, “Overview of the independent ASTEC V2.0 validation by SARNET partners”, *Nuclear Engineering and Design*, **272**, pp.136-151(2014)
2. P. CHATELARD, N. REINKE, S.ARNDT, S. BELON, L.CANTREL, L.CARENINI, K.CHEVALIER-JABET, F.COUSIN, J.ECKEL, F.JACQ, C.MARCHETTO, C.MUN, L.PIAR, “ASTEC V2 severe accident integral code main features, current V2.0 modelling status, perspectives”, *Nuclear Engineering and Design*, **272**, pp.119-135(2014)
3. G.BANDINI, M.BUCK, W.HERING, L.GODIN-JACQMIN, G.RATEL, P.MATEJOVIC, M.BARNAK, G.PAITS, A.STEFANOVA, N.TRÉGOURÈS, G.GUILLARD, V.KOUNDY, “Recent

- advances in ASTEC validation on circuit thermal-hydraulic and core degradation”, *Progress in Nuclear Energy* **52**, 148–157.(2014)
4. I. KLJENAK, M.DAPPER, J.DIENSTBIER, L.E.HERRANZ, M.K.KOCH, J.FONTANET, “Thermal-hydraulic and aerosol containment phenomena modelling in ASTEC severe accident computer code”, *Nuclear Engineering and Design* **240**, pp 656–667 (2010)
  5. P. CHATELARD, J. FLEUROT, O. MARCHAND, P. DRAI, “Assessment of ICARE/CATHARE V1 severe accident code”, ICONE-14 conference, July17–20, Miami, FL, USA. (2006).
  6. M. CRANGA, R. FABIANELLI, F. JACQ, M. BARRACHIN, F. DUVAL, "The MEDICIS code, a versatile tool for MCCI modelling", *ICAPP'05*, Seoul (Korea), May 15-19, (2005)
  7. “The JEFF-3.1 Nuclear Data Library”, *JEFF Report 21, OECD-NEA Data Bank* (2006).
  8. G. BRILLANT, C. MARCHETTO, W. PLUMECOCQ “Fission product release from nuclear fuel I. Physical modelling in the ASTEC code”, *Annals of Nuclear Energy*, **61**, pp 88–95 (2013)
  9. G. BRILLANT, C. MARCHETTO, W. PLUMECOCQ “Fission product release from nuclear fuel II. Validation of ASTEC/ELSA on analytical and large scale experiments”, *Annals of Nuclear Energy* **61**, pp 96–101(2013)
  - 10.F. COUSIN, M. KISSANE, N. GIRAULT, “Modelling of fission product transport in the reactor coolant system”, *Annals of Nuclear Energy*, Vol.**61**, p.135-142 (2013)
  - 11.LE MAROIS G., “Expérience HEVA Essai HEVA 4”, *CR DMG n° 64/87*, (1987)
  - 12.LE MAROIS G., “Expérience HEVA Essai HEVA 5”, *CR DMG n° 58/88*, (1988)
  - 13.DUCROS G. et al. “Expérience HEVA Essai HEVA 6”, *CR DMG 34/89*, (1989)
  - 14.DUCROS G. et al., “Expérience HEVA Essai HEVA 8”, *CR DRN/SECC 05/90*, (1990)
  - 15.PONTILLON Y., DUCROS G., MALGOUYRES P.P., “Behaviour of fission products under severe PWR accident conditions VERCORS experimental programme Part 1: General description of the programme”, *Nuclear Engineering and Design*, **240, Issue 7**, pp 1843–1852 (2010)
  16. “Synthesis of the VERCORS experimental programme: Separate-effect experiments on Fission Product release, in support of the PHEBUS-FP programme”, *Annals of Nuclear Energy* **61** pp 75–87 (2013)
  - 17.M.F. OSBORNE et al., “Data summary report for fission product release test HI-1”, *ORNL/TM-8500- NUREG/CR-2928*, Oak Ridge National Laboratory, (1982)
  - 18.OSBORNE M.F. et al., “Data summary report for fission product release test HI-3”, *ORNL/TM-8793- NUREG/CR-3335*, Oak Ridge National Laboratory, (1984)
  - 19.OSBORNE M.F. et al., “Data summary report for fission product release test HI-4”, *ORNL/TM-9001- NUREG/CR-3600*, Oak Ridge National Laboratory, (1984)
  - 20.OSBORNE M.F. et al., “Data summary report for fission product release test HI-5”, *ORNL/TM-9437- NUREG/CR-4037*, Oak Ridge National Laboratory, (1985)
  - 21.OSBORNE M.F. et al., “Data summary report for fission product release test VI-1”, *ORNL/TM-11104- NUREG/CR-5339*, Oak Ridge National Laboratory, (1989)
  - 22.OSBORNE M.F. et al., “Data summary report for fission product release test VI-2”, *ORNL/TM-11105- NUREG/CR-5340*, Oak Ridge National Laboratory, (1989)

- 23.OSBORNE M.F. et al., “Data summary report for fission product release test VI-3”, *ORNL/TM-11399- NUREG/CR-5480*, Oak Ridge National Laboratory, (1990)
- 24.OSBORNE M.F. et al., “Data summary report for fission product release test VI-4”, *ORNL/TM-11400- NUREG/CR-5481*, Oak Ridge National Laboratory, (1991)
- 25.OSBORNE M.F. et al., “Data summary report for fission product release test VI-5”, *ORNL/TM-11743- NUREG/CR-5668*, Oak Ridge National Laboratory, (1991)
- 26.OSBORNE M.F. et al., “Data summary report for fission product release test VI-6”, *ORNL/TM-12416- NUREG/CR-6077*, Oak Ridge National Laboratory, (1994)
- 27.KHABENSKY V. B., et al., “Late Phase Source Term Phenomena: Oxidic Melt Experiments (WP2)”, *Leningrad Specialised Integrated Plant “RADON”, St. Petersburg, SAM-LPP-D010*, 2002.
- 28.RABU B., “EMAIC : synthèse des résultats des essais A-B-C et E\*“, *CR DEC/SECI/99-002* (1999)
- 29.LEWIS B. J., COX D.S., IGLESIAS F.C., “A kinetic model for fission-product release and fuel oxidation behaviour for Zircaloy-clad fuel elements under reactor accident conditions”, *Journal of Nuclear Material* **00710** (1993)
- 30.LEWIS B. J., IGLESIAS F.C., C.E.L. HUNT, COX D.S., *Nucl. , Technol.* **99** p330 (1992)
- 31.L.CANTREL, F.COUSIN , L. BOSLAND, K.CHEVALIER-JABET, C.MARCHETTO, “ASTEC V2 severe accident integral code: Fission product modelling and validation”, *Nuclear Engineering and Design*, **272**, pp.195-206(2014)
- 32.L. BOSLAND, L. CANTREL, N. GIRAULT,B. CLEMENT, “Modeling of iodine radiochemistry in the ASTEC severe accident code: Description and application to FPT-2 PHEBUS test”, *Nuclear Technology*, **171**, pp 88-107 (2010)
- 33.T. DURIN , J.DENIS, E.RAIMOND, Y.GUIGUENO, “Very fast running codes for the characterization of severe accident radiological consequences and the results presentation in level 2 PSA”, conference PSAM 11, Helsinki,(2011)
- 34.E. RAIMOND, B. CLÉMENT, J. DENIS, Y. GUIGUENO, D. VOLA, “Use of Phébus FP and other FP programs for atmospheric radioactive release assessment in case of a severe accident in a PWR (deterministic and probabilistic approaches developed at IRSN)”, *Annals of Nuclear Energy* , **61** 190–198(2013)

## IN WHAT EXTENT THE IODINE REACTIVITY IN THE ATMOSPHERE CAN IMPACT THE RADIOLOGICAL CONSEQUENCES

J. Trincal<sup>(1,3)\*</sup>, L. Cantrel<sup>(1,3)</sup>, F. Cousin<sup>(1,3)</sup>, V. Fèvre-Nollet<sup>(2,3)</sup>, P. Lebègue<sup>(2,3)</sup>

<sup>(1)</sup>Institut de Radioprotection et de Sûreté Nucléaire, Saint-Paul Lez Durance, France, <sup>(2)</sup>Laboratoire de PhysicoChimie des Processus de Combustion et de l'Atmosphère (PC2A), UMR 8522 CNRS/Lille 1, France, <sup>(3)</sup>Laboratoire de Recherche Commun IRSN-CNRS-Lille1 "Cinétique Chimique, Combustion, Réactivité" (C3R), Saint-Paul Lez Durance, France

\*Corresponding author, tel: (+33) 4.42.19.91.87, Email: julien.trincal@irsn.fr

**Abstract** – *Following a severe accident on a nuclear reactor, the main radiological consequences are due to the quantity of deposited radionuclides, and more specifically iodine. These quantities can be evaluated by several simulation codes, through deposition velocities of each involved species.*

*However, significant differences between measurements and modeling of iodine radiation levels resulting from the Fukushima nuclear accident have been observed. The gap could be at least partially explained by the fact that the IRSN dispersion tool considers no chemical transformation during transport in the atmosphere, which can appear as a rough assumption because some parameters like the deposition velocity or the dose-effect factor depend on iodine chemical speciation as well as physical forms (gas or particle).*

*In order to quantify the behaviour of the iodine reactivity in the atmosphere, a chemical mechanism of 246 gas phase reactions has been implemented in OD simulation software. For simulations, iodine is injected as gaseous I<sub>2</sub> and/or CH<sub>3</sub>I, which are some iodine species potentially released during a nuclear incident. The calculations are made on 10 days in representative atmospheric conditions, and the influence of many parameters are evaluated, such as the pollution levels (O<sub>3</sub>, NO<sub>x</sub>, VOC), the photolysis conditions, the form and the rate of the injected iodine and the reaction mechanism (inorganic, organic).*

*Concerning the inorganic simulations, result analysis revealed that depending on the simulation parameters, the iodine speciation could be very different. Indeed, iodine is distributed between HI and HIO during the day and between I<sub>2</sub> and IONO<sub>2</sub> the night, which highlights the important impact of day/night cycle. The modification of the photolysis rates (calculated for another date) indicates that the iodinated species photolysis is a fundamental element of the mechanism, leading to the formation of I and IO radicals, which are the central species of the iodine reactivity.*

*Moreover, I<sub>2</sub>O<sub>5</sub> is produced all along the calculation from iodine reactions with O<sub>3</sub>, pointing out the pollutant role in iodine reactivity, especially the O<sub>3</sub>/NO<sub>x</sub> ratio, O<sub>3</sub> being produced from the NO<sub>x</sub> (Chapman cycle).*

*The iodine injection rate variation also showed that iodine reactions with NO<sub>x</sub> constitute a high reactive cycle, involving I, I<sub>2</sub>, IO, IONO<sub>2</sub> and IONO<sub>2</sub>. With a low injection rate (10<sup>-4</sup> ppt.s<sup>-1</sup>), the iodine is mainly under IONO<sub>2</sub> form, I<sub>2</sub>O<sub>5</sub> becomes predominant for higher rate (1 ppt.s<sup>-1</sup>).*

*Regarding the organic simulations, results were very different. In these cases, the iodine reacts with the VOC to form iodocarbons. However, the organic mechanism is still not very well known, several species can be produced without any destruction reaction like photolysis process, leading to an accumulation in the simulations. The results revealed that the main iodine forms are iodo-cyclopentane, iodo-methylbenzene and some other iodo-alkanes.*

*Radioactive iodine speciation in the atmosphere appears to be very dependent on the conditions, and in particular the photolysis process, the pollutant levels and the iodine injection rate. The species form being important in the determination of the radiological consequences, it is relevant to include the iodine reactivity in the dispersion tools. In parallel, the organic mechanism has to be improved to reduce the lack of knowledge around the iodo-carbons.*



### III. 0D SIMULATIONS

#### 1. Inorganic Base Case

In a first step, only the inorganic mechanism has been used ({I-H-O-N} elementary system) to study the impact of the initial pollutant levels ( $O_3$ ,  $NO_x$ ), the photolysis conditions and the iodine injection rate on iodine chemical speciation.

The Inorganic Base Case is a reference simulation for atmospheric iodine behaviour, the parameters are described in Table 1. In this case, iodine is injected as  $I_2$ , a gaseous species which may be released outside during a nuclear accident. The injection rate of  $0.01 \text{ ppt.s}^{-1}$  is arbitrary, but the total injected iodine over the 10 days ( $\approx 1\text{g}$ ) is in the order of magnitude of an expected potential release in case of severe accident. The molecular iodine reacts with pollutant, which are not injected during the simulation.

To preserve the atmospheric pollution conditions, all the non-iodine species quantities are fixed. For this base case, the  $O_3$  and  $NO_2$  quantities are set to 25 ppb, which roughly corresponds to measured background levels.

Photolysis location	Gravelines (2.11°E, 51.0°N)	
Beginning	2013-08-08, 00:00	
Duration	10 days	
Pressure	$10^5 \text{ Pa}$	
Temperature	298 K	
Volume	$10^4 \text{ m}^3$	
Initial quantities (ppb)	$O_3$ 25	$NO_2$ 25
	H $2.5 \times 10^{-10}$	$H_2$ $5.5 \times 10^{-02}$
	HO $2.5 \times 10^{-04}$	$H_2O_2$ 1.0
	$HNO_2$ 0.25	$HNO_3$ 0.25
	$H_2O$ 73.4 % RH	$HO_2$ $2.5 \times 10^{-02}$
Injection - Emission	$I_2$ , $0.01 \text{ ppt.s}^{-1}$	
Non-iodine species	Fixed quantities	

Table 1: Box-Model parameters, Inorganic Base Case

The results (reported in Table 2) show that iodine, injected as  $I_2$ , rapidly reacts with the atmospheric species  $NO_x$  and  $O_3$  to form  $IONO_2$  during the night and HI during the day. Moreover,  $I_2O_5$  accumulates all along the simulation, mainly produced during the day period. A second observation concerns the importance of the day/night cycle, linked to the photolysis reaction kinetics.

The analysis of the reactional paths show that this behaviour can be explained by the formation of the I and IO radicals by photolysis, these radicals being very reactive.

#### 2. Inorganic Parameters Sensitivity Studies

From the Base Case, several parameters have been studied, to define their impact on the iodine speciation. First, the pollutant ratio  $[O_3]/[NO_2]$  have been modified from 1.0 to 1/500 and 500, in order to represent typical conditions (rural or urban with wind). Secondly, the photolysis reactions have been moderated (rates calculated for January or completely removed). Finally, the injection rates of  $I_2$  has been either multiplied or divided by 100. The results of the different cases are gathered in Table 2.

Spe.	Base Case	$[O_3]/[NO_2]$		Photolysis		Injection	
		1/500	500	Jan.	No	/100	x100
$I_2$	6.66	13.7	0.01	17.2	5.75	0.64	20.0
	9.45	48.7	0.41	10.5	5.84	0.30	15.9
HI	30.8	82.2	0.65	33.5	0.01	14.6	7.34
	2.66	12.0	0.07	0.86	0.01	0.95	0.95
HOI	0.42	0.53	0.12	2.24	4.48	0.11	0.80
	7.69	36.8	1.15	8.64	4.55	0.29	12.2
$IONO_2$	3.41	0.03	0.14	3.48	88.4	83.8	0.01
	22.3	2.25	1.23	37.5	88.1	98.4	0.03
$I_2O_5$	56.2	0.01	96.6	40.6	0.55	0.05	43.5
	56.7	0.01	94.7	41.2	0.61	0.05	42.7
$I_4O_{10}$	0.46	-	1.37	0.24	-	-	27.9
	0.50	-	1.39	0.26	-	-	28.2

Table 2: Iodine distribution (%) at the last day of simulation (10d.), at 12 am (white) and 12 pm (gray)

It has been observed that the iodine speciation can widely vary, depending on the atmospheric conditions (pollution, photolysis, injection). The most important impact concerns the repartition between the iodine oxides ( $I_xO_y$ ), the iodine nitroxides ( $INO_x$ ) and the molecular forms (HI, HOI,  $I_2$ ). Indeed, when there are no photolysis reactions, the iodine predominant form is  $IONO_2$ . With photolysis, and for  $[O_3] \gg [NO_2]$ , the  $I_xO_y$  forms become predominant. On the contrary, for  $[O_3] \ll [NO_2]$ , the iodine is mainly under HI, HOI and  $I_2$  forms.

With a low iodine injection rate, the iodine is under  $IONO_2$  form, which turns to  $I_xO_y$  with higher injection, highlighting a reaction cycle between iodine and the  $NO_x$ .

Assuming that the iodine oxides and nitroxides could nucleate to form aerosols (with different deposition rates), the iodine reactivity in the atmosphere could influence the iodine predicted deposits.

### 3.3. Global Mechanism Base Case

The inorganic mechanism was completed with some organic reactions and coupled to RACM (Regional Atmospheric Chemical Mechanism, [1]), to be more realistic of the overall iodine reactivity.

The parameters of the Global Base Case are identical to the inorganic one (Table 1), to which were added volatil organic compounds (VOC) emission rates (Kuhn & al. [11]) and VOC initial concentrations. The pollutant reactivity being included in RACM, the non-iodine species concentrations are not fixed but calculated. RACM regroup the species in 72 categories, so the non-iodine species have been converted to the RACM chemical categories. The initial VOC concentrations have been obtained with a simulation in the same conditions without iodine, including the VOC emissions rates from Kuhn & al. [11], by averaging the last day concentrations, the resulting values are detailed in Table 3. For this case, the iodine speciation is mainly under iodocarbon forms, such as  $C_2H_4I$ ,  $cC_5H_9I$  (iodocyclopentane) or benzMI (iodomethylbenzene), that highlights the predominance of the organic part of the mechanism.

ALD	1.50	HC5	1.20	OLI	$5.10^{-4}$	SO <sub>2</sub>	3.50
CSL	0.01	HC8	1.00	OLT	$1.5.10^{-2}$	CO	80.0
ETE	0.12	HCHO	4.00	TOL	0.25		
HC3	8.00	KET	10.0	XYL	0.50		

Table 3: Initial VOC concentrations (ppb) for the Global Base Case

The iodocarbons are formed by several reactions of I and  $I_2$  with the VOC (HC3, HC5, ALD, TOL, ...). However it remains an important lack of knowledge concerning the mechanism, with 25 unknown products, 11 non-destroyed species and only 13 photolysis reactions. Possible consequence would be to enhance the persistence of iodocarbons in the atmosphere.

### 3.4. Global Parameters Sensibility Studies

In order to study the impact of the VOC on the iodine speciation, several cases have been examined with VOC initial concentrations only (IC only) and with VOC emission rates only (Em only). The iodine inlet as  $I_2$  has also been changed to  $CH_3I$  ( $0.02 \text{ ppt.s}^{-1}$ ) to get the iodine inlet form importance,  $CH_3I$  being an other potential released gaseous species. The last day repartitions of iodine for this cases are presented in Table 4.

Species - Reactions	Base Case	VOC		Injection
		Em Only	IC Only	CH <sub>3</sub> I
CH <sub>2</sub> CH <sub>2</sub> I and CH <sub>3</sub> CHI	21.5	20.2	8.17	20.1
	21.6	20.3	7.79	20.2
cC <sub>5</sub> H <sub>9</sub> I	11.5	12.3	0.54	16.5
	11.3	12.1	0.52	15.8
benzMI	9.17	10.1	0.68	10.1
	8.88	9.79	0.65	9.84
IO + HC3P* products	6.48	5.75	3.01	6.78
	6.47	5.81	2.86	6.72
CH <sub>3</sub> CH <sub>2</sub> I	6.82	6.81	0.24	6.08
	6.20	6.20	0.20	5.38
CH <sub>3</sub> COI	4.78	3.97	10.8	5.30
	4.77	3.98	10.3	5.08
CH <sub>3</sub> I	0.26	0.30	-	2.55
	-	-	-	0.11
Inorganic Sum	2.44	1.65	68.4	3.61
	3.98	3.25	70.0	8.66

Table 4: Iodine distribution (%) at the last day of simulation (10d.), at 12 am (white) and 12 pm (gray). HC3P : RACM family (peroxides with 3 carbons or less)

With VOC initial concentrations only, iodine species react to form iodocarbons until consuming all the VOC inventory. The pollutant reactivity (O<sub>3</sub>, NO<sub>x</sub>, VOC) lead to the formation of inorganic species like I<sub>2</sub>O<sub>5</sub> and IONO<sub>2</sub>, which accumulates after the VOC consumption. With only VOC emission rates, the final iodine speciation is similar to the global base case. In the case with CH<sub>3</sub>I injection, the final speciation of iodine is also under iodocarbon forms. It is worth noticing the lower reactivity of CH<sub>3</sub>I with VOC compare to I<sub>2</sub>, due to a lower photolysis oxidation reaction.

The relevant impact is an increase of the inorganic sum fractions (I<sub>2</sub>O<sub>5</sub>, IONO<sub>2</sub>) and cC<sub>5</sub>H<sub>9</sub>I (iodocyclopentane), and a decreasing of the CH<sub>2</sub>CH<sub>2</sub>I and CH<sub>3</sub>CHI fraction.

### 3.5. Conclusions on the 0D Simulations

Through the 0D simulations, iodine reactivity in atmospheric conditions is high and appears to be influenced by several parameters, such as the pollutant levels (O<sub>3</sub>, NO<sub>x</sub>, VOC), the photolysis rates (location, season, day/night cycle) and the iodine level. Concerning the inorganic behaviour, iodine is able to form iodine oxides (I<sub>x</sub>O<sub>y</sub>), iodine nitroxide (IONO<sub>x</sub>) or molecular species (I<sub>2</sub>, HI, HOI), depending on the conditions. When VOC are added to the box-model, iodocarbon forms become the dominant iodine species, which can be interpreted as a high reactivity of iodine with VOC. The dose-effect factor being different for organic than for inorganic compounds, the iodocarbon formation could be a relevant point.

However the lack of reactional paths for iodocarbons could also lead to their accumulation, which can bias the simulation results. Future theoretical works and experiments in atmospheric chamber has been planned to improve this iodine mechanism.

## IV. 3D SIMULATIONS

In order to study the iodine reactivity in more relevant conditions, the 3D-chemical-transport code Polair3D-Chemistry [2] has been used, supported by the Polyphemus platform [3]. The selected 3D simulation domain is presented in Figure 3. The simulation are based on the same parameters than for the box-model studies, with the global iodine mechanism, a continuous inlet of CH<sub>3</sub>I at Gravelines location in France, during the 10 days duration of the simulation. The pollutant concentrations come from MOZART ([www2.acd.ucar.edu](http://www2.acd.ucar.edu)), the emission rates from EMEP ([www.emep.int](http://www.emep.int)), and the meteorological fields are calculated with WRF ([wrf-model.org/index.php](http://wrf-model.org/index.php)).

The Figure 4 illustrate the dispersion calculated by the code. The analysis of the time concentrations shows that the iodocarbon forms are predominant, the inorganic fraction being insignificant (1.5 % the night). The calculated differences between day and night highlight the importance of the photolysis reactions, especially for the highest vertical levels where the photolysis rates are more consequent. The 3D simulations give the same trend than 0D ones.

However, the observed iodocarbons are not exactly the same, the differences being due to the more realistic VOC emissions used. It then appears in particular a relevant concentration of  $iC_3H_5I$  ( $CH_2CHCH_2I$ ), coming from the reaction of I or  $I_2$  with toluene.

Because of the high reactivity of the iodine in the atmosphere, the speciation can be very different at a short distance from the accident location (few tens of kilometers), depending on the wind speed essentially.

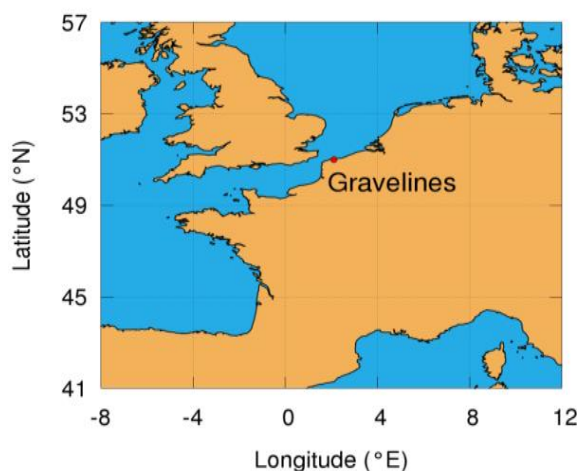


Fig. 3: 3D simulation domain. Gravelines nuclear powerplant : iodine injection point

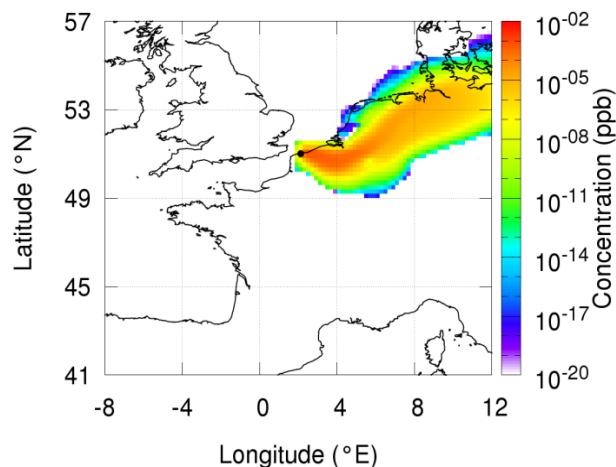


Fig. 4: Concentration of  $CH_3I$ , after 12 hours of release, altitude : 0-50 m

## V. CONCLUSIONS

The 0D and 3D simulation results show that when the iodine reactivity is activated, the accident source term (ST) speciation is

drastically changed during the iodine transport in the atmosphere.

In the ideal case without organic species, from an initial  $I_2$  ST, the final formation of iodine oxides  $I_xO_y$  and  $IONO_x$  has been obtained, with a repartition depending on the conditions such as the pollutant levels ( $O_3$ ,  $NO_x$ ), the photolysis rates (location, season, day/night cycle) and the iodine injection rate. These iodine oxides and nitroxides can nucleate by heterogeneous processes to form aerosols with different transport properties. For the inorganic part, the stability of iodine oxides in the atmosphere has to be deep because some possible reactions, for instance reduction of  $I_xO_y$  by CO into  $I_2$ , should be included but kinetic parameters are still unknown.

However, in the more realistic case with organic species, the iodine speciation becomes very different with the predominance of the iodocarbon forms. With the current knowledge, the results show an accumulation of the organic iodine, for which there remains a lot of uncertainties, such as 25 unknown reaction products, 11 non-destroyed species, and only 13 photolysis reactions. It means some works remains to do to get a firm conclusion.

To sum-up, the chemical mechanism may be further improved by a combination of experimental data and theoretical chemistry works. A last, the development of an aerosol modeling module has to be considered, to treat first radioactive iodine aerosol behaviour in the dispersion softwares as well as interactions between gaseous iodine and atmospheric aerosols knowing that  $I_2(g)$  is adsorbed onto aerosol surfaces.

## ACKNOWLEDGMENTS

This work is realised in the C3R common research laboratory (IRSN/CNRS/Lille 1), and is co-funded by the Bel-V institute.

## REFERENCES

1. W.R. Stockwell, F. Kirchner, M. Kuhn and S. Seefeld, "A New Mechanism for Regional Atmospheric Chemistry Modeling", *J GeophysicResearch*, (1997).

2. J. Boutahar, S. Lacour and V. Mallet, “Development and validation of a fully modular platform for numerical modelling of air pollution: POLAIR”, *Int J Env Pollut*, **22**, pages 17–28 (2004).
3. D. Quelo, M. Krysta, M. Bocquet, O. Isnard, Y. Minier and B. Sportisse, “Validation of the Polyphemus platform on the ETEX, Chernobyl and Algeciras cases”, *Atm Environment*, **41**, pages 5300–5315, (2007).
4. R. Vogt, R. Sander, R. Von-Glasow and P. Crutzen, “Iodine chemistry and its role in halogen activation and ozone loss in the marine boundary layer: a model study”, *J Atmospheric Chemistry*, **32**, pages 375–395 (1999).
5. G. McFiggans, J. Plane, J. Beverley and L. Carpenter, “A modeling study of iodine chemistry in the marine boundary layer”, *J Geophysic Research*, **105**, pages 14371–14385 (2000).
6. J. Calvert and S. Lindberg, “Potential influence of iodine-containing compounds on the chemistry of the troposphere in the polar spring. I ozone depletion”, *Atm Environment*, **38**, pages 5087–5104 (2004).
7. A. Mahajan, H. Oetjen, A. Saiz-Lopez, J. Lee, G. McFiggans and J. Plane, “Reactive iodine in a semi-polluted environment”, *Geophys Res Lett*, **36**, page L16803 (2009).
8. A. Saiz-Lopez, J. Plane, A. Baker, L. Carpenter, R. Von-Glasow, J. Gomez-Martin, G. McFiggans and R. Saunders, “Atmospheric Chemistry of Iodine”, *Chemical Reviews* (2011).
9. C. Ordonez, J. Lamarque, S. Tilmes, D. Kinnison, E. Atlas, D. Blake, G. Sousa-Santos, G. Brasseur and A. Saiz-Lopez, “Bromine and iodine chemistry in a global chemistry–climate model: description and evaluation of very short-lived oceanic sources”, *Atmos Chem Phys*, **12**, pages 1423–1447 (2012).
10. R. Sommariva, W. Bloss and R. Von-Glasow, “Uncertainties in the gas-phase atmospheric iodine chemistry”, *Atm Environment*, **57**, pages 219–232 (2012).
11. M. Kuhn, P.J.H. Builtjes, D. Poppe, D. Simpson, W.R. Stockwell, Y. Andersson-Skold, A. Baart, M. Das, F. Fiedler, O. Hov, F. Kirchner, P.A. Makar, J.B. Milford, M.G.M. Roemer, R. Ruhnke, A. Strand, B. Vogel and H. Vogel, “Intercomparison of the gas-phase chemistry in several chemistry and transport models”, *Atm Environment*, **32**, pages 693–70 (1998)..